IMPROVING THE CONTROL STRUCTURE OF A HIGH PRESSURE LEACHING PROCESS

by

Pieter Daniël Knoblauch

Thesis presented in partial fulfillment
of the requirements for the Degree

of

MASTER OF ENGINEERING
(EXTRACTIVE METALLURGICAL ENGINEERING)

in the Faculty of Engineering
at Stellenbosch University

Supervisor

Prof S.M. Bradshaw

Co-Supervisors

Dr C. Dorfling
Dr L. Auret

March 2015

DECLARATION

By submitting this thesis electronically, I declare that the entirety of the work contained therein is my own, original work, that I am the sole author thereof (save to the extent explicitly otherwise stated), that reproduction and publication thereof by Stellenbosch University will not infringe any third party rights and that I have not previously in its entirety or in part submitted it for obtaining any qualification.

20 February 2015
Date

Copyright © 2015 Stellenbosch University

All rights reserved

ABSTRACT

The main purpose of the base metal refinery (BMR) as operated by Lonmin at their Western Platinum Ltd BMR, is to remove base metals – such as copper and nickel – from a platinum group metal (PGM) containing matte. The leaching processes in which this is done pose several challenges to the control of the process. The most significant of these is the slow dynamics of the process, due to large process units, as well as the continuously changing composition of the first stage leach residue, which is not measured on-line. This is aggravated by the fact that the exact leaching kinetics (and therefore the effect of the disturbances) are not understood well fundamentally. The slow process dynamics mean that controllers cannot be tuned aggressively, resulting in slow control action. The large residence times and off-line composition analyses of major controlled variables also mean that the effects of operator set point changes are visible only the following day, often by a different shift of operators.

Dorfling (2012) recently developed a fundamental dynamic model of the pressure leach process at Lonmin's BMR. This dynamic model incorporates 21 chemical reactions, as well as mass and energy balances, into a system of 217 differential equations. The model provides a simulation framework within which improved control strategies can be investigated.

The primary aims of this study are twofold. The first is to validate the model for the purpose of the investigation and development of control structure improvements. This is done by comparing the model to plant data, and adapting it if necessary. The second aim to reconsider the current control philosophy to the extent that is allowed by the model's determined validity.

The current plant control philosophy aims to maintain a PGM grade of 65%, while the copper in the solids products of the second and third leaching stages should be below 25% and 3.5% by mass, respectively. Two areas of particular concern in this process that have been raised by Lonmin are the control of the temperature of the first compartment and the addition of pure sulphuric acid to control the acid concentration in the second stage leach.

Dynamic plant data were used to calibrate the model, which was migrated from its received MATLAB platform to Simulink, to assist with control development. Flow rates were imported from the data, with some data values adapted for this purpose, due to mass balance inconsistencies. The outputs from the calibrated model were compared with corresponding data values. The model was found to be suitable for the investigation and development of the control structures of pressure, temperatures and inventories (termed basic regulatory control) and the acid concentration and solids fraction in the preparation tanks (termed compositional regulatory control). It was, however, found to be inadequate for the investigation and development of supervisory control, since it does not provide accurate compositional results. The leaching of copper is especially under-predicted, with the predicted copper concentration in the second stage product being approximately 46% lower than data values.

The basic and compositional regulatory control structures were investigated. For each of these a base case was developed which aimed to represent the relevant current control structure, assuming optimal tuning. The variable pairings for the basic regulatory control were reconsidered using a method proposed by Luyben and Luyben (1997), since this part of the process does not permit the generation of a relative gain array (RGA) for variable pairing. The resulting pairing corresponds with Lonmin's current practice. Considering the temperature control of compartment 1, it was found that the addition of feed-forward control to the feedback control of the level of the flash tank improves the temperature control. More specifically, during an evaluation where the temperature's set point is varied up to 1%, the IAE of the temperature of compartment 1 was decreased with 7.5% from the base case, without disturbing the flash tank. The addition of feed-forward control allows for more rapid control and more aggressive tuning of this temperature, removing the current limit on ratio between the flash recycle stream and the autoclave feed.

The compositional control was investigated for the second stage leach only, due to insufficient flow rate and compositional information around the third stage preparation tank. Variable pairing showed that three additive streams are available for the preparation tanks of the second and third stage leach to control the acid concentration and solids fraction in those tanks. Focussing on the second stage, the aim was to determine whether the acid concentration in the flash tank can be successfully controlled without the addition of pure acid to the tank. With four streams available around the second stage preparation tank to control its mass/level, the acid concentration and solids fraction, three manipulated variables were derived from these streams. The resulting pairings were affirmed by an RGA. Control loops for the control of acid concentration and solids fraction in the flash tank were added as cascade controllers, using the preparation tank's control as secondary loops. The added compositional control was evaluated in two tests. The first of these entailed the adding of typical disturbances, being the flash recycle rate, the solids and water in the feed to the second stage preparation tank and the acid concentration in copper spent electrolyte. In the second test the control system was tested for tracking an acid concentration set point. It was found that the cascade structure controls the acid concentration in the flash tank less tightly than the base case (with an IAE that is 124% and 80.6% higher for the two tests), but that it decreases the variation of solids fraction (lowering the IAE with 40.8% with the first test) in the same tank and of the temperature in the first compartment (lowering the IAE with 73.6% in the second test). It is recommended that the relative effects of these three variables on leaching behaviour should be investigated with an improved model that is proven to accurately predict leaching reactions in the autoclave.

Key words: Simulation, Pressure Leach, Autoclave, Simulink.

OPSOMMING

The hoofdoel van die basismetaal-raffinadery (BMR), soos dit bestuur word deur Lonmin by hulle Western Platinum Ltd BMR, is om basismetale – soos koper en nikkel – te verwyder uit ’n mat wat platinum groep metale (PGM) bevat. Die logingsprosesse waarin dit gedoen word hou talle uitdagings in vir die beheer van die proses. Die mees beduidende hiervan is die proses se stadige dinamika, wat veroorsaak word deur groot proseseenhede, sowel as die deurlopend veranderende samestelling van die eerste stadium residue (wat nie aanlyn gemeet word nie). Dit word vererger deur die feit dat die presiese logingskinetika (en daarom ook die effek van versteurings) nie fundamenteel goed verstaan word nie. Die stadige dinamika beteken dat die beheerders die aggressief verstel kan word nie, en dit lei tot stadige beheeraksies. Die groot verblyftye en aflyn samestellingsanalises van die belangrikste beheerde veranderlikes beteken dat die gevolge van ’n operateur se stelpunt veranderinge slegs die volgende dag sigbaar is – dikwels in die skof van ’n ander operateur.

Dorfling (2012) het onlangs ‘n fundamentele, dinamiese model van die drukloog proses by Lonmin se BMR ontwikkel. Hierdie dinamiese model inkorporeer 21 chemiese reaksies, sowel as massa- en energiebalanse, in ’n stelsel van 217 differensiaalvergelykings. Die model bied ’n simulasie-raamwerk waarbinne verbeterde beheerstrategieë ondersoek kan word.

Die hoofdoel van hierdie studie is tweeledig. Die eerste hiervan is om die model te valideer vir die ondersoek en ontwikkelling van beheerstruktuur verbeteringe. Dit is gedoen deur die model met aanlegdata te vergelyk en dit aan te pas, indien nodig. Die tweede doel is om die huidige beheerfilosofie te heroorweeg tot op ’n punt wat toegelaat word deur die bepaalde geldigheid van die model.

Die huidige beheerfilosofie van die aanleg mik om ’n gehalte van 65% te handhaaf, terwyl die koper in die vastestof produk van die tweede en derde logingsstadia onderskeidelik onder 25% en 3.5% op ’n massa basis moet wees. Twee probleem-areas, soos ge-opper deur Lonmin, is die beheer van die temperatuur in die eerste kompartement en die byvoeging van suiwer swaelsuur om die suurkonsentrasie van die tweede stadium te beheer.

Dinamiese aanlegdata is gebruik om die model te kalibreer. Hierdie model is van die oorspronklike MATLAB platform na Simulink gemigreer, ten einde beheerontwikkelling te vergemaklik. Vloeitempo’s is van die data af ingevoer na die model toe, met sekere data waardes wat aangepas is vanweë massabalans inkonsekwenthede. Die uitsette van die gekalibreerde model is met die ooreenstemmende data waardes vergelyk. Daar is bevind dat die model geskik is vir die ondersoek en ontwikkelling van die beheer van druk, temperature en tenks (basiese reguleringsbeheer), sowel as die beheer van suurkonsentrasies en vastestoffraksies in die bereidingstenks (reguleringsbeheer van die samestelling). Daar is egter bevind dat die model nie

geskik is vir die ondersoek en ontwikkelling van toesigbeheer nie, aangesien dit nie akkurate samestellingsresultate genereer nie. Die voorspelde loging van koper is veral te laag, met die model wat koperkonsentrasies vir die tweede stadium voorspel wat ongeveer 46% laer is as ooreenstemmende data waardes.

Die basiese en samestelling reguleringsbeheer strukture is ondersoek. Vir elkeen is 'n basisgeval ontwikkel wat poog om die huidige beheerstruktuur te verteenwoordig, met optimale verstellings aanvaar. Die paring van veranderlikes vir die basiese reguleringsbeheer is heroorweeg met deur middel van 'n metode wat deur Luyben en Luyben (1997) voorgestel is, aangesien hierdie deel van die proses nie die opstel van 'n relatiewe winsmatriks (RWM) vir die paring toelaat nie. Die uiteindelike paring stem ooreen met Lonmin se huidige praktyk. Met die heroorweging van die temperatuurbeheer van kompartement 1 is daar bevind that die byvoeging van vooruitvoer beheer by die terugvoerbeheer van die flitstenk die temperatuurbeheer verbeter. Meer spesifiek het die IAE van hierdie temperatuur met 7.5% verlaag van die basisgeval af nadat die temperatuur se stelpunt tot met 1% gevariëer is – sonder om die flitstenk te versteur. Die byvoeging van vooruitvoer beheer laat vinniger beheer en meer aggressiewe verstellings van die temperatuur toe, aangesien die huidige beperking op die verhouding tussen die flitsstroom en die outoklaaf voer verwyder word.

Die samestellingsbeheer is slegs ondersoek in die geval van die tweede loogstadium as gevolg van onvoldoende vloeitempo- en samestellingsinligting om die bereidingstenk van die derde stadium. Die paring van veranderlikes het gewys dat drie voerstrome onderskeidelik beskikbaar is vir beide die bereidingstenks van die tweede en derde stadia, om die suurkonsenstrasies en vastestoffraksies in hierdie tenks te beheer. Met die fokus op die tweede stadium was die doel om te bepaal of die suurkonsentrasie in die flitstenk suksesvol beheer kan word sonder dat suiwer suur by hierdie tenk gevoeg word. Met vier strome beskikbaar rondom die bereidingstenk van die tweede stadium om die massa/vlak, die suurkonsentrasie en die vastestoffraksie te beheer, is drie manipuleerde veranderlikes vanuit hierdie strome afgelei. Die uiteindelike paring is bevestig deur 'n RWM. Beheerlusse is ingevoeg vir die beheer van die suurkonsentrasie en vastestoffraksie in die flitstenk, met die bereidingstenk se beheer wat dien as sekondêre lusse in kaskadebeheer. Die kaskadebeheer is geëvalueer in twee toetse. Die eerste hiervan behels die invoer van tipiese versteurings, soos die vloeitempo van die flitsstroom, die vastestof en water in die voer na die tweede stadium se bereidingstenk en die suurkonsentrasie in die gebruikte elektroliet. In die tweede toets is die vermoë van die beheerstelsel om 'n suurkonsentrasie stelpunt te volg getoets. Daar is bevind dat die kaskadestruktuur die suurkonsentrasie minder nougeset beheer as die basisgeval (met 'n IAE wat 124% en 80.6% hoër is vir die twee toetse), maar dat dit die variasie in die vastestoffraksie in dieselfde tenk (40.8% vermindering van die IAE in die eerste toets) en in die temperatuur van die eerste kompartement (73.6% vermindering van die IAE in die tweede toets) beduidend verminder. Daar word aanbeveel dat die relatiewe

effekte van hierdie drie veranderlikes op logingsoptrede ondersoek moet word, met die gebruik van 'n model wat logingsreaksies in die outoklaaf akkuraat voorspel.

Sleutelwoorde: Simulasie, Drukloog, Outoklaaf, Beheerstruktuur.

ACKNOWLEDGEMENTS

I want to thank the following persons for their roles in this project and in my life in 2013/2014:

Firstly my parents (Kobus and Riana), my brother (Stefan) and Alisa – for giving me perspective, especially in frustrating times. I will not even attempt to say anything more that this: your unconditional love is the light that helps me see.

My friends, my small groups of 2013 and 2014, and especially Herman Franken – for willing ears, for prayers and for encouraging me not only with words, but also by sharing a drink and being wonderful witnesses to my life.

My supervisors – for guidance throughout this project. Prof Bradshaw, for your ability to always keep a project's bigger picture in sight. Dr. Auret, for the wealth of knowledge you brought to the table. Dr. Dorfling, for your help in clarifying difficult concepts, especially at the start of this project. It was an honour to work with the three of you.

My fellow post-graduate students – for every soccer game and for good times in the office. Doing this on my own would not have been possible.

Adriaan Haasbroek and Dr. JP Barnard, as well as fellow students Brian Lindner, Jason Miskin and Adriaan Henning – for helping me with various parts of this project (especially concerning the model). Sometimes one needs help and other times sympathy and you guys were generous with both of these.

Mintek, especially the measurements and control division – for giving me a bursary to be able to do this project.

Lonmin, and especially Nico Steenekamp and John Burchell – for answering my numerous questions, welcoming me to the plant in 2013 and giving me the data I need to do this project.

And finally, the Almighty *I Am* – by the grace of Whom I can take part in this thing called life. I am forever in awe... I did this project for You.

"The real voyage of discovery consists not in seeking new landscapes,
but in having new eyes." – *Marcel Proust*

TABLE OF CONTENTS

Abstract .... **iv**
Opsomming .... **viii**
Acknowledgements .... **xii**
List of Figures .... **xx**
List of Tables .... **xxxii**
Chapter 1: Introduction **38**
1.1 Background and Process Description 40
1.1.2 The Base Metal Refinery 41
1.1.3 Atmospheric and Pressure Leach 42
1.2 Project Description 43
1.2.1 Background 43
1.2.2 Purpose of Project 43
1.2.3 Project Methodology 43
1.3 Objectives, Scope and Deliverables 45
1.3.1 Aims and Objectives 45
1.3.2 Hypothesis 45
1.3.3 Scope 45
1.3.4 Thesis Overview 45
Chapter 2: Pressure Leach Process & Current Control **46**
2.1 Chapter Introduction 48
2.2 Process Description 49
2.2.1 Summary: First Stage 49
2.2.2 Pressure Leach 49
2.3 Current Control Philosophy and Variables 52
2.3.1 Process & Control Objectives 52
2.3.2 Challenges to Control 52
2.3.3 Key Variables 53
2.3.4 Control Loops 53
2.3.5 Control Hierarchy 57
2.3.6 Recommendations 58
Chapter 3: Data Processing & Model Validation **60**
3.1 Chapter Introduction 62
3.2 Literature Review 63
3.2.1 Data Analysis and Processing 63
3.2.2 Model Validation & Verification 64
3.3 Data Generation & Processing 69

3.3.1 Data Acquisition 69
3.3.2 Data Processing 70
3.3.3 Data Summary & Completeness 70
3.3.4 Internal Consistency 74
3.4 Dynamic Model Description 80
3.4.1 Original Purpose 80
3.4.2 Form and Working 80
3.4.3 Previously Added Control 81
3.4.4 Differential Equation Solver Used 82
3.5 Model Migration & Verification 83
3.5.1 Model Migration to Simulink 83
3.5.2 Computer Model Verification 84
3.6 Conceptual Model Validation 85
3.6.1 Model Purpose & Required Accuracy 85
3.6.2 Applicability of Conceptual Model to Purpose 85
3.6.3 Conceptual Model Changes 86
3.6.4 Validation Input Conditions 94
3.7 Sanity Checks 98
3.8 Operational Validation 100
3.8.1 Adaptions to Model for Validation 100
3.8.2 Validation Overview 102
3.8.3 Operational Validation Findings 106
3.8.4 Sensitivity Analysis 108
3.8.5 Copper Reaction Rate Adaption 111
3.9 Section Conclusions 113
Chapter 4: Regulatory Control Development & Evaluation 116
4.1 Chapter Introduction 118
4.2 Literature Review 119
4.2.1 Control Objectives 119
4.2.2 Challenges to Control in the Chemical Process Industry 121
4.2.3 Process Control Development 123
4.2.4 Control Selection 124
4.2.5 Feedback Control Structure & Tuning 125
4.2.6 Variable Pairing & Controllability 130
4.2.7 Enhancements to Feedback Control 131
4.3 Base Case Model For Basic Regulatory Control 135
4.3.1 Base Case Mass Controllers 135
4.3.2 Other PID Controllers 136

4.3.3 Controller Fine-tuning 137
4.4 Basic Regulatory Control Variable Pairing 140
4.4.1 Introduction & Method 140
4.4.2 Control Degrees of Freedom 141
4.4.3 Valve for Production Rate 142
4.4.4 MVs for Influential Variables 143
4.4.5 Inventory Control 144
4.4.6 Controller Tuning 145
4.5 Alternative Control on 400-TK-20 146
4.5.1 Design 146
4.5.2 Evaluation & Comparison 150
4.5.3 Model Predictive Control 156
4.6 Section Conclusions 158
Chapter 5: Compositional & Supervisory Control 160
5.1 Chapter Introduction 162
5.2 Literature Review 163
5.2.1 Advanced Regulatory Control on Autoclaves 163
5.2.2 Enhancements to Feedback Control 164
5.2.3 Model Predictive Control 166
5.3 Base Case Structure of Compositional Control 167
5.3.1 Introduction 167
5.3.2 Tuning and Fine-Tuning 167
5.4 Variable Pairing for Compositional Control 168
5.4.1 Allocation of Remaining CVs 168
5.4.2 Introduction to Compositional Control in 400-TK-10 & 400-TK-20 170
5.5 Compositional Control on 400-TK-10 172
5.5.1 Preliminary MV Allocation 172
5.5.2 Proposed Design 173
5.5.3 Split-range Control Design Criteria 174
5.5.4 MV Definitions 174
5.5.5 Pairing & Controllability Evaluation by RGA 175
5.5.6 Mass Controller Tuning 176
5.5.7 Solids Fraction Controller Initial Tuning 176
5.5.7 Split-Range Acid Controller Tuning 176
5.5.8 Removal of Stream 23 177
5.5.9 Controller Fine Tuning 178
5.6 Cascade Control on 400-TK-20 & 400-TK-10 179
5.6.1 Desirability & Design Criteria 179

    5.6.2 Cascade Controller Tuning 179
  5.7 Compositional Control Evaluation 182
    5.7.1 Disturbance Rejection: Procedure 182
    5.7.2 Disturbance Rejection: Evaluation 182
    5.7.3 Set Point Tracking: Procedure 189
    5.7.4 Set Point Tracking: Evaluation 190
    5.7.5 Second Stage Compositional Control Structure: Best Practice 193
    5.7.6 400-TK-050 Control Discussion 194
  5.8 Supervisory Control 196
    5.8.1 Identification of Key Variables 196
    5.8.2 CV Selection & Development 197
    5.8.3 Recommendations for Future Work 198
  5.9 Section Conclusions 199
Chapter 6: Conclusions & Recommentations 202
  6.1 Summary of Conclusions 204
  6.2 Recommendations & Future Work 207
References 208
Appendix A: Current Lonmin Process 216
Appendix B: Model m-File Actions 219
Appendix C: Pressure Leach Reactions 225
Appendix D: Operational Validation Plots 229
  D1 Validation: 400-TK-10 & 400-TK-20 232
  D2 Validation: Second Stage Leach 240
  D3 Validation: 400-TK-040 & 400-TK-050 251
  D4 Validation: Third Stage Leach 256
Appendix E: Model Inputs for Investigation in Section 3.8.5 263
Appendix F: Controller Tuning for Chapter 4 267
  F1 Controller Tuning for Chapter 4 Base Case 269
    F1.1 Mass Controllers 269
    F1.2 Other Controllers 270
    F1.3 Fine Tuning 278
  F2 Controller Fine-Tuning for Re-Paired Model 296
  F3 Controller fine-Tuning for Model vir FF Control 297
Appendix G: Controller Tuning for Chapter 5 301
  G1 Controller Tuning for the Base Case of Chapter 5 303
    G1.1 Initial Tuning 303
    G1.2 Fine-tuning of Compositional Control Base Case 304
  G2 Controller Tuning for Model with Compositional Regulatory Control 307

G2.1 Solids Controller ... 307
G2.2 Acid Controller ... 309
G2.3 Fine-Tuning of Control on 400-TK-10 ... 312
G2.4 Outside Solids Controller ... 316
G2.5 Outside Acid Controller ... 318
G2.6 Fine-Tuning of Compositional Control on 400-TK-20 ... 320
Appendix H: Compositional Control Evaluation for Chapter 5 ... 327
H1 Plots for Compositional Regulatory Control Evaluation – Disturbance Rejection ... 329
H1.1 Evaluation of Base Case – Disturbance Rejection ... 329
H1.2 Evaluation Cascade Compositional Control – Disturbance Rejection ... 334
H2 Plots for Compositional Regulatory Control Evaluation – Acid Set Point Tracking 341
H2.1 Evaluation of Base Case – Acid Set Point Tracking ... 341
H2.2 Evaluation of Cascade Compositional Control – Acid Set Point Tracking. 345
Appendix I: Simulink Models for chapters 4 & 5 on Disk ... 351

LIST OF FIGURES

Figure 1: Schematic representation of the PGM refining process sequence (drawn from information by Crundwell et al, 2011) 40
Figure 2: Schematic representation of the stages at a base metal refinery (drawn from information by Crundwell et al, 2011) 41
Figure 3: Simplified schematic representation of the pressure leach process at Lonmin, with basic control loops and stream numbers indicated. 50
Figure 4: Simplified schematic representation of the pressure leach process at Lonmin, with basic control loops and stream numbers indicated. 54
Figure 5: Simplified diagram of the model validation & verification process (redrawn from Sargent, 2013) 65
Figure 6: Simplified schematic representation of the pressure leach process at Lonmin, with basic control loops and stream numbers indicated. 72
Figure 7: Plot of the level of 400-TK-10 over the total data range (in 10 second intervals) 75
Figure 8: Plot of the mass balance error around 400-TK-10 for a region of minimal level change 76
Figure 9: Plot of the level of 400-TK-20 over the total data range (in 10 second intervals) 77
Figure 10: Plot of mass balance error into 400-TK-20 for a region of minimal level change 78
Figure 11: Flow Chart of Dorfling's Original Second/Third Stage Leach Dynamic Model 81
Figure 12: The setup of the PI controller of 400-TIC-2001 in Simulink 84
Figure 13: Diagram of the pressure leach process, with the relevant process variable tags added. 87
Figure 14: Simplified schematic representation of the pressure leach process at Lonmin, with basic control loops and stream numbers indicated 103
Figure 15: Block diagram of a feedback control system (Redrawn from Marlin, 2000) 125
Figure 16: Block diagram of a PID control system, as typically implemented in Simulink. 126
Figure 17: Block diagram of a cascade control system (Redrawn from Marlin, 2000) 132
Figure 18: Block diagram of a feedback control system with feed-forward control (Redrawn from Marlin, 2000) 133
Figure 19: Block diagram of a typical mass controller in this project 136
Figure 20: Block diagram of the 400-TIC-2001 controller, with the flash recycle flow rate as MV. 138
Figure 21: Block diagram as the autoclave's pressure controller, with the total oxygen additional rate as MV. 139
Figure 22: Diagrammatic representation of the interconnectedness of pressure, as representative variable of the vapour space. 140

Figure 23: Simplified schematic representation of the pressure leach process at Lonmin, with basic control loops and stream numbers indicated 141
Figure 24: Block diagram of a feedback control system with feed-forward control (Redrawn from Marlin, 2000) 147
Figure 25: Block diagram of the feed-forward and feedback temperature controller. 149
Figure 26: Plot of the base case model's SP (red) and measured value (blue) of the temperature in the first compartment (°C) vs time (hours). There is not offset at steady-state. Maximum deviation = 1.01%. nIAE = 2.997e-4. 151
Figure 27: Plot of the base case model's flash recycle flow rate (kg/h) vs time (h) 152
Figure 28: Plot of the base case model's mass flow rate of stream 7 (kg/h) against time (h) 152
Figure 29: Plot of the base case model's mass inside 400-TK-20 versus time (h). Steady-state offset. Maximum deviation = 0.04%. nIAE = 1.716e-5. 153
Figure 30: Plot of the FF model's SP (red) and measured value (blue) of the temperature in the first compartment (°C) vs time (hours). There is no offset at the new steady-state. Maximum deviation = 1.01%. nIAE = 2.773e-4. 154
Figure 31: Plot of the FF model's flash recycle flow rate (kg/h) vs time (h). Offset at steady-state. 154
Figure 32: Plot of the FF model's mass flow rate of stream 7 (kg/h) against time (h). Offset at steady-state. 155
Figure 33: Plot of the FF model's mass inside 400-TK-20 versus time (h). There is a steady-state offset of -0.0036%. Maximum deviation = 0.046%. nIAE = 2.764e-5. 155
Figure 34: Block diagram of a split-range control system (Redrawn from Marlin, 2000) 164
Figure 35: Block diagram of a feedback control system with inferential control (redrawn from Marlin (2000)). 165
Figure 36: Block diagram of a simple MPC control system (Redrawn from Marlin, 2000) 166
Figure 37: Simplified schematic representation of the pressure leach process at Lonmin, with basic control loops and stream numbers indicated 168
Figure 38: Diagrammatic representation of a cascade control structure that can be applied to the control of acid concentration and density for the second stage leach. 171
Figure 39: Block diagram of the proposed split-range controller used for the control of acid in 400-TK-10. It is a snap shot of the simulation in Simulink 177
Figure 40: Block diagram of the proposed mass control structure for 400-TK-10 180
Figure 41: Block diagram of the proposed solids fraction cascade control structure for the second stage leach. A and B refer to the primary and secondary loops, respectively. 180
Figure 42: Block diagram of the proposed acid concentration cascade control structure for the second stage leach. A and B refer to the primary and secondary loops, respectively. 181

Figure 43: Plot of the set point (red) and measured (blue) base case acid concentration values for 400-TK-20 (g/L), versus time (hours). IAE = 0.0042, Maximum deviation = 0.56%. No steady-state offset. 183
Figure 44: Plot of the set point (red) and measured (blue) developed model's acid concentration values for 400-TK-20 (g/L), versus time (hours). IAE = 0.0094, Maximum deviation = 0.80%. No steady-state offset. 184
Figure 45: Plot of the set point (red) and measured (blue) base case solids fraction values for 400-TK-20, versus time (hours). IAE = 0.038, Maximum deviation = 1.64%. 184
Figure 46: Plot of the set point (red) and measured (blue) developed model's solids fraction values for 400-TK-20, versus time (hours). IAE = 0.0225, Maximum deviation = 1.08%. 185
Figure 47: Plot of the base case model's mass of the contents of 400-TK-20 (kg), versus time (hours). IAE = 7.487e-5, Maximum deviation = 0.0053%. 186
Figure 48: Plot of the developed model's mass of the contents of 400-TK-20 (kg), versus time (hours). IAE = 7.65e-5, Maximum deviation = 0.0023% 186
Figure 49: Plot of the developed model's temperature of compartment 1 (°C) versus time (hours). IAE = 0.0023, Maximum deviation = 1%. No steady-state offset. 187
Figure 50: Plot of the developed model's temperature of compartment 1 (°C) versus time (hours). IAE = 0.0022, Maximum deviation = 1%. No steady-state offset. 187
Figure 51: Plot of the percentage of the solid copper leached in the second stage leach in the base case model versus time (hours). Maximum deviation =4.3% 188
Figure 52: Plot of the percentage of the solid copper leached in the second stage leach in the newly developed model versus time (hours). Maximum deviation =2.75% 189
Figure 53: Plot of the set point (red) and measured (blue) base case acid concentration values for 400-TK-20 (g/L), versus time (hours). IAE = 0.0284, Maximum deviation= 4.01%. 191
Figure 54: Plot of the set point (red) and measured (blue) developed model's acid concentration values for 400-TK-20 (g/L), versus time (hours). IAE = 0.0513, Maximum deviation = 4.2%. 191
Figure 55: Plot of the set point (red) and measured (blue) values for the temperature of compartment 1 (°C) versus time (in hours). IAE = 1.171e-4, Maximum deviation= 0.006%. 192
Figure 56: Plot of the set point (red) and measured (blue) values for the temperature of compartment 1 (°C) versus time (in hours). IAE = 3.096e-5, Maximum deviation= 0.001%. 193
Figure 57: Diagram of the section between the second and third stage leach. 195
Figure 58: Diagram of the proposed supervisory control parameters, showing the true and inferential CVs, along with the supervisory control MVs, which are the SPs of the regulatory control. % Solids is maintained within predefined ranges. 198
Figure 59: Diagram of the pressure leach process at Lonmin's BMR, as on 30 August 2013. 218
Figure 60: Plot of the extent to which 400-TK-10 is full in the data and the model, with the instantaneous error percentages given. 232

Figure 61: Plot of the volumetric flow rate of stream 1 against time, with the instantaneous error percentages given. 233
Figure 62: Plot of the acid concentration in 400-TK-10 against time. 234
Figure 63: Plot of the volumetric flow rate of stream 2 against time. 234
Figure 64: Plot of the volumetric flow rate of stream 7 against time, with the instantaneous error percentages given. 235
Figure 65: Plot of the volumetric flow rate of stream 9 against time, with the instantaneous error percentages given. 236
Figure 66: Plot of the extent to which 400-TK-20 is full in the data and the model, with the instantaneous error percentages given. 237
Figure 67: Plot of the model's calculated acid concentration in 400-TK-20 against time. 238
Figure 68: Plot of the mass flow rate of the pure acid stream entering 400-TK-20 238
Figure 69: Plot of the acid concentration in 400-TK-20, as it is in the data, against time. 239
Figure 70: Plot of the temperature of compartment 1 against time, with the instantaneous error percentages given. 240
Figure 71: Plot of the temperature of compartment 2 against time, with the instantaneous error percentages given. 241
Figure 72: Plot of the temperature of compartment 3 against time, with the instantaneous error percentages given. 242
Figure 73: Plot of the autoclave pressure against time, with the instantaneous error percentages given. 243
Figure 74: Plot of the mass flow rate of stream 10 against time, with the instantaneous error percentages given. 244
Figure 75: Plot of the volumetric flow rate of stream 14 against time, with the instantaneous error percentages given. 245
Figure 76: Plot of the extent to which compartment 3 is full in the data and the model, with the instantaneous error percentages given. 246
Figure 77: Plot of model values for percentage base metals and PGMs in the second stage leach residue vs time 247
Figure 78: Plot of model values for concentration of base metals and PGMs in the second stage leach residue vs time 249
Figure 79: Plot of model values of the acid concentration in the third autoclave compartment, versus time. 250
Figure 80: Plot of the extent to which 400-TK-040 is full in the data and the model, with the instantaneous error percentages given. 251
Figure 81: Plot of the volumetric flow rate of stream 15 against time, with the instantaneous error percentages given. 251

Figure 82: Plot of the extent to which 400-TK-050 is full in the data and the model, with the instantaneous error percentages given. 252
Figure 83: Plot of the volumetric flow rate of stream 18 against time, with the instantaneous error percentages given. 253
Figure 84: Plot of the volumetric flow rate of stream 19 against time, with the instantaneous error percentages given. 253
Figure 85: Plot of the model's acid concentration for 400-TK-050. 254
Figure 86: Plot of the data's acid concentration for 400-TK-050. 254
Figure 87: Plot of the temperature of compartment 4 against time, with the instantaneous error percentages given. 256
Figure 88: Plot of the extent to which compartment 4 is full in the data and the model, with the instantaneous error percentages given. 257
Figure 89: Plot of model values for percentage base metals and PGMs in the third stage leach residue vs time 258
Figure 90: Plot of model values for concentration of base metals and PGMs in the third stage leach residue vs time 260
Figure 91: Plot of the model's calculated acid concentration in compartment 4, versus time. 261
Figure 92: Plot of the data's acid concentration in compartment 4, versus time. 262
Figure 93: Plot of the mass flow rate of the water in the cooling coils of compartment 3 (in kg/h) vs time (in hours) 270
Figure 94: Plot of the temperature of compartment 3 (in °C) vs time (in hours) 271
Figure 95: Plot of the mass flow rate of the steam entering compartment 4 (in kg/h) vs time (in hours) 272
Figure 96: Plot of the temperature of compartment 4 (in °C) vs time (in hours) 273
Figure 97: Plot of the total oxygen mass flow rate into the autoclave (in kg/h) vs time (in hours) 274
Figure 98: Plot of the absolute autoclave pressure (in bar) vs time (in hours) 275
Figure 99: Plot of the set point of the temperature of compartment 1 versus time (in hours) 276
Figure 100: Plot of the temperature of compartment 1 versus time (in hours) 277
Figure 101: Plot of set point sent to the mass controller of 400-TK-10 vs time (in hours) 278
Figure 102: Plot of the mass flow rate of stream 1 vs time (in hours) 278
Figure 103: Plot of the mass of 400-TK-10 vs time (in hours) 279
Figure 104: Plot of set point (red) and measured (blue) values of the mass in 400-TK-20 vs time (in hours) 280
Figure 105: Plot of the mass flow rate of stream 7 vs time (in hours) 280
Figure 106: Plot of set point (red) and measured (blue) values of the mass in compartment 3 vs time (in hours) 281
Figure 107: Plot of the mass flow rate of stream 14 vs time (in hours) 281

Figure 108: Plot of set point (red) and measured (blue) values of the mass in compartment 3 vs time (in hours) ... 282
Figure 109: Plot of the mass flow rate of stream 14 vs time (in hours) ... 282
Figure 110: Plot of set point (red) and measured (blue) values of the mass in compartment 4 vs time (in hours) ... 283
Figure 111: Plot of the mass flow rate of stream 22 vs time (in hours) ... 283
Figure 112: Plot of set point (red) and measured (blue) values of the mass in 400-TK-040 vs time (in hours) ... 284
Figure 113: Plot of the mass flow rate of stream 15 vs time (in hours) ... 284
Figure 114: Plot of set point (red) and measured (blue) values of the mass in 400-TK-040 vs time (in hours) ... 285
Figure 115: Plot of the mass flow rate of stream 15 vs time (in hours) ... 285
Figure 116: Plot of set point (red) and measured (blue) values of the mass in 400-TK-050 vs time (in hours) ... 286
Figure 117: Plot of the mass flow rate of stream 18 vs time (in hours) ... 286
Figure 118: Plot of set point (red) and measured (blue) values of the temperature of compartment 1 (^{o}C) vs time (in hours) ... 287
Figure 119: Plot of the mass flow rate of stream 9 vs time (in hours) ... 287
Figure 120: Plot of the mass flow rate of stream 9 (limited to 95% of stream 7) vs time (in hours) ... 288
Figure 121: Plot of set point (red) and measured (blue) values of the temperature of compartment 1 (^{o}C) vs time (in hours) ... 288
Figure 122: Plot of the mass flow rate of stream 9 vs time (in hours) ... 289
Figure 123: Plot of the mass flow rate of stream 9 (limited to 95% of stream 7) vs time (in hours) ... 289
Figure 124: Plot of set point (red) and measured (blue) values of the temperature of compartment 3 (^{o}C) vs time (in hours) ... 290
Figure 125: Plot of the mass flow rate of the cooling water for compartment 3 vs time (in hours) ... 290
Figure 126: Plot of set point (red) and measured (blue) values of the temperature of compartment 3 (^{o}C) vs time (in hours) ... 291
Figure 127: Plot of the mass flow rate of the cooling water for compartment 3 vs time (in hours) ... 291
Figure 128: Plot of set point (red) and measured (blue) values of the temperature of compartment 4 (^{o}C) vs time (in hours) ... 292
Figure 129: Plot of the mass flow rate of the steam into compartment 4 vs time (in hours) ... 292
Figure 130: Plot of set point (red) and measured (blue) values of the temperature of compartment 4 (^{o}C) vs time (in hours) ... 293

Figure 131: Plot of the mass flow rate of the steam into compartment 4 vs time (in hours) 293
Figure 132: Plot of set point (red) and measured (blue) values of the autoclave pressure (bar) vs time (in hours) 294
Figure 133: Plot of the mass flow rate of stream 10 vs time (in hours) 294
Figure 134: Plot of set point (red) and measured (blue) values of the autoclave pressure (bar) vs time (in hours) 295
Figure 135: Plot of the mass flow rate of stream 10 vs time (in hours) 295
Figure 136: Plot of set point (red) and measured (blue) values of the mass 400-TK-050 vs time (in hours) 296
Figure 137: Plot of the mass flow rate of stream 21 vs time (in hours) 296
Figure 138: Plot of set point (red) and measured (blue) values of the temperature of compartment 1, versus time (hours) 297
Figure 139: Plot of the mass flow rate of stream 9 (kg/h) versus time (in hours) 298
Figure 140: Plot of set point (red) and measured (blue) values of the mass in 400-TK-20 (kg), versus time (in hours) 298
Figure 141: plot of the mass flow rate of stream 7 (kg/h) versus time (in hours) 299
Figure 142: Plot of the set point (red) and measured (blue) values of the acid concentration in 400-TK-20 (g/L) versus time (in hours). 303
Figure 143: Plot of the mass flow rate of stream 23 (kg/h) versus time (in hours). 304
Figure 144: Plot of the set point (red) and measured (blue) values of the acid concentration in 400-TK-20 (in g/L) versus time (in hours). 304
Figure 145: Plot of the mass flow rate of stream 23 (kg/h). 305
Figure 146: Plot of the set point (red) and measured (blue) values of the acid concentration in 400-TK-20 (in g/L) versus time (in hours). 305
Figure 147: Plot of the mass flow rate of stream 23 (kg/h). 306
Figure 148: Plot of the ratio between the mass flow rates of stream 1 and streams 2 to 4, versus time (hours) 307
Figure 149: Plot of the solids fraction in 400-TK-10 (kg/kg) versus time (hours) 307
Figure 150: Plot of the ratio between the mass flow rates of streams 3 and 2, versus time (hours) 309
Figure 151: Plot of the acid concentration in 400-TK-10 (in kg/L) versus time (h) 309
Figure 152: Plot of the ratio between the mass flow rates of streams 4 and 2, versus time (hours) 310
Figure 153: Plot of the acid concentration in 400-TK-10 (in kg/L) versus time (h) 311
Figure 154: Plot of set point (red) and measurement (blue) of the acid concentration in 400-TK-10 vs time (in hours). 312
Figure 155: Plot of ratio between the mass flow rates of streams 4 and 2 vs time (in hours), with the ratio between flow rates 3 and 2 at zero. 312

Figure 156: Plot of set point (red) and measurement (blue) of the acid concentration in 400-TK-10 vs time (in hours) 313
Figure 157: Plot of ratio between the mass flow rates of streams 4 and 2 vs time (in hours) 313
Figure 158: Plot of set point (red) and measurement (blue) of the solids fraction in 400-TK-10 vs time (in hours) 314
Figure 159: Plot of ratio between the mass flow rates of stream 1 and the sum of streams 2 to 4, vs time (in hours) 314
Figure 160: Plot of set point (red) and measurement (blue) of the solids fraction in 400-TK-10 vs time (in hours) 315
Figure 161: Plot of ratio between the mass flow rates of stream 1 and the sum of streams 2 to 4, vs time (in hours) 315
Figure 162: Plot of the set point (red) and measurement (blue) values of the solids fraction in 400-TK-10 vs time (in hours). This is the MV of the primary controller and CV of the secondary controller. 316
Figure 163: Plot of the set point (red) and measurement (blue) values of the solids fraction in 400-TK-20 vs time (in hours). This is the CV of the primary controller. 316
Figure 164: Plot of the ratio between the mass flow rates of streams 1 and the sum of streams 2-4 versus time (in hours). This is the MV of the secondary controller. 317
Figure 165: Plot of the set point (red) and measurement (blue) values of the acid concentration in 400-TK-10 vs time (in hours). This is the MV of the primary controller and CV of the secondary controller. 318
Figure 166: Plot of the set point (red) and measurement (blue) values of the acid concentration in 400-TK-20 vs time (in hours). This is the CV of the primary controller. 318
Figure 167: Plot of the ratio between the mass flow rates of streams 4 and 2 versus time (in hours). This is an MV of the secondary controller. 319
Figure 168: Plot of set point (red) and measured (blue) values for the acid concentration of 400-TK-20 (g/L) versus time (in hours). 320
Figure 169: Plot of set point (red) and measured (blue) values for the acid concentration of 400-TK-20 (g/L) versus time (in hours). 320
Figure 170: Plot of the ratio between the mass flow rates of streams 4 and 2 (kg/kg) versus time (in hours). 321
Figure 171: Plot of set point (red) and measured (blue) values for the solids fraction in 400-TK-20 (kg/kg) versus time (in hours). 321
Figure 172: Plot of set point (red) and measured (blue) values for the solids fraction in 400-TK-10 (kg/kg) versus time (in hours). 322
Figure 173: Plot of the ratio between the mass flow rates of streams 1 and 2 to 4 (kg/kg) versus time (in hours). 322

Figure 174: Plot of set point (red) and measured (blue) values for the acid concentration of 400-TK-20 (g/L) versus time (in hours). 323
Figure 175: Plot of set point (red) and measured (blue) values for the acid concentration of 400-TK-20 (g/L) versus time (in hours). 323
Figure 176: Plot of the ratio between the mass flow rates of streams 4 and 2 (kg/kg) versus time (in hours). 324
Figure 177: Plot of the ratio between the mass flow rates of streams 3 and 2 (kg/kg) versus time (in hours). 324
Figure 178: Plot of set point (red) and measured (blue) values for the solids fraction in 400-TK-20 (kg/kg) versus time (in hours). 325
Figure 179: Plot of set point (red) and measured (blue) values for the solids fraction in 400-TK-10 (kg/kg) versus time (in hours). 325
Figure 180: Plot of the ratio between the mass flow rates of streams 1 and 2 to 4 (kg/kg) versus time (in hours). 326
Figure 181: Plot of the set point (red) and measured (blue) base case acid concentration values for 400-TK-20 (g/L), versus time (hours). IAE = 0.0042, Maximum deviation = 0.56%. No steady-state offset. 329
Figure 182: Plot of the mass flow rate of stream 23 (kg/h) versus time (in hours). 329
Figure 183: Plot of the set point (red) and measured (blue) base case solids fraction values for 400-TK-20, versus time (hours). IAE = 0.038, Maximum deviation = 1.64%. 330
Figure 184: Plot of the mass of 400-TK-10 versus time (hours). IAE = 6.762e-6, Maximum deviation = 0.0005%. 330
Figure 185: Plot of the flow rate of stream 1 (kg/h) versus time (in hours). 331
Figure 186: Plot of the base case model's mass of the contents of 400-TK-20 (kg), versus time (hours). IAE = 7.487e-5, Maximum deviation = 0.0053%. 331
Figure 187: Plot of the flow rate of stream 1 (kg/h) versus time (in hours). 332
Figure 188: Plot of the developed model's temperature of compartment 1 (oC) versus time (hours). IAE = 0.0023, Maximum deviation = 1%. No steady-state offset. 332
Figure 189: Plot of the flow rate of stream 9 (kg/h) versus time (in hours). 333
Figure 190: Plot of the percentage of the solid copper leached in the second stage leach in the base case model versus time (hours). Maximum deviation =4.3% 333
Figure 191: Plot of the set point (red) and measured (blue) developed model's acid concentration values for 400-TK-20 (g/L), versus time (hours). IAE = 0.0094, Maximum deviation = 0.80%. No steady-state offset. 334
Figure 192: Plot of the set point (red) and measured (blue) developed model's acid concentration values for 400-TK-10 (g/L), versus time (hours). 334
Figure 193: Plot of the ratio between the mass flow rates of streams 4 and 2 versus time (in hours). 335

Figure 194: Plot of the ratio between the mass flow rates of streams 3 and 2 versus time (in hours) 335
Figure 195: Plot of the set point (red) and measured (blue) developed model's solids fraction values for 400-TK-20, versus time (hours). IAE = 0.0225, Maximum deviation = 1.08% 336
Figure 196: Plot of the set point (red) and measured (blue) developed model's solids fraction values for 400-TK-10, versus time (hours). 336
Figure 197: Plot of the ratio between the mass flow rates of streams 1 and 2 to 4 versus time (in hours). 337
Figure 198: Plot of the mass of 400-TK-10 versus time (hours). IAE = 2.918e-6, Maximum deviation = 0.0002%. 337
Figure 199: Plot of the sum of the mass flow rates of streams 1 to 4 (kg/h) versus time (in hours). 338
Figure 200: Plot of the developed model's mass of the contents of 400-TK-20 (kg), versus time (hours). IAE = 7.65e-5, Maximum deviation = 0.0023% 338
Figure 201: Plot of the mass flow rate of stream 7 (kg/h) versus time (in hours). 339
Figure 202: Plot of the developed model's temperature of compartment 1 (°C) versus time (hours). IAE = 0.0022, Maximum deviation = 1%. No steady-state offset. 339
Figure 203: Plot of the mass flow rate of stream 9 (kg/h) versus time (in hours). 340
Figure 204: Plot of the percentage of the solid copper leached in the second stage leach in the newly developed model versus time (hours). Maximum deviation =2.75% 340
Figure 205: Plot of the set point (red) and measured (blue) base case acid concentration values for 400-TK-20 (g/L), versus time (hours). IAE = 0.0284, Maximum deviation= 4.01%. 341
Figure 206: Plot of the mass flow rate of stream 23 (kg/h) versus time (in hours). 341
Figure 207: Plot of the set point (red) and measured (blue) base case solids fraction values for 400-TK-20, versus time (hours). IAE = 0.0103, Maximum deviation = 0.55%. 342
Figure 208: Plot of the base case model's mass of the contents of 400-TK-20 (kg), versus time (hours). IAE = 3.54e-5, Maximum deviation = 0.0022%. 342
Figure 209: Plot of the flow rate of stream 1 (kg/h) versus time (in hours). 343
Figure 210: Plot of the set point (red) and measured (blue) values for the temperature of compartment 1 (°C) versus time (in hours). IAE = 1.171e-4, Maximum deviation= 0.006%. 343
Figure 211: Plot of the flow rate of stream 9 (kg/h) versus time (in hours). 344
Figure 212: Plot of the set point (red) and measured (blue) developed model's acid concentration values for 400-TK-20 (g/L), versus time (hours). IAE = 0.0513, Maximum deviation = 4.2%. 345
Figure 213: Plot of the set point (red) and measured (blue) developed model's acid concentration values for 400-TK-20 (g/L), versus time (hours). 345
Figure 214: Plot of the ratio between the mass flow rates of streams 4 and 2 versus time (in hours). 346

Figure 215: Plot of the ratio between the mass flow rates of streams 3 and 2 versus time (in hours). 346
Figure 216: Plot of the set point (red) and measured (blue) developed model's solids fraction values for 400-TK-20, versus time (hours). IAE = 0.007, Maximum deviation = 0.46%. 347
Figure 217: Plot of the developed model's mass of the contents of 400-TK-20 (kg), versus time (hours). IAE = 3.13e-5, Maximum deviation = 0.0022%. 347
Figure 218: Plot of the mass flow rate of stream 7 (kg/h) versus time (in hours). 348
Figure 219: Plot of the set point (red) and measured (blue) values for the temperature of compartment 1 (°C) versus time (in hours). IAE = 3.096e-5, Maximum deviation= 0.001%. 348
Figure 220: Plot of the mass flow rate of stream 9 (kg/h) versus time (in hours). 349

LIST OF TABLES

Table 1: Element-wise composition of molten converter matte at Western Platinum BMR........ 41
Table 2: Mineralogy of the matte entering the first stage leach 49
Table 3: List of the process variables for which a set point is given during automatic operation, as well as disturbance-, manipulated and controlled variables. 53
Table 4: Allowable ranges used by process operator to control compositions 56
Table 5: List of control loops that form part of the current control 57
Table 6: Lists of data tags available (for the two aligned data sets), with corresponding locations (model stream or tank) given. 71
Table 7: Second stage leach variables that are in cascade mode and not in it during the data gathering. 72
Table 8: Lists of compositional data available around pressure leach process 73
Table 9: More frequently available process stream information of different process units in and around the pressure leach process 74
Table 10: Table of densities for stream around 400-TK-10 75
Table 11: Table of densities for stream around 400-TK-10 78
Table 12: List of files that make up the received model, along with the purpose of each............ 80
Table 13: Simulink block numbers, with input and output links, as well as the parameters calculated in each. 83
Table 14: Conceptual model changes, with a summary of the reason for each.............................. 86
Table 15: Summary of typical dead times in the piping of the pressure leach................................ 91
Table 16: Sample composition of formic filtrate 92
Table 17: Inventory volumes, as provided by Lonmin 94
Table 18: Autoclave dimensions as required by the model 94
Table 19: Flow rates and densities for streams 1 to 5, and its phases. 95
Table 20: Flow rates and densities for streams from the second stage leach, and its phases. 96
Table 21: Compounds in which metallic elements occur in the first stage leach residue 97
Table 22: Stepped input variables, with step sizes given, along with the responses of several output variables – by Dorfling (2012) and in this project.. 98
Table 23: Table of data arrays imported into the model for validation 100
Table 24: Control loops added to the validation model, with reasons therefor 101
Table 25: Tuning parameters used in validation model 101
Table 26: Variables for which a comparison is done between model and data values, with units, means and absolute error values are given, along with the ordinary and normalised root mean square error (RMSE) values and an indication of the trend match. 104
Table 27: A summary of the data and model values for acid concentrations in 5 process inventories. 105

Table 28: Minimum, mean and maximum values for the fractions different metal components make up of the second and third stage residue from 22 to 24 April 2013, with corresponding model values given. 105
Table 29: Minimum, mean and maximum values for the concentrations of metal components of the second and third stage residue from 22 to 24 April 2013, with corresponding model values given. 105
Table 30: List of variables changed for each sensitivity analysis run, with initial and final values displayed 108
Table 31: Selected list of responses to each of the test runs done. 109
Table 32: Flow rates added into the model 111
Table 33: Responses in key variables to the two steady-state model runs done, with the old and new pre-exponential factors. 112
Table 34: Normalised standard deviations of the MV flow rates and tank levels in the data, used for the tuning of mass controllers in the base case model. 135
Table 35: Control loops given with manipulated and controlled variables 136
Table 36: Tuning parameters for all basic regulatory control loops, before and after fine-tuning. Old T_t values are equal to the old T_I values. 138
Table 37: Summary of the flows representing the potential control valves 142
Table 38: List of inventories, with the flow controllers of the streams that will serve as MVs 145
Table 39: Summarised comparison between the performance of the controllers for the first temperature compartment and mass of 400-TK-20, for the base case and controller with feed-forward control. 150
Table 40: Tuning constants before and after fine-tuning for the acid controller in 400-TK-20. 167
Table 41: List of variables that remain to serve as MVs after MV allocations to basic regulatory control. 168
Table 42: Lists of proposed manipulated & controlled variables for the advanced regulatory control level 170
Table 43: List of the controlled and manipulated variables for around 400-TK-10 172
Table 44: Solids fractions for each of the streams entering 400-TK-10 172
Table 45: Acid concentrations of each of the streams entering 400-TK-10 173
Table 46: Transfer matrix determined for the compositional control on 400-TK-10. 175
Table 47: RGA determined for the compositional control on 400-TK-10. 175
Table 48: Tuning parameters for the two components of the acid concentration split range controller 176
Table 49: Tuning parameters for all basic regulatory control loops, with controller gains before and after fine-tuning 178
Table 50: Tuning parameters for the primary cascade compositional controllers. 180
Table 51: Qualitative comparative measures for the rejection of disturbances 183

Table 52: Set point values sent to the acid concentration controller for 400-TK-20 (g/L) and its time ranges. 190
Table 53: Quantitative comparative measures for responses to acid concentration set point tracking. 190
Table 54: Comparison drawn between the additive streams of the preparation tanks for the second and third stage leach, respectively. 195
Table 55: Summary of measured variables in the pressure leach process that can be used for automated supervisory control 197
Table 56: Variables for which a comparison is done between model and data values, with units, means and absolute error values are given, along with the ordinary and normalised root mean square error (RMSE) values and an indication of the trend match. 231
Table 57: Minimum, mean and maximum values for the fractions different metal components make up of the second stage residue from 22 to 24 April 2013, with corresponding model values given. 248
Table 58: Minimum, mean and maximum values for the concentrations of metal components of the second stage residue from 22 to 24 April 2013, with corresponding model values given. 249
Table 59: Minimum, mean and maximum values for the fractions different metal components make up of the third stage residue from 23 to 24 April 2013, with model values alongside it. 259
Table 60: Minimum, mean and maximum values for the concentrations of metal components of the third stage residue from 22 to 24 April 2013, with model values alongside it. 261
Table 61: Composition of copper spent electrolyte 265
Table 62: Composition of formic filtrate 265
Table 63: Composition of solids feed 265
Table 64: Mineralogy of solids feed 266
Table 65: Flow rates added into the model 266
Table 66: Maximum variations for mass control MV flow variations and mass variations for mass controller tuning 269
Table 67: Tuning parameters calculated for the PI mass controllers in the base case model 269

NOMENCLATURE

Symbol	Name	More information
A	Area	The area is typically given in m^2
$\boldsymbol{C_p}$	Heat capacity	Energy required to increase the temperature of a material with 1°C
$\boldsymbol{c_{uy}}$	Covariance coefficient	Indication of a time delay between variables
G_c	Controller TF	Transfer function of a controller in the Laplace domain
G_d	Disturbance TF	Transfer function of a disturbance in the Laplace domain
G_{ff}	Feed-forward TF	Transfer function of a feed-forward controller in the Laplace domain
G_{fbs}/G_s	Feedback sensor TF	Transfer function of a feedback controller sensor in the Laplace domain
G_p	Process TF	Transfer function of the process in the Laplace domain
G_v	Valve TF	Transfer function of a valve in the Laplace domain
K_c	Controller gain	Tuning parameter for the proportional function of a PID controller
K_{ij}	Steady-state gains	The gain values in the gain matrix
K_p	Process gain	Steady-state change component of the process TF
L	Length	The length is typically given in meters
$\dot{\boldsymbol{m}}$	Mass flow rate	The mass flow rate of a stream, typically in kg/h
P	Pressure	The pressure is typically given in bar absolute
$\dot{\boldsymbol{Q}}$	Heat transfer rate	Rate of heat addition or removal, typically in kJ/h
R	Gas constant	Used in the ideal gas law: 8.314 J/mol.K
T_d/T_D	Differential time	Tuning parameter for the differential function of a PID controller
T_I	Integral time	Tuning parameter for the integral function of a PID controller
T_t	Anti-reset windup time	Tuning parameter for the anti-reset windup in PI controllers
T	Temperature	The temperature is typically given in $^{\circ}$C
V	Volume	The volume is typically given in m^3
$\dot{\boldsymbol{V}}$	Volumetric flow rate	The volumetric flow rate of a stream, typically L/h
z	Compressibility factor	Factor used in the ideal gas law to account for non-ideal behaviour
θ	Dead time	Time delay due to flow in pipes
ξ	Damping coefficient	A parameter set for the tuning of mass or level controllers
λ	Relative gain	Ratio between open and closed loop behaviour
μ	Mean	The average value of a data set
$\boldsymbol{\rho}$	Density	The density is usually given in kg/L
σ	Standard deviation	Statistic variable with the same units as the parameter in question
τ	Time constant	The time constant is a time parameter, given in hours for example

CHAPTER 1

INTRODUCTION

1.1 BACKGROUND AND PROCESS DESCRIPTION

Platinum group metals (PGMs) are a group of precious metals that include platinum, palladium, rhodium, osmium, iridium and ruthenium. PGMs are in high demand, due to their valuable chemical and thermal characteristics – giving them a premium market value. Uses range from being raw materials in the manufacturing industry and catalysts in a wide variety of chemical processes to smaller products and tools. Platinum and palladium are also used in jewellery applications, giving them an elite status (Platinum Group Metals, 2009). In this flourishing market, increased re-use and recycling of PGMs is putting pressure on the PGM refining industry. This is aggravated by the cost of deep mining and the complex mineralogy of PGMs - demanding continuous improvement in the efficiency of the extraction and refining processes. This translates to an on-going demand for better control in the field.

PGM Refining Process

The typical PGM refining process can be divided into a number of principal stages. These stages are shown in Figure 1, with the typical intermediate products:

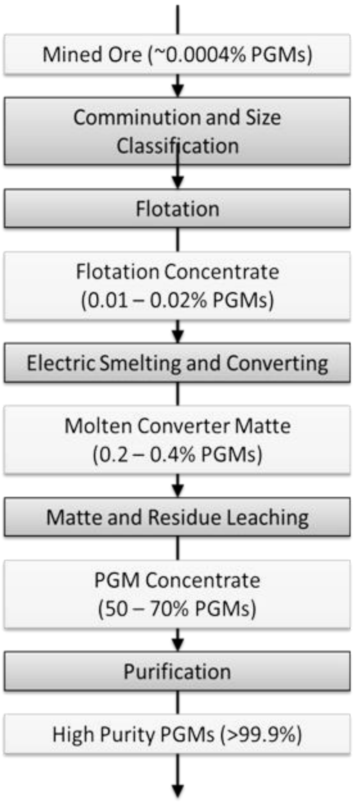
Mined Ore (~0.0004% PGMs)
Comminution and Size Classification
Flotation
Flotation Concentrate (0.01 – 0.02% PGMs)
Electric Smelting and Converting
Molten Converter Matte (0.2 – 0.4% PGMs)
Matte and Residue Leaching
PGM Concentrate (50 – 70% PGMs)
Purification
High Purity PGMs (>99.9%)

Figure 1: Schematic representation of the PGM refining process sequence (drawn from information by Crundwell et al, 2011)

Figure 1 shows that mined ore enters a process of size reduction and classification, where-after it undergoes flotation (where the more valuable metals are recovered). The resulting concentrate is smelted and converted to Ni-Cu matte, which is fed to the first stage leach. The solids phase of the third stage leach (with 50-70% PGMs) goes to the PGM refining area, where it is purified to specification.

1.1.2 The Base Metal Refinery

A base metal refinery (BMR) is an important component in the PGM refining industry. Its main purpose is to remove base metals (copper, nickel and iron), as well as selenium, from PGM-containing matte. Below is the typical composition of the matte entering the first stage leach (Steenekamp & Mrubata, Control and Specifications of the BMR, 2013):

Table 1: Element-wise composition of molten converter matte at Western Platinum BMR

Element	**Composition (mass %)**
Nickel	48
Copper	28
Sulphur	20
Iron	1
Cobalt	0.5
PGM's	0.5 - 0.6

Designs of BMRs vary globally – mainly due to differences in the composition of the available ore. The following is a representation of the layout of a typical South African BMR. Note that the diagram is based on the design of Lonmin's Western Platinum BMR.

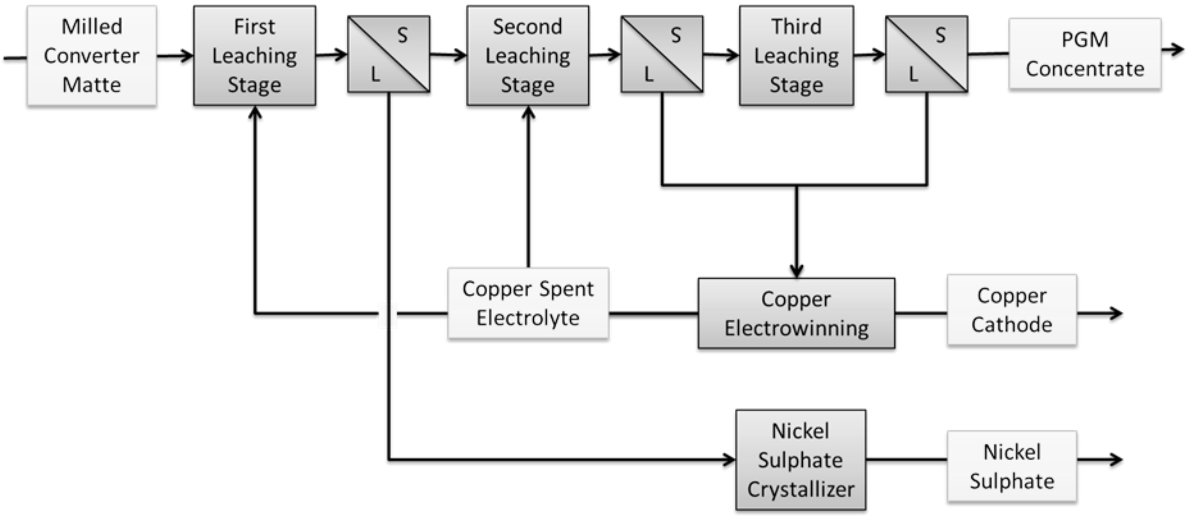
Milled Converter Matte
First Leaching Stage
S
L
Second Leaching Stage
S
L
Third Leaching Stage
S
L
PGM Concentrate
Copper Spent Electrolyte
Copper Electrowinning
Copper Cathode
Nickel Sulphate Crystallizer
Nickel Sulphate

Figure 2: Schematic representation of the stages at a base metal refinery (drawn from information by Crundwell et al, 2011)

It can be seen that leaching makes up a large part of the BMR. The first stage leach is typically an atmospheric pressure leach, with the second and third leaching stages taking place at a high pressure inside an autoclave. The reason for the separate stages is to improve the separation efficiency. Each leach stage takes the solids from the previous stage, since the aim is to purify the PGM-containing solids as much as possible.

1.1.3 Atmospheric and Pressure Leach

While the objectives of each leaching stage are currently rather well understood, the leaching processes are complex in the sense that they involve a large number of reactions. This is partly due to the complex mineralogy of the matte. Moreover, each of these elements/compounds can typically react with the added reagents in a number of ways – adding to the complexity of the process (see Appendix D).

The first stage leach is an atmospheric pressure, oxygen leach that takes place in 5 stirred tanks in series. The main objective of this step is to remove most of the nickel (as well as iron and cobalt) from the matte, in order for it to be sent to the nickel crystallisers, and to remove copper from solution by means of cementation reactions (Olivier, 2012). The latter is done in order for the copper to be leached out in the second and third leaching stages. A thickener is used to separate the effluent slurry into a solid and liquid phase. The solid underflow is sent to the second leaching stage, with a certain fraction recycled to the first stage. The reactions identified for the second and third leaching stages are given in Appendix D.

The two pressure leach stages take place in one autoclave, with a dividing wall between the stages. The autoclave is fed with slurry that is made up of wet matte (50 wt% water), to which copper spent electrolyte and formic filtrate (or water) is added to specification. The overarching aim of the control on the plant (especially the reactions taking place in both stages) is to maximise the leaching of copper, while limiting the loss of PGMs to the liquid phase.

Note that a more detailed process description is given in section 2.2.

1.2 PROJECT DESCRIPTION

1.2.1 Background

Due to the variability of the composition of the entering matte and other process streams, and the low levels of PGMs in it, the control of the leaching circuit is a very challenging task. This problem is aggravated by the fact that – until recently – the complex leaching reactions taking place at the BMR (and the reaction kinetics) were not fundamentally understood very well. The personnel at Lonmin's BMR have determined that the leaching circuit often operates outside its desired bounds. Much of the plant is currently controlled using an iterative approach, based on operator experience – making changes to certain variables in response to deviations of certain key variables from their set points. Due to the fact that the control is not based on sound fundamental principles, it is very limited.

Such a fundamental model had recently been developed by Dorfling for the second and third leaching stages at Lonmin's BMR (Dorfling, Bradshaw, & Akdogan, Characterisation and dynamic modelling of the behaviour of platinum group metals in high pressure sulphuric acid/oxygen leaching systems, 2012). This dynamic model has been created in MATLAB, taking reaction specifics and kinetics into account, as well as mass and energy balances, heat transfer and local process limitations. It is covers all four compartments of the autoclave, as well as the tanks and flows in pressure leach area. The model creates the possibility of developing, simulating and evaluating improved control structures/strategies for the BMR.

1.2.2 Purpose of Project

Taking the aforementioned information into account, the main purpose of this project can be summarised as follows:

- To use plant data from Lonmin to calibrate and validate the model to the extent required by the development of improved control structures/strategies.
- To use the validated model as "plant" to evaluate control structure against performance measures and to sequentially develop improvements on it.

1.2.3 Project Methodology

Due to the multi-facetted nature of this project, it is divided into a number of main phases that will form the backbone of the project's planning. These phases are the following:

- Data acquisition, processing and analysis: the process of getting process data from Lonmin, extracting from it what is useful and analysing the data to determine its internal consistency and usefulness.

- Model migration to Simulink: the process of transcribing the dynamic model, from its current MATLAB code format, to Simulink's interface.
- Model validation and adaption: the process of identifying key differences between the model and Lonmin's plant data, and making changes to the model accordingly.
- Control development & evaluation: the process of adding different kinds of control loops and structures to the Simulink model, as well as evaluating the ability of the different control methods to nullify different process disturbances and choosing the best thereof.

1.3 OBJECTIVES, SCOPE AND DELIVERABLES

1.3.1 Aims and Objectives

The aims of this project comprise the following five points:

1. To identify possible control strategies for leaching circuits, as well as improved control techniques, from literature.
2. To validate the pressure leach simulation model presented by Dorfling (2012) by means of comparing the model with plant data and implementing the required improvements on the model.
3. To implement an analogue of the current industrial control structure on the pressure stage leach simulation model and the assessment of control performance.
4. To develop and implement of control structure improvements on the simulation model and the assessment of control performance.
5. To evaluate the performance of the different control structures.

1.3.2 Hypothesis

Improved control structures can be developed for the pressure leach at Lonmin's BMR, which will outperform the current control technique – by improving the product quality, while still maintaining the desired production rates and safety standards.

1.3.3 Scope

The scope of this project was confined to the pressure leach process at Lonmin's Western Platinum BMR. No control development was done on the actual plant. Instead, the pressure leach simulation model presented by Dorfling (2012) was used as the "plant", from which control was developed and on which it was tested. Note that no empirical model was developed, and that only the provided fundamental simulation was used.

1.3.4 Thesis Overview

This thesis composes of six chapters, of which the first is the introduction. In the second chapter the pressure leach process is introduced, along with the current control. This serves both as a means of becoming familiar with the process, and of identifying the scope for improvement. In chapter 3 the model is introduced, along with the data used in this project. The main aim of chapter 3 is to validate the model and to calibrate and adapt it in the means necessary. In chapters 4 and 5 two parts of regulatory control is considered, with a base case developed for each and improvements made and evaluated. Note that the findings of each of these chapters are independent from one another and can be implemented either separately or together. Each of the last 3 chapters has its own conclusion, with a summary of the conclusions, as well as recommendations given in chapter 6.

CHAPTER 2

PRESSURE LEACH PROCESS & CURRENT CONTROL

2.1 CHAPTER INTRODUCTION

In order to be able to develop improvements of the manner in which a process is controlled, it is important to get to know the process. Developing process control from a fundamental understanding requires that the developer should become well acquainted with the plant's current setup, operation, challenges and control. In this chapter the process is introduced and described – both broadly and in more detail. The focus then shifts to the current control of the plant – focusing both on the overall strategy, as well as the specifics. This chapter aims to create a platform from which improvements to the current process and its control can be developed.

2.2 PROCESS DESCRIPTION

2.2.1 Summary: First Stage

Because the first stage precedes the pressure leach, it is the source of the main disturbances to the pressure leach circuit. It is therefore important to understand (albeit briefly) the reactions taking place in the atmospheric leach tanks. These reactions can typically be summarised by following main reactions (Crundwell et al, 2011):

$$Ni_3S_2\ (s) + 2Cu\,SO_4(aq) \rightarrow 2NiSO_4(aq) + \ Cu_2S\ (s) + NiS\ (s)$$

[1]

$$Ni_3S_2\ (s) + H_2SO_4\ (aq) + 0.5O_2(g) \rightarrow CuSO_4(aq) + CuS\ (s) + \ H_2O(l)$$

[2]

$$Ni\ (s) + \ H_2SO_4\ (aq) + 0.5O_2(g) \rightarrow NiSO_4(aq) + H_2O\ (l)$$

[3]

$$Cu_2S\ (s) + \ H_2SO_4\ (aq) + 0.5O_2(g) \rightarrow CuSO_4(aq) + CuS\ (s) + \ H_2O\ (l)$$

[4]

The mineralogy of the matte taking part in these reactions is given below (Olivier, 2012). Note that additional copper sulphates enter the feed, along with acid, with the copper spent electrolyte.

Table 2: Mineralogy of the matte entering the first stage leach

Mineral		**Composition (%)**
Heazlewoodite	Ni_3S_2	51.88
Chalcocite	Cu_2S	32.11
Metal Alloy		14.11
Nickel	*Ni*	*10.01*
Copper	*Cu*	*2.76*
Iron	*Fe*	*1.02*
Cobalt	*Co*	*0.32*
Copper Selenide	Cu_2Se	0.11
Copper Telluride	Cu_2Te	0.03

2.2.2 Pressure Leach

As mentioned, the second and third leaching stages take place at a high pressure. A PFD (with current control loops indicated) is shown below, with a larger version provided in Appendix A.

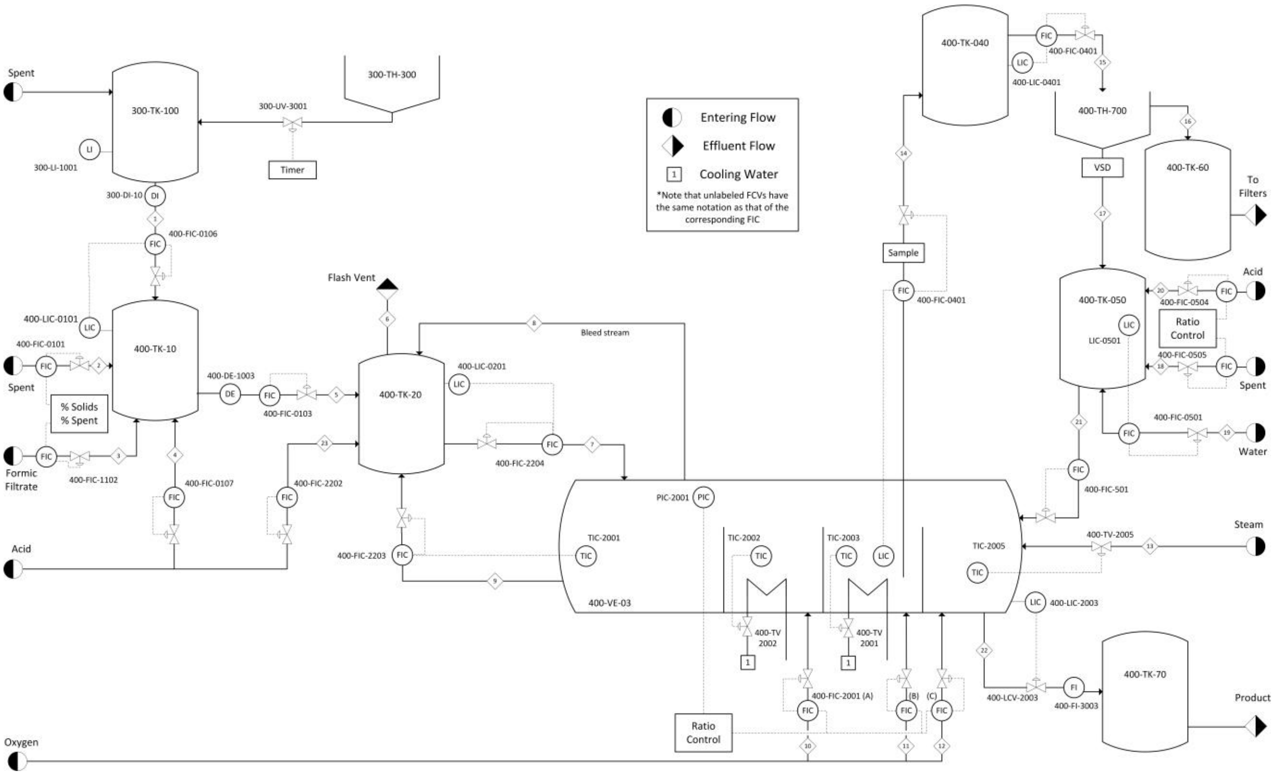
Spent
300-TK-100
LI
300-LI-1001
300-DI-10
DI
300-TH-300
300-UV-3001
Timer
1
FIC
400-FIC-0106
400-LIC-0101
LIC
400-FIC-0101
2
Spent
400-TK-10
% Solids
% Spent
FIC
3
Formic
Filtrate
400-FIC-1102
4
400-FIC-0107
Acid
400-DE-1003
DE
400-FIC-0103
5
Flash Vent
6
8
Bleed stream
400-TK-20
400-LIC-0201
LIC
23
400-FIC-2202
400-FIC-2204
7
400-FIC-2203
9
Entering Flow
Effluent Flow
Cooling Water
*Note that unlabeled FCVs have the same notation as that of the corresponding FIC
400-TK-040
400-FIC-0401
400-LIC-0401
15
400-TH-700
16
VSD
400-TK-60
To
Filters
14
17
Sample
400-FIC-0401
400-TK-050
LIC-0501
Acid
20
400-FIC-0504
Ratio
Control
400-FIC-0505
18
Spent
400-FIC-0501
19
Water
21
400-FIC-501
PIC-2001
PIC
TIC-2001
TIC
TIC-2002
TIC-2003
TIC-2005
400-VE-03
Steam
400-TV-2005
13
400-LIC-2003
400-TV
2002
400-TV
2001
1
400-FIC-2001 (A)
(B)
(C)
Ratio
Control
10
11
12
22
400-LCV-2003
FI
400-FI-3003
400-TK-70
Product
Oxygen

Figure 3: Simplified schematic representation of the pressure leach process at Lonmin, with basic control loops and stream numbers indicated.

The pressure leach will be explained next, with current control being discussed in section 2.3.

The underflow of a thickener (300-TH-300) – which is 50% solids – is added to 300-TK-100, where copper spent electrolyte (spent) is added to decrease the density of the pulp. From here it is pumped to a slurry preparation tank (400-TK-10), where spent, pure sulphuric acid and formic filtrate (or pure water, if the filtrate is depleted) is added to reach a predefined % solids and % spent specification. The contents of 400-TK-10 are pumped, along with pure sulphuric acid, into the flash recycle tank (400-TK-20), which receives a flash recycle stream, as well as a vapour bleed stream, from the autoclave. The contents of 400-TK-20 are pumped into the autoclave.

The autoclave has four compartments, of which the first three make up the second stage leach and the last is used for the third stage leach. The slurry moves between the first three compartments by means of overflow, while the contents of the third compartment are pumped out. Cooling in the first compartment is done by means of flash cooling, where part of the slurry is continuously flashed to a lower pressure. Compartments 2 and 3 are cooled by means of cooling coils, through which cooling water flows. The last autoclave compartment is heated by means of steam addition. Note that oxygen is sparged into the last three compartments.

The contents of compartment 3 are pumped to a discharge tank (400-TK-040), which feeds a thickener (400-TH-700) or centrifuge. The overflow of the thickener goes to filters, while the underflow is pumped to the third stage slurry preparation tank (400-TK-050). Here, sulphuric acid, spent and water is added, to ensure the correct fraction of solids and acid. The contents of the preparation tank are returned to the autoclave's last compartment, from where the product is pumped to a discharge tank (400-TK-70).

2.3 CURRENT CONTROL PHILOSOPHY AND VARIABLES

In this project, the control philosophy was determined primarily by communicating with process experts (as opposed to using data as main source of information). This was done to get more generally applicable knowledge of the process. The information provided is deemed "current control" in this project.

2.3.1 Process & Control Objectives

The unit downstream form the pressure leach process is a batch process, which means that smooth production is not as important as the production rate and product quality. While the production rate is limited by the process' design and has not been made available by Lonmin, the pressure leach products have to adhere to the following specifications (Steenekamp & Mrubata, Control and Specifications of the BMR, 2013):

- A PGM grade of 65% needs to be maintained at the end of the pressure leach.
- The copper in the second and third stage leach residues need to be below 18 - 25 wt% and below 3.5 wt%, respectively.

The process objectives directly influence the objectives for the control system. Specific process knowledge is required to ensure that these objectives are met. More specifically, the exact effects of certain process variables, such as pressure, temperatures and stream compositions, on the leaching reactions that determine the product compositions need to be determined. The current aim at Lonmin is to attempt to control the pressure, acid concentration and temperatures tightly, while the control of densities – for example – is controlled much less tightly, if at all.

The role of a control system is to keep these variables at their respective set points, while rejecting the disturbances that enter the process. This therefore emphasises the importance of the structural design and the tuning of the plant's control.

2.3.2 Challenges to Control

The lack of measurement of key process variables means that they cannot be controlled directly, but only inferentially. The inference is done by operator experience, rather than mathematically from fundamental principles. The following are the main factors leading to the suboptimal operation:

- The pressure leach process has large residence times (due to large inventories), meaning that the effect of any change made by the operator will only be seen after a significant time.
- The process operators work in shifts. The large time constants mean, then, that some changes made by the previous operator will have an effect on the process – whilst the new operator may be unaware of what these changes entailed. This phenomenon is aggravated by the

tendency of these operators not to react to compositional data analyses made in a shift prior to their own (Steenekamp & Mrubata, Control and Specifications of the BMR, 2013).

- The operators have no tool that they can use to anticipate the exact consequences of the made changes. They need to wait for key response variables to change, before reacting once more.

Most control loops are capable of operating successfully under a *cascade* mode. In many cases, these loops need to be overridden by the operator. The exact reason for this is unknown.

2.3.3 Key Variables

One of the main reasons for the difficulty faced when controlling the pressure leach process is the fact that inferential control is mainly used, with no established relationship between the inferential and true variables – as well as a large amount of disturbances. Below is a list of the most important variables:

Table 3: List of the process variables for which a set point is given during automatic operation, as well as disturbance-, manipulated and controlled variables.

Set Point Inputs	Disturbances	Manipulated Variables	Controlled Variables
Autoclave Pressure	Spent composition & density	Acid feed rate into preparation tanks (streams 4, 23 & 20)	Autoclave pressure
All tank levels	Spent temperature	Cooling water flow rates (compartments 2 & 3)	All tank levels
Autoclave compartment temperatures	Acid concentration & density	Flash recycle flow rate (stream 9)	Autoclave compartment temperatures
Pulp feed rate (stream 5)	Formic composition	Formic filtrate flow rate (stream 3)	Base metal, acid & PGM concentrations in compartments 3 & 4
% Solids in preparation tanks (400-TK-10 & -050)	Matte composition	Matte feed rate (stream 1)	
% Spent entering 400-TK-10	Oxygen temperature	Oxygen feed rate/ratio (streams 10-12)	
% Acid in 400-TK-050	Steam temperature	Pulp feed rate (stream 5)	
	Any MV disruptions	Spent feed rate (streams 2 & 19)	
		Steam flow rate (stream 13)	
		Vapour bleed flow rate (stream 8)	

2.3.4 Control Loops

The control of the different identified controlled variables (CVs) will now be discussed separately. Refer to the following diagram (or the larger version given in Appendix A) throughout this section:

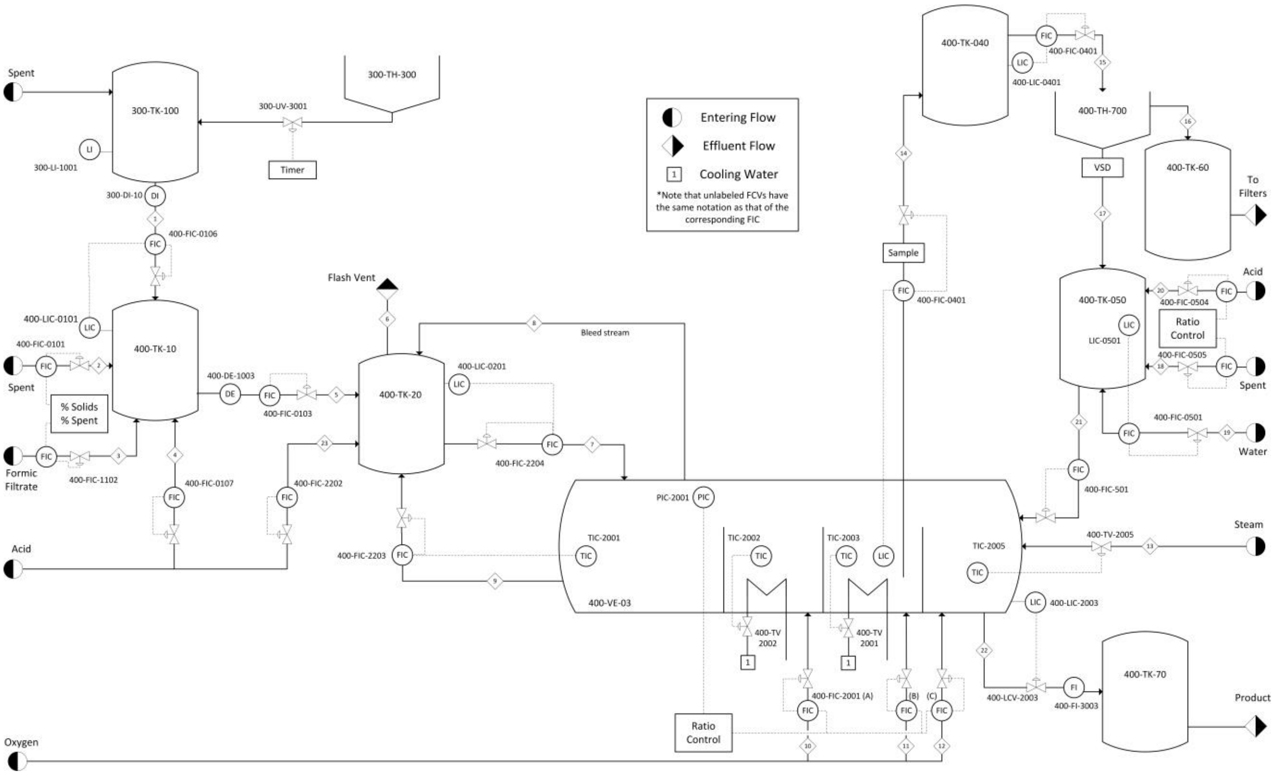
Spent
300-TK-100
300-TH-300
300-UV-3001
LI
300-LI-1001
Timer
300-DI-10
DI
400-FIC-0106
FIC
400-LIC-0101
LIC
400-TK-10
400-FIC-0101
Spent
% Solids
% Spent
Formic Filtrate
400-FIC-1102
400-FIC-0107
Acid
400-DE-1003
DE
400-FIC-0103
Flash Vent
400-TK-20
400-LIC-0201
Bleed stream
400-FIC-2202
400-FIC-2204
400-FIC-2203
PIC-2001
PIC
TIC-2001
TIC
TIC-2002
TIC-2003
TIC-2005
400-VE-03
400-TV 2002
400-TV 2001
400-FIC-2001 (A)
(B)
(C)
Ratio Control
Oxygen
Entering Flow
Effluent Flow
Cooling Water
*Note that unlabeled FCVs have the same notation as that of the corresponding FIC
400-TK-040
400-FIC-0401
400-LIC-0401
400-TH-700
VSD
400-TK-60
To Filters
Sample
400-FIC-0401
Acid
400-TK-050
400-FIC-0504
Ratio Control
LIC-0501
400-FIC-0505
Spent
400-FIC-0501
Water
400-FIC-501
Steam
400-TV-2005
400-LIC-2003
400-TK-70
400-LCV-2003
FI
400-FI-3003
Product

Figure 4: Simplified schematic representation of the pressure leach process at Lonmin, with basic control loops and stream numbers indicated

Level Control

400-TK-10: The level of this tank is controlled by manipulating the flow rate of the entering slurry (400-FIC-0106). The fact that the flow rates of spent and formic filtrate (or water) depend on the composition and density of the tank's contents, means that the level of 400-TK-10 will never really be steady. However, at the time of gathering data for this project, the flow rates of these two streams were set to operate in a fixed ratio with the slurry stream – meaning that the total entering flow rate served as MV for level control. Note that the set point of 400-FIC-0103 is set constant, in order to ensure that the flow entering the autoclave is as stable as possible.

400-TK-20: The level of this tank is controlled by varying its outflow (400-FIC-2204). The main disturbance is the entering flash recycle stream. No advanced control is said to be present, but the flow rate of the flash recycle stream is said to be limited to 95% of this tank's outflow (400-FIC-2204), in order to ensure a net inflow into the autoclave between these streams.

Autoclave: The levels of compartments 1 and 2 are automatically regulated by the overflow into the next compartment. The level of compartment 3 is controlled by changing 400-FIC-0402. The level of the last compartment is controlled by the outflow from the autoclave.

400-TK-040: The level of this tank is controlled by its outflow (400-FIC-0402).

400-TH-700: The level of this thickener is not controlled directly. Its inflow is used to control the level of 400-TK-040, while the variable speed drive (VSD) of the underflow pump is changed according to the level of 400-TK-050. There is – therefore – potential for large improvements in the operation of this thickener (and the parallel centrifuge). Note, however, that this process unit falls outside the scope of this project.

400-TK-050: The VSD is operated manually to keep the level of 400-TK-050 constant. The addition rate of acid, spent and water is said to be changed according to the acid concentration and density of the tank's contents. There is an option of automatically controlling the addition of the three flows via level control, but this is often overridden, because of the VSD control. The outflow of the tank (400-FIC-501) is changed manually and kept constant over long periods. Keeping all these factors in mind, it is clear that 400-TK-050 is controlled in a similar fashion to 400-TK-10.

Temperature Control

The only temperature control done in the pressure leach is in the autoclave. The first three compartments are cooled, while the last compartment requires the addition of heat.

The first compartment is cooled by means of flash cooling. A feedback controller uses the temperature (400-TIC-2001) measurement and adjusts the flow rate of the flash recycle stream (400-FIC-2001). In this flash recycle stream, a portion of the autoclave contents is flashed continuously from the pressurised autoclave to the flash tank, which is at atmospheric pressure. This leads to the cooling of a part of the slurry. The flashed slurry is then returned to the autoclave from 400-TK-20. As mentioned, a limit is placed on the flow rate of the flash recycle stream.

The second and third compartments are controlled by means of circulating cooling water through coils. One of these water coils is currently blocked, leading to temperatures being higher than set point values (Steenekamp & Mrubata, Control and Specifications of the BMR, 2013).

The last compartment is heated by means of steam addition. Theoretically, 400-TV-2005 should be automatically controlled by 400-TIC-2005, but this valve is currently changed by hand (Steenekamp & Mrubata, Control and Specifications of the BMR, 2013).

Pressure Control

All the tanks – except for the autoclave – are kept at atmospheric pressure by means of the necessary ventilation. The autoclave, however, is kept at pressures between 6 and 7 bar absolute by means of oxygen addition. Oxygen is sparged into the last three compartments. The ratio between the compartments is periodically reset by the operator, in response to hourly sampled compositional data that provides information on the extent of leaching taking place. However, since the whole autoclave shares one vapour space, the ratio has a negligible effect on the pressure.

The reading of 400-PIC-2001 automatically adjusts the overall oxygen addition rate and it operates satisfactorily, according to process engineers (Steenekamp & Mrubata, Control and Specifications of the BMR, 2013).

Control of Acid and Metal Concentrations

While the tank levels, temperatures and pressure can be easily controlled, the control of the concentrations of acid and metals is more difficult. The only automatic control of the latter group is at tanks 400-TK-10 and 400-TK-050. Here the acid concentration is controlled by changing the addition rate of spent, formic filtrate and pure acid. At 400-TK-10, the percentage that spent makes up of the overall entering flow is set. This is also true for the formic filtrate. This means that the spent and formic filtrate, in the absence of an acid stream, is controlled by means of ratio control. Note that the acid concentration cannot be controlled separately from the slurry density, since the three mentioned streams available for controlling acid concentration should be simultaneously used for density control.

In the case of 400-TK-050, the actual acid concentration is said to be used to determine the necessary adjustments to the flow rates of acid and spent. Except for the automatic control, the plant operator also examines compositional data in order to change the set points of the automatic control or manually change the flow rates of the fed pulp, acid, spent and/or water. Note that, again, the control of acid concentration is done hand-in-hand with the control of the pulp density,

The control of metal concentrations in the process is mainly done by the process operator, but – as mentioned – there is automatic control on the density in 400-TK-10 and 400TK-050. The most important control of metal concentrations is done by looking at the *total metal* values (sum of concentrations of base metals) in the compositional data results, as well as the concentration of metals like copper alone (Lonmin, 2013). The operator responds to significant deviations from allowable pre-defined ranges by changing above-mentioned process parameters, such as the underflow discharge rate of the thickener 300-TH-300. The following is an excerpt from the spreadsheet that the process operator uses to control the plant.

Table 4: Allowable ranges used by process operator to control compositions

Compositional Ranges	**400TK020**	**400 - VE - 300**		**2nd Stage Residue**	**400TK150**	**400TK110**
		Compartment 3	**Compartment 4**			
Acid (g/l)	20-25	10 - 20	25-30		35 - 45	30 - 35
Total Metals (g/l)	100- 120	135 - 145	<50		0	
Copper (g/l)					< 30	< 60
mV		450 - 480	520 - 550			
%Pt				12 - 18		
%Cu				18 - 25		

This is the part of control that needs the most input from the operator and is, therefore, an important area of improvement. Note that the manner in which these values are used to control the plant could not be clearly defined by Lonmin and therefore cannot be quantified here. It can, however, be noted that the acid concentration measurements are responded to by manipulating the amount of acid entering the autoclave (Burchell, 2014). This refers the acid concentration in the feed entering the autoclave. The total metals concentration readings are responded to changing the water and spent flow rates into the pressure leach (Burchell, 2014).

Summary

Table 5 provides a brief summary of the current control mentioned.

Table 5: List of control loops that form part of the current control

CV	MV	Control Type	Potential Disturbances
Level of 400-TK-10	400-FIC-0106	Automated feedback	Flow rate change: streams 1-5
Level of 400-TK-20	400-FIC-2204	Automated feedback	Flow rate change: streams 5, 7-9, 23
Level of Comp 3	400-FIC-0402	Automated feedback	Reactions change, flow rate change: streams 7-11
Level of 400-TK-040	400-FIC-0401	Automated feedback	Flow rate change: stream 14
Level of 400-TK-050	more than 1	Unsure	Flow rate change: streams 17-21
Level of Comp 4	400-FIC-2003	Automated feedback	Reaction change, flow rate change: streams 12, 13, 21, 22
Temperature of Comp 1	400-FIC-2203	Automated feedback	Reaction change, upstream temperature change
Temperature of Comp 2	Cooling coils	Automated feedback	Reaction change, upstream temperature change
Temperature of Comp 3	Cooling coils	Automated feedback	Reaction change, upstream temperature change
Temperature of Comp 4	400-TV-2005	Manual	Reaction change, upstream temperature change
Autoclave Pressure	400-FIC-2001	Automated feedback	Reaction change, flow rate change: streams 8, 10-13
%Solids in 400-TK-10	400-FIC-1102	Unsure	Change in ratio between streams 1-4
%Spent in 400-TK-10	more than 1	Unsure	Change in ratio between streams 1-4
%Solids in 400-TK-040	more than 1	Unsure	Change in ratio between streams 17-20
Acid conc in 400-TK-040	more than 1	Unsure	Change in ratio between streams 17-20

2.3.5 Control Hierarchy

The control structure of a process can be divided into two different levels: regulatory and supervisory control.

Regulatory control refers to the control level that regulates a process during normal operation. It ensures that all controlled variables are kept at their respective set points, and this is done by manipulating one or more manipulated variables (Wang, 2011). For the sake of clarity in this project, regulatory control can be further divided into what will be called basic and compositional regulatory control in this project.

In this project, basic regulatory control refers to the control of temperature, pressure and inventory levels in the pressure leach process, and will be dealt with in chapter 4. On the other hand, compositional regulatory control refers to the control of density and acid concentration – as is the case in tanks 400TK10 and 400TK050. This will be the focus of chapter 5.

Supervisory control supervises the regulatory control by determining and entering the set points thereof. This is done in order to reach certain, predefined process performance objectives. At Lonmin, this control level is currently done by the operator – but it is possible to incorporate it into an automated supervisory control strategy. Supervisory control is also part of chapter 5.

2.3.6 Recommendations

From this chapter, the potential areas of interest can be identified.

Basic Regulatory Control

This part of the control is done the best of the control levels on the plant. The strengths include the control of pressure and the inventory control. The temperature control on the first compartment has been identified by Lonmin as an area of concern, and therefore it will be an area of focus in this project. The temperature of the second compartment is not controlled, due to the mentioned cooling malfunction, but since this project focuses on control only, it will not be focussed on.

Compositional Regulatory Control

The procedures surrounding compositional control could not be clearly defined by Lonmin. In 400-TK-10 the ratio between the flow rates of spent/formic and stream 1 is kept constant to attempt to keep the solids fraction and acid concentration in this tank constant. The manner in which these ratios are changed is unclear. The clearest part of compositional control is the fact that pure acid is added to 400-TK-20 to control the acid concentration in this tank. However, it has been noted by Lonmin that this stream is not desired. This will therefore also be an area of focus in this project.

The compositional control before the third stage leach is a weakness on the plant, partly due to the fact that the solids-liquid separation phase between the second and third leaching stages is controlled from a different control room. The compositional control on 400-TK-050 is therefore less clearly defined than that of 400-TK-10. While this is a significant weakness, it will not be an area of focus in this project. The reason for this is that the problem is not yet well enough defined, with more information required to be able to accurately simulate the process section. Given this fact, the methodology developed for 400-TK-10 should be helpful as a first approximation for future control developments on 400-TK-050.

Supervisory Control

The supervisory control on the plant is done by process operators, who follow rules that could not be clearly stipulated for use in this project. Inferential variables (to be defined in chapter 4) are measured and used to control the project. This is an area with much scope for improvement, but it can only be investigated in this project if the model is to be found valid for this control. This validity is investigated in chapter 3.

CHAPTER 3

DATA PROCESSING & MODEL VALIDATION

3.1 CHAPTER INTRODUCTION

In order to use the model as a representative simulation of the pressure leach process, the extent to which the model matches the actual process needs to be determined. This should be done keeping in mind the fact that the match should be sufficient for the investigation of current and improved of control structures on the process. This is the central aim of this chapter.

The plant data from Lonmin's BMR are first introduced and discussed, focussing on the manner in which it was acquired and processed, as well as its potential for use in this project. The model – in the form it was received at the onset of this project – is then introduced and discussed, after which its migration from MATLAB to Simulink is explained. The validation, verification and adaption of this model are then done.

The findings of this chapter, specifically the model's validity for its intended use, are given – along with the scope for control development that is allowed by the results.

3.2 LITERATURE REVIEW

3.2.1 Data Analysis and Processing

While it is essential to understand a plant in terms of fundamentals (e.g. reactions and kinetics), as well as operating conditions and control, the dynamic behaviour of a plant can only truly be known by examining data drawn from a number of important variables. Process data therefore have to be accurate and adhere to a number of requirements before it can be used as a reliable source of information.

Data Requirements

The data gathered from a plant, before it is processed, are to adhere to a number of requirements in order for it to be deemed sufficient for doing model validation. The most important of these requirements is that it has to give a good and complete representation of the relevant process and it should not contain any bad data. In order for a data set to be a good and complete representation of a process, it firstly needs to consist of a sufficient number of data points. Roffel and Betlem (2006) recommend that the number of data points should be at least 10-20 times the number of model parameters (for a model with the complexity of the one at hand). It is also important for the data points to span a sufficient range, contain a sufficient amount of low-frequency information (slower changes) and should be sampled at a high enough frequency to pick up as much as possible of the dynamic process characteristics. “Bad” data should also be removed, while the remaining data should be examined to determine whether the inputs and outputs of the process adhere to the law of mass conservation. (Roffel & Betlem, 2006)

Detection and Removal of Bad Data

Bad data are defined as being data that is incomplete or incorrect (Chen, Kwon, Rice, Skabardonis, & Varaiya, 2002). Data can have the following possible deficiencies (Ljung, 1999):

- High-frequency disturbances (above frequencies of interest)
- Occasional outliers, missing data or discontinuities in data records
- Drift/offset and unexplainable low-frequency disturbances

The most common method of removing such data from a data set is by graphical analysis. While sufficient in most cases, other methods (such as principal component analysis) can help in identifying bad data that may not be directly visible. (Roffel & Betlem, 2006)

Data Filling

Roffel and Betlem (2006) propose three ways of filling empty zones in the data. The first of these is to interpolate between data, either using splines (Friedman, Grosse, & Stuetzle, 1982) or time-series modelling (Box, Jenkins, & Reinsel, 2008). In the latter method a time series model is created and then used to determine the unknown values. A second approach is to use linear interpolation between the data points on the boundaries of the gap. While very simple, this often gives satisfactory results (Roffel & Betlem, 2006). Finally, a matching pattern approach can be used. This means that a region in the data is found which resembles the region with missing points – and that the observed trend is applied to fill the gaps. Roffel and Betlem (2006) propose that the second approach is used.

It should be noted that – in the case of very small gaps in the data – these methods may prove unnecessarily complex. For such a case the most basic approach would be to hold the previous value for the duration of each gap, creating steps in the data.

Data Validation

Data that is appropriately gathered, filled and sufficient in number may still have internal inconsistencies. Such inconsistencies typically refer to violations of mass balances and are often caused by faulty sensor readings. It is therefore important to do mass balances on the process and its sub-systems – if not to change the data, then only to be able to comment on the quality of the data that will be used for model validation.

Dead Time Identification

Time lags (dead time and time constants) are very important in the analysis of dynamic time series data. The time delay between an input change and a corresponding response in output variables can be determined graphically or by means the cross-correlation coefficients between input and outputs (Roffel & Betlem, 2006). For a given input series (u_1, u_2, …, u_n) and output series (y_1, y_2, …, y_n), the cross covariance coefficients (c_{uy}) can be calculated with the following equation (Roffel & Betlem, 2006):

$$c_{uy}(k) = \frac{1}{N-k}\sum_{t=1}^{N-k}(u_t - \bar{u})(y_{t+k} - \bar{y})$$

[5]

In this equation k is an integer starting from 0. Moreover, $\bar{u}$ and $\bar{y}$ refer to the respective means and N to the number of samples. While the calculation of cross correlation is a linear technique, it can also be used to a certain extent with non-linear processes (Roffel & Betlem, 2006).

3.2.2 Model Validation & Verification

Model validation is defined as the process of determining the degree to which a model is an accurate representation of the real world from the perspective of the intended use of the model (AIAA, 1998). More directly (in terms of this project): it is the confirmation that a computerised model is sufficiently accurate within a suitable range and in the light of the model's intended purpose (Schelsinger, et al., 1979). From both these definitions, it can be seen that the purpose of the model is key to its validation. This stems from the view that the philosophy of model validation in the field of system dynamics correlates with the holistic or relativist field of science – which means that models cannot be deemed absolutely true or false, but rather has a certain degree of usefulness with respect to a predefined purpose (Barlas, 1994) This implies that the purpose of the model with regards to this project has to be stated clearly before model validation can be done. This will be done in section 3.6.1. Note that model verification refers to the confirmation that the computerised model is correctly implemented on a software platform (Sargent, 2013).

Concepts & Process

Sargent (2013) proposes that model validation and verification consists of three components that need to be considered. These components, as well as the links between them, are displayed in the following figure:

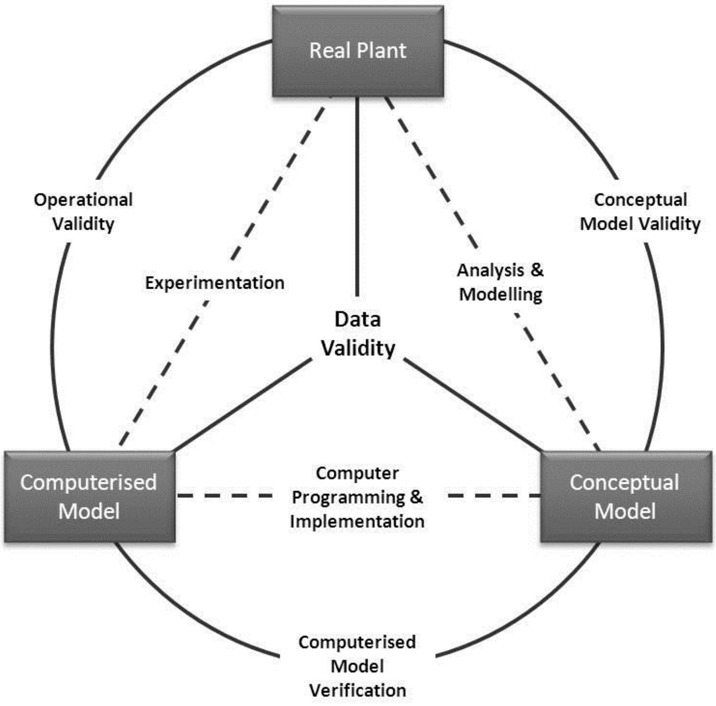
Real Plant
Operational Validity
Conceptual Model Validity
Experimentation
Analysis & Modelling
Data Validity
Computerised Model
Computer Programming & Implementation
Conceptual Model
Computerised Model Verification

Figure 5: Simplified diagram of the model validation & verification process (redrawn from Sargent, 2013)

In this figure, it can be seen that a valid and accurate data set lies at the centre of model validation and verification. This emphasises the importance of the data acquisition and processing step. Note that at the top there is the real plant, which the model looks to represent. By analysis and modelling, a conceptual model is developed. This is the mathematical representation of the real plant. From this model a computerised model is programmed and implemented on a relevant software package. By experimentation, the computerised model and the real plant are compared.

During conceptual model validation the assumptions and principles on which the conceptual model is built are reconsidered and it is ensured that – within the purpose of the model – the mathematical expression of the process is correct to a satisfactory degree (Sargent, 2013). During the computerised model verification stage, the implementation of the conceptual model in computerised form is evaluated. During the operational validation step, the model's key output variables are compared to that of the real plant and evaluated within the bounds set by the limitations on the model's purpose and range of operation.

Conceptual Model Validation

According to Sargent (2013) this leg of model validation consists of two components: the testing of the theories and assumptions that underlie the conceptual model and the evaluation of the model if it is reasonable for its intended purpose.

During this project, the reaction kinetics and its related parameters determined by Dorfling (2012) is not revisited – and therefore in-depth investigation into the derivation of these parameters from experimental test work lies outside the scope of this project. This means that the first component of conceptual model validation is limited to an evaluation of the assumptions made in the setting up of the conceptual model – as well as other discrepancies encountered during comparisons between the true process and the rationale of the model. After defining the model's exact purpose in this project in section 3.6.1, the suitability of the structure of the model will be commented on. Sargent (2013) recommends that face validation should be used for these evaluations, which means that process experts (or people who are familiar with the real plant's operation) should comment on the reasonableness of the model – keeping in mind its intended purpose. Flow charts are typically examined, along with model equations.

Computerised Model Verification

This is a very important step in the total model validation procedure, since in it the implementation of the model in terms of computer programming is verified. Errors arising in this step are typically independent of the conceptual model and pertain to the programming philosophy and structure used, as well as the details in the programming text and blocks (in the case of a visual programming language such as Simulink) – often referred to as "bugs" in the program. Sargent (2013) proposes two possible methods of testing for the computer model's correctness. The first of these is a static method, wherein the program is gone through systematically – typically by walking through it with other knowledgeable people. The second method entails dynamic testing, where the model runs and process-specific checks are done on the model. Checks can be built into the model to ensure that internal consistency limitations aren't violated – stopping the model with an error message in the case of such a violation. Note that the dynamic testing ties in with operational validation, which is discussed next.

Operational Validation

Operational validation is the most important part of model validation, since the majority of errors are detectable in and has an influence on this step. In this step the model's performance and outputs are compared with that of the available data from the real plant. There are numerous ways in which this can be done, and the best methods depend on whether it is possible to collect data on the operational behaviour of modelled system or not, and on the nature of the model's outputs. Sargent (2013) recommend using both a qualitative and quantitative method of comparison.

The qualitative method is the more important of the two, due to the fact that the model's validity (with regards to a specific purpose) is evaluated, and not an absolute measure of accuracy. Sargent (2013) recommend a graphical comparison between the model outputs and the data. In this method, the two sets of values are plotted on the same graph, with comments made from it. Sargent (2013) note that such comparisons should be made for variables that have relationships that are important to the model's purpose. A consequence of this is that it would be good practice during such a validation procedure to go through the process sequentially (one process subsystem at a time) and comment on what can be observed. Since such a qualitative method is subjective, it is important that it is done by someone who is knowledgeable of the process and the plant.

Due to the fact that model validation of system dynamics is purpose-dependent, hypothesis tests are not included in the quantitative validation step (Barlas, 1994). This consideration also has implications for other statistical methods, such as confidence intervals – which are recommended by Sargent (2013). Instead, the differences between two time series data can be compared by means of well-established statistical measures. An example of this is the root mean squared error (RMSE), which is defined as follows (Chai & Draxler, 2014):

$$RMSE = \sqrt{\frac{1}{n}\sum_{i=1}^{n}(A_i - B_i)^2} \tag{6}$$

Here, *A* represents the values predicted/calculated by the model and *B* represents actual measured values. *n* is the number of data points in question. Such an RMSE value has the same units as the variables compared. It can also be normalised to become a dimensionless number, as follows:

$$nRMSE = \frac{RMSE}{max(\mathrm{B}) - min(\mathrm{B})} \tag{7}$$

Here, *B* is defined the same is in the previous equation.

A perfect quantitative match between the model and the data would lead to an RMSE, and therefore also an nRMSE, of zero. Less correlated model and data values lead to larger RMSE and nRMSE values. While hypothesis tests are not relevant for this application, a reference RMSE or nRMSE value needs to be defined to enable sensible interpretations to be made.

The RMSE can be viewed as the standard deviation of the residuals between two data sets (Schmee & Opperlander, 2010). A reference value for the RMSE can therefore be set as the standard deviations of the sets of model and data values. While an RMSE value smaller than these standard deviations would indicate a good correlation, larger RMSE values cannot be deemed as bad. A value of 30% is chosen as a crude baseline value for the normalised RMSE. These two interpretation methods will aid in the evaluation of the correlation between model and data sets.

3.3 DATA GENERATION & PROCESSING

In order to be able to be able to evaluate and adapt the model in this project, a sufficient amount of plant data is necessary. The data requirements listed in section 3.2.1 have an impact on both the requirements for the conditions under which process data are generated and how it is processed. These two steps are now discussed separately.

3.3.1 Data Acquisition

General Information

In terms of acquiring plant data for this project, it is important to recognise the fact that Lonmin's BMR is a fully functioning, large-scale production plant. This means that the manipulations of different variables on the plant are limited, if not prohibited. It is for this reason that it was impossible for the author to do the tests that would be necessary to ensure that there are sufficient low frequency variations, with large enough amplitudes, to cause changes in intermediate and output variables such that causal relationships can be verified beyond the uncertainty of noise. Instead, the data obtained for this project were generated by external control consultants who focussed on a small part of the second stage leach, namely the flash recycle tank and first autoclave compartment. Process manipulations were therefore not sufficient to be able to characterise the whole pressure leach process. This means that that, while it was ensured that all necessary data tags were logged and acquired – over a sufficiently long time period of 60 hours – there are some important limitations to the data.

Data Generation Limitations

The first limitation on the data is caused by the fact that the people that made the process alterations and gathered the data at the plant did not have the same purpose for it as this project does. This means that data logging outside of their scope – that is, the part of the process beyond the second stage leach – is done much less frequently than is the case for the second stage leach. This also means that process alterations were made mainly to characterise the second stage leach.

The second limitation is caused by the fact that the plant's control system was in full operation at the time of the data acquisition. The fact that the exact specifications of the control on the plant are not known means that much uncertainty is introduced in terms of the plant's dynamic characteristics. Literature supports the fact that system identification is more difficult under closed loop conditions (Bitmead & de Callafon, 2003). This is arguably worsened by the fact that, instead of doing step tests, the tests were done in the form of a pseudo-random binary sequence, making it challenging to derive low frequency information on process dynamics.

3.3.2 Data Processing

The data received for the second stage leach varied in terms of sampling/logging times and were therefore not aligned to the same time intervals. This was addressed by creating an matrix with 10-second intervals. This interval size was chosen, as it represented the shortest logging rate among the data points. The data was fitted onto this matrix, with empty zones left among the values of the less frequently logged variables. A suitable interpolation method had to be applied to fill the empty zones.

As a first approach, the last logged was held until the next one is reached – creating data that changes in a stepwise fashion. From the matrix a smaller, complete data set for the second stage leach was chosen for which the time range wherein there are values for all variables. This time range was approximately 48 hours long, which is sufficient for the data's purpose.

The logged data received for the third stage leach were logged every 5 minutes, making it less ideal than the second stage data in terms of dynamic analyses. This data was treated in a similar manner to that of the second stage leach, with values held over the 5 minute intervals.

By inspection of graphs of the data it could be seen that some of the variables had outliers, which can be attributed to sensor or transmission faults. These outliers were removed by setting it equal to the last non-outlying value.

3.3.3 Data Summary & Completeness

The data provided by Lonmin, logged during the execution of pseudo-random binary sequence tests, can be split into two categories: online measurements and analysis data. The former is sampled several times per hour (down to every 10 seconds), while the latter is available much less frequently. Before these categories are discussed, a summary of the data set – and how it corresponds to model names – are given below.

Online Measurements

Most of the available data for the pressure leach process has been logged. As mentioned, the data tags around the second stage leach were logged at a higher frequency than that of the third stage leach. This includes volumetric flow rates, tank levels (percentage-wise), temperatures and pressures. The available tags are given in the table below, with the two aligned data sets listed separately. Note that the flow rates of streams 17, 21 and 22 (see the flow diagram below) – which are important – are not available.

Table 6: Lists of data tags available (for the two aligned data sets), with corresponding locations (model stream or tank) given.

Available				**Not available**	
10 seconds		**5 minutes**			
Data Tag	***Location***	***Data Tag***	***Location***	***Data Tag***	***Location***
400-FIC-0101	Stream 2	400-LIC-0401	400-TK-040	400-FIC-501	Stream 21
400-FIC-0103	Stream 5	400-FIC-0401	Stream 15	400-FIC-2003	Stream 22
400-FIC-0106	Stream 1	400-FIC-0501	Stream 19	$\text{FI}_{\text{stream17}}$	Stream 17
400-FIC-0107	Stream 4	400-FIC-0504	Stream 20		
400-FIC-0402	Stream 14	400-FIC-0505	Stream 18		
400-FIC-1102	Stream 3	400-LIC-0501	400-TK-050		
400-FIC-2001A	Stream 10	400-LIC-2003	Comp 4		
400-FIC-2001B	Stream 11	400-TIC-2005	Comp 4		
400-FIC-2202	Stream 23				
400-FIC-2203	Stream 9				
400-FIC-2204	Stream 7				
400-LIC-0101	400-TK-10				
400-LIC-2002	Comp 3				
400-LIC-2201	400-TK-20				
400-PIC-2001	Autoclave				
400-TIC-2001	Comp 1				
400-TIC-2002	Comp 2				
400-TIC-2003	Comp 3				

The data tags provided in the above table can be seen in the following figure:

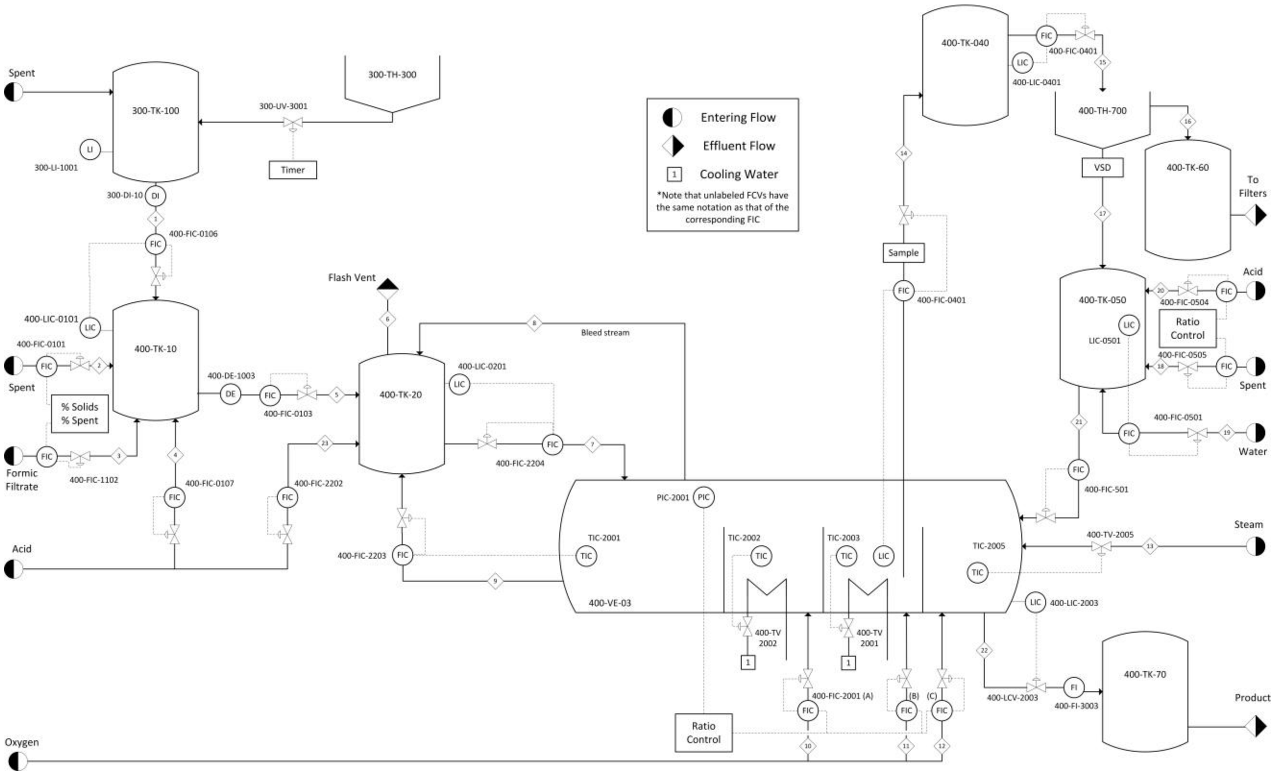
Spent
300-TK-100
300-LI-1001
LI
300-DI-10
DI
300-UV-3001
Timer
300-TH-300
400-FIC-0106
FIC
400-LIC-0101
LIC
400-FIC-0101
400-TK-10
Spent
% Solids
% Spent
Formic
Filtrate
400-FIC-1102
400-FIC-0107
400-DE-1003
DE
400-FIC-0103
Flash Vent
Bleed stream
400-TK-20
400-LIC-0201
400-FIC-2204
400-FIC-2202
400-FIC-2203
Acid
Entering Flow
Effluent Flow
1
Cooling Water
*Note that unlabeled FCVs have the same notation as that of the corresponding FIC
400-TK-040
400-FIC-0401
400-LIC-0401
400-TH-700
VSD
400-TK-60
To
Filters
Sample
400-FIC-0401
400-TK-050
LIC-0501
Ratio
Control
Acid
400-FIC-0504
400-FIC-0505
Spent
400-FIC-0501
Water
400-FIC-501
PIC-2001
PIC
TIC-2001
TIC
TIC-2002
TIC-2003
TIC-2005
400-VE-03
400-TV
2002
400-TV
2001
400-TV-2005
Steam
400-LIC-2003
400-FIC-2001 (A)
(B)
(C)
Ratio
Control
400-LCV-2003
FI
400-FI-3003
400-TK-70
Product
Oxygen
1
2
3
4
5
6
7
8
9
10
11
12
13
14
15
16
17
18
19
20
21
22
23

Figure 6: Simplified schematic representation of the pressure leach process at Lonmin, with basic control loops and stream numbers indicated

Control Modes

The exact modes of the controllers were determined by inspecting the data. Process variables that made straight lines are in manual mode, while noisy process variables indicate that it is automatically controlled. In a similar manner, variables with noisy set point values are in a cascade mode, with set point values determined by another controller. The flow rates of streams 4 and 23 are found to be in manual mode throughout the time of the data's gathering. The following variables are split into those in and not in cascade mode:

Table 7: Second stage leach variables that are in cascade mode and not in it during the data gathering.

In cascade mode	Not in cascade mode
400-FIC-0106	400-FIC-0104
400-FIC-0101	400-LIC-2201
400-FIC-0402	400-TIC-2001
400-FIC-2009	400-TIC-2002
400-FIC-2010	400-TIC-2003
400-FIC-1102	400-LIC-2002
400-FIC-2204	400-PIC-2001
	400-LIC-0101

It should be noted that the control modes is only available for the second stage leach, since the third stage leach data is not logged frequently enough to be able to comment on the control modes. Since it is a running plant, however, the third stage was indeed controlled.

The flow rate of streams 9 seems to be switched between cascade and non-cascade mode at the time of the data gathering. The reason for this is that, while the set point of the flow rate of stream 9 is typically determined by the temperature controller of compartment 1, the set point is temporarily manually changed by the process operators.

Compositional Analysis Data

The available analysis data comprise of compositional data of the solids residues (mass fractions) and liquid filtrates (concentration) for the second and third stage leach. This is also available for the first stage leach residue and the formic filtrate. It is summarised in the following table, along with the rate at which it is sampled.

Table 8: Lists of compositional data available around pressure leach process

Compositional Data		
Once a shift	**Daily**	**Process Unit**
1st stage residue		
2nd stage residue		Compartment 3
2nd stage filtrate		Compartment 3
3rd stage residue		Compartment 4
3rd stage filtrate		Compartment 4
	Formic filtrate	Formic Leach

Other data that is more directly used by plant operators to control the process are available for the process units around the pressure leach process. These include density, redox potential and different component concentration measurements. The table below summarises it, along with the frequency at which the information is available.

Table 9: More frequently available process stream information of different process units in and around the pressure leach process

Process Unit	Density	Concentration (g/L)			Redox
	(kg/L)	Acid	Copper	Total metals	potential (mV)
300-TK-100	hourly				
400-TK-10	hourly	2/shift		2/shift	
400-TK-20	hourly	hourly		hourly	
Comp 3		1/shift	1/shift	1/shift	hourly
Comp 4		1/shift	1/shift	1/shift	hourly
400-TK-050		hourly	hourly	hourly	

3.3.4 Internal Consistency

In order to be able to confidently use the data as bench mark for model validation, its internal consistency needs to be verified. This is typically done by means of a mass balance – but the setting up of a mass balance for the data proved to be difficult. This can be attributed to the following factors:

- An operator shift is typically 7 hours long. The instantaneous compositional analysis data that are used to set up a component balance could therefore have been sampled at any time during such a shift.
- A mass balance cannot be done throughout a transient process at one time step. While a mass balance can be done over a unit during a period in the data where there is no accumulation in the unit, it cannot be done for the process as a whole. For the larger process, dead times and time constants need to be taken into account to attempt to follow the same portion of contents throughout the process. While the typical values for these times can be calculated using typical or mean flow rates, the variability in these flow rates cause a large (especially cumulative) uncertainty in the times throughout the process at which data should be chosen for comparison.

With the two sources of uncertainty just mentioned, it is clear that the setting up of a complete mass balance is limited, if not impossible. Due to its importance the mass balances that have been done are, however, shown in this section.

Mass Balances

The flow rates around 400-TK-10 are inspected at a stage where the tank level is reasonably stable, since this indicates a period of no accumulation. In the following plot of the level of 400-TK-10, it can be seen that this stable region lies between 10-second intervals 4000 and 6000 (666.7 and 1000 minutes).

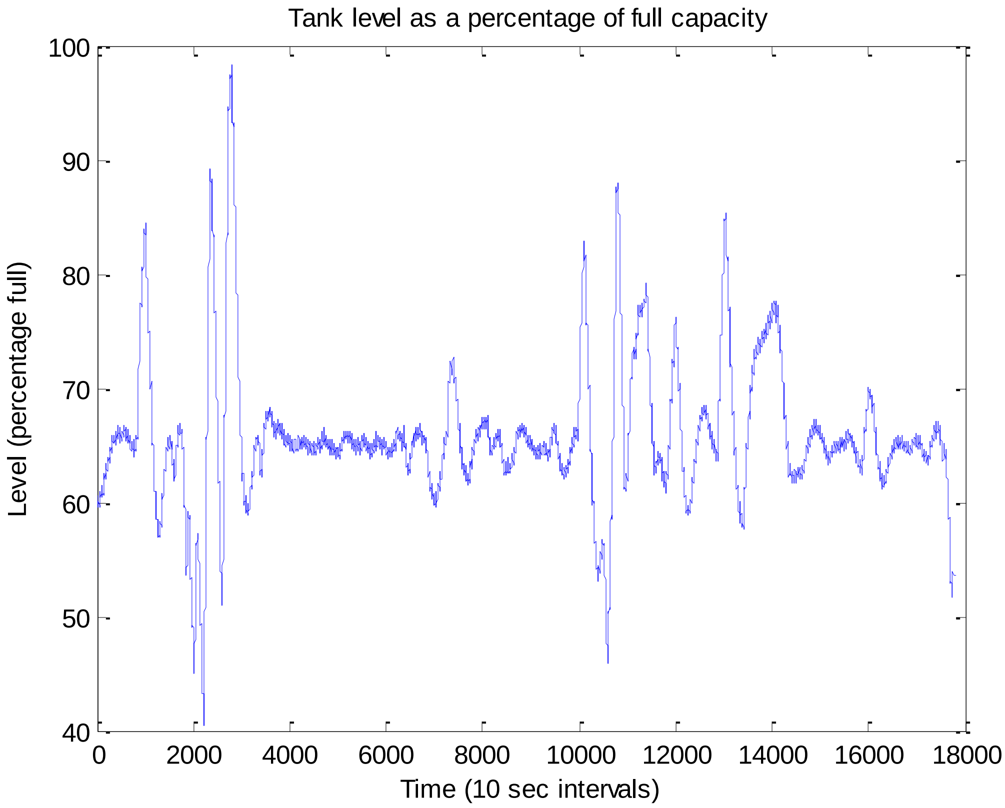

Figure 7: Plot of the level of 400-TK-10 over the total data range (in 10 second intervals)

For this range, the mass flow rates to and from 400-TK-10 should be the same, as can be seen in the following equation:

$$\frac{dm_{tank}}{dt} = 0 = \dot{m}_{in} - \dot{m}_{out} \tag{8}$$

In this equation, the $\dot{m}$ terms refer to mass flow rates. In order to test whether the difference between these variables are indeed zero, the respective mass flow rates need to be determined. The following densities are available:

Table 10: Table of densities for stream around 400-TK-10

Stream	Density (kg/L)	Assumed	Data
1	1.5		x
2	1.15	x	
3	1.15	x	
4	1.836	x	
5	1.18		x

The densities for stream 1 and 5 are available in the compositional data. These values are taken as an average of the chosen data range. The densities of streams 2 and 4 are typical values given in literature for the respective streams (Dorfling, Bradshaw, & Akdogan, Characterisation and dynamic modelling of the behaviour of platinum group metals in high pressure sulphuric acid/oxygen leaching systems, 2012). The density of the formic filtrate is approximated as being similar to that of copper spent electrolyte.

The following equation is used to determine the values plotted in the figure below:

$$\dot{V}_1\rho_1 + \dot{V}_2\rho_2 + \dot{V}_3\rho_3 + \dot{V}_4\rho_4 - \dot{V}_5\rho_5 = \Delta_{m,400TK10} \tag{9}$$

Here, $\dot{V}$ refers to the volumetric flow rates as they are given in the data and the delta term is the mass balance error, also called the net mass flow rate (in kg/h). These errors are plotted in the following figure:

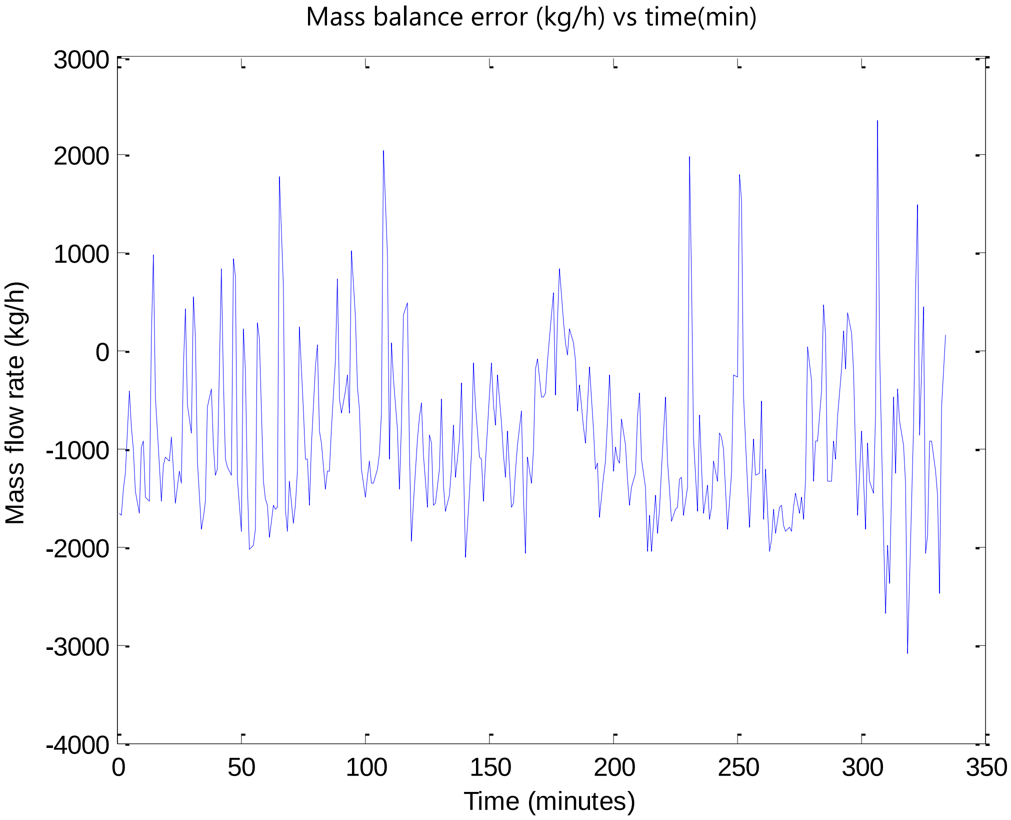

Figure 8: Plot of the mass balance error around 400-TK-10 for a region of minimal level change

From this figure it can be seen that there is generally a net flow out of the tank (with a mean value of 897 kg/h). This mean value is 10.86% of stream 5's mean value for the range (representing the tank's throughput), which is very large for a value that should be zero. The logged density values provided by Lonmin vary with less than 2%, which means that either the assumed densities are very far from correct or the data provided is incorrect to the extent that the mass balance around the tank in question does not hold.

The same can be done for the flash tank, 400-TK-20, as can be seen in the equation below:

$$F_5\rho_5 - F_6\rho_6 - F_7\rho_7 + F_8\rho_8 + F_9\rho_9 = \Delta_{m,400TK20}$$ [10]

It should be noted that the case of this tank is more complex than for 400-TK-10, since streams 6 and 8 are vapour streams, of which the densities are unknown. Moreover, there is evaporation and condensation taking place in 400-TK-20, which means that a constant level does not necessarily indicate a tank with no accumulation.

From the following plot it can be seen that a stable region lies between the 6900th and 7400th 10-second intervals (1150 and 1233.3 minutes, respectively):

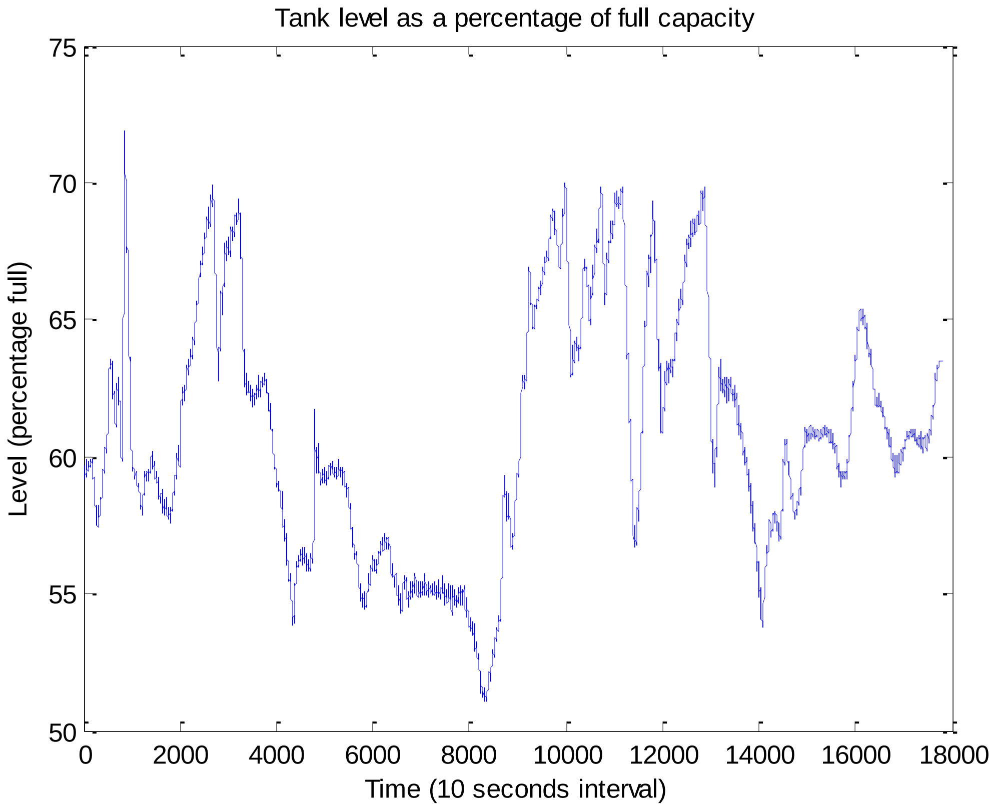

Figure 9: Plot of the level of 400-TK-20 over the total data range (in 10 second intervals)

In the identified region, the tank level stays between the bounds of 54.8% and 55.7%.

The streams relevant to this comparison are streams 5 to 9. Streams 6 and 8 are the vapour streams that exit and enter the tank, respectively. Similarly, streams 7 and 9 are the non-vapour streams that exit and enter the tank. It should be noted that neither flow nor density data are available for the vapour streams and that a mass balance around 400-TK-20 is limited by this fact. The slurry stream densities are given below:

Table 11: Table of densities for stream around 400-TK-10

Stream	Density (kg/L)	Assumed	Data
5	1.21		x
6	-		
7	1.27		x
8	-		
9	1.2	x	

As with the previous mass balance, the density values are in the data are averaged over the chosen time range. The flash recycle stream density of 1.2 kg/L is predicted by the model when the inputs that Dorfling (2012) used are entered into the model.

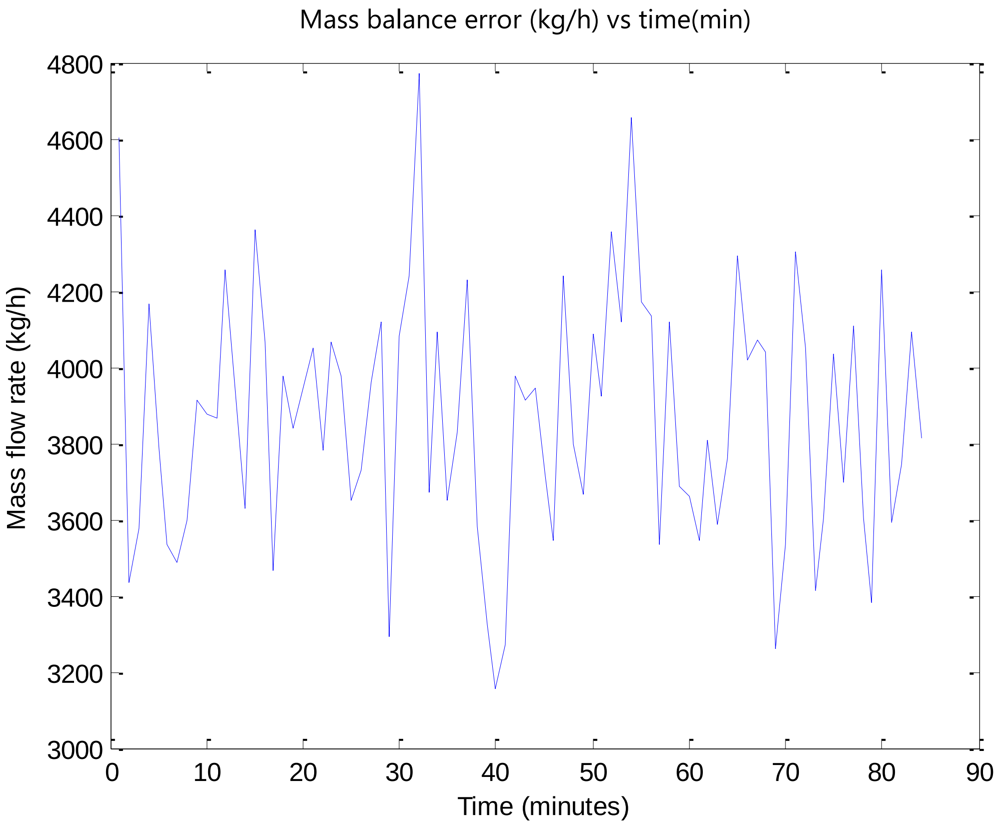

Figure 10: Plot of mass balance error into 400-TK-20 for a region of minimal level change

It can be seen from this figure that there is a net flow into the flash tank (with a mean value of 3865.5 kg/h). This is 9.9% of stream 7's flow rate (representing the tank's throughput) in this time range. It is clear that the vapour flow rates are important and that clear conclusions cannot be drawn from this mass balance.

The methods used to do the mass balances in this section cannot be applied to the second stage leach as a whole. The reason for this is that the reactions taking place consume unknown amounts of oxygen, while steam is also added into the system. While such a mass balance could be set up with a sufficient amount of assumptions, its use is limited and the fact that the data are not complete enough to formally check whether its mass balances hold has to be accepted.

Goal Driven Data Validation

The fact that the data are not sufficient for checking whether the mass balances in the pressure leach process hold means that the validation of the data has to be evaluated by other means. Ljung (1999) mentions that a model can be validated by using it for its intended purpose and evaluating its performance.

The purpose of this project is to design and evaluate control structures for the BMR pressure leach. This means that the model must be sufficient to enable the design and evaluation of control structures on it. Continuing this goal driven approach, the data in this project, in turn, have to be sufficient for enabling the development or verification of the mentioned model. The requirements for data validation are therefore determined by the requirements of model validation, and therefore data validation will be continued as part of the model validation procedure in this project.

3.4 DYNAMIC MODEL DESCRIPTION

3.4.1 Original Purpose

The dynamic model received at the onset of this project was developed by Dorfling (2012) in MATLAB, in order to present the results from experimental batch test work done. The model was therefore created as a supplementary project to a larger project – as a means of incorporating reaction kinetic findings into a structure that to a large degree resembles that of the real pressure leach process. The manner in which the model reacts to disturbances was evaluated qualitatively by Dorfling, in order to show that that the results obtained correlate well with the trends that can be expected from process knowledge. With this in mind, it is therefore important to recognise that the model delivered at the onset of this project is by no means an exact (or quantitatively verified) simulation of the pressure leach process at Lonmin.

3.4.2 Form and Working

The MATLAB model consists of the following 7 files:

Table 12: List of files that make up the received model, along with the purpose of each

Model file name	Purpose of file
autoclave_model	Calls other functions and plots required outputs
input_data	Sets predetermined parameter values (e.g. flow rates, temperatures, pressure, compositions, process component sizes and other constants)
calculate_steady_state_operation	Calculates all unspecified steady-state conditions (e.g. temperatures, flow rates and compositions)
calculate_oxygen_solubility	Calculates the oxygen solubility in the leach solution
calculate_reaction_rates	Calculates the reaction rate constants
calculate_autoclave_odes	Contains the model's ordinary differential equations of mass and energy balances
calculate_dynamic_behaviour	Determines all time domain profiles

The manner in which these files connect, and the order in which they execute, is displayed in the following flow chart. A more detailed list of their functions is given in more detail in Appendix B.

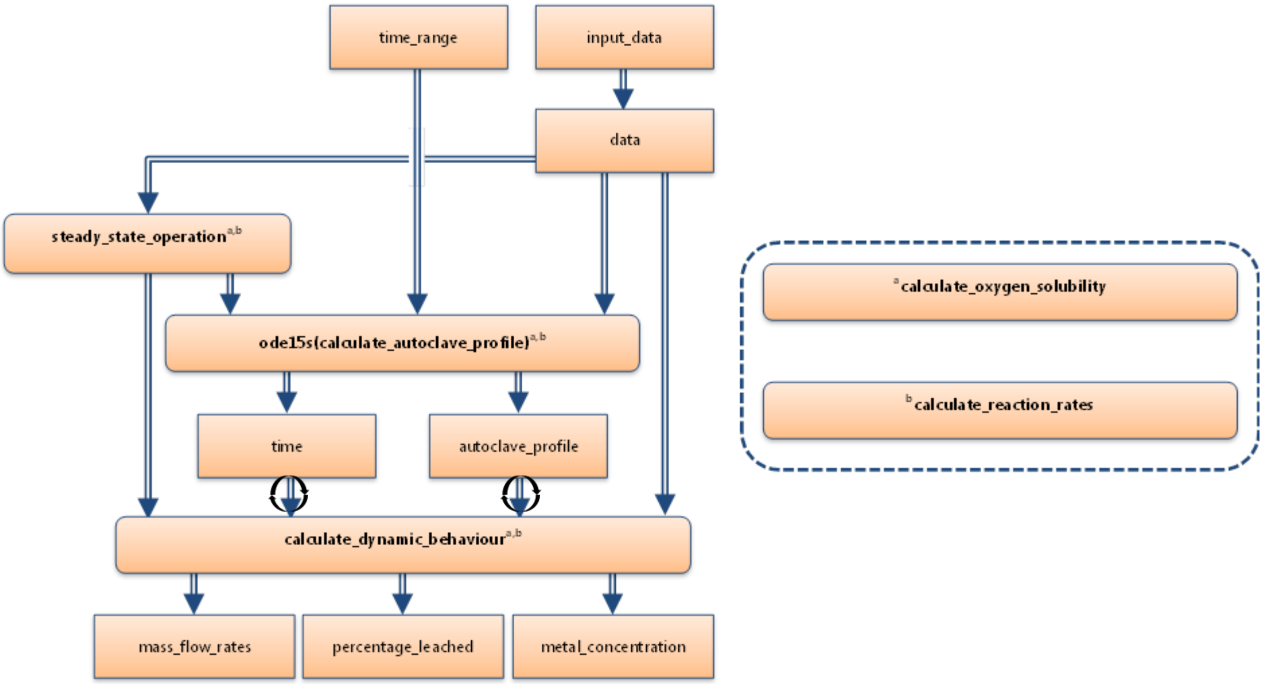
time_range
input_data
data
steady_state_operation a,b
ode15s(calculate_autoclave_profile) a,b
time
autoclave_profile
calculate_dynamic_behaviour a,b
mass_flow_rates
percentage_leached
metal_concentration
a calculate_oxygen_solubility
b calculate_reaction_rates

Figure 11: Flow Chart of Dorfling's Original Second/Third Stage Leach Dynamic Model

It can be seen in this figure how the input data (containing the necessary physical and numerical data) are used to calculates the steady-state values. These values, along with the input data and the time range over which the process runs, are used to solve the ODEs. The results from the ODE-solver, as well as the steady-state values and input data are used to calculate the requested mass flow rates, leaching results and metal concentrations.

3.4.3 Previously Added Control

The possibility of adding control to the dynamic model in the above-mentioned form has been researched by the author (Knoblauch & Bradshaw, 2012). PI control loops were added to provide dynamic control of the following variables (see Appendix A for a flow sheet of the process):

- Temperature in the first (400-TIC-2001) and (400-TIC-2005) last autoclave compartments
- Mass control of 400-TK-10, 400-TK-20, 400-TK-040 and 400-TK-050

Tuning was done by means of tuning correlations proposed by Marlin & Ciancone (Marlin, 2000), using process curve derived information. The details of this tuning method are provided in sections 4.2 and 4.3. The control proved to be successful at rejecting different disturbances (both in the form of stepwise and sinusoidal inputs). However, the added control was limited to being preliminary test work by the following two facts:

- Control was added and tuned without the consideration/inclusion of dead time in the model – which is important in the process of control implementation.

- The added control is far too limited in its scope to accurately represent the pressure leach process at Lonmin.

3.4.4 Differential Equation Solver Used

MATLAB and Simulink provide a number of ordinary differential equation (ODE) solvers which can be used in models such as the one in this project. Dorfling (2012) used ODE15s, which can solve stiff ODE's and uses a variable order method (Mathworks, 2014).

The size of the model, along with the different dynamics in it (with some variables changing more rapidly than others, makes it important to consider system stiffness in the selection of an ODE solver. While system stiffness is a complex principle to define briefly, a very slow execution speed (using a non-stiff solver) often indicates stiffness in a simulation (Moler, 2004). One source notes that a system that has time constants which vary significantly in magnitude is prone to stiffness (plexim, 2014). This is the case with the model used in this project. According to Mathworks (2014) ODE45 should be the first ODE solver attempted, and if the system is stiff, ODE15s should be used. ODE15s ran the model in a significantly shorter time, and therefore it is used.

3.5 MODEL MIGRATION & VERIFICATION

3.5.1 Model Migration to Simulink

The dynamic model received at the start of this project was developed by Dorfling (2012 and changed by the author (Knoblauch & Bradshaw, 2012). For its working, see section 3.4.2. Due to the fact that MATLAB's Simulink platform provides more comprehensive and helpful tools in terms of controller development and implementation, it has been decided that the model would be migrated from its received MATLAB code format to Simulink. Note that Dorfling's initial model was migrated in its published form, and that sanity checks are done in section 3.7 to compare the outputs of the Simulink model with the received model.

The following table summarises the interconnection between the resulting Simulink blocks, along with the function of each block.

Table 13: Simulink block numbers, with input and output links, as well as the parameters calculated in each.

Block #	Input Links	Output Links	Variables/parameters calculated
A	K	B, C, E, F-I	Flow rates to 400-TK-10
B	A	J, K	Flow rates to 400-TK-050
C	K, A	F-I, K	Oxygen & heat transfer in autoclave
D	K	E, K	Heat capacities & mass fractions in various streams
E	A, D	J, K	Energy removal & water evaporation in flash recycle stream
F-I	A, C	J, K	Reactions in autoclave compartment 1-4
J	B, E, F-I	K	Outstanding variables
K	B, C, D, E, F-I, J	A, C, D	Solving of differential equations

Once the model was migrated, the control mentioned in section 2.3 was added to it. The controllers in question are PI controllers having the same format. The controller for the temperature of the first autoclave compartment (400-TIC-2001) is shown below:

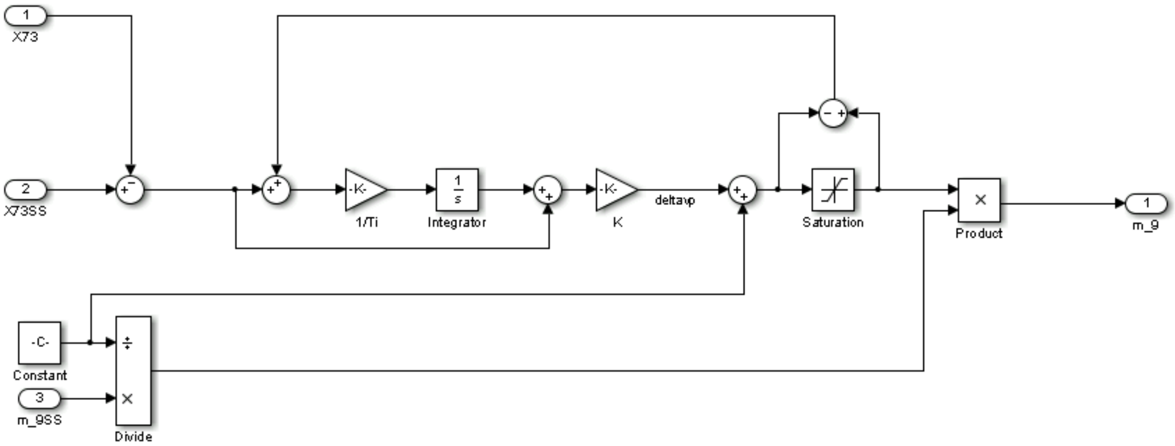

Figure 12: The setup of the PI controller of 400-TIC-2001 in Simulink

In this diagram it can be seen that the current and set point values of the CV – in this case the temperature in compartment 1, X(73) – are entered into the control block. Note that the CV values at steady-state are chosen to be the set point values during the simulations. The difference between the two values makes up the error, which is sent to the proportional (bottom) and integrator (middle) routes. This generates the required change in the position of the relevant valve (Δv). This Δv value is added to the initial valve position to give the new position. Before translating this valve position to a flow rate, it is limited to a predetermined range, with anti-windup added. The correlation between the flow rate and the valve position is assumed to be linear and is calculated by dividing the steady-state value of the MV by the initial valve position. This value is multiplied by the new valve position to give the iteration's new flow rate.

3.5.2 Computer Model Verification

As mentioned in the literature section, there are two methods of doing model verification: static and dynamic. While section-focussed walk-throughs through the model have been done with researchers knowledgeable in the area of programming and modelling, no single, thorough walk-though (which is an important part of static verification) was done by a third party. For this reason, dynamic verification will be the main means of verifying the computer model.

The dynamic part of the computer model verification is lumped in with the operational validation section, since this serves as the single, rigorous testing of the model. Note that Dorfling (2012) added tests in the model for reactions proceeding past their stoichiometric limitations, while tests have been added in this project for checking for tanks running dry and the pressure moving outside its allowable range.

3.6 CONCEPTUAL MODEL VALIDATION

3.6.1 Model Purpose & Required Accuracy

The aim of this project, as stated, is to investigate and develop improvements on the control structure of the pressure leach process. This means that the purpose of the model is to serve as a plant simulation that adheres to the following criteria:

1. It should be set up in such a way that control can be successfully implemented and tested on it.
2. It should be sufficiently similar to the real plant that conclusions and developments made in terms of control structure should apply to the real plant.

Such a model would enable the testing of control structures for the pressure leach process.

It is important to note that the required accuracy of the model depends on the nature of the control development. However, the control that can be developed is limited by the accuracy of the model. With this dilemma in mind, it makes sense that Barlas (1994) states that model validity is achieved by means of a "conversational", instead of a confrontational, process. This means that instead of unceasingly attempting to eliminate errors between the model and the real plant, model validation as a whole in this project entails a process wherein the following two questions are asked continuously (and in a sense iteratively):

- Is the model similar to the real process in the sense and to the extent that control can be developed on the model?
- How does the current model validity limit the control that can be developed, and is it sufficient for this project?

The result of this process is given in this document.

3.6.2 Applicability of Conceptual Model to Purpose

Preliminary test work done by Dorfling (2012) suggested and work by the author (Knoblauch & Bradshaw, 2012) showed that the model's overall structure is suitable for the implementation and evaluation of control. Model validation for the investigation of control structures is sufficient for the purpose of this project, but it must be noted that a more rigorous conceptual model validation – including the reconsideration of how reaction kinetics were derived and of the manner in which reaction rates are calculated – would be necessary for a detailed design of control for the process. The difference between the structural and a detailed design of control lies therein that the latter requires accurate tuning that can be applied to the real plant, and this in turn requires a model that quantitatively provides a near exact match of plant performance.

3.6.3 Conceptual Model Changes

In the process of migrating the model to Simulink, it was found that a number of the assumptions made both by Dorfling (Dorfling, Bradshaw, & Akdogan, Characterisation and dynamic modelling of the behaviour of platinum group metals in high pressure sulphuric acid/oxygen leaching systems, 2012) and the author (Knoblauch & Bradshaw, 2012) in the development of the controlled model are not justifiable. This called for some changes to be made to the model, which will now be discussed separately.

The following assumptions made by Dorfling (2012) still hold for this project:

- All mixed tanks and autoclave compartments are perfectly mixed.
- There are no reactions taking place outside the autoclave.
- The flash recycle stream has the same composition as the contents of compartment 1.

The following table summarises the conceptual model changes in this section:

Table 14: Conceptual model changes, with a summary of the reason for each

Conceptual Model Changes	**Reason for change**
Addition of cooling of compartments 2 and 3	The temperature of compartments 1 to 3 are not the same
Addition of level control in the autoclave	Compartment levels do not stay constant
Change of the level control of 400-TK-050	Implementation in model did not correlate with statements
Addition of pressure control	Pressure is incorrectly assumed to be constant
Addition of dead time	Delays due to piping were not accounted for in model
Addition of stream 23	Acid stream was not in previous models
Addition of non-leaching components	The omission of Pt and Pd is incorrect
Addition of water to stream 1	Solids are fed at a solids fraction of 0.5.
Addition of formic filtrate	Stream 3 was assumed to be water, but is not
Changed oxygen feed fractions	Data and stoichiometry requirements do not correlate well
Correction of compartment 1 calculations	This was not done correctly
Correction of inventory sizes	All inventories were assumed to be 1 m^3

Each of these changes will now be discussed separately. Note that the following flow diagram can be used as reference for the discussion of the changes made:

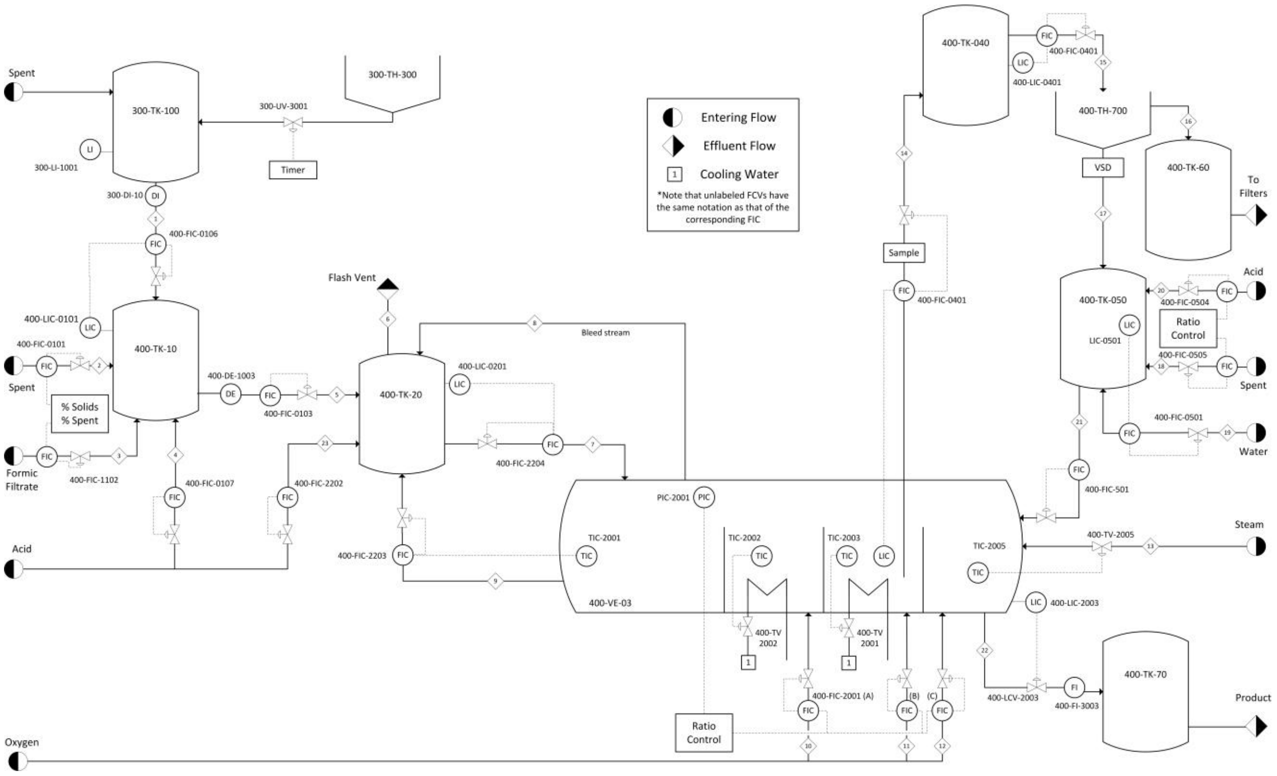
Spent
300-TK-100
300-LI-1001
LI
300-UV-3001
300-TH-300
Timer
300-DI-10
DI
400-FIC-0106
FIC
400-LIC-0101
LIC
400-FIC-0101
400-TK-10
Spent
% Solids
% Spent
Formic
Filtrate
400-FIC-1102
400-FIC-0107
Acid
400-DE-1003
DE
400-FIC-0103
400-FIC-2202
Flash Vent
Bleed stream
400-TK-20
400-LIC-0201
400-FIC-2204
400-FIC-2203
Entering Flow
Effluent Flow
Cooling Water
*Note that unlabeled FCVs have the same notation as that of the corresponding FIC
PIC-2001
PIC
TIC-2001
TIC
TIC-2002
TIC-2003
TIC-2005
400-VE-03
400-TV 2002
400-TV 2001
400-FIC-2001 (A)
(B)
(C)
Ratio Control
Oxygen
400-TK-040
400-FIC-0401
400-LIC-0401
400-TH-700
VSD
400-TK-60
To Filters
Sample
400-FIC-0401
400-TK-050
LIC-0501
Acid
400-FIC-0504
Ratio Control
400-FIC-0505
Spent
400-FIC-0501
Water
400-FIC-501
Steam
400-TV-2005
400-LIC-2003
400-LCV-2003
FI
400-FI-3003
400-TK-70
Product

Figure 13: Diagram of the pressure leach process, with the relevant process variable tags added.

Addition of Cooling of Compartments 2 & 3

In previous work on the MATLAB model, it was assumed that the cooling coils in the autoclave's second and third compartments do not have the capacity to sufficiently cool these compartments down to set point values (Knoblauch & Bradshaw, 2012). During an inspection of the autoclave on the plant, it was found that this was not the case, and that the cooling in the second compartment was not operational – leading to the overheating of the second stage leach. Taking into account for the existing cooling coils' capacity to bring the respective temperatures down to its set points, these coils were added – along with the control of the flow of cooling water (Steenekamp & Mrubata, Control and Specifications of the BMR, 2013).

Assuming perfect mixing and heat transfer, the following equation is used to determine the heat removed by the cooling coils in each compartment (Cengel & Ghajar, 2010):

$$\dot{Q} = \dot{m}_{H_2O} C_{p,H_2O} (T_{AC2} - T_{H_2O}) \tag{11}$$

In this equation, the $\dot{m}$ term refers to the mass flow rate of cooling water through the cooling coils, the C_p values is the water's heat capacity and the two temperatures are those of the second autoclave compartment and of the cooling water, respectively. It is assumed that the flow rate of the cooling water will be high enough that the temperature increase thereof will be small enough that its heat capacity remains approximately constant.

It should be noted that the manner in which the temperature of the second and third compartments are calculated was changed with the addition of the cooling coils. Dorfling assumed in his model that, at steady-state, these two temperatures would be the same as that of compartment 1 (Dorfling, Bradshaw, & Akdogan, Characterisation and dynamic modelling of the behaviour of platinum group metals in high pressure sulphuric acid/oxygen leaching systems, 2012). After an inspection of the data from Lonmin this assumption is found to be unjustified. For the steady-state condition, an energy balance is solved for each autoclave compartment, as can be seen below for compartment 3:

$$T_{14} = 25 + \frac{P_{agitator} + Q_{loss}l_{comp3} + C_{p,AC2}m_{AC2}(T_{AC2} - 25) + Q_{evp,3} - Q_{removed,3} - \sum Q_{Rxn3}}{C_{p,14}m_{14} - (O_{2\_cons})C_{p,O_2}}$$

[12}

Here, $P_{agitator}$ is the energy added by the agitator, Q_{loss} is the rate of heat loss through the compartment's wall, stream AC2 is the flow into the compartment, Q_{evap} is the rate of heat loss through evaporation, $Q_{removed}$ is the rate of heat removal by the cooling coils and the $O_{2\ cons}$ term is in kg/h.

Addition of Level Control in the Autoclave

At the onset of this project, no level control has yet been added to the third (400-LIC-2002) and fourth (400-LIC-2003) autoclave compartments in the model – while it is present at the Lonmin plant. The reason for this is that it was wrongly assumed that the masses of these compartments remain constant, while the respective outflows vary to maintain this condition. This was corrected by changing the two compartments in the model in such a way that with each time step in Simulink a new compartment content mass is calculated for a given instantaneous outflow, in the form of a differential equation. The equation for compartment 3 is given below:

$$\frac{dm_{comp3}}{dt} = m_{AC2} - m_{14} + (O_{2,cons3}) + (H_2O_{cons3})$$

[13}

In this equation m_{AC2} and m_{14} refer to the mass flow rate of the streams flowing in from compartment 2 and out of compartment 3, respectively. Moreover, the O_2 and H_2O terms refer to the rate at which oxygen is taken up into the tank contents (by reactions) and water condenses into the contents (which can also be a negative term). The resulting compartment contents mass is then used in the calculation of the reactions in each compartment.

A PI mass controller was then added, which operates in the same manner as those already implemented, with the effluent flow rate being the manipulated variable in each case. The tuning of these controllers is discussed in more detail in section 4.3.

Change of Level Control of 400-TK-050

While it was known that the level of 400-TK-050 is controlled by varying the flow rate of the entering acid, water and spent, this was not yet implemented on the model (Knoblauch & Bradshaw, 2012).

This problem was rectified by changing the MV of the level controller from the tank's outflow (400-FIC-501) to the sum of the three added streams (400-FIC-0504, -0505 and -0501, also called streams 18 to 20). The flow rate of the outflow was then changed to be constant – making the operation of 400-TK-050 more similar to that of 400-TK-10.

Addition of Pressure Control

An important assumption made by Dorfling was that the pressure in the autoclave remains constant (Dorfling, Bradshaw, & Akdogan, Characterisation and dynamic modelling of the behaviour of platinum group metals in high pressure sulphuric acid/oxygen leaching systems, 2012). The flow rate of the vapour bleed was calculated to be the net sum of the vapour flow rates from the autoclave compartments, thus varying as is required to maintain a constant pressure. In practice, the vapour bleed stream's flow rate is more constant than is assumed in the provided model (Steenekamp & Mrubata, Control and Specifications of the BMR, 2013). The pressure in the autoclave does change and is controlled on the plant by varying the total flow rate of the sparged oxygen into the last three compartments. It is important that this is included in the model, due to the fact that fluctuations in pressure influence a number of factors, such as reaction kinetics. The addition of pressure as a variable therefore introduces to the autoclave's control a potential source of instability and loop interaction.

The first step in adding pressure variation and control was to decide on a manner in which the pressure would be calculated from known process parameters. A correlation between the temperature, volume, mass of components and pressure of the vapour phase in the autoclave was needed. While there are a number of comprehensive correlations available in literature, it should be noted that the low level of precision of the known parameters mean that a crude, approximated correlation is sufficient. With this in mind, the ideal gas law with a compressibility factor is deemed sufficient for this purpose. The adapted ideal gas law of a mixture is given below (Felder & Rousseau, Elementary Principles of Chemical Processes, 2005):

$$P_{tot}V_{tot} = z_{avg}n_{tot}RT_{avg} = \frac{z_{avg}m_{tot}RT_{avg}}{M_{avg}} \tag{14}$$

Here, V_{tot} is the total space in the autoclave available for filling with vapour, while z_{avg} is the compressibility factor of the mixture. At the provided typical autoclave conditions, the compressibility factor of water is approximately 0.94 (Sandler, 2006). T_{avg} is set to be a 100°C, which is a reasonable representation of the autoclave's vapour space, of which the temperature is influenced by the temperature of the autoclave contents and tank walls. In order to simplify the process of determining the total amount of moles in the vapour space, the adapted ideal gas law is used in the steady-state calculations to determine the total mass in the vapour space at a specific pressure. Since the vapour phase is assumed to be a saturated mixture between water and oxygen, the molar mass of the mixture is set to be a weighted average of the molar masses of these two components. The steady-state pressure is set to the typical pressure in the data.

Dorfling (2012) assumed that the flow rate of the autoclave's vapour bleed stream would be the sum of the vapour streams from each autoclave compartment However, the introduction of pressure control necessitates the occurrence of accumulation in the vapour space. The first approach to this problem would be to assume a constant bleed rate. However, correspondence with Lonmin personnel revealed that the bleed stream flows through a valve that opens and closes at a set frequency (Burchell, 2014). This frequency is not available, but is said to be very high. Noting that each time the valve opens the flow through it is a function of the pressure difference over it, along with assuming that the open-close frequency is very high, the bleed flow rate can be assumed to change linearly with autoclave pressure. The following equation describes how the bleed stream is calculated at time step *i*:

$$\dot{m}_{8,i} = \dot{m}_{8,0}\frac{P_i}{P_0}$$

[15]

Here, the ratio between the current and initial pressure is multiplied by the initial mass flow rate through the bleed stream to calculate the current flow rate thereof.

A new differential equation is also added to the model,

$$\frac{dm_{vapour\ space}}{dt} = m_{vap,in} - m_8$$

[16]

Here, $m_{vap,in}$ is the total vapour given off by the four compartments, while m_8 is the mass flow rate of the bleed stream. The resulting vapour space mass is then used to determine the pressure for each iteration.

A PI controller is added which uses this pressure as CV, while the total oxygen flow rate is the MV. This control is discussed later in more detail.

Addition of dead time

The addition of dead time in the model is an important step in the refining of the dynamic model, due to its potentially significant influence on controller design. This was done by calculating it from plant specifications. Pipe lengths and diameters were provided by Lonmin, allowing the calculation of the pipes' approximate volumes. Using the mean values of the flow rates in the gathered data, along with the pipe volumes, the following equation is used to determine the typical dead time values. The calculated values are called typical values, since flow rate variations will let the exact dead times vary.

$$\theta = \frac{V}{\dot{V}}$$

[17]

It is important to note that, since the model has to be compared with the data, the positions of the sensors are important. This means that – along with the dead times between tanks – the dead times of the pipe sections before sensors are also important. The dead time calculation for each pipe is therefore separated into *before* and *after* the sensing point. Dead times are calculated from steady-state values, since small changes are not important. Dead time values for typical input data are shown below:

Table 15: Summary of typical dead times in the piping of the pressure leach

Tank Before	Tank After	Flow Sensor	Relation to Sensor	θ (s)
400-TK-10	400-TK-20	400-FIC-0103	Before	<0.001
			After	<0.001
400-TK-20	Autoclave C1	400-FIC-2204	Before	3.60
			After	22.68
Autoclave C1	400-TK-20	400-FIC-2203	Before	30.96
			After	5.04
Autoclave C3	400-TK-40	400-FIC-0402	Before	28.80
			After	5.40
400-TK-40	400-TH-700	400-FIC-0401	Before	6.48
			After	6.48
400-TH-700	400-TK-150	(stream 17)	Before	21.60
			After	53.64
400-TK-15	Autoclave C4	400-FIC-501	Before	6.48
			After	25.92

It can be seen that not one of the dead times are in excess of 2 minutes, which is magnitudes smaller than the large time constants noted by Lonmin (Steenekamp & Mrubata, Control and Specifications of the BMR, 2013).

The dead times are added into the continuous Simulink model by means of *Transport Delay* blocks. A first set of delays are made which represent the dead times in the pipe sections before the sensor positions. After this first set, all controllers receive its necessary information – as would be done by the sensors in the plant. Note that this does not include flow sensors, since incompressible flow is assumed – meaning that there will be no delay in flow rate changes in the pipes.

Thereafter, a second set of delays are made, which represent the pipe sections from the sensors to the next tank. After this second delay, the respective variables are used in the model's calculations and differential equations – before the next iteration receives its same delays.

Addition of Stream 23

The received model does not contain a pure acid stream entering 400-TK-20, while acid is in fact added at this point. A pure sulphuric acid stream is therefore added to the dynamic model and named stream 23. On the real plant, this stream serves as a manipulated variable with which the acid concentration in 400-TK-20 is controlled. Its measurements are available in the data, so its flow rate can be simulated realistically.

Addition of Non-leaching Components

The received model contains only Ir, Rh and Ru as PGMs. The reason for this is that is that platinum and palladium is assumed not to leach in the autoclave. These two species were added to the model, assuming that it does indeed not react. This is done to provide a more realistic representation of stream compositions.

Addition of Water to Stream 1

The received model assumes that the first stage leach residue enters the second stage area as a solid mass. Lonmin, however, noted that this stream is 50% solids (Steenekamp & Mrubata, Control and Specifications of the BMR, 2013). Water is therefore added to the model's first stream in a mass flow rate that matches that of the total entering solids.

Addition of Formic Filtrate

The model in its received form does not have a formic filtrate stream flowing into 400-TK-10. Instead, it approximates it as being 100% water. With compositional data of formic filtrate being available, this stream's composition was corrected, as can be seen below:

Table 16: Sample composition of formic filtrate

Element	Concentration	
Cu	0.024	g/L
Ni	2.239	g/L
Fe	4.56	g/L
Co	~0	g/L
Te	~0	g/L
Pt	~0	g/L
Pd	~0	g/L
Au	~0	g/L
Rh	1.802	ppm
Ru	166.108	ppm
Ir	323.455	ppm
Se	~0	g/L

Changed Oxygen Feed Fractions

The total flow rate values of oxygen into the autoclave in the data are much lower than the stoichiometrically required amount, as calculated by simulating the process with inputs that correspond with those of the data. Since only the flow rate of the oxygen into the second compartment is available in the data, it is assumed that the low oxygen flow rate in the data is caused by a small fraction of the total oxygen fed going to compartment 2. This means that only 20% of the total oxygen goes into the second compartment. In this manner, a compromise is found between adhering to the input data and letting the model reach the plant's performance.

Correction of Compartment 1 Calculations

An error was picked up in the manner in which the reactions in (and flow from) compartment 1 are calculated in the received model. It was assumed, in the calculation of the reactions in the compartment, that the products leave the compartment only via the flash recycle stream, where in fact it also exits via the overflow to compartment 2. Correcting this error introduced the need for a *while* loop, since the flow rate of the overflow stream (and therefore also the reaction rates) has to be determined iteratively. This method was correctly present in the calculations of compartment 2.

Discrete Controllers Considered

The PI controllers implemented on the model receives set point and CV values continuously, and the resulting MV change is also applied continuously. This is typically not ideal, since controllers on a plant are generally discrete – meaning that it receives values sampled at certain time steps and also executes at certain times, known as the controller execution rate. Typical values for this controller execution rate were received from Lonmin, showing that it is typically in the order of 100 milliseconds (Burchell, 2014). In the light of the fact that the Simulink model's step sizes are almost never below 1 second, it can be confirmed that the controllers can be approximated as being continuous.

Inventory Sizes

The sizes of the inventories surrounding the autoclave assumed by Dorfling (2012) were found to be incoherent with the true sizes on the plant. After a plant visit these sizes were updated to be the following (Steenekamp & Mrubata, Control and Specifications of the BMR, 2013):

Table 17: Inventory volumes, as provided by Lonmin

Inventory Name	Dorfling (2012) (m^3)	V_{Tank} (m^3)	Normal Level (%)	V_{Liquid} (m^3)
Compartment 1	14.00	18.67	75	14.00
Compartment 2	4.67	6.23	75	4.67
Compartment 3	4.67	6.23	75	4.67
Compartment 4	4.67	6.23	75	4.67
400-TK-10	1	15.00	60	9.00
400-TK-20	1	35.00	55	19.25
400-TK-040	1	15.70	40	6.28
400-TK-050	1	8.30	60	4.98

In addition to the above volumes, the model requires additional information in terms of the autoclave's dimensions. It is assumed that the space filled by the cooling coils is negligible. These are given below (Steenekamp & Mrubata, Control and Specifications of the BMR, 2013):

Table 18: Autoclave dimensions as required by the model

Compartment	Length (m)	Outer Diameter (m)
1	5.5	2.5
2	1.8	2.5
3	1.8	2.5
4	1.8	2.5

3.6.4 Validation Input Conditions

In order for the model to operate in the same operational ranges as the real plant did at the time of the gathering of the data, the inputs of the model need to be matched with that of the data. This has to be done by setting up mass balances, since much of the required flow rate and compositional information is missing in the data. This is first done for the second stage leach and thereafter the third stage. A number of assumptions are necessary to be able to do the balance, and these include the following:

- The solid and liquid phases mix in an ideal fashion in 400-TK-10
- The densities of formic filtrate and copper spent electrolyte are both 1.15 kg/L
- The solids phase has a density of 4.45 kg/L (Dorfling, Bradshaw, & Akdogan, Characterisation and dynamic modelling of the behaviour of platinum group metals in high pressure sulphuric acid/oxygen leaching systems, 2012)

Due to the fact that the composition of the contents of stream 1 is unknown, the first step is to determine it from the data. The balance set up around 400-TK-10 can be seen below:

Table 19: Flow rates and densities for streams 1 to 5, and its phases.

Phase	Stream	1	2	3	4	5
Liquid	**Mass Flow (kg/h)**	947.5	2390	3841	0	7178
	Density (kg/L)	1.1	1.15	1.15	-	1.143
	Volume Flow (L/h)	861.3	2078	3340	0	6279
Solid	**Mass Flow (kg/h)**	521	0	0	0	521
	Density (kg/L)	4.45	-	-	-	4.45
	Volume Flow (L/h)	117.0787	0	0	0	117.0787
Total	**Mass Flow (kg/h)**	1468.5	2389.7	3841	0	8498.36
	Density (kg/L)	1.5	1.321006	1.15	-	1.18
	Volume Flow (L/h)	979	1809	3340	0	7202

The values used in this balance are means of the first range identified in section 3.3.4. The solids fraction of stream was chosen in such a way that the mass balance in stream 1 is satisfied under perfect mixing conditions. It can, however, be calculated that the total mass flow rates across the table (streams 1 to 4) add up to 7699.2 kg/h, which gives a 9.4% error. This error value can be caused by mistakes in either flow measurements or density readings, as mentioned in section 3.3.4.

With the phase fractions of stream 1 determined, and the element composition of the respective phases set – it is important to note that the compounds in which the element occur in the solids remains to be determined. Due to uncertainties about additional compounds that may be present in the first stage leach residue, a component balance on the solids compositional data is not sufficient to determine the exact component fractions. Instead, a mass balance is used, in which the following assumption is made:

The base metal reactions in the second stage leach can be approximated by the following four (Dorfling, Akdogan, Bradshaw, & Eksteen, Determination of the relative leaching kinetics of Cu, Rh, Ru and Ir during the sulphuric acid pressure leaching of leach residue derived from Ni-Cu converter matte enriched in platinum group metals, 2010):

1. $NiS + 2O_2 \rightarrow Ni^{2+} + SO_4^{2-}$
2. $2Ni_3S_4 + 2H_2O + 15O_2 \rightarrow 6Ni^{2+} + 4H^+ + 8SO_4^{2-}$
3. $Cu_9S_5 + 8H^+ + 2O_2 \rightarrow 4Cu^{2+} + 5CuS + 4H_2O$
4. $CuS + 2O_2 \rightarrow Cu^{2+} + SO_4^{2-}$

Using the entering flow rates and compositions as were specified for the previous table, the following table was set up:

Table 20: Flow rates and densities for streams from the second stage leach, and its phases.

Phase	Stream	1	2	3	4	5	14
Liquid	**Mass Flow (kg/h)**	947.5	2389	3841	0	7177.5	7903.547
	Density (kg/L)	1.070	1.150	1.150	1.840	1.139	1.200
	Volume Flow (L/h)	890	2080	3340	0	6300	6586
Solid	**Mass Flow (kg/h)**	521	0	0	0	521	6.54
	Density (kg/L)	4450	-	-	-	4450	4450
	Volume Flow (L/h)	0.1170787	0	0	0	0.117079	0.00147
Total	**Mass Flow (kg/h)**	1468.5	2389	3841	0	7698.5	7910.089
	Density (kg/L)	1500	1150	1150	-	1199.146	1200.725
	Volume Flow (L/h)	0.98	2.08	3.34	0.00	6.42	6.59
Element Mass Flow Rates (kg/h)	**Cu**	306.42	0.00	0.00	0.00	306.42	1.59
	Ni	64.97	0.00	0.00	0.00	64.97	0.00
	H2SO4	0.00	0.00	0.00	0.00	0.00	0.00
	H2O	0.00	0.00	0.00	0.00	0.00	0.00
	O2	0.00	0.00	0.00	0.00	0.00	0.00
	Fe	1.21	0.00	0.00	0.00	1.21	1.21
	Pt	1.71	0.00	0.00	0.00	1.71	1.71
	Pd	0.84	0.00	0.00	0.00	0.84	0.84
	Rh	0.30	0.00	0.00	0.00	0.30	0.30
	Ru	0.69	0.00	0.00	0.00	0.69	0.69
	Ir	0.19	0.00	0.00	0.00	0.19	0.19
	S	127.85	0.00	0.00	0.00	127.85	0.00

The fraction of copper as Cu_9S_5 (rest is CuS) and of nickel as NiS (rest is Ni_3S_4) is assumed and the extent of each of the assumed reactions is set to 100%. The latter is done for the following reason: for the correct ratio's – disregarding the PGM compounds – such complete reactions would ensure that no sulphur is left in the solids phase. With this in mind, the chosen values are solved with Excel's solver function, setting the sulphur in the solids phase as the end of the reaction to zero. The following values result from this, with PGM values still being at the values provided by Dorfling (2012):

Table 21: Compounds in which metallic elements occur in the first stage leach residue

Element	Major Compound	Fraction	Rest
Cu	Cu_9S_5	0.914	CuS
Ni	NiS	0.903	Ni_3S_4
Rh	Rh_2S_3	0.5	Rh
Ru	RuS_2	0.7	Ru
Ir	Ir_2S_3	0.6	Ir

With stream 1 characterised, a number of variables need to be set from the data in order to have a completely specified system. Two such variables are the flow rate and ratio of oxygen into the autoclave, and the manner in which the thickener/centrifuge split the contents of stream 15 into 16 and 17. Dorfling (2012) recommends that oxygen is fed at a rate that is 20% more than what is required stoichiometrically. Data are only available for the oxygen flow rate into compartments 2 and 3. As mentioned, if the flow rate into compartment 4 would be the same as that of the other two, the total oxygen flow rate would be much too low, if compared with the amount calculated by the model. There are three possible explanations for this situation:

1. The model wrongly predicts the amount of oxygen that is necessary
2. The real plant does not sparge enough oxygen
3. The total oxygen flow rate is split in such a way that the majority of it (approximately 60%) goes to the last compartment

Scenario's 1 and 2 are outside the scope of this project, which leaves the assumption that scenario 3 is true as the only possibility for this project. The recommendation is that scenarios 1 and 2 should be investigated in future work.

Due to the shortage of data for the third leaching stage leach (more specifically, the lack of data for the effluent stream of 400-TK-050), the composition of the underflow of the thickener/centrifuge (stream 17) cannot be determined with a mass balance. Since the solid-liquid separation step is outside the scope of this project, the operation of this step is assumed to be perfect, and that the contents of stream 17 is the solids in stream 15. This same assumption is made by Dorfling (2012).

3.7 SANITY CHECKS

Before commencing with operational validation, it is important to ensure that in principle the model performs as is expected. This can be done by doing sanity checks in the form of step tests on the model, noting the effect it has on several key model variables. In this comparison the results of tests done by Dorfling (2012) are used as the expected responses – and therefore the tests done in this section (along with the step sizes of each test) are made similar to those by Dorfling. It is important to note here that, due to the complexity of the model, no other expected responses can be given as a third option. A thorough comparison of the model responses with experimental knowledge has been done by Dorfling (2012), and therefore those results are expected to be matched in this section.

Note that the input conditions of the model are set to match those of Dorfling (2012) for this comparison. Each effect is only noted as an increase or decrease, to verify that the model responds as expected. It should be noted that sanity checks are not limited to this section, and that throughout the use of the model – whether during model validation or controller tuning – the manner in which output variables respond to different input changes are continually considered in the light of process knowledge.

In this section, steady-state tests are done, which means that the noted responses refer to the changes in steady-state ranges of operation. The results can be seen below:

Table 22: Stepped input variables, with step sizes given, along with the responses of several output variables – by Dorfling (2012) and in this project.

Step	Size	Dorfling (2012) Response						Current Response					
		T_1	T_3	Cu_3	Cu_4	Rh_3	Rh_4	T_1	T_3	Cu_3	Cu_4	Rh_3	Rh_4
S_1	+6.7%	∧	∨	∨	∧	∨	∧	∧	∨	∨	∧	∨	∧
m_4	+ 25%	-	∨	∨	∧	∨	∧	-	∨	∨	∧	-	∧
m_9	- 40%	∧	∨	∨	∧	∨	∧	∧	∨	∨	∧	∨	∧
P	+6.7%	∧	∨	∧	-	∧	∨	∧	∨	∧	-	∧	∨

In this table S_1, m_4 and m_9 refer to the solids flow rate in stream 1, and the mass flow rates of stream 4 and 9, respectively. The response variables are the temperatures of compartments 1 and 3, the copper concentration in compartments 3 and 4, and the rhodium concentrations in compartments 3 and 4.

It can be seen that all the given response variables – in each of the runs – change in the same direction as has been found by Dorfling (2012). This shows that the model used in this project performs in a manner that is in line with experimental knowledge. One exception is the fact that the rhodium concentration in the third autoclave compartment does not change in response to the acid feed change, while it is expected to decrease. Dorfling (2012) mentions that the rate of rhodium leaching does not depend directly on the acid concentration, but rather on the dissolved oxygen concentration. Therefore, while the responses do not correlate well (due to one or more of the changes made in section 3.6.3), the current response is in line with experimental knowledge.

3.8 OPERATIONAL VALIDATION

The purpose of this section, as was discussed in the literature review, is to evaluate the performance of the model by comparing it to the data. The aim is not to achieve an exact quantitative match between the model and the data, but to systematically demonstrate how suitable the model is to its intended purpose.

3.8.1 Adaptions to Model for Validation

The dynamic model was adjusted in a number of ways in order to facilitate the comparison with the data.

Differences between the model and data can be due to the following factors:

1. Differences in plant specifications and reaction kinetics (collectively referred to as model errors).
2. Differences in controller performance (including setup and tuning).

In order to minimise the effect of point 2, the decision was made to bypass the effect of control by importing actual MV values into the model as inputs. During this process, the fact that the mass balances in the data do not hold was encountered again. For the sake of mass conservation, therefore, some flow rate values are calculated instead of being imported, in order to ensure that all relevant flow rates balance. The variables imported are listed below:

Table 23: Table of data arrays imported into the model for validation

Variable	Stream Number	Manner in which imported
400-FIC-0101	2	Directly
400-FIC-1102	3	Directly
400-FIC-0107	4	Directly
400-FIC-0103	5	Adapted: outliers removed & moving average of 1 minute taken
400-FIC-2204	7	Adapted: data values for 400-FIC-2203 multiplied by 1.18
400-FIC-2203	9	Adapted: data values divided by 1.1
400-FIC-0505	18	Adapted: data values multiplied by 0.85 to aid mass balance
400-FIC-0504	20	Directly
400-FIC-2202	23	Directly

Note that the reasoning behind the given factors with which some of the data values have been multiplied, are given below:

- The flow rate of stream 7 is imported as 1.18 times the data values of the flash recycle stream. This is due to the fact that a large enough ratio between the flow rates has to be kept at all times in order to ensure that the net effect of these two streams is an inflow into the autoclave. The value of 1.18 is chosen, since multiplying it with the flash recycle stream values produced flow rates of stream 7 that best approximated the data values for this stream.

- The flow rate of the flash recycle stream is divided by 1.1 in order to aid in ensuring that the ratio between this stream and stream 7 is large enough (see previous point) without resulting in a stream 7 flow rate that is too large.
- The data values of stream 18 are multiplied by 0.85 to minimise the times where a negative flow rate of stream 19 is required to prevent accumulation in 400-TK-050.

Some variables could not be imported and rather had to be set as an MV by a control loop. The following values are determined in this manner:

Table 24: Control loops added to the validation model, with reasons therefor

MV	CV	Reason for control addition
400-FIC-0103	Mass in 400-TK-10	Mass balance around tank
400-FIC-2001(A-C)	Autoclave pressure	Pressure control needed to run model
m_{13} (steam)	400-TIC-2005	MV flow rate not in data
400-FIC-0402	Mass in compartment 3	Compartment mass should drive outflow (response variable)
400-FIC-0401	Mass in 400-TK-040	Mass throughput more important than exact flow
400-FIC-0501	Mass in 400-TK-050	Mass balance around tank
400-FIC-2003	Mass in compartment 4	MV flow rate not in data
Water in coils (comp 3)	400-TIC-2003	MV flow rate not in data

The added controllers were tuned and fine-tuned in the manner described in section 4.3. Examples of such a tuning procedure are shown in Appendix F. The following tuning parameters are used:

Table 25: Tuning parameters used in validation model

CV	K_c	$1/T_I$
Mass in 400-TK-10	N/A	N/A
Autoclave pressure	18.75	0.9
400-TIC-2005	2	5
Mass in compartment 3	-0.12	0.3
Mass in 400-TK-040	-0.027	0.7
Mass in 400-TK-050	N/A	N/A
Mass in compartment 4	-0.005	0.3
400-TIC-2003	-6	0.1

Note that – for the model validation phase – the mass controllers of 400-TK-10 and 400-TK-050 are replaced by manual calculations. This means that the MV values are calculated such that there is a minimal change in the mass of the tank's contents. For 400-TK-10 the mass flow rate of stream 1 is calculated as follows:

$$\dot{m}_1 = \dot{m}_5 - \dot{m}_2 - \dot{m}_3 \tag{18}$$

Note that the mass flow rates of streams 2, 3 and 5 are imported from the data. In the case of 400-TK-050, stream 19 is chosen to be the stream that will be calculated from other imported values. The following equation shows how this is done:

$$\dot{m}_{19} = \dot{m}_{21} - \dot{m}_{17} - \dot{m}_{18} - \dot{m}_{20} \tag{19}$$

The compositions of the streams entering the pressure leach process are sampled too infrequently to be able to continuously import these compositions into the simulation. With this in mind, the compositions of formic filtrate, copper spent and first stage leach residue are taken to be the average of the sampled values over the timespan of the data gathered. The flow rates entered for the calculation of initial values (under steady-state assumptions) are taken to be the mean of the first few hours' values in the data set.

Note again that the data are provided for a period stretching from 11:38 on 22 April to 12:09 on 24 April 2013. For the generation of the validation plots that is to be discussed, the model was run for 24 hours simulation time, from the start of the data set. A script file was written to automatically import the input data, run the steady-state model, import the variables to be added as flow rates into the model, run the dynamic model using the *Sim* function, import the data values and plot the model and data values below one another.

3.8.2 Validation Overview

Due to the large number of variables to be compared for this validation, the operational model validation is done in Appendix D, with a summary of the statistics and the resulting findings presented in this section.

The following diagram can be referred to throughout the operational validation section:

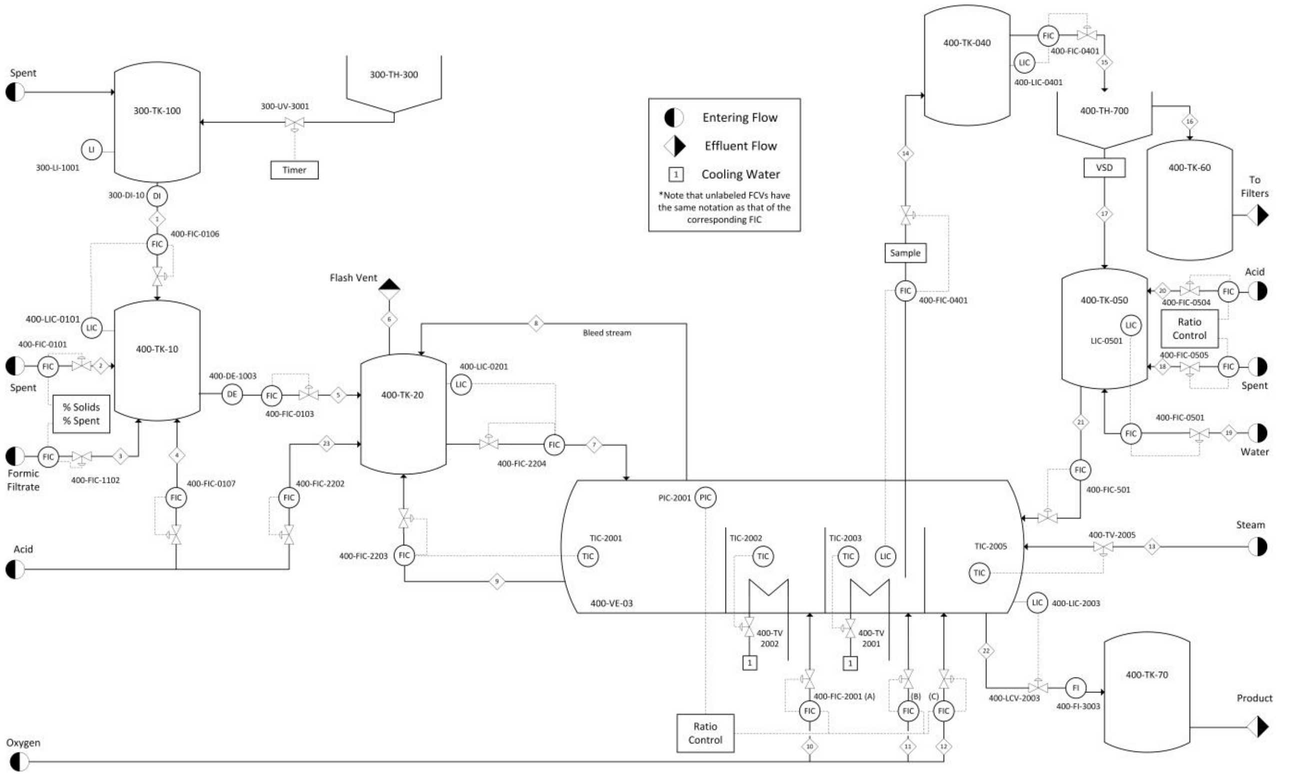
Spent
300-TK-100
300-UV-3001
300-TH-300
LI
300-LI-1001
Timer
300-DI-10
DI
400-FIC-0106
FIC
Entering Flow
Effluent Flow
1
Cooling Water
*Note that unlabeled FCVs have the same notation as that of the corresponding FIC
400-TK-040
FIC
400-FIC-0401
LIC
400-LIC-0401
400-TH-700
VSD
400-TK-60
To Filters
Sample
400-FIC-0401
Flash Vent
400-LIC-0101
LIC
400-TK-10
400-FIC-0101
Spent
% Solids
% Spent
400-DE-1003
DE
400-FIC-0103
Formic Filtrate
400-FIC-1102
400-FIC-0107
400-FIC-2202
400-TK-20
400-LIC-0201
Bleed stream
400-FIC-2204
Acid
400-FIC-2203
PIC-2001
PIC
TIC-2001
TIC-2002
TIC-2003
TIC-2005
TIC
LIC
400-VE-03
400-TV 2002
400-TV 2001
400-FIC-2001 (A)
(B)
(C)
Ratio Control
Oxygen
400-TK-050
LIC-0501
400-FIC-0504
Ratio Control
400-FIC-0505
Acid
Spent
400-FIC-0501
Water
400-FIC-501
Steam
400-TV-2005
400-LIC-2003
400-LCV-2003
FI
400-FI-3003
400-TK-70
Product
1
2
3
4
5
6
7
8
9
10
11
12
13
14
15
16
17
18
19
20
21
22
23

Figure 14: Simplified schematic representation of the pressure leach process at Lonmin, with basic control loops and stream numbers indicated

Table 26 contains the key variables for the comparison of flow rates, temperatures, pressure and tank levels:

Table 26: Variables for which a comparison is done between model and data values, with units, means and absolute error values are given, along with the ordinary and normalised root mean square error (RMSE) values and an indication of the trend match.

Tag (400-)	Stream / Tank	Unit	Mean		Standard Dev.		Error		RMSE	nRMSE	Trend match
			Data	Model	Data	Model	Min	Max			
FIC-0106	Stream 1	L/h	1143.8	2641.1	778.53	1613.4	0.403	6961.0	2674.5	40.94%	Fair
FIC-0101	Stream 2	L/h	2357.3	2357.2	1720.5	1720.5	0	80.530	2.2250	0.02%	Match
FIC-1102	Stream 3	L/h	2892.4	2893.3	1872.7	1872.6	0	663.61	21.235	0.22%	Match
LIC-0101	400-TK-10	%full	65.372	65.846	6.6322	12.311	0.0246	38.95	13.063	23.02%	Bad
FIC-0103	Stream 5	L/h	7445.2	7453.7	482.14	421.68	0	6322.3	254.19	3.40%	Match
FIC-2202	Stream 23	L/h	42.072	42.136	64.028	64.009	0	46.24	1.7227	0.73%	Match
LIC-2201	400-TK-20	%full	58.904	60.831	4.3599	8.9655	0.0024	27.395	11.799	57.37%	Bad
FIC-2204	Stream 7	L/h	28352	31355	42969	3854.8	3.0906	162530	42996	2.64%	Good
FIC-2203	Stream 9	L/h	26548	24120	3424.1	2964.7	1.8385	16720	2764.0	9.97%	Match
TIC-2001	Comp 1	°C	136.34	106.44	1.8437	2.2718	23.603	39.460	30.055	269.1%	Bad
TIC-2002	Comp 2	°C	141.62	124.25	1.5410	4.0681	9.029	27.133	17.824	245.4%	Bad
TIC-2003	Comp 3	°C	125.17	124.93	2.8060	3.2923	0.0033	18.697	2.980	23.01%	Good
LIC-2002	Comp 3	%full	65.241	65.367	2.1939	0.7708	0.0008	23.893	2.425	8.38%	Bad
FIC-0402	Stream 14	L/h	7954.5	7502.0	2084.9	888.47	0.9173	7123.3	2518.5	23.42%	Bad
LIC-0401	400-TK-040	%full	49.654	49.654	6.1035	1.5988	0.0139	22.823	6.329	15.23%	Bad
FIC-0401	Stream 15	L/h	7346.1	7720.3	2335.8	875.90	0.0987	7349.3	2741.6	21.53%	Bad
LIC-151	400-TK-050	%full	72.28	72.28	10.614	13.314	0.0013	44.525	20.654	39.33%	Bad
FIC-0505	Stream 18	L/h	1095.2	932.13	48.181	42.910	48.401	180.99	164.24	95.98%	Good
FIC-0501	Stream 19	L/h	107.16	66.88	343.95	119.71	0	1595.5	382.73	23.99%	Bad
FIC-0504	Stream 20	L/h	0	0	0	0	0	0	0	N/A	N/A
TIC-2005	Comp 4	°C	139.97	139.71	2.9852	2.9018	0.0073	17.543	4.820	30.71%	Fair
LIC-2003	Comp 4	%full	66.385	61.331	15.455	1.2170	0.0089	43.667	15.364	28.93%	Bad
PIC-2001	Autoclave	bar	650.00	646.29	6.5036	8.3318	0.0027	63.996	11.363	11.72%	Bad
FIC-2009	Stream 10	kg/h	88.127	85.574	6.4333	7.2751	0.0081	34.349	9.2935	19.29%	Bad

From this table it can be seen that for some of the variables there is a good correlation between model and data values, while large errors are evident for others. This is discussed in Appendix D, with the findings of the analysis given in the next section.

A summary of the acid concentrations in key process inventories are given in Table 27, both for data and model values.

Table 27: A summary of the data and model values for acid concentrations in 5 process inventories.

Inventory	Data Values (g/L)			Model Values (g/L)		
	Min	Mean	Max	Min	Mean	Max
[Acid]$_{\text{400-TK-10}}$	31.0	41.5	55.9	24.2	32.6	41.9
[Acid]$_{\text{400-TK-20}}$	13.0	19.2	32.4	23.3	28.4	35.7
[Acid]$_{\text{comp 3}}$	9.0	19.6	39.0	13.6	17.3	21.1
[Acid]$_{\text{400-TK-050}}$	36.9	42.2	49.1	76.5	89.5	98.3
[Acid]$_{\text{comp 4}}$	30.4	35.8	44.0	51.5	56.8	60.1

It is evident that the acid concentration ranges overlap for the second stage leach inventories, but not for those of the third stage. For the analysis of these results, see Appendix D.

Lastly, the solids and liquid compositional values for the second and third stage leach products are given in the two tables below:

Table 28: Minimum, mean and maximum values for the fractions different metal components make up of the second and third stage residue from 22 to 24 April 2013, with corresponding model values given.

		Data Values				Model Values			
		% Cu	% Ni	% Fe	% PGMs	% Cu	% Ni	% Fe	% PGMs
2nd Stage	**Min**	4.50	5.54	4.34	28.07	27.55	6.64	0.004	4.90
	Mean	10.27	7.35	5.70	36.27	59.93	10.53	0.010	5.53
	Max	14.41	9.52	7.14	42.82	65.13	32.18	0.037	9.83
3rd Stage	**Min**	1.47	5.46	8.39	48.07	29.51	4.64	1.0E-4	7.19
	Mean	1.89	5.80	8.48	48.33	51.63	12.59	5.8E-4	9.05
	Max	2.31	6.15	8.57	48.59	65.36	26.40	1.6E-3	13.21

Table 29: Minimum, mean and maximum values for the concentrations of metal components of the second and third stage residue from 22 to 24 April 2013, with corresponding model values given.

		Data Values (g/L)				Model Values (g/L)			
		[Cu]	[Ni]	[Fe]	[PGMs]	[Cu]	[Ni]	[Fe]	[PGMs]
2nd Stage	**Min**	83.19	38.35	0.47	0.22	50.62	19.39	2.11	4.5E-3
	Mean	97.32	43.15	0.57	0.23	52.76	25.30	2.34	0.04
	Max	153.03	52.25	0.66	0.25	57.39	28.28	2.72	0.19
3rd Stage	**Min**	25.36	11.49	0.18	0.07	28.26	31.75	0.68	0.04
	Mean	63.62	33.88	0.48	0.23	56.76	41.14	0.78	0.61
	Max	78.33	42.28	0.61	0.29	76.56	51.27	0.88	1.73

From the solids table it can be clearly seen that there are significant differences between the data and model values, with only the percentage ranges of nickel that overlap. In the case of the liquid compositions, the third stage values compare better than those of the second stage. The results are discussed in more depth in Appendix D, of which the findings are given below:

3.8.3 Operational Validation Findings

Data Comments

While working with the data, it was clear that the mass balances over several process sections do not hold. While such mass balance errors have specifically been found for 400-TK-10 and 400-TK-20 in section 3.3.4, due to an incomplete data set it could not be confirmed to be as a result of faulty data. This model validation step, however, affirms the internal inconsistency of the data in terms of mass balances. In response to this, adaptions were made to several flow rates in the data before importing it into the model. This was done to ensure that mass balance errors in the model did not interfere with the model validation procedure by wrongly causing inventories to run dry or overflow.

It would be more ideal if the compositional data was available more frequently than once a shift (or once a day, in some cases), so that trends could be compared along with value ranges. The lack of flow data for streams 8, 12, 13, 17, 21 and 22 and high-frequency compositional data (especially densities) for streams 1, 3, 7, 9, 14, 17, 21 and 22 prevents the setting up of a complete mass balance. Other important information that is lacking is the compounds that are present in the first to third stage solid residue. It is recommended that – for future projects – this information is retrieved from Lonmin before commencing a more rigorous data and model validation.

Model Comments

During the setup of the model validation plots, it became very clear that the model does not execute for certain combinations of input data. Due to the long execution time of both the steady-state and dynamic models, it was not possible to determine the exact combinations or code structures (as set up by Dorfling (2012)) that cause these failures. It is recommended that the steady-state model's programming structure be reviewed in order to find the root of this problem. Moreover, it is recommended that the dynamic model is migrated from its current form – in Simulink, with function blocks – into a Simulink-only form. This would ensure that the model runs more quickly and perhaps more accurately.

Validation Plot Findings

The performance of the model, as evaluated from comparisons with plant data, can be divided into two sections. The first section deals with the responses of process variables such as temperature and calculated flow rates to the variables added from the data (whether directly or after being altered) and those controlled to approximate the corresponding variables in the data. The temperatures of the autoclave compartments 1 and 2, as well as the flow rate of stream 10 and 14, are the most important ones to consider in this first section. While these temperatures displayed a clear offset between model and data values and trends were not followed very well, the model's outputs prove to be satisfactory in the light of this project. It was mentioned that the main cause of the differences could either be differences between the compositions of the autoclave contents (which, in turn, would be caused by inaccurate stream compositions) or by an inaccurate correlation in the model between the flow rate of the flash recycle stream and the resulting energy loss in compartment 1. Differences between model and data values for stream 14 showed that what happens in the autoclave differ to a significant extent, but that this too can be attributed to compositional (as well as temperature) differences. Trends were, however, followed to satisfaction – with the omission of noise in the model.

This first section impacts a division of control that is called regulatory control. It is the control of inventories, temperatures and pressure (to be termed *basic* regulatory control) as well as of acid concentrations and densities (to be termed *compostional* regulatory control). Note that the latter is not called supervisory control, since the aim of this control is to eventually be employed under another supervisory control level. For the sake of model validation, however, and in the light of the aforementioned definitions, it can be said that for the purpose of investigating and improving the control structure of basic regulatory control, this model is sufficient, for the following reasons:

- The flow rates of the streams around each inventory influence the contents of these inventories in a correct manner, showing that mass control can be implemented on the model.
- While not matching the data's temperatures, the model's temperatures respond as expected to by flow rates (most notably those of the flash recycle stream, cooling coils and steam addition) and other process variables, such as stream compositions. The model therefore allows for the structural control of temperatures. The sources of temperature errors identified in this section need to be resolved before the model can be used for the detailed design of temperature control on the model.
- The pressure responds as expected to changes in oxygen feed, and therefore – as with temperature – allows for a structural control investigation.

Moreover, in terms of compositional regulatory control, it can be seen that – while the model's acid values do not correlate well with data values (due to incorrect assumptions, flow rates and/or model kinetics) – it is clear that the entering flow rates lead to sensible acid concentrations in the mixing tanks and that these concentrations have a notable impact of the acid concentrations in the autoclave. This observation – along with the fact that solids compositions are calculated by means of mixing rules – deems the model appropriate for the investigation of advanced regulatory control.

The second section of the data-model comparisons pertain to the leaching reactions and the resulting solid and liquid compositions. Since leaching is the main purpose of the autoclave, and the compositional information is the best source of information on leaching performance, the accuracy of the model's calculated compositions are directly linked to the its usability for the development of supervisory control. Due to the observation that the leaching performance – especially in terms of the under-prediction of copper leaching – is not well simulated, it is preliminarily recommended that control structure investigation and development be limited to regulatory control. In order to confirm this, sensitivity analyses are done in the next section.

3.8.4 Sensitivity Analysis

Introduction & Preparation

In order to see which variables can be changed that will simultaneously increase the leaching of copper and nickel, a steady-state sensitivity analysis is done. The purpose of this sensitivity analysis is not to find exact mathematical correlations for different sensitivities, but to determine whether certain particular changes lead to large enough changes in key output variables for these changes to be considered as possible solutions for fixing model errors. For this reason a one-way sensitivity analysis is done (Clemen & Reilly, 2004), specifically in the direction which is expected to improve the base metal leaching, in this case. Moreover, only the variables that are examined for improved responses to the changes are added in this section as response variables. These include the fraction of base metals and PGMs in the solid products of the second and third stage leach.

The decision of the percentages with which each variable is changed is influenced by the amount with which this variable typically varies in the data. Run 2 is an exception to this, since mineralogical data is not available. The fraction used by Dorfling is therefore chosen as a reasonable test value.

Table 30: List of variables changed for each sensitivity analysis run, with initial and final values displayed

Run Nr	Run Name	Tested Variable	Unit	Initial Value	Test Value	% Change
1	Δm_9	Flash recycle stream (400-FIC-2203)	kg/h	27000	20000	-25.9
2	ΔCu_{Min}	Fraction Cu as Cu_9S_5 (rest as CuS)	-	0.914	0.85	-7
3	ΔCu_{Frac}	Percentage Cu in 1st Stage Residue	%	59.31	50	-15.7
4	$\Delta Spent_1$	Spent in stream 1	L/h	421.95	500	18.5
5	Δm_{23}	Acid addition to 400-TK-20 (400-FIC-2202)	kg/h	46.24	50	8.13
6	ΔP	Pressure	kPa	660	700	6.06

In each of these tests all other variables are kept at their respective base case values, with only the one in question changed.

Table 31 contains responses to the tests that best display the process' sensitivity to it.

Table 31: Selected list of responses to each of the test runs done.

Run	Base	Δm_9	ΔCu_{Min}	ΔCu_{Frac}	$\Delta Spent_1$	Δm_{23}	ΔP
400-TIC-2001 (°C)	104.3	105.4	105.6	104.0	104.2	104.5	104.8
[Acid] in 400-TK-20 (g/L)	20.09	21.25	20.45	20.01	20.44	20.66	19.77
% Cu (comp 3)	27.55	31.39	11.60	6.145	21.18	20.29	20.55
% Ni (comp 3)	32.19	29.43	42.44	48.33	36.45	36.90	35.29
% Fe (comp 3)	0.037	0.032	0.044	0.054	0.041	0.040	0.048
% PGM (comp 3)	9.826	9.427	12.00	11.20	10.83	11.12	12.58
% Cu (comp 4)	26.40	24.22	34.22	40.71	30.20	30.74	29.73
% Ni (comp 4)	9.82	9.19	12.30	13.75	11.06	11.32	12.36
% Fe (comp 4)	0.001	0.001	0.001	0.002	0.001	0.001	0.001
% PGM (comp 4)	29.57	32.48	18.98	10.72	24.39	23.58	23.88

The results of each of these tests are now discussed separately.

Sensitivity to Flash Recycle Rate

In the first test the effect of the temperature of the first autoclave compartment is tested by changing the flash recycle flow rate. The latter is decreased with 25.9% (in terms of mass flow), which results in a 1.05°C change in temperature. This, in turn, leads to an increase in copper % in the second stage residue from 27.6% to 31.4%, while the nickel percentage decreases. The sum of copper and nickel in the second and third leaching stages change from 58.74% and 36.23%, to 60.82% and 33.41%, respectively. This means that the effect of the change introduced in test run 1 does not have the potential of improving the leaching kinetics.

Sensitivity to Copper Mineralogy

In this test the fraction of copper that that is prevalent in the residue of the first stage leach as Cu_9S_5 (with the rest as CuS) is changed from 0.914 to 0.85 (a 7% change). This leads to a significant change in copper fraction (from 27.6% to 11.6%). Meanwhile, nickel increases from 32% to 42%. However, the sum of copper and nickel for the second stage leach decrease from 58.74% to 54.034% - showing that the mineralogy of the pressure leach process feed is of great importance, and that more information regarding it is required for more accurate model validation. Note that the change made in this test has a more significant impact on the temperature of compartment 1 than the flash recycle flow has.

Sensitivity to Copper in Solid Feed

In this test the percentage copper in the solids feed to the pressure leach process is changed from 59.31% to 50%. This led to an 11.6% decrease in the stoichiometric oxygen requirement. Moreover, this caused the copper percentage to change from 27.6% to 6.15% for the second stage leach, while nickel changed from 32% to 48%. This means an overall decrease of the percentage made up by copper and nickel, allowing the PGM fraction to climb to 11.2%. While the change is significant, it is small relative to the input change during this test – indicating that the leaching is not very sensitive to the copper fraction in the solids feed.

Sensitivity to Spent Addition before Second Stage

For this test an 18.5% increase was made in the flow rate of spent in stream 1. Looking at the results, it can be seen that the impact of this change on the sum of copper and nickel in the second stage leach (from 59.74% to 57.63%) is negligible.

Sensitivity to Pure Acid Addition

This test entailed increasing the mass flow rate of pure sulphuric acid to 400-TK-20 from 46.24 to 50 kg/h. It can be seen that, although it has only a slightly more significant impact than that of test run 4, the change in this case was due to an 8% change (instead of 18.5%). This means that the leaching in the process is very sensitive to the acid addition rate to 400-TK-20.

Sensitivity to Autoclave Pressure

In this test the pressure inside the autoclave is changed from 660 to 700 kPa. This is a 6.1% change, which leads to the PGM fraction changing from 9.8% to 12.6% in the second stage leach, but decreases it from 29.6% to 23.9% in the third stage. This result indicates that the process reactions are sensitive to the pressure in the autoclave, and can be explained by the importance of dissolved oxygen in the system and the direct link between pressure and oxygen solubility.

Sensitivity Analysis Findings

It is clear from these analyses that the acid addition rate and process pressure, as well as the first stage leach residue's mineralogy, are factors to which the process is reasonably sensitive, while other factors – such as the flash recycle rate seems to have a small impact. Due to the fact that none of the tests give a solution to the problem of the difference between the product solids compositions in the model and data, the last finding of section 3.7.7 has to be accepted: the current model, with process inputs resembling that of the data, under-predicts the leaching of copper and nickel in the process – and thereby deems the model in its current form not suitable to be used for the investigation and design of supervisory control strategies. This, however, does not hamper the model's use as tool for investigating and designing regulatory control structure improvements.

3.8.5 Copper Reaction Rate Adaption

While good conclusions have been made thus far, with the model's validity evaluated in terms of its purpose in this project – covering a host of variables and the interactions between them – there is one issue that has yet to be addressed. That is the fact that in the operational validation thus far, the temperatures calculated by the model for the autoclave could not come near the temperatures in the data. There is always a constant offset that is unaccounted for. During this project it was proposed by the model's author that the pre-exponential factor for the reaction rate constants for reactions 4 and 5 (see Appendix C) are too low and the reaction rate can be adjusted by merely increasing these factors (Dorfling, Bradshaw, & Akdogan, Characterisation and dynamic modelling of the behaviour of platinum group metals in high pressure sulphuric acid/oxygen leaching systems, 2012). The reason for this stems from the fact the reaction kinetic parameters used in the model were determined by doing batch experiments, while the actual plant is a continuous process. Due to this difference, it is probable that the dissolved oxygen concentration in the autoclave is higher than it would be in the batch experiments. The copper leaching reactions are assumed to be mass transfer dependent and the rate at which they proceed is limited by the amount of dissolved oxygen available.

Due to the fact that the steady-state model with the current inputs does not converge to reach its predefined tolerances when these factors are increased, another set of inputs are used to demonstrate the effect such an increase would have. These inputs can be seen in Appendix E, of which an excerpt is given below:

Table 32: Flow rates added into the model

Stream	Units	Value
Solids in stream 1	kg/h	1400
Water in stream 1	L/h	1400
Spent in stream 1	L/h	730
Stream 2	L/h	3600
Stream 3	L/h	900
Stream 4	L/h	0
Stream 23	L/h	46.24
Stream 9	kg/h	27000
Stream 18	L/h	88.5
Stream 19	L/h	6
Stream 20	L/h	0

It is important to remember that, due to the change in input conditions, the results obtained in this test are not comparable to the data, but only serves to investigate the effect of the proposed change on key process variables. First a test is done with the same kinetic parameters, but with the new input conditions, for the sake of a local base case. The second run is then done by multiplying each pre-exponential factor with a factor that leads to the best approximation of the temperatures in the second stage leach. After varying this factor between its initial value of 1 and a very high value of 20, a factor of 9 gave the best results. It should be noted here that the exact value is not of importance, since this rate adaption is merely done to crudely adjust the model for this project, and the improvements of reaction kinetics for this project lies outside its time frame. The effects of the change on key variables are given below:

Table 33: Responses in key variables to the two steady-state model runs done, with the old and new pre-exponential factors.

Variable	Old Factors	New Factors	Data Range
400-FIC-2203	21552	22316	7500-32000
400-PIC-2001	660.000	660.000	600-690
400-TIC-2001	107.573	130.456	**132-145**
400-TIC-2002	127.414	146.009	**137-146**
400-TIC-2003	116.953	132.675	**119-131**
[Acid] in 400-TK-20	34.544	22.924	23-36
% Cu (comp 3)	64.431	49.839	4.5-14.4
% Ni (comp 3)	7.898	20.057	5.5-9.5
% Fe (comp 3)	0.002	0.010	4.3-7.1
% PGM (comp 3)	1.569	3.575	28.1-42.8
% Cu (comp 4)	4.291	18.833	1.4-2.3
% Ni (comp 4)	1.762	6.230	5.4-6.2
% Fe (comp 4)	0.000	0.001	8.4-8.6
% PGM (comp 4)	67.982	47.782	48.0-48.6

From Table 33 it can be seen that the changes in the pre-exponential factors clearly lead to an increase in steady-state temperatures, moving it into the ranges seen in the data. The change leads to more complete leaching reactions, as can be seen from the acid concentration difference in 400-TK-20. The sum of copper and nickel for the second and third leaching stages change from 72.329% and 6.053%, to 69.896% and 25.063%, respectively. This improvement is insufficient to overturn the conclusion that the model in its current form is not suitable for investigating supervisory control. However, the change does improve the response of the variables that have an influence on the regulatory control system. Hence the model is adapted at this point, for the sake of this project, with the recommendation that the reaction kinetic parameters that form the backbone of the model be reconsidered for the sake of model accuracy.

3.9 SECTION CONCLUSIONS

In this chapter the manner in which plant data are gathered and processed is discussed, as well as its completeness and internal consistency. Due to the fact that key variables and values are missing from the data, and that compositional data is not available at a high enough frequency, a complete process mass balance is not possible. Data validation is therefore primarily lumped with model validation.

After the data's discussion, the model used in this project is described, focussing on the purpose, form and adaptions of it, after which its migration from the normal MATLAB workspace to Simulink is discussed. This follows into the validation of the model, which is done in 3 steps – as recommended by Sargent (2013): computer model verification, conceptual model validation and operational validation.

As part of the conceptual validation stage, several changes are made to the model. These include the addition of cooling for compartment 2 and 3, level control in the autoclave, pressure control, dead time, stream 23, non-leaching components, formic filtrate to stream 3 and water to stream 1, as well as calculation corrections and the correction of inventory sizes. It was noted in this stage that the oxygen flow rate in the data is much lower than what is required stoichiometrically, as calculated by the model. This can be the result of a wrong calculation in the model of the amount of oxygen required, the sparging of an insufficient amount of oxygen on the plant or the oxygen flow rate into the autoclave is split in such a way that more than 50% of it is sparged into the last compartment. After conceptual validation sanity checks are done, which serves as a qualitative comparison with experimental knowledge, as presented by Dorfling (2012). The model's performance was found to correspond well with what is expected.

A sensitivity analysis is done in order to determine which changes have the potential of solving the copper and nickel dissolution inconsistency. None of the tested changes have this potential, but the acid addition rate, pressure and the first stage leach residue's mineralogy have significant influences on the process. The effect of a recommended adjustment to the copper leaching reaction kinetics presents a solution to the temperature bias found in the validation plots, but should not be used outside this project.

During operational validation, certain input flow rates were imported from data into the model, in order to bypass the control system as much as possible and to view the model's response to real, dynamic process inputs. Due to inconsistent data, some flow rates had to be calculated – either explicitly or by a controller. Model outputs and data values were compared to each other, noting the errors qualitatively and quantitatively. The propagation of trends through the system – both in the case of the data and model output – are investigated and discussed. A number of conclusions were made from these comparisons, and they include the following:

- Data values around 400-TK-10 and 400-TK-20 do not balance.
- The model's current structure (with function blocks in Simulink) does not execute for all input data combinations, due to values not converging. It is recommended that the model is migrated to a Simulink-only platform, with its structure reconsidered.
- There is a near-constant temperature offset between model and data values, due to compositional differences in the autoclave or an inaccurate correlation in the model between the flow rate of the flash recycle stream and the resulting energy loss. It is recommended that this is examined in a future project.

Moreover, the model is validated for the investigation and improvement of the structure of basic regulatory control, due to the following observations:

- The inventory contents change in a correct manner in response to adjacent flow rate changes.
- The model's temperatures respond qualitatively as expected (though with an offset) to the flow rates of the flash recycle stream, the water in the cooling coils and the steam into the last compartment, as well as to compositional changes.
- The autoclave pressure changes as expected to changes in the oxygen sparging rate.

It is noted that the quantitative discrepancies between the model and data values need to be resolved before a detailed design of the basic regulatory control structure can be done. Until then the model is validated for structural research only.

The model is validated for the investigation and improvement of the structure of compositional control. This is due to the observation that flow rate changes in the model lead to sensible changes in the acid concentration and solids fraction, despite offsets between model and data values. The model is, however, not validated for the development of improved supervisory control structures. This is due to the fact that the leaching behaviour of the plant is not well predicted by the model, with the copper leaching especially being under-predicted. The mean concentration of copper in the second stage leach product is approximately 46% less than in the data mean, for example. It is recommended that the reaction kinetics of the model be improved in a follow-up project before investigating supervisory control. Until then the model is only valid for structure investigations on regulatory control. For such an investigation it is recommended that more complete data is made available (in terms of variables measured/logged and the frequency at which it is done) to be able to better validate the data and model for this purpose.

CHAPTER 4

REGULATORY CONTROL DEVELOPMENT & EVALUATION

4.1 CHAPTER INTRODUCTION

In this project the control on the pressure leach process has been divided into two levels: supervisory and regulatory control. In chapter 3 it has been found that the model is sufficient for use in the investigation and development of control structures in the latter. Regulatory control has been defined as consisting of basic regulatory control (referring to the control of temperatures, pressure and inventories) and compositional control.

In this chapter the structure of the basic regulatory control level is considered. This is done by first creating a base case, which has control that is structurally equivalent to that of the currently employed, basic regulatory control. Hereafter a series of steps are followed to reconsider several aspects of this structure. This involves reconsidering the variable pairings, as well as the control of areas of interest. All recommended improvements are evaluated against the base case in order to comment on its success.

4.2 LITERATURE REVIEW

4.2.1 Control Objectives

Marlin (2000) notes several objectives that a control system should aim to ensure. These are discussed separately, with the relevance of each to the project noted.

Safe operation

It is important that the process is always controlled in such a manner that all forms of risk to personnel are minimised. The autoclave is the part of the pressure leach process that poses the biggest threat in terms of safety. In order to ensure that the autoclave operates within safe limits, the temperature and pressure inside it should not exceed 155°C and 10 bar, respectively (Steenekamp & Mrubata, Control and Specifications of the BMR, 2013). Moreover, tank levels should not rise above a safe maximum height, in order to prevent spillages in the form of an overflow.

Emergency control procedures need to be developed to ensure that the correct/necessary valves close/open, or that the whole plant shuts down if needed. More specifically, Marlin notes that there are five "layers" in a control system when controlling for safety. They are the following (Marlin, 2000):

1. Basic Process Control System
2. Alarms (high, medium and low)
3. Safety Interlock System
4. Safety Valves
5. Containment

Note that only layer *i* falls into the scope of this project.

Environmental protection

Compounds such as concentrated sulphuric acid, which pose a threat to the environment, are used in large quantities at the base metal refinery. This means that – along with careful "steady state" control of the plant – start-up, shut-down and cleaning procedures should proceed in such a way as to ensure that process fluids are correctly disposed of. This is very important to a designed control system, but lies outside the scope of this project.

Equipment protection

Process equipment need to be protected for economic, as well as safety and environmental reasons. The process fluid in the leaching circuit is very acidic and is particulate in nature, which makes for a very erosive and corrosive environment. Fluid densities are also high, putting high loads on piping and pumps. For this reason it is important to keep the limitations of the materials used for specific sections in mind when controlling the plant. The control of pumps and feed flows should prevent pumps from running dry and pipes from clogging. As mentioned, the stated maximum temperature and pressure of the autoclave should not be exceeded, in order to prevent material/seal failure. Lastly, the action of the controller should not be too erratic; otherwise the generated stresses may cause additional damage.

Smooth operation and production rate

As noted, the actions of the controller should be executed smoothly in order to minimise the stress on valves, pipes and pumps. Because of the solids content of the process fluid, it is prone to settling. Since settling in a pipe may cause blockages – which may lead to plant shut-down – it is critical that all flow should be kept above its critical settling velocity. Note that these velocities are unknown in this project, and therefore it cannot be included. It is worth noting that the pressure leach process forms part of the larger base metal refinery, with the efficiency of downstream processes directly depending on production by the leaching circuit.

Profit

Because of the fact that the operation of the BMR is economically driven, it is important that the plant is operated and controlled in such a way that the BMR as a whole is profitable. This means that – for example – as little PGMs as possible should be leached from the solid phase, and that the separation of additional valuable metals should be as close to complete as possible. Lastly, the production rate should not be limited by the leaching circuit. Rather, the production rate should be as high as the rate at which the provided ore is milled.

Monitoring and diagnostics

Sensors and final control elements need to be positioned in a manner that makes the monitoring of key variables and the identification of faults a relatively easy task. The processes in the BMR are prone to pipe blockages – which is a fault that would need to be quickly picked up by the control system. Note that this is outside the scope of this project.

Additional Note: Simplicity

In the process of designing a control system to meet the above-mentioned objectives, Luyben and Luyben (1997) mention that – on an industrial scale – the simplest control system that achieves the desired aims is the best.

4.2.2 Challenges to Control in the Chemical Process Industry

The chemical process industry poses unique challenges to process control, which will have to be considered and overcome in this project.

Non-Linear Processes

The first of these is the fact that similar processes are typically rather complex – behaving non-linearly (Rhinehart, Darby, & Wade, 2011). This means that the control of these processes should be more advanced and capable of handling non-linearities.

Non-Stationary Processes

Chemical processes never really reach a steady state, because of the fact that the entering reagent grade (or solid residue, in this case) typically keeps changing with time (Rhinehart, Darby, & Wade, 2011). Fouling or blockages can also occur, leading to process disruptions. On a less regular basis, there may also be planned changes to the process (in terms of piping, tank/pump bypassing or unit switching). The control of the plant should be able to take care of the regular disturbances and should not be rendered ineffective in the case of process changes.

Challenging Dynamics

The large tank sizes and long pipes on industrial scale processes typically lead to large residence- and dead times (Rhinehart, Darby, & Wade, 2011). These times make it difficult to successfully implement feedback control. This is typically overcome by introducing cascade, feed-forward or other advanced control.

Multiple Variables

Chemical processes tend to have a large amount of MVs that affect and interact with several CVs (Rhinehart, Darby, & Wade, 2011). This makes control much more complex than the case where a process has clear MV-CV pairs without interaction. It is also improbable that the amount of MVs and CVs are the same. If the former is more than the latter, the controller has extra degrees of freedom, which requires additional decision-making or calculations in order to use the MVs optimally. On the other hand, if there are more CVs than MVs, a compromise on one or more of the CVs will have to be made. This is often the case in industry, and a developed control system should be able to do this.

Constraints

There are numerous constraints on both the process and the product. The whole process is designed to reach a certain product specification. This aim needs to be upheld at all times – except perhaps during start-up and shut-down periods. Process constraints include the following (Rhinehart, Darby, & Wade, 2011):

- Operational limits on equipment (e.g. vibrations, valve positions, temperatures and pressures)
- Tank sizes/levels
- Occupational health and safety considerations

Such constraints influence control by setting "soft" boundaries from which the MVs and CVs should steer clear, as well as "hard" limits, which requires interlocks on the process.

Uniqueness

Each industrial process is unique in a number of ways. This leads to the situation where a different control system needs to be developed for each process. The fact that this project focusses on Lonmin's BMR is a clear example of this challenge.

Disturbances

Disturbances in plants in the chemical process industry (CPI) can be very complicated in nature – partly due to the fact that there is a large amount of important variables. There is a wide variety of possible forms that disturbances can come in. These include the following (Rhinehart, Darby, & Wade, 2011):

- Disruptions or errors due to human actions
- Equipment failures or fouling
- Environmental upsets
- Changes to upstream processes

Each of these disturbance types will affect one or more CVs and its effect will need to be nullified (or minimised) by the control system.

Noise

Noise is a nearly unavoidable challenge on industrial scale processes. It can be divided into two types: process noise and measurement noise. The latter is introduced by a sensor, while the former can be due to vibrations, flow turbulence, etc. Note that high frequency disturbances may also be picked up as noise (Rhinehart, Darby, & Wade, 2011).

Cost Involved

Any change to control on the plant should be economically justifiable, since the making of a profit is arguably the main reason for the plant's existence. Theoretically, a control system can be developed that will control the process close to perfection – but the sensors and other equipment needed to implement it may be expensive. While the aim of this project is not to create an economical APC, but merely recommend structural control improvements, it should be kept in mind that the current sensors and MVs should be used as much as possible. In other words, the theoretical cost of any proposed process changes should be kept in mind.

4.2.3 Process Control Development

Marlin (2000) proposes an integrated control design procedure, which combines important concepts like sequence, hierarchy and design decisions. It will be discussed briefly in this section.

At the onset of the project it is important to acquire information about the process. This pertains to process equipment, flow structure, sensor locations and operating conditions. It is also important to understand the aims of the process and the desired product quality. Hereafter, the feasibility of the proposed project needs to be determined. This is done by means of a degrees of freedom (DOF) analysis, as well as evaluating the controllability of the plant. In the case of this project, the BMR is already being controlled in a certain manner. The controllability of different subsections of it – in the way that is desired – will be discussed in the sections where the relevant control is dealt with.

Next, it is important to develop an understanding of the process as a whole, to be able to make “bigger picture” decisions. The following need to be considered:

- Key production rate variables
- Inventories for control
- Open-loop unstable processes
- Any complex dynamics (e.g. long delays, strong interactions, etc.)
- Key product qualities
- Key constraints
- Key disturbances

Hereafter, the actual design of the control strategy commences. Luyben and Luyben (1997) present a more practical sequence of this process control development. The following five steps are recommended:

1. Count the number of available control valves. This is the number of control degrees of freedom.
2. Determine which valve will be used to set the production rate, taking into account the availability of different feed streams and limitations on production rate by downstream processes.
3. Select the MVs which can most tightly control important process variables influencing the product quality and plant safety.
4. Determine the valves for inventory control.
5. Assign other control valves with component balances and other optimisation criteria.

Note that this designed control structure applies to single-input single-output control methods, but can also serve as foundation for more advanced control.

4.2.4 Control Selection

Advanced process control (APC) is an umbrella term for a wide variety of methods to control processes. It generally refers to control methods that are more complex than the more classical PID-based methods, but often also include methods such as gain scheduling, ratio- and cascade control. In the chemical process industry (CPI), APC typically refers to model predictive control (MPC), but the field is much broader and the control options more numerous today (Rhinehart, Darby, & Wade, 2011).

A guideline is given in literature for the selection of control in the CPI (Rhinehart, Darby, & Wade, 2011). A clear distinction is made between *single input single output* (SISO) and *multiple input multiple output* (MIMO) processes. While the pressure leach process to be considered is a MIMO process, there are sub-processes that can be considered as SISO processes within the larger framework.

SISO Control

For a linear SISO system with dynamics that is well-behaved (having small dead times relative to other time constants and open-loop stability, for example) and well understood, PID control is recommended. This is the simplest and most often used method, and should be used as first approach. If the process is linear, but has ill-behaved dynamics, one is to use internal model control (IMC) – a simple version of MPC. In the case of a non-linear process with well-behaved dynamics, it is recommended that a gain scheduled PI(D) controller is used. For a non-linear process that is only qualitatively understood, but adequately understood for manual control, it is recommended that fuzzy logic control (FLC) is used. (Rhinehart, Darby, & Wade, 2011)

MIMO Control

For a linear MIMO process, which is interactive and subject to simple constraints (and that has less than 4 MVs), it is recommended that advanced regulatory control is used (Rhinehart, Darby, & Wade, 2011). This includes cascade, feed-forward and ratio control. For a linear process with non-zero degrees of freedom, a large number of MVs, loops that switch between manual and automatic and similar dynamics for all CVs, one should use MPC. If the dynamics of the CVs are dissimilar, a hierarchical control structure should be used.

In the case of a process that is interactive, subject to constraints and non-linear/non-stationary, it is recommended that one considers nonlinear MPC or a hierarchical structure.

Control Shortlisting

As mentioned, control in large scale chemical process plants should be as simple as possible (Luyben & Luyben, 1997). With available control methods becoming increasingly complex, this fact is often disregarded. With this in mind, the first approach to control would be SISO control. For processes showing linear behaviour, PID controllers will be used as first approach. Other methods will be considered if the SISO dynamics are ill-behaved and PID controllers are unable to achieve satisfactory performance.

Process subsystems that can be well defined as a MIMO system, and that cannot be controlled well when subdivided into SISO systems, will be provided with MIMO control. Depending on the nature of such a subsystem, one of the recommended MIMO control methods will be used.

4.2.5 Feedback Control Structure & Tuning

Definition

Feedback control is the most widely used online control method used in the industry. In its simplest form, a control variable (CV) is compared to an entered set point (SP) value – of which the difference (*E*) is sent to a controller (G_c). The general block diagram is shown below:

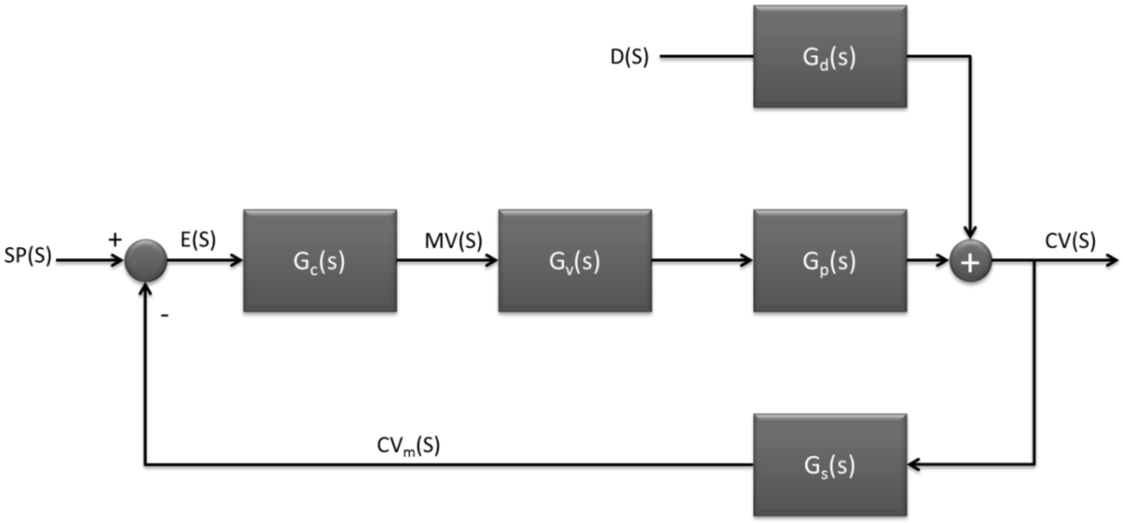

Figure 15: Block diagram of a feedback control system (Redrawn from Marlin, 2000)

Here, *D* and G_d refer to the disturbance and disturbance transfer function, respectively. G_v and G_p are the transfer functions of the valve and the process. The sensor also has its transfer function, denoted as G_s.

PID Control: Introduction & Open Loop Tuning

The most common feedback controller is a PID controller, which has a proportional, integral and derivative function. The general Laplace-domain transfer function for a PID controller is as follows (Marlin, 2000):

$$G_c(s) = \frac{MV(s)}{E(s)} = K_c\left(1 + \frac{1}{T_I s} + T_d s\right)$$

[20]

Note that there are three parameters that need to be determined: K_c, T_I and T_d. This is done by means of controller tuning. These parameters are typically employed as shown in the figure below:

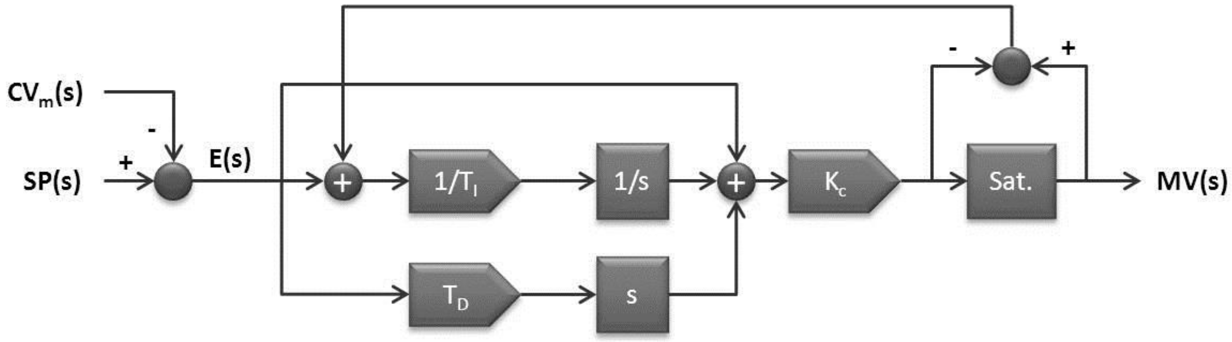

Figure 16: Block diagram of a PID control system, as typically implemented in Simulink.

In this figure, CV_m is the measured CV, while the saturation block is a feature that will be discussed at the end of this subsection. The *1/s* term is an integrator, while the *s* term refers to a derivative block. The information in the figure is based on information provided by Marlin (2000).

There is a wide variety of tuning methods available in literature. The method most applicable to industrial chemical processes with significant dead times, according to Marlin (2000) is the use of tuning correlations that are based on generated process reaction curves. The Ziegler-Nichols (Z-N) tuning method (or adaptions thereof) is considered to be the benchmark for such tuning correlations and is often used in industry (Shamsuzzoha, 2013). One improvement on the Z-N tuning method is the tuning method developed by Marlin and Ciancone, which typically leads to more robust performance with model errors (Marlin, 2000). This method determines suitable tuning constants from the process' time constant (τ) and dead time (θ). These can be derived directly for first-order systems, but higher order processes need to be approximated by a first order system with dead time before the Ciancone correlations are useful. For a first-order system with dead time, the time constant and dead time of a process is related to the process transfer function by the following equation (Marlin, 2000):

$$G_p(s) = \frac{K_p e^{-\theta s}}{\tau s + 1}$$

[21]

From this equation it can be seen that G_p should be a first order transfer function (with dead time).

The aforementioned approximation can be done in two ways: mathematically or graphically. The mathematical method consists of linearizing the differential equation(s) that describe the sub-process in question. Due to the large number of differential equations in the model received at the onset of this project, the graphical method is preferred.

The graphical method is typically employed by making a step change in the manipulated variable (MV) and noting the dynamic response of the controlled variable (CV). Both variables are plotted as functions of time. The following three values can be determined from these plots (Marlin, 2000):

$$K_P = \frac{\Delta CV_{SS}}{\Delta MV_{SS}} \tag{22}$$

$$\tau = 1.5(t_{63\%} - t_{28\%}) \tag{23}$$

$$\theta = t_{63\%} - \tau \tag{13}$$

Here, K_p, is the ratio between the CV and MV changes, using steady-state values. The two t values in these equations are the times the CV takes to teach 28% and 63% of its final value. With these two factors known, the Ciancone tuning correlation charts given in literature can be used to determine the PID controller tuning constants. Note that the goals of these tuning correlations are to minimise the IAE of the CV, to be robust to model errors and to prevent unnecessarily large MV variations.

For these correlations to produce usable tuning parameters, two assumptions need to be met (Marlin, 2000):

1. The controlled variable in question must have a response to a MV step that at least resembles a first order (plus dead time) response.
2. All control loops in the process must be open during the step test. This means that no control should be present.

In the figure depicting a PID controller, a saturation block could be seen. The purpose of this saturation block is to prevent reset windup by the PID controller's integrator mode. The MV is bounded to a certain range. The reset value (RS) that is returned to the integral path of the controller is calculated as follows:

$$RS = MV_{lim} - MV_0 \tag{24}$$

Here, MV_{lim} refers to the MV that is limited to the saturation block's predefined bounds, while MV_0 refers to the MV without limits applied. This reset value is added to the integrator path before being multiplied by the reciprocal of the integral time. This is done since the reset time for anti-reset windup by back calculation is often approximated as being the same as that of the integral time (Visioli, 2006).

PID Level & Mass Control

It is important to note that the inventories are integrators and do not adhere to the aforementioned assumptions. Any flow rate change that is upstream from an inventory will cause the inventory in question to either overflow or run dry after a certain amount of time, without propagating the flow change to the rest of the process. A consequence of this is that open loop tests will not be able to be used for process characterisation. An alternative tuning method is recommended for inventories, where the maximum variations in tank level and flow rate determine the necessary parameters.

For level control, Marlin (2000) recommends the following tuning equations:

$$K_c = \frac{-0.736 \cdot \Delta F_{max}}{\Delta L_{maxi}}$$ [25]

$$T_I = \frac{4\xi^2 A}{-K_c}$$ [26]

Here, the damping coefficient (ξ) is normally set to one, while A is the area of the liquid surface.

These methods are adjusted to apply to a mass (instead of level) controller by means of the following equations are relevant:

$$\Delta L = \frac{\Delta m}{\rho \mathrm{A}}$$ [27]

$$\dot{m} = \rho F$$ [28]

$$\Delta F_{max} = var(F) \cdot F_{mean}$$ [29]

$$\Delta m_{max} = var(m) \cdot m_{mean}$$ [30]

This leads to a new equation for the mass controller gain:

$$K_c = -0.736 \cdot \frac{var(F)}{var(m)} \cdot \frac{\dot{m}_{mean} A}{m_{mean}}$$ [31]

Here, *var* refers to the maximum variation. The areas in these equations are approximated by assuming that the tank height is equal to 1.5 times its diameter for all tanks, except the autoclave compartments. Compartments 3 and 4 are approximated as being perfect cubes. The rest of the symbols are defined in the nomenclature section.

Note that the above equations apply to mass controllers of which the MV is the flow rate out of the tank. If the MV were to be an inlet of the tank, the negative sign of equation 31 would fall away, with the T_I value remaining a positive value.

Closed Loop PID Controller Tuning

In the tuning of PID controllers, there might be a non-inventory case where process characteristics make it impossible to derive process reaction curves under open loop conditions. A method proposed to overcome this challenge has recently been developed by Shamsuzzoha (2013). This is a closed-loop tuning method, which means that all other available controllers need to be in operation as this process characterisation and tuning method takes place. The method will now be discussed in more detail.

With all other control loops closed, the PID controller to be tuned is changed into a proportional-only controller. This is done by setting the $1/T_I$ and T_d values to zero. The controller gain is chosen so that a step change in the set point of the controlled variable brings about an overshoot between 10% and 60% (with 30% being ideal). This overshoot is defined as follows:

$$OS = \frac{\Delta y_p - \Delta y_\infty}{\Delta y_\infty}$$

[32]

Here, Δy_p refers to the difference between the first peak's maximum value and the initial CV value and Δy_∞ refers to the difference between the new steady state CV value and the initial value.

When achieved, the tuning parameters are determined as follows:

$$K_c = K_{c0}[1.55(OS)^2 - 2.159(OS)^2 + 1.35]$$

[33]

$$T_I = min\left(0.645A\left|\frac{b}{1-b}\right| t_p\,, 2.44t_p\right)$$

[34]

$$T_d = 0.14t_p$$

[35]

Here, A is the ratio between K_c and K_{c0} and t_p is the time to the peak of the overshoot. The b value is defined as follows:

$$b = \frac{\Delta y_\infty}{\Delta y_s}$$

[36]

Note that Δy_s is defined as the difference between the final and initial set point values.

Controller Fine Tuning

The tuning parameters determined during one of the aforementioned tuning methods serve only as initial values, and should be adjusted to give the required controller performance. This is done by means of fine tuning, which entails the adjustment of the tuning parameters based on the controller's initial dynamic responses. It is recommended that the controller to be fine-tuned, should be set in its automatic mode and a set point change be made. The main reason for a set point change is that, in the case of a PI controller, the effects of the proportional and integral modes can be split and examined separately. (Marlin, 2000)

The fine tuning of the proportional mode is aided by the fact that the immediate change in the MV (MV_{imt}) results due to the following equation (Marlin, 2000):

$$\Delta MV_{imt} = K_c \Delta E(t) = K_c \Delta SP(t)$$

[37]

This immediate change is usually 50% to 150% of the final steady-state MV change. The integral time is reconsidered if a controller with a suitable gain leads to unsatisfactory performance.

Note that, while this method should lead to suitable results, the objectives for the controller in question need to be taken into account to ensure that CV or MV limits are not breached, for example.

4.2.6 Variable Pairing & Controllability

Variable Pairing

The advanced regulatory control methods discussed in the previous section are ways of improving a basic, existing feedback control structure. It is important to note that any advanced regulatory methods applied to a control system with undesirable MV-CV pairings will not be able to make for good control. Luyben and Luyben's (1997) approach to this step has been introduced in section 4.2.2. The following method is more rigorous and is advisable to be used if allowed by the nature of the model.

This method employs the relative gain array (RGA), which is a matrix that consists of a process' relative gains (RG). The latter is defined as the ratio between the open-loop and closed-loop gains. It is defined as follows (Marlin, 2000):

$$\lambda_{ij} = \frac{\left(\frac{\delta CV_i}{\delta MV_j}\right)_{MV_{k=constant,k\neq j}}}{\left(\frac{\delta CV_i}{\delta MV_j}\right)_{CV_{k=constant,k\neq i}}} = \frac{\left(\frac{\delta CV_i}{\delta MV_j}\right)_{other\ loops\ open}}{\left(\frac{\delta CV_i}{\delta MV_j}\right)_{other\ loops\ closed}}$$

[38]

From this equation it can be seen that a relative gain of 1 will mean that the process gain is not affected by the other control loops and that no interaction is therefore prevalent. Deviation from unity means that there is process interaction – the extent to which is indicated by the value of the RG.

Using the above equation directly, doing open- and closed-loop tests for all variable parings can be a tedious process – especially if there are more than 3 MVs (or CVs) to be tested. This is avoidable due to the fact that the RGA can be calculated by using open-loop tests only (Marlin, 2000). This is done as follows, where the second equation indicates an element by element multiplication, called the Hadamard product:

$$K_{ij} = \left(\frac{\delta CV_i}{\delta MV_j}\right)_{MV_{k=constant,k\neq j}}$$

[39]

$$\lambda_{ij} = K_{ij} \cdot \left(K_{ij}^{-1}\right)^T$$

[40]

The K-matrix in these equations is called the gain matrix – which should be set up first. Before using this matrix to calculate the gain array, the condition number (CN) thereof is first calculated. This is done in order to determine whether the process can be decoupled. A CN below 50 is regarded as a good indication of decouplability (Carey, van Kuiken, Longcore, & Yeung, 2007). The RGA can then be determined from the gain matrix.

In the case where the process in question contains an integrator, such as a non-self-regulating tank, the gain matrix is replaced by a transfer matrix. This matrix contains the transfer functions between each MV and CV in a similar manner as a gain matrix. From this transfer matrix, the RGA can be determined as follows (Hu, Cai, & Xiao, 2010):

$$\lambda_{ij} = G_{ij}(s) \cdot \left(G_{ij}^{-1}(s)\right)^{T} |_{\, s=0} \qquad [41]$$

Here the *G(s)* values represent the respective transfer functions. The RGA is calculated in terms of *s*, which is in the Laplace domain, and the *s*-terms in the solution are then multiplied by zero.

Loop pairings are done in response to the RGA. MV-CV pairings that result in real, positive RG's are considered. The closer the RG value is to 1, the better, since this indicates little transmission interaction (Marlin, 2000).

Process Controllability

Marlin (2000) mentions the importance of ensuring that a process is controllable. If the controlled variables of a process can be kept at its respective set points under steady-state conditions, even with disturbances entering the system, it is deemed controllable. In other terms a system is said to be controllable if its gain matrix is invertible (Marlin, 2000).

4.2.7 Enhancements to Feedback Control

Cascade Control

In cascade control two or more feedback control loops are used in a hierarchal fashion. It is often used when a second MV is available that may aid in improving control – especially in processes with slow dynamics (caused by significant dead times, for example). The second variable should have quicker dynamics than the primary variable, since the main aim of cascade control is to detect and nullify errors faster than single loop feedback control can (Marlin, 2000). A block diagram of a typical cascade block diagram is shown below:

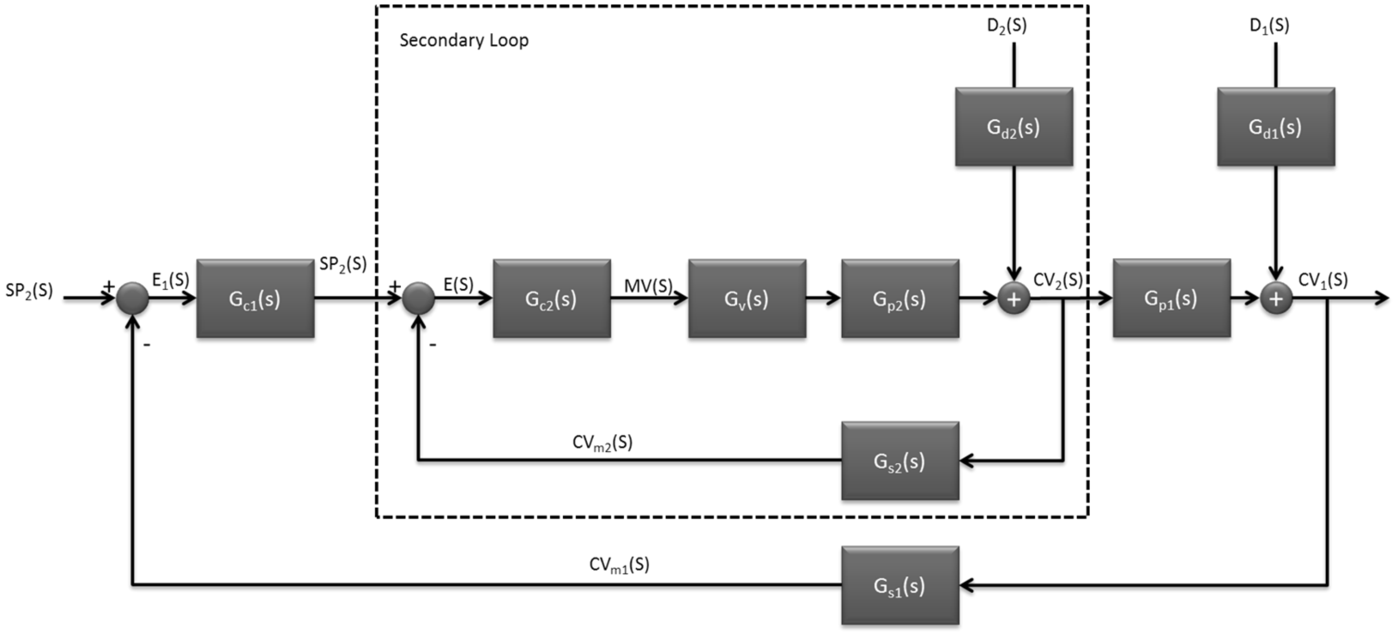

Figure 17: Block diagram of a cascade control system (Redrawn from Marlin, 2000)

It can be seen that cascade control is a combination of two feedback control systems. The primary controller's output is the set point for the secondary controller. Tuning a cascade controller is done in a similar fashion to a normal feedback controller, with the only detail to be noted being that the secondary controller should be tuned first. This control loop should then be closed while tuning the primary, outer control loop.

Feed-forward Control & Decoupling

Feed-forward control uses the measurement of a disturbance to adjust an MV. The main purpose of this control method is therefore to aid in rejecting disturbances. It is may be necessary when feedback control is not satisfactory – and when an additional MV is available (Marlin, 2000). The appeal of feed-forward control is that it can decrease the time a process takes to respond to and rectify a disturbance-induced error. The following block diagram displays the control structure:

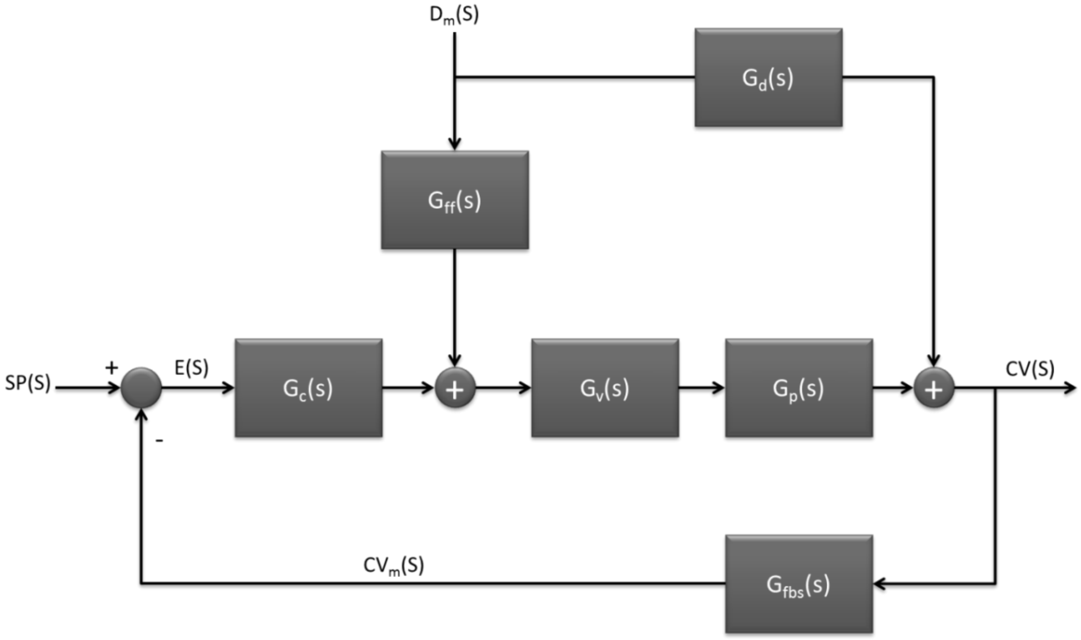

Figure 18: Block diagram of a feedback control system with feed-forward control (Redrawn from Marlin, 2000)

It is clear how the feed-forward transfer function (G_{ff}) is added between the measured disturbance (D_m) and the measured variable – thereby aiding the feedback control system by contributing to it as the disturbance influences the controlled variable.

Note that the feed-forward controller's transfer function is defined as follows (Marlin, 2000):

$$G_{ff}(s) = -\frac{G_d(s)}{G_p(s)}$$

[42]

Marlin (2000) lays out a design criteria that have to be met before implementing feed-forward control:

- The identified feed-forward variable must detect and clearly indicate the occurrence of an important process disturbance.
- There should not be a causal link between the MV and feed-forward variable.
- The dynamics between the MV and the output variable should not be significantly slower than the disturbance dynamics in the presence of feedback control.

In the light of these criteria, feed-forward control is implemented by the following procedure:

1. Identify disturbances in the plant which the current control system does not successfully reject.
2. Identify potential feed-forward variables and apply the design criteria to determine the best one.
3. Design and tune the feed-forward controller.

It is important to note that, while decoupling is a separate control method, it can be approximated as being rather similar to feed-forward control. The most notable difference is that – in the case of a decoupler – an MV from another MV-CV paring acts as the disturbance in the process subsystem at hand. The main purpose of a decoupler, therefore, is to counteract the interaction effects between two control loops. The similarities between decoupling and feed-forward control becomes clear when it is noted that the transfer function for the former is the same as for the latter, except that the disturbance term is replaced by the transfer function representing the interaction.

4.3 BASE CASE MODEL FOR BASIC REGULATORY CONTROL

In order for control to be evaluated, a base case needs to be defined, which represents the current control structure, against which model developments can be compared. Since this base case is to serve as benchmark, the manner in which it is set up has a significant influence on subsequent comparisons. Since all improvements are to be made on the current control, it is clear that the base case control should best represent the current control structure (at the time of data acquisition), as employed on the plant.

The base case control version of this chapter includes only the current basic regulatory control, which refers to the control of the temperatures, inventory masses and the autoclave pressure. Compositional control is therefore not included in this base case, but a constant ratio between the mass flow rates of streams 2 to 4 and stream 1 is maintained in the base case, as this is what is done by the control system on the plant.

This base case control will be made up of PID controllers, with loop pairings made as discussed in chapter 2. The manner in which it is tuned is discussed next.

4.3.1 Base Case Mass Controllers

The tuning of the mass controllers was done according to the method recommended by Marlin (2000), as presented in the literature section. In order to do this the allowed variation in the MV flow rate and the tank mass needed to be determined. Due to the fact that the values should best represent the data, it was decided that the coefficients of variance (CoV) of the relevant variables should be used. This is calculated as follows for each of the parameters (Zady, 2009):

$$CoV_i = \frac{\sigma_i}{\mu_i} \tag{43}$$

Here, σ refers to the standard deviation, and μ is the mean. Table 34 displays the resulting values:

Table 34: Normalised standard deviations of the MV flow rates and tank levels in the data, used for the tuning of mass controllers in the base case model.

Inventory	Flow CoVs(%)	Level CoVs (%)
400-TK-10	70	10
400-TK-20	9	7
400-TK-040	30	10
400-TK-050	50	10
Comp 3	27	3.4
Comp 4	79	10

These values were used along with the mean tank mass and flow rate values, as well as with a calculated tank area, to determine the tank's tuning parameters. These parameters are given in Appendix F1.

A typical block diagram for the mass controllers is shown below:

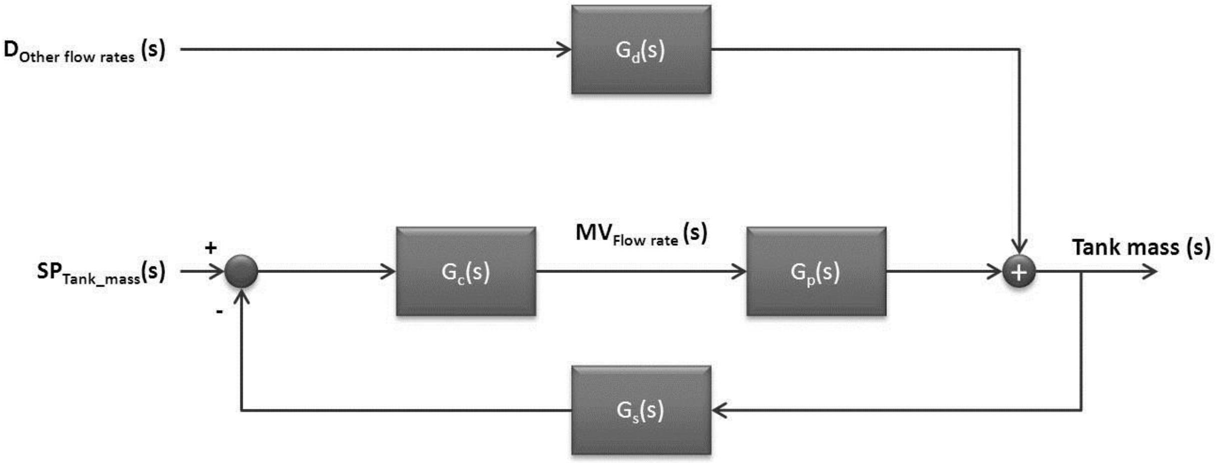

Figure 19: Block diagram of a typical mass controller in this project

It should be noted that the MV is the flow rate that is used to control the tank mass. Typically there would be valve dynamics included, but it is omitted from this diagram since the relationship between the controller outputs and the corresponding flow rates are assumed to be linear.

4.3.2 Other PID Controllers

With the mass controllers tuned, the other PI controllers need to be tuned using Ciancone's correlations. This includes the following control loops:

Table 35: Control loops given with manipulated and controlled variables

#	MV	CV
1	Flash recycle stream (m_9)	Temperature of compartment 1
2	Cooling coils in compartment 2	Temperature of compartment 2
3	Cooling coils in compartment 3	Temperature of compartment 3
4	Steam addition rate (m_{13})	Temperature of compartment 4
5	Total oxygen addition rate	Autoclave pressure

In order for these control loops to be tuned by means of the Ciancone tuning correlations, all control loops should be open – including the mass controllers already tuned (Marlin, 2000). This can be done for control loops 2 to 5. In each case, a step change is made in the MV and the response in the CV is noted. These plots are given in Appendix F1. From this response, the K_p value is derived, as well as the approximate time constant and dead time. Using the tuning correlations developed by Marlin and

Ciancone (Marlin, 2000), the loops are tuned. Fine-tuning of the control loops (to account for process interaction) is discussed in the next section.

Control loop 1 requires a different tuning method, since a step change in the flow rate of the flash recycle stream would significantly change the mass/level in 400-TK-20. With the mass controller in manual mode, this would mean that the tank's contents would simply increase and that the cooled slurry would not return to the autoclave. This shows that the temperature control cannot be tuned under open loop conditions. The method recommended by Shamsuzzoha (2013) is used.

Starting with an arbitrary controller gain, and refining it in response to the resulting CV overshoot – in a manner proposed by Shamsuzzoha (2013) – an initial controller gain of -70 is found. A set point change of 0.5% (130.456 to 131.1°C) is made, and the methodology introduced in section 4.2.4 is used. Giving an overshoot of 32.39%, which is very close to the mentioned optimal value of 30%, the K_c, T_I and T_d are calculated to be -56.96, 0.07 h and 0.004 h, respectively. The plots from which these values are deduced are given in Appendix F1.

4.3.3 Controller Fine-tuning

It is important to note that the methods just mentioned are generic methods, meaning that the methods have been developed to provide suitable tuning parameters for a wide variety of processes. The fine-tuning approach mentioned in section 4.2.4 is therefore applied here. It should be noted that the aim is not to ensure that the base case control reflects the control behaviour of the actual plant. Rather, the aim is to have a base case control structure that is similar to that of the real plant, with tuning done well to prevent structural comparisons to be hampered by suboptimal tuning.

Due to the presence of process interaction, the change of the tuning parameters of one control loop will change the control performance – and therefore the required tuning parameters. This means that it would be best practice for a fine controller tuning step to entail iterative retuning of all the relevant control loops. However, since the basic regulatory control level of this process alone has 11 control loops, reconsidering all tuning parameters for each adjustment is an overly complex and time consuming step. This is especially true in the light of the fact that mere fine tuning is done, as opposed to complete controller tuning.

Fine tuning is started with the CV that is the earliest in the pressure leach process and then the order from there follows the order of its appearance along the process. This method is good practice, since the control loops that have an influence in the largest part of the process are tuned first. Note that the fine-tuning is done in Appendix F1.3, according to the method described in section 4.2.4. Below are the tuning parameters before and after fine-tuning:

Table 36: Tuning parameters for all basic regulatory control loops, before and after fine-tuning. Old T_t values are equal to the old T_I values.

CV	MV	Old K_c	New K_c	Old $1/T_I$ (h)	Old $1/T_I$ (h)	New T_t (h)
Mass in 400-TK-10	400-FIC-0106	1.896	1.896	0.155	0.155	T_I
Mass in 400-TK-20	400-FIC-2204	-4.655	-2.327	0.145	0.145	T_I
400-TIC-2001	400-FIC-2203	-56.960	-18.990	14.286	14.286	T_I
400-TIC-2002	Coils in comp 2	N/A	N/A	N/A	N/A	N/A
400-TIC-2003	Coils in comp 3	-847.458	-169.492	5.556	5.556	$0.025T_I$
400-PIC-2001	400-FIC-2001	128.205	64.103	3.968	19.840	T_I
Mass in Comp 3	400-FIC-0402	-7.150	-7.150	1.070	1.070	$0.1T_I$
Mass in 400-TK-040	400-FIC-0401	-2.646	-0.132	0.276	0.276	$0.1T_I$
Mass in 400-TK-050	Streams 18-20	0.385	0.385	0.047	0.047	T_I
400-TIC-2005	Stream 13	13.640	68.200	4.762	47.620	T_I
Mass in Comp 4	400-FIC-2003	-1.0134	-1.0134	0.1517	0.1517	$0.18T_I$

In this table the T_t value refers to the anti-reset windup time, initially approximated to be equal to T_I.

Below the block diagrams are given for the temperature controller of compartment 1 and the pressure controller:

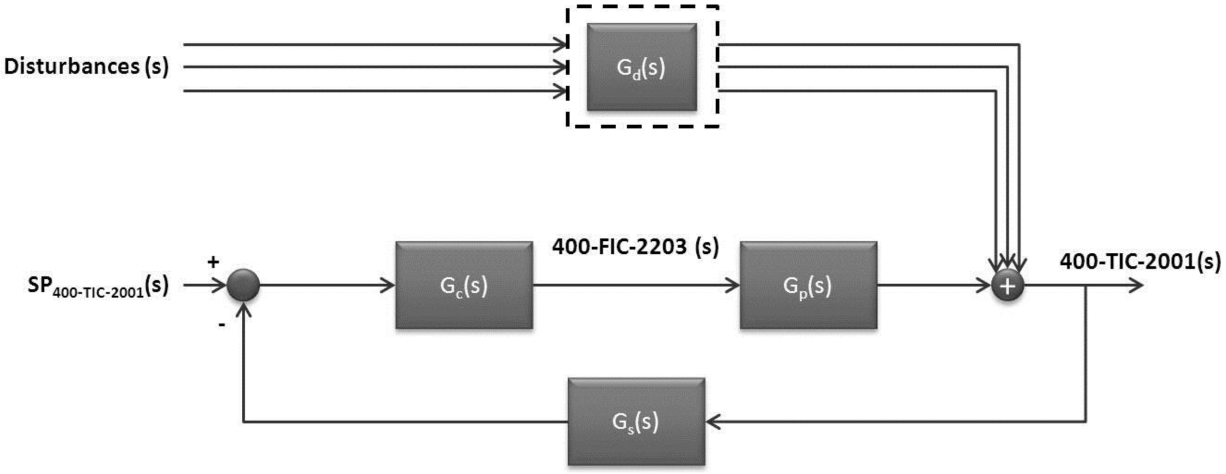

Figure 20: Block diagram of the 400-TIC-2001 controller, with the flash recycle flow rate as MV.

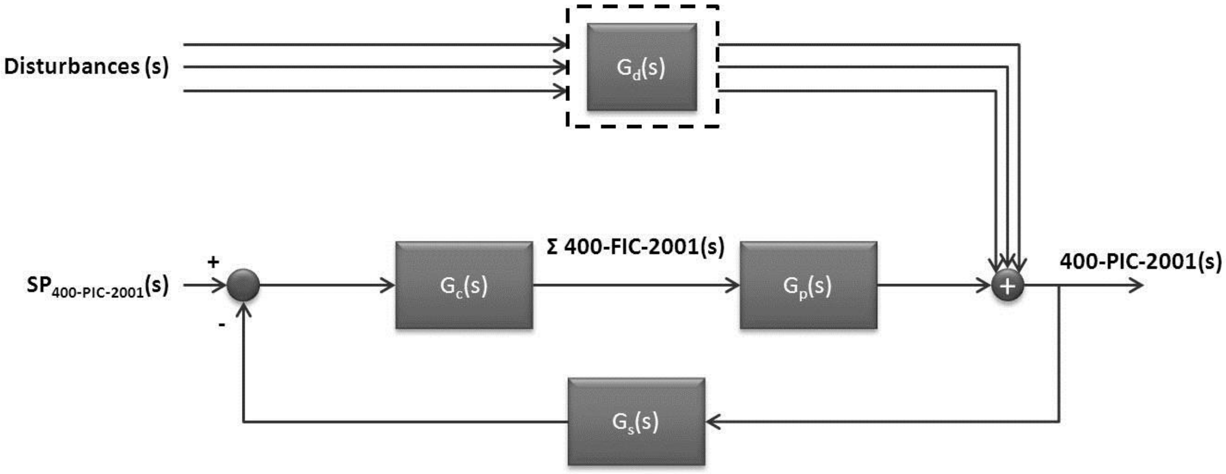
Disturbances (s)
G_d(s)
SP_400-PIC-2001(s)
+
-
G_c(s)
Σ 400-FIC-2001(s)
G_p(s)
+
400-PIC-2001(s)
G_s(s)

Figure 21: Block diagram as the autoclave's pressure controller, with the total oxygen additional rate as MV.

For both these controllers, it is assumed that the valve dynamics are linear and instantaneous. Note also that the G_d block refers to a collection of disturbance transfer functions – one for each disturbance.

4.4 BASIC REGULATORY CONTROL VARIABLE PAIRING

4.4.1 Introduction & Method

Having a working base case control structure, improved control can be developed and compared with it. The first step in improving the control is to reconsider the variable pairings and changing these if necessary. Note that the manner in which control is applied – that is, using PID controllers – will not be changed.

As mentioned, the method recommended by literature for setting up MV-CV pairings in the model starts with setting up a RGA (Marlin, 2000). This approach was followed at first, but challenges arose which led to the decision of determining optimal pairings by other means. The RGA was initially developed for processes without integrators. While there are methods available for calculating the RGA for a process with integrators in the form of inventories, the model contains another integrator – namely the vapour space in the autoclave – which cannot be treated as an inventory.

The reason why this integrator prevents the development of a usable gain matrix and RGA is that it impacts the rest of the process to a large extent, in contrast with a tank, which can be isolated to a large extent. The rates at which oxygen and water enter the vapour space are dependent on the temperatures and reactions inside all of the autoclave compartments. The contents of the vapour space directly influence the pressure in the autoclave, which – in turn – influences the reactions. This is displayed in the following diagram:

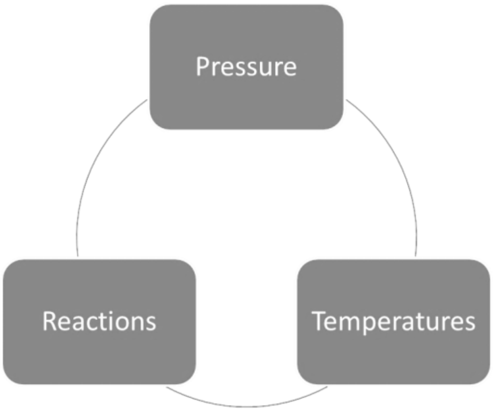

Figure 22: Diagrammatic representation of the interconnectedness of pressure, as representative variable of the vapour space.

It is clear that the vapour space is an integrator that cannot be treated as an ordinary inventory. Under open-loop conditions (as is required for generating an RGA) the oxygen flow rate into the autoclave is constant, while the vapour bleed stream from it is also relatively constant. This would cause the pressure to increase or decrease (depending on the inputs changed) to a large extent, in turn changing the leaching reactions and autoclave temperatures.

An alternative, simpler approach to variable pairings (as part of a plant wide control design procedure) by Luyben and Luyben (1997) has been introduced in the literature section and is chosen as alternative to the RGA approach.

The consequences of the above statement for an investigation into the process' controllability should first be noted. The factors preventing the generating of an RGA for the process also prevent the setting up of a gain matrix. In order to check the controllability of the process by way of a gain matrix, all of the process gains need to be determined. Since this is not possible for the whole process, the controllability cannot be formally determined according to the method proposed by Marlin (2000). It should, however, be noted that the analysis of a process' controllability forms part of its design stage and that the process dealt with in this project is already in operation and is controlled. With this in mind the process will be assumed to be controllable in the manners that are desired in chapter, and the control will be reconsidered while taking into account process knowledge from Lonmin and fundamental leaching knowledge from the work of Dorfling (2012).

4.4.2 Control Degrees of Freedom

The first step entails the counting of the number of valves available to be used as control valves. This can be done from Figure 23:

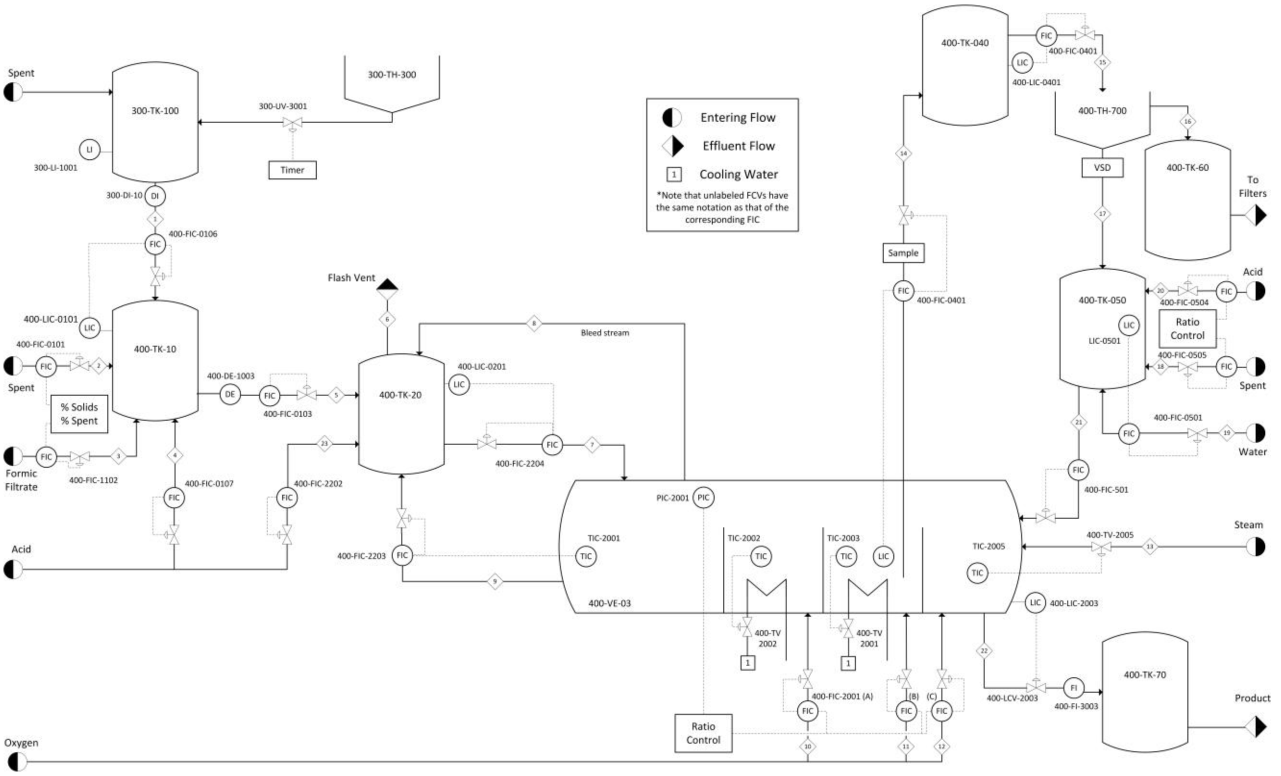
Spent
300-TK-100
300-LI-1001
LI
300-UV-3001
300-TH-300
Timer
300-DI-10
DI
400-FIC-0106
FIC
Entering Flow
Effluent Flow
1
Cooling Water
*Note that unlabeled FCVs have the same notation as that of the corresponding FIC
400-TK-040
FIC
400-FIC-0401
LIC
400-LIC-0401
15
400-TH-700
16
VSD
400-TK-60
To Filters
14
17
Sample
FIC
400-FIC-0401
Flash Vent
6
8
Bleed stream
400-LIC-0101
LIC
400-FIC-0101
FIC
2
Spent
400-TK-10
% Solids
% Spent
400-DE-1003
DE
FIC
400-FIC-0103
5
400-TK-20
400-LIC-0201
LIC
FIC
400-FIC-2204
7
23
3
4
Formic Filtrate
400-FIC-1102
400-FIC-0107
400-FIC-2202
Acid
400-TK-050
LIC
LIC-0501
Acid
20
400-FIC-0504
Ratio Control
400-FIC-0505
18
Spent
21
400-FIC-0501
19
Water
400-FIC-501
PIC-2001
PIC
TIC-2001
TIC
TIC-2002
TIC-2003
LIC
TIC-2005
Steam
400-TV-2005
13
400-FIC-2203
9
400-VE-03
400-TV 2002
400-TV 2001
LIC
400-LIC-2003
22
400-LCV-2003
FI
400-FI-3003
400-TK-70
Product
400-FIC-2001 (A)
(B)
(C)
Ratio Control
10
11
12
Oxygen

Figure 23: Simplified schematic representation of the pressure leach process at Lonmin, with basic control loops and stream numbers indicated

From this figure, the following flow rates can be identified:

Table 37: Summary of the flows representing the potential control valves

#	Representing Flow Rate	Stream number
1	400-FIC-0106	1
2	400-FIC-0101	2
3	400-FIC-1102	3
4	400-FIC-0107	4
5	400-FIC-0103	5
6	400-FIC-2203	9
7	400-FIC-2204	7
8	400-FIC-2001A	10
9	400-FIC-2001B	11
10	400-FIC-2001C	12
11	Water in coils	Compartment 2
12	Water in coils	Compartment 3
13	Steam	13
14	400-FIC-0402	14
15	400-FIC-0401	15
16	400-FIC-0504	20
17	400-FIC-0505	18
18	400-FIC-0501	19
19	400-FIC-501	21
20	400-FIC-2003	22

From this table it can be seen that the pressure leach process has a control degrees of freedom of 20, according to the definition of Luyben and Luyben (1997).

4.4.3 Valve for Production Rate

The production rate is limited by the rate of solids addition into the process. There are therefore three flow rates that can serve as candidates for determining the production rate:

- 400-FIC-0106 (referred to as m_1 in this discussion)
- 400-FIC-0103 (referred to as m_5)
- 400-FIC-2204 (referred to as m_7)

A prerequisite for the process is that the net flow rates into compartments 1 and 2 cannot be negative. This is caused by the assumption that the volumes of these compartments remain constant, due to their overflows as outlet streams. This, in turn, leads to a limitation on the ratio between m_7 and the flash recycle rate. If m_7 were to be fixed to determine the production rate, and the flash recycle rate would vary to control the temperature of compartment 1, there would be no simple way of preventing a net outflow from the compartment. This means that m_1 and m_5 are the only real alternatives.

It is important to note that, while one of these variables will be used to control the production rate, the other will control the level of 400-TK-10, for example. If the simplification of control was the only aim, it would be best if m_1 would determine the production rate, with additions made in 400-TK-10, and m_5 controlling the level of this tank. However, even if m_1 were to remain at a fixed flow rate, changes in the composition thereof would result in changes to the flow rates of streams 2 to 4 (in the presence of a proper advanced composition controller). This would result in ongoing variations in m_5, making its way directly into the flash tank and onward. This is undesirable, since – due to the nature of the mass balance around 400-TK-20 – a constant m_5 ensures that the difference between m_7 and the flash recycle stream remains at a safe value. Fixing the flow rate of m_5, on the other hand, necessitates the design of good and advanced control on 400-TK-10, to ensure that all flow- and compositional criteria are met by the streams entering the tank. Taking all of this into account, m_5 remains the stream determining the production rate – as is currently the case at Lonmin.

4.4.4 MVs for Influential Variables

According to Khan (2009) the following variables significantly influence leaching performance:

- Temperature in the autoclave compartments
- Pressure in the autoclave
- Acid concentration
- Solids percentage

In terms of temperature, each compartment has its own cooling or heating mechanism. The MVs for the control of each of the compartment's temperatures therefore do not require reconsideration.

From the previous discussion of the pressure in the autoclave acting as a special type of integrator, it can be deduced that the control of pressure is a very important part of the control of the pressure leach process. Possible MVs are the vapour bleed stream (henceforth called m_8) and the total addition rate of oxygen into the autoclave. m_8 is the flow rate through a vapour bleed valve that opens and closes at a set frequency. Assuming therefore that it is not available as easily adjustable MV, the total oxygen flow rate is the only MV for pressure control.

The acid concentration and solids percentage are also important variables, but the control of these variables is more complex than merely making an SISO pairing with a flow rate. It will therefore be considered at a later stage.

4.4.5 Inventory Control

The first inventory in the pressure leach process is 400-TK-10, for which m_5 (its effluent stream) has been ruled out as MV for inventory control. The remaining streams around this tank are streams 1 to 4. A more advanced control development around this tank may lead to the inventory not being controlled by one stream (SISO). For the sake of this design step, however, one stream needs to be chosen – and the currently used m_1 is appropriate.

The flash recycle tank (400-TK-20) has one unallocated solids/liquids stream, namely m_7. It is therefore chosen by default as the MV for this tank.

The levels of the first and second compartments in the autoclave are automatically controlled by means of overflow. This is not true for the third and fourth compartments, meaning that MVs need to be selected for controlling these inventories. For the third compartment, this can only be its outflow, stream 14. For compartment 4, it can be either its inflow (m_{21}) or outflow (m_{22}). This will be returned to.

400-TK-040 can only be controlled by its outflow (stream 15), since its inflow is already allocated to compartment 3.

The current control of the level of 400-TK-050 at Lonmin is not clearly defined. The flow rate of m_{17} (its solids feed stream) is manipulated with a variable speed drive (VSD). According to the plant operator this flow rate is changed according to the level of 400-TK-050 (Steenekamp & Mrubata, Control and Specifications of the BMR, 2013). However, the other feeds to the tank also affect the level, the acid concentration and the density. The effluent flow rate (stream 21) is adjusted manually by the operator. This method seems to have been developed organically (as opposed to systematically) and may benefit from a logical redesign. The thickener (in parallel with centrifuges) lies outside the scope of this project, since it does not form part of area 400 (the pressure leach area). In the plant simulation, the flow rate of stream 17 was therefore set as being flow rate of the solids in stream 15. Moreover, due to the similarities between the two setups, the control around 400-TK-050 is approached in a manner that is similar to what is done around 400-TK-10. Streams 18 to 20 are preliminarily assigned to compositional adaptions and will be reconsidered during the design of more advanced control. This leaves the tank's outflow (stream 21) as the only MV for inventory control of 400-TK-050.

This, in turn, means that the inventory of the fourth autoclave compartment will be controlled by manipulating the exit stream, stream 22.

Below is a table that summarises the allocated MV flow rates, alongside the respective inventories:

Table 38: List of inventories, with the flow controllers of the streams that will serve as MVs

Inventory	Flow Controllers
400-TK-10	400-FIC-0106
400-TK-20	400-FIC-2204
Autoclave compartment 3	400-FIC-0402
Autoclave compartment 4	400-FIC-2003
400-TK-040	400-FIC-0401
400-TK-050	400-FIC-501

4.4.6 Controller Tuning

The tuning methodology applied to this control structure is the same as was the case for the base case model. This means that all the tuning parameters remained the same as the fine-tuned base case, except for the mass controller on 400-TK-050, where stream 21 replaces streams 18 to 20 as the MV for mass control.

When the level control of an inventory is designed, one of the first steps is to define the control as averaging or tight control. The definition has consequences for the maximum variation of the tank's level and the flow rate that is used to control the level. For the base case, these parameters were set to the coefficients of variance (CoV) of the relevant variables. For this section, the tanks can either be defined as averaging or tight, or the base case values can be used. Due to the fact that there is a range of degrees of tightness a level controller can be, knowledge is required of what acceptable level and flow rate variations is. Since the main source of information for these parameters are the data, it is decided that the initial mass controller tuning parameters for the control in this section are calculated using the same CoV values used for the initial tuning of the base case.

Note that in the case of 400-TK-050 the flow rate variation value used in the base case for flow rates 18 to 20 is still applied to stream 21. Fine-tuning is done in Appendix F2, which shows that the initially determined values of K_c and T_I (-0.522 and 0.064 h, respectively) provide satisfactory performance.

4.5 ALTERNATIVE CONTROL ON 400-TK-20

4.5.1 Design

Conceptual Design

Because the cooling of the first compartment depends on both the flashing of part of the compartment's content and return of colder slurry, it is important to note that the mass control of the flash tank is an important part of the temperature control of the first compartment. Defining the control of the temperature of compartment 1 and the mass of the flash tank as two separate loops that need to be tuned separately is therefore not ideal. At Lonmin, tuning is done separately, while the flow rate of the flash recycle stream (m_9) is limited to 95% of the returning flow (m_7). While this ensures that the net rate into the first compartment is positive, the temperature control of this compartment is limited by limiting its MV.

A better approach would be to design a controller that can react rapidly to changes in flow rate of flash recycle stream (m_9), while also ensuring that the flash tank does not overflow or run dry due to changes in the other flow rates. Incorporating these two aspects into one PI controller is done by establishing feed-forward feedback control on the flow controller.

Before formally designing a feed-forward controller, it is important to ensure that this control form is indeed desired and, if so, that it is possible to implement it. According to Marlin (2000) feed-forward control is desired when feedback control does not provide satisfactory control performance, and if a measured feed-forward variable is available. As mentioned, the first criterion as satisfied, due to the limitation placed on the cooling of compartment when using only feedback control. The second criterion is met by the fact that the flash recycle flow rate can serve as feed-forward variable.

Marlin (2000) further recommends three criteria that have to be satisfied by the chosen feed-forward variable in order for feed-forward control to be possible. The first of these is that the feed-forward variable has to indicate the occurrence of an important disturbance. Since the flash recycle stream typically makes up the bulk of the stream entering the flash tank, changes in this flow rate will be an important disturbance to the level control system. The second criterion notes that there must not be causal relationship between the MV (of the level controller, in this case) and the feed-forward variable. A change in the flash tank's effluent stream (m_7) does not change the flow rate of the flash recycle stream under open-loop conditions, and hence the second criterion is met. Lastly, the disturbance dynamics should not be significantly faster than the dynamics between the CV and the MV when the feed-forward control is added to the feedback control. Note that the CV is the tank level, while the MV and the feed-forward variables are entering (m_9) and exit (m_7) streams, respectively. In order to be able to properly comment on this criterion, the unsteady state mass balance for the flash tank needs to be examined. The unsteady state mass balance of 400-TK-20 is as follows:

$$\frac{dX_{25}}{dt} = m_5 + m_9 - m_{H_2O\,flash\,evaporated} - m_7 + m_{23}$$

[44]

Here, m_9 represents the flash recycle stream (measured disturbance), while m_7 refers to the exit stream. The other variables follow the same numbering system as is used in Figure 23. It can be seen that a change in m_9 would result in similar dynamic response in the mass of the tank's contents, as a change in the effluent flow would have, albeit opposite in sign. With this, the final criterion of Marlin (2000) is met – affirming the flash recycle stream as a suitable feed-forward variable, in an application suitable to receive feed-forward control.

The design of a feed-forward controller starts with defining the feed-forward transfer function (in the Laplace domain), as the following equation shows (Marlin, 2000):

$$G_{ff}(s) = \frac{-G_d(s)}{G_p{}'(s)}$$

[45]

Here, G_d is the disturbance transfer function, while $G_p{}'$ is the product of the transfer functions of the valve and the process. Below is a diagram illustrating the control structure in question:

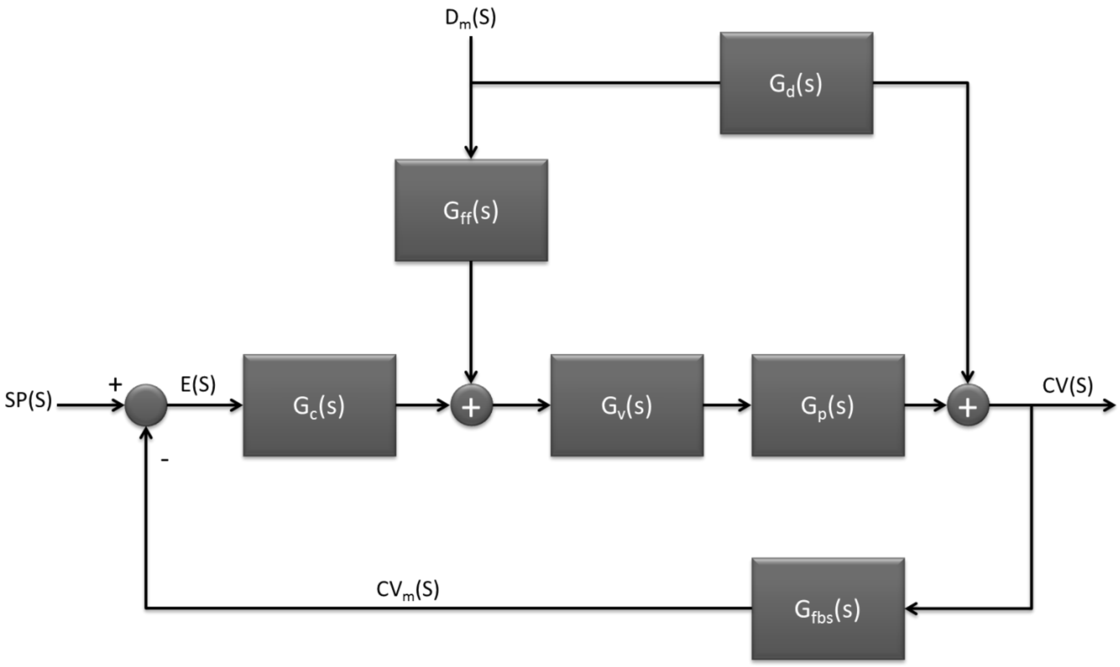

Figure 24: Block diagram of a feedback control system with feed-forward control (Redrawn from Marlin, 2000)

Note that in this case D_m represents the flash recycle stream, while CV represents the level or mass of the flash tank (400-TK-20). The disturbance transfer function is therefore defined as follows:

$$G_d(s) = \frac{CV(s)}{D_m(s)} = \frac{X(25)(s)}{m\_9(s)}$$

[46]

Here, X(25) is the mass of 400-TK-20 and m_9 is the flash recycle flow rate.

Similarly, the process transfer function is defined as follows:

$$G_p'(s) = G_v(s)G_p(s) = \frac{v_{MV}(s)}{MV(s)} \cdot \frac{CV(s)}{v_{MV}(s)} = \frac{CV(s)}{MV(s)} = \frac{X(25)}{m\_7(s)}$$

[47]

It is important to note that, while the flow rate of stream 7 (the flow rate from the flash tank) is controlled by a cascade controller on the plant, the inner loop of this cascade controller is assumed to be very fast and in automatic mode during this derivation.

With these terms defined, the transfer functions thereof need to be defined, in order to determine the feed-forward transfer function. This is done by reviewing the differential equation wherein the tank mass is calculated:

$$\frac{dX_{25}}{dt} = m_5 + m_9 - m_{H_2O\ flash\ evaporated} - m_7 + m_{23}$$

[48]

In the Laplace domain, this translates into the following equations:

$$sX_{25}(s) = m_5(s) + m_9(s) - m_{H_2O\ flash\ evaporated}(s) - m_7(s) + m_{23}(s)$$

[49]

$$G_p'(s) = \frac{X_{25}(s)}{m_9\ (s)} = -\frac{1}{s}$$

[50]

Similarly,

$$G_d(s) = \frac{X_{25}(s)}{m_7\ (s)} = \frac{1}{s}$$

[51]

These two equations make sense, since a tank serves as an integrator in a process, and it has been stated that the flash recycle stream and effluent stream have the same type of effect on the tank mass, albeit opposite in its signal. The feed-forward controller transfer function can now be calculated by equation 45, giving the following result:

$$G_{ff}(s) = \frac{-G_d(s)}{G_p'(s)} = -1 \cdot \frac{1}{s} \cdot \frac{s}{-1} = 1$$

[52]

The fact that this transfer function is unity means that the measured mass flow rate of the flash recycle stream is to be added to the output of the feedback controller. This means that the initial MV output of the mass controller of 400-TK-20 is the difference between the initialisation terms of m_7 and m_9.

This ensures that there will always be a positive ratio between m_7 and m_9, that the temperature control of the first compartment will work quickly and efficiently and that the mass controller will work as designed. It should be noted that the feedback controller should not be a tight mass controller and should rather be tuned loosely, since only the flash recycle stream variations will be quickly rejected. If it is found that large deviations in the flash recycle stream lead to undesired deviations in m_7, a signal sampler (in the form of a zero-order hold) can be added in the place of a feed-forward transfer function, to ensure lower frequency changes.

Below a block diagram of the controller is given:

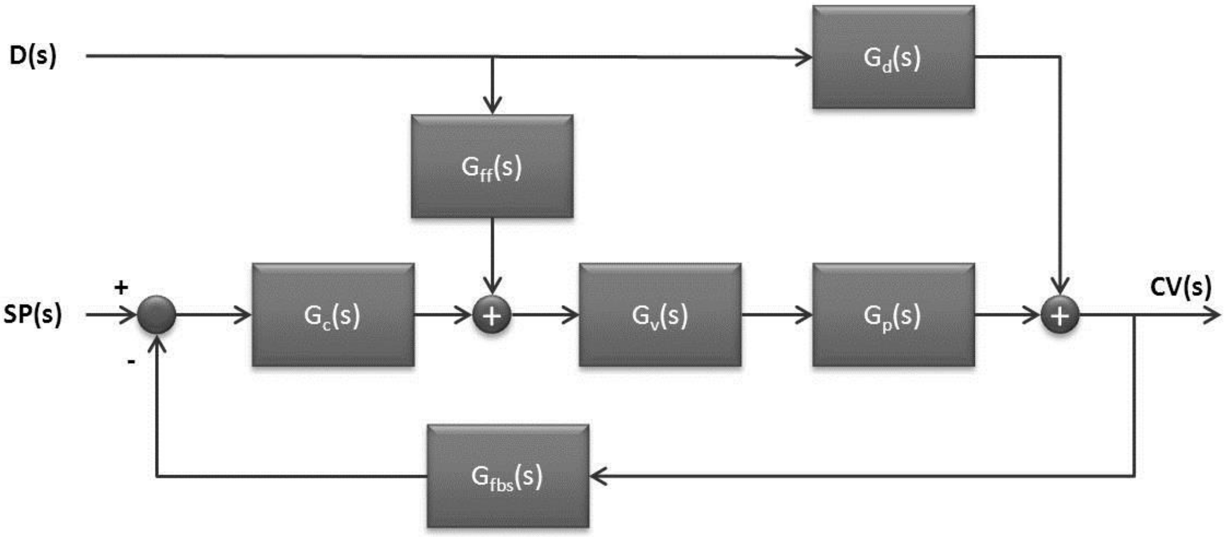

Figure 25: Block diagram of the feed-forward and feedback temperature controller.

Note that valve dynamics are replaced by a linear correlation and are therefore not included in the diagram.

Tuning

Marlin (2000) notes that the best practice for tuning a feed-forward-feedback controller is to tune each controller separately. Having already designed the feed-forward control component, the feedback controller has to be tuned. Since this is entails inventory control, the same tuning method is used as with the mass controllers in the base case model. Instead of using the coefficients of variance of data values to determine the maximum variation in the tank mass and flow rate of stream 7, for tuning, the tank is tuned for averaging mass control. According to Marlin (2000) a maximum change of 40% in both directions is noted to given averaging behaviour. The maximum change in flow rate of stream 7 is maintained at the base case value. The difference between the initial flow rates of streams 7 and 9 is used as mean flow rate. The resulting tuning parameters are a K_c value of -0.1755 and $1/T_I$ of 0.0055 hours.

The plots used for the fine-tuning of the feedback component of the mass controller and the temperature controller in compartment are shown in Appendix F3. Note that no adaption of the tuning parameters was found to be necessary.

4.5.2 Evaluation & Comparison

In order to show how the addition of feed-forward control improves the performance of the first compartment's temperature control (T1) and the control of the mass in 400-TK-20, a test was done which highlights the improvement. This test entails a sequence of changes in the set point (SP) of T1. Since the MV of the temperature controller is the flash recycle stream, these SP changes will result in flash recycle fluctuations, which in turn will introduce an important disturbance to 400-TK-20. Since the addition of feed-forward control aims that improving the response of the mass controller to this disturbance, the test done in this section showcases the success of the FF control. Starting with the steady state value as the SP, at 12 minutes into the run the SP is multiplied by 0.99, to return to its initial value after 1.2 minutes. After another 1.2 minutes the SP is multiplied by 0.995, and is kept there. While this is a small temperature change, the resulting change in flash recycle rate is large. These quick changes between reasonable values allow for a demonstration of the addition of feed-forward control.

Table 39 summarises the results from this evaluation:

Table 39: Summarised comparison between the performance of the controllers for the first temperature compartment and mass of 400-TK-20, for the base case and controller with feed-forward control.

Controller	Comparative Measure	Base Case	FF-Feedback Controller
Temperature (400-TIC-2001)	Maximum Deviation	1.01%	1.01%
	Normalised IAE	2.997e-4	2.773e-4
	SS Offset	No	No
Mass of 400-TK-20	Maximum Deviation	0.040%	0.046%
	Normalised IAE	1.716e-5	2.764e-5
	SS Offset	Yes	Yes

In this table it can be seen that the addition of feed-forward control improves the control of the first compartment's temperature. The normalised IAE is decreased by 7.5% from the base case, while the maximum deviation remains unchanged. The larger maximum deviation and IAE values for the FF-feedback control is caused by the fact that this mass controller is tuned to averaging control, whereas the base case is tuned using the variance of the tank's level in the data.

Note that, during the fine-tuning of the FF-feedback controller, it has been observed that tighter control on 400-TK-20 does not worsen the performance of the temperature controller, and therefore the above improvement in temperature control can be confirmed not be caused by a more loosely controlled 400-TK-20.

The analysis of the plots generated for this evaluation can be seen below.

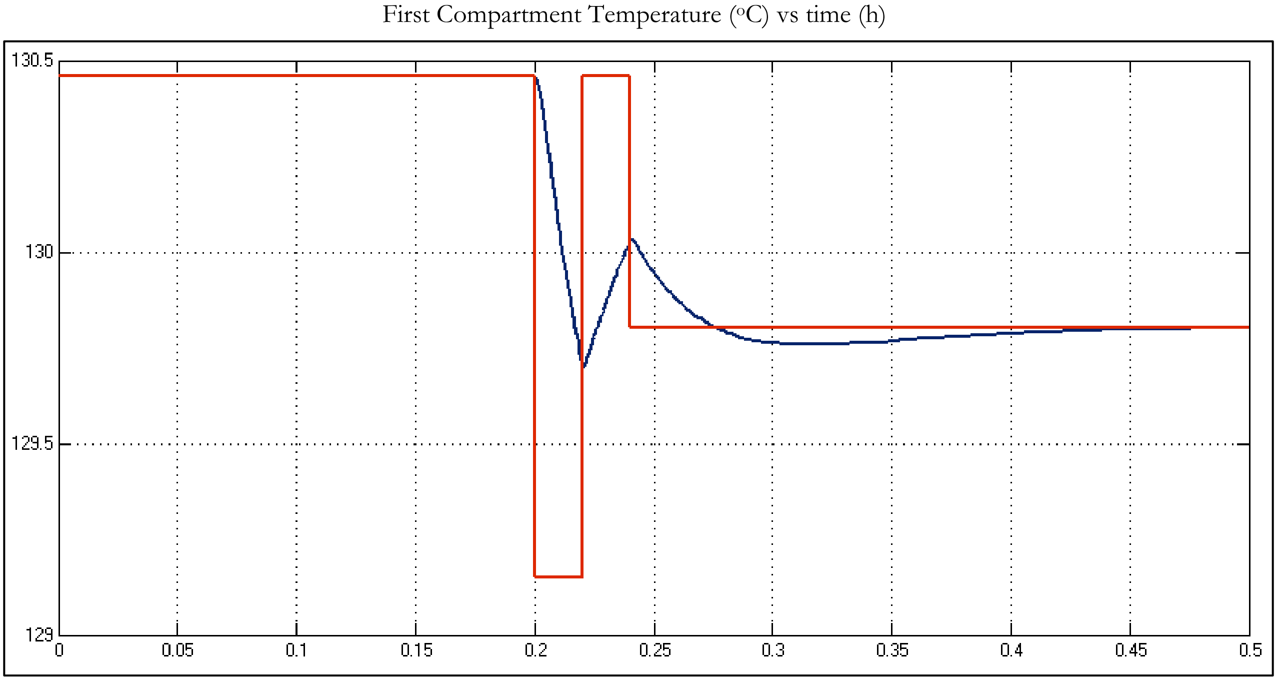

Figure 26: Plot of the base case model's SP (red) and measured value (blue) of the temperature in the first compartment (°C) vs time (hours). There is not offset at steady-state. Maximum deviation = 1.01%. nIAE = 2.997e-4.

In this figure the SP changes in the temperature can be clearly seen. While the temperatures move toward the SPs, it reaches it only again at 0.45 hours. The normalised IAE is less than 0.0003, which is a small value. The following plots show the flow rates of the flash recycle stream and of stream 7.

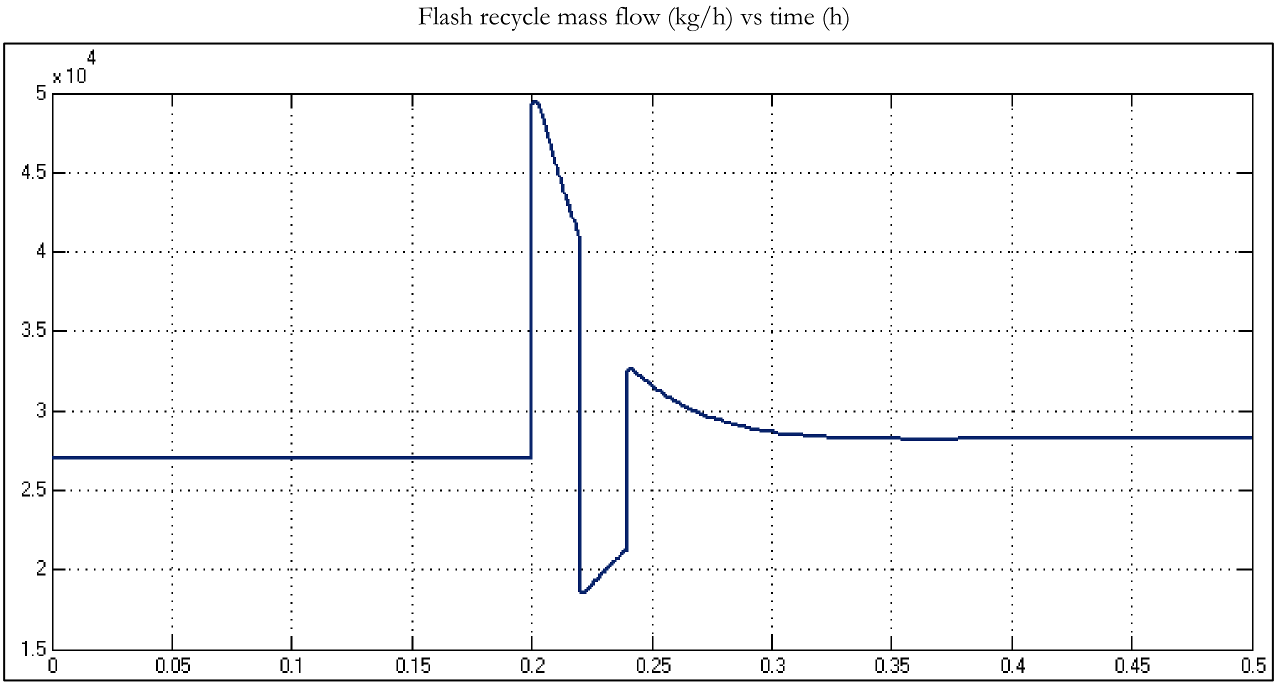

Flash recycle mass flow (kg/h) vs time (h)

Figure 27: Plot of the base case model's flash recycle flow rate (kg/h) vs time (h)

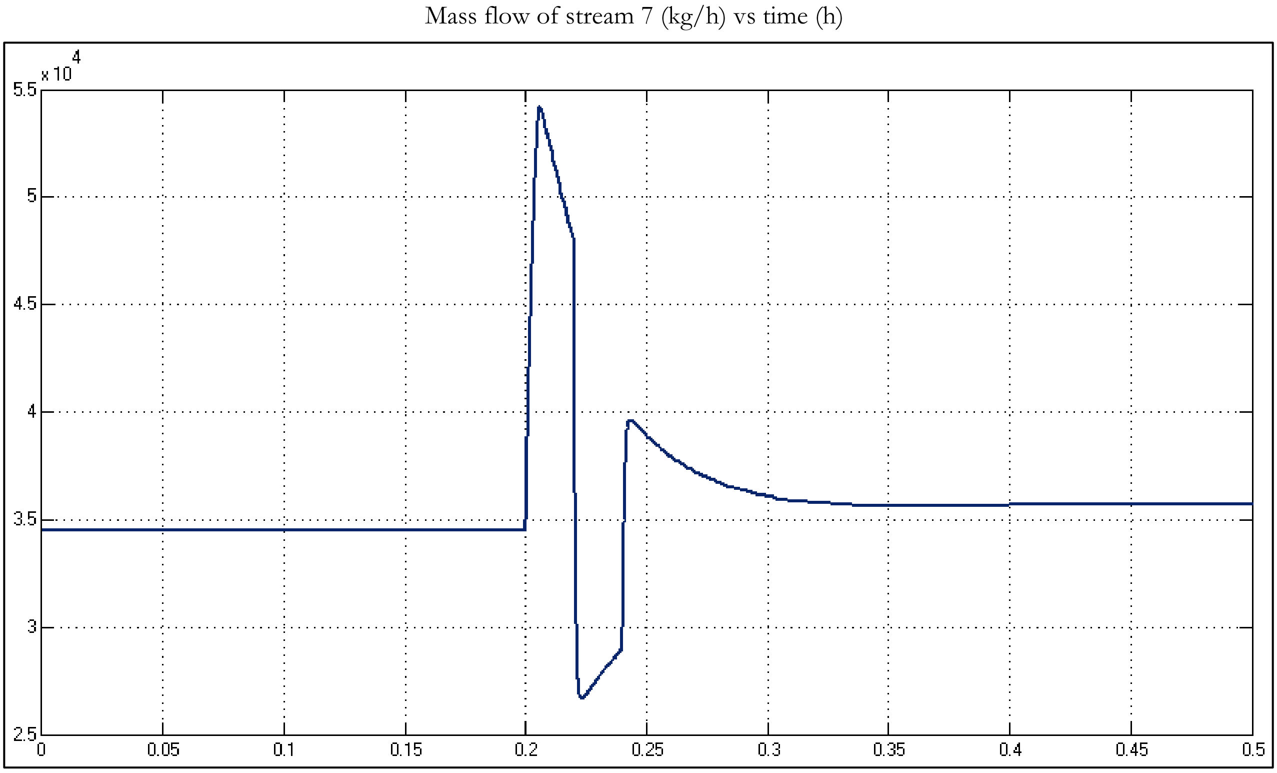

Mass flow of stream 7 (kg/h) vs time (h)

Figure 28: Plot of the base case model's mass flow rate of stream 7 (kg/h) against time (h)

It can be seen from these figures how the outflow of 400-TK-20 resembles that of the flash recycle stream. This is due to the fact that the flow rate of the latter is limited by that of the former (to a ratio of 0.9 in this exercise). This problem has been identified and is the main motivation for the inclusion of feed-forward control. The mass in 400-TK-20 is given below:

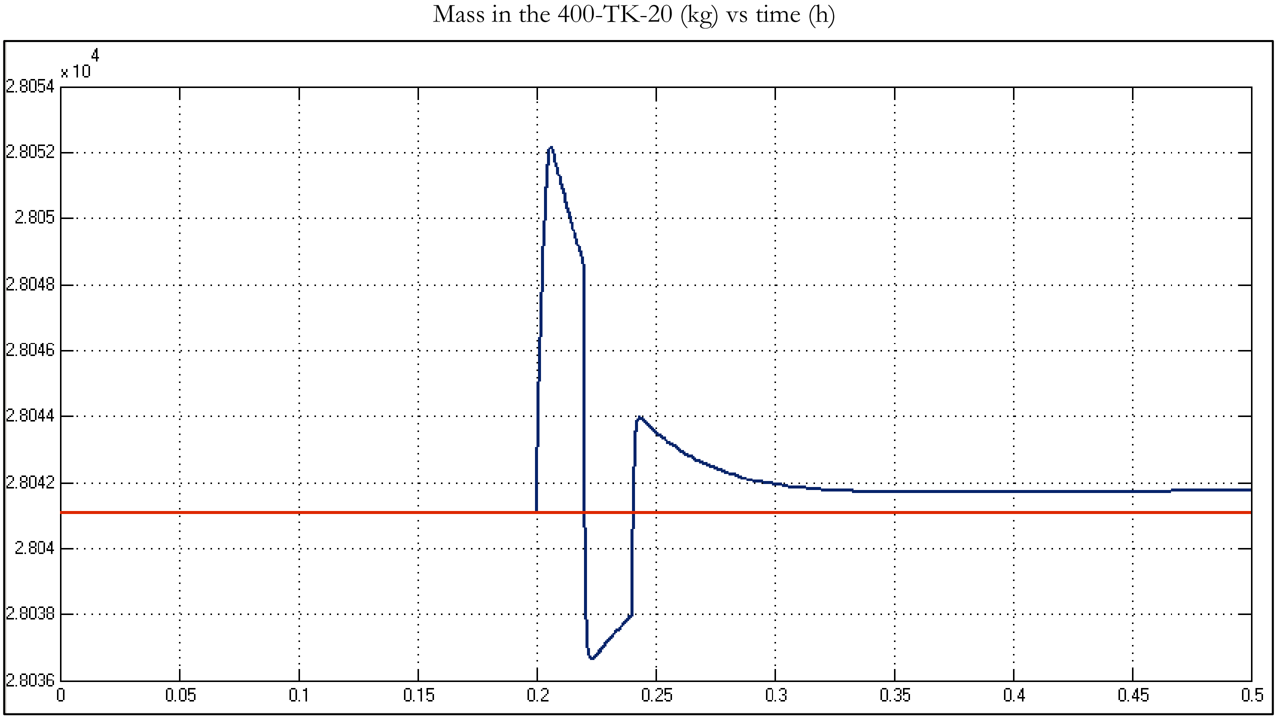

Figure 29: Plot of the base case model's mass inside 400-TK-20 versus time (h). Steady-state offset. Maximum deviation = 0.04%. nIAE = 1.716e-5.

It can be seen how the maximum deviation is 0.04% of the SP. It can be noted that there is a steady-state offset, but this offset is negligibly small.

In the case of the model with feed-forward control, the same test is done.

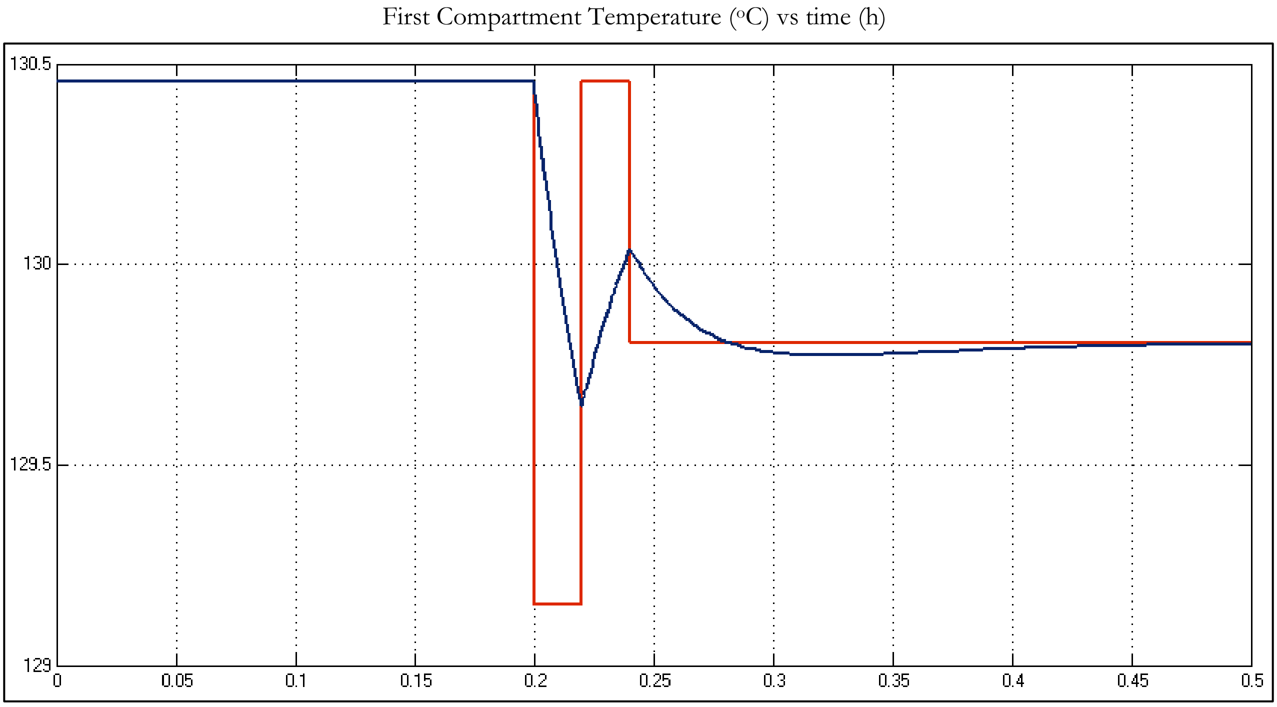
First Compartment Temperature (°C) vs time (h)

Figure 30: Plot of the FF model's SP (red) and measured value (blue) of the temperature in the first compartment (°C) vs time (hours). There is no offset at the new steady-state. Maximum deviation = 1.01%. nIAE = 2.773e-4.

From Figure 30 it can be seen that the temperatures proceed closer to the SP values than it does in the base case. A zero steady-state offset is again reached.

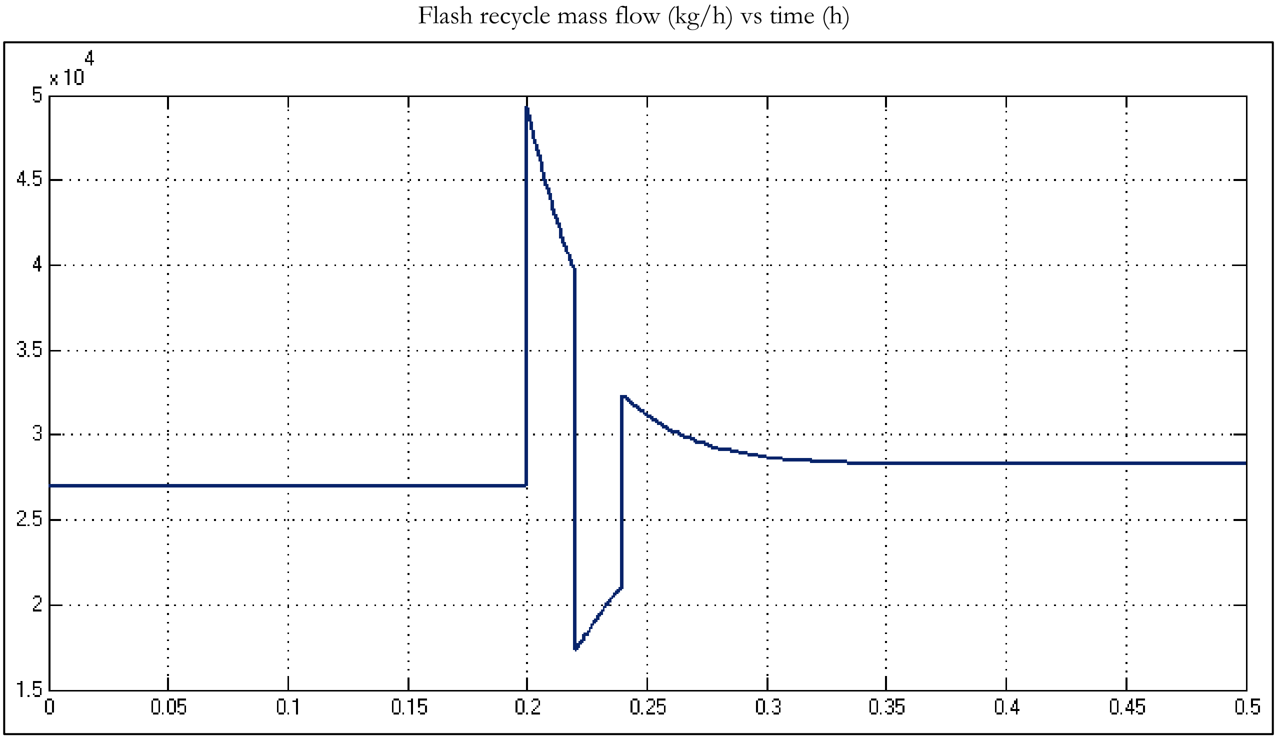
Flash recycle mass flow (kg/h) vs time (h)

Figure 31: Plot of the FF model's flash recycle flow rate (kg/h) vs time (h). Offset at steady-state.

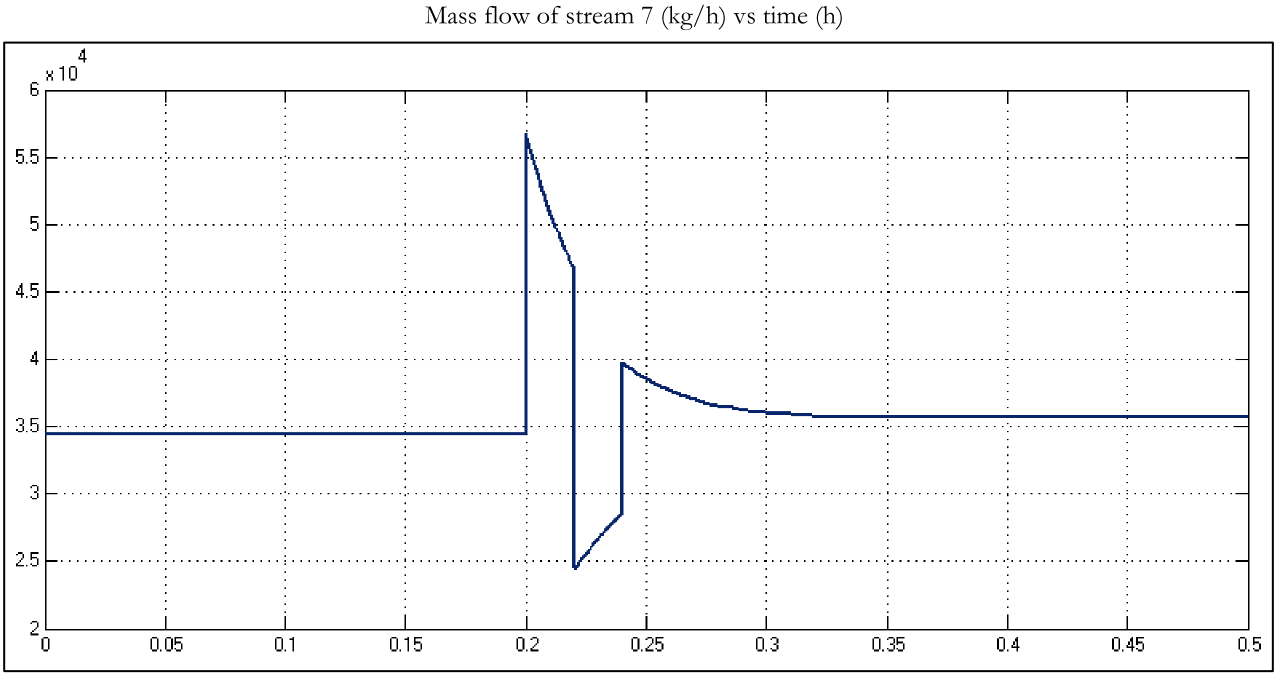

Figure 32: Plot of the FF model's mass flow rate of stream 7 (kg/h) against time (h). Offset at steady-state.

As in the case of the base case model, the two mass flow rates resemble one another. However, its shape differs from that of the base case plots in that there is a sharp initial change (compared to the slightly delayed one of the base case). The reason for this is the fact that the flash recycle flow rate is not inhibited by the flow rate of stream 7, but rather immediately changes its flow rate.

The mass in 400-TK-20 is plotted below.

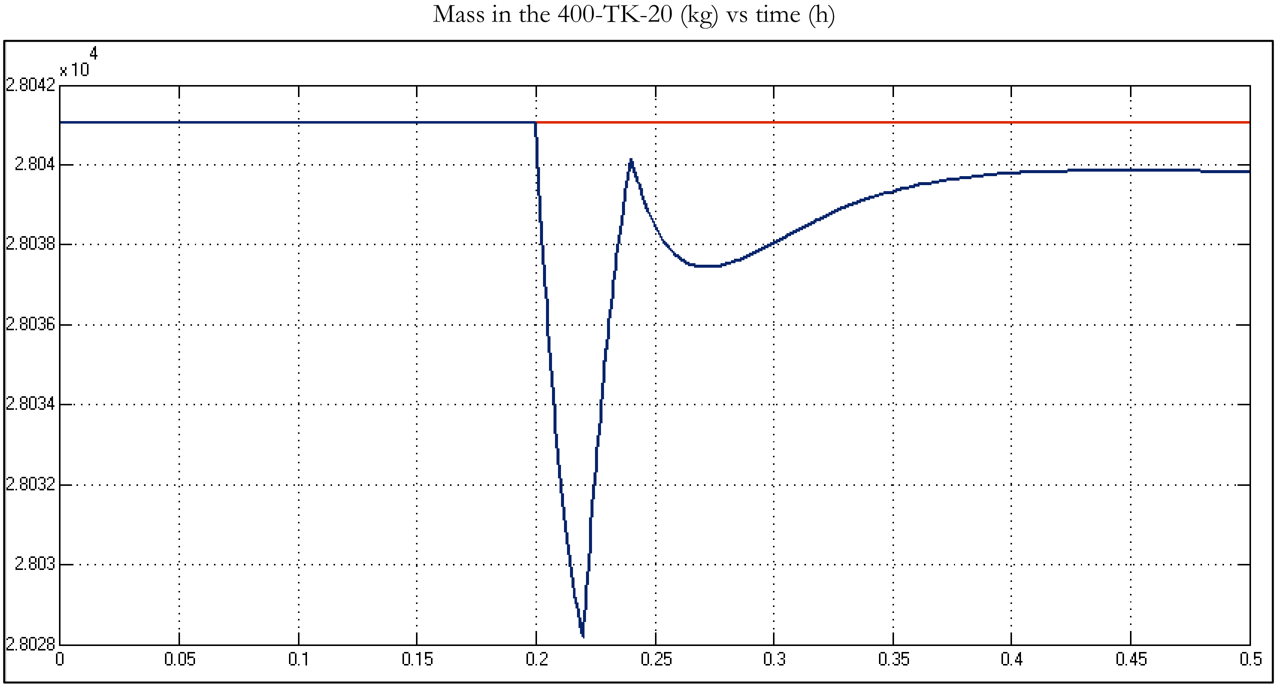

Figure 33: Plot of the FF model's mass inside 400-TK-20 versus time (h). There is a steady-state offset of -0.0036%. Maximum deviation = 0.046%. nIAE = 2.764e-5.

It can again be seen that 400-TK-20 has a steady-state offset. This is caused by the averaging control on this tank. The offset is less than 0.001% of the tank's mean, and is therefore negligible.

It can also be seen that the tank's mass does not follow the same trend as that of the flow rates entering and leaving the tank. These observations can be explained by the fact that an increase in the flash recycle stream's flow rate immediately causes the outflow to increase with the same amount. In the absence of controller lag (which is assumed to be zero in this project) the tank mass will not be influenced notably by the control of the first compartment's temperature.

From what has been shown, the following observations can be made:

- The fact that the mass flow rate of stream 7 immediately changes in response to the change in the flash recycle rate (in the model with FF control) leads to a smaller disruption in the mass in 400-TK-20
- In the absence of feed-forward control the response of the flash recycle rate is slow, due to the fact that it is limited by a mass controller which has one gain term by which it has to reject the disturbance constantly introduced by changes in the flash recycle rate. Introducing feed-forward control allows the mass control to be more effective, which in turn allows the temperature control to proceed without limitations on the MV.

Note that the temperature controller can be tuned much more aggressively for the model with feed-forward control without interfering with the mass controller. The reason for this is that the MV of the temperature controller is not limited by an externally enforced ratio. The same cannot be said for the model(s) without feed-forward control.

It is recommended that feed-forward control, as introduced and designed in this section, is used as supplementation to the feedback mass (or level) control of 400-TK-20.

4.5.3 Model Predictive Control

An alternative, more advanced approach to the control about 400-TK-20 would be to implement a model predictive controller. Before looking to MPC as in "improved" control method, the following this should be noted in this case:

- Marlin (2000) notes that the simplest control method that gives satisfactory results is the best. If a control strategy therefore gives acceptable results, it is not advisable to look to more complex solutions.
- The feed-forward-feedback control combination works well on the sub-process at hand.
- The nature of the control problem surrounding 400-TK-20 and the temperature of compartment 1 makes it a challenge to isolate the effects each stream on the tank's level and the temperature of the first compartment. Since the success of a model predictive controller

depends on the accuracy of the derived process transfer functions, the control problem is not ideally suited to an MPC solution.

4.6 SECTION CONCLUSIONS

This chapter is the first of two that make up the crux of this thesis, with the current control structure being reconsidered and new approaches recommended on several levels. This chapter focuses in the evaluation and development of the basic regulatory control structure.

Before reconsidering the current system, a base case is developed, which represents the current structure of this control level. Mass controllers are tuned using variances in the relevant variables in the data, in an attempt to match real plant performance as closely as possible. PI controllers are used throughout the process and tuning is assumed to be done optimally.

The manner in which the controlled and manipulated variables are paired on the basic regulatory control level is investigated. It was found that this cannot be done by setting up an RGA, since the process contains an integrator of which its effects on the process cannot be isolated. This integrator is the vapour space in the autoclave, which directly influences the pressure and therefore indirectly influences the reactions and temperatures in the autoclave. An alternative procedure is followed, as recommended by Luyben and Luyben (1997). It is found that the current variable pairing is appropriate, with the only recommended adaption being that 400-TK-050 should be controlled with its outflow, instead of some of its entering flows (which is currently the case), to allow for the addition of compositional control to this tank. More specifically, stream 5 is affirmed as being the best stream for determining the production rate.

The control of the temperature of compartment 1 and the level control of the flash recycle tank is examined, since this has been identified by Lonmin as a point of concern. Instead of using independent control loops for the control of the aforementioned variables, a feed-forward feedback controller for 400-TK-20 is developed which can improve control performance. The feedback component is tuned to be an averaging mass controller.

A comparison is done with the developed base case model, where the set point of the temperature of compartment 1 is changed several times. It is found that the addition of feed-forward control improves the temperature control, decreasing the IAE with 7.5% from the base case, without introducing unwanted tank level fluctuations via the flash recycle stream. Lastly the recommended control structure allows more room for aggressive controller tuning than the base case, since there is not external limit imposed on the flash recycle flow rate in the former. It is therefore recommended that feed-forward control is used to supplement the feedback control on 400-TK-20.

CHAPTER 5

COMPOSITIONAL & SUPERVISORY CONTROL

5.1 CHAPTER INTRODUCTION

In the previous chapter the control structure of the basic regulatory control level has been investigated, with improvements recommended. This section deals with compositional control, which has been defined as the second part of regulatory control in this project. In chapter 3 the model has been found sufficient for use in the investigation and development of control structures in compositional control.

In this chapter a base case is developed for compositional control. This base case is an adaption of one of the structures in chapter 4, with the current compositional control of the second stage leach simulated as best possible. Note that the compositional control on the third stage leach is omitted due to insufficient process information and data. All new control developments are evaluated against the base case in order to comment on its success.

Since the model in its current form was not found to be valid for the investigation of supervisory control, this control level is merely discussed, with recommendations made, in this chapter and cannot be simulated.

5.2 LITERATURE REVIEW

The literature provided in this section is an extension of the literature review in chapter 4, focussing especially on control methods relevant to compositional and supervisory control.

5.2.1 Advanced Regulatory Control on Autoclaves

While Lonmin's Western Platinum BMR does not have an overarching advanced process control (APC) system (see chapter 2), such types of control have already been developed and implemented globally on similar processes. The best example in literature is the development of pH APC at the first stage pressure leach at Impala Platinum's BMR (Khan, Spandiel, van Schalkwyk, & Rademan, 2009). It was identified that temperatures, pressures and tank levels (basic regulatory control variables) can be tightly controlled by means of simpler control methods, such as PID control, and that there is evidence of a strong relationship between the control of the final metal concentrations and pH control (Marlin, 2000). This process closely resembles the one to be modelled and controlled in this project – showing that much is to be learnt from it. The main difference is the fact that the aims of Impala's first stage leach include leaving copper in the solids form, while it should be leached out in Lonmin's second and third stages.

Key Variables

Due to the fact that there are a significant number of disturbances, as well as controlled and manipulated variables, the control of the pressure leach can become very complicated in principle. It is therefore useful to look at the variables identified as important by Khan (2009).

The main disturbance variables are identified as being the matte composition, the composition of the spent electrolyte, as well as the pulp feed. The main disturbances at Lonmin's pressure leach are similar in nature – with the main compositional disturbances at Lonmin's BMR being compositions of the first stage leach residue and the copper spent electrolyte.

The main variables used to monitor the state of the process at Impala are identified to be the pulp density and the copper in solution (Khan, Spandiel, van Schalkwyk, & Rademan, 2009). Keeping in mind that these variables are chosen to be the most important indicators with the aim of controlling the pH, it again looks to be applicable to Lonmin's process. The main manipulated variable is given to be the addition rate of spent electrolyte (Khan, Spandiel, van Schalkwyk, & Rademan, 2009). This is also the case for the Lonmin process, except that sulphuric acid addition can be included as an MV. Lastly, the controlled variable is the pH in the first compartment of the autoclave. For the Lonmin process, the acid concentration in the mixing tanks and product streams would be the CVs.

Note that a more detailed analysis of the key process variables, as it pertains to the Lonmin process, has been done by Dorfling (2012). These variables are discussed in section 5.8.1.

Control Philosophy

It is advised that the temperature and pressure in the autoclave should be set to constant, appropriate values – perhaps changed periodically by a supervisory control system – and that the pulp density should not vary much, as it is prepared to enter the autoclave (Khan, Spandiel, van Schalkwyk, & Rademan, 2009). The consequence of this is that the temperature and pressure control should be tuned tightly on both the autoclave and the tanks around it, so that these two variables do not unnecessarily disturb the more difficultly controllable variables, such as acid concentration. It is advised that the pulp feed rate should be used to change the production rate, as is the case at Lonmin. The reason for setting these variables up in this manner is to ensure that the acid-containing streams can be used exclusively as primary MV for pH control in the autoclave.

5.2.2 Enhancements to Feedback Control

Split-Range Control

The feedback control structures mentioned up to this point applied to cases where one valve (from one MV) is used to control one CV (SISO). In a case where two control valves should be used to control one CV, split-range control (an alteration of feedback control) is typically applied. In chemical process plants, such control is typically used when two different control modes are employed at different times, such as in the case of an air temperature regulator with both heating and cooling functions. Below is a block diagram of a typical split-range controller:

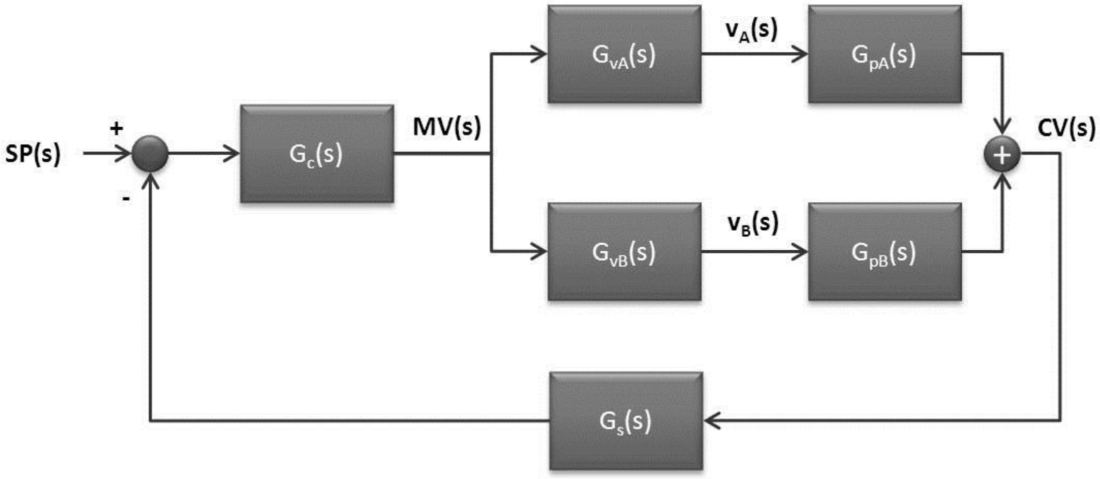

Figure 34: Block diagram of a split-range control system (Redrawn from Marlin, 2000)

From this diagram it can be seen that a split-range controller is a single controller with one set of tuning constants. The output of the controller determines in which way the available valves must operate to serve as total MV. Marlin (2000) mentions that split range control is only possible if

1. There is one CV and more than one MVs.
2. There is a causal relationship between each MV and the CV.

3. There is a fixed hierarchy which determines the order in which the MVs are adjusted.

The last criterion refers to the fact that there should be a fixed correlation between the controller output and the resulting change in the control valves.

Inferential Control

There are some cases on a plant where the CV is not measurable or not measured at a high enough rate. This is typically the case for compositional data, which is often sampled and analysed in a laboratory, instead of by an online sensor. In order to overcome this, these unmeasured (or infrequently measured) variables can be inferred from other available measurements (called inferential variables). The following diagram shows how an inferential controller is implemented in principle:

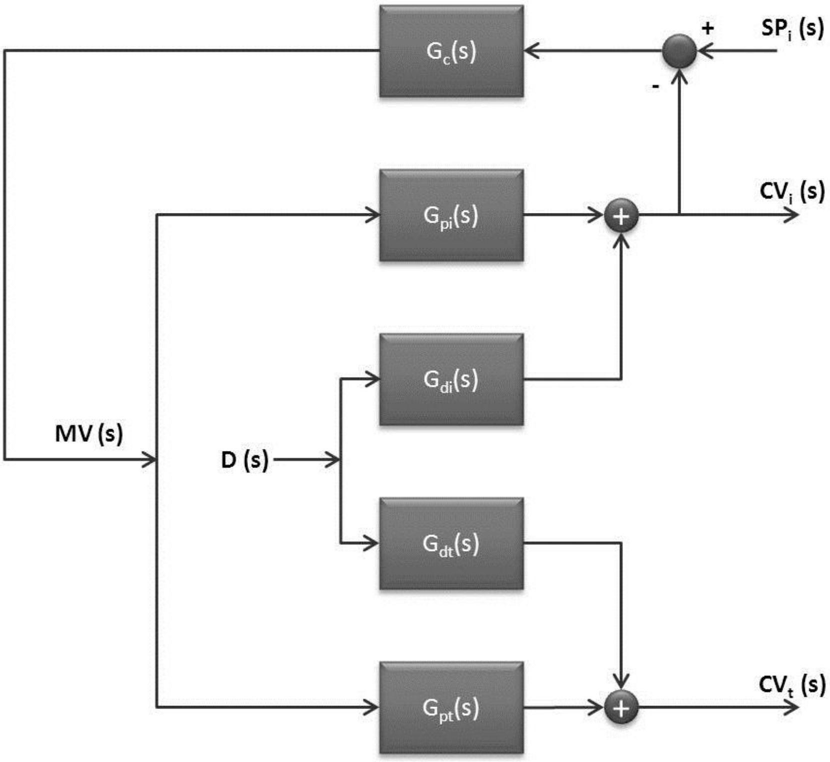

Figure 35: Block diagram of a feedback control system with inferential control (redrawn from Marlin (2000)).

Here, the *t* subscript refers to the true, unmeasured variable and the *i* subscript refers to the inferential variables. It can be seen that a disturbance has an effect on both the true and inferential processes, but that only the inferential CV compared to a corresponding SP, for use by a controller. If the true CV is indeed measured, but just infrequently so, it is often used to adjust or reset the inferential controller. This is the only manner in which a zero steady-state offset can be achieved by an inferential controller. (Marlin, 2000)

5.2.3 Model Predictive Control

Model predictive control (MPC), often referred to as receding horizon control, is a form of control where the current control action is found by solving a finite horizon open-loop control problem online – at each moment of sampling (with the plant's current state as starting point) (Mayne, Rawlings, Rao, & Scokaert, 2000). The optimisation brings about a more optimal control strategy. Linear models therefore are used to predict system dynamics – even though constraints cause the closed-loop system dynamics to be non-linear (Findeisen & Allgöwer, 2002). The following is a very simple block diagram representation of an MPC control system (Marlin, 2000):

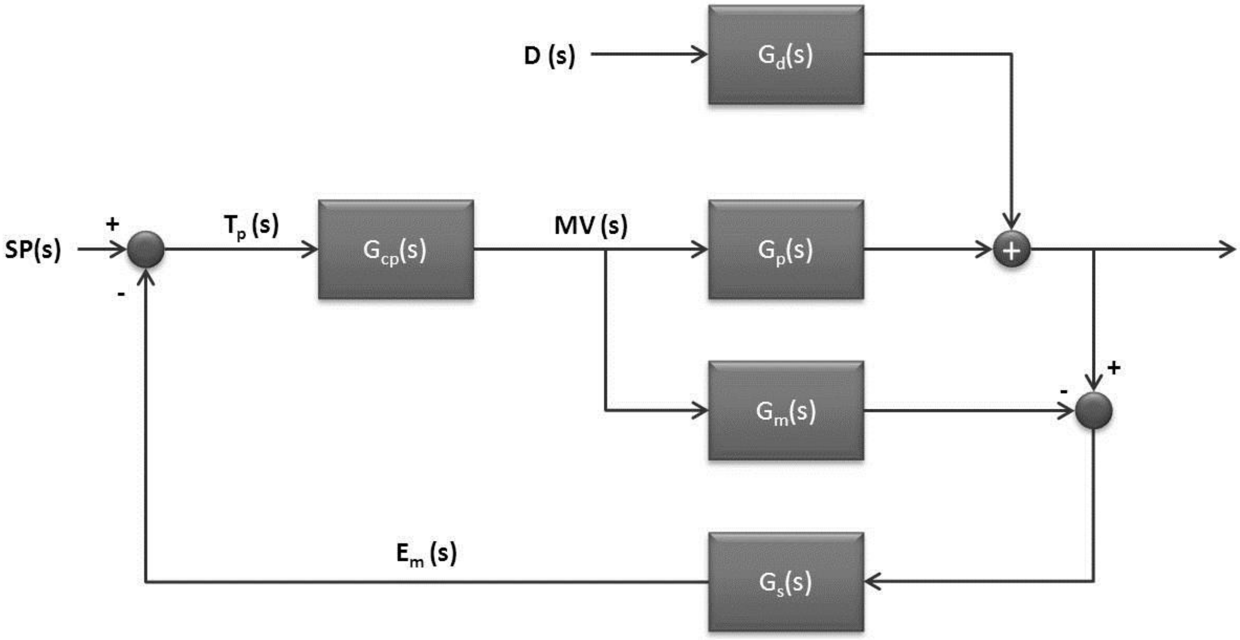

Figure 36: Block diagram of a simple MPC control system (Redrawn from Marlin, 2000)

In this figure, G_p is the true process, G_{cp} represents the controller and G_m is the dynamic model of the process. The returned error term is the difference between the measured and predicted CVs, which represents the effect of the disturbance and the model-plant mismatch. This therefore serves as a model correction, adjusting the set point as to provide a better target value (T_p). This target value is then sent to the controller, which contains a predictive control algorithm.

It should be noted that MPC is in fact an umbrella term for a large number of similar control strategies. The model used for MPC can be linear or non-linear, and can be in a large variety of forms.

5.3 BASE CASE STRUCTURE OF COMPOSITIONAL CONTROL

5.3.1 Introduction

In order to be able to evaluate the control designed in this chapter, a structural base case model is developed for the compositional control. This is an adapted version of the version developed in section 4.4, where the pairing of the basic regulatory control was redone.

Stream 23 (the sulphuric acid stream into 400-TK-20) is set as the MV for the control of the acid concentration inside 400-TK-20, with no additional acid concentration or solids fraction control – except for the fact that a constant ratio is maintained between each of streams 2 to 4 and stream 1. At steady state, the flow rate of stream 23 is therefore restored. It is important to note that, while it is known that the acid concentration in this tank (the CV) is sampled and logged only once an hour, an inspection of the acid controller shows an execution frequency of 1 minute. The set point values of this controller are not available and therefore it is assumed that the base case acid controller continuously receives the CV measurement and continuously executes.

5.3.2 Tuning and Fine-Tuning

The added acid controller on 400-TK-20 is tuned in the same manner as that of other PI controllers in this project, with a step change made in the MV (which in this case is the mass flow rate of stream 23). A +10% step change is made in the MV – with all control in the model in manual mode – and the CV response curve is analysed to derive the PID controller tuning constants (Marlin, 2000). Note that the tuning parameters are set in the same manner as that of section 4.4, after fine-tuning op this version has been done.

Since the only difference between this base case and the version of section 4.4 is the addition of stream 23, fine-tuning is limited to the evaluation of the acid control in 400-TK-20. This fine-tuning is done by closing all the control loops on the model, making a step change in the set point of the tuned control loop. The response is checked, with adaptions made if necessary, based on the procedure in section 4.2.4. The tuning and fine-tuning procedures are shown in Appendix G1. The following tuning constants result:

Table 40: Tuning constants before and after fine-tuning for the acid controller in 400-TK-20.

Tuning Constants	**K_c**	**T_I**
Initial tuning	20.285	1.36
Fine-tuning	304.275	1.36

It can be seen that the controller was made more aggressive during fine-tuning.

5.4 VARIABLE PAIRING FOR COMPOSITIONAL CONTROL

5.4.1 Allocation of Remaining CVs

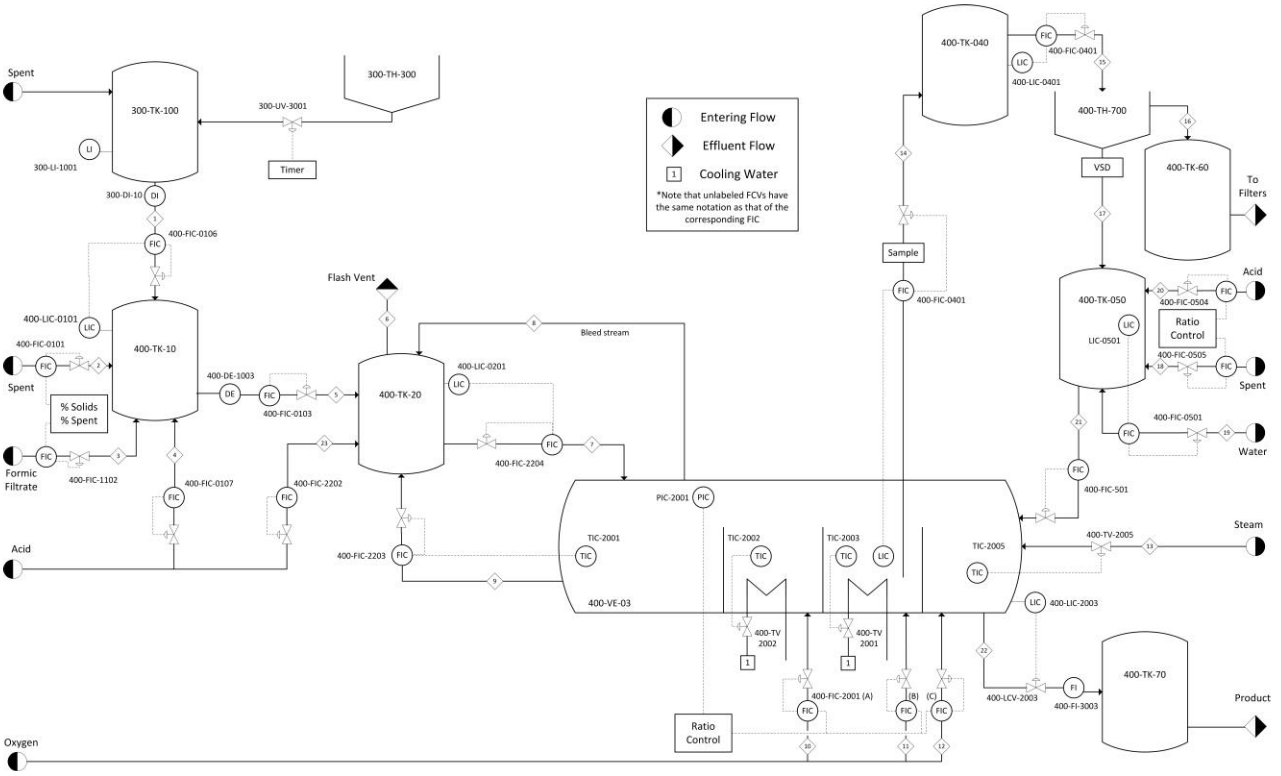
Spent
300-TK-100
300-TH-300
300-UV-3001
Timer
LI
300-LI-1001
300-DI-10
DI
400-FIC-0106
FIC
400-LIC-0101
LIC
400-FIC-0101
400-TK-10
Spent
% Solids
% Spent
Formic
Filtrate
400-FIC-1102
400-FIC-0107
Acid
400-DE-1003
DE
400-FIC-0103
Flash Vent
Bleed stream
400-TK-20
400-LIC-0201
400-FIC-2204
400-FIC-2202
400-FIC-2203
Entering Flow
Effluent Flow
Cooling Water
*Note that unlabeled FCVs have the same notation as that of the corresponding FIC
PIC-2001
PIC
TIC-2001
TIC
TIC-2002
TIC-2003
TIC-2005
400-VE-03
400-TV 2002
400-TV 2001
400-FIC-2001 (A)
(B)
(C)
Ratio Control
Oxygen
400-TK-040
400-FIC-0401
400-LIC-0401
400-TH-700
VSD
400-TK-60
To Filters
Sample
400-TK-050
LIC-0501
Acid
400-FIC-0504
Ratio Control
400-FIC-0505
Spent
400-FIC-0501
Water
400-FIC-501
Steam
400-TV-2005
400-LIC-2003
400-LCV-2003
FI
400-FI-3003
400-TK-70
Product

Figure 37: Simplified schematic representation of the pressure leach process at Lonmin, with basic control loops and stream numbers indicated

There are 8 control valves available for compositional regulatory or supervisory control. Note that these are the valves that remain to serve as MVs after the variable pairing in chapter 4 has been done. They pertain to the following flows:

Table 41: List of variables that remain to serve as MVs after MV allocations to basic regulatory control

Controller tag	Stream on diagram	Description
400-FIC-0101	m_2	Addition of spent
400-FIC-1102	m_3	Addition of formic filtrate
400-FIC-0107	m_4	Addition of pure acid
400-FIC-2001	2 of $m_{10} – m_{12}$	Oxygen feed ratio's
400-FIC-0504	m_{20}	Addition of pure acid
400-FIC-0505	m_{18}	Addition of spent
400-FIC-0501	m_{19}	Addition of water

There are several possible ways in which these possible MVs can be paired with CVs in the regulatory and supervisory control levels. The first step in determining the best pairings is investigating which variables most influence the reaction rates in the autoclave, according to the original dynamic model. More specifically, the reaction rate equations – as developed by Dorfling (2012) – are inspected, taking note of all the variables on which the reaction rates depend. The following four variables are identified as having the greatest influence on reaction rates:

- Temperature
- Acid concentration
- Oxygen concentration
- Pressure

Noting that the pressure in the autoclave directly influences the oxygen dissolution, and that the pressure is controlled by sparging oxygen into the autoclave, these four factors can be roughly summarised into three terms: temperature, acid concentration and pressure. These factors are supported by Dorfling (2012), who found that temperature and pressure are the factors with the most significant influence on PGM leaching, while the acid concentration and temperature have the most significant influence on copper leaching.

Keeping in mind the fact that a PGM grade of 65% needs to be maintained at the end of the pressure leach, while the copper in the second and third stage leach residues need to be 18 - 25 wt% and below 3.5 wt%, respectively, it would be advisable that the mentioned variables should serve as CVs of the regulatory control layer. Other important variables to consider for this purpose are the density of the pulp added into the autoclave (representing the solids fraction) and the ratio in which oxygen is fed into the autoclave. Note that the set points of all these identified CVs should not automatically be viewed as the MVs for a supervisory control level. While the set points of autoclave pressure, temperature and acid concentration are affirmed by literature to be suitable as MVs to supervisory control the pressure leach, it has been found that variations in the density have a much less significant influence on the leaching of copper and PGMs than the temperature and acid concentration (Dorfling, Akdogan, Bradshaw, & Eksteen, Kinetics of Rh, Ru, and Ir dissolution during the sulfuric acid pressure leaching of first stage leach residue, 2012). It is therefore appropriate to keep the density (or solids fraction) in the mixing tanks within suitable ranges, instead of serving as MVs for supervisory control.

Since temperatures and the autoclave pressure are already controlled in the basic regulatory control level, only the remaining CVs need to be controlled by the compositional regulatory control level. The following table summarises the CVs and MVs that have been identified for use in this control level. Note that the variables are not yet paired and that the table represents two adjacent lists.

Table 42: Lists of proposed manipulated & controlled variables for the advanced regulatory control level

MVs	CVs
m_2	Density in 2nd Stage Leach
m_3	Acid Concentration in 2nd Stage
m_4	Density in 3rd Stage Leach
m_{20}	Acid Concentration in 3rd Stage
m_{18}	
m_{19}	

5.4.2 Introduction to Compositional Control in 400-TK-10 & 400-TK-20

Introduction

The purpose of 400-TK-10 (called the second stage slurry preparation tank) is to prepare slurry for the autoclave – ensuring that it has the correct properties for the next leaching step. As mentioned, the composition in 400-TK-10 is currently controlled mainly by adjusting the flow rates of the added copper spent electrolyte, formic filtrate and acid to reach a certain set point in *% spent* and *% solids*. This is done with a cascade control system which is not well understood and frequently overridden by the process operator. However, from process data it can be seen that – under typical operating conditions – the ratio between the flow rates of the spent and formic filtrate, and that of stream one, are kept constant. The values of these ratios are changed by the process operator in order to keep acid concentrations and densities within allowable ranges.

It should be noted that, even when the acid concentration and density of 400-TK-10 are within its desired ranges, the large flow rate of the flash recycle stream (which is typically more than twice that of the feed from 400-TK-10) necessitates the addition of pure acid to 400-TK-20. This means that, even though the contents of stream 5 has the correct acid concentration and density, its properties are severely altered as it is mixed with the flash recycle stream. The contents of the stream entering the autoclave's first compartment would therefore typically have an acid concentration that is too low, were additional acid not added.

However, it has been stated by Lonmin that the addition of this pure acid stream to 400-TK-20 is undesirable and should be avoided, if possible (Steenekamp & Mrubata, Control and Specifications of the BMR, 2013).

Proposed Design

In the light of the effect of the flash recycle stream on the acid concentration and density, it can be deduced that set point (SP) values or desired ranges for the acid concentration and density need to be set for 400-TK-20, and not 400-TK-10, as is currently being done. This would ensure that the effect of the flash recycle stream is taken into account. Since the pure acid addition to 400-TK-20 is undesirable, it means that the acid concentration and density of 400-TK-20 should be controlled via the streams added to 400-TK-10. This would give rise to a cascade control structure, as can be seen in the following diagram:

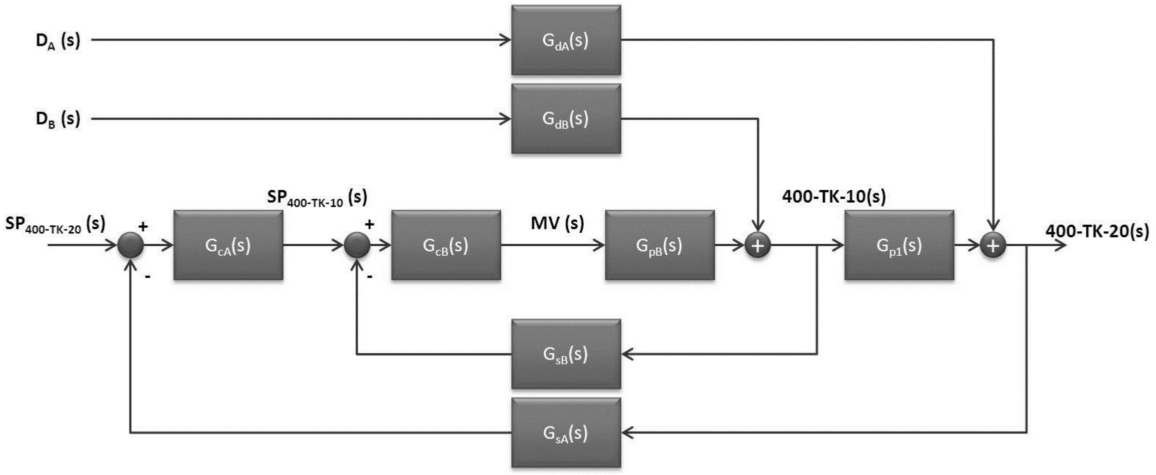

Figure 38: Diagrammatic representation of a cascade control structure that can be applied to the control of acid concentration and density for the second stage leach.

Here it can be seen that a SP value for the acid concentration or density in 400-TK-20 is entered – either by a supervisory control system or by a process operator – and that a primary controller translates this into a corresponding SP for 400-TK-10. The secondary controller then makes an appropriate MV change. Note that this system should remove the need for a pure acid stream into 400-TK-20, as per comments made by Lonmin personnel (Steenekamp & Mrubata, Control and Specifications of the BMR, 2013). The formal design of such a cascade system will be done in the next section.

It should now be noted that there are 3 CVs around 400-TK-10: the tank's mass/level and its contents' acid concentration and solids fraction. Moreover, there are four streams that enter 400-TK-10, all of which can serve as MVs. This means that the control problem around 400-TK-10 has non-zero degrees of freedom. Moreover, the three identified CVs cannot be controlled in isolation – meaning that individual pairings cannot be made for some of the identified variables. These two mentioned factors mean that a SISO control approach (such as ordinary PID control) would not be an appropriate control strategy around 400-TK-10. A more advanced, multivariable control method is required, and will be investigated in the next section.

5.5 COMPOSITIONAL CONTROL ON 400-TK-10

5.5.1 Preliminary MV Allocation

As mentioned, the compositional control around 400-TK-10 consists of the following MVs and CVs:

Table 43: List of the controlled and manipulated variables for around 400-TK-10

CVs	MVs
Mass in 400-TK-10	400-FIC-0106 (stream 1)
Acid concentration in 400-TK-10	400-FIC-0101 (stream 2)
Solids fraction in 400-TK-10	400-FIC-1102 (stream 3)
	400-FIC-0107 (stream 4)

While the mass control of 400-TK-10 forms part of basic regulatory control, which was done in chapter 4, it is returned to in this section, since its MV (the flow rate of stream 1) has an influence on the compositional control of this section.

It can be seen in Table 43 that the flow rates of four streams need to be manipulated in such a way that the contents of 400-TK-10 has the correct acid concentration, solids fraction and that it does not overflow or run dry. While the mass in the tank can be easily controlled by means of flow rate manipulation, it is clear that the other two CVs are interdependent and cannot simply be assigned different flow rates as SISO MVs. The characteristics of the respective MV streams are important.

In order to control the solids fraction in the tank, a change in the assigned MV would have to be able to bring about a change in the tank's solids contents. The solids fractions of each of the 4 streams (during the simulations used for the control developments in this section) are given below.

Table 44: Solids fractions for each of the streams entering 400-TK-10

Stream Number	Solids Fraction (%)
1	38.47
2	0
3	0
4	0

It can be seen here that stream 1 is the only stream entering 400-TK-10 that contains solids. Increasing the flow rate of stream 1 would increase the solids fraction in the tank, while increasing the flow rate of either or all of streams 2 to 4 would decrease the solids fraction. From this it can be deduced that changing the ratio between stream 1 and the sum of the rest of the streams would lead to a corresponding change in the solids fraction of 400-TK-10. This finding will be returned to.

Since the acid concentration is defined as the mass of acid divided by the volume of liquid, acid concentration can be controlled by manipulating the acid concentration of the liquid entering the tank. The acid concentrations of each of the four streams are given below.

Table 45: Acid concentrations of each of the streams entering 400-TK-10

Stream Number	[Acid] (g/L)
1	31.488
2	84
3	0
4	1835.5

The liquid component of stream 1 is a mixture of spent and water, and stream 4 is pure sulphuric acid. Since stream 1 has already been identified as key to the control of the solids fraction in 400-TK-10, streams 2 to 4 are left to manipulate the acid concentration. The addition of spent (via stream 2) is the main liquid addition to 400-TK-10 on the plant, while streams 3 and 4 are added in smaller quantities (or not at all). From the acid concentrations in provided in the above table, it can be seen that – in a manner similar to the ratio's between stream 1 and stream 2-4 influencing the solids fraction of 400-TK-10 – the ratio between streams 3 and 2 (with no pure acid added) would lead to a decrease in the tank's acid concentration. The opposite would be the case if the ratio between streams 4 and 2 were to be increased, with no formic filtrate added.

5.5.2 Proposed Design

With the control principles mentioned above for each of the three CVs around 400-TK-10, the next challenge is to incorporate these interdependent control practices into a working strategy. To summarise the above section, the following should apply to such a strategy:

- The mass in 400-TK-10 should be controlled by one or more of the entering flow rates.
- The solids fraction in the tank should be controlled by the relationship/ratio between stream 1 and one or more of the other streams.
- The acid concentration should be controlled by changing the ratio between streams 3 and 2, or 4 and 2.

Taking these points into account, it is recommended that the total flow rate into 400-TK-10 (the sum of streams 1 to 4) is used as MV to control the mass in the tank. This method ensures that the mass control does not interfere with the compositional control by introducing changes in the ratios between flow rates. The is further recommended that the solids fraction in the tank is controlled by using the ratio between the flow rates of stream 1 and the sum of streams 2 to 4 as MV. While stream 1 contains water and spent, along with the solids, of which the ratios could change – a properly tuned

PID controller would be able to be robust enough to cope with such changes. The last recommendation then is to control the acid concentration by using the ratio between streams 3 and 2 (with stream 4 at zero) and between streams 4 and 2 (with stream 3 zero). The acid controller proposed is a split-range controller, which first has to be formally evaluated and designed.

5.5.3 Split-range Control Design Criteria

Marlin (2000) notes that, in order for a split-range controller to be implemented, the following criteria should be met:

1. The should be one CV and more than one MV
2. The should be a causal relationship between each MV and the CV
3. The proper order of adjusting the MV should adhere to a fixed priority ranking

It is clear and has been established that points 1 and 2 are indeed met. Point 3 refers to the design of the split-range controller, and will be met by the manner in which it operates. In the case that it operates with a fixed ranking, the problem is suitable for the application of split-range control.

5.5.4 MV Definitions

The four MVs used to control the mass of 400-TK-10, as well as the acid concentration and solids fraction in this tank, are defined below.

$$\dot{m}_{in} = \dot{m}_1 + \dot{m}_2 + \dot{m}_3 + \dot{m}_4 \tag{53}$$

$$Ratio_{\frac{m1}{liquids}} = \frac{\dot{m}_1}{\dot{m}_2 + \dot{m}_3 + \dot{m}_4} \tag{54}$$

$$\mathrm{Ratio}_{\frac{\mathrm{m3}}{\mathrm{m2}}} = \frac{\dot{m}_3}{\dot{m}_2} \tag{55}$$

$$\mathrm{Ratio}_{\frac{\mathrm{m4}}{\mathrm{m2}}} = \frac{\dot{m}_4}{\dot{m}_2} \tag{56}$$

In these equations m denotes the mass flow rate of a stream, while the ratios are self-evident. From the controller outputs these four MVs are translated into the flow rates of streams 1 to 4.

5.5.5 Pairing & Controllability Evaluation by RGA

Gain Matrix & RGA

With the MVs and CVs of the compositional control level defined, the preliminary pairing done for compositional control thus far can be evaluated by means of the method introduced in section 4.2.5. This entails the development of a transfer matrix, which is found to be the following:

Table 46: Transfer matrix determined for the compositional control on 400-TK-10.

CVs (400-TK-10) → MVs	Tank mass	Acid concentration	Solids fraction
m_{in}	$\frac{1}{s}$	0	0
$\frac{m_1}{\sum m_{2-4}}$	0	$\frac{-6.926}{1.763s+1}$	$\frac{-1.064}{1.715s+1}$
$\frac{m_3}{m_2}$	0	$\frac{-32.075}{1.711s+1}$	0

The first of these variables (top-left) is determined from the differential equation of the mass in 400-TK-10 as follows:

$$\frac{dm_{TK10}}{dt} = \dot{m}_{in} - \dot{m}_5$$ [57]

$$\frac{m_{TK10}(s)}{\dot{m}_{in}(s)} = \frac{1}{s}$$ [58]

The other transfer functions (including the zeros) are determined in Appendix G2. Note that the ratio between streams 3 and 2 are chosen (and not the ratio between streams 4 and 2), since the initial conditions are the time of tuning is done with a zero flow rate for stream 4. By equation 4.x the RGA is determined to be the following:

Table 47: RGA determined for the compositional control on 400-TK-10.

CVs (400-TK-10) → MVs	Tank mass	Acid concentration	Solids fraction
m_{in}	1	0	0
$\frac{m_1}{\sum m_{2-4}}$	0	0	1
$\frac{m_3}{m_2}$	0	1	0

The first fact to take note of is that an invertible transfer matrix – as with a gain matrix – shows that a process (or subsystem, in this case) is controllable. It can also be seen that the pairings recommended in this section are affirmed by the RGA. From the transfer matrix it can be seen that the MV of the solids controller influences the acid concentration.

5.5.6 Mass Controller Tuning

The PI mass controller of 400-TK-10, with the sum of the entering flow rates as MV, is tuned in the same manner as that of the mass controllers in the base case model of chapter 4. The maximum percentage variations in flow rate and in tank mass are kept the same as that of 400-TK-10 in the base case model, with the coefficients of variance of data values used. The only change is that the mean flow rate is the total entering mass flow rate instead of the mass flow rate of stream 1 only. This results in a K_c value of 4.5415 kg/h per kg and an integral time of 0.3702 hours.

5.5.7 Solids Fraction Controller Initial Tuning

A SISO PI controller is used for the control of the solids fraction in 400-TK-10. Since the MV for this controller is the is the ratio between the mass flow rate of stream 1 and the other three streams, the MV's initial value in the model is set to the value of this ratio at the calculated steady state. The PI controller has the same structure as those used in the base case model of chapter 4, with anti-reset windup.

In order to tune the model, a process reaction curve is generated. With all control on the model switched off, the MV is stepped and the response in the solids fraction is noted. The resulting plots are given in Appendix G2.1. The result is a K_c value of 11.52 and an integral time of 0.402 hours.

5.5.7 Split-Range Acid Controller Tuning

The tuning of the acid controller is more complex than that of the solids controller. First, the effect of each MV on the acid concentration in 400-TK-10 is evaluated. This is done by treating the split-range control as two PI controllers, with each one tuned in the same manner as that of the solids fraction controller. The resulting plots are shown in Appendix G2.2. The resulting tuning parameters are shown below:

Table 48: Tuning parameters for the two components of the acid concentration split range controller

MV	K_c	T_I (h)
Ratio between m_3 & m_2	-0.0578	0.45
Ratio between m_4 & m_2	0.0033	0.40

From this table it can be seen that the gains of the two acid controller components have opposite signs. It should be emphasised that these controller components are mutually exclusive and therefore do not execute simultaneously.

A split-range controller has only one set of tuning parameters, which means that the two controllers presented above have to be incorporated into one controller. Noting that the integral times are very similar, and that one controller gain can be multiplied to give the other one, the following is proposed:

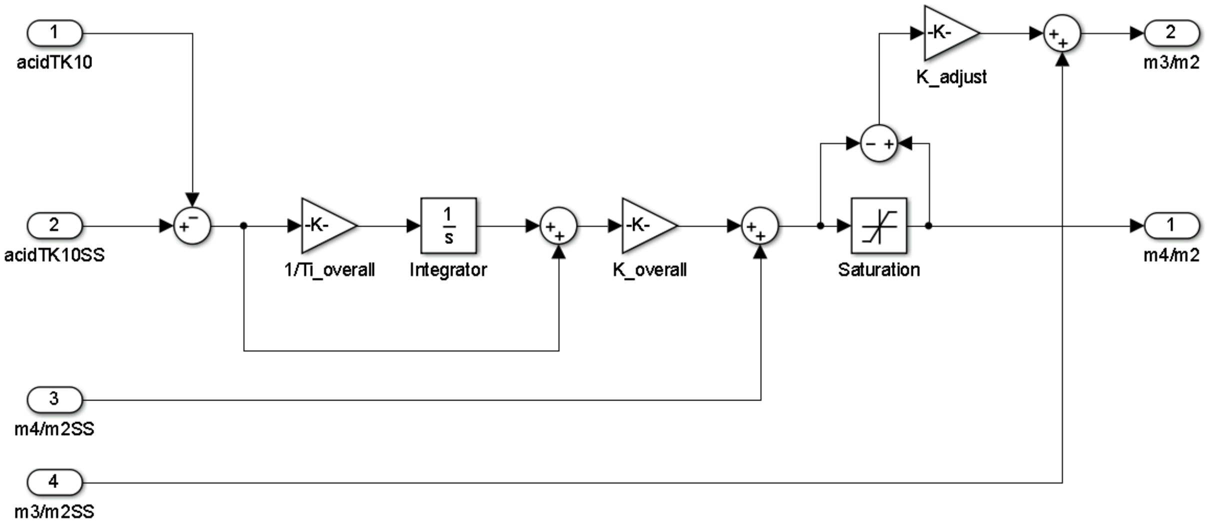

Figure 39: Block diagram of the proposed split-range controller used for the control of acid in 400-TK-10. It is a snap shot of the simulation in Simulink.

One of the MVs is used as the first-approach in what the design criteria call a fixed priority ranking. This is chosen to be the ratio between the mass flow rates of streams 4 and 2. The controller gain and the smaller of the integral times are used. In the figure above, these are called the *overall* terms. The output of this part of the controller goes through a saturation block, which limits it to a positive value. If the initial controller output is smaller than zero, its absolute value is sent to be multiplied by an adjustment gain, which is the quotient of the two determined gain values. Since any controller output leads to an appropriate MV change, there are no bounds on the MVs. The single split-range controller output therefore determines which ratio has to be non-zero and what its value should be. A consequence of this is that no anti-reset windup is necessary for this controller.

5.5.8 Removal of Stream 23

One important remark made by Lonmin at the start of this project was that the addition of pure acid to 400-TK-20 should ideally be removed.

In order to test whether the recommended compositional control can provide satisfactory control without sulphuric acid addition to 400-TK-20, a version of the process model is created where this pure acid addition does not take place. In order to achieve such a process model, the input data were changed by setting the flow rate of this acid stream to zero, while the additive streams to 400-TK-10 were adapted to still reach a similar steady-state acid concentration in 400-TK-20. More specifically, the volumetric flow rates of streams 2, 3 and 4 were changed from 3600, 900 and 0 L/h to 4382.6, 0 and 10 L/h, respectively – changing the ratios between streams 4 and 2, and 3 and 2 from 0.25 and 0 to 0 and 0.0023, respectively. This adaption changed the steady-state acid concentration in 400-TK-20 from 22.9245 g/L to 23.4454 g/L, which is similar.

5.5.9 Controller Fine Tuning

The transfer matrix in section 5.5.5 showed that there the MV of solids control influences the acid concentration. This, along with other possible interactions, necessitates that fine-tuning should be done under closed-loop conditions. This is done by making a step change in the set point of the controller being evaluated. The results for this procedure are given in Appendix G2.3. The resulting tuning constants are given below:

Table 49: Tuning parameters for all basic regulatory control loops, with controller gains before and after fine-tuning

CV in 400-TK-10	Old K_c	New K_c	Old T_I (h)	New T_I (h)
Acid concentration (pure acid)	0.0034	0.187	0.41	0.451
Acid concentration (formic)	-0.0468	-2.573	0.41	0.451
Solids fraction	14.1	21150	0.409	0.136

It can be seen that the all the controllers are made more aggressive by the fine-tuning. The most possible reason for this is the fact that, during the initial changes, it could be seen that both the acid concentration and solids fraction in 400-TK-10 take approximately 10 hours to reach a new steady state after a step change has been made. Fine-tuning these controllers to reach new set point values within 1 hour required that the initial MV should be more than 50 times that of the steady-state change. This is contrasted with the recommended factor of 0.5 to 1.5 recommended by Marlin (2000) for fine-tuning. The initial tuning parameters therefore did not lead to rapid enough performance, requiring the fine-tuning stage to make it much more aggressive.

5.6 CASCADE CONTROL ON 400-TK-20 & 400-TK-10

5.6.1 Desirability & Design Criteria

The purpose of designing the compositional control around 400-TK-10 is to be able to control the composition of the contents that enter the autoclave (that is the contents of 400-TK-20). This means that the respective set points of the acid concentration and solids fraction in 400-TK-20 should be translated by some means into corresponding set points for 400-TK-10. This is typically done by means of cascade control.

According to Marlin (2000) cascade control is desired when single-loop control does not lead to control performance that is satisfactory, and when a measured secondary variable is available. The first statement is valid, due to the fact that the usage of stream 23 is undesirable, while the second statement is also true – with the acid concentration and solids fraction (inferred from a measured density) being measured.

Marlin (2000) however further states three criteria which must be satisfied by the secondary variable(s) to be useful for cascade control. The first of these is that it must indicate the occurrence of an important disturbance. Since the new contents entering 400-TK-20 via stream 5 all come from 400-TK-10, meaning that the first criterion is satisfied. The second is that there must be a causal relationship between the MV and the secondary controlled variable. It has been demonstrated that the acid concentration and solids fraction can be controlled by the MV flow rates. Lastly, the dynamics of the secondary variable must be faster than that of the primary variable. That is indeed the case, since the time it will take for adjustments in the MV flow rates to lead to a change in the composition of 400-TK-20 includes the time it will take to change that of 400-TK-10. All the criteria are therefore met.

5.6.2 Cascade Controller Tuning

The secondary (or inner) control loops for the acid and solids control are those designed and tuned in the previous section. The set points of these control loops become the MVs for the corresponding controllers on 400-TK-20. These outer loops are added into the model as PI controllers of the same structure as has been used in this section 4.3, without the inclusion of saturation or anti-reset windup.

The standard procedure for tuning a cascade controller is to first tune the secondary loop and then, with only the secondary loop closed, tune the primary loop (Marlin, 2000). With the secondary loops already tuned, only the compositional controllers of 400-TK-20 are left to be tuned. This is done by making step changes in the MV of the primary controllers (which are the set points of the 400-TK-10 compositional controllers), generating plots of the CV responses and tuning it accordingly by means of the Ciancone tuning correlations (Marlin, 2000). While these “outer MVs” do not make an exact step change, it approximates it to a reasonable extent. The resulting plots are shown in Appendix

G2.4 and G2.5. The results of fine-tuning, done in accordance with the information given in section 4.2.4, are also shown in this Appendix. The tuning parameters for the acid concentration and solids fraction controllers for 400-TK-20 are shown below:

Table 50: Tuning parameters for the primary cascade compositional controllers.

Control in 400-TK-20	**K_c**	**T_I**
Acid concentration	12.12	0.5265
Solids fraction	1.558	1.298

The block diagrams developed in this section are given below:

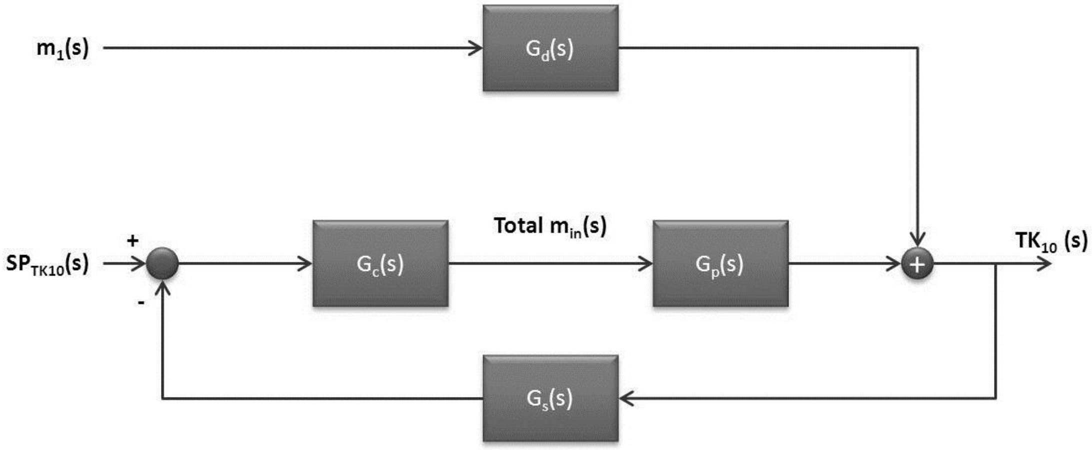
$m_1(s)$
$G_d(s)$
Total $m_{in}(s)$
$SP_{TK10}(s)$
+
-
$G_c(s)$
$G_p(s)$
TK_{10} (s)
$G_s(s)$

Figure 40: Block diagram of the proposed mass control structure for 400-TK-10

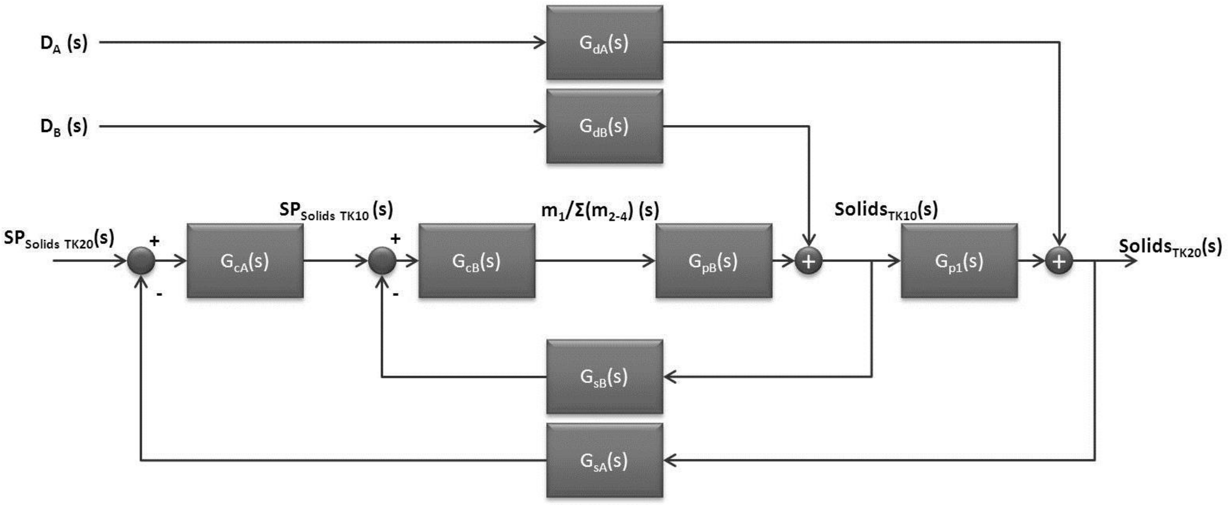
D_A (s)
$G_{dA}(s)$
D_B (s)
$G_{dB}(s)$
$SP_{Solids\ TK10}$ (s)
$m_1/\Sigma(m_{2\text{-}4})$ (s)
$Solids_{TK10}(s)$
$SP_{Solids\ TK20}(s)$
+
-
$G_{cA}(s)$
+
-
$G_{cB}(s)$
$G_{pB}(s)$
$G_{p1}(s)$
$Solids_{TK20}(s)$
$G_{sB}(s)$
$G_{sA}(s)$

Figure 41: Block diagram of the proposed solids fraction cascade control structure for the second stage leach. A and B refer to the primary and secondary loops, respectively.

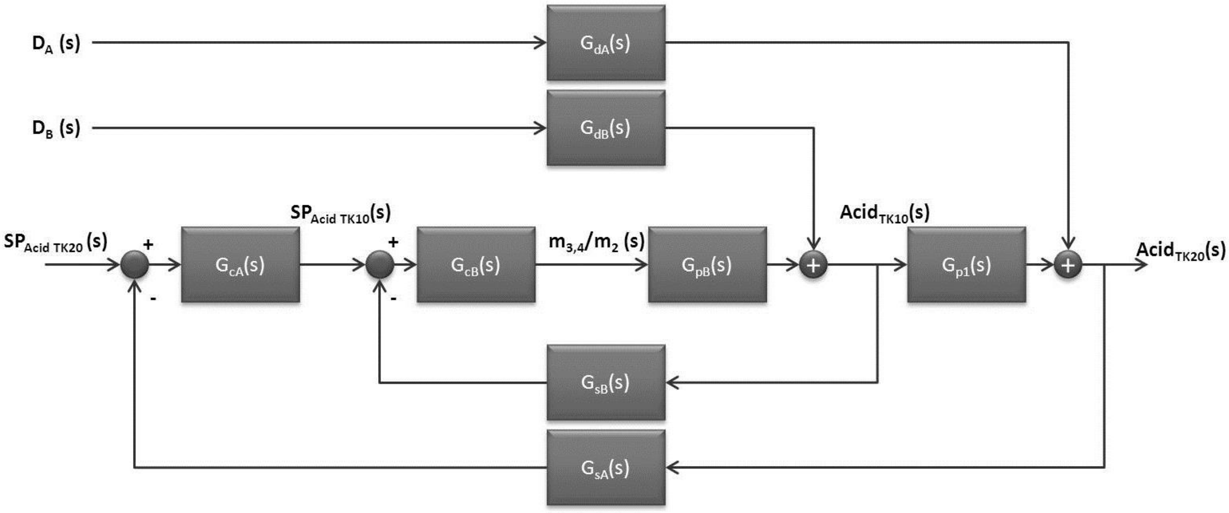
D_A (s)
D_B (s)
$G_{dA}(s)$
$G_{dB}(s)$
$SP_{Acid\ TK20}$ (s)
+
-
$G_{cA}(s)$
$SP_{Acid\ TK10}(s)$
+
-
$G_{cB}(s)$
$m_{3,4}/m_2$ (s)
$G_{pB}(s)$
+
$Acid_{TK10}(s)$
$G_{p1}(s)$
+
$Acid_{TK20}(s)$
$G_{sB}(s)$
$G_{sA}(s)$

Figure 42: Block diagram of the proposed acid concentration cascade control structure for the second stage leach. A and B refer to the primary and secondary loops, respectively.

The flow rates of streams 1 to 4 into 400-TK-10 are calculated from the respective MVs of these control loops. The exact manner in which the split-range controller switches between streams 3 and 4 has been displayed in a separate block diagram.

5.7 COMPOSITIONAL CONTROL EVALUATION

5.7.1 Disturbance Rejection: Procedure

In order to evaluate the proposed control, typical plant disturbances need to be imposed on the system. These disturbances are identified as being the solids fraction and acid concentration in stream 1, the flow rate of the flash recycle stream and the acid concentration in the copper spent electrolyte. The first and last of these change continuously on the plant, so they are chosen to be approximated by sine waves. The wavelength of the solids fraction is chosen to be 1 hour, since that is something that should not change very quickly. The wavelength of the acid concentration in copper spent is chosen to be 15 minutes. The amplitude of the solids fraction wave is set to 2% of the mean value, since this is the standard deviation of the 400-TK-10 density measurements in the data. The amplitude of the acid concentration is taken to be the same, for the lack of other guidelines. The acid concentration in stream 1 is controlled roughly by the addition of spent to the tank preceding 400-TK-10, and therefore it is added in the form a step up and down. This is done by multiplying the flow rate of the water accompanying the solids by 1.1 over a certain time period. Finally, the set point of the temperature of compartment 1 is increased by a factor of 1% and decreased again. The total evaluation procedure is given below:

- At time step 0, multiply the set point of the temperature of compartment 1 with 1.01, until 1 hour is reached. The temperature controller increases the flow rate of the flash recycle stream.
- At 1 hour, multiply the flow rate of the water into the tank preceding 400-TK-20 with 1.1, until 1.7 hours are reached. This decreases the solids fraction and the acid concentration in stream 1.
- At 2 hours start adding the described sine wave to the solids entering via stream 1, until the end of the simulation.
- At 2.5 hours start adding a sine wave to the acid concentration in copper spent electrolyte, until the end of the simulation.

5.7.2 Disturbance Rejection: Evaluation

The structural base case and developed compositional control models are evaluated. The following table summarises the quantitative measures, after which a number of plots are included for discussion.

Table 51: Qualitative comparative measures for the rejection of disturbances

CV	Comparative Measure	Base Case	Cascade System
Acid Concentration (400-TK-20)	Maximum Deviation	0.56%	0.80%
	Normalised IAE	0.0042	0.0094
	SS Offset	No	No
Solids Fraction (400-TK-20)	Maximum Deviation	1.64%	1.08%
	Normalised IAE	0.038	0.0225
	SS Offset	Unsure	Unsure
Tank mass (400-TK-20)	Maximum Deviation	0.0053%	0.0023%
	Normalised IAE	7.487e-5	7.65e-5
	SS Offset	Yes	Yes
Temperature (Compartment 1)	Maximum Deviation	1%	1%
	Normalised IAE	0.0023	0.0022
	SS Offset	No	No

The contents of this table are discussed below. Note that a more complete set of plots are given in Appendix H1.

The first and most important of these is the plot of the acid concentration in 400-TK-20. Note that all IAE and maximum deviation values are given as it was after 6 hours.

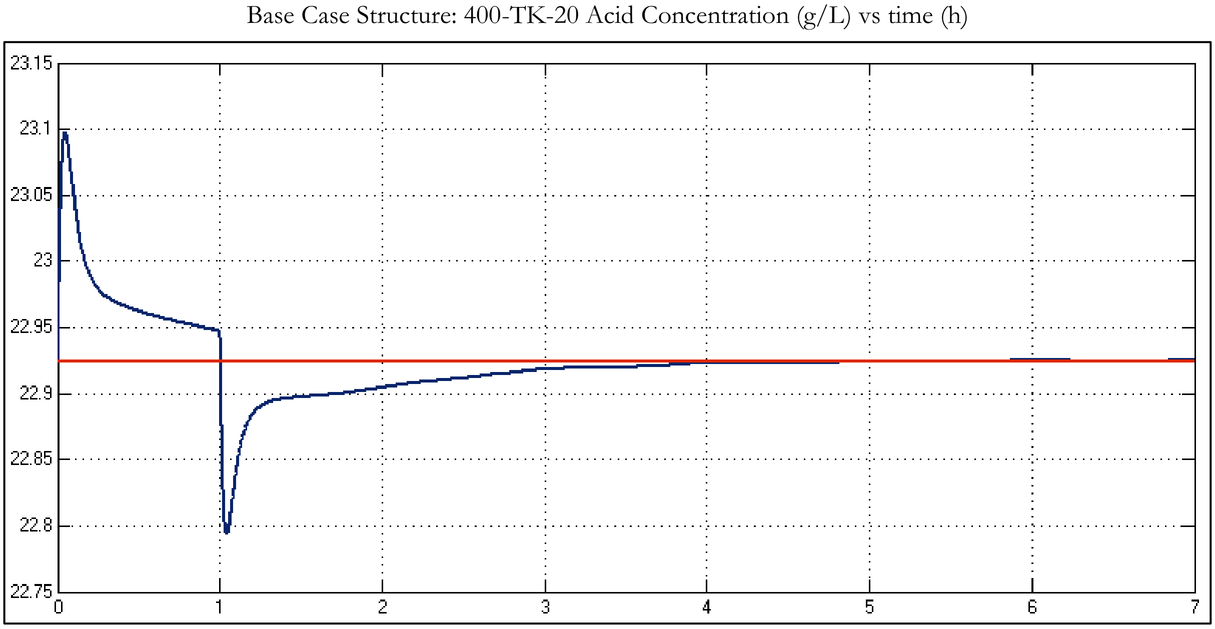

Figure 43: Plot of the set point (red) and measured (blue) base case acid concentration values for 400-TK-20 (g/L), versus time (hours). IAE = 0.0042, Maximum deviation = 0.56%. No steady-state offset.

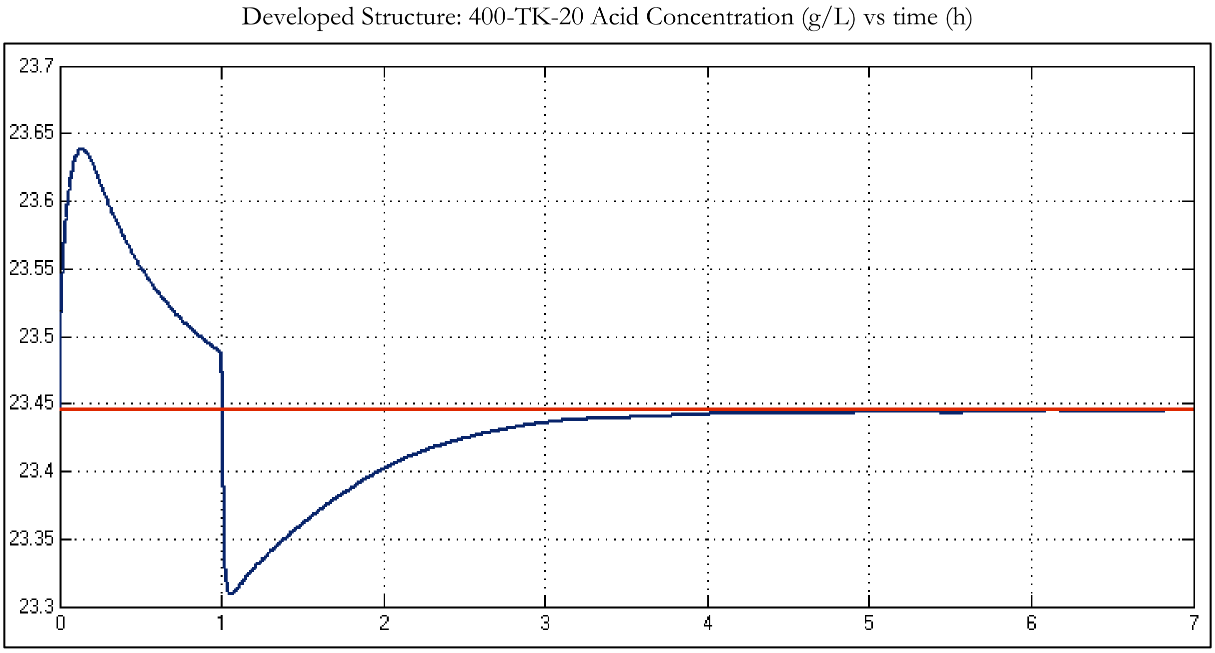

Figure 44: Plot of the set point (red) and measured (blue) developed model's acid concentration values for 400-TK-20 (g/L), versus time (hours). IAE = 0.0094, Maximum deviation = 0.80%. No steady-state offset.

From these plots it's clear that the newly developed structure reacts significantly slower. This can be attributed to the fact that the set point of the acid concentration in 400-TK-10 is not tracked perfectly, resulting in the direct acid control of the base case performing better. Except for this difference, however, the control looks similar, with neither having an offset at its new steady state. The aim of the compositional controller is not only to maintain the acid concentration set point values, but also that of the solids fraction. This is shown for 400-TK-20 below:

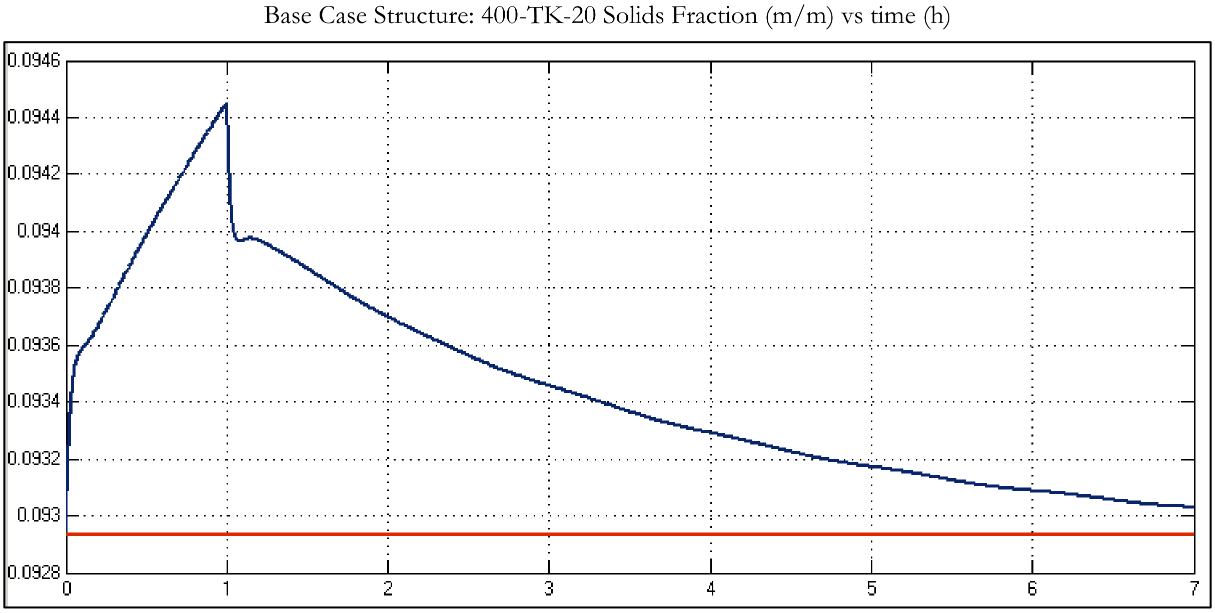

Figure 45: Plot of the set point (red) and measured (blue) base case solids fraction values for 400-TK-20, versus time (hours). IAE = 0.038, Maximum deviation = 1.64%.

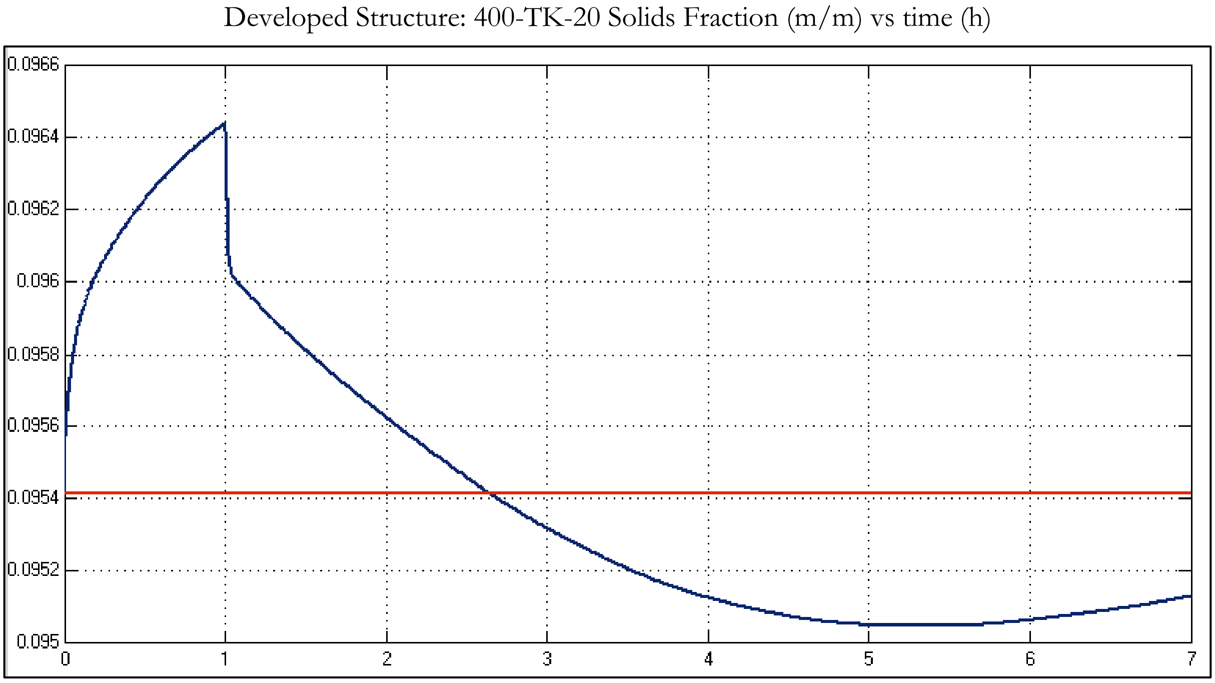

Figure 46: Plot of the set point (red) and measured (blue) developed model's solids fraction values for 400-TK-20, versus time (hours). IAE = 0.0225, Maximum deviation = 1.08%.

The solids fraction values display a similar trend. In contrast with the acid concentration values, the developed structure is an improvement on the base case, with the IAE and maximum deviation values being 40.8% and 34.1% lower in the cascade control structure. Since no allowable solids fraction ranges are provided by Lonmin, it is not possible to comment on the sufficiency of the performance of either of the cases. However, it is important to notice the possible play-off between the acid and solids control that arises. The base case structure has no direct solids control (as is the case on the real plant), so it is expected that it should perform worse.

Except for acid concentration and solids fraction, the structural difference has a potential effect on the mass control of 400-TK-20. These values are compared next:

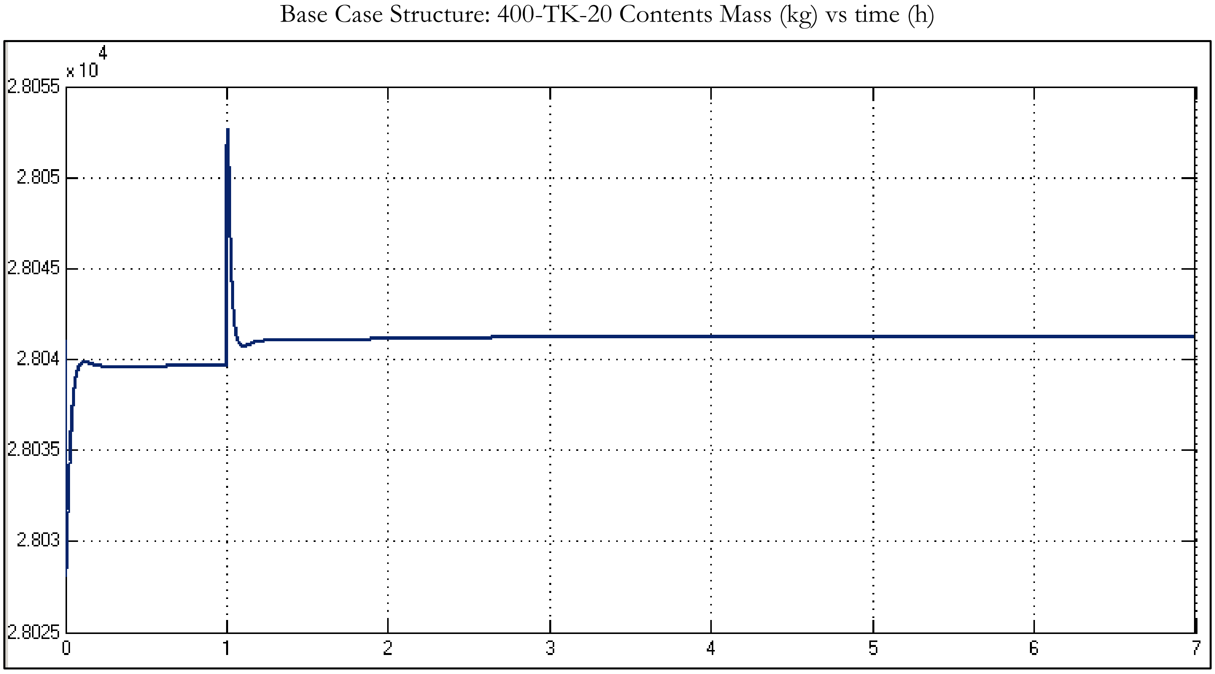

Figure 47: Plot of the base case model's mass of the contents of 400-TK-20 (kg), versus time (hours). IAE = 7.487e-5, Maximum deviation = 0.0053%.

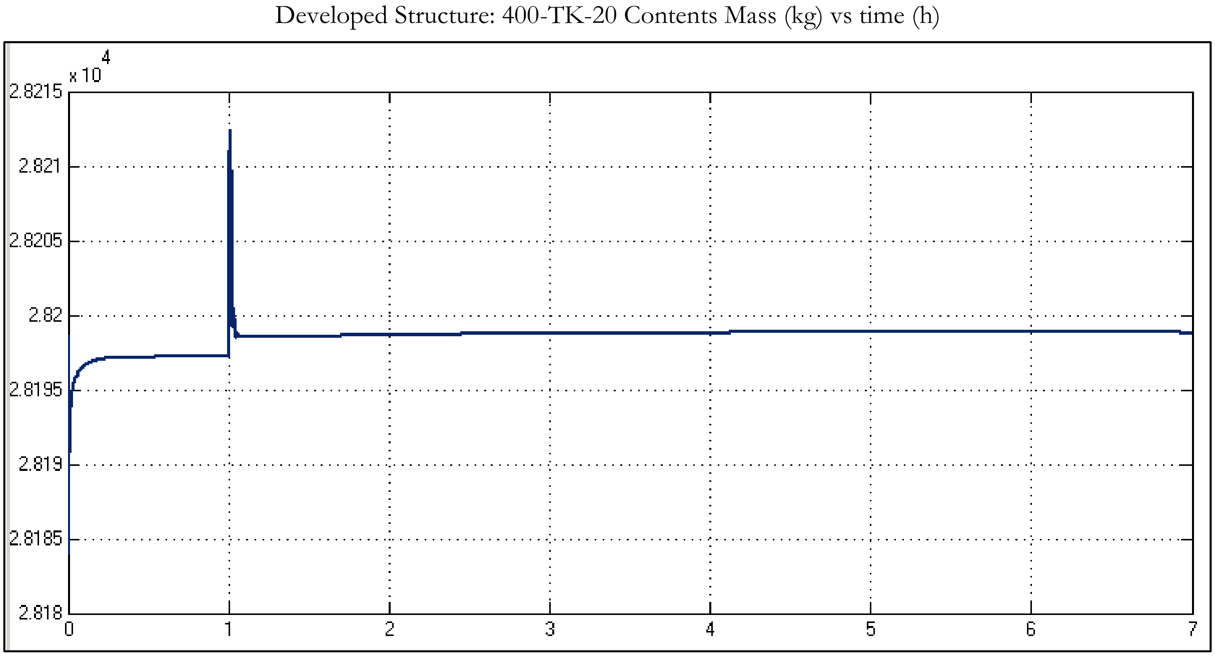

Figure 48: Plot of the developed model's mass of the contents of 400-TK-20 (kg), versus time (hours). IAE = 7.65e-5, Maximum deviation = 0.0023%

It can be seen that the mass in 400-TK-20 has a similar shape for both control structures. The developed control structure, however, leads to a 2% increase in the IAE and a 56.6% decrease in the maximum deviation, respectively. It can therefore be said that there is not a clear winner in this case.

While the developed control structure leads to a better control of solids fraction, it performs worse in terms of acid concentration control. These factors need to be weighed in some manner in order to be able to comment on the total success of the control methods. Such a factor is chosen to be the temperature of the first compartment, since it is indicative of the reactions taking place in the compartment, as well as the flow rates (in and out) influencing it.

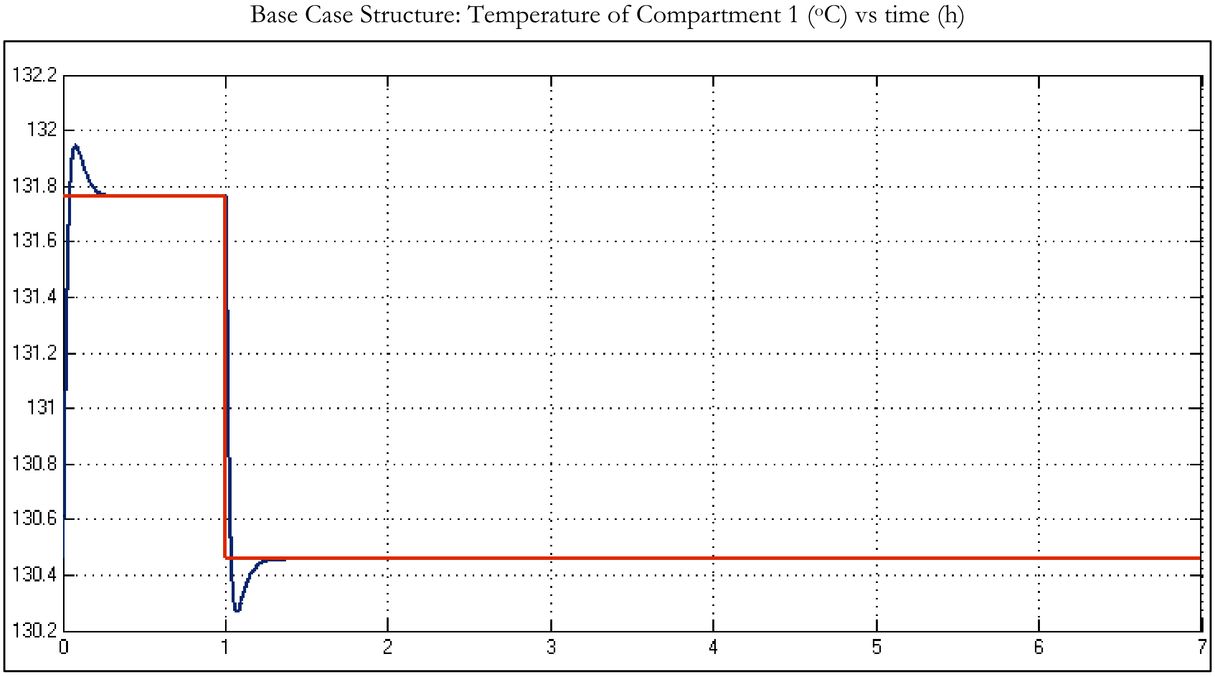

Figure 49: Plot of the developed model's temperature of compartment 1 (°C) versus time (hours). IAE = 0.0023, Maximum deviation = 1%. No steady-state offset.

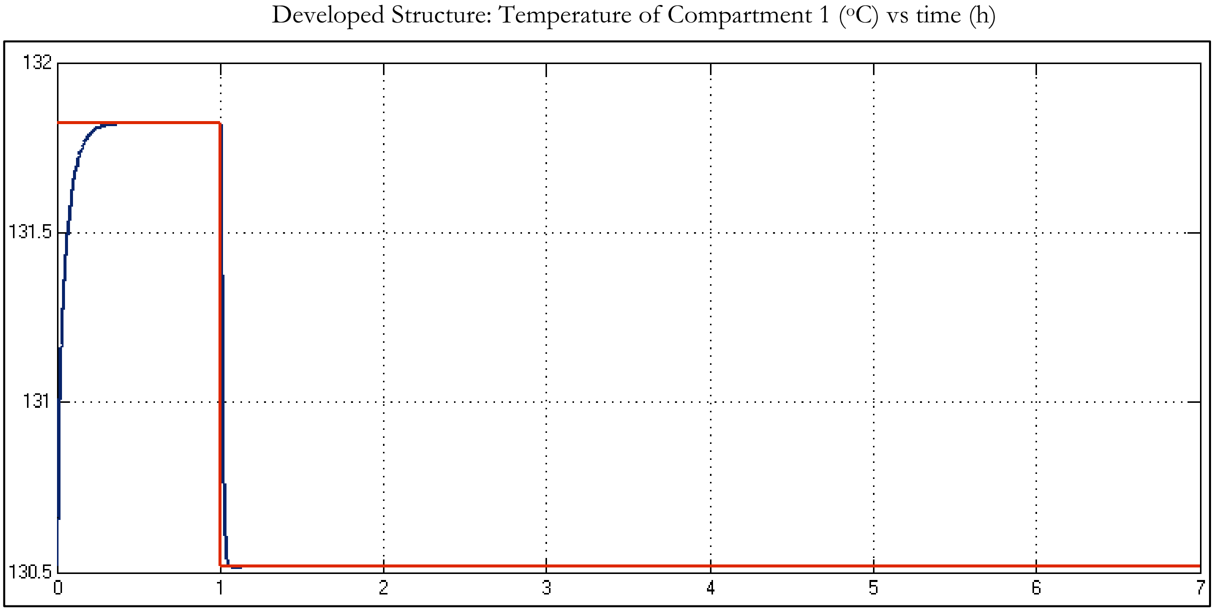

Figure 50: Plot of the developed model's temperature of compartment 1 (°C) versus time (hours). IAE = 0.0022, Maximum deviation = 1%. No steady-state offset.

From these plots it can be seen that the identically tuned temperature controller performs more aggressively in the base case than in the cascade system. This can be explained by the fact that both the solids fractions and the acid concentration would have an influence on the reactions, and therefore on the temperature. Considering the IAE and maximum deviation values it can be concluded that another parameter needs to be chosen for the purpose of an overall comparison of disturbance rejection.

In spite of the fact that the model validation step has deemed the prediction of leaching results to be insufficiently accurate for the use in this project, the copper leaching can be a good indicator of the state of the process (Burchell, 2014). The copper dissolution in the second leaching stage for the two runs is therefore compared next:

Base Case Structure: % Copper Dissolution in 2nd Stage Leach vs time (h)

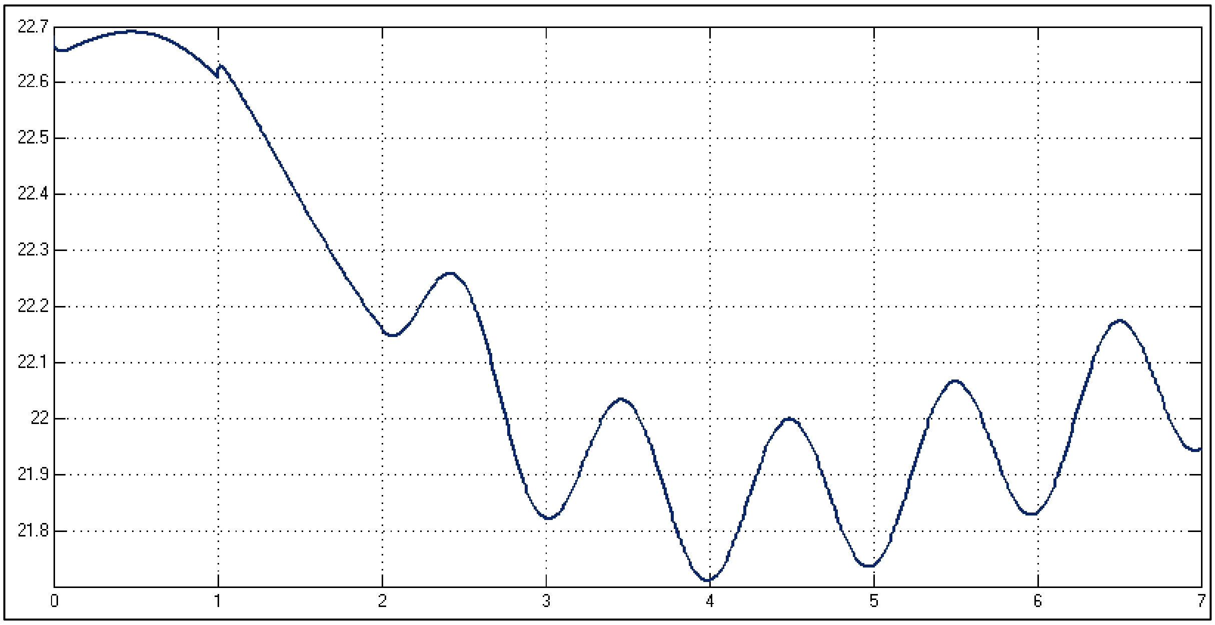

Figure 51: Plot of the percentage of the solid copper leached in the second stage leach in the base case model versus time (hours). Maximum deviation =4.3%

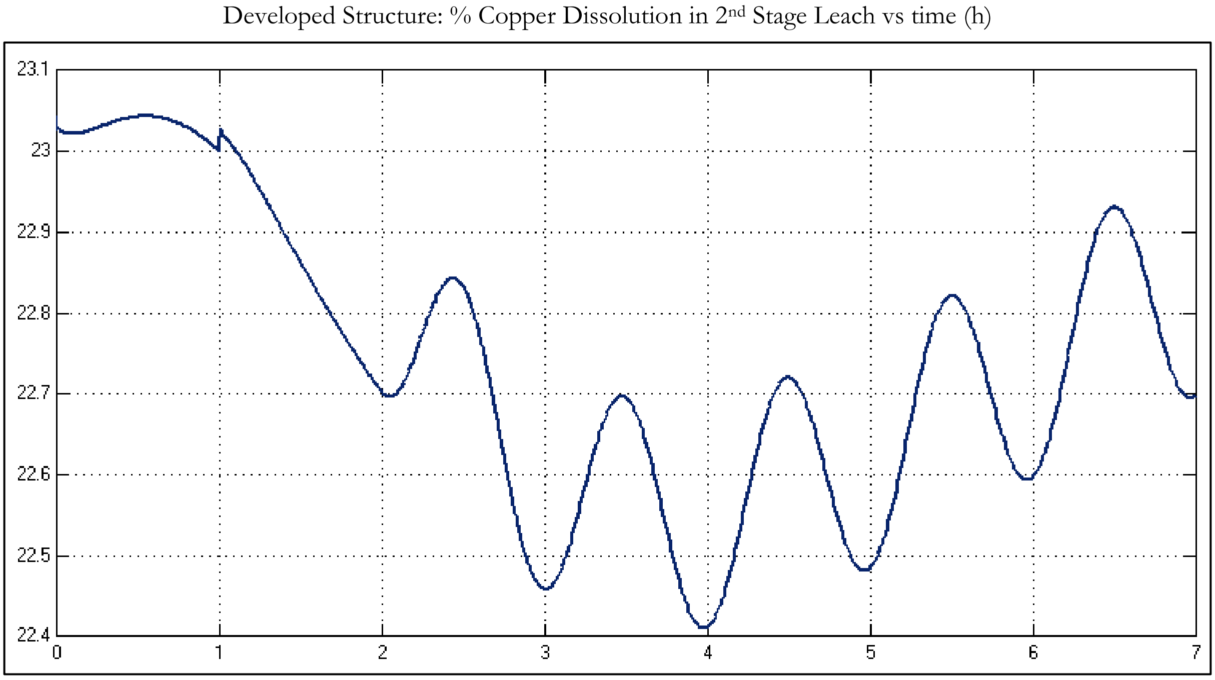

Figure 52: Plot of the percentage of the solid copper leached in the second stage leach in the newly developed model versus time (hours). Maximum deviation =2.75%

From these plots it can be seen that the maximum deviation from the steady-state (initial) value is 36% lower in the newer control than in the base case, showing that the effect of the added disturbances on the process performance is better rejected in the cascade control system.

From the two control methods' ability to reject disturbances, the newer control proves to be more effective – in spite of the fact that it does not control the acid concentration in 400-TK-20 as well as the base case structure. Before drawing final conclusions, the ability of the two control methods to track the acid concentration's set point is also evaluated.

5.7.3 Set Point Tracking: Procedure

The set point of the acid concentration in 400-TK-20 is constantly changed in response to the leaching performance of the second stage leach. This is currently done by the process operators, but can also be done by a supervisory control system. It is therefore important that a compositional control system should not only be able to reject disturbances, but also track acid concentration set points – while not disturbing inventories, temperatures and the solids fraction to a large extent.

The initial, steady-state values of each of the control structures are multiplied by a sequence of factors which results in set points that could typically be sent to the acid controllers. For an initial value of between 22 and 24, these factors results in values that correlate well with the acid concentration data in 400-TK-20. This sequence of factors is shown below:

Table 52: Set point values sent to the acid concentration controller for 400-TK-20 (g/L) and its time ranges.

Time range (h)	Multiplication Factor
0-1	1
1-1.5	1.02
1.5-2	1.04
2-3	1
3-3.5	0.98
3.5-4	0.96
4-4.5	1

The values in Table 52 result in step change lengths varying between 30 minutes and an hour, and a maximum change of 40% in both directions are tested for in 20% steps.

5.7.4 Set Point Tracking: Evaluation

The same two control structures are evaluated in this section as in the previous one. The following table summarises the quantitative parameters, while a discussion of key plots follows.

Table 53: Quantitative comparative measures for responses to acid concentration set point tracking.

CV	Comparative Measure	Base Case	Cascade System
Acid Concentration (400-TK-20)	Maximum Deviation	4%	4.2%
	Normalised IAE	0.0284	0.0513
	SS Offset	No	Unsure
Solids Fraction (400-TK-20)	Maximum Deviation	0.55%	0.46%
	Normalised IAE	0.0103	0.007
	SS Offset	Unsure	Unsure
Tank mass (400-TK-20)	Maximum Deviation	0.0022%	0.0022%
	Normalised IAE	3.54e-5	3.13e-5
	SS Offset	Unsure	Unsure
Temperature (Compartment 1)	Maximum Deviation	0.006%	0.001%
	Normalised IAE	1.171e-4	3.096e-5
	SS Offset	Unsure	Unsure

Note that a more complete set of plots given in Appendix H2. The IAE and maximum deviation values are again given at a time of 6 hours.

The most important plots to compare in this evaluation are those of the acid concentration in 400-TK-20. These are provided below:

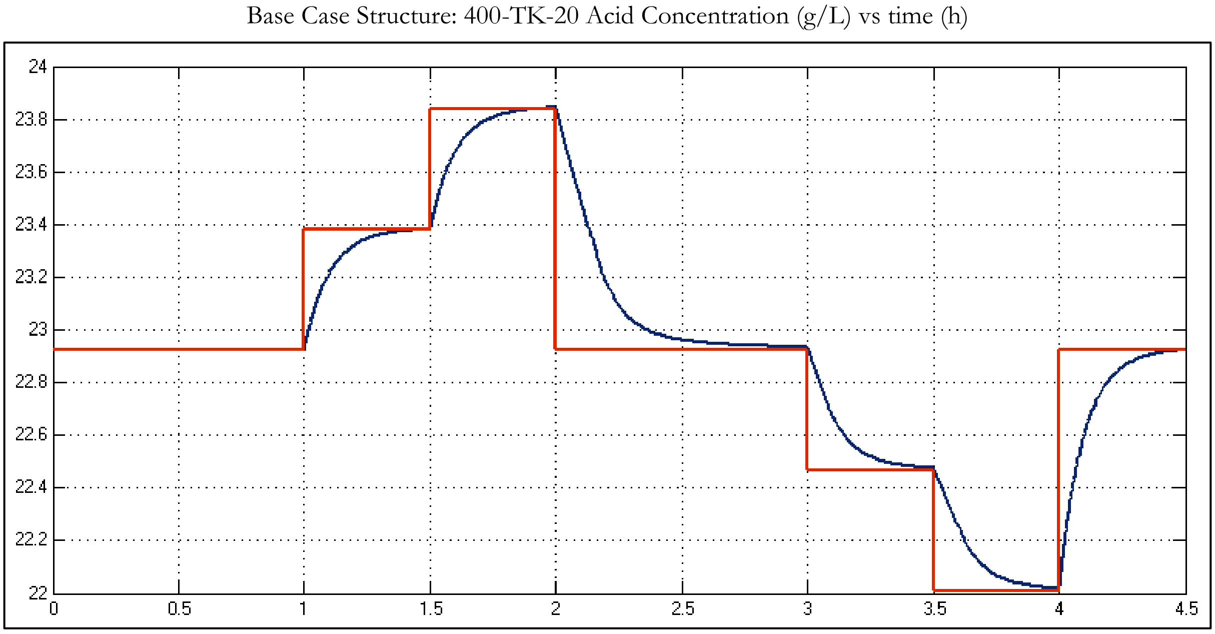

Figure 53: Plot of the set point (red) and measured (blue) base case acid concentration values for 400-TK-20 (g/L), versus time (hours). IAE = 0.0284, Maximum deviation= 4.01%.

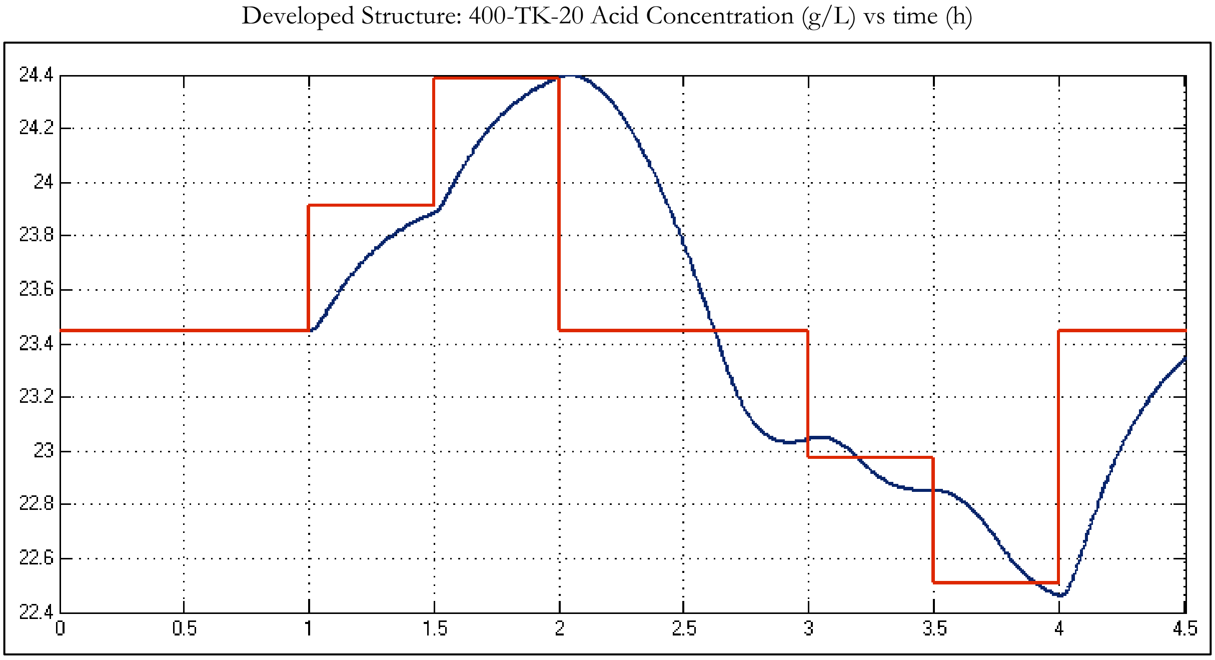

Figure 54: Plot of the set point (red) and measured (blue) developed model's acid concentration values for 400-TK-20 (g/L), versus time (hours). IAE = 0.0513, Maximum deviation = 4.2%.

From these plots it can be clearly seen how well the set point in the base case is tracked, while the same cannot be said for the cascade control structure. The reason for this, as with the disturbance rejection evaluation, is that the SP of the acid concentration in 400-TK-10 is not tracked closely enough to result in good performance in 400-TK-20. The control of the base case has no such limitations, except for the fact that the flow rate of stream 23 cannot be less than zero. The cascade system leads to IAE and maximum deviation values that are 80.6% and 4.7% higher than that of the base case, respectively. This shows that – as is the case with the control of acid concentration during disturbance rejection – the base case structure is better at tightly controlling the acid concentration in 400-TK-20.

Note that the slow change between 2 and 2.7 hours in Figure 54 is caused by the solids controller decreasing the ratio between the flow rate of streams 1 and 2 to 4. This change causes the sum of streams 2 and 3 (with stream 4 zero at this stage) to decrease, which, in turn, means that the increased ratio between streams 3 and 2 has a much smaller effect that it would have had if the sum of these flow rates were to remain the same. The solids control therefore negatively impacts the acid control. This interaction was predicted by the RGA, developed in section 5.5.5

Due to the fact that the temperature control of the base performed worse than the newer control in the previous section, the temperature responses of the first compartment are compared below:

Base Case Structure: Temperature of Compartment 1 (°C) vs time (h)

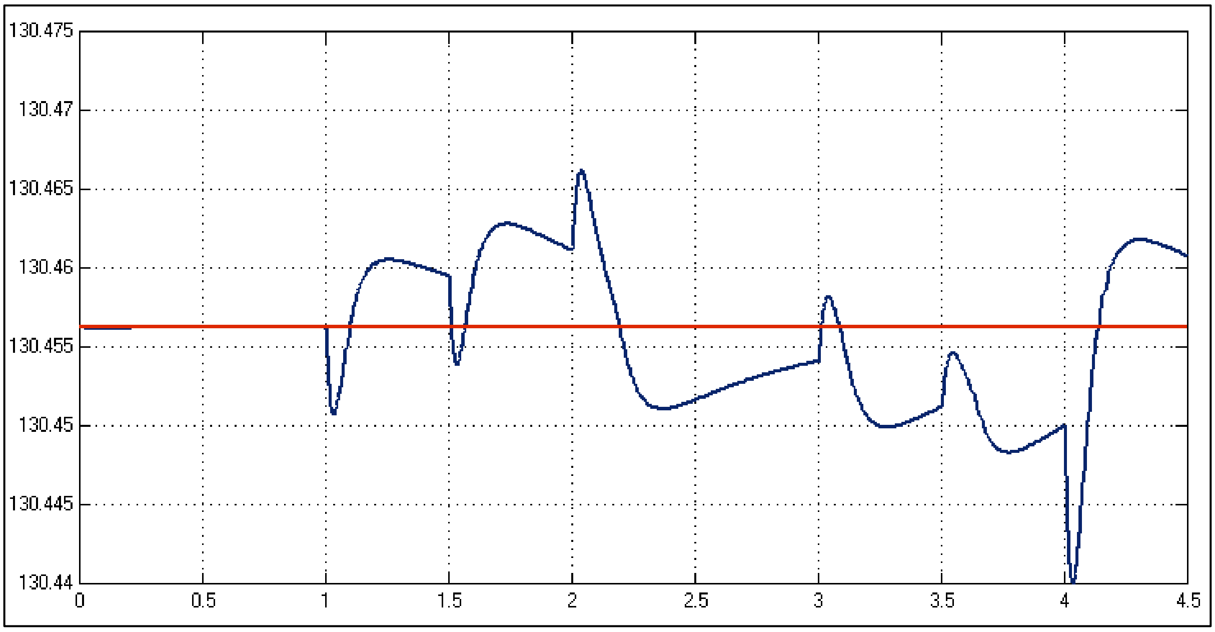

Figure 55: Plot of the set point (red) and measured (blue) values for the temperature of compartment 1 (°C) versus time (in hours). IAE = 1.171e-4, Maximum deviation= 0.006%.

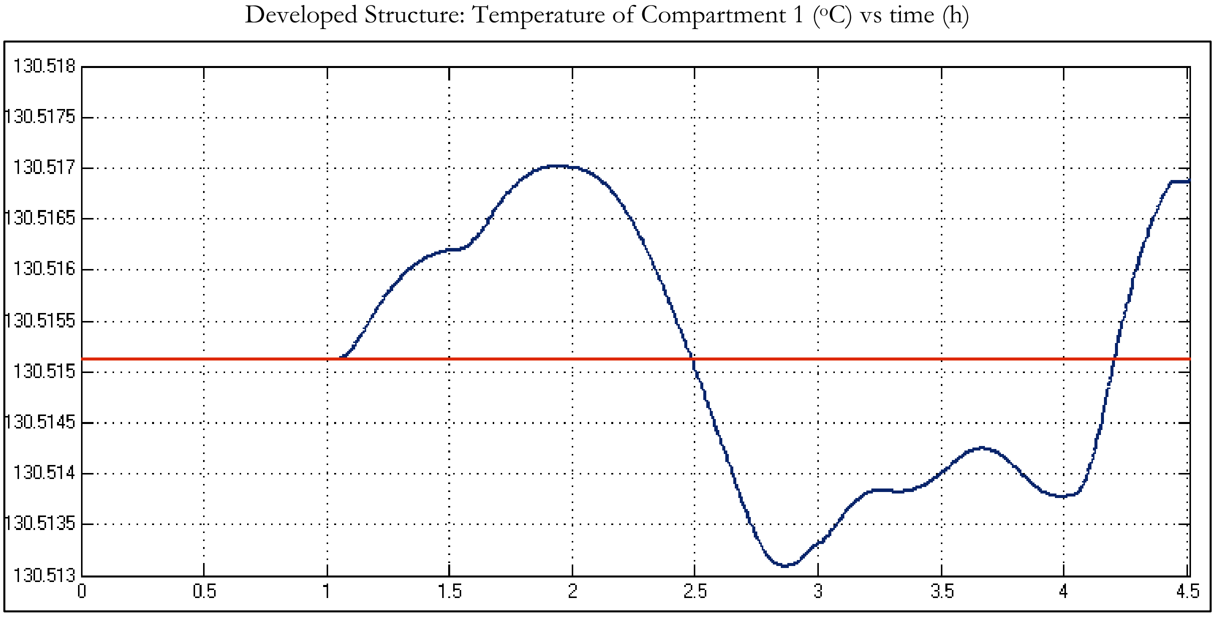

Figure 56: Plot of the set point (red) and measured (blue) values for the temperature of compartment 1 (°C) versus time (in hours). IAE = 3.096e-5, Maximum deviation= 0.001%.

As with the disturbance rejection evaluation, these plots show that the newly developed control leads to smaller temperature fluctuations. More specifically, it leads to IAE and maximum deviation values that are 73.6% and 83.3% lower than that of the base case. The shape of Figure 55 closely resembles the flow rate of stream 23, indicating that the tight control of the acid concentration in 400-TK-20 disturbs the temperature control of compartment 1. From literature it is known that the acid concentration has a significant effect on the reactions in the autoclave, which in turn influences its temperature (Dorfling, Bradshaw, & Akdogan, Characterisation and dynamic modelling of the behaviour of platinum group metals in high pressure sulphuric acid/oxygen leaching systems, 2012).

5.7.5 Second Stage Compositional Control Structure: Best Practice

The most notable finding of the previous section is that the acid concentration of in 400-TK-20 can be controlled better by manipulating a sulphuric acid stream added directly into it than by manipulating the ratio between additive streams into 400-TK-10 via cascade control. This is an expected result, since in the latter scenario the residence times of both 400-TK-10 and 400-TK-20 delay the influences of the changes on the acid concentration in 400-TK-20. The main incentive for removing the pure acid feed to 400-TK-20 is the fact that this has been mentioned by Lonmin as a desirable move. The aim of the control evaluation, therefore, was to determine whether the proposed control structure can be viewed as a means of removing stream 23, while not compromising plant performance (rather than attempting to necessarily providing overall better performance).

The direct conclusion that can be drawn from the results is that the base case structure is better at controlling the acid concentration in 400-TK-20, while the newly developed control improves the behaviour of the solids fraction in this tank and the temperature of compartment 1. A more careful examination of the results, however, reveals that the solids control impacts the acid control, which in turn influences the mentioned temperature control. The best practice for compositional control before the second stage leach can therefore not be determined before the relative importance of variations in the acid concentration, solids fraction and temperature are determined.

It is recommended that the effect of each of these parameters should be quantified using the model. Since it was found in chapter 3 that the model is its current form is not valid for research on the leaching behaviour in the autoclave, this should form part of a project where un updated model is used that has been validated for this purpose. On such a model the base case and the developed cascade system can be implemented and the response of the leaching behaviour can be quantified.

5.7.6 400-TK-050 Control Discussion

In this section only the compositional control before the second stage leach was considered, since there is not sufficient information available for the third stage (that is, for 400-TK-050). However, the findings of this section are applicable to the compositional control before the third stage.

In the variable pairings done in section 4.4 the MV for the mass control in 400-TK-050 was changed from the sum of streams 18 to 20 to stream 21. The reason for this was that this freed up streams 18 to 20 for doing compositional control.

Figure 57 shows the streams surrounding 400-TK-050 and how it forms part of the pressure leach process.

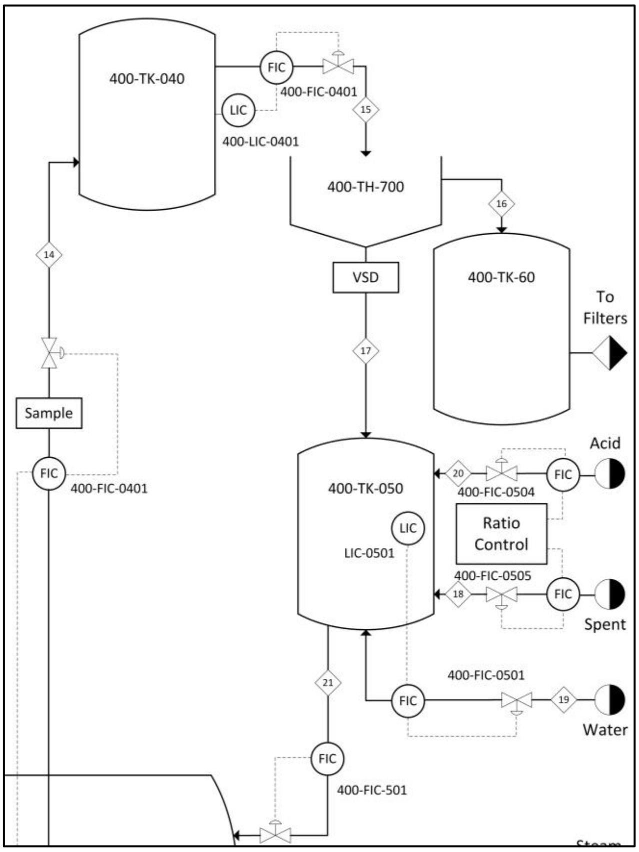
400-TK-040
FIC
400-FIC-0401
LIC
400-LIC-0401
15
400-TH-700
16
14
VSD
400-TK-60
To Filters
17
Sample
FIC
400-FIC-0401
Acid
400-TK-050
20
FIC
400-FIC-0504
LIC
LIC-0501
Ratio Control
400-FIC-0505
18
FIC
Spent
21
400-FIC-0501
FIC
19
Water
FIC
400-FIC-501

Figure 57: Diagram of the section between the second and third stage leach.

The main difference between 400-TK-050 and 400-TK-10 is the fact that the solids stream in the latter can be controlled. In 400-TK-050 the flow rate of stream 17 is determined by the solids-liquid separation (by means of a thickener or centrifuges), and it is therefore viewed as an entering disturbance. With stream 21 being used for the tank's mass control, a comparison can be drawn between streams 18 to 20 and streams 2 to 4 in 400-TK-10. This is done in Table 54:

Table 54: Comparison drawn between the additive streams of the preparation tanks for the second and third stage leach, respectively.

	400-TK-10	**400-TK-050**
Copper Spent Electrolyte	Stream 2	Stream 18
Formic Filtrate/Water	Stream 3	Stream 19
Sulphuric Acid	Stream 4	Stream 20

With this similarity in mind, the compositional control structure on 400-TK-10 can be adapted for 400-TK-050. More specifically, the mass control can be omitted from the developed compositional control, retaining only the acid concentration and solids fraction control. The ratio between the total flow rate of streams 18 to 20 and that of stream 17 can be the MV for the acid control, while the ratio among stream 18 to 20 can be manipulated (with a split range controller) in the manner that has been developed for the solids control in 400-TK-10.

5.8 SUPERVISORY CONTROL

5.8.1 Identification of Key Variables

Supervisory control forms the top level of control of a plant, and its main purpose is to ensure that the plant's main performance criteria are met. In order to design supervisory control, therefore, variables need to be identified that will best represent the plant's performance if it were to serve as CVs for top level control. It should be noted that the metal compositions in the solids phase and concentrations in the liquid phase are available only once per shift, which means that – while it best characterises the state of the process, it can't be used directly for automated control. One possible alternative is to investigate which measured variables are used as CVs by process operators to do manual supervisory control on the process.

There are four places in the process that are of critical importance to controlling the process at a supervisory level. Two of these are the mixing tanks (400-TK-10, -20 and -050), and the other two are the third and fourth compartments in the autoclave. These compartments are important since it contain the products of the second and third leaching stages, respectively.

For the mixing tanks the densities are measured, along with the concentrations of total metals and acid. The total metals values are defined as the sum of the concentrations of the base metals in the liquid phase (Burchell, 2014). In the autoclave's third and fourth compartments the reduction potential is measured, along with the concentration of copper, total metals and acid. All these measurements are said to be measured every hour (Steenekamp & Mrubata, Control and Specifications of the BMR, 2013).

Note that the readings for reduction potential, although important at the plant, are omitted in this study. The reason for this is that the inclusion of reduction potential would, by the following equation, require the reactions in the model to be more accurate than is currently the case (Boundless Chemistry, 2014):

$$E = E_0 - \frac{RT}{nF}\ln(Q) \tag{59}$$

$$E_0 = -\frac{RT}{nF}\ln\left(K_{eq}\right) = -\frac{\Delta G^0}{nF} \tag{60}$$

Here, E and E_0 refer to the cell potential and standard cell potential, respectively. R and F refer to the gas and Faraday constants, while n and ΔG^0 are the number of electrons transferred and the Gibbs energy change for a system under standard conditions, respectively. Q and K_{eq} are the reaction quotient and equilibrium constants. These equations are two different forms of the Nernst equation.

A model that is validated for the use in supervisory control – that is, a model which predicts the leaching reactions more accurately – can be used to calculate and incorporate the reduction potential. The current model is, however, not valid for this purpose.

Keeping this in mind, the main top-level CVs that remain are the concentrations of copper, total metals and acid. There are compositional data of the solids phase as well, but – as mentioned – it's is sampled once a shift (Steenekamp & Mrubata, Control and Specifications of the BMR, 2013) and is therefore not helpful in terms of the development of an automatic control system. The following table summarises measured variables that can currently be used for automated supervisory control:

Table 55: Summary of measured variables in the pressure leach process that can be used for automated supervisory control.

Mixing tanks	Autoclave compartments 3 & 4
Density	Copper concentration
Total metals concentration	Total metals concentration
Acid concentration	Acid concentration

5.8.2 CV Selection & Development

Having identified the measured variables around the most important process components, the potential of these variables as process CVs need to be discussed.

Since these variables are used by the process operators to control the process at a supervisory level, two questions arise that need to be answered for the sake of developing automatic supervisory control. The first of these is determining how the measurements are interpreted and used by the operator, and the second is which MVs are used to correct any deviations picked up from these measurements. These two questions will now be dealt with in more detail.

As mentioned previously, the products produced by the pressure leach process are drawn off from the third and fourth autoclave compartments. Due to the fact that the variables in Table 55 are the frequently measured variables that are most closely linked to the metal composition/concentrations in these tanks, they are very important as CVs for supervisory control. Of these, the acid concentration measurements are used to manipulate the amount of acid entering the autoclave (Burchell, 2014), meaning that it is currently corrected by manipulating the sulphuric acid concentration in the feed into the respective stages. The total metals concentrations are currently corrected by changing the feed rate of water or copper spent into the leaching stages (Burchell, 2014).

With more fundamental knowledge of the degree of influence the variables in Table 55 have on the system provided by Dorfling (2012), the current strategy can be reconsidered. The proposed approach is that the identified inferential supervisory control CVs are to be paired in a cascade system with the acid concentration, as well as the set points (SPs) of temperatures and the pressure. This is shown in the diagram below:

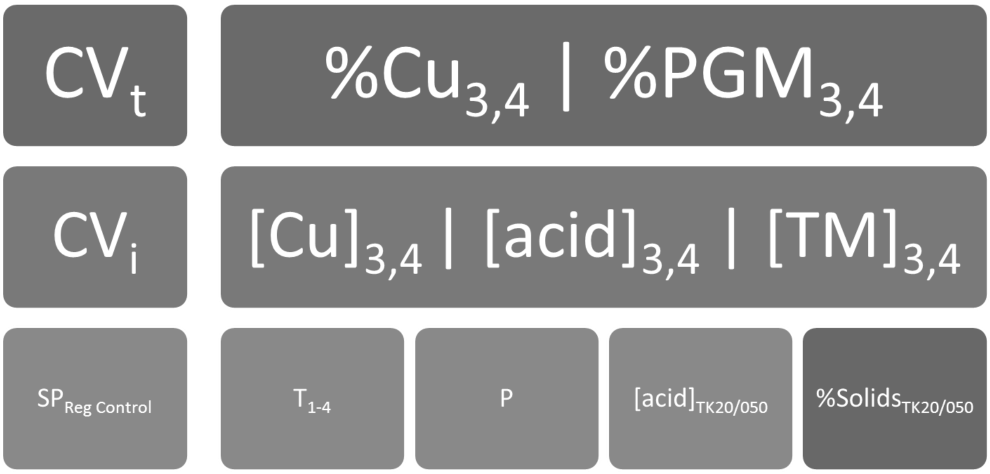

Figure 58: Diagram of the proposed supervisory control variables, showing the true and inferential CVs, along with the supervisory control MVs, which are the SPs of the regulatory control. % Solids is maintained within predefined ranges.

Here CV_t and CV_i refer to the true and inferential CVs of the supervisory control, respectively. The percentage terms refer to the solids phase, and the bracketed terms refer to the concentrations of ions in the liquid phase. Subscripts 1 to 4 refer to the autoclave compartment number and TM refers to the total metals concentration.

The total metals concentration measurements can be used to calculate an approximate of the percentage dissolution of base metals, which in turn will indicate to what extent the reactions are proceeding. The SPs of the acid concentration and solids fraction (or density) can be sent to the compositional controllers in 400-TK-20 and 400-TK-050. Along with this, the adjustments to the SPs in pressure and temperature can be sent to the relevant controllers.

The recommendations of this section are similar to those made by Khan (2009), who notes that the SPs of temperature and pressure should be set to constant values and the variation of the pulp density should be limited, leaving the SP of the acid concentration as main MV for supervisory control.

5.8.3 Recommendations for Future Work

In the chapter on model validation it has been found that the model in its current form is not yet suitable to be used for the development of supervisory control. This means that the link between the identified true supervisory CVs and the potential inferential CVs cannot be verified or quantified. It is recommended that, when the model is validated for developing supervisory control, these inferential relationships be investigated and designed. The compositional data can therefore be used to periodically reset the inferential control, in order to enable zero steady-state offsets – as mentioned in section 5.2.2.

5.9 SECTION CONCLUSIONS

Following from chapter 4, where the basic regulatory control structure has been investigated and improvements developed, in this chapter this is done for compositional regulatory control. This pertains to the control of solids fraction (which is directly linked to the density) and acid concentration of the streams that enter the second and third leaching stages, respectively.

A compositional control base case is first developed, which uses the control structure of section 4.4. Focusing on the second stage leach, due to a lack of data on the third stage, the acid stream into 400-TK-20 is added as MV for the base case control of acid concentration in this tank.

The variables remaining after the variable pairing of chapter 4 are allocated to compositional control. Streams 2 to 4 and streams 18 to 20 are identified as being available for the compositional control of 400-TK-10 and 400-TK-050, respectively.

Focussing on 400-TK-10, it is identified that streams 1 to 4 should be used to control the mass, the acid concentration and the solids fraction in this tank. The MVs for these variables are decided to be the total flow of the four streams, the ratio between stream 4 or 3 and stream 2, and the ratio between stream 1 and the sum of streams 2 to 4, respectively. The acid concentration control entails the use of a split-range controller. These pairings are affirmed by an RGA, which also showed that the identified subsystem is controllable. After the design of the compositional control on 400-TK-10, control loops are added for the acid concentration and solids fraction of 400-TK-20. This serves as the primary loop, with the corresponding control loops for 400-TK-10 being the secondary loops. Note that these primary loops are tuned while assuming that the set point of 400-TK-10 is sufficiently closely tracked to resemble a step change.

The developed compositional control is evaluated by two means: disturbance rejection and set point tracking. For the first of these, the flash recycle rate, the water and solids in stream 1 and the acid concentration of spent electrolyte are identified as disturbances. It was found that the cascade control cannot control the acid concentration in 400-TK-20 as rapidly as the base case, leading to an increase in the IAE of 124%. It does, however, lead to a smaller deviation in the solids fraction – decreasing the IAE of this parameter with 40.8%. This indicated that there is a play-off between the acid and solids control, and the relative importance of these need to be determined to determine which method is best. The copper dissolution was, however, less disturbed by the disturbances in the cascade control, with the maximum deviation being 36% lower than with the base case.

This was followed by a set point tracking evaluation, where the initial acid concentration in each case was multiplied by a sequence of factors to simulate set points received from a supervisory control system. The base case again proved better at controlling the acid concentration in 400-TK-20, with the newer structure leading to an IAE value that is 80.6% higher than the base case. It was observed that the acid control in the cascade structure was limited by the control of solids fraction, as predicted by the developed RGA. Although the temperature controller in the two cases had the same tuning parameters, the newer structure decreased its IAE by 73.6% from the base case. It is deduced that tight acid control (leading to quick acid concentration changes) disturbs the temperature of compartment 1.

It is recommended, from these evaluations, that the relative effects of acid concentration, solids fraction (or density) and temperature on leaching in the autoclave should be quantified. This should be done using an improved model, which has been proven to accurately predict the actual leaching behaviour.

Supervisory control could not be evaluated, since the model was found in chapter 3 not to be valid for this purpose. However, from literature it was found that the leaching of copper and PGMs can be inferred by the concentration of copper, acid and other base metals (cumulatively known as *total metals*) in the third and fourth autoclave compartments. A supervisory control system could aim to control these inferential variables by keeping the solids fraction at a fixed set point, while adjusting the set points of the temperatures and pressure in the autoclave, along the with the acid concentrations in the preparation tanks. The inferential links between the liquid concentrations and leaching behaviour can be determined with a model that has been validated for the development of supervisory control on it. The recommendation that the ability of the model to correctly predict the leaching on the plant should be improved in subsequent projects, is therefore emphasised.

CHAPTER 6

CONCLUSIONS & RECOMMENTATIONS

6.1 SUMMARY OF CONCLUSIONS

The conclusions from this study are divided into three sections, being conclusions from chapters 3 to 5. The conclusions of each of these sections are presented at the end of each chapter, with a summary given here.

In chapter 3 the model was migrated from its initial MATLAB platform to Simulink and it was calibrated by reconsidering initial assumptions made by Dorfling (2012). Using dynamic plant data that was acquired from Lonmin's BMR, model validation was done by importing input variables from the data into the model and comparing the outputs. Note that some of these imported variables had to be calculated to correct mass balance inconsistencies. The following was concluded in terms of the model's adequacy:

- It is suitable for the investigation and development of the structure of basic regulatory control. This pertains to the control of pressure, temperatures and inventories and is the focus of chapter 4.
- It is suitable for the investigation and development of the structure of compositional regulatory control. This concerns the control of acid concentration and solids fraction in the preparation tanks for the second and third leaching stages. It is the focus of chapter 5.
- It is not suitable for the investigation and development of supervisory control, since a model with similar inputs to the data predicts compositional results that are not within the same range as that of the data. An example of this is the copper concentration in the third compartment for which the mean of the model values is 46% lower than the corresponding data value. The leaching of copper is especially found to be under-predicted.

In chapter 4 a base case was first developed for the basic regulatory control, which aims to be a representation of the current control structure. This was set up assuming optimal tuning. Due to the fact that the vapour space of the autoclave behaves as an integrator that affects the majority of the process, it is found to be impossible to set up a relative gain array (RGA) for the purpose of reconsidering the basic regulatory control variable parings. A method proposed by Luyben and Luyben (1997) is followed instead, which leads to a set of pairings that corresponds well with Lonmin's current practice. The only difference is the control on the preparation tank for the third stage leach, which has been changed to allow for the addition of compositional control on this tank. The addition of feed-forward control to the control of the flash recycle tank yielded the following results:

- It was found that the addition of feed-forward control improves the temperature control of the first autoclave compartment. An evaluation was done where the set point of this temperature was varied up to a 1% change, and the IAE of the temperature was decreased by

7.5% from the base case. This more rapid control does not disturb the flash tank, since the tank's outflow changes rapidly in response the changes in the flash recycle rate.

- The addition of feed-forward control allows the temperature to be controlled more aggressively, since the need for the externally imposed limit of 0.95 on the ratio between the flash recycle stream and the autoclave feed is removed.

These findings confirm the hypothesis of this project.

Chapter 5 followed on from chapter 4, with the variable pairing for compositional regulatory proceeding from the pairing done for the basic regulatory control. A base case was first developed for the compositional control of the preparation for the second stage leach, which is a structure from chapter 4 to which the control of acid concentration in the flash tank, by means of the addition of sulphuric acid, was added. Note that the compositional control of the third stage leach preparation tank is not added, due to insufficient information on the flow rates and compositions of the streams surrounding this tank. The variable pairing showed that three additive streams are available for the compositional control on the preparation tanks of each of the two pressure leach stages. This compositional control refers to the control of the acid concentration and the solids fraction. Due to the fact that Lonmin indicated the addition of pure acid to the flash tank is undesirable, a control structure was developed to control the acid concentration and solids fraction in the flash tank. This was done by developing a cascade control structure, where the set points of the acid concentration and solids fraction in the second stage preparation tank serves as the manipulated variables for the control of the corresponding variables in the flash tank. The compositional control on the second stage preparation tank therefore serves as the secondary loop for the cascade control. On this tank, four streams are available for the control of the tank's mass, acid concentration and solids fraction. Pairings between manipulated variables derived from the available streams and these controlled variables were done and were affirmed by a generated RGA. Two tests were done on the developed compositional control. In the first the set point of the temperature is varied, resulting in variations in the flash recycle rate, along with the solids and liquids in the feed to the second stage preparation tank and the acid concentration in the copper spent electrolyte. This is therefore an evaluation of disturbance rejection. In the second test the set point of the acid concentration in the flash tank is varied in order to evaluate the set point tracking capability of the control. The following conclusions are made:

- The cascade control structure controls the acid concentration in the flash tank less tightly than the base case does. The former increases the IAE with 124% and 80.6% for the two tests, respectively.
- The cascade control structure decreases the variation of the solids fraction in the flash tank. Its IAE is 40.8% lower than that of the base case in the first test. It is found that the control

of the solids fraction limits the acid control and that there is therefore a potential play-off between the control of the solids fraction and acid concentration.

- The cascade control structure decreases the variation of the temperature in the first autoclave compartment, despite the fact that the temperature controllers in the two cases are identical. The newer structure leads to an IAE that is 73.6% lower than that of the base case. It is found that the tighter control of the acid concentration increases the disturbance of the temperature control of compartment 1.

6.2 RECOMMENDATIONS & FUTURE WORK

From the conclusions in this project, a number of recommendations can be made for the pressure leach process and future projects. These are listed below, with the context for the recommendations given in the conclusions section of each chapter.

The following recommendations are made in chapter 3:

- The model should be migrated to a Simulink-only platform and its structure reconsidered, since the current inclusions of MATLAB function blocks in the Simulink framework does not execute and solve for all input data combinations.
- The cause of the temperature offset between the model and data values require investigation. It can either be caused by inaccurate prediction of leaching reactions or by an inaccurate correlation between the flash recycle rate and the resulting energy loss. It is recommended that the true cause should be determined.
- The reaction kinetics of the model requires improvement, with the current reaction rate parameters not producing accurate compositional predictions. It is recommended that the derivation of these parameters from experimental test work are revised and improved.

From chapter 4 the following recommendations follow:

- The level of the preparation tank for the third stage leach (400-TK-050) should be controlled by its outflow (stream 21), instead using the additive flow rates (streams 18 to 20), as is currently the practice. The reason for this is that the new method allows for the addition of compositional control to this tank.
- The level controller on the flash recycle tank (400-TK-20) should be a feed-forward feedback controller, so that the outflow of the tank (stream 7) changes rapidly in response to changes in the flash recycle rate (stream 9).

In chapter 5 it is recommended that the relative effects of the acid concentration and solids fraction (or density) in the preparation tanks and the temperatures in the autoclave on the leaching behaviour and performance of the second stage leach need to be quantified. This should be done using a model that has proven to accurately predict leaching behaviour of the pressure leach process.

REFERENCES

AIAA. (1998). *Guide for the Verification and Validation of Computational Fluid Dynamics Simulations, American Institute of Aeronautics and Astronautics.* Reston, VA: AIAA-G-077-1998.

Barlas, Y. (1994). Model Validation in Systems Dynamics. Stirling: The 12th International Conference of the System Dynamics Society .

Bitmead, R. R., & de Callafon, R. A. (2003). Control related topics in identification - closed loop experiments and identification for control. *System Identification, I*(13), 1561-1566.

Boundless Chemistry. (2014). *Thermodynamics of Redox Reactions.* Retrieved November 24, 2014, from https://www.boundless.com/chemistry/textbooks/boundless-chemistry-textbook/electrochemistry-18/standard-reduction-potentials-129/thermodynamics-of-redox-reactions-517-3631/

Box, G. E., Jenkins, G. M., & Reinsel, G. C. (2008). *Time Series Analysis: Forecasting and Control* (4th ed.). Hoboken: John Wiley & Sons.

Burchell, J. (2014). Personal Communication: Operation specifics of Lonmin BMR.

Carey, J., van Kuiken, B., Longcore, C., & Yeung, A. (2007). MIMO Control Using RGA. Ann Arbor: Michigan University.

Cengel, Y., & Ghajar, A. (2010). *Heat and Mass Transfer* (4th SI Units ed.). Reno: McGraw Hill.

Chai, T., & Draxler, R. R. (2014). Root mean square error (RMSE) or mean absolute error (MAE) - Arguments against avoiding RMSE in the literature. *Geoscientific Model Developement*(7), 1247–1250.

ChemWiki. (2014). *Connection between Ecell, ΔG, and K.* Retrieved November 24, 2014, from http://chemwiki.ucdavis.edu/Analytical_Chemistry/Electrochemistry/Electrochemistry_and_Thermodynamics#.E2.88.86G:_Gibbs_Free_Energy

Chen, C., Kwon, J., Rice, J., Skabardonis, A., & Varaiya, P. (2002). *Detecting errors and imputing missing data for single-loop surveillance systems.* Berkeley: University of California.

Clemen, R. T., & Reilly, T. (2004). *Making Hard Decisions with Decision Tools* (3rd ed.). Boston: Cengage Learning.

Crundwell et al. (2011). *Extractive Metallurgy of Nickel, Cobalt and Platinum Group Metals.* Amsterdam: Elsevier.

Dorfling, C., Akdogan, G., Bradshaw, S. M., & Eksteen, J. J. (2010). *Determination of the relative leaching kinetics of Cu, Rh, Ru and Ir during the sulphuric acid pressure leaching of leach residue derived from Ni-Cu converter matte enriched in platinum group metals.* Stellenbosch: Elsevier.

Dorfling, C., Bradshaw, S. M., & Akdogan, G. (2012). *Characterisation and dynamic modelling of the behaviour of platinum group metals in high pressure sulphuric acid/oxygen leaching systems.* Stellenbosch: Faculty of Engineering, Stellenbosch University.

Felder, R. M., & Rousseau, R. W. (2005). *Elementary Principles of Chemical Processes* (3rd ed.). Hoboken: John Wiley & Sons.

Felder, R. M., & Rousseau, R. W. (2005). *Elementary Principles of Chemical Processes* (3rd ed.). Raleigh: John Wiley & Sons.

Findeisen, R., & Allgöwer, F. (2002). An Introduction to Nonlinear Model Predictive Control. 21st Benelux Meeting on Systems and Control.

Franklin, G. F., Powell, J. D., & Emami-Naeini, A. (2009). *Feedback Control of Dynamic Systems* (6th ed.). New Jersey: Pearson Education.

Friedman, J. H., Grosse, E., & Stuetzle, W. (1982). Multidimentional Additive Spline Approximation. *Journal of Scientific and Statistical Computing, 4*, 291-301.

Gopal, M. (2002). *Control Systems: Principles and Design* (2nd ed.). Columbus: McGraw Hill.

Gopal, M. (2009). *Digital Control and State Variable Methods* (3rd ed.). Delhi: McGraw Hill.

Haasbroek, A. L., Steyn, W. H., & Auret, L. (2013). *Advanced Control with Semi-Empirical and Data Based Modelling for Falling Film Evaporators.* Stellenbosch: Stellenbosch University.

Hillston, J. (2003). Model Validation and Verification. Edinburgh: University of Edinburgh.

Hofirek, Z., & Kerfoot, D. (1992). *The chemistry of the nickel-copper matte leach and its application to process control and optimisation.* Amsterdam: Elsevier.

Hu, W., Cai, W. J., & Xiao, G. (2010, December 7). Relative Gain Array for MIMO Processes Containing Integrators and/or Differentiators. *11th International Conference on Control, Automation, Robotics and Vision*, pp. 231-235.

Jemwa, G. T., & Aldrich, C. (2003). *Multivariate Nonlinear Time Series Analysis of Dynamic Process Systems.* Stellenbosch: Stellenbosch University.

Jolliffe, I. T. (2002). *Principal Component Analysis* (2nd ed.). New York: Springer.

Joshi, N. V., Murugan, P., & Rhinehart, R. R. (1997). Experimental Comparison of Control Strategies. *Control Engineering Practice, 5*(7), 885-896.

Khan, A. F., Spandiel, T., van Schalkwyk, T., & Rademan, J. (2009). pH advanced process control solution for Impala BMR first stage high pressure acid-oxygen leach. *Hydrometallurgy Conference 2009*. The Southern African Institute of Mining and Metallurgy.

Knoblauch, P. D., & Bradshaw, S. M. (2012). *Preliminary Implementation and Analysic of Second and Third Stage Leach*. Stellenbosch: Stellenbosch University.

Kosko, B. (1992). *Neural Networks and Fuzzy Systems* (1st ed.). Eaglewood Cliffs, NJ: Prentice-Hall International.

Ling, Y., & Mahadevan, S. (2012). *Quantitative model validation techniques: new insights*. Nashville: Vanderbilt University.

Ljung, L. (1999). *System Identification: Theory for the User* (2nd ed.). Upper S: Prentice Hall PTR.

Lonmin. (2013). Mill & Leach Logsheet. Marikana.

Luyben, M. L., & Luyben, W. L. (1997). *Essentials of Process Control* (1st ed.). Bethlehem, PA: McGraw-Hill.

Marlin, T. E. (2000). *Process Control: Designing Processes and Control Systems for Dynamic Performance* (Second ed.). Ontario: McGraw Hill.

Mathworks. (2014). *MATLAB Ordinary Differential Equations: ode15s*. Retrieved September 18, 2014, from http://www.mathworks.com/help/matlab/ref/ode15s.html

Mayne, D. Q., Rawlings, J. B., Rao, C. V., & Scokaert, P. O. (2000). Constrained Model Predictive Control: Stability abd Optimality. *Automatica, 36*, 789-814.

Mitra, P. P., & Bokil, H. (2008). *Observed Brain Dynamics* (1st ed.). Oxford: Oxford University Press.

Moler, C. B. (2004). *Numerical Computing with MATLAB* (1st ed.). Natick: Society for Industrial and Applied Mathematics.

Oberkampf, W. L., & Trucano, T. G. (2002). *Verification and Validation in Computational Fluid Dynamics*. Livermore: Sandia National Laboratories.

Olivier, M. (2012). *Induction Report: Lonmin Process Division (BMR).* Marikana: Lonmin.

Pellissippi State Community College. (2011). Expansion of Gasses. Knoxville.

Platinum Group Metals. (2009). *About Platinum*. Retrieved Junie 13, 2012, from Platinum Group Metals Home: http://www.platinumgroupmetals.net/about_platinum/

plexim. (2014). *What does it mean by "stiff" and "non-stiff" when choosing a solver?* Retrieved November 16, 2014, from http://www.plexim.com/support/solutions/158

Rebba, R., & Mahadevan, S. (2008). Computational methods for model reliability assessment. *Reliability Engineering and System Safety, 93*(8), 1197–1207.

Rhinehart, R. R., Darby, M. L., & Wade, H. L. (2011). Choosing Advanced Control. *ISA Transactions*, pp. 2-10.

Roffel, B., & Betlem, B. (2006). *Process Dynamics and Control: Modeling for Control and Prediction* (1st ed.). Chichester: John Wiley & Sons Ltd.

Sandler, S. I. (2006). *Chemical, Biochemical, and Engineering Thermodynamics* (4th ed.). John Wiley & Sons.

Sargent, R. G. (2013). Verification and Validation of Simulation Models. *Journal of Simulation, 7*(20), 12-24.

Schelsinger, S., Crosby, R. E., Cagne, R. E., Innis, G. S., Lalwani, C. S., Loch, J., et al. (1979). Terminology for model credibility. *Simulation, 32*(3), 103-104.

Schmee, J., & Opperlander, J. E. (2010). *JMP Means Business: Statistical Models for Management* (1st ed.). New York: SAS Institute.

Steenekamp, N. (2011). *Draft Operating Philosophy: Lonmin Autoclaves.* Rustenburg: Lonmin Platinum.

Steenekamp, N. (2012, August 16). The operation of the Lonmin Base Metal Refinery at Marikana. (P. D. Knoblauch, S. M. Bradshaw, & C. Dorfling, Interviewers)

Steenekamp, N., & Mrubata, Z. (2013, March 11-14). Control and Specifications of the BMR.

Visioli, A. (2006). *Practical PID Control* (1st ed.). London: Springer.

Wang, J. (2011, July). What is the Outlook for Advanced Control Engineering? *Hydrocarbon Processing*, pp. 79-84.

Zady, M. F. (2009). *Z-Stats: Mean, Standard Deviation, And Coefficient Of Variation*. Retrieved November 18, 2014, from http://www.westgard.com/lesson34.htm

APPENDIX A

CURRENT LONMIN PROCESS

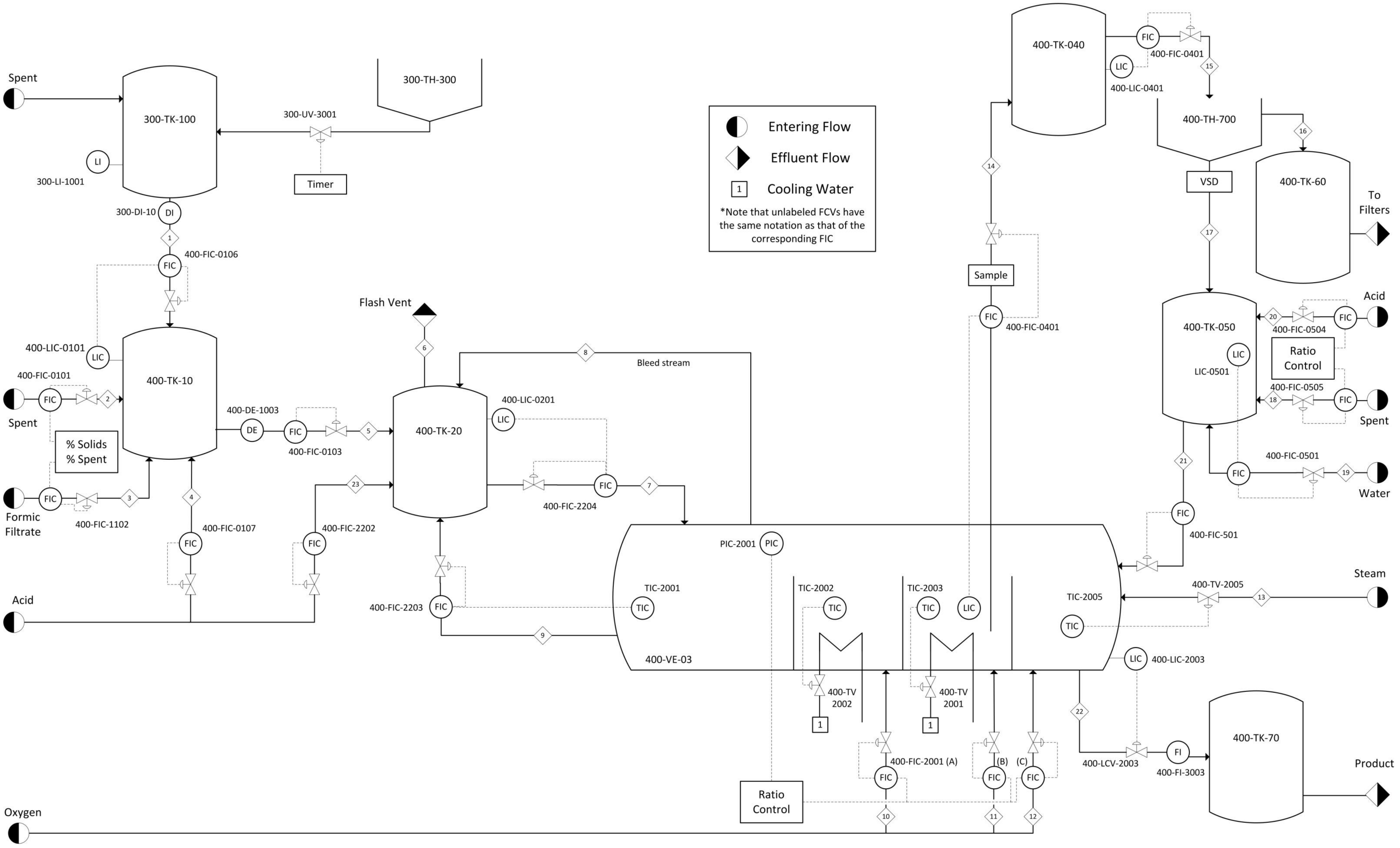
Spent
300-TK-100
300-TH-300
300-UV-3001
Timer
LI
300-LI-1001
300-DI-10
DI
1
FIC
400-FIC-0106
400-LIC-0101
LIC
400-TK-10
400-FIC-0101
FIC
2
Spent
% Solids
% Spent
FIC
3
Formic
Filtrate
400-FIC-1102
4
FIC
400-FIC-0107
Acid
400-DE-1003
DE
FIC
5
400-FIC-0103
Flash Vent
6
8
Bleed stream
400-TK-20
400-LIC-0201
LIC
23
FIC
400-FIC-2202
FIC
7
400-FIC-2204
400-FIC-2203
FIC
9
PIC-2001
PIC
TIC-2001
TIC
400-VE-03
TIC-2002
TIC
TIC-2003
TIC
LIC
400-TV
2002
400-TV
2001
1
1
FIC
400-FIC-2001 (A)
(B)
(C)
FIC
FIC
10
11
12
Ratio
Control
Oxygen
Entering Flow
Effluent Flow
1
Cooling Water
*Note that unlabeled FCVs have the same notation as that of the corresponding FIC
400-TK-040
FIC
400-FIC-0401
LIC
400-LIC-0401
15
400-TH-700
16
14
Sample
FIC
400-FIC-0401
VSD
17
400-TK-60
To
Filters
400-TK-050
LIC
LIC-0501
Acid
20
FIC
400-FIC-0504
Ratio
Control
400-FIC-0505
18
FIC
Spent
400-FIC-0501
FIC
19
Water
21
FIC
400-FIC-501
TIC-2005
TIC
Steam
400-TV-2005
13
LIC
400-LIC-2003
22
400-LCV-2003
FI
400-FI-3003
400-TK-70
Product

Figure 59: Diagram of the pressure leach process at Lonmin's BMR, as on 30 August 2013.

APPENDIX B

MODEL M-FILE ACTIONS

Calculate_steady_state_operation.m

From data

1) Composition of first stage solid residue
2) Composition of spent electrolyte
3) Component properties (densities, heat capacities, molecular weights etc.)
4) Heats of state changes (heats of reactions, heat of evaporation)
5) Stream information (flow rates, temperatures)
6) Autoclave conditions (pressure, volume, etc.)

Actions

1) Determine properties of the stream entering the flash recycle tank, stream 5
2) Calculate theoretical oxygen requirements and oxygen flow rates
3) Perform mass and energy balances for compartments 1-4
4) Calculate the flow rate constant for the slurry tanks
5) Calculate the percentage metals leached
6) Assign calculated values to function output

Calculate_autoclave_odes.m

From data (same as for calculate_steady_state_operation)

1) Composition of first stage solid residue
2) Composition of spent electrolyte
3) Component properties (densities, heat capacities, molecular weights etc.)
4) Heats of state changes (heats of reactions, heat of evaporation)
5) Stream information (flow rates, temperatures)
6) Autoclave conditions (pressure, volume, etc.)

From steady_state_conditions (flow_constants)

1) Estimate the constants to relate the outlet flow rate from a tank to the mass of slurry in the tank

Actions

1) Calculate flow rates of streams fed to second stage slurry preparation tank, TK-10
2) Calculate the flow rates of solid elemental species & liquids and dissolved species entering the second stage slurry preparation tank, TK-10, kg/h
3) Calculate the molar & mass amounts of the solid phases entering the second stage slurry preparation tank, TK-10 (NiS, Ni_3S_4, Cu_9S_5, CuS, $Fe(OH)SO_4$, Rh_2S_3, Rh, RhO_2, RuS_2, Ru, RuO_2, Ir_2S_3, Ir, IrO_2)
4) Calculate the total flow rates of liquids and dissolved species entering the third stage slurry preparation tank, TK-50, kg/h
5) Calculate the fraction oxygen in the vapour space of the autoclave
6) Estimate heat losses from respective autoclave compartments due to convection and radiation

7) Calculate the theoretical amount of oxygen required for complete dissolution of NiS and Cu9S5 in feed to process (assuming all copper present as Cu9S5 and all nickel present at NiS)
8) Calculate actual flow rates of the oxygen feed streams
9) Estimate the heat capacities of the liquid phase in the respective streams
10) Normalise mass fractions of NiS, Ni_3S_4, CuS, and Cu_9S_5 in solid phase in the respective streams
11) Estimate heat capacity of the solid portion of the respective streams
12) Calculate energy removal to cool solid & liquid portions of stream 9 to 100°C
13) Calculate total energy removal to cool stream 9 to 100°C
14) Calculate rate of water evaporation from stream 9 upon entering the flash recycle tank
15) Compartment 1-4 reaction rates and extents of reactions
16) Calculate differential equations to specify autoclave conditions as a function of time
17) Assign differential equations to function output

Calculate_dynamic_behaviour.m

From data

1) Composition of first stage solid residue
2) Composition of spent electrolyte
3) Component properties (densities, heat capacities, molecular weights etc.)
4) Heats of state changes (heats of reactions, heat of evaporation)
5) Stream information (flow rates, temperatures)
6) Autoclave conditions (pressure, volume, etc.)

From steady_state_conditions (flow_constants)

1) Estimate the constants to relate the outlet flow rate from a tank to the mass of slurry in the tank

Actions

1) Calculate flow rates of streams fed to second stage slurry preparation tank, TK-10
2) Calculate the flow rates of solid elemental species & liquids and dissolved species entering the second stage slurry preparation tank, TK-10
3) Calculate the molar & mass amounts of the solid phases entering the second stage slurry preparation tank, TK-10 (NiS, Ni_3S_4, Cu_9S_5, CuS, Fe(OH)SO_4, Rh_2S_3, Rh, RhO_2, RuS_2, Ru, RuO_2, Ir_2S_3, Ir, IrO_2)
4) Calculate the total flow rates of liquids and dissolved species entering the third stage slurry preparation tank, TK-50
5) Calculate the fraction oxygen in the vapour space of the autoclave
6) Calculate the theoretical amount of oxygen required for complete dissolution of NiS and Cu9S5 in feed to process (assuming all copper present as Cu_9S_5 and all nickel present at NiS)
7) Calculate actual flow rates of the oxygen feed streams
8) Estimate the heat capacities of the liquid phase in the respective streams

9) Normalise mass fractions of NiS, Ni_3S_4, CuS, and Cu_9S_5 in solid phase in the respective streams
10) Estimate heat capacity of the solid portion of the respective streams
11) Calculate energy removal to cool solid & liquid portions of stream 9 to 100°C
12) Calculate total energy removal to cool stream 9 to 100°C
13) Calculate rate of water evaporation from stream 9 upon entering the flash recycle tank
14) Compartment 1-4 reaction rates and extents of reactions
15) Assign calculated values to function output

APPENDIX C

PRESSURE LEACH REACTIONS

Main base metal reactions

$4NiS + 2H^+ + ½O_2 \rightarrow Ni^{2+} + Ni_3S_4 + H_2O$ [C1]

$NiS + 2O_2 \rightarrow Ni^{2+} + SO_4^{2-}$ [C2]

$2Ni_3S_4 + 2H_2O + 15O_2 \rightarrow 6Ni^{2+} + 4H^+ + 8SO_4^{2-}$ [C3]

$Cu_9S_5 + 8H^+ + 2O_2 \rightarrow 4Cu^{2+} + 5CuS + 4H_2O$ [C4]

$CuS + 2O_2 \rightarrow Cu^{2+} + SO_4^{2-}$ [C5]

$Fe(OH)SO_4 + H^+ \rightarrow Fe^{3+} + SO_4^{2-} + H_2O$ [C6]

PGM Reactions

$8Rh^{3+} + 3Cu_9S_5 + 38O_2 \rightarrow 8RhO_2 + 27Cu^{2+} + 15SO_4^{2-}$ [C7]

$2Rh^{3+} + Ni_3S_4 + 4H_2O + 8O_2 \rightarrow 2RhO_2 + 3Ni^{2+} + 8H^+ + 4SO_4^{2-}$ [C8]

$8Ru^{3+} + 3Cu_9S_5 + 38O_2 \rightarrow 8RuO_2 + 27Cu^{2+} + 15SO_4^{2-}$ [C9]

$2Ru^{3+} + Ni_3S_4 + 4H_2O + 8O_2 \rightarrow 2RuO_2 + 3Ni^{2+} + 8H^+ + 4SO_4^{2-}$ [C10]

$8Ir^{3+} + 3Cu_9S_5 + 38O_2 \rightarrow 8IrO_2 + 27Cu^{2+} + 15SO_4^{2-}$ [C11]

$2Ir^{3+} + Ni_3S_4 + 4H_2O + 8O_2 \rightarrow 2IrO_2 + 3Ni^{2+} + 8H^+ + 4SO_4^{2-}$ [C12]

$Rh_2S_3 + 6O_2 \rightarrow 2Rh^{3+} + 3SO_4^{2-}$ [C13]

$4Rh + 3O_2 + 12H^+ \rightarrow 4Rh^{3+} + 6H_2O$ [C14]

$2RhO_2 + 6H^+ \rightarrow 2Rh^{3+} + 3H_2O + 0.5O_2$ [C15]

$4RuS_2 + 2H_2O + 15O_2 \rightarrow 4Ru^{3+} + 6SO_4^{2-} + 4H^+ + 2SO_4^{2-}$ [C16]

$4Ru + 3O_2 + 12H^+ \rightarrow 4Ru^{3+} + 6H_2O$ [C17]

$2RuO_2 + 6H^+ \rightarrow 2Ru^{3+} + 3H_2O + 0.5O_2$ [C18]

$Ir_2S_3 + 6O_2 \rightarrow 2Ir^{3+} + 3SO_4^{2-}$ [C19]

$4Ir + 3O_2 + 12H^+ \rightarrow 4Ir^{3+} + 6H_2O$ [C20]

$2IrO_2 + 6H^+ \rightarrow 2Ir^{3+} + 3H_2O + 0.5O_2$ [C21]

Reaction Rate Expressions

$r_1 \;=\; k_1 \cdot [H^+] \cdot [O_2] \cdot \left(n_0^{1/f_{sh}} \cdot n^{1-1/f_{sh}}\right)_{NiS}$ [C22]

$r_2 \;=\; k_2 \cdot [O_2]^2 \cdot \left(n_0^{1/f_{sh}} \cdot n^{1-1/f_{sh}}\right)_{NiS}$ [C23]

$r_3 \;=\; k_3 \cdot [O_2] \cdot \left(n_0^{1/f_{sh}} \cdot n^{1-1/f_{sh}}\right)_{Ni_3S_4}$ [C24]

$r_4 \;=\; k_4 \cdot [H^+] \cdot [O_2]$ [C25]

$r_5 \;=\; k_5 \cdot [O_2]^2$ [C26]

$r_6 \;=\; k_6 \cdot [H^+] \cdot \left(n_0^{1/f_{sh}} \cdot n^{1-1/f_{sh}}\right)_{Fe(OH)SO_4}$ [C27]

$r_7 \;=\; k_7 \cdot [Rh^{3+}] \cdot [O_2] \cdot \left(n_0^{1/f_{sh}} \cdot n^{1-1/f_{sh}}\right)_{Cu_9S_5}$ [C28]

$$r_8 = k_8 \cdot [Rh^{3+}] \cdot [O_2] \cdot \left(n_0^{1/f_{sh}} \cdot n^{1-1/f_{sh}}\right)_{Ni_3S_4} \tag{C29}$$

$$r_9 = k_9 \cdot [Ru^{3+}] \cdot [O_2] \cdot \left(n_0^{1/f_{sh}} \cdot n^{1-1/f_{sh}}\right)_{Cu_9S_5} \tag{C30}$$

$$r_{10} = k_{10} \cdot [Ru^{3+}] \cdot [O_2] \cdot \left(n_0^{1/f_{sh}} \cdot n^{1-1/f_{sh}}\right)_{Ni_3S_4} \tag{C31}$$

$$r_{11} = k_{11} \cdot [Ir^{3+}] \cdot [O_2] \cdot \left(n_0^{1/f_{sh}} \cdot n^{1-1/f_{sh}}\right)_{Cu_9S_5} \tag{C32}$$

$$r_{12} = k_{12} \cdot [Ir^{3+}] \cdot [O_2] \cdot \left(n_0^{1/f_{sh}} \cdot n^{1-1/f_{sh}}\right)_{Ni_3S_4} \tag{C33}$$

$$r_{13} = k_{13} \cdot [O_2] \cdot \left(n_0^{1/f_{sh}} \cdot n^{1-1/f_{sh}}\right)_{Rh_2S_3} \tag{C34}$$

$$r_{14} = k_{14} \cdot [O_2] \cdot \left(n_0^{1/f_{sh}} \cdot n^{1-1/f_{sh}}\right)_{Rh} \tag{C35}$$

$$r_{15} = k_{15} \cdot \left(n_0^{1/f_{sh}} \cdot n^{1-1/f_{sh}}\right)_{RhO_2} \tag{C36}$$

$$r_{16} = k_{16} \cdot [O_2] \cdot \left(n_0^{1/f_{sh}} \cdot n^{1-1/f_{sh}}\right)_{RuS_2} \tag{C37}$$

$$r_{17} = k_{17} \cdot [O_2] \cdot \left(n_0^{1/f_{sh}} \cdot n^{1-1/f_{sh}}\right)_{Ru} \tag{C38}$$

$$r_{18} = k_{18} \cdot \left(n_0^{1/f_{sh}} \cdot n^{1-1/f_{sh}}\right)_{RuO_2} \tag{C39}$$

$$r_{19} = k_{19} \cdot [O_2] \cdot \left(n_0^{1/f_{sh}} \cdot n^{1-1/f_{sh}}\right)_{Ir_2S_3} \tag{C40}$$

$$r_{20} = k_{20} \cdot [O_2] \cdot \left(n_0^{1/f_{sh}} \cdot n^{1-1/f_{sh}}\right)_{Ir} \tag{C41}$$

$$r_{21} = k_{21} \cdot \left(n_0^{1/f_{sh}} \cdot n^{1-1/f_{sh}}\right)_{IrO_2} \tag{C42}$$

APPENDIX D

OPERATIONAL VALIDATION PLOTS

In this section, all flow rates are volumetric flow rates (in litres per hour), except for the oxygen, pure acid and steam flow rates, which are expressed in kg/h. Temperatures are in degrees Celsius and pressures in kPa absolute. Tank contents are given in terms of % full. In the data this is on a level basis and on the model it is the tank mass divided by the tank's maximum capacity.

The following table is given in chapter 3, but is repeated here to refer to.

Table 56: Variables for which a comparison is done between model and data values, with units, means and absolute error values are given, along with the ordinary and normalised root mean square error (RMSE) values and an indication of the trend match.

Tag (400-)	Stream / Tank	Unit	Mean		Standard Dev.		Error		RMSE	nRMSE	Trend match
			Data	Model	Data	Model	Min	Max			
FIC-0106	Stream 1	L/h	1143.8	2641.1	778.53	1613.4	0.403	6961.0	2674.5	40.94%	Fair
FIC-0101	Stream 2	L/h	2357.3	2357.2	1720.5	1720.5	0	80.530	2.2250	0.02%	Perfect
FIC-1102	Stream 3	L/h	2892.4	2893.3	1872.7	1872.6	0	663.61	21.235	0.22%	Perfect
LIC-0101	400-TK-10	%full	65.372	65.846	6.6322	12.311	0.0246	38.95	13.063	23.02%	Bad
FIC-0103	Stream 5	L/h	7445.2	7453.7	482.14	421.68	0	6322.3	254.19	3.40%	Perfect
FIC-2202	Stream 23	L/h	42.072	42.136	64.028	64.009	0	46.24	1.7227	0.73%	Perfect
LIC-2201	400-TK-20	%full	58.904	60.831	4.3599	8.9655	0.0024	27.395	11.799	57.37%	Bad
FIC-2204	Stream 7	L/h	28352	31355	42969	3854.8	3.0906	162530	42996	2.64%	Good
FIC-2203	Stream 9	L/h	26548	24120	3424.1	2964.7	1.8385	16720	2764.0	9.97%	Perfect
TIC-2001	Comp 1	°C	136.34	106.44	1.8437	2.2718	23.603	39.460	30.055	269.1%	Bad
TIC-2002	Comp 2	°C	141.62	124.25	1.5410	4.0681	9.029	27.133	17.824	245.4%	Bad
TIC-2003	Comp 3	°C	125.17	124.93	2.8060	3.2923	0.0033	18.697	2.980	23.01%	Good
LIC-2002	Comp 3	%full	65.241	65.367	2.1939	0.7708	0.0008	23.893	2.425	8.38%	Bad
FIC-0402	Stream 14	L/h	7954.5	7502.0	2084.9	888.47	0.9173	7123.3	2518.5	23.42%	Bad
LIC-0401	400-TK-040	%full	49.654	49.654	6.1035	1.5988	0.0139	22.823	6.329	15.23%	Bad
FIC-0401	Stream 15	L/h	7346.1	7720.3	2335.8	875.90	0.0987	7349.3	2741.6	21.53%	Bad
LIC-151	400-TK-050	%full	72.28	72.28	10.614	13.314	0.0013	44.525	20.654	39.33%	Bad
FIC-0505	Stream 18	L/h	1095.2	932.13	48.181	42.910	48.401	180.99	164.24	95.98%	Good
FIC-0501	Stream 19	L/h	107.16	66.88	343.95	119.71	0	1595.5	382.73	23.99%	Bad
FIC-0504	Stream 20	L/h	0	0	0	0	0	0	0	N/A	N/A
TIC-2005	Comp 4	°C	139.97	139.71	2.9852	2.9018	0.0073	17.543	4.820	30.71%	Fair
LIC-2003	Comp 4	%full	66.385	61.331	15.455	1.2170	0.0089	43.667	15.364	28.93%	Bad
PIC-2001	Autoclave	bar	650.00	646.29	6.5036	8.3318	0.0027	63.996	11.363	11.72%	Bad
FIC-2009	Stream 10	kg/h	88.127	85.574	6.4333	7.2751	0.0081	34.349	9.2935	19.29%	Bad

D1 VALIDATION: 400-TK-10 & 400-TK-20

400-TK-10

The flow rates of streams 2, 3, 4, and 5 are imported into the model. This makes stream 1 (400-FIC-0106) the dependent variable that should ensure that the net flow rate into 400-TK-10 remains close to zero. The difference is calculated and, if the flow rate of stream 1 is required to be negative, it is set to a value just above zero. This, however, does not happen often meaning that the process always has solids flowing into 400-TK-20.

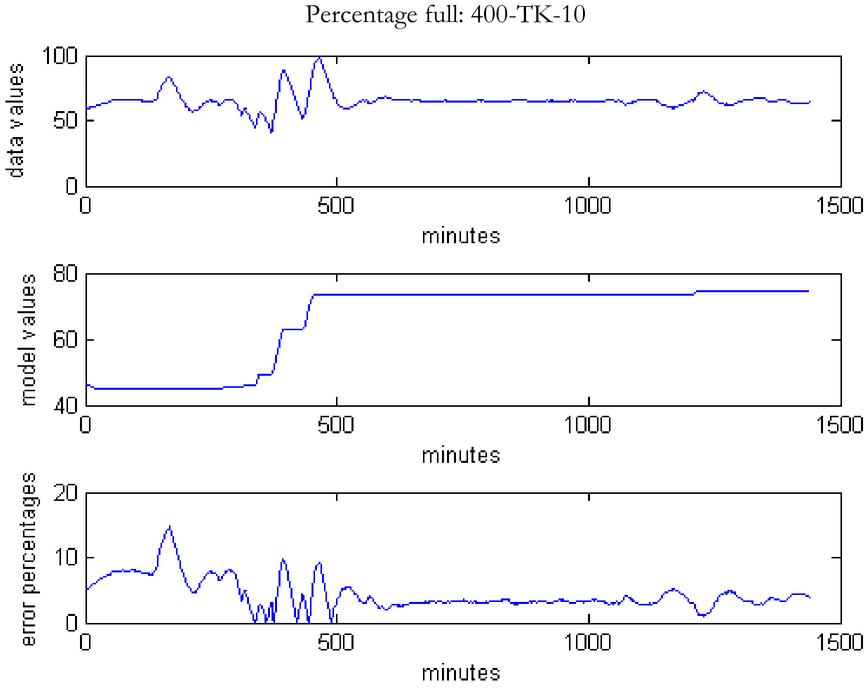

Figure 60: Plot of the extent to which 400-TK-10 is full in the data and the model, with the instantaneous error percentages given.

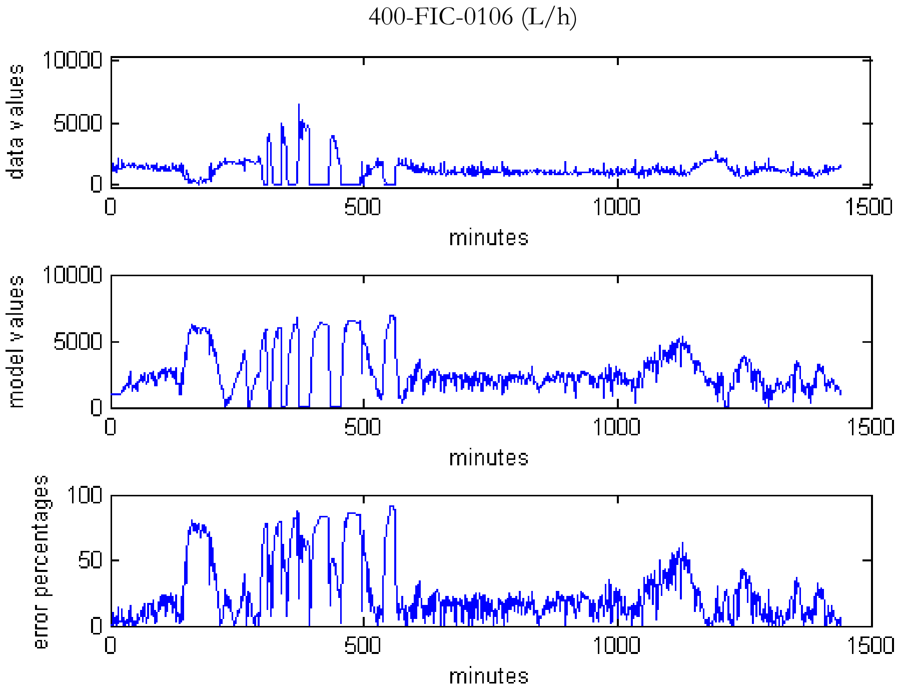

Figure 61: Plot of the volumetric flow rate of stream 1 against time, with the instantaneous error percentages given.

It can be seen from these plots that the moments when the tank level increases corresponds to the periods when the model values are set to a value just above zero (meaning that a negative value for this stream is required to keep the tank level constant). This slow increase of the tank level should have a negligible influence on the process, since it serves only as inventory and it is assumed that no reactions take place in it.

The significant difference between the model and data values can be attributed to the fact that in these validation plots the mass flow rates of stream 1 are calculated to prevent accumulation in the tank, while regions of accumulation can be seen in the data. Assuming no accumulation, while introducing model-data mismatches, proved to lead to results that are more comparable to the data than when a controller attempts to track the data values for the tank's level. The difference in stream 1 might be the largest source of differences between model and data during the validation, and therefore it is important to note the trends. Three zones in the data can be identified, and they correspond well in the above figure. These zones are from approximately 100 to 600 minutes, from 600 to 1000 minutes, and from 1000 onward, and they correspond to the data values for the mass in 400-TK-10. In terms of exact trends, there is a bad correlation – with especially zones 1 and 3 (the zones with accumulation in the data) leading to large errors.

An important parameter to take note of is acid concentration.

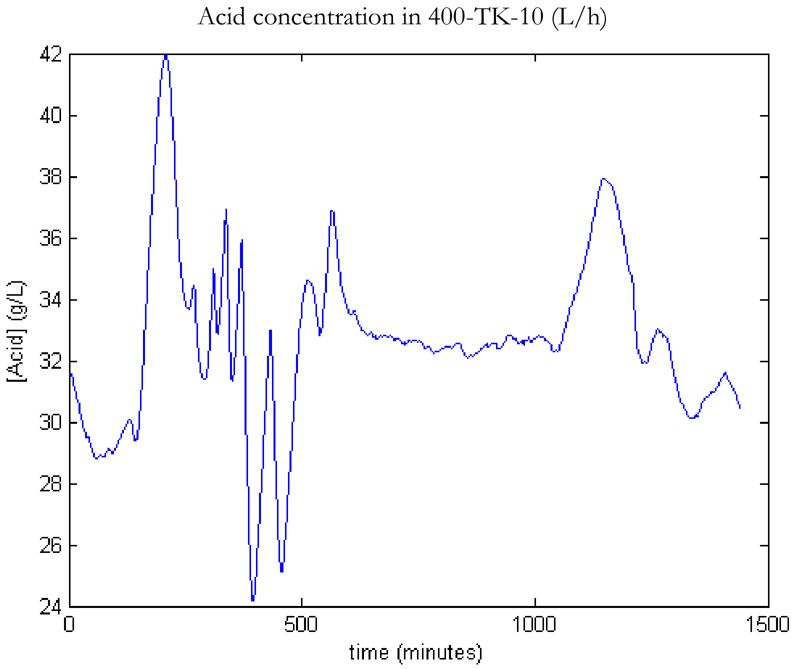

Figure 62: Plot of the acid concentration in 400-TK-10 against time.

The acid concentration in the data is logged only twice per shift, making it insufficient for comparing trends. However, ranges can be compared. From 22 to 24 April the minimum, mean and maximum of the acid concentrations are 31, 41.53 and 55.9 g/L, respectively. The acid concentrations in the model overlap with the data's range, showing that the model is operating within an acceptable range. However, there is an error of approximately 20% between the means of the data and the model, showing that it is not a very good match. The main source of acid in 400-TK-10 is the spent stream (stream 2), for which the flow rate is plotted below:

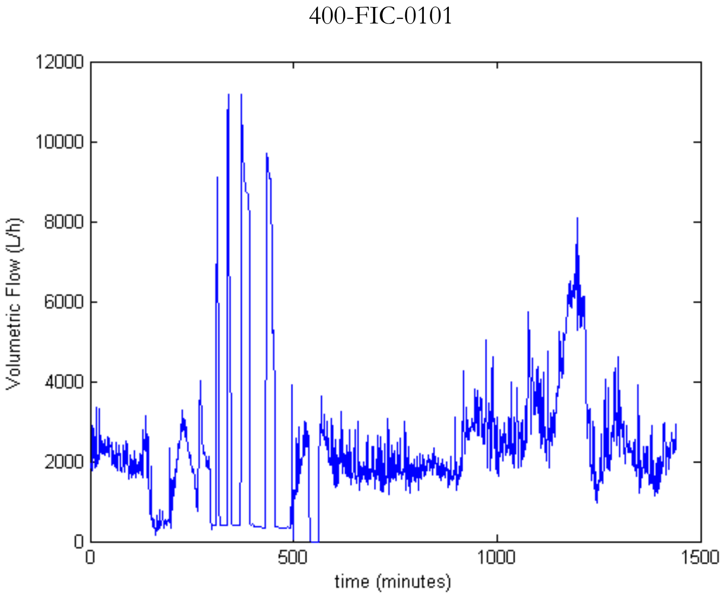

Figure 63: Plot of the volumetric flow rate of stream 2 against time.

Note that these data values are imported into the model and that the error for it between the data and the model is zero. The correlation between the flow rate of stream 2 and the acid concentration can be clearly seen – more so after 1000 minutes. The early peak in the concentration is caused by a similar peak in 400-FIC-0106, which also contains copper spent electrolyte.

400-TK-20

The flow rate of stream 7 is imported 1.18 times the flow rate of the flash recycle stream. The reason for this is that the latter has the biggest influence on the former, and that a fixed ratio between the flow rates has to be kept at all times – in order to ensure that the net effect of these two streams is an inflow into the autoclave. The value of 1.18 is chosen, since multiplying it with the flash recycle stream values produced flow rates of stream 7 that best approximated the data.

400-FIC-2204 (L/h)

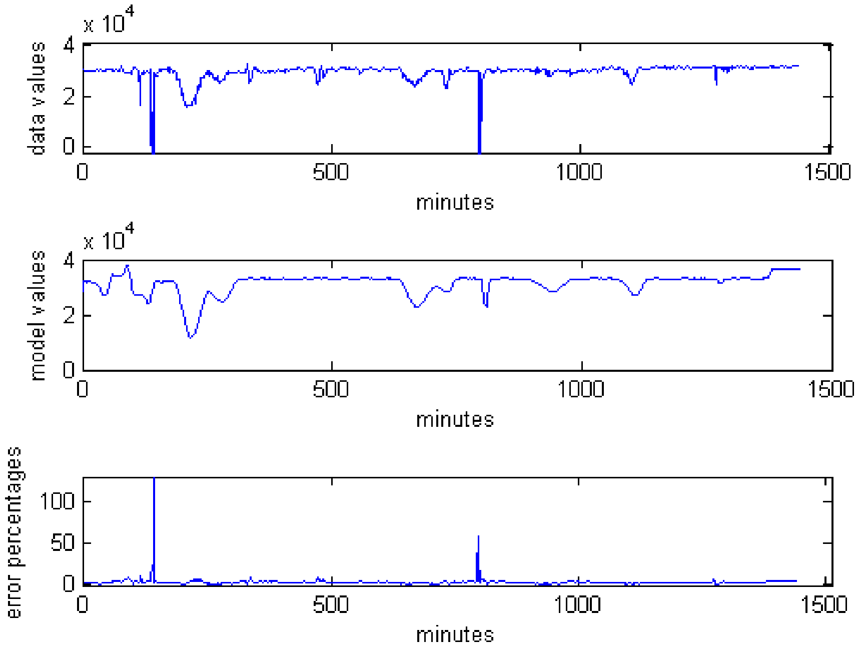

Figure 64: Plot of the volumetric flow rate of stream 7 against time, with the instantaneous error percentages given.

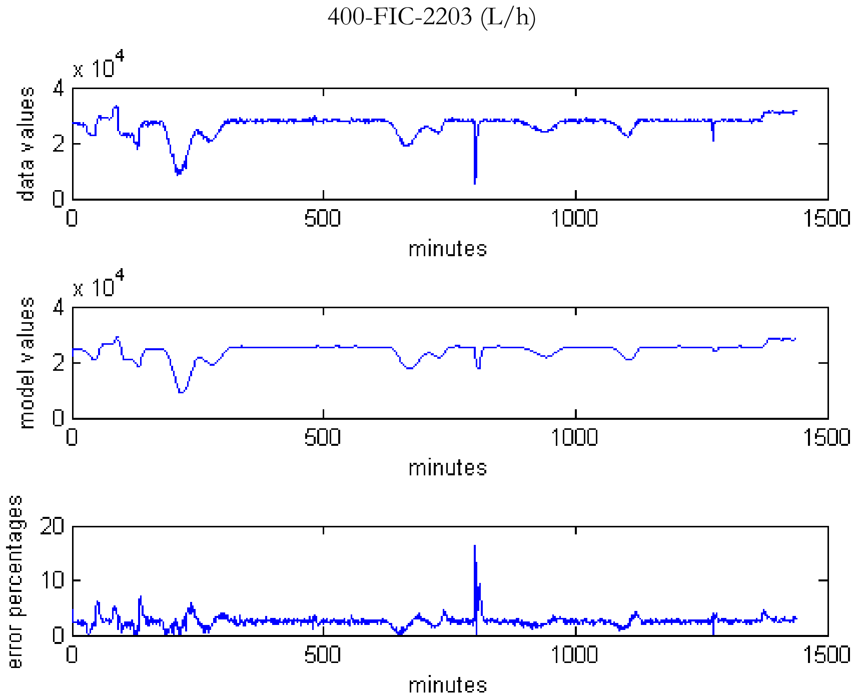

Figure 65: Plot of the volumetric flow rate of stream 9 against time, with the instantaneous error percentages given.

It can be seen that there is a good, but non-exact agreement between data and model values for the flash recycle stream. The reason for this is that there is a near constant offset of approximately 2%, which is caused by the fact that the data values are divided by 1.1 before imported and a constant density of 1.2 kg/L is assumed. Note that the values are smoothed before it is imported by taking a moving average of the data values. For 400-FIC-2204 a slight difference can be picked up, caused by the fact that the data values are set by a level controller on the plant – introducing noise to the variable. While trends are slightly different, corresponding peaks can be clearly seen. Except for extreme outliers at two times, the instantaneous relative error remain below 10%.

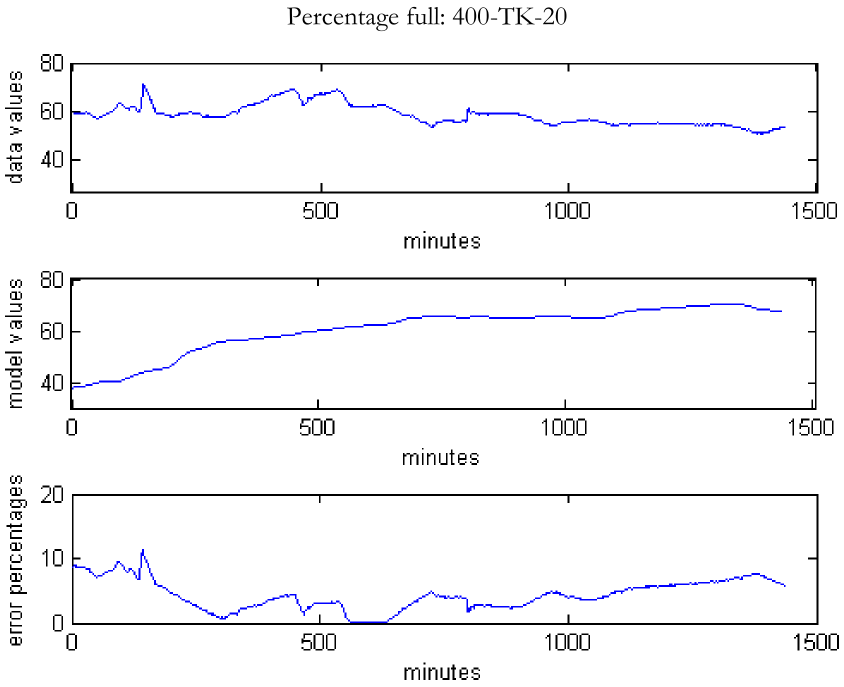

Figure 66: Plot of the extent to which 400-TK-20 is full in the data and the model, with the instantaneous error percentages given.

In this figure it can be seen that there is a drift in the tank level in the cases of both the data and the model, and that these drifts are in opposite directions. The increase in the model's case can be caused by an incorrectly chosen ratio between streams 9 and 7. The slopes on the model's tank levels correspond with the peaks in the flow rates of the mentioned streams, showing that the chosen ratio of 1.18 between the flow rates of streams 7 and 9 is too small. Due to the assumption of no reactions in 400-TK-20, however, the resulting error should not have a notable influence on the process performance.

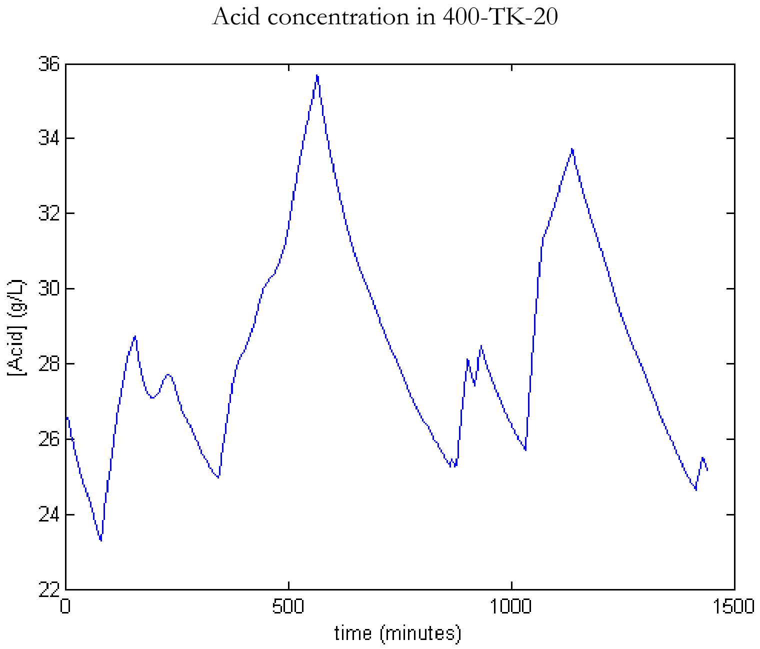

Figure 67: Plot of the model's calculated acid concentration in 400-TK-20 against time.

Comparing this acid concentrations to that of 400-TK-10, it is clear that it is lower. This is expected, since the flash recycle stream – with a lower acid concentration – is added in large quantities to 400-TK-20. However, it is not as significantly lower, since pure acid is added to the process.

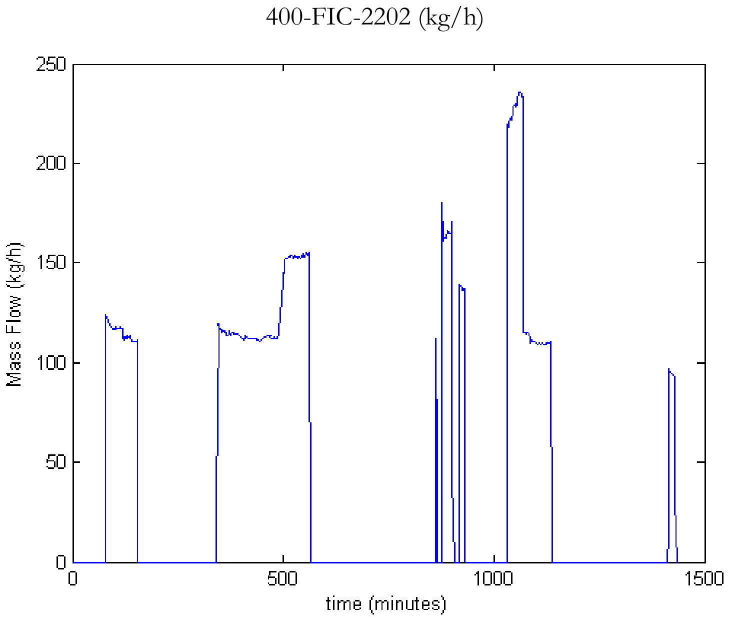

Figure 68: Plot of the mass flow rate of the pure acid stream entering 400-TK-20

The above figure shows why the acid concentration plot of 400-TK-20 is displaying the trends it does. The slope of the concentration plot is directly related to the mass flow rate of the pure acid. This shows that the pure acid is the variable used on the plant to ensure that the acid concentration remains within acceptable bounds. In contrast with the data for 400-TK-10, the acid concentration in the data is typically logged once an hour, allowing trend comparisons. Below are the data points for the times corresponding to the plot of the model's values:

Acid concentration in 400-TK-20

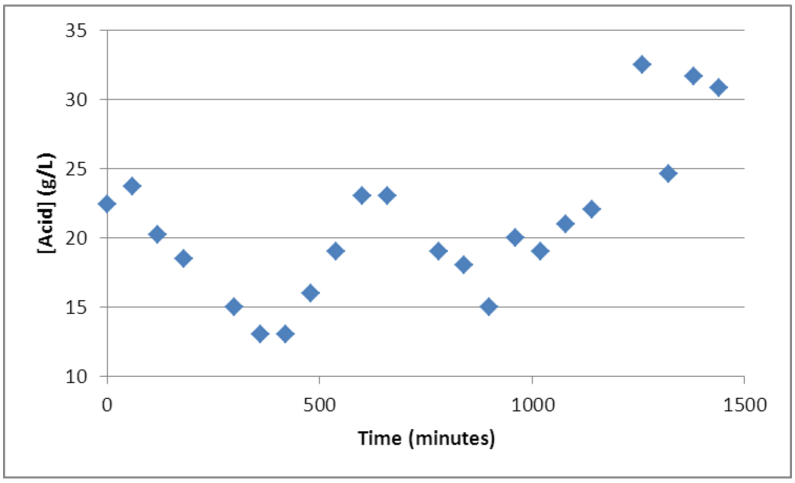

Figure 69: Plot of the acid concentration in 400-TK-20, as it is in the data, against time.

It can be seen that there is a slight difference in acid concentrations between the model (24-26 g/L) and data (13-33 g/L), but that the ranges do overlap. This can be caused by the fact that, while the pure acid fed in the model is exactly the same as that of the data, the acid concentration in the flash recycle stream can differ significantly. This will be discussed in more detail when the acid concentrations of the third compartment are compared. It can be seen that the same peaks are prevalent in the data, although these peaks do not align with those seen in the model. Note that hourly samples are insufficient for drawing clear conclusions from it, and therefore a discussion of the shift in the peaks is limited.

D2 VALIDATION: SECOND STAGE LEACH

Compartment 1

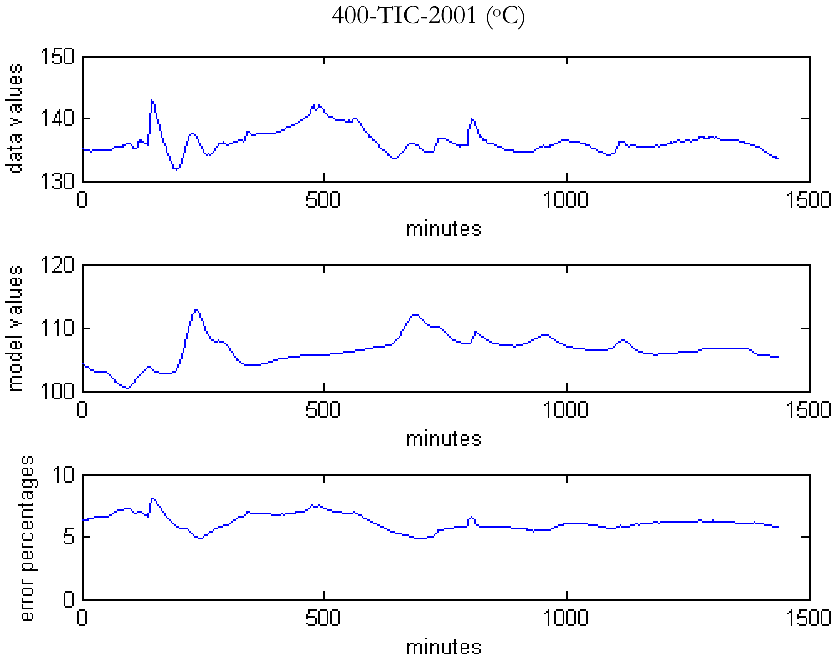

Figure 70: Plot of the temperature of compartment 1 against time, with the instantaneous error percentages given.

From this plot it can be seen that there is a near-constant, significant offset of 5-8% and an RMSE value of 30°C. This gives rise to an nRMSE of 269%, showing that it is a very large error. This can be caused by one of the following factors:

- There is an inaccurate correlation in the data between the flow rate of the flash recycle stream and the resulting rate of energy removal from compartment 1.
- Differences in flow rates/compositions or process specifications, such as autoclave pressure.

These factors will be returned to at a later stage. In spite of the offset, clear trends are visible in both the data and model values. Looking at the flow rate of the flash recycle stream, it can be seen that peaks in the temperature are the inversion of the recycle flow rate. This demonstrates to a large extent that the cooling mechanism in the model qualitatively represents what is known from the plant. Secondary trends in the data – such as the flat peak around the 500th minute – cannot be explained by the flow rates of streams 7 and 9, but a similar flat peak in the level of 400-TK-20 might lead to a suitable explanation. This may point to the occurrence of reactions in this tank, with a higher level referring to a larger residence time. Alternatively the peak can be caused by a higher solids fraction, caused by an increase in the flow rate of stream 1.

Compartment 2

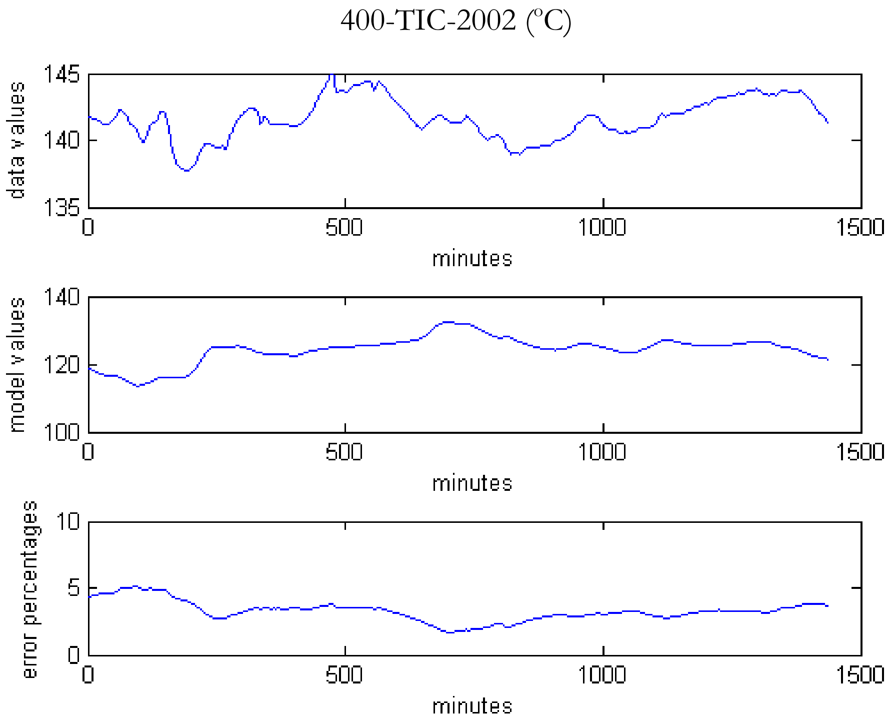

Figure 71: Plot of the temperature of compartment 2 against time, with the instantaneous error percentages given.

It can be seen in this figure that there is in compartment 2 – as with compartment 1 – a clear offset of 2-5% between the data and model values, with the data values being the higher one. Its nRMSE of 245%, is lower than that of compartment 1, but remains very large. It is worth noting that the temperature in this compartment is not controlled – neither in the data, not the model. Clear similarities in the trends can be seen between the plots of compartment 1 and 2, which the peaks flattened in compartment 2. Moreover, the temperature between compartments 1 and 2 increase with approximately 10°C for both data sets.

Compartment 3

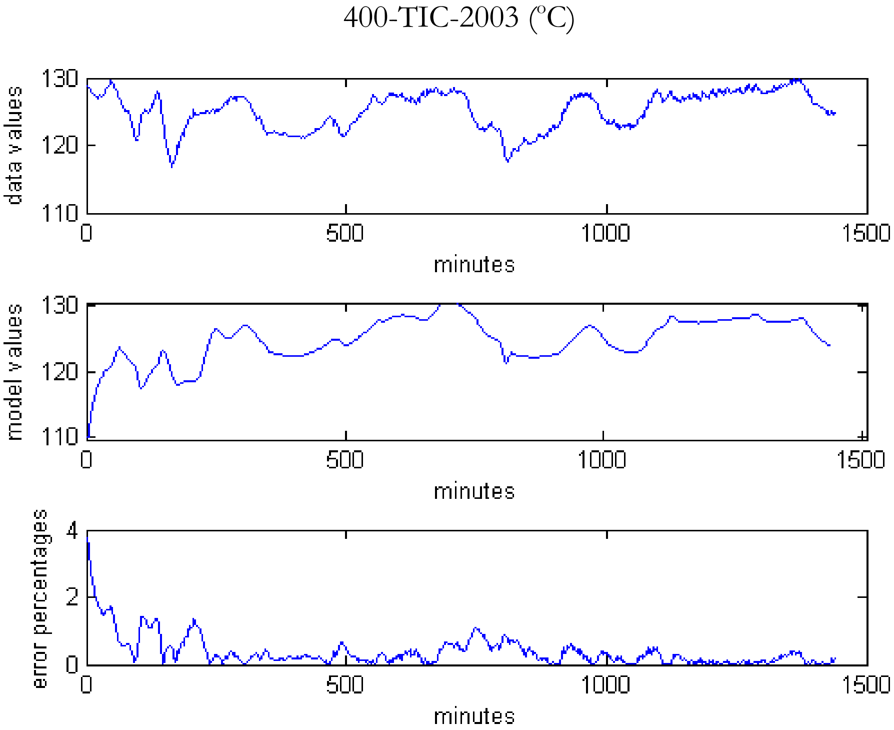

Figure 72: Plot of the temperature of compartment 3 against time, with the instantaneous error percentages given.

In this figure it can be seen that the trends in the data is being followed approximately by the model values. The reason for this is that the data values were imported as the set point of the controller of the temperature of compartment 3. It can be seen that after 1-2 hours the error is decreased from 4% to below 1%. The resulting RMSE value of 2.98°C gives rise to an nRMSE of 23%, which puts it in an allowable range.

Pressure

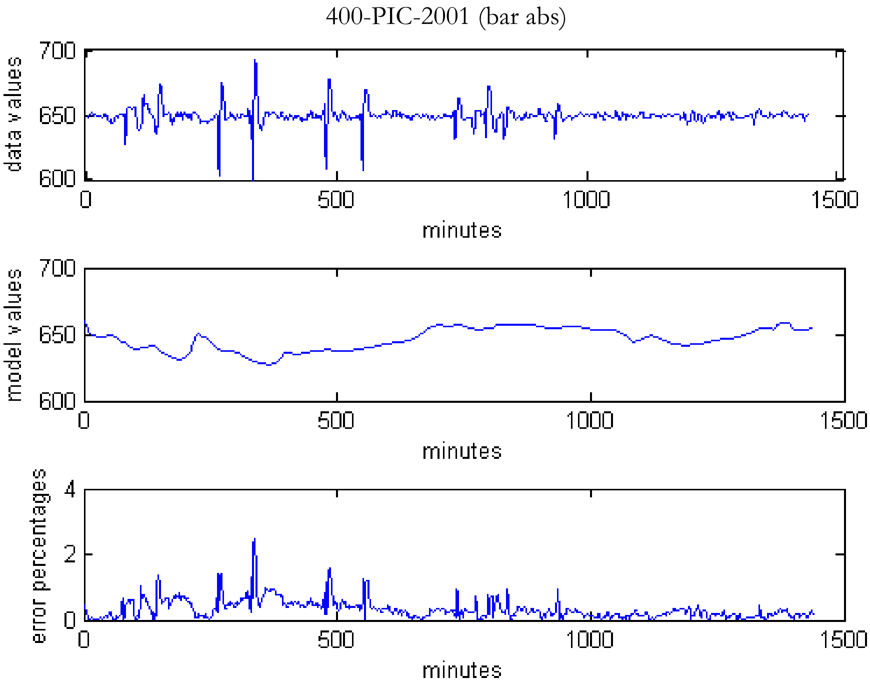

Figure 73: Plot of the autoclave pressure against time, with the instantaneous error percentages given.

It can be seen that the pressures in the data and model outputs lie within the same range (if outliers are disregarded) of 630 to 670 kPa. When outliers are considered the errors do not exceed 2%. The nRMSE value of 11.72% shows that the errors are acceptable. The reason for this performance is the fact that the pressure is controlled in the model at a set point of 650 kPa absolute, which is the same set point that the pressure controller on the plant is fed. The fact that the data values are noisy is due to tighter controller tuning on the plant, as well as noise – which is not a factor in the model.

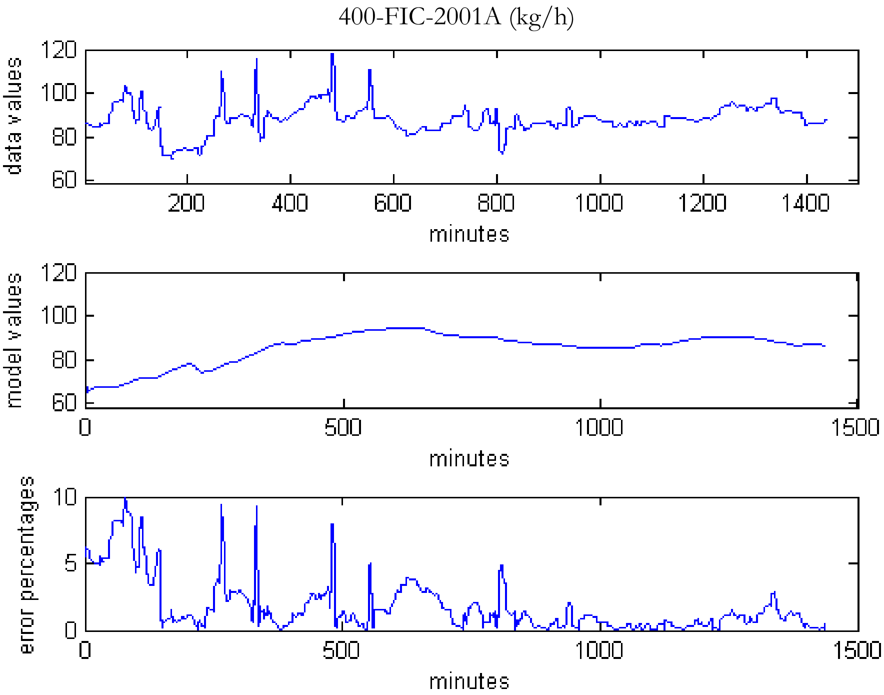

Figure 74: Plot of the mass flow rate of stream 10 against time, with the instantaneous error percentages given.

The oxygen in the above plot represents the total oxygen addition rate, since the oxygen feed ratios are kept constant. It can be seen that the error between the data and model values vary between 0 and 10%. The calculated nRMSE value of 19% shows that the errors are acceptable. It can be clearly seen in this plot, as with the previous one, that the pressure control on the plant is much tighter than in the model. However, this should not have a notable influence on the plant's performance, due to small error percentages.

Second Stage Product

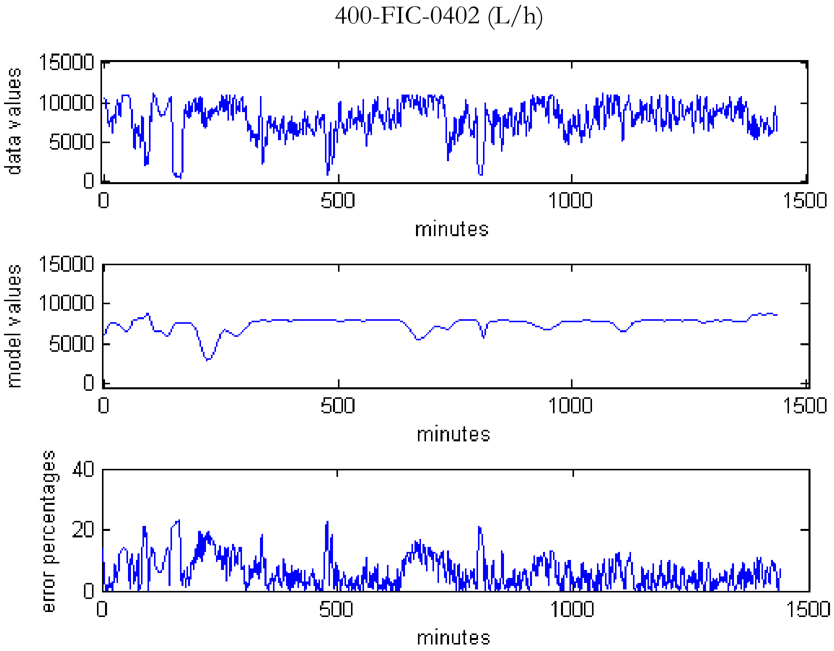

Figure 75: Plot of the volumetric flow rate of stream 14 against time, with the instantaneous error percentages given.

The slurry stream leaving the third autoclave compartment is the product stream of the second stage leach. Its flow rate and composition is a very important variable for validation, since it is influenced by the reactions (and therefore the process variables, like flows, sizes, temperatures and pressure) in the process. From the above plot it can be seen that the model flow rate of stream 14 corresponds well to that of stream 7 (shown earlier). Due to the fact that this flow rate is calculated by the mass controller of the third autoclave compartment, it can be deduced – as would be expected – that the slurry feed stream into the autoclave has a significant influence on the autoclave throughput. The data values do not have such a clear correlation – and in order to comment on it, the following plot is needed:

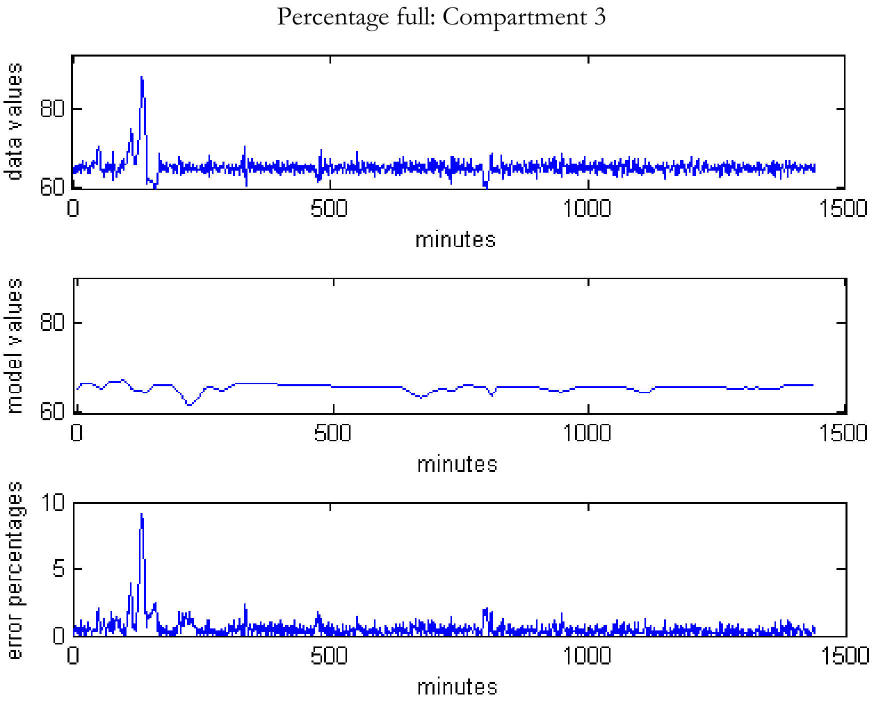

Figure 76: Plot of the extent to which compartment 3 is full in the data and the model, with the instantaneous error percentages given.

It can be seen that the real plant has more noise, and that it is more tightly controlled than the compartment mass in the model. The model values follow the trends of the outflow, while in the data the compartment level remains at a noisy constant value – except for a peak at approximately 2 hours. The error between the flow values reach a maximum of 20%, and it has an nRMSE value of 23%, which seems acceptable, but taking into account the fact that the RMSE (2518 L/h) is much larger than the standard deviation values of both the model and the data, this is a significant difference. In contrast with this, the compartment level error only reaches above 2% once and it has an nRMSE value of 8.4%, which is good. Taking into account that the error for stream 7 rarely ever reaches above 10%, the difference in results for stream 14 may originate in compositional – and therefore reaction – differences.

In terms of the solids fractions of the most noteworthy components, the following figure is generated for model values:

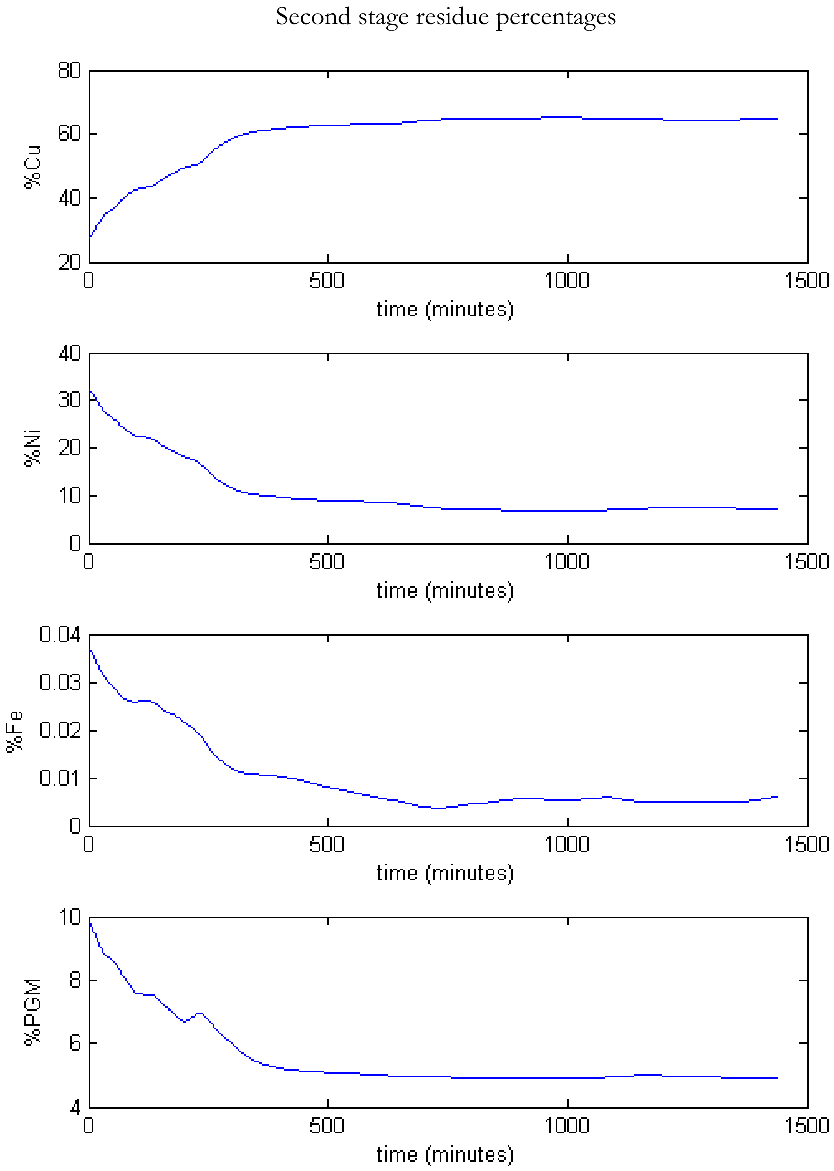

Figure 77: Plot of model values for percentage base metals and PGMs in the second stage leach residue vs time

One of the first things that can be noted from this plot is that there is an inverse correlation between copper and nickel in the residue. This can be explained by the fact that copper and nickel are leached in similar reactions and therefore in a sense compete for the available lixiviants. Note that the percentage iron and PGMs also decreases.

The most important aspect of the composition section is to compare the model values with data values. Since this data is made available only once a shift, it does not allow for comparisons of trends. The data from the shifts that correlate with the range in which data was gathered is chosen, and the minimum, maximum and average of the above variables are given below:

Table 57: Minimum, mean and maximum values for the fractions different metal components make up of the second stage residue from 22 to 24 April 2013, with corresponding model values given.

	Data Values				Model Values			
	% Cu	**% Ni**	**% Fe**	**% PGMs**	**% Cu**	**% Ni**	**% Fe**	**% PGMs**
Minimum	4.50	5.54	4.34	28.07	27.55	6.64	0.004	4.90
Mean	10.27	7.35	5.70	36.27	59.93	10.53	0.010	5.53
Maximum	14.41	9.52	7.14	42.82	65.13	32.18	0.037	9.83

From this table it can be seen that there is a clear difference between the range of the percentage copper in the data and the model. The same cannot be said for nickel, since after 500 minutes the model values are below 10%, which is adjacent to the range in the data (with a maximum of 9.5%). The earlier observation that copper and nickel change inversely to one another means that it might be useful rather to compare the percentages of the sum of these metals. The data range then becomes 10-23.9%, while in the model it goes from around 65% to approximately 74%. This is a very significant error, and it necessitates further investigation. As a preliminary step, it can be noted that one or more of the following factors may cause the error:

- The flow rates and compositions of the entered streams are not correct.
- Process variables of which there is not a clear match between data and model values, such as temperatures and pressure, may directly lead to leaching performance that is dissimilar to that on the plant.
- The leaching kinetics derived by Dorfling (2012) and used in the model are not correct.

Proceeding onto iron, it can be seen that this metal too is far outside the range of the process data. While the model values vary between 0.04 and 0.005%, iron makes up 4.3 to 7.1 % in the second stage leach residue on the plant. The PGMs make up the bulk of the residue on the plant, being 28-42.8% of the residue – while it is 5-10% in the model. Note that more complete leaching of copper and nickel should be enough to bring PGM values into the correct range.

In order to confirm and elaborate on the aforementioned discussion, the concentration of these elements in the liquid phase is plotted below:

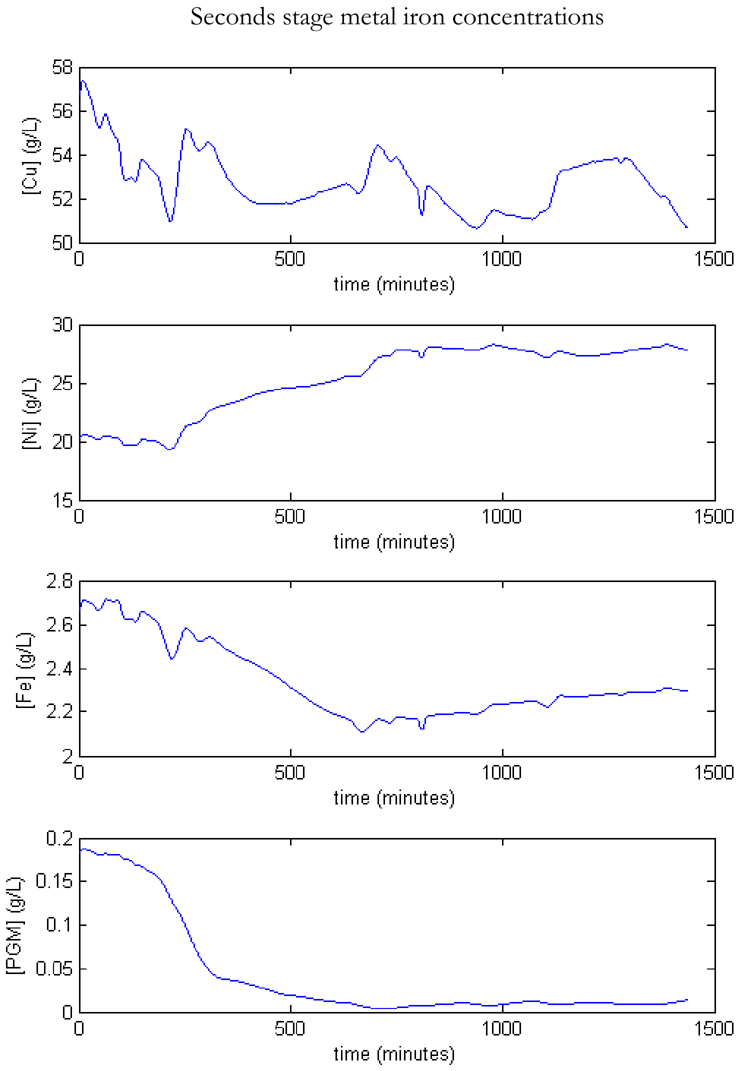

Figure 78: Plot of model values for concentration of base metals and PGMs in the second stage leach residue vs time

In this figure it can be seen that there are clearer trends than in the solid residue plots. Some of the peaks – most visible in the plots for copper and iron – correlate well with the flow rates of streams 7 and 14 in the model. Unfortunately, these values in the data are also sampled merely once a shift, which means that – as with the solids comparisons – only the ranges can be compared.

Table 58: Minimum, mean and maximum values for the concentrations of metal components of the second stage residue from 22 to 24 April 2013, with corresponding model values given.

	Data Values (g/L)				**Model Values (g/L)**			
	[Cu]	**[Ni]**	**[Fe]**	**[PGMs]**	**[Cu]**	**[Ni]**	**[Fe]**	**[PGMs]**
Minimum	83.19	38.35	0.47	0.22	50.62	19.39	2.11	4.5E-3
Mean	97.32	43.15	0.57	0.23	52.76	25.30	2.34	0.04
Maximum	153.03	52.25	0.66	0.25	57.39	28.28	2.72	0.19

Comparing the data values of the copper concentration with that of the model values it can be seen that the former are much higher than the latter. With the reverse being the case in the solid fractions, there is a high probability that the leaching of copper is under-predicted by the model. The nickel concentrations range between 19.4 and 28.3 g/L, while data values lie between 38.4 and 52.3 g/L. Again the model's concentrations are too low. In the case of iron, for which it was found that iron's leaching might be over-predicted, rather than under-predicted, the concentration according to the model is much higher than in the data. PGM concentrations differ marginally, with model values being below 0.2 g/L, while data values lie within the narrow range of 0.22-0.25 g/L.

Another species of which the concentration is very important is that of acid. Its concentration in the third compartment, as calculated by the model, is given below:

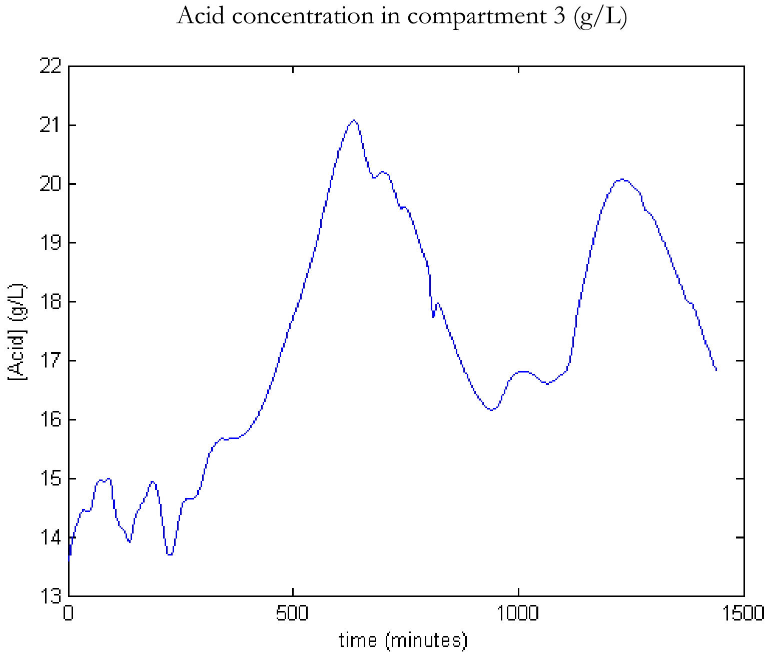

Figure 79: Plot of model values of the acid concentration in the third autoclave compartment, versus time.

The two main peaks (with the smaller on in between) in this plot correlate with the peaks in the acid concentration of 400-TK-20. This result can be expected. Moreover, it is clear that the acid concentration decreased from 24-36 g/L to 14-21g/L and this can be attributed to the leaching reactions that require and consume sulphuric acid. The concentration for the third compartment is sampled once every shift, meaning that only range comparisons can be made. Note that for a more rigorous validation of this model, more detailed compositional data is necessary. The minimum, mean and maximum values for the data are 9, 19.63 and 39 g/L, respectively. The model's values lie well within these bounds and have a similar mean, meaning that the acid concentration is well predicted. This is a surprising result, since it would be expected that under-leaching of copper would correspond to a higher effluent acid concentration.

D3 VALIDATION: 400-TK-040 & 400-TK-050

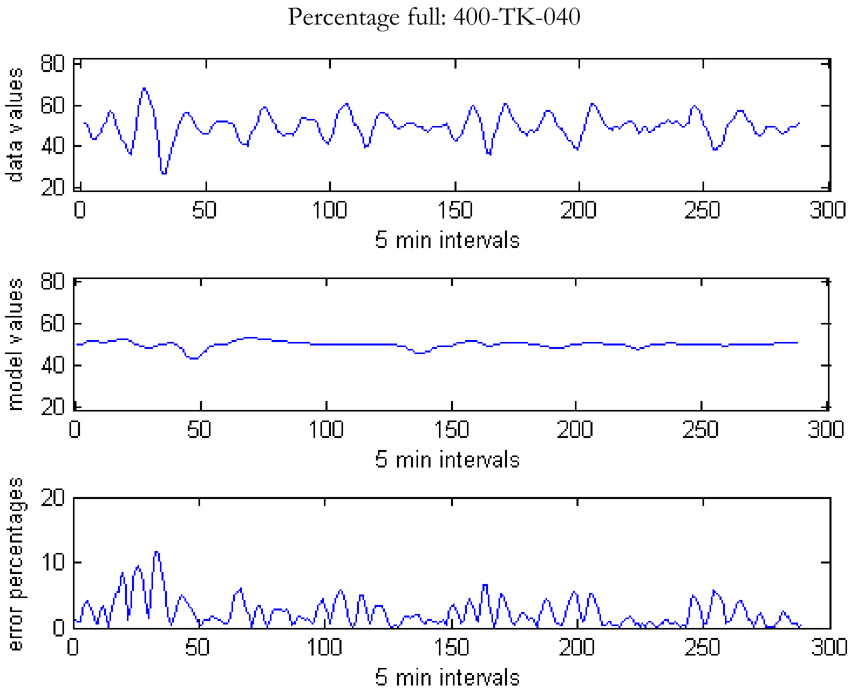

Figure 80: Plot of the extent to which 400-TK-040 is full in the data and the model, with the instantaneous error percentages given.

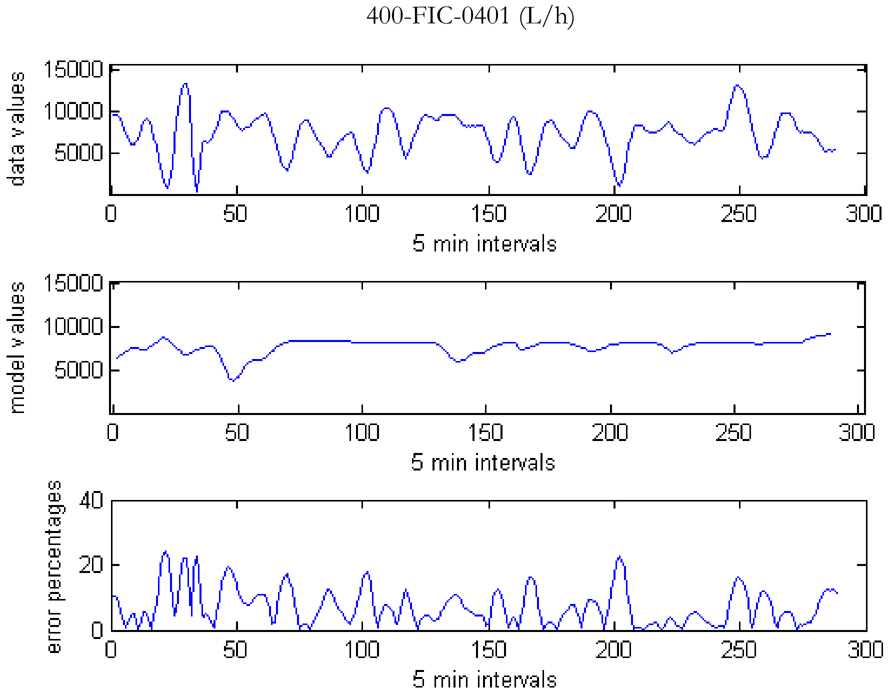

Figure 81: Plot of the volumetric flow rate of stream 15 against time, with the instantaneous error percentages given.

It can be seen from the above figures that the flow rate trends of stream 15 in the model closely follow the trends of stream 14. The peaks are clearly recognisable and can be most clearly seen between 0 and 1000 minutes. The same type of correlations in peaks and other trends can also be seen for the data values, but it is more difficult due to the noise in the stream leaving compartment 3. In terms of a comparison between model and data values, the nRMSE value for stream 15 is 21.5%. Note that the qualitative similarity between the flow rates to and from 400-TK-040 is more important in this case than the instantaneous correlation between model and data values. The trends in the data and model values of stream 15 are reflected in the contents of 400-TK-040, respectively. This indicates that the inventory control in the two cases may be tuned to a similar degree of tightness.

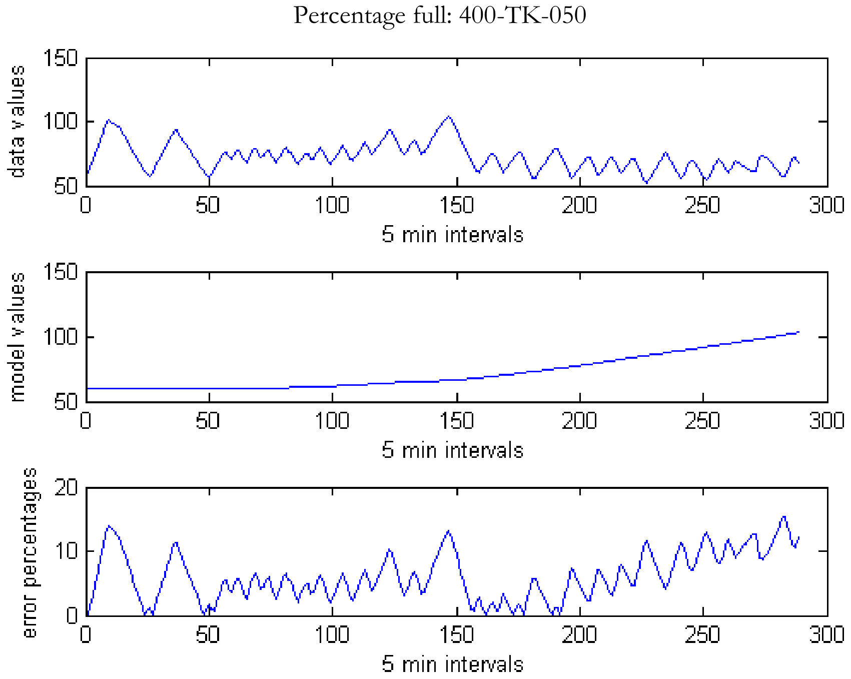

Figure 82: Plot of the extent to which 400-TK-050 is full in the data and the model, with the instantaneous error percentages given.

In 400-TK-050 the level much less in the case of the model values than for the data values. The reason for this is that the flow rate of stream 19 is determined with a mass balance around this tank. If the flow rate of stream 18 were to be imported from the data, and from process knowledge the flow rate of stream 21 were to be assumed as constant, stream 19 would be required to have a negative flow rate to prevent accumulation in the tank in question. This explains the increase in the mass of 400-TK-050's contents in the model. Note that this is for the case that the pure acid addition is zero.

It was decided that the assumption of a constant flow rate of stream 21 should not be overturned, and that the flow rate of stream 18 (the copper spent electrolyte addition) should rather be lowered to attain a reconciled mass balance. The flow rate of stream 19 is then set to be the dependent variable that ensures that the flows into and out of 400-TK-050 add up to zero.

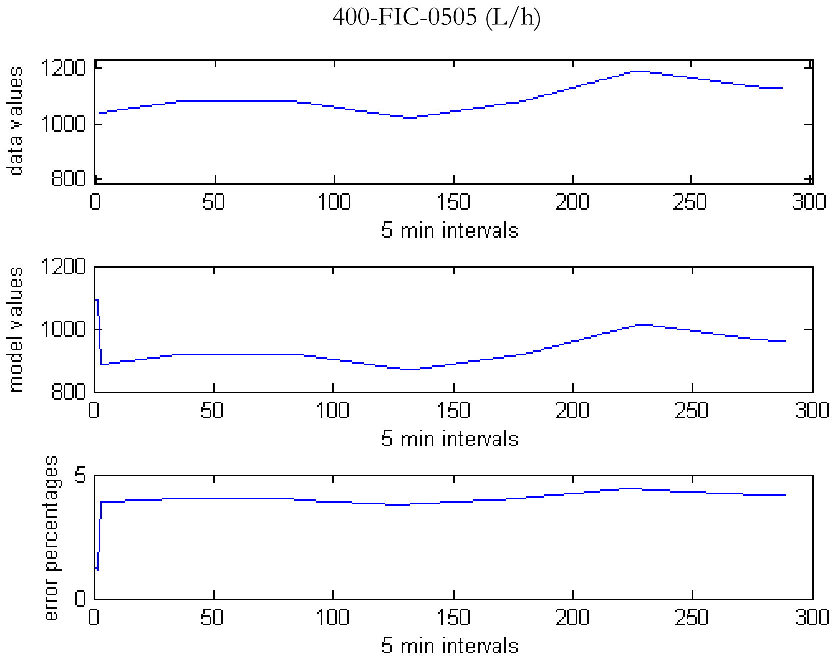

Figure 83: Plot of the volumetric flow rate of stream 18 against time, with the instantaneous error percentages given.

It can be seen, as is expected from the discussion above, that the trends of stream 18 in the data and model are similar, but that it differs with approximately 4%. The nRMSE is 96%, which is very large.

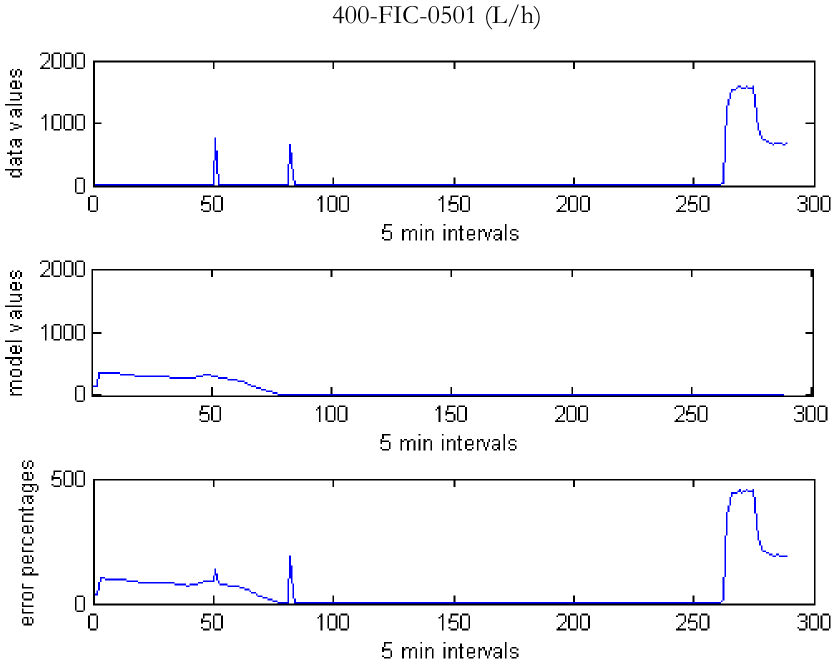

Figure 84: Plot of the volumetric flow rate of stream 19 against time, with the instantaneous error percentages given.

Predictably, there is a significant difference between the model and data values. The fact that the flow rate of stream 21 is constant means that such variations in stream 19 would introduce minor compositional errors into the process. With respective mean values of 66.88 L/h and 107.164 L/h for the model and data values respectively, the total influence should be minimal and will not prevent validation for the purpose of the model.

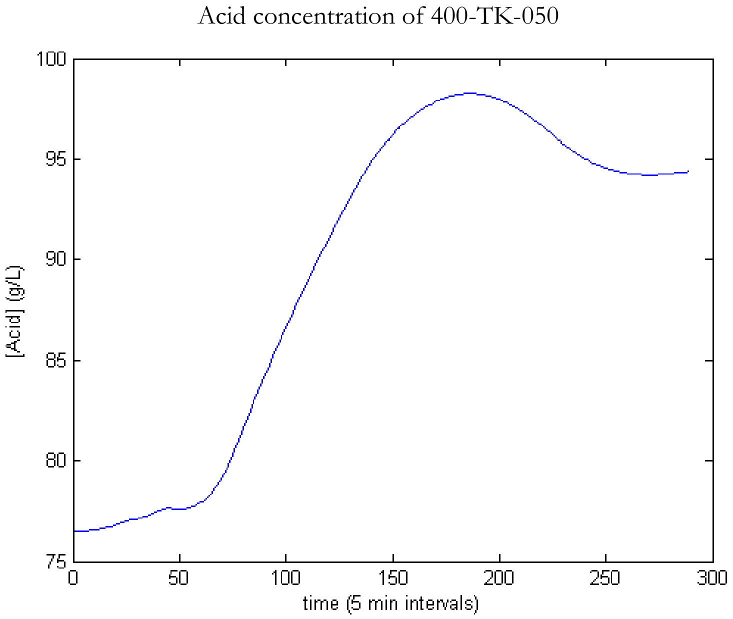

Figure 85: Plot of the model's acid concentration for 400-TK-050.

The only source of acid entering 400-TK-050 in the model is the spent entering in stream 18. The trends of this flow rate is, however, not visible in the acid concentration plot. Instead, there is a climb and settling of the acid concentration value. A possible reason for this is the fact that the acid concentration not only depends on the amount of acid in the system, but also the total amount of liquid. The decreasing amount of water (which is zero after 75 minutes) may cause the trend seen in the above figure. The data values are sampled hourly, allowing a reasonable comparison between the model and data values.

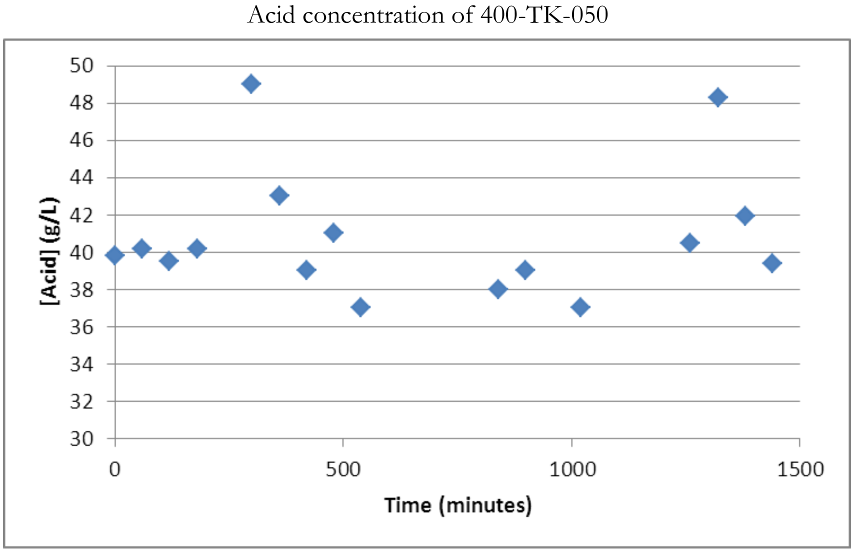

Figure 86: Plot of the data's acid concentration for 400-TK-050.

A comparison between the model and data values shows the significance of the solid-liquid separation step in the pressure leach process. It can be seen that the approximation of a solids-only stream 17 lead to a significant difference in the acid concentrations calculated by the model (76-98 g/L) and what is available in the data (37-50 g/L). It can, however, not be confirmed that this – and not faulty data – is the source of the problem, but it is an important factor to take note of in subsequent projects.

D4 VALIDATION: THIRD STAGE LEACH

Temperature and Level

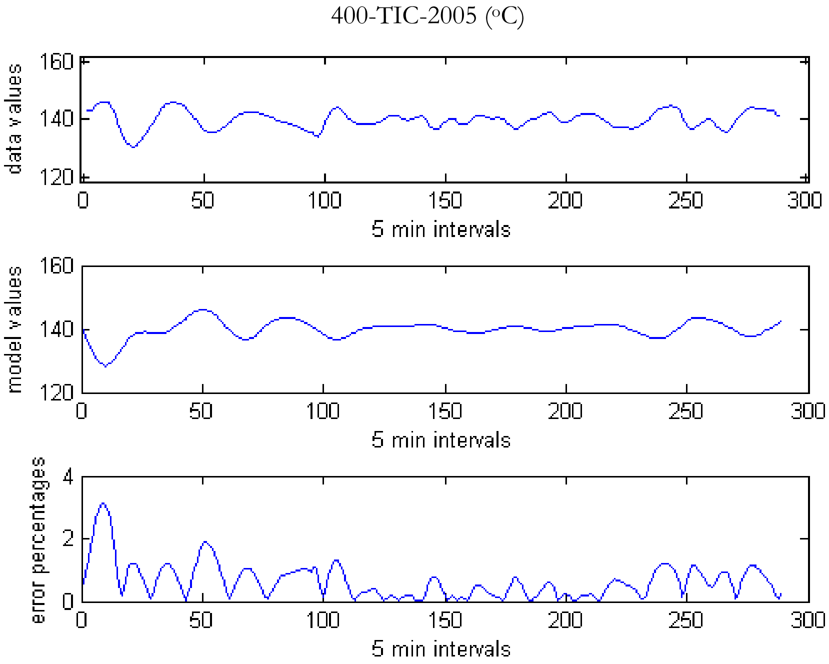

Figure 87: Plot of the temperature of compartment 4 against time, with the instantaneous error percentages given.

The temperature of compartment 4 is controlled by means of steam addition. Due to the lack of data for stream 21 the focus of this comparison step is on how close the model gets to approximate the data values. The error percentages are all below 3%, while the nRMSE of is 30.7%, which is large, due to the small variance in the data values. It can, however, be seen that the temperature of the fourth compartment is very similar.

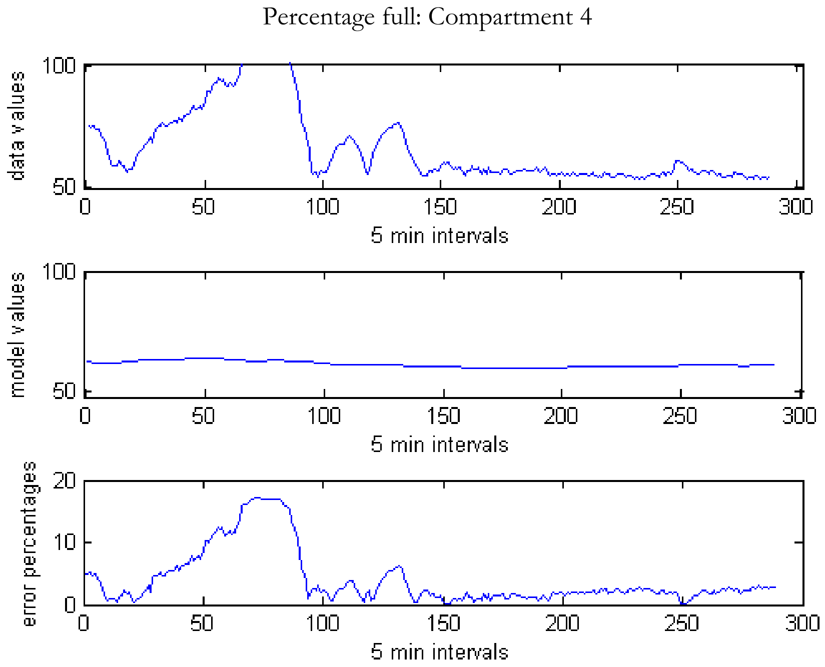

Figure 88: Plot of the extent to which compartment 4 is full in the data and the model, with the instantaneous error percentages given.

It can be seen that the compartment mass in the model is controlled more tightly than in the data, which reaches values above 100% for its level. Due to a lack of flow rate data around compartment 4 much more cannot be said. Note, however, that the nRMSE value of 29% is significant.

4.7.6.2 Compositions

In terms of the solids fractions of the most noteworthy components, the following figure is generated for model values:

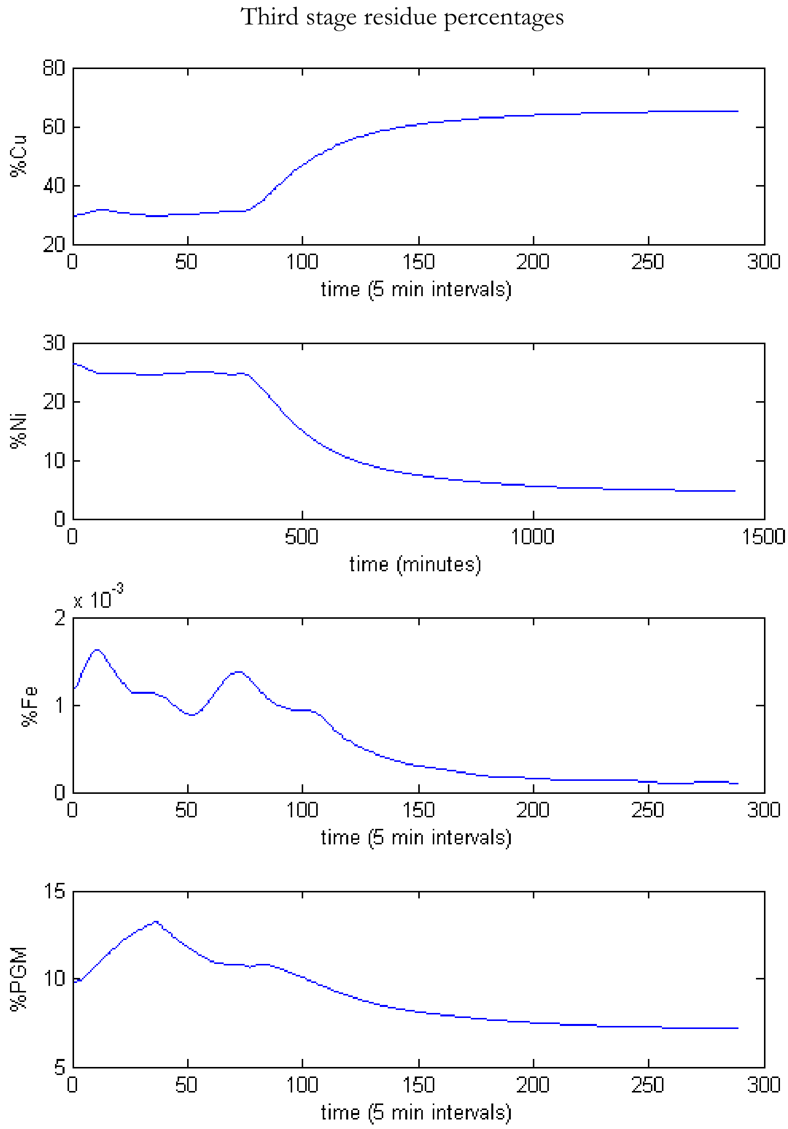

Figure 89: Plot of model values for percentage base metals and PGMs in the third stage leach residue vs time

It can be clearly seen in this figure that the copper and nickel percentages change with what resembles a first-order response with dead time. It can therefore be deduced that the shift in solids composition is due to an upstream change of some kind. The most probable cause of this is the fact that the mean values of the flow rates imported from the data do not exactly match the initial input data given to the model. Since the time series comparisons consider only the model once the new MVs are imported, and the compositional comparisons are limited to value ranges, this does not pose a problem for this operational validation section.

It can be seen that, again, the copper and nickel fractions change in an inverse proportion to one another. As for the second stage leach residue, iron and PGM fraction decrease with time, and do not display the same shape as the first two metals. The corresponding values in the data are given below. Note that only one reading was available per day, with 22 April excluded. This means the following table is based on a table with two readings per element.

Table 59: Minimum, mean and maximum values for the fractions different metal components make up of the third stage residue from 23 to 24 April 2013, with model values alongside it.

	Data Values				Model Values			
	% Cu	**% Ni**	**% Fe**	**% PGMs**	**% Cu**	**% Ni**	**% Fe**	**% PGMs**
Minimum	1.47	5.46	8.39	48.07	29.51	4.64	1.0E-4	7.19
Mean	1.89	5.80	8.48	48.33	51.63	12.59	5.8E-4	9.05
Maximum	2.31	6.15	8.57	48.59	65.36	26.40	1.6E-3	13.21

From this table it can be seen that there is an even clearer difference between the range of the percentage copper in the data and the model. The reason for this is than the copper fraction in the third stage residue is the same as that of the second stage, except that the change takes place after a certain delay. As with the second stage leach same is not true nickel, which reaches below 5% after the first order change. The data fractions are between 5.46% and 6.15%. Comparing the sum of these metals, the data values are between 6.93% and 8.48%. The model values lie between 55% and 70%. As with the second stage leach, this is a big difference. One should keep in mind that, since all the solids proceed from the second stage leach into the third stage, the second stage leach is a source of much of the errors seen in the third stage.

The iron in the data makes up 8.39-8.57% of the third stage leach residue, while model values are below 0.002%. This is a larger difference than in the second stage leach and strengthens the suspicion that iron leaching is over-predicted in the model. While the PGM fraction is higher in the third stage residue than in that of the second stage, it still remains below 14% - while data values are above 48%.

The concentration of these elements in the liquid phase is plotted below:

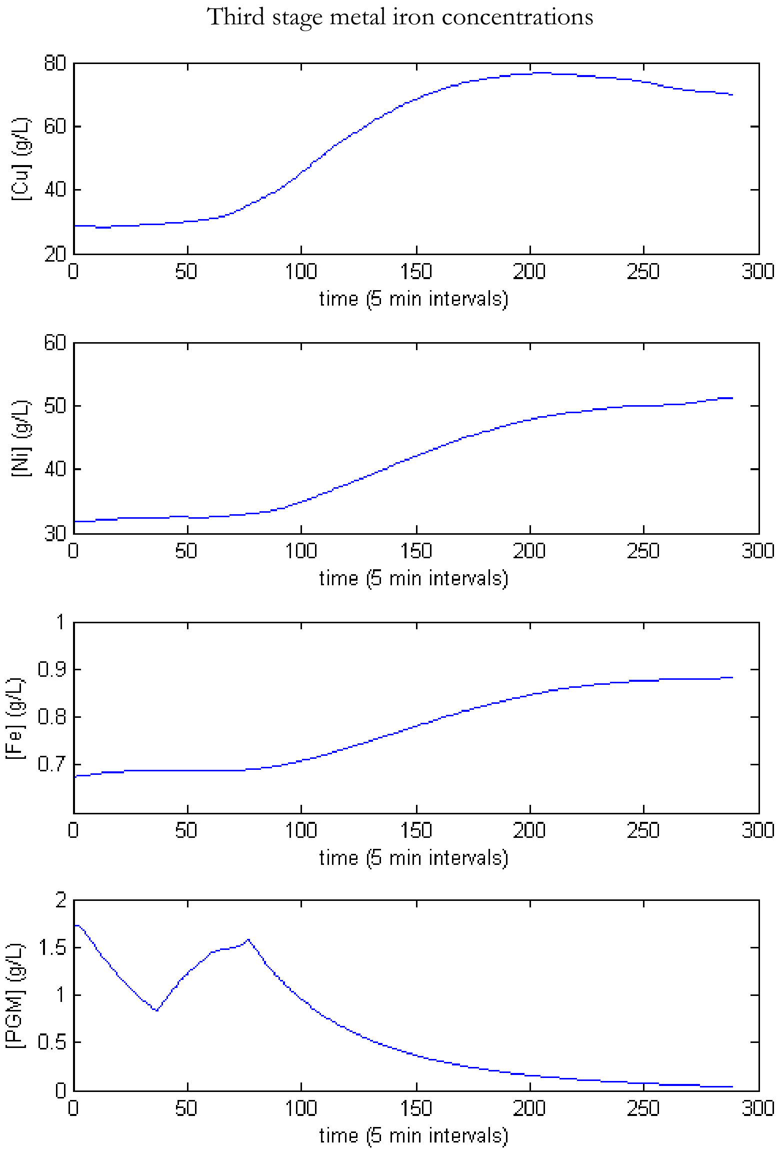

Figure 90: Plot of model values for concentration of base metals and PGMs in the third stage leach residue vs time

In this figure it can be seen that the trends are much flatter than it is the case for the second stage concentrations. The copper, nickel and iron concentrations climb in the form of an s-curve, while the PGM concentration changes less steadily. The data values, sampled once a shift, are given below. Note that for these values, as well as for the second stage values, the PGM concentrations are calculated from ppm values assuming a bulk density of 1.2 kg/L.

Table 60: Minimum, mean and maximum values for the concentrations of metal components of the third stage residue from 22 to 24 April 2013, with model values alongside it.

	Data Values (g/L)				Model Values (g/L)			
	[Cu]	[Ni]	[Fe]	[PGMs]	[Cu]	[Ni]	[Fe]	[PGMs]
Minimum	25.36	11.49	0.18	0.07	28.26	31.75	0.68	0.04
Mean	63.62	33.88	0.48	0.23	56.76	41.14	0.78	0.61
Maximum	78.33	42.28	0.61	0.29	76.56	51.27	0.88	1.73

Comparing the third stage data values of the copper concentration with that of the second stage values, it can be seen that it is significantly lower. Moreover, the data values (25.36-78.33 g/L) are, contrary to what is the case for the second stage values, in the same range as the model values (28.3-75.6 g/L). The bad data-model correlation in the case of the solids residue, in the light of a good liquid correlation, is not a wholly surprising phenomenon, since the solids-liquid separation step allows the solids to proceed into the third stage, while the liquid is made up new in 400-TK-050. The model's nickel concentrations range between 31.8 and 51.3 g/L, while data values lie between 11.5 and 42.3 g/L. Again the model's concentrations acceptably close to the data values. In the case of iron, the concentration according to the model (0.68-0.89 g/L) is higher than in the data (0.18-0.61 g/L), but not to a significant degree. PGM concentrations are in the same ballpark, with model values being below 2 g/L, while data values lie between 0.07 and 0.29 g/L.

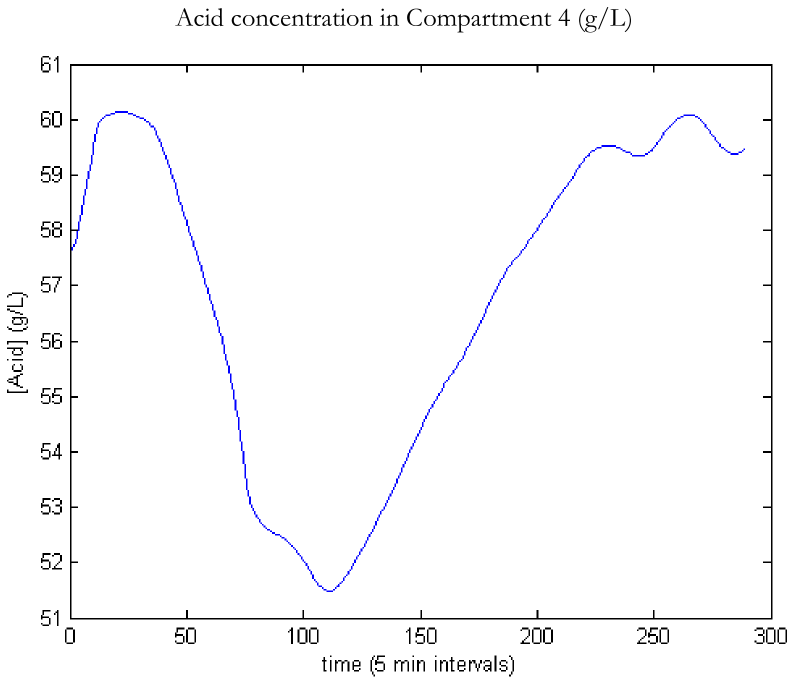

Figure 91: Plot of the model's calculated acid concentration in compartment 4, versus time.

The trends of the acid concentration in compartment 4 do not correlate with the concentrations of the metal species, which is a surprising result. The trend can be caused by the fact that the entering acid shows an upward S curve, while increasing copper and nickel concentrations indicate that the usage of acid by the leaching reactions should also display what approximates an upward S curve. The two competing S-curves may be what cause the shape of the plot above. It should be noted that, since entering acid concentration in the model is much higher than the corresponding data values, the outflow should also be much higher. This is, in fact, the case – as can be seen from the following plot:

Acid concentration in Compartment 4 (g/L)

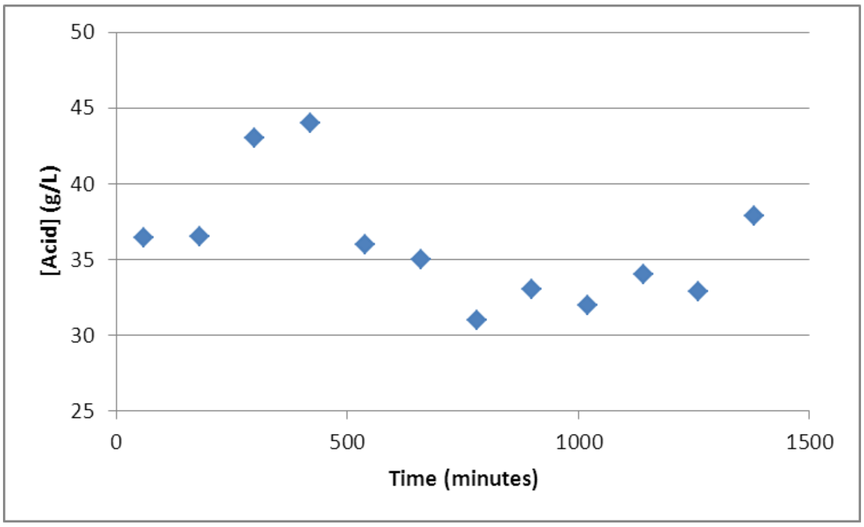

Figure 92: Plot of the data's acid concentration in compartment 4, versus time.

The data logging is too infrequent to make significant comments on the trends, but it is confirmed that the data (30-45 g/L) and model (51-60 g/L) are not in the same range.

APPENDIX E

MODEL INPUTS FOR INVESTIGATION IN SECTION 3.8.5

The following tables list the input conditions for the analysis done in section 3.8.5.

Table 61: Composition of copper spent electrolyte

Component	Concentration (mg/L)
Cu	32440
Ni	33000
Fe	855
Rh	50
Ru	210
Ir	45
Acid	84000

Table 62: Composition of formic filtrate

Component	Concentration (mg/L)
Cu	24
Ni	2239
Fe	4560
Rh	1.802
Ru	191
Ir	372

Table 63: Composition of solids feed

Component	Mass Fraction
Cu	59.529 %
Ni	12.645 %
Fe	0.221 %
S	25.057 %
Rh	574.5 ppm
Ru	1371.5 ppm
Ir	388.8 ppm
Pt	3314 ppm
Pd	1650 ppm

Table 64: Mineralogy of solids feed

Component	Fraction
Cu as Cu9S5	0.914
Ni as NiS	0.903
Rh as Rh2S3	0.5
Ru as RuS2	0.7
Ir as Ir2S3	0.6
Fe as FeOHSO4	0.1

Table 65: Flow rates added into the model

Stream	Units	Value
Solids in stream 1	kg/h	1400
Water in stream 1	L/h	1400
Spent in stream 1	L/h	730
Stream 2	L/h	3600
Stream 3	L/h	900
Stream 4	L/h	0
Stream 23	L/h	46.24
Stream 9	kg/h	27000
Stream 18	L/h	88.5
Stream 19	L/h	6
Stream 20	L/h	0

APPENDIX F

CONTROLLER TUNING FOR CHAPTER 4

F1 CONTROLLER TUNING FOR CHAPTER 4 BASE CASE

F1.1 Mass Controllers

Coefficients of Variance

The following values are the coefficients of variance in the respective parameter's data values, used to calculate the tuning parameters for the mass controllers.

Table 66: Maximum variations for mass control MV flow variations and mass variations for mass controller tuning

Inventory	Flow variation (%)	Mass variation (%)
400-TK-10	70	10
400-TK-20	9	7
400-TK-040	30	10
400-TK-050	50	10
Comp 3	27	3.4
Comp 4	79	10

Results of Tuning

The following tuning parameters result from applying these variations in the mass controller tuning equations given in section 4.2.6.

Table 67: Tuning parameters calculated for the PI mass controllers in the base case model

Inventory	K_c	$1/T_I$
400-TK-10	1.8960	0.1554
400-TK-20	-4.4715	0.1402
400-TK-040	-2.5939	0.2702
400-TK-050	0.2994	0.0365
Comp 3	-7.5364	1.1282
Comp 4	-1.1799	0.1766

F1.2 Other Controllers

The plots used for the tuning of the other variables mentioned in section 4.3.2 are given below, along with the deduced tuning parameters.

Temperature of Compartment 3 (400-TIC-2001)

Cooling water of compartment 3 (kg/h) vs time (h)

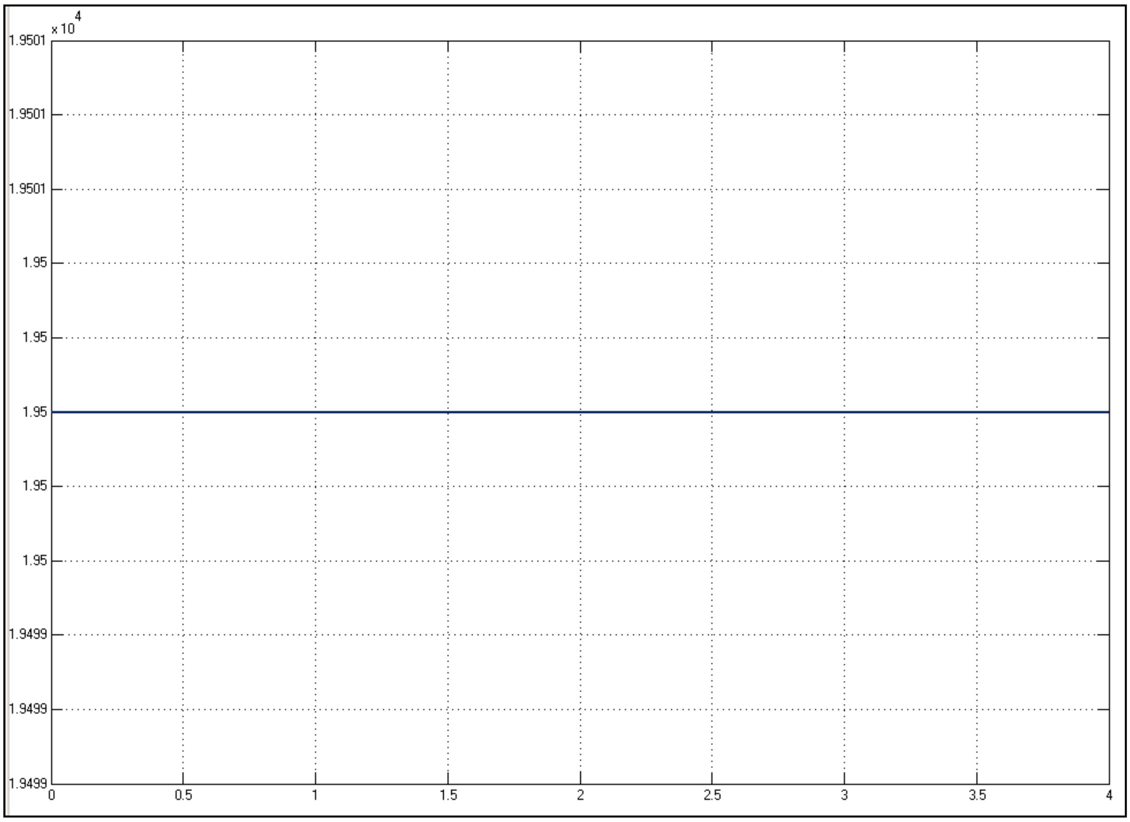

Figure 93: Plot of the mass flow rate of the water in the cooling coils of compartment 3 (in kg/h) vs time (in hours)

400-TIC-2003 readings (°C) vs time (h)

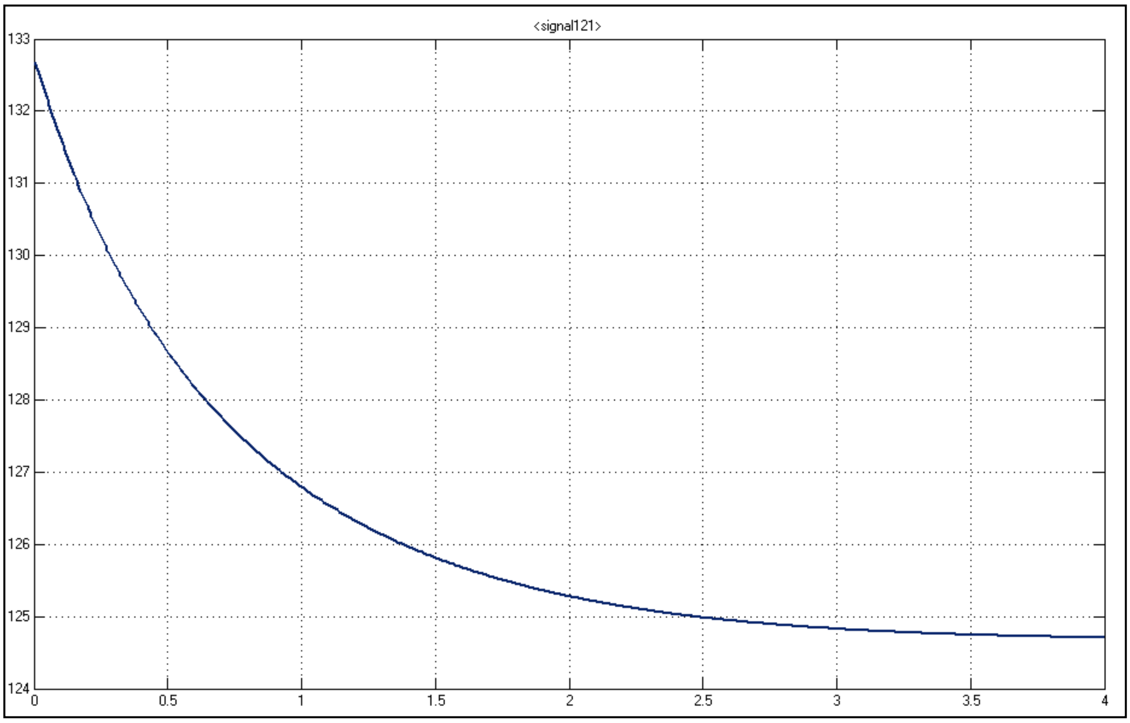

Figure 94: Plot of the temperature of compartment 3 (in °C) vs time (in hours)

$\Delta m_{coils3} = 19500 - 15000 = 4500$

$\Delta T_{comp3} = 124.706 - 132.677 = -7.971$

$K_p = -0.00177$

$t_{63\%} = 0.728$

$t_{28\%} = 0.228$

$K_c K_p = 1.5$

$\frac{T_I}{t_{63\%}} = 0.24$

$\frac{T_d}{t_{63\%}} = 0$

$\tau = 0.75$

$\theta = 0$

$\boldsymbol{K_c = -847.458}$

$\boldsymbol{T_I = 0.18}$

$\boldsymbol{T_d = 0}$

Temperature of Compartment 4 (400-TIC-2005)

Maas flow of stream 13 (kg/h) vs time (h)

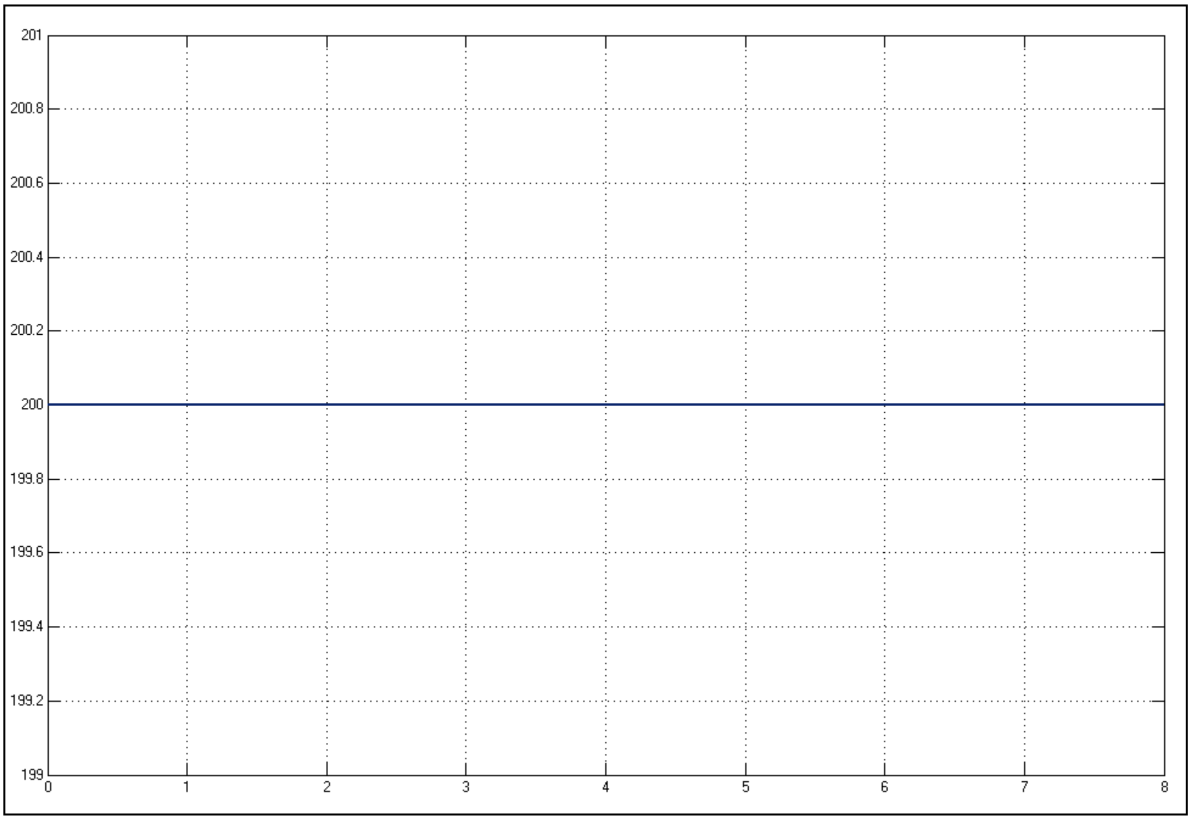

Figure 95: Plot of the mass flow rate of the steam entering compartment 4 (in kg/h) vs time (in hours)

400-TIC-2005 readings (°C) vs time (h)

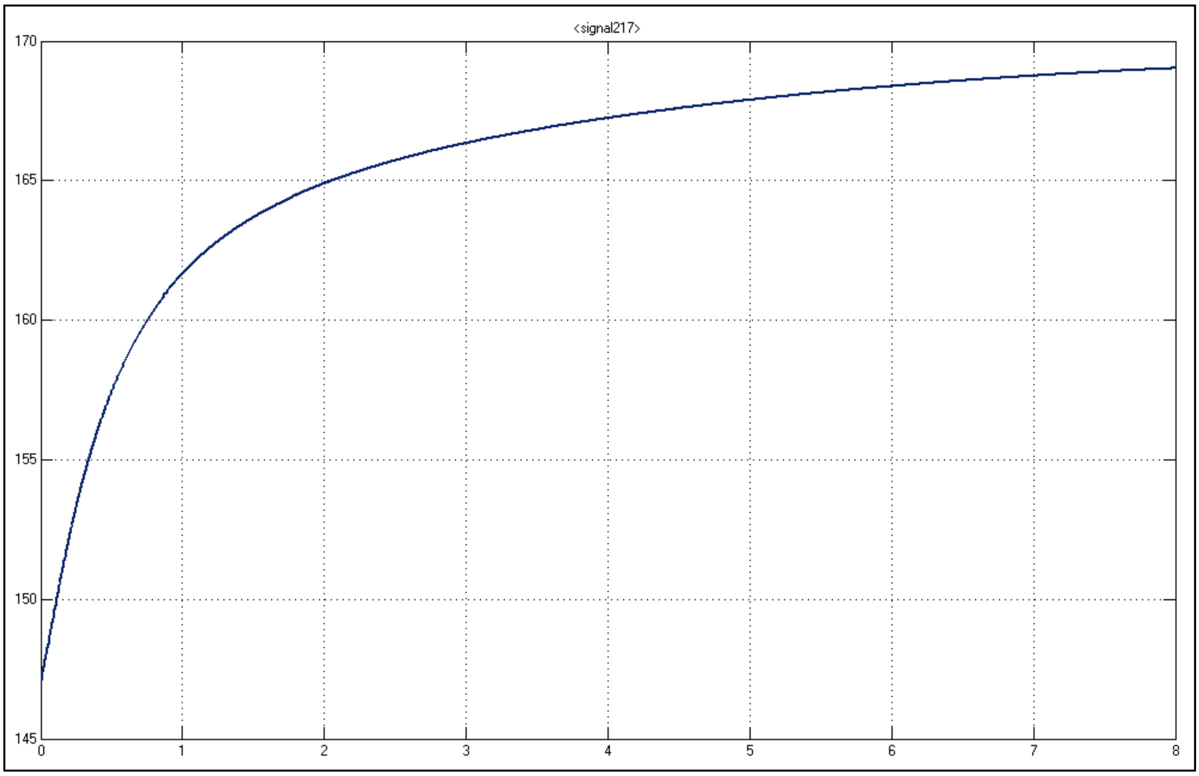

Figure 96: Plot of the temperature of compartment 4 (in °C) vs time (in hours)

$\Delta m_{13} = 200 - 0 = 200\ kg/h$

$\Delta T_{comp4} = 169.025 - 147.062 = 21.963^{o}C$

$K_p = 0.11$

$t_{63\%} = 0.871$

$t_{28\%} = 0.246$

$K_c K_p = 1.5$

$\frac{T_I}{t_{63\%}} = 0.24$

$\frac{T_d}{t_{63\%}} = 0$

$\tau = 0.938$

$\theta = 0$

$\boldsymbol{K_c = 13.64}$

$\boldsymbol{T_I = 0.21}$

$\boldsymbol{T_d = 0}$

Autoclave Pressure (400-PIC-2001)

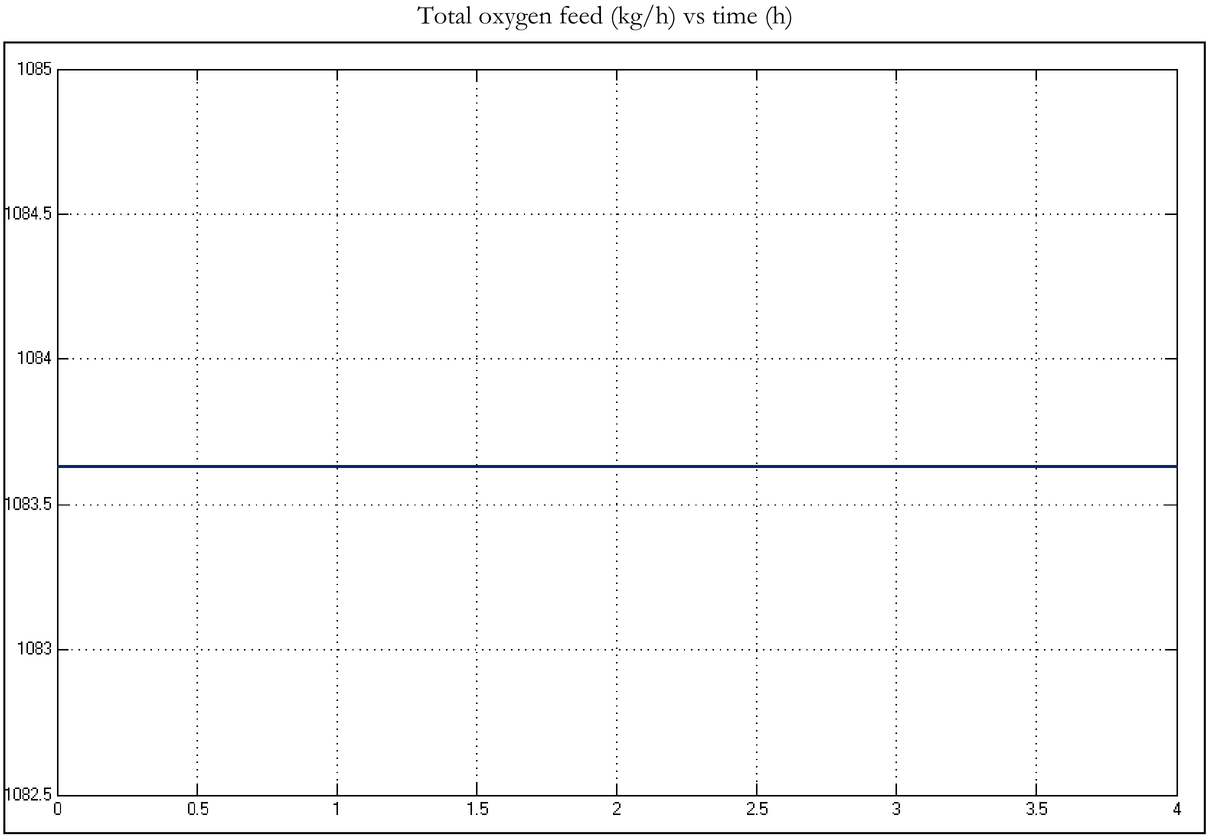

Figure 97: Plot of the total oxygen mass flow rate into the autoclave (in kg/h) vs time (in hours)

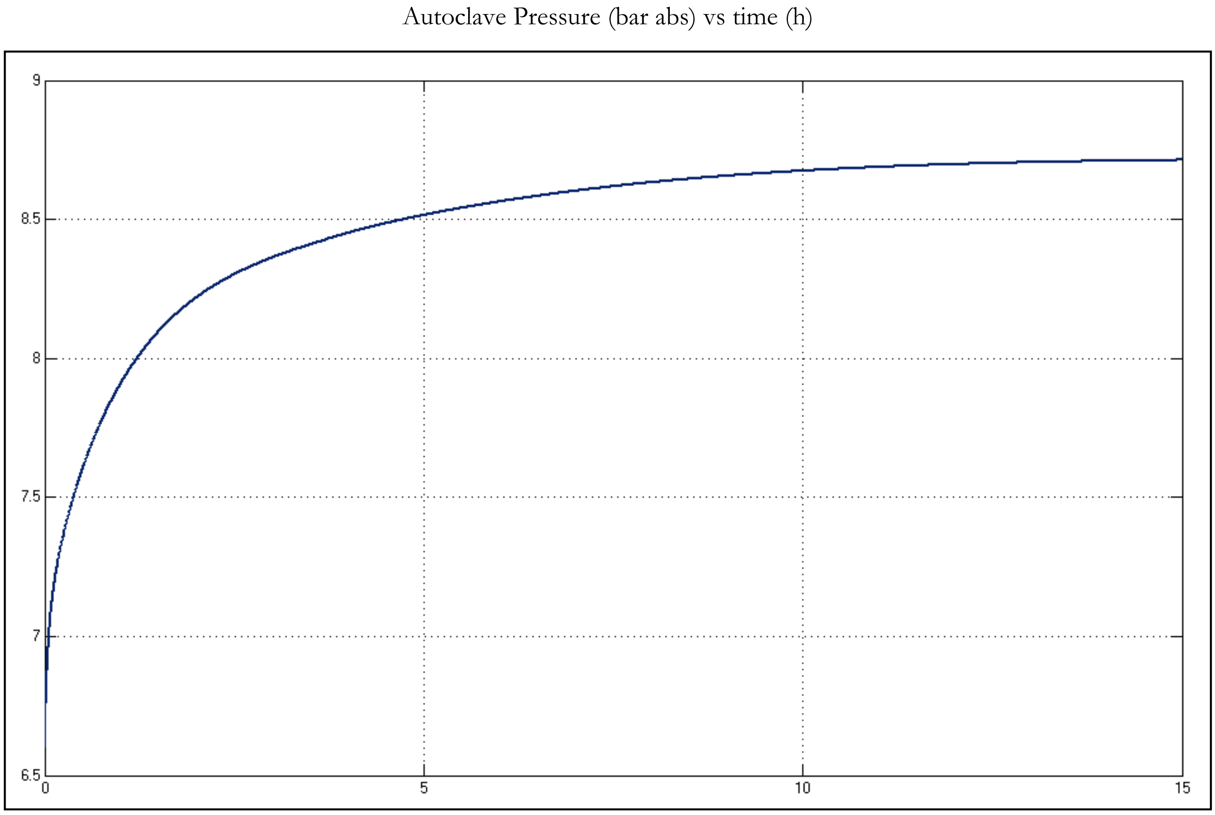

Figure 98: Plot of the absolute autoclave pressure (in bar) vs time (in hours)

$\Delta m_{O2} = 1083.63 - 903.0232 = 180.607\ kg/h$

$\Delta P = 8.713 - 6.6 = 2.113\ bar$

$K_p = 0.0117$

$t_{63\%} = 1.048\ h$

$t_{28\%} = 0.131\ h$

$\tau = 1.376$

$\theta = 0$

$K_c K_p = 1.5$

$\frac{T_I}{t_{63\%}} = 0.24$

$\frac{T_d}{t_{63\%}} = 0$

$\boldsymbol{K_c = 128.205}$

$\boldsymbol{T_I = 0.252}$

$\boldsymbol{T_d = 0}$

Temperature of Compartment 1 (400-TIC-2001)

Set point for 400-TIC-2001 (°C) vs time (h)

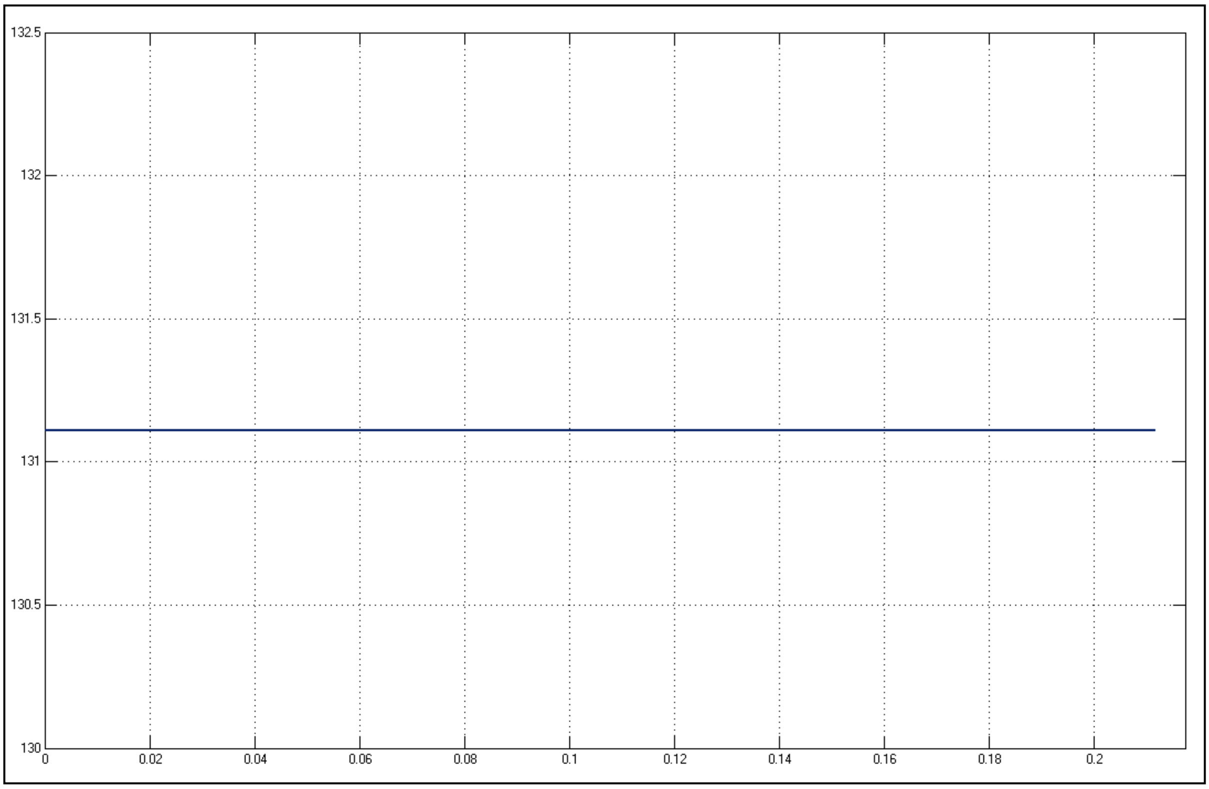

Figure 99: Plot of the set point of the temperature of compartment 1 versus time (in hours)

400-TIC-2001 (°C) vs time (h)

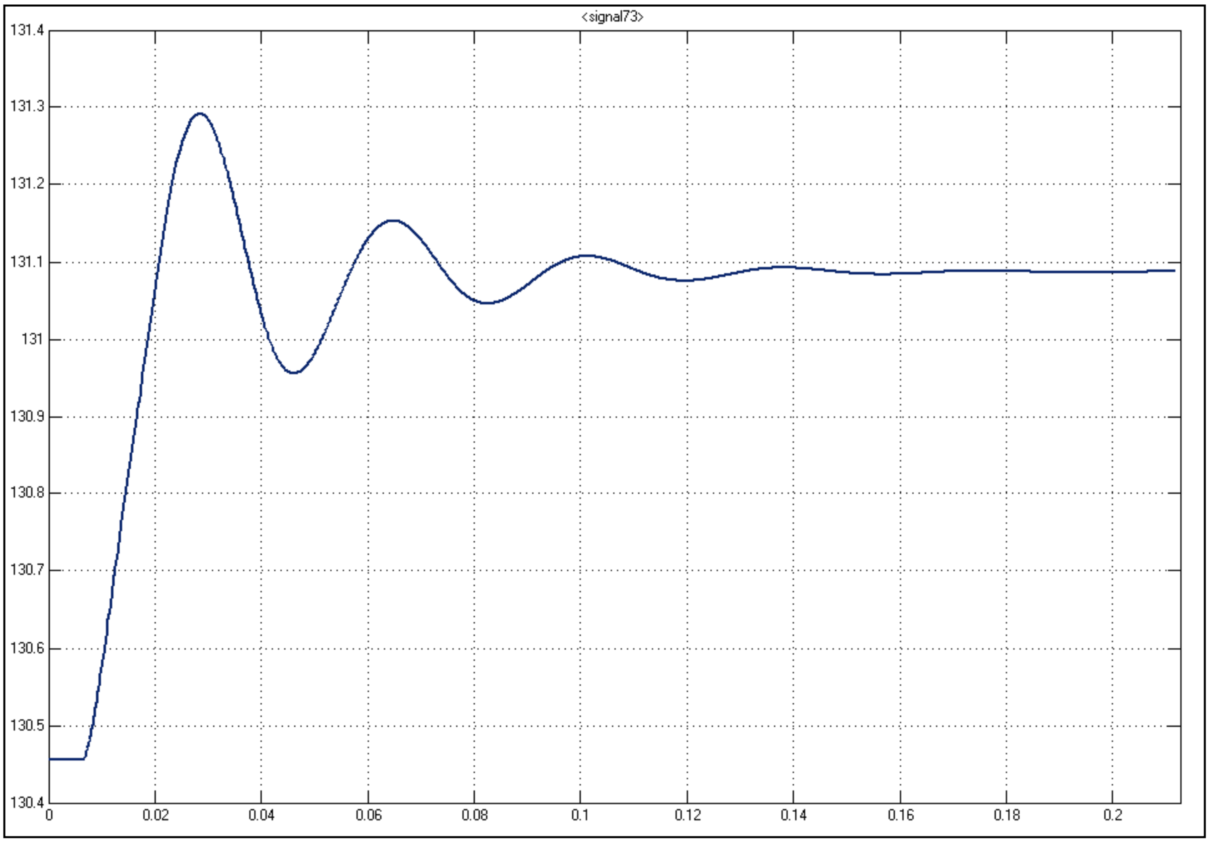

Figure 100: Plot of the temperature of compartment 1 versus time (in hours)

$\boldsymbol{n}(\mathbf{0}$ $\mathbf{07})$

F1.3 Fine Tuning

Mass Controller on 400-TK-10

In this test, the set point of the mass in 400-TK-10 is multiplied by 1.05 at time step 0.2. The set point, as well as the MV and CV responses, is plotted below.

Set point values for the mass in 400-TK-10 (kg) vs time (h)

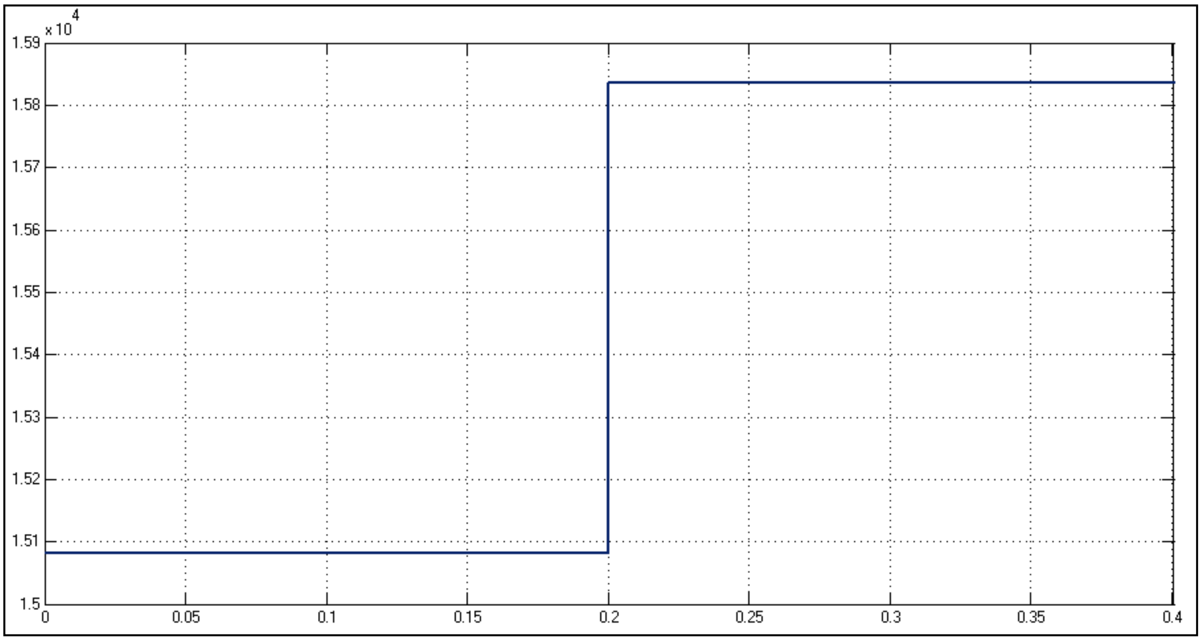

Figure 101: Plot of set point sent to the mass controller of 400-TK-10 vs time (in hours)

Mass flow rate of stream 1 (kg/h) vs time (h)

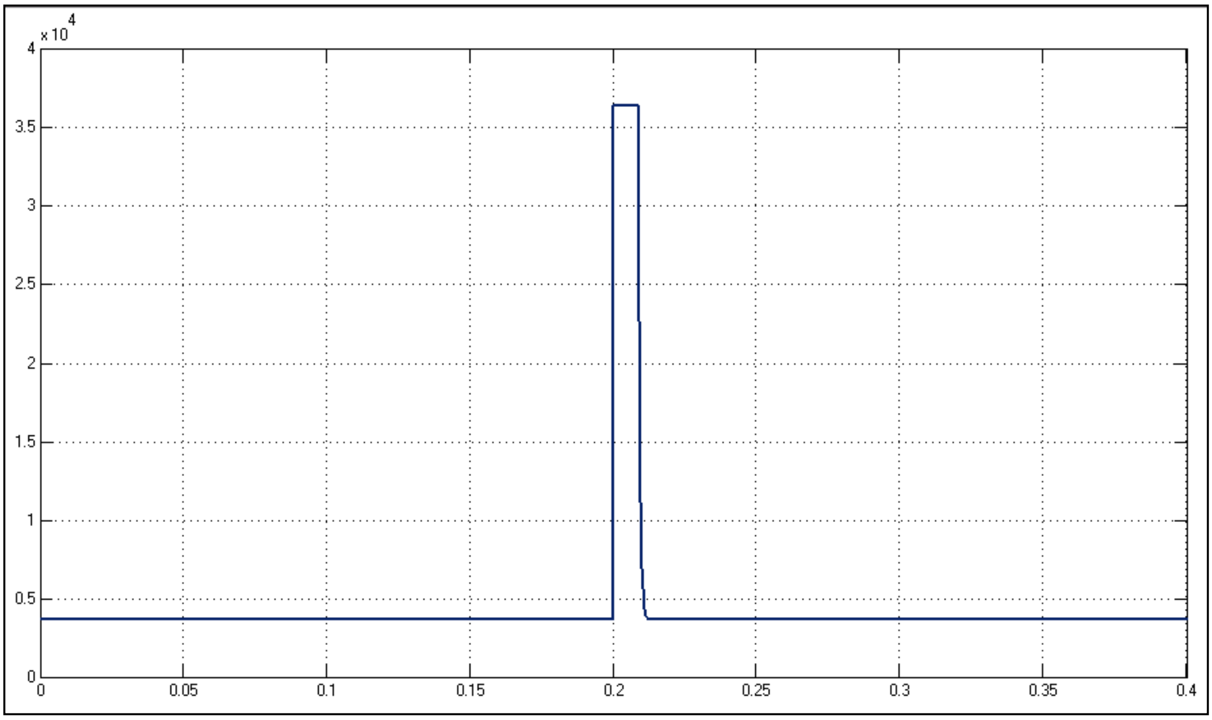

Figure 102: Plot of the mass flow rate of stream 1 vs time (in hours)

Mass in 400-TK-10 (kg) vs time (h)

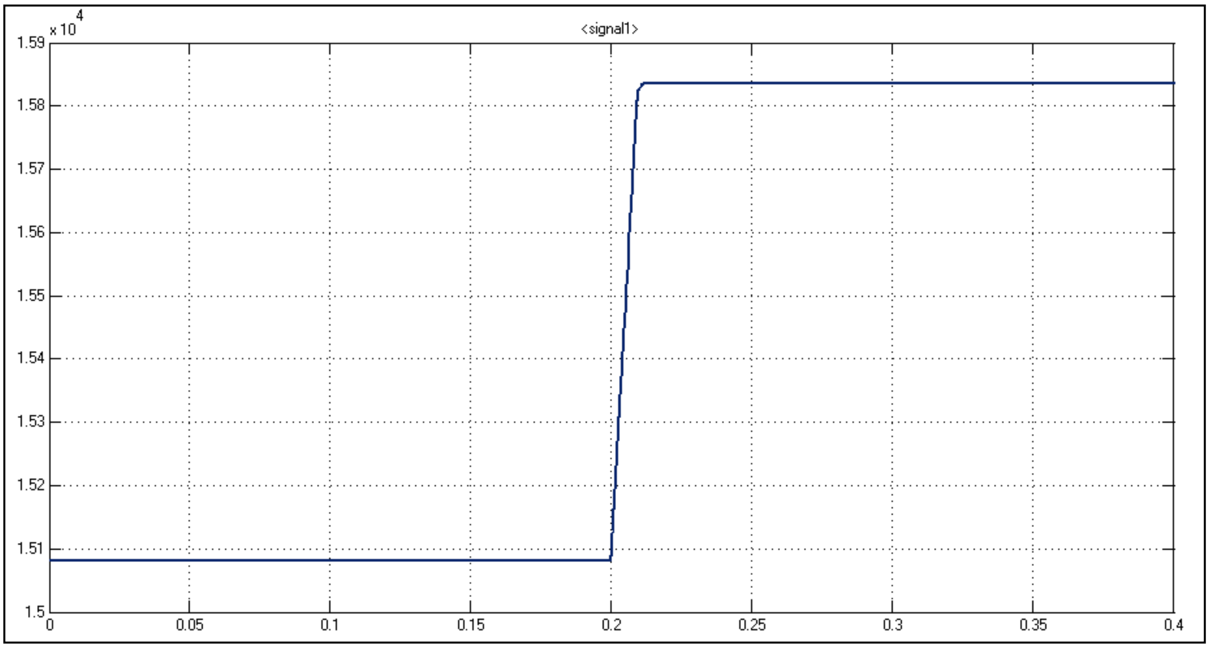

Figure 103: Plot of the mass of 400-TK-10 vs time (in hours)

Due to the fact that this is a controller of an integrator, the proportional and integral controller modes cannot be separated. The maximum deviation in the MV and the time the CV takes to reach the new set points are the main factors taken into consideration for this fine tuning. While it can be seen that the MV is limited just after the change is made at 0.2 hours, and still the CV reaches its new set point in less than 1 minute. This is satisfactory behaviour.

Note that Lonmin could not provide flow rate limits, and therefore reasonable, arbitrary values are used in these tests.

Mass Controller on 400-TK-20

In this test, the set point of the mass in 400-TK-20 is multiplied by 0.95 at time step 0.2. Note that at the start of this test, the original K_c value was divided by 2 to allow the model to run within a reasonable time frame.

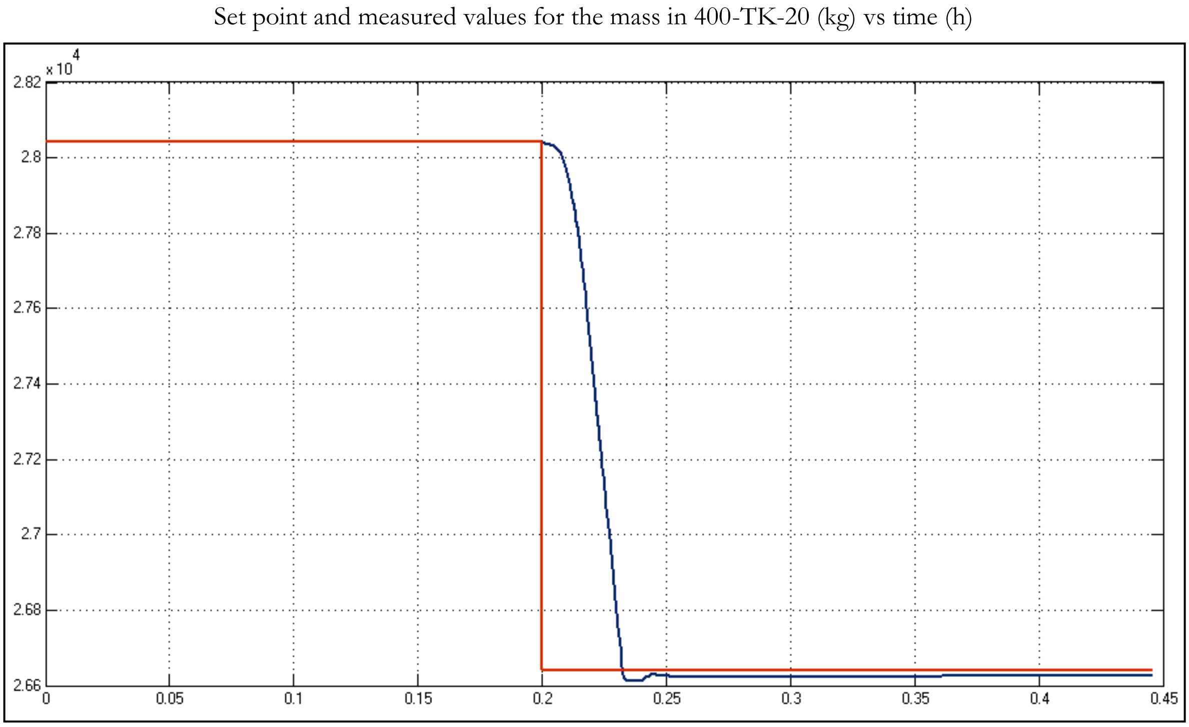

Set point and measured values for the mass in 400-TK-20 (kg) vs time (h)

Figure 104: Plot of set point (red) and measured (blue) values of the mass in 400-TK-20 vs time (in hours)

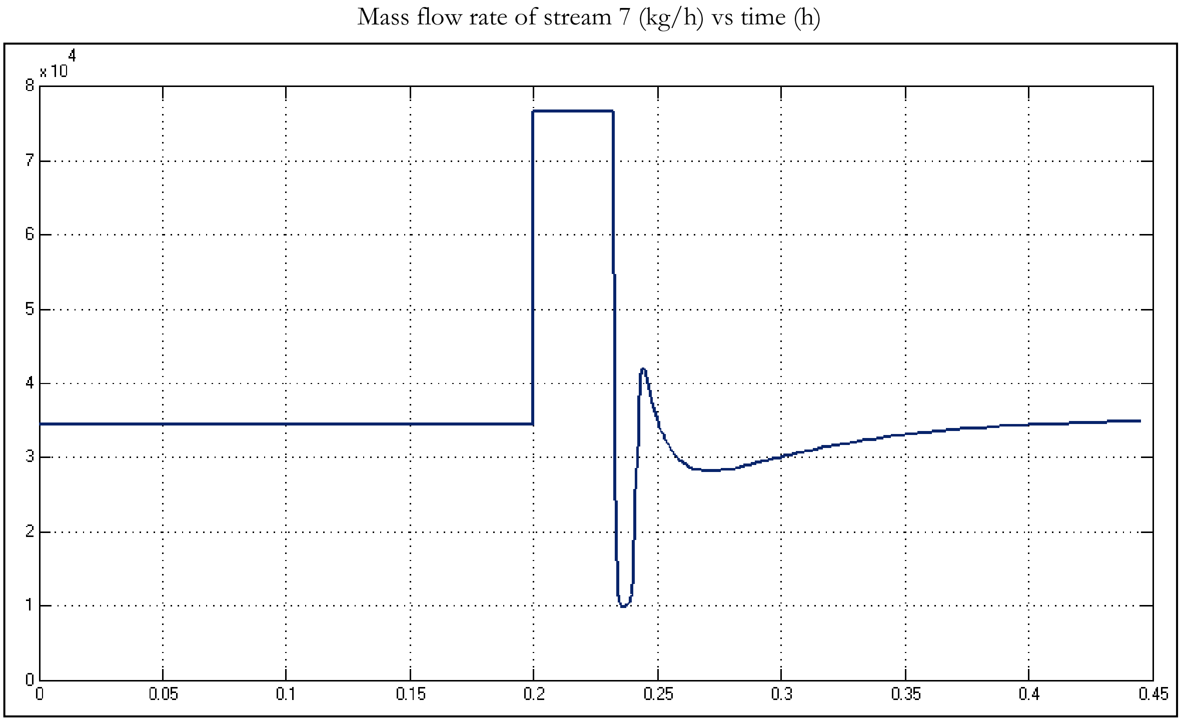

Mass flow rate of stream 7 (kg/h) vs time (h)

Figure 105: Plot of the mass flow rate of stream 7 vs time (in hours)

In this fine-tuning test the maximum deviation and settling time of the CV are again the important parameters, since an integrator is controlled. It can be seen from the plot of stream 7 that MV change is limited, and this leads to the CV only crossing its SP after 2 minutes. This control is deemed acceptable.

Mass Controller on Compartment 3

In this test, the set point of the mass in compartment 3 is multiplied by 0.95 at time step 0.2.

Set point and measured values for the mass in compartment 3 (kg) vs time (h)

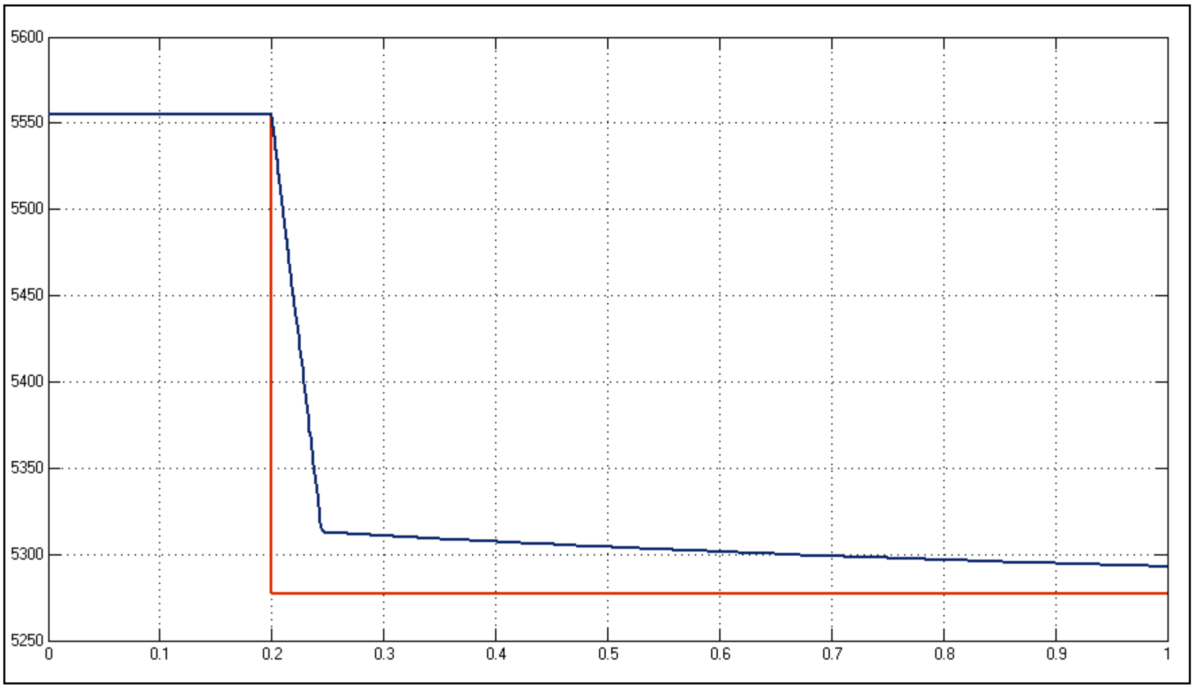

Figure 106: Plot of set point (red) and measured (blue) values of the mass in compartment 3 vs time (in hours)

Mass flow rate of stream 14 (kg/h) vs time (h)

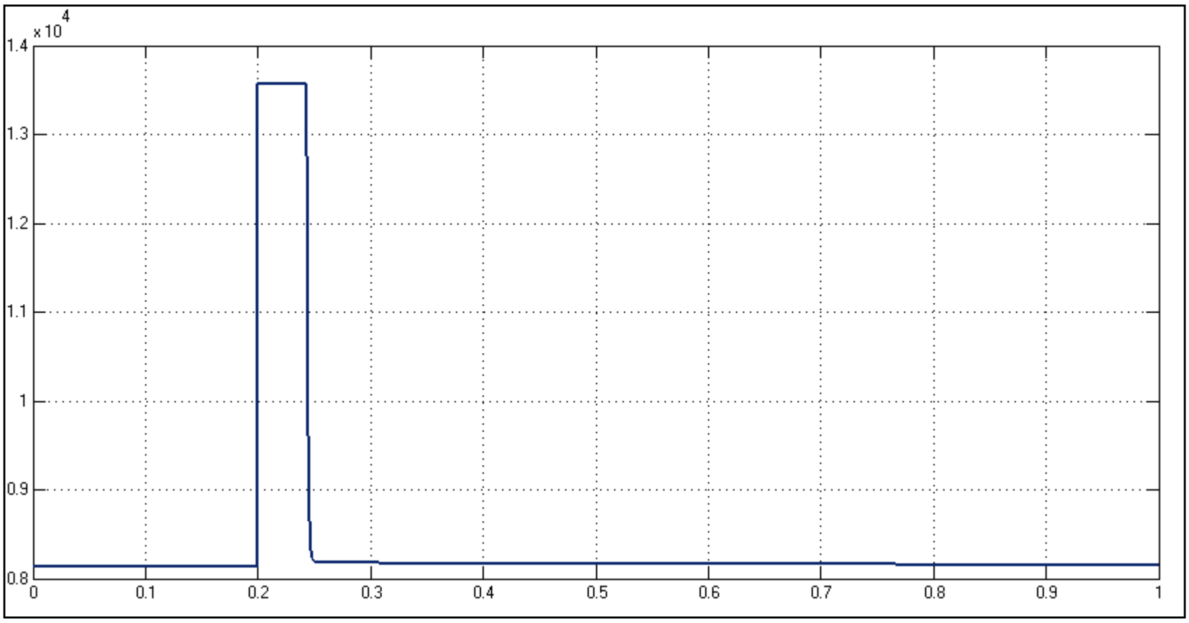

Figure 107: Plot of the mass flow rate of stream 14 vs time (in hours)

From these plots it can be clearly seen that the CV is not reached within 1 hour. The reason for this is the anti-reset windup that inhibits the controller action to a too large extent. The anti-reset windup time (T_t) is changed from the T_I value to $T_I/9$, and the test is repeated.

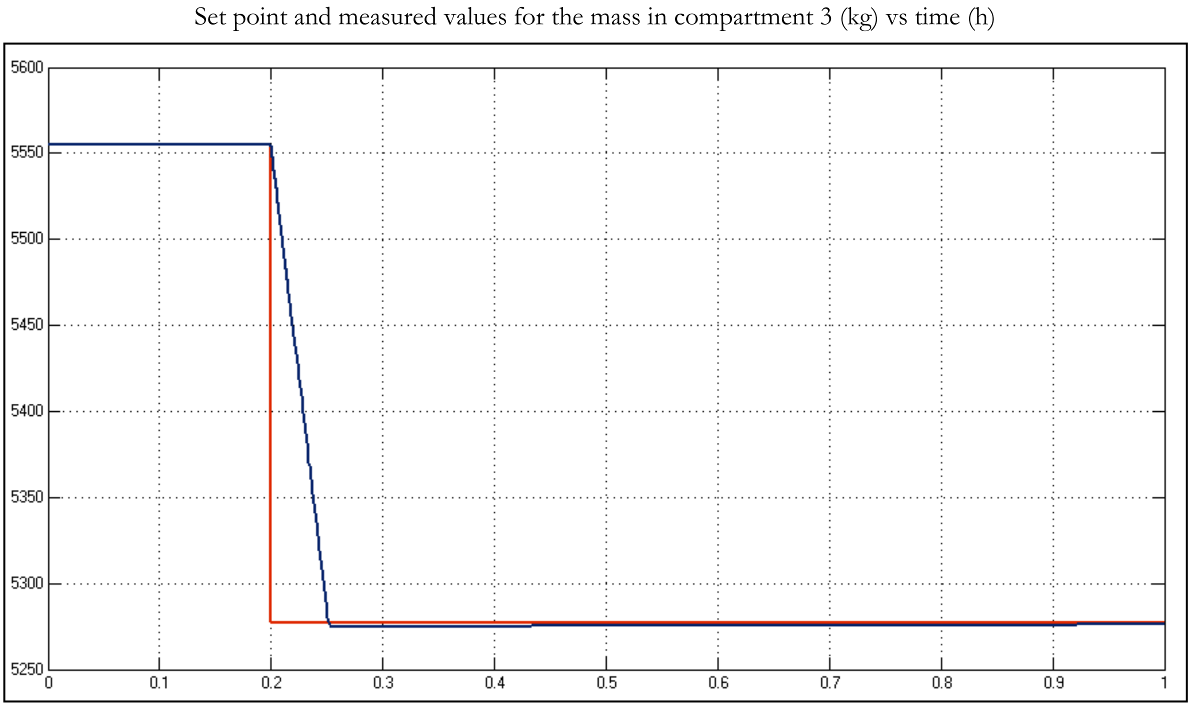

Figure 108: Plot of set point (red) and measured (blue) values of the mass in compartment 3 vs time (in hours)

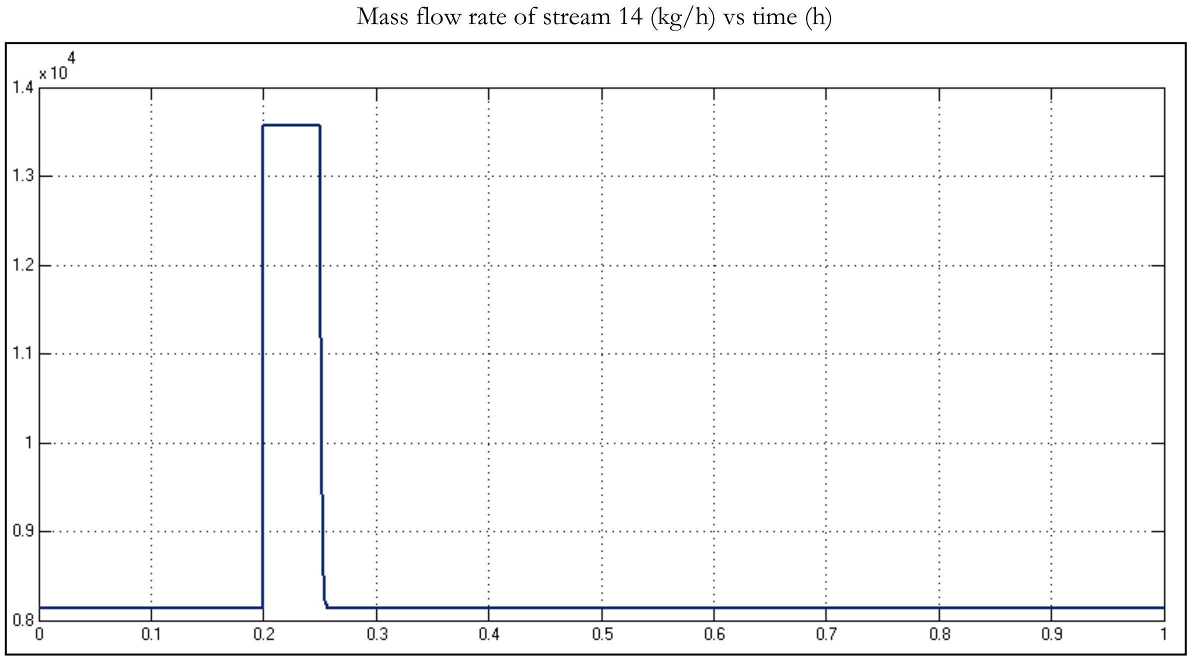

Figure 109: Plot of the mass flow rate of stream 14 vs time (in hours)

While it can be seen that the MV reaches its upper limit, the CV reaches the new SP much faster with the adapted T_t value.

Mass Controller on Compartment 4

In this test, the set point of the mass in compartment 4 is multiplied by 0.95 at time step 0.01.

Set point and measured values for the mass in compartment 4 (kg) vs time (h)

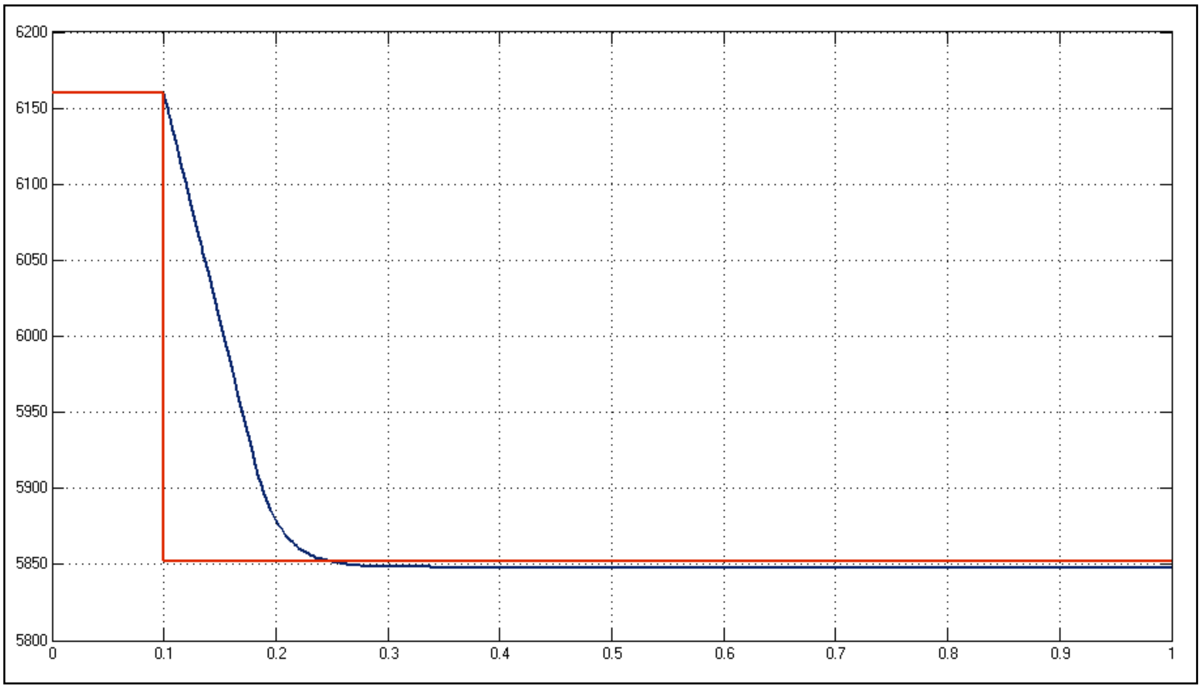

Figure 110: Plot of set point (red) and measured (blue) values of the mass in compartment 4 vs time (in hours)

Mass flow rate of stream 22 (kg/h) vs time (h)

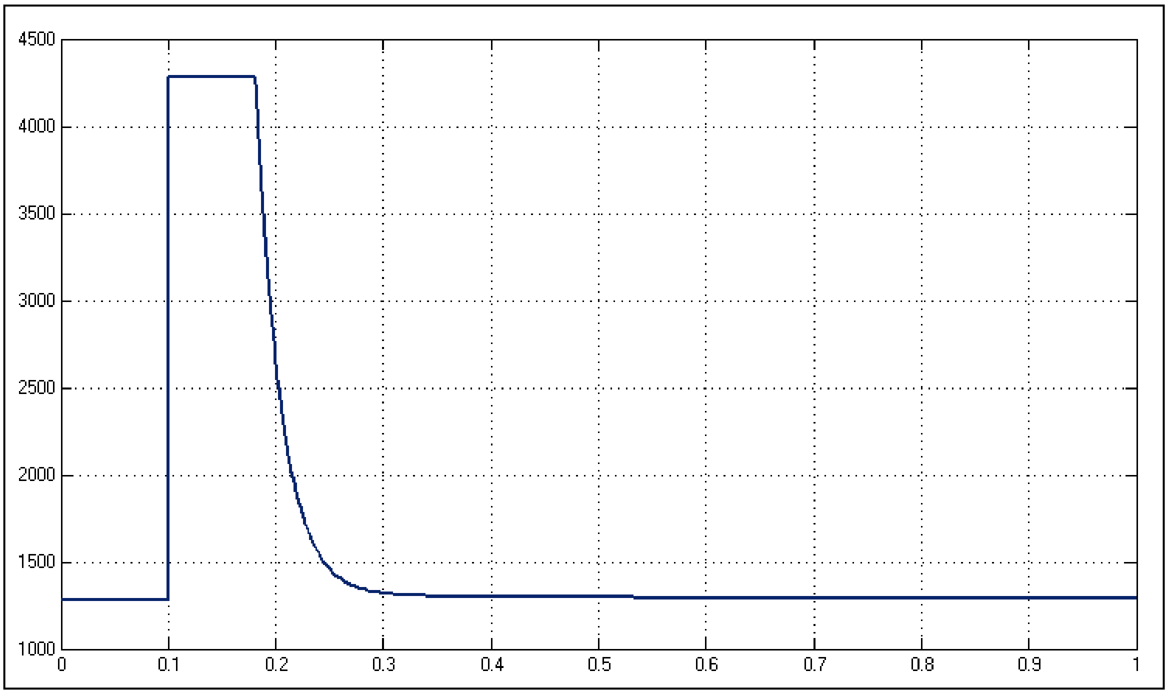

Figure 111: Plot of the mass flow rate of stream 22 vs time (in hours)

The steady-state offset of the CV is approximately 0.1% of its mean, and therefore it is negligible. This control is deemed satisfactory and is not in clear need of adaption.

Mass Controller on 400-TK-040

In this test, the set point of the mass in 400-TK-040 is multiplied by 0.95 at time step 0.1.

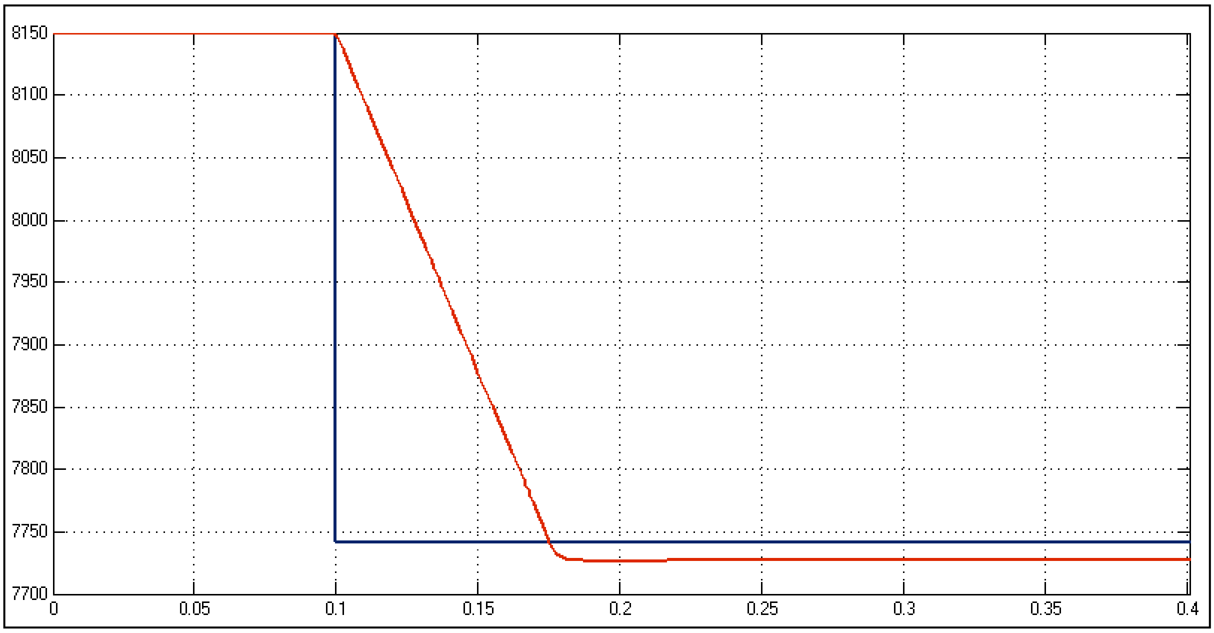
Set point and measured values for the mass in 400-TK-040 (kg) vs time (h)

Figure 112: Plot of set point (red) and measured (blue) values of the mass in 400-TK-040 vs time (in hours)

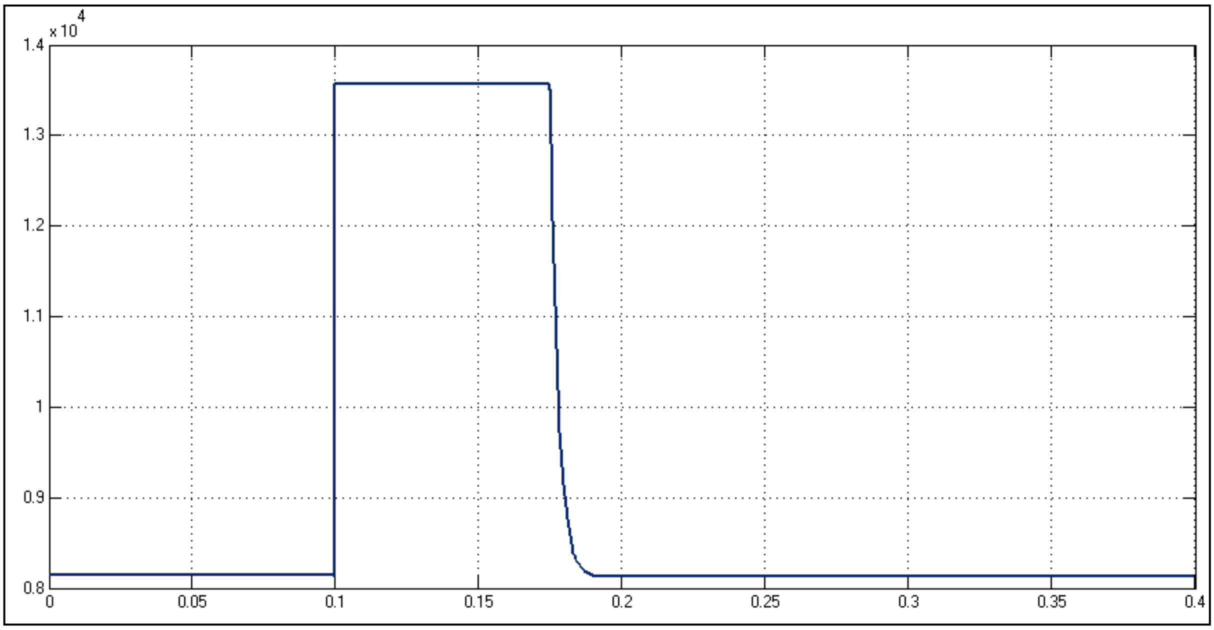
Mass flow rate of stream 15 (kg/h) vs time (h)

Figure 113: Plot of the mass flow rate of stream 15 vs time (in hours)

It can be seen from these figures that there is a steady-state offset in the CV. This is found to be caused by suboptimal tuning of the anti-reset windup time (T_I). It is changed from T_I to $T_I/10$, and the test is repeated.

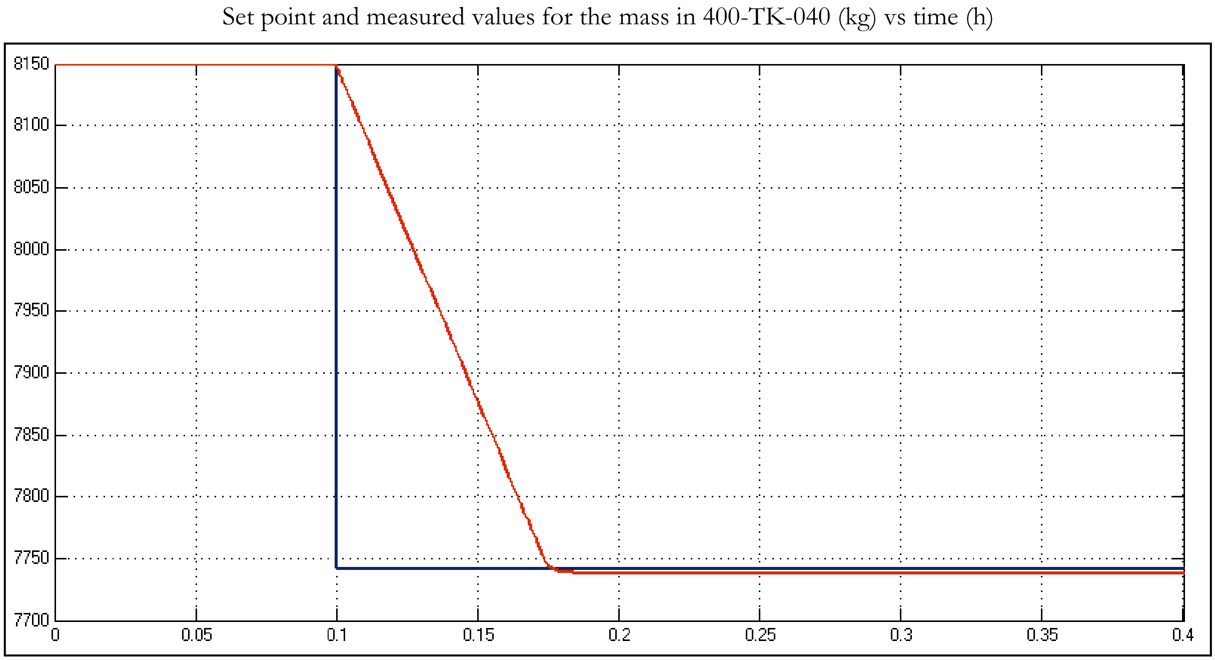

Figure 114: Plot of set point (red) and measured (blue) values of the mass in 400-TK-040 vs time (in hours)

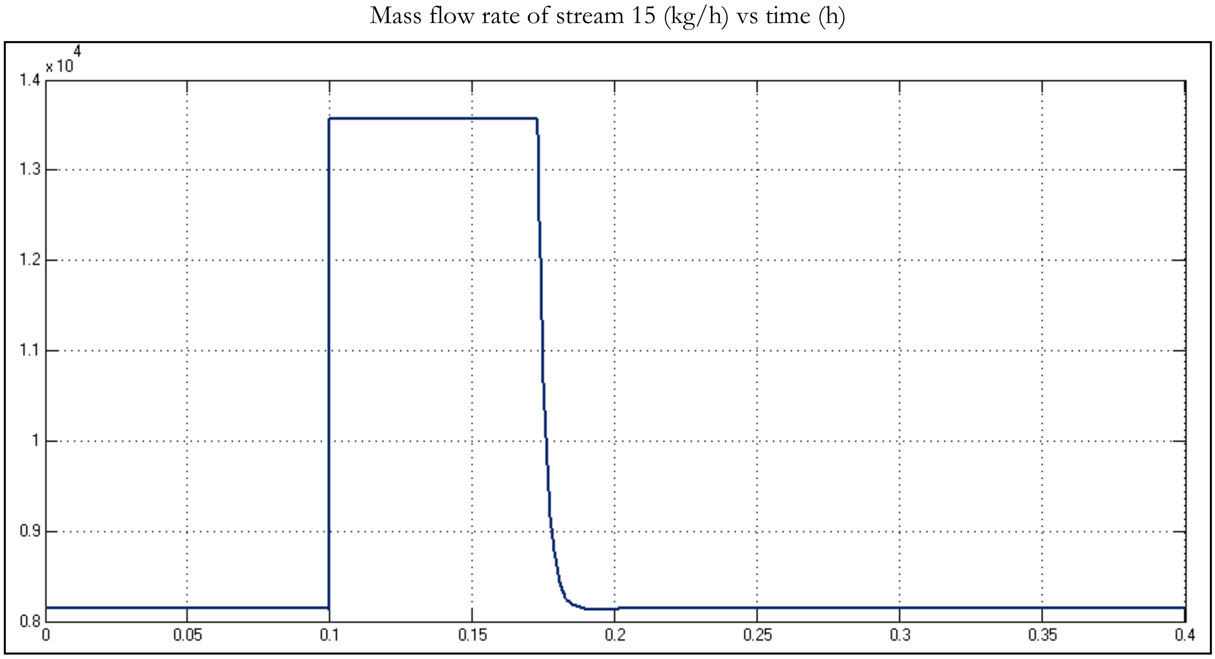

Figure 115: Plot of the mass flow rate of stream 15 vs time (in hours)

This is a much improved response. Note that the slow CV change is caused by the MV reaching its upper limit.

Mass Controller on 400-TK-050

In this test, the set point of the mass in 400-TK-050 is multiplied by 1.05 at time step 0.1.

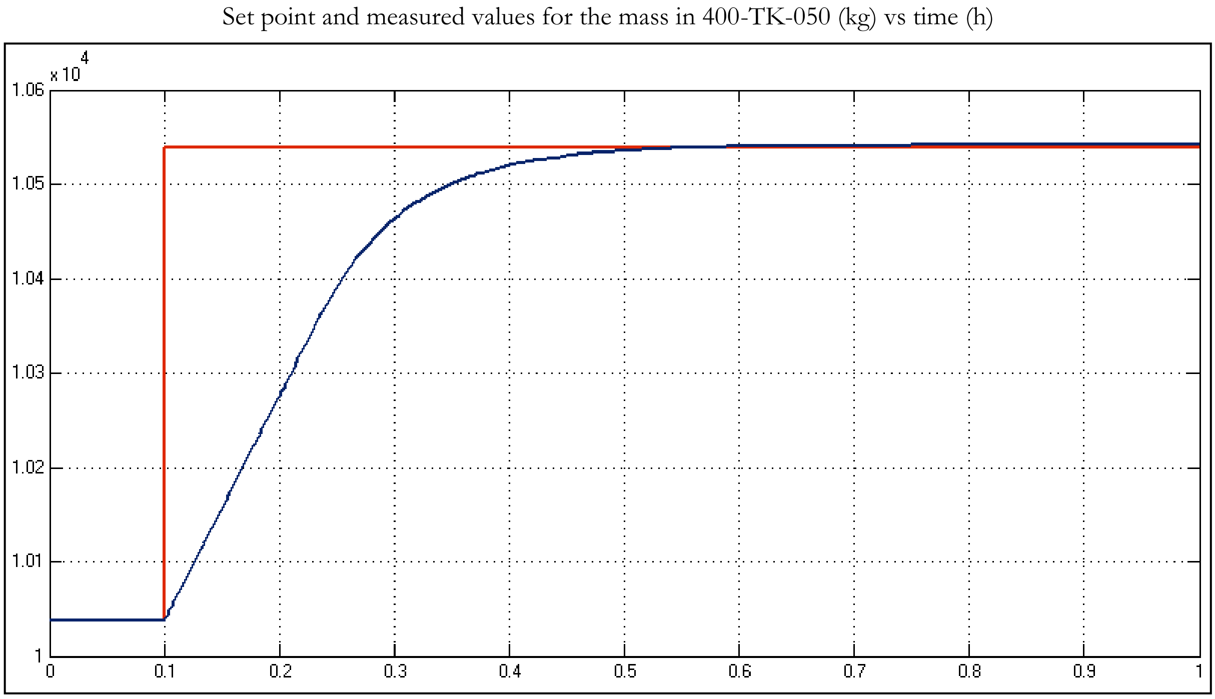
Set point and measured values for the mass in 400-TK-050 (kg) vs time (h)

Figure 116: Plot of set point (red) and measured (blue) values of the mass in 400-TK-050 vs time (in hours)

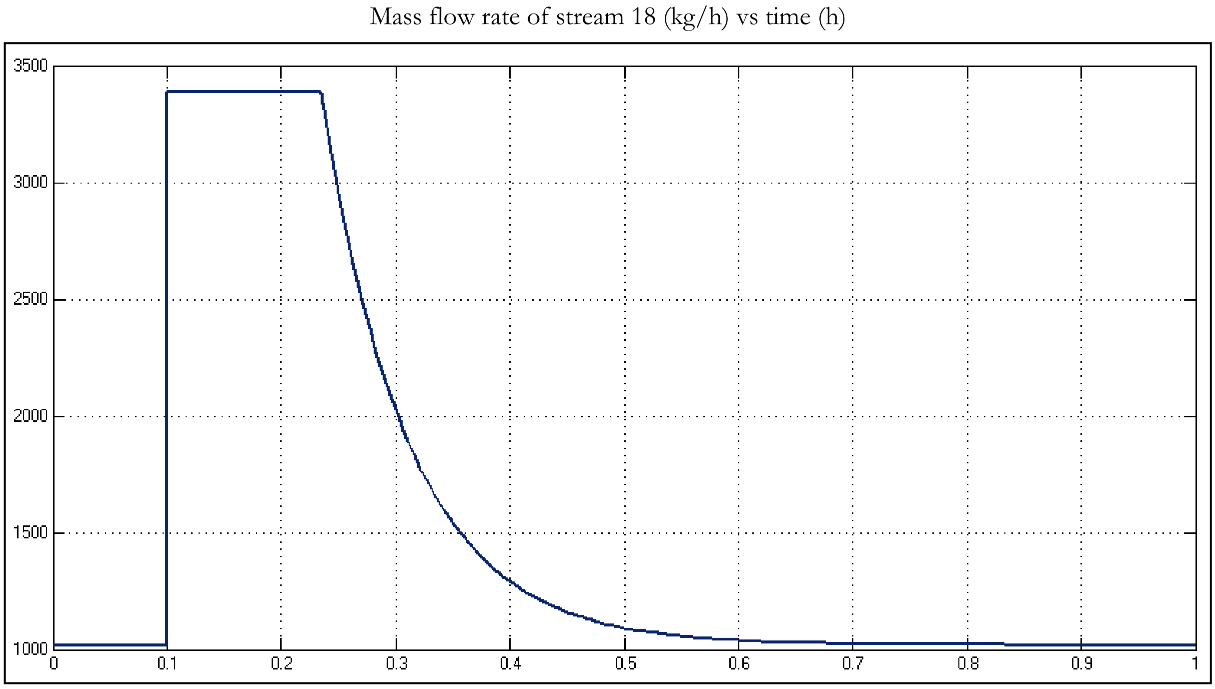
Mass flow rate of stream 18 (kg/h) vs time (h)

Figure 117: Plot of the mass flow rate of stream 18 vs time (in hours)

From the above figures it can be seen that the MV streams (represented by stream 18) reach their upper limits. This is due to the fact that the initial valve positions for all of these streams are assumed to be the same, and that the maximum flow rate of each of these additive streams has the same ratios as the initial flow rates. The steady-state offset of the CV can be seen to be negligible, and therefore the control is satisfactory.

Temperature of Compartment 1 (400-TIC-2001)

In this test, the set point of the temperature of compartment 1 is multiplied by 0.99 at time step 0. It should be noted that there is the limitation on the flash recycle stream to be a maximum of 95% of stream 7.

Set point and measured values for the temperature of compartment 1 (°C) vs time (h)

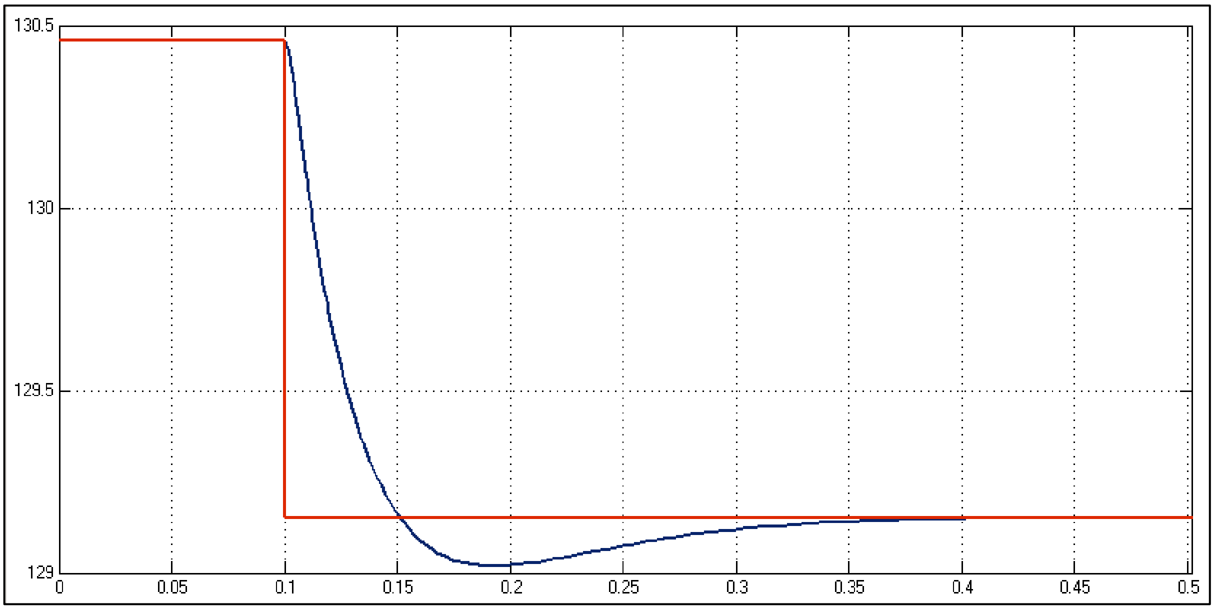

Figure 118: Plot of set point (red) and measured (blue) values of the temperature of compartment 1 (°C) vs time (in hours)

Non-limited mass flow rate of stream 9 (kg/h) vs time (h)

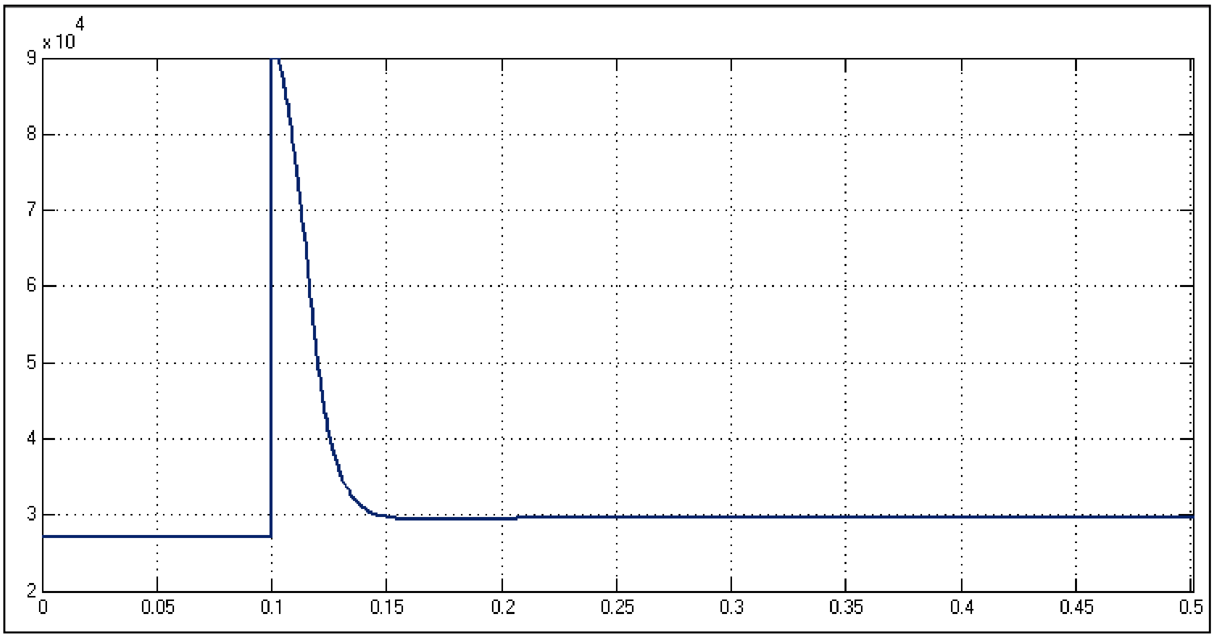

Figure 119: Plot of the mass flow rate of stream 9 vs time (in hours)

Limited mass flow rate of stream 9 (kg/h) vs time (h)

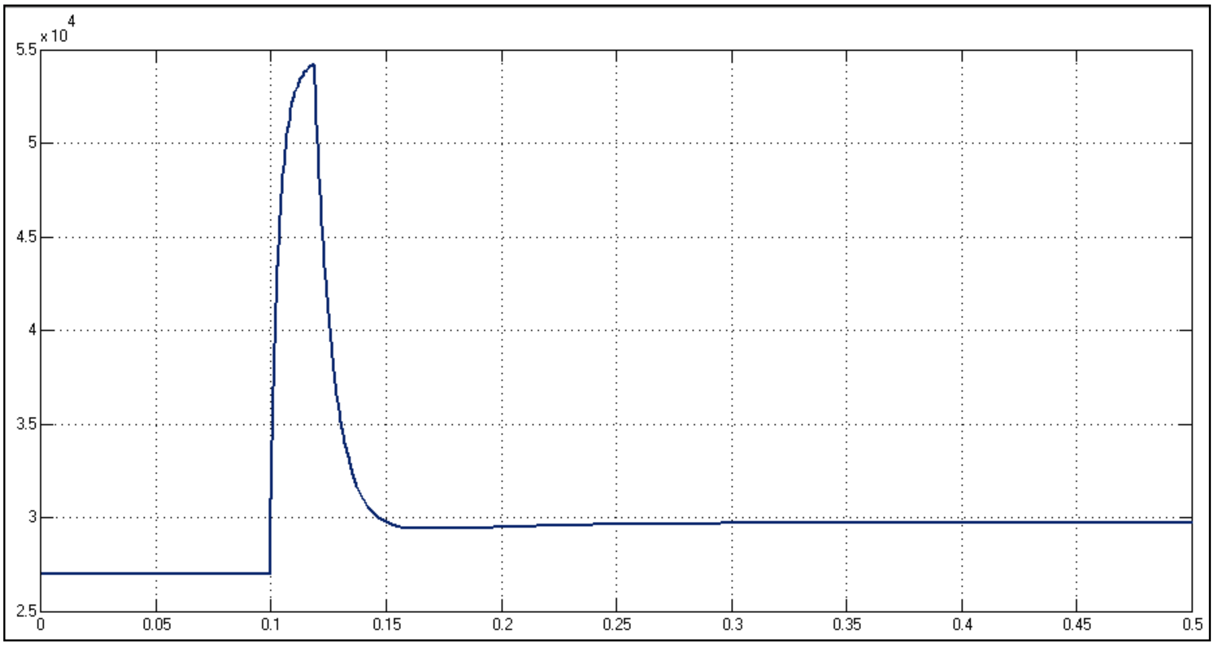

Figure 120: Plot of the mass flow rate of stream 9 (limited to 95% of stream 7) vs time (in hours)

From the two MV plots it can be seen that the peak of the limited flash recycle rate is much smaller than the one not limited. The one not limited gives an MV overshoot of more than 30 times that of its steady-state change. The controller can therefore be detuned without leading to poorer CV behaviour.

This test is repeated after the Kc value is divided by a factor of 3:

Set point and measured values for the temperature of compartment 1 (°C) vs time (h)

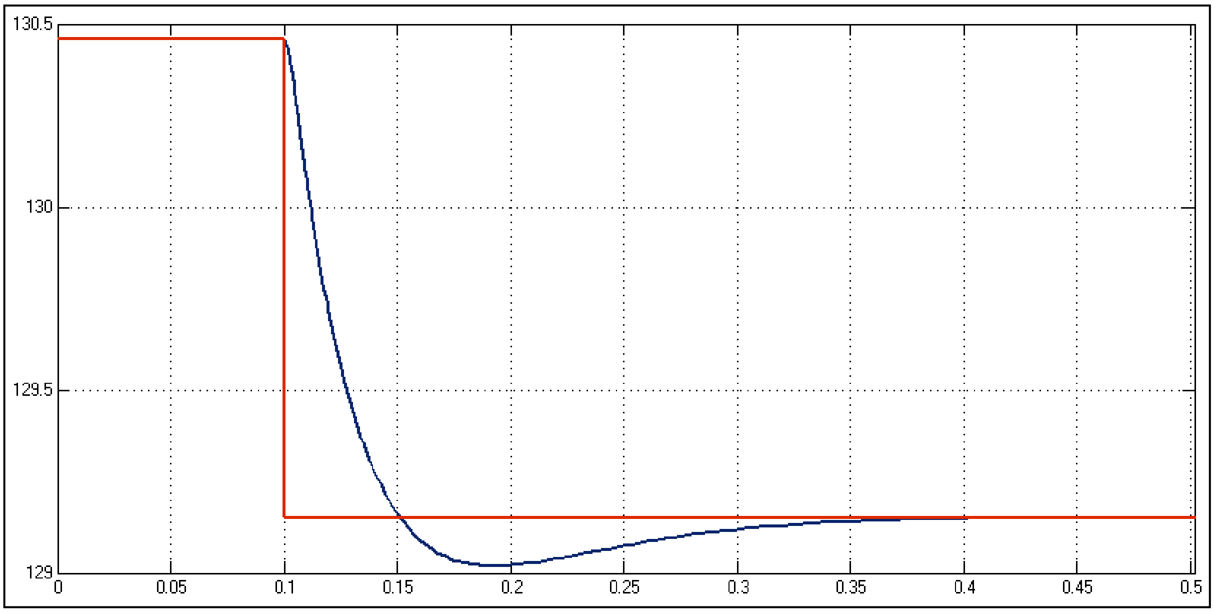

Figure 121: Plot of set point (red) and measured (blue) values of the temperature of compartment 1 (°C) vs time (in hours)

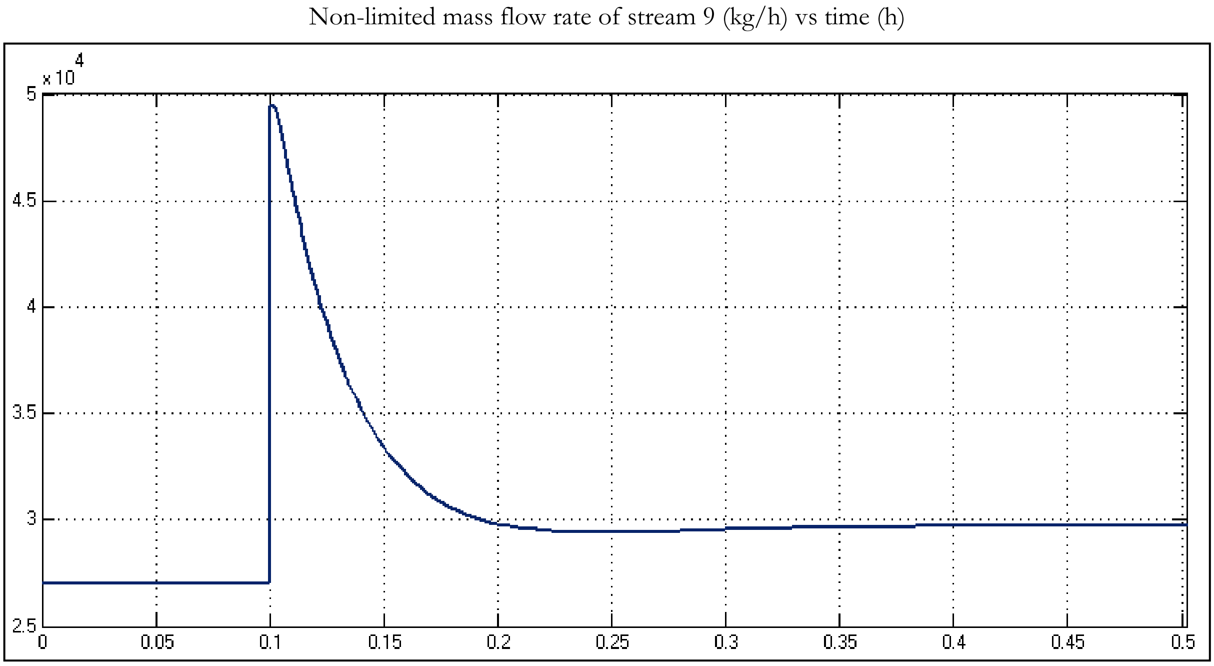
Non-limited mass flow rate of stream 9 (kg/h) vs time (h)

Figure 122: Plot of the mass flow rate of stream 9 vs time (in hours)

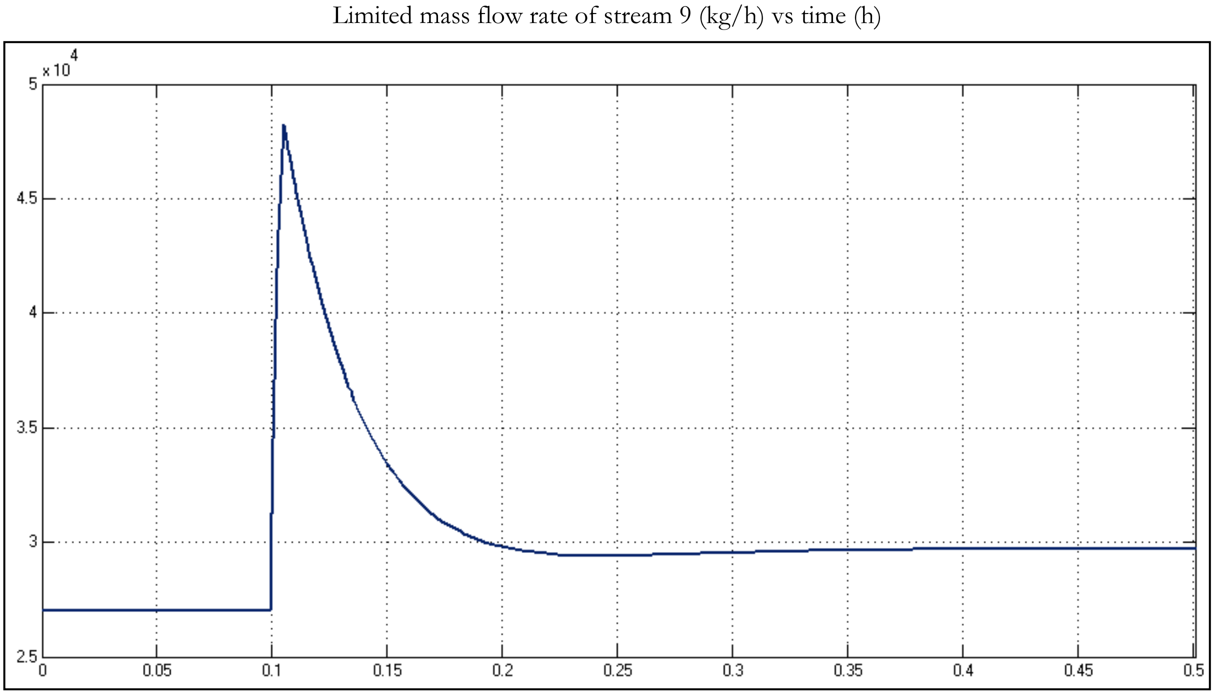
Limited mass flow rate of stream 9 (kg/h) vs time (h)

Figure 123: Plot of the mass flow rate of stream 9 (limited to 95% of stream 7) vs time (in hours)

It can clearly be seen that both the limited and non-limited MV behaviour are more acceptable, while the CV response does not change noticeably. While the initial MV change is more than 150% of the final, steady-state change, the fact that this control is limited by the mass control on 400-TK-20 deems it satisfactory. Note that the new SP is crossed 3 minutes after it is introduced.

Temperature of Compartment 3 (400-TIC-2003)

In this test, the set point of the temperature of compartment 3 is multiplied by 0.98 at time step 0.1. Note that the Kc value is divided by 5 from the start in order to ensure that the model runs within a reasonable time frame.

Set point and measured values for the temperature of compartment 3 (°C) vs time (h)

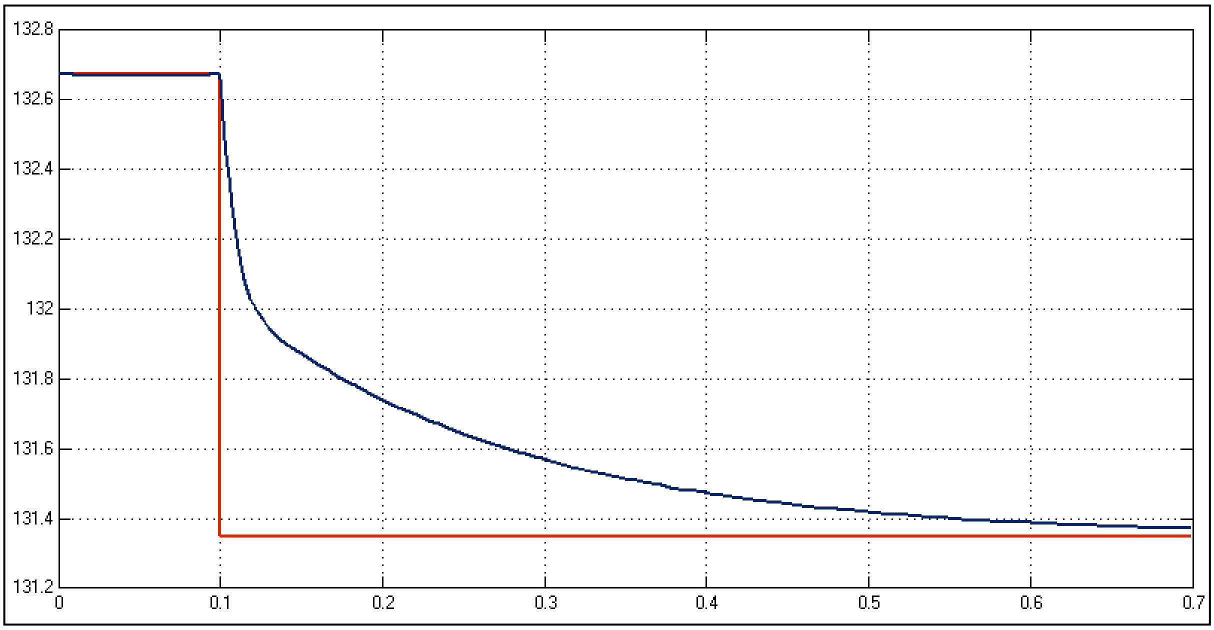

Figure 124: Plot of set point (red) and measured (blue) values of the temperature of compartment 3 (°C) vs time (in hours)

Mass flow rate of cooling water for compartment 3 (kg/h) vs time (h)

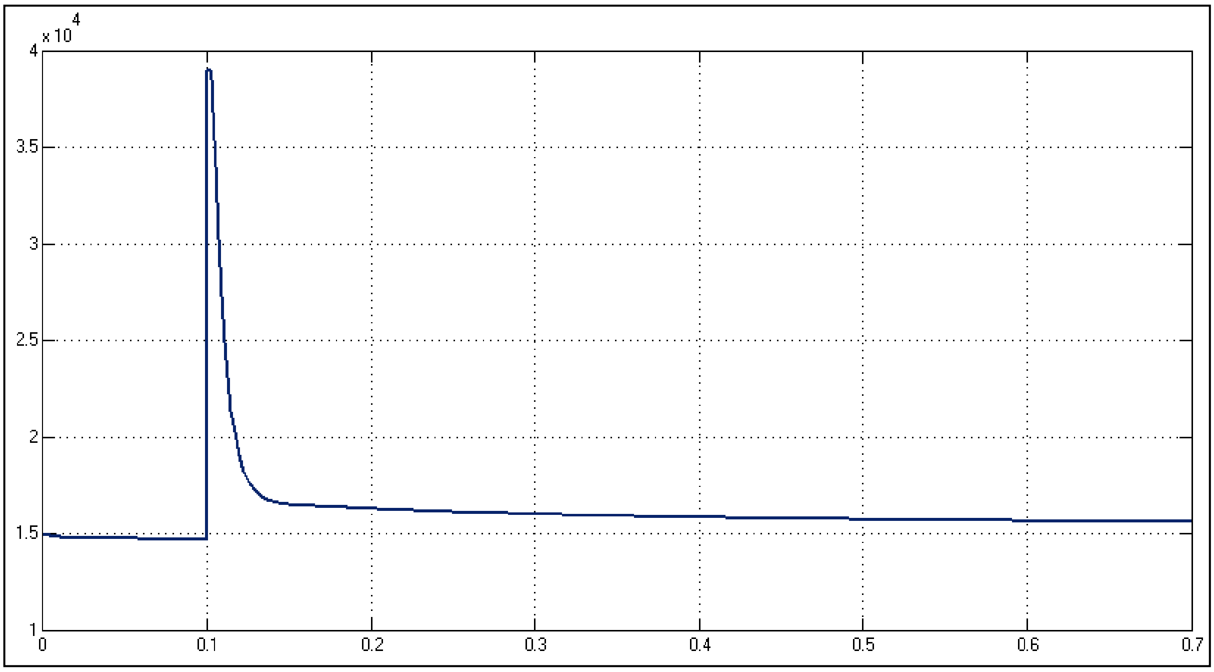

Figure 125: Plot of the mass flow rate of the cooling water for compartment 3 vs time (in hours)

From these plots it can be seen that the MV reaches an upper limit, and that the anti-reset windup that results inhibits the CV performance. The anti-reset windup time (T_t) is changed from T_I to $T_I/40$, and the test is redone.

Set point and measured values for the temperature of compartment 3 (°C) vs time (h)

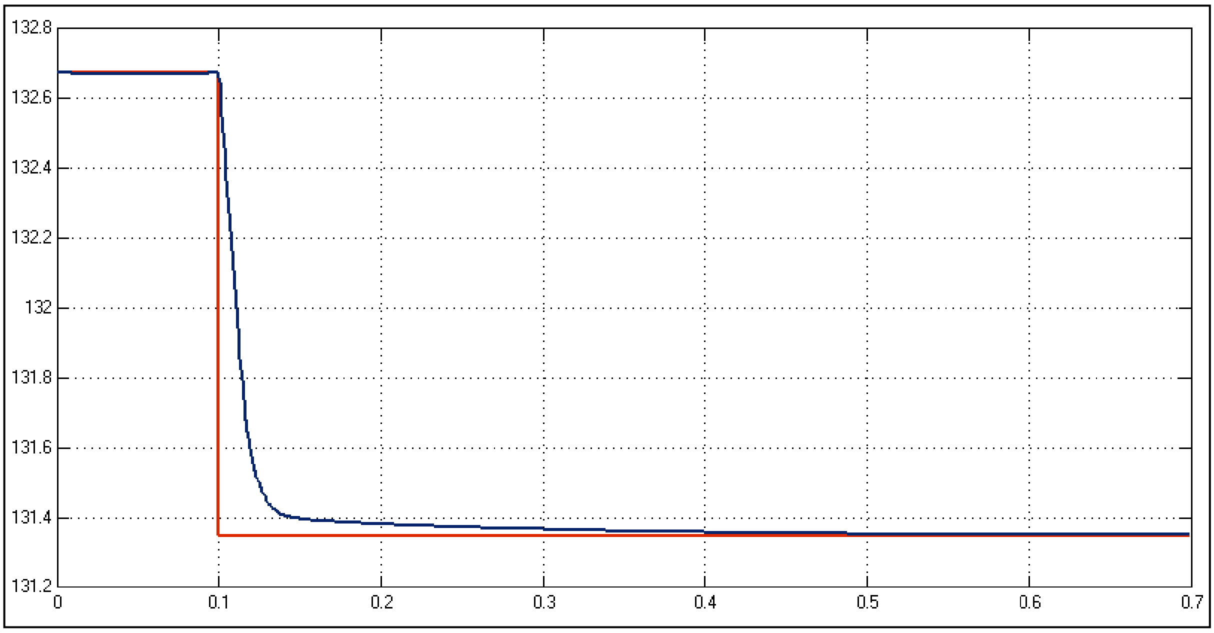

Figure 126: Plot of set point (red) and measured (blue) values of the temperature of compartment 3 (°C) vs time (in hours)

Mass flow rate of cooling water for compartment 3 (kg/h) vs time (h)

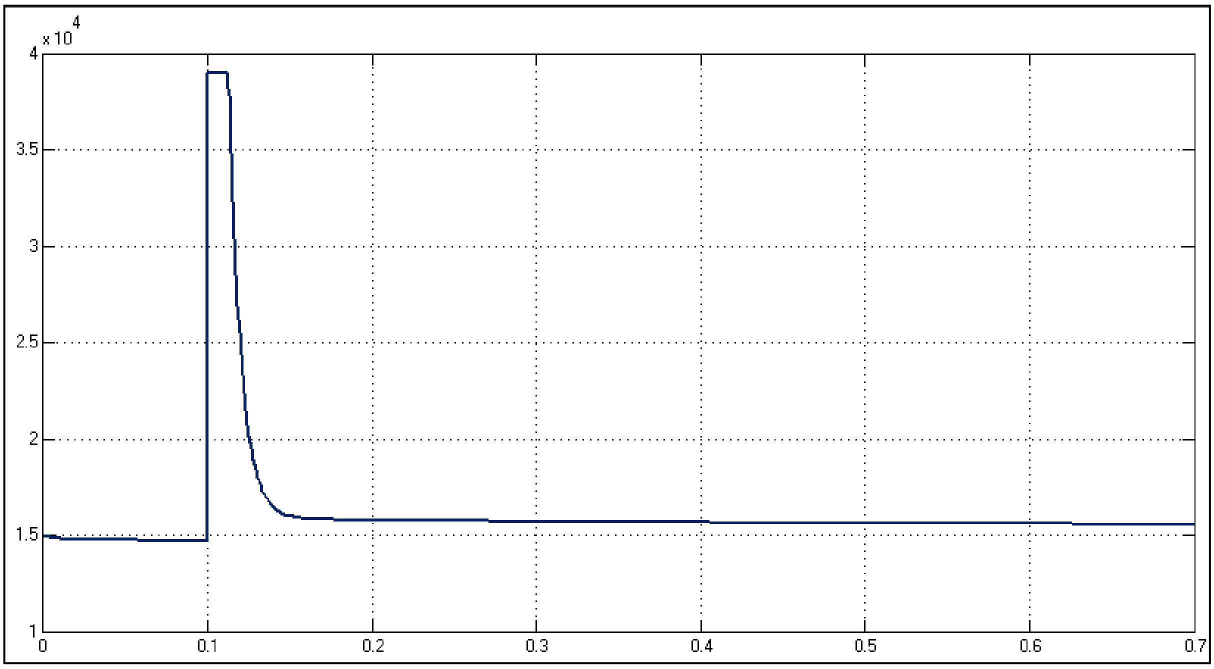

Figure 127: Plot of the mass flow rate of the cooling water for compartment 3 vs time (in hours)

It can be seen that the adjusted T_t value leads to much improved control, even with the MV reaching its upper limit.

Temperature of Compartment 4 (400-TIC-2005)

In this test, the set point of the temperature of compartment 4 is multiplied by 1.1 at time step 0.1.

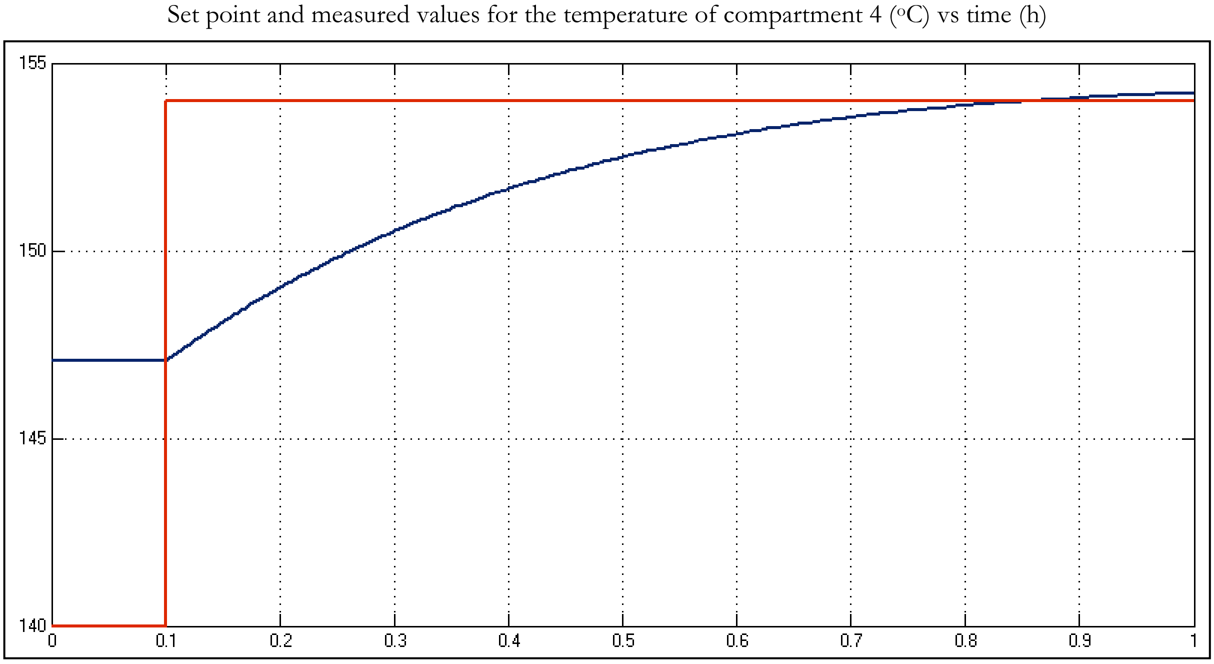

Figure 128: Plot of set point (red) and measured (blue) values of the temperature of compartment 4 (°C) vs time (in hours)

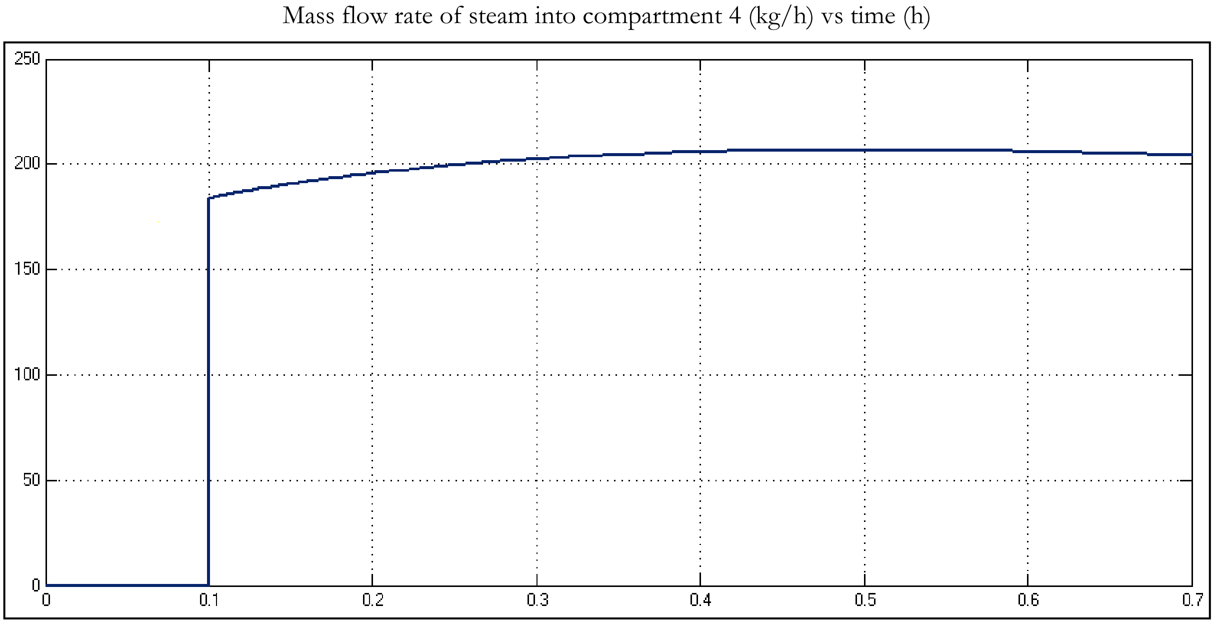

Figure 129: Plot of the mass flow rate of the steam into compartment 4 vs time (in hours)

The most notable feature of these plots is the fact that at steady-state, the temperature of compartment 4 is not at its set point, since the MV cannot be lower than 0 kg/h.

It is clear that the controller is not aggressive enough. The fact that the initial MV change has a similar size as the steady-state change shows that the integral time is too large. The integral time is divided by 10 and the controller gain is multiplied by 5 to give the following results:

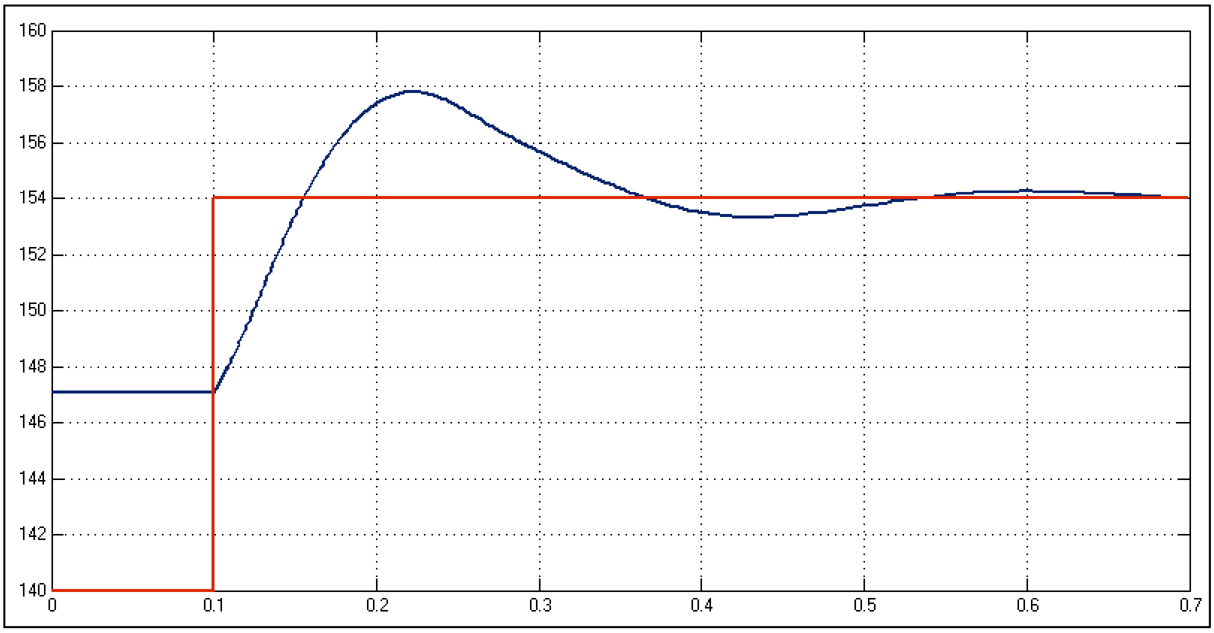
Set point and measured values for the temperature of compartment 4 (^oC) vs time (h)

Figure 130: Plot of set point (red) and measured (blue) values of the temperature of compartment 4 (^oC) vs time (in hours)

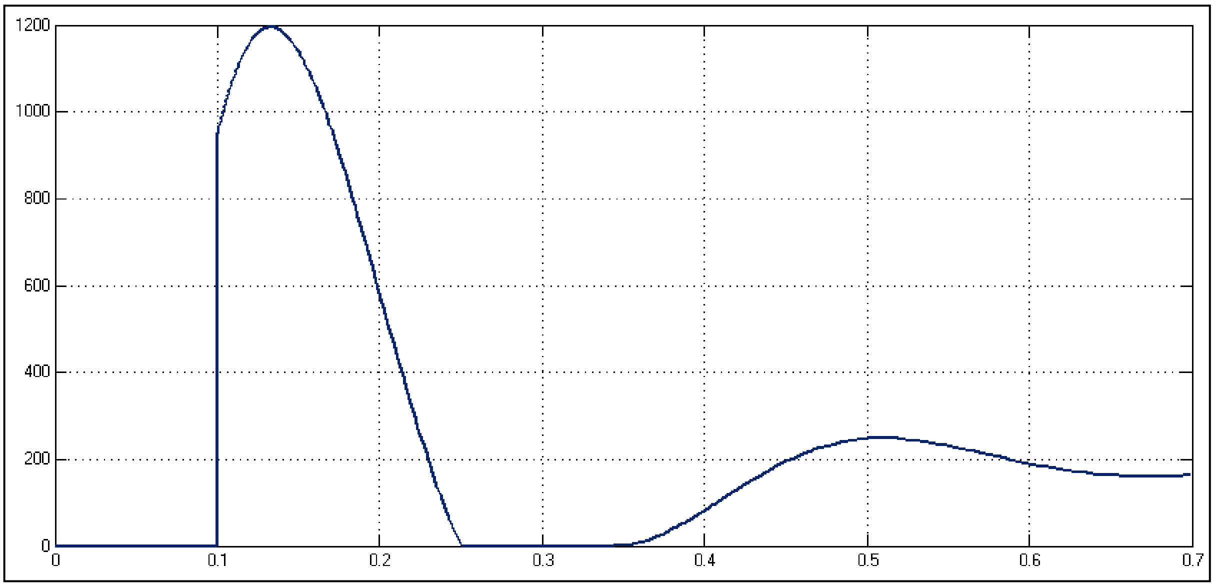
Mass flow rate of steam into compartment 4 (kg/h) vs time (h)

Figure 131: Plot of the mass flow rate of the steam into compartment 4 vs time (in hours)

The large overshoot of the CV is caused mainly by the large controller gain. Making this gain smaller, however, leads to longer settling times. Since it is desired that the temperatures of the autoclave are controlled tightly, this control is deemed satisfactory.

Autoclave Pressure (400-PIC-2001)

In this test, the set point of the autoclave pressure is multiplied by 1.1 at time step 0.

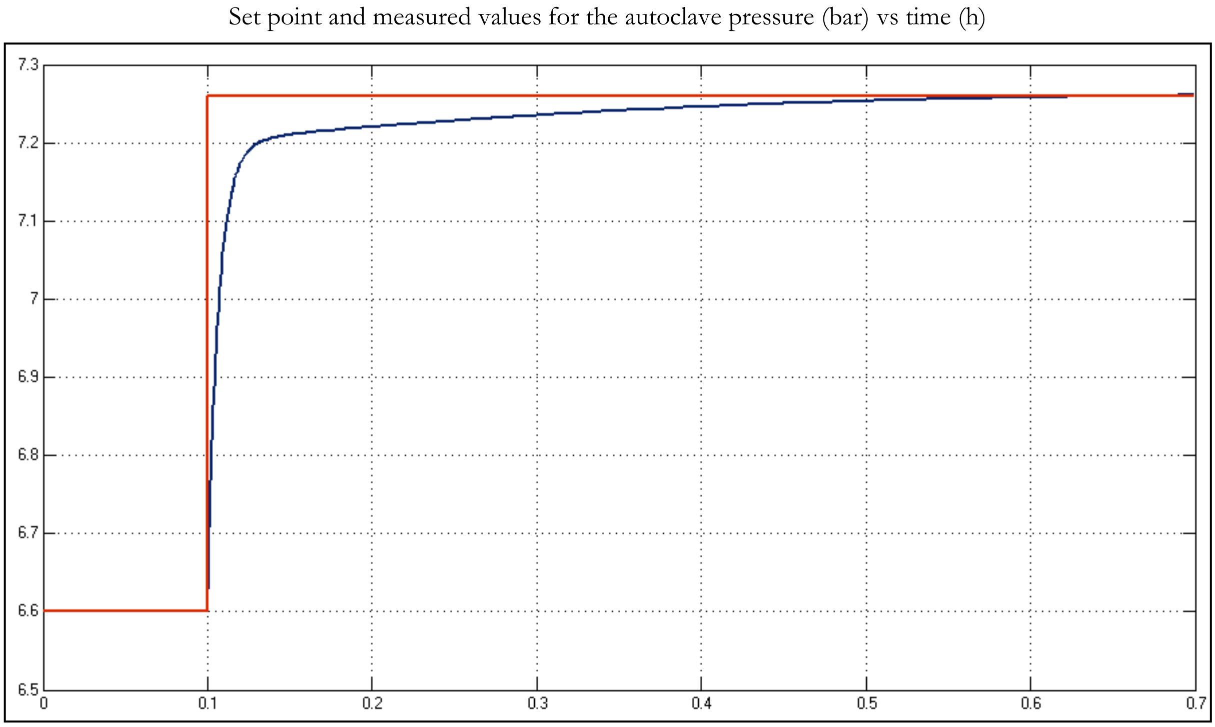

Figure 132: Plot of set point (red) and measured (blue) values of the autoclave pressure (bar) vs time (in hours)

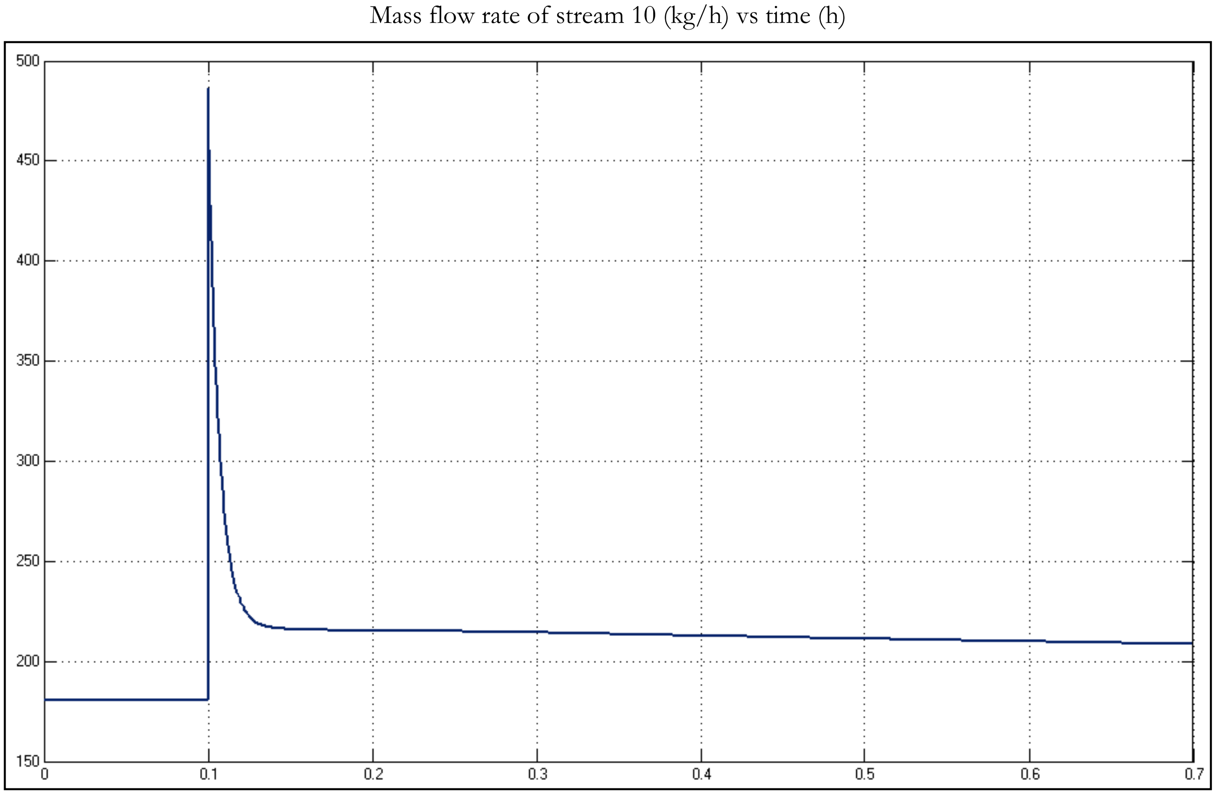

Figure 133: Plot of the mass flow rate of stream 10 vs time (in hours)

The oxygen sparging rate (represented by the mass flow rate of stream 10) can be seen to make a large spike, while the pressure takes a long time to reach the new SP. In response to the first observation, the K_c is made smaller (divided by 2), while the integral time is divided by 5 in response to the second observation. The test is repeated.

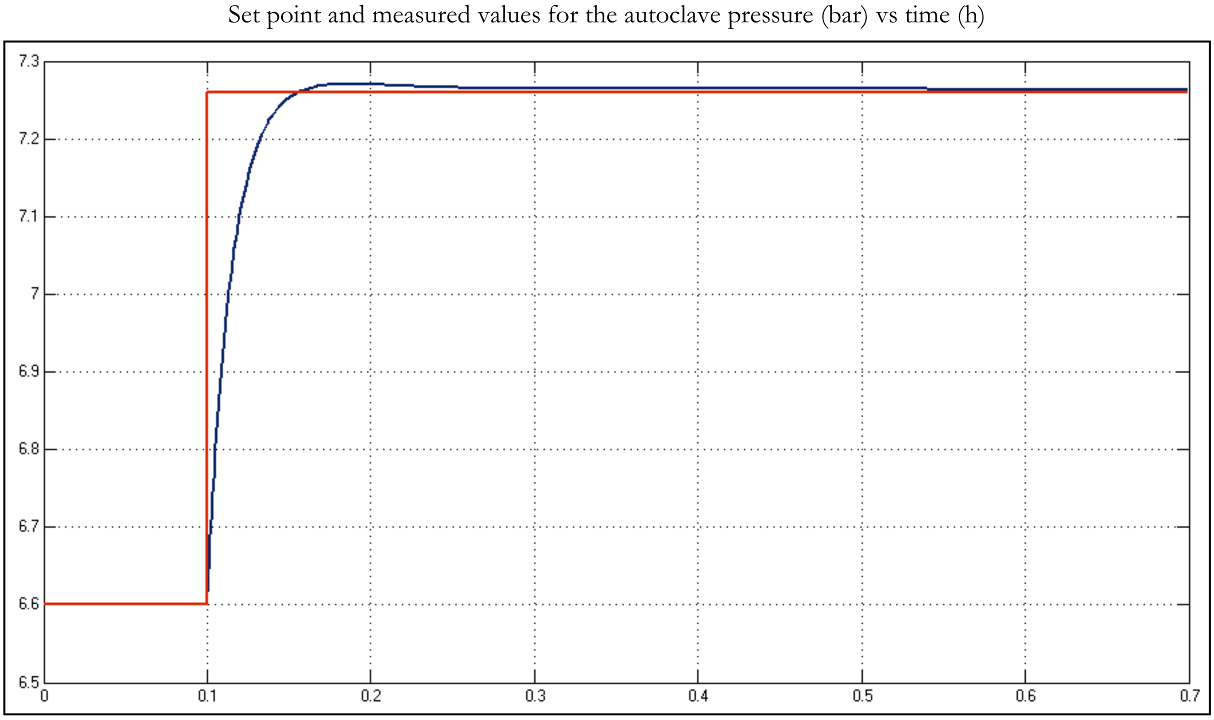

Figure 134: Plot of set point (red) and measured (blue) values of the autoclave pressure (bar) vs time (in hours)

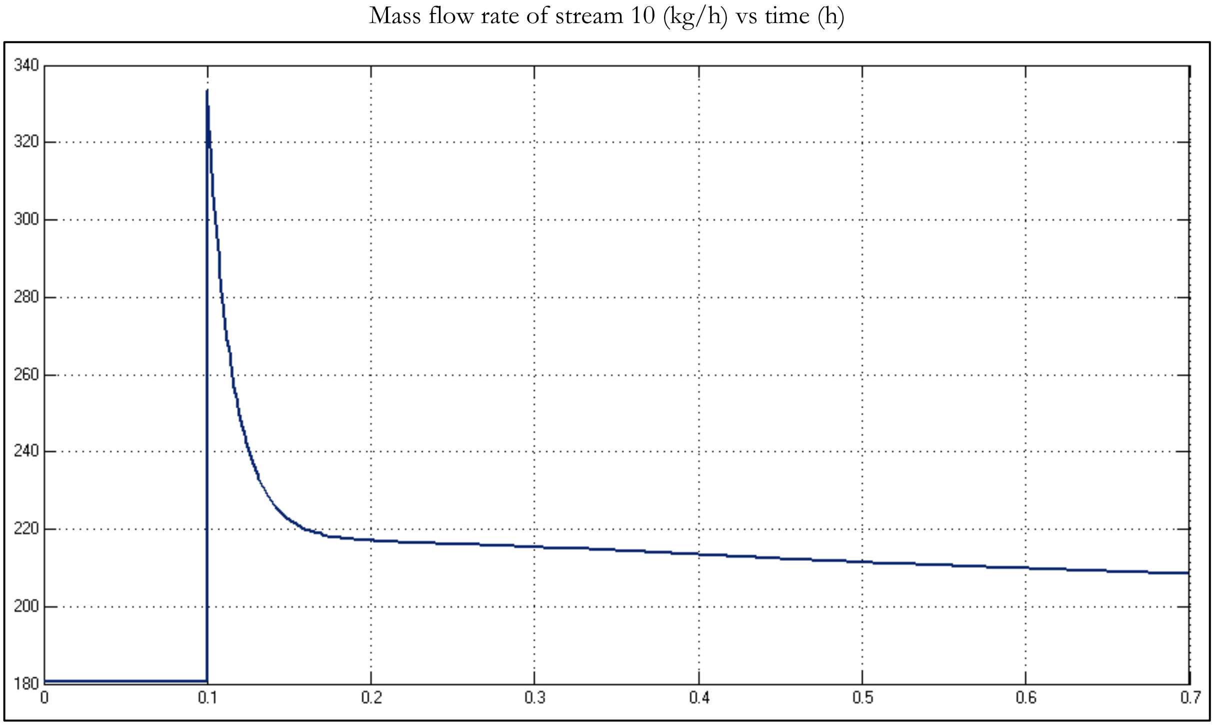

Figure 135: Plot of the mass flow rate of stream 10 vs time (in hours)

It can be seen that this change improves the CV response, while dramatically decreasing the size of the spike made by the oxygen flow. This response is acceptable.

F2 CONTROLLER FINE-TUNING FOR RE-PAIRED MODEL

All controller tuning parameters in this section are set to be the same as that of the base case (after fine-tuning). The initial tuning parameters of the mass controller of 400-TK-050, however, is set by the controller tuning method given in section 4.2.4. The anti-reset windup time of $0.1T_I$ is kept for this controller.

In this fine-tuning step, the SP of the mass in 400-TK-050 is multiplied by 0.95 at time step 0.1.

Set point and measured values for the mass in 400-TK-050 (kg) vs time (h)

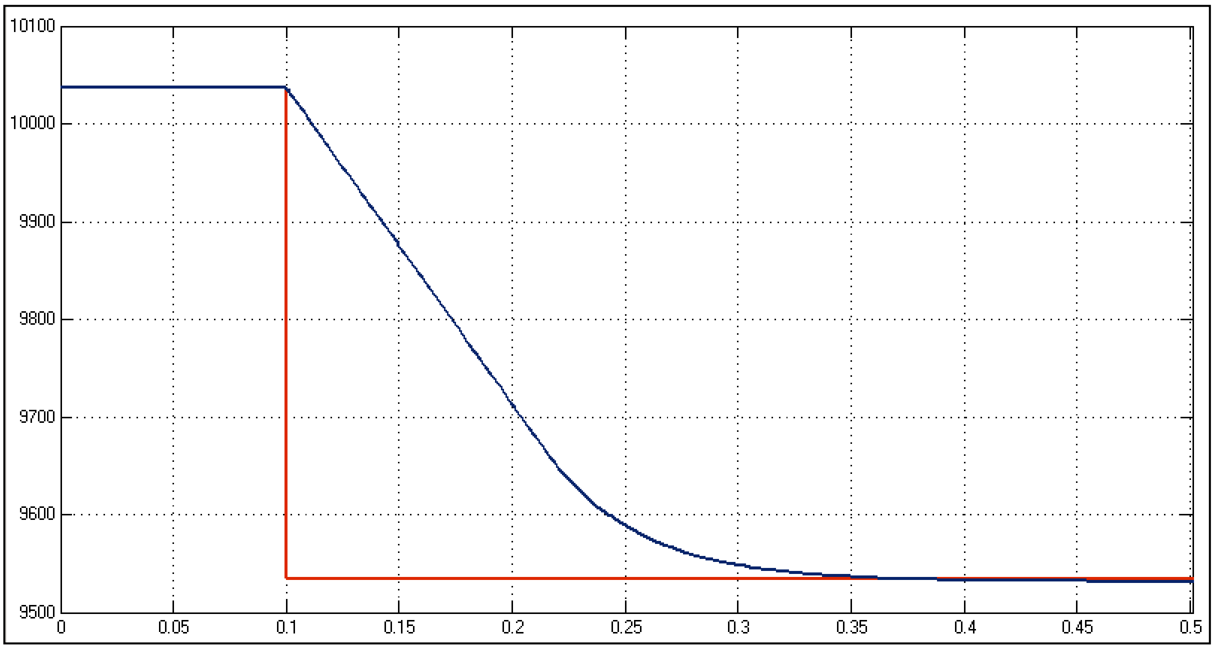

Figure 136: Plot of set point (red) and measured (blue) values of the mass 400-TK-050 vs time (in hours)

Mass flow rate of stream 21 (kg/h) vs time (h)

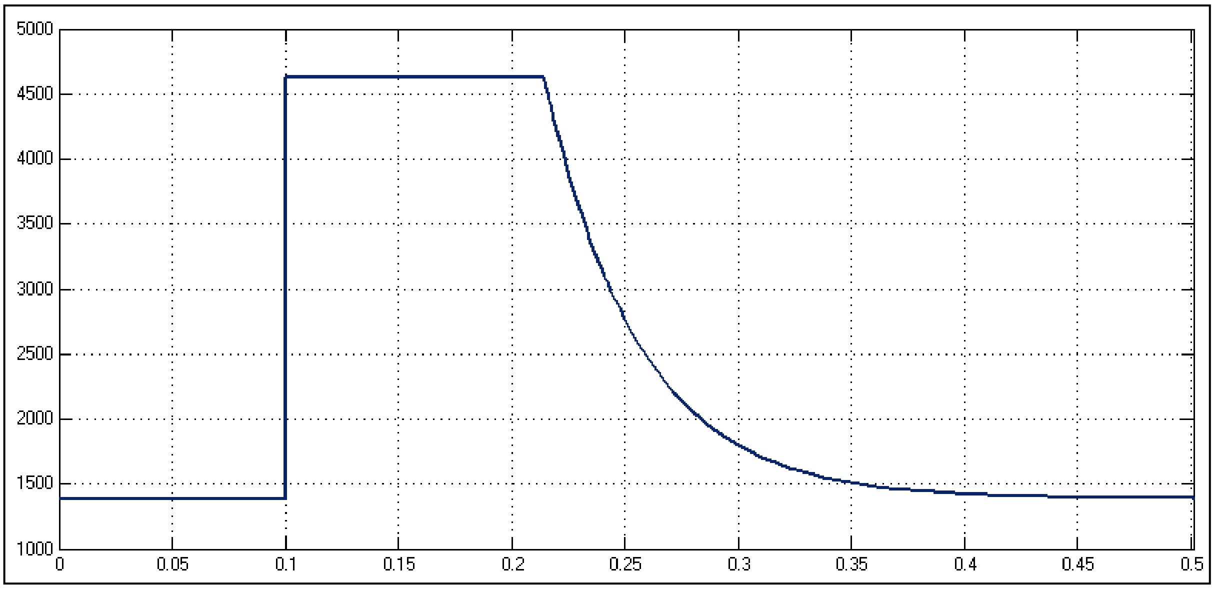

Figure 137: Plot of the mass flow rate of stream 21 vs time (in hours)

This response is satisfactory, even though the MV reaches its maximum flow rate for a while.

F3 CONTROLLER FINE-TUNING FOR MODEL VIR FF CONTROL

As with the tuning of the re-paired model, the tuning parameters in this model are kept the same as that of the fine-tuning results of the base case. This pertains also to the Tt values for the anti-reset windup. In this fine-tuning procedure, only the mass controller on 400-TK-20 and the temperature of compartment 1 are fine-tuned.

In this test, the set point of the first compartment's temperature is multiplied by 0.99 after 0.1 hours.

Set point and measured values for the temperature of compartment 1(°C) vs time (h)

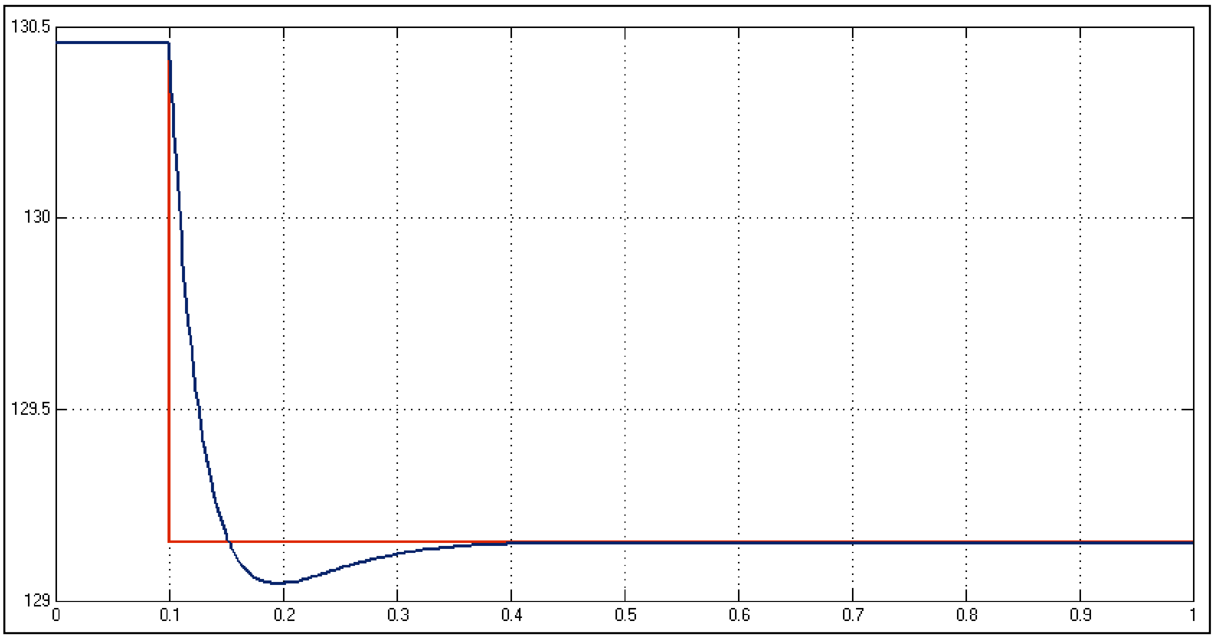

Figure 138: Plot of set point (red) and measured (blue) values of the temperature of compartment 1, versus time (hours)

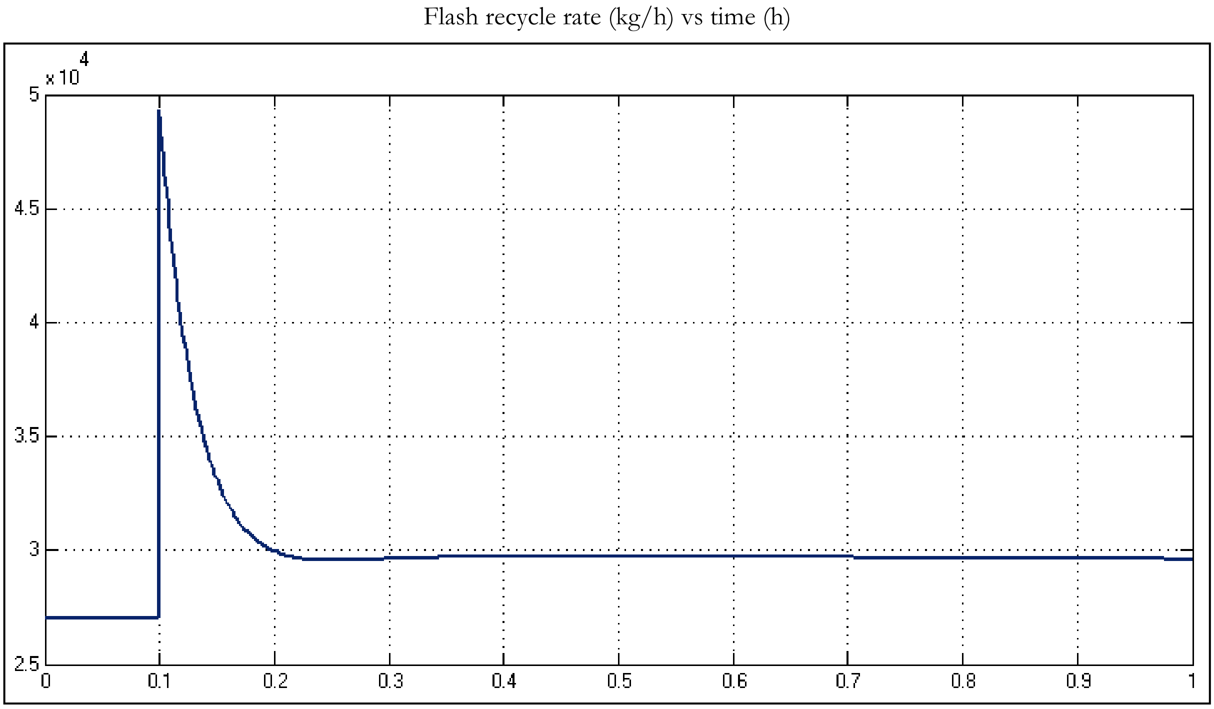

Flash recycle rate (kg/h) vs time (h)

Figure 139: Plot of the mass flow rate of stream 9 (kg/h) versus time (in hours)

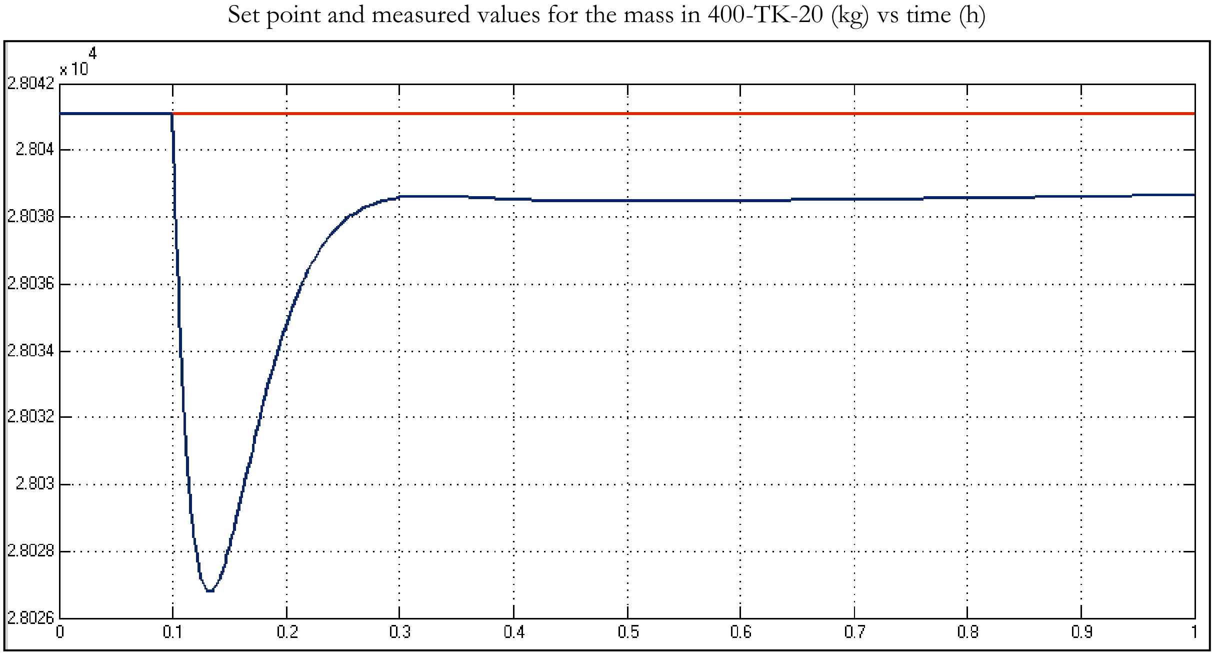

Set point and measured values for the mass in 400-TK-20 (kg) vs time (h)

Figure 140: Plot of set point (red) and measured (blue) values of the mass in 400-TK-20 (kg), versus time (in hours)

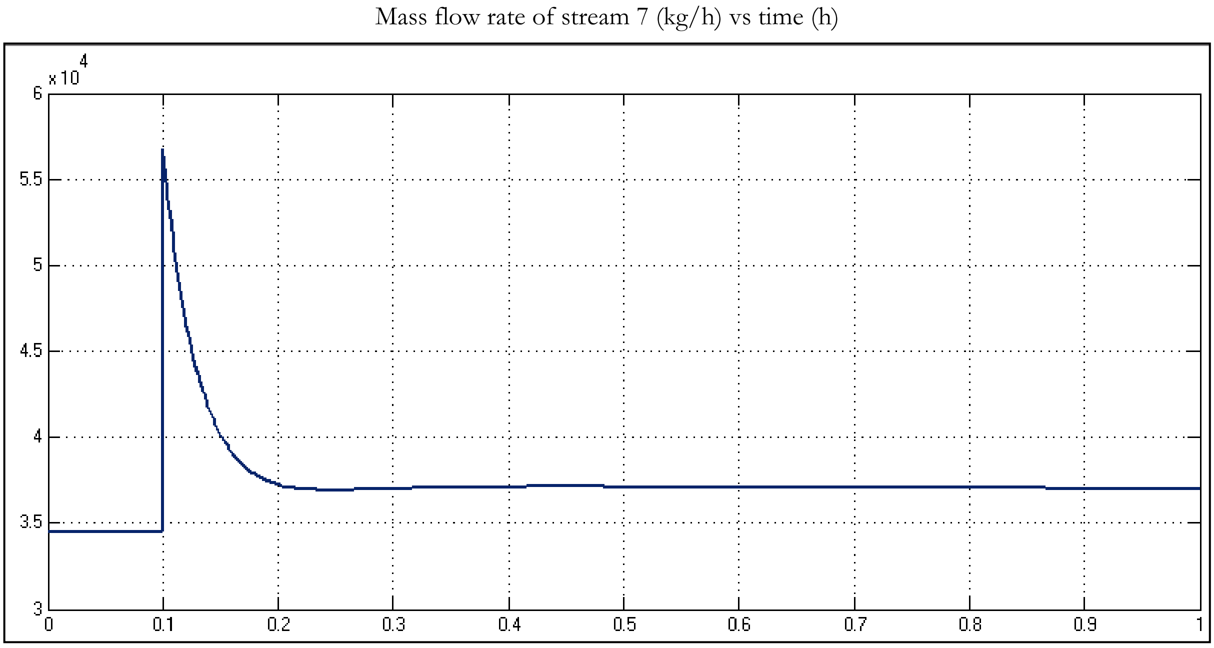

Figure 141: plot of the mass flow rate of stream 7 (kg/h) versus time (in hours)

From these plots it can be seen that the temperature in the first compartment in very tightly controlled. While the fine-tuning rules of Marlin (2000) would recommended a detuning of this controller, from process knowledge it is known that this controller should indeed be tightly tuned. The temperature controller is therefore deemed satisfactory.

The mass controller limits the maximum deviation of the tank's mass to less than 0.05% of the initial/SP value. Due to the averaging tuning done on the tank, there is an offset at steady state, but the magnitude of this offset is less than 0.01% of the initial/SP value and is therefore acceptable.

APPENDIX G

CONTROLLER TUNING FOR CHAPTER 5

G1 CONTROLLER TUNING FOR THE BASE CASE OF CHAPTER 5

This section shows the plots used to tune and fine-tune the acid controller on 400-TK-20 added as part of the base case for chapter 5.

G1.1 Initial Tuning

In this tuning the flow rate of pure acid (stream 23) is multiplied by 1.1 and the open loop behaviour of the acid concentration in 400-TK-20 is noted.

Acid concentration (g/L) in 400-TK-20 vs time (h)

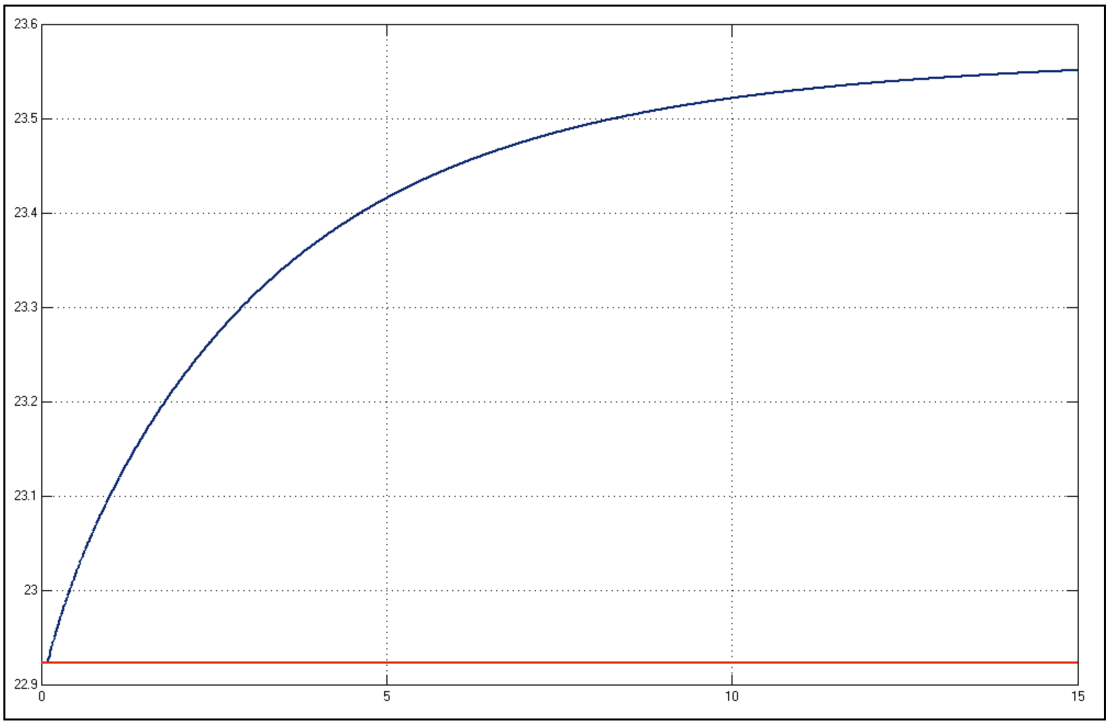

Figure 142: Plot of the set point (red) and measured (blue) values of the acid concentration in 400-TK-20 (g/L) versus time (in hours).

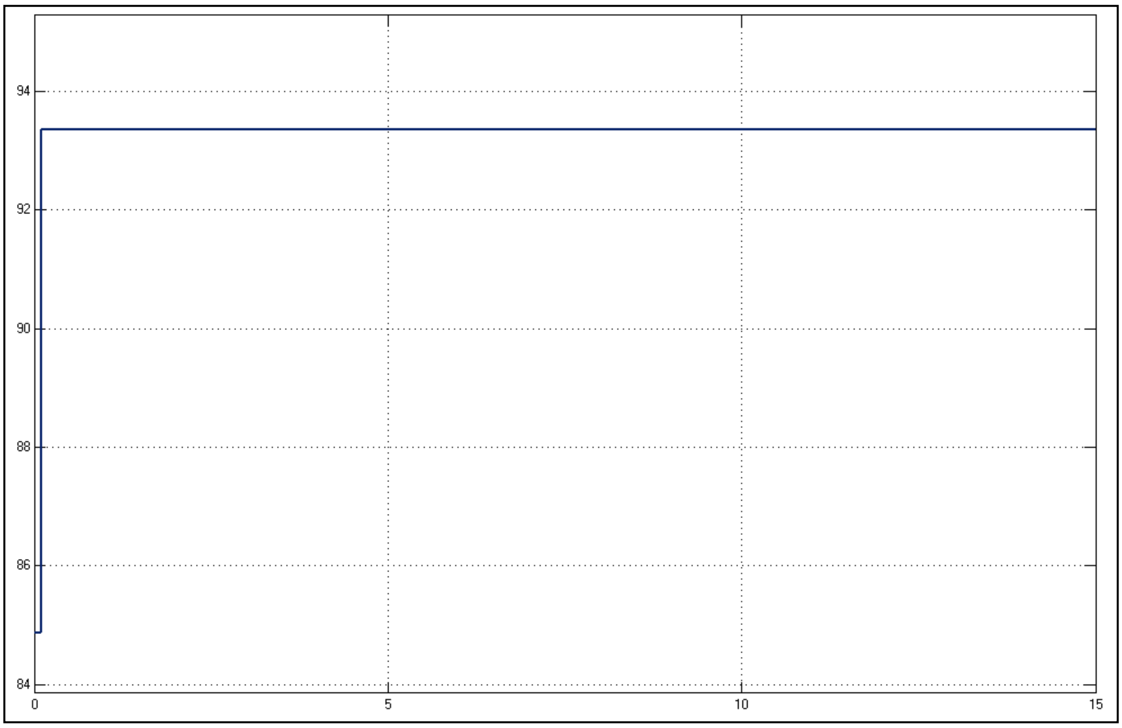
Mass flow rate of pure acid into 400-TK-20 (kg/h) vs time (h)

Figure 143: Plot of the mass flow rate of stream 23 (kg/h) versus time (in hours).

G1.2 Fine-tuning of Compositional Control Base Case

In this test the mass flow rate of stream 23, the acid addition to 400-TK-20, is multiplied by 1.1 at 0.1 hours.

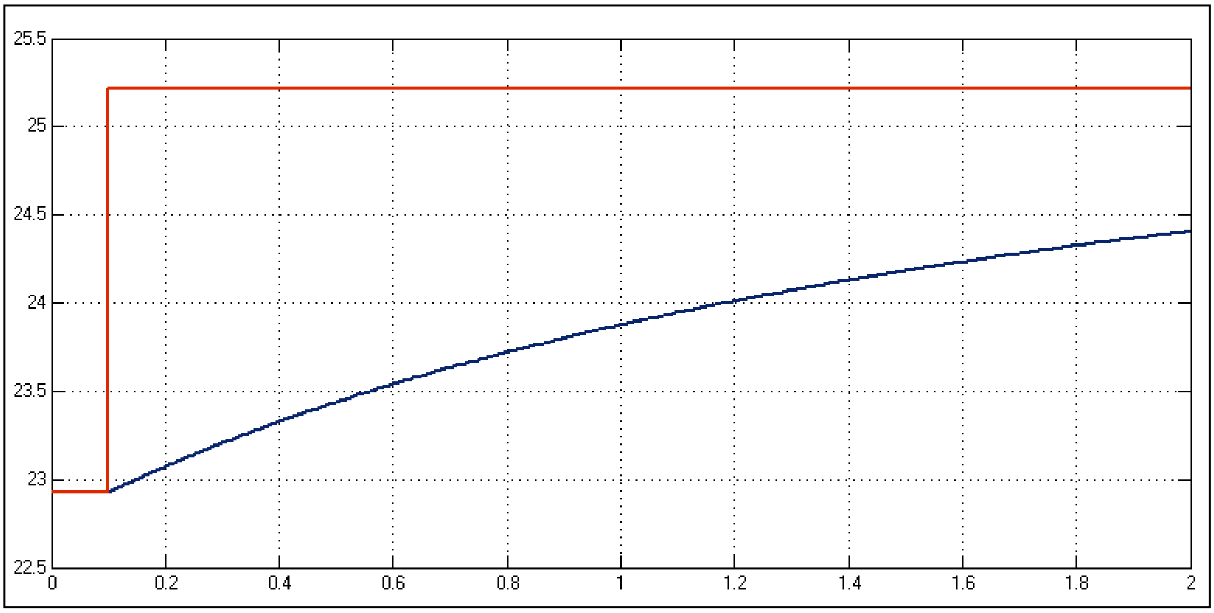
Acid concentration (g/L) in 400-TK-20 vs time (h)

Figure 144: Plot of the set point (red) and measured (blue) values of the acid concentration in 400-TK-20 (in g/L) versus time (in hours).

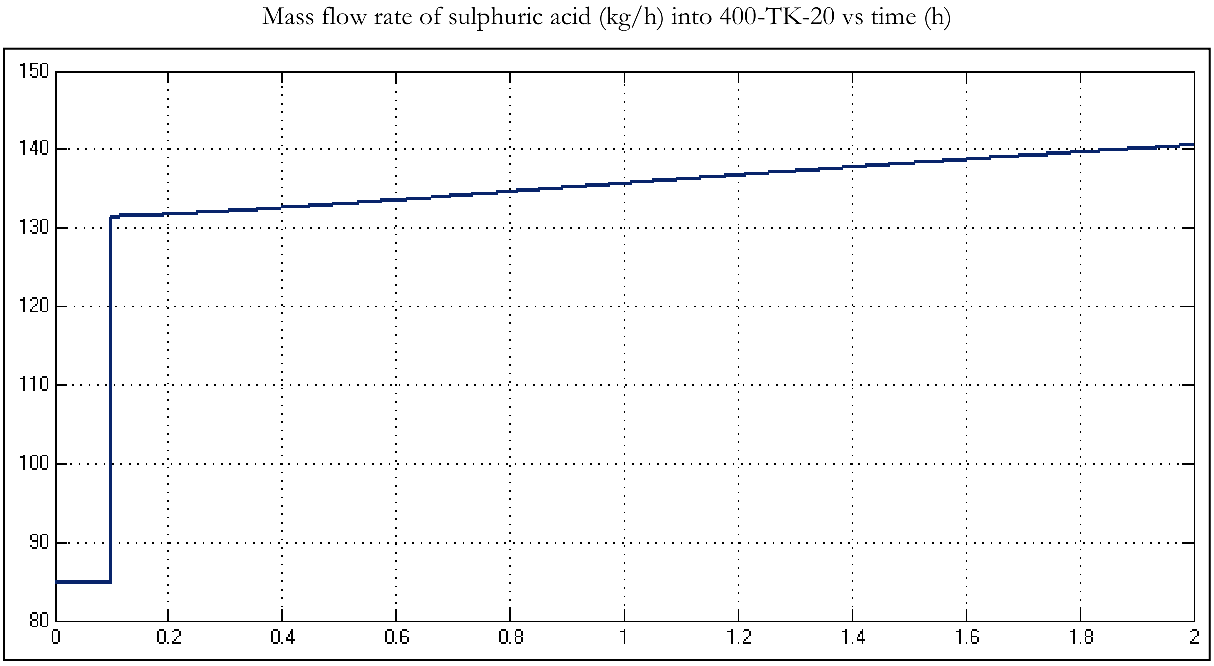

Figure 145: Plot of the mass flow rate of stream 23 (kg/h).

From these plots it can be seen that the acid concentration does not approach the new set point as fast as would be desired. From the MV plot the new steady-state value cannot be seen.

The controller gain is multiplied by 15 and the test is repeated:

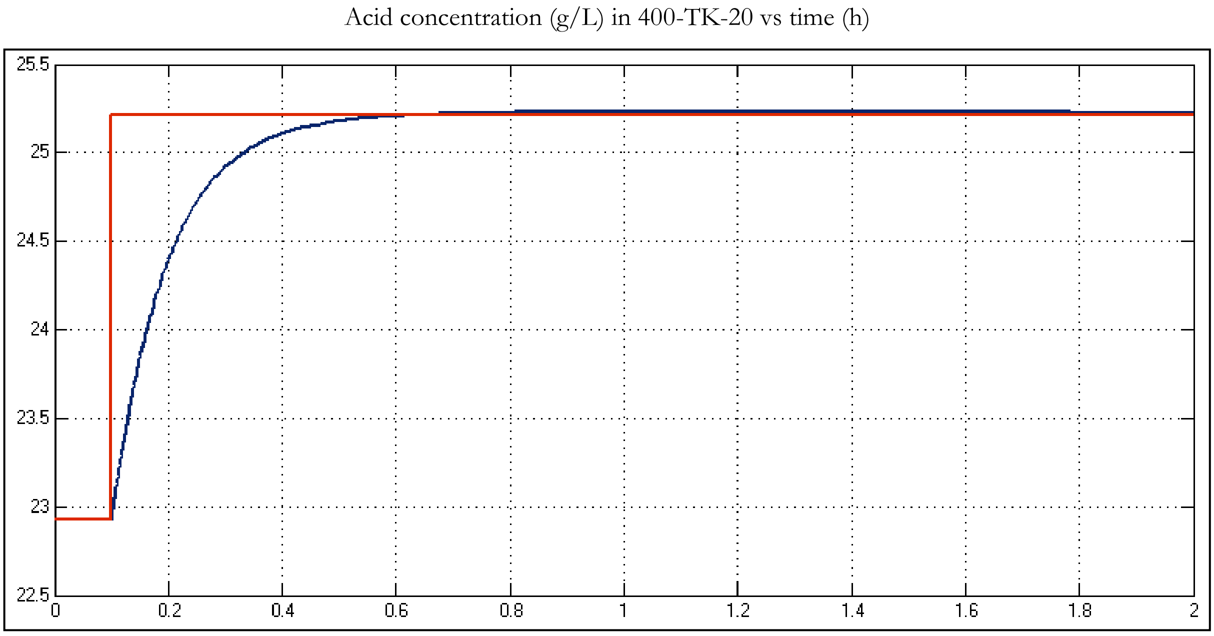

Figure 146: Plot of the set point (red) and measured (blue) values of the acid concentration in 400-TK-20 (in g/L) versus time (in hours).

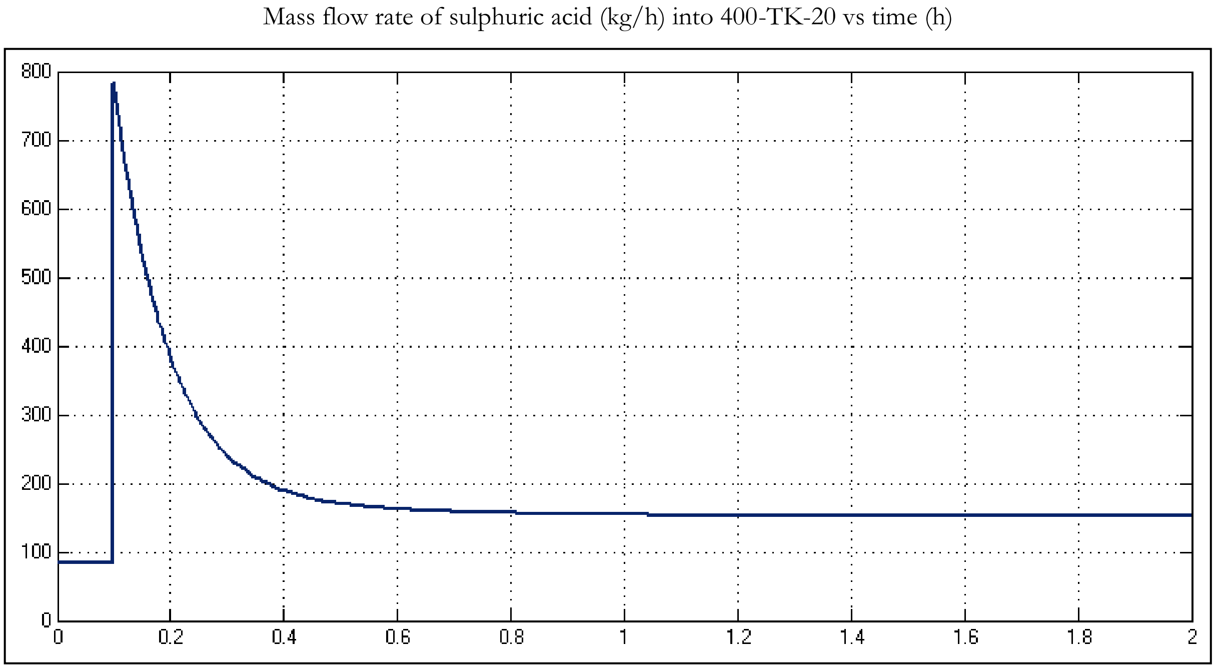

Figure 147: Plot of the mass flow rate of stream 23 (kg/h).

It can be seen that the change results in the acid concentration reaching its new set point after 30 minutes, which is reasonable for a compositional controller. The MV response shows that the controller gain is very high – but its spike is not too large, making the resulting control satisfactory.

G2 CONTROLLER TUNING FOR MODEL WITH COMPOSITIONAL REGULATORY CONTROL

G2.1 Solids Controller

The tuning of the mass controller is done by manipulating the flow rates in such a way that the ratio between the mass flow rates of streams 1 and 2 to 4 changes with 57.75%. This is done under open-loop conditions.

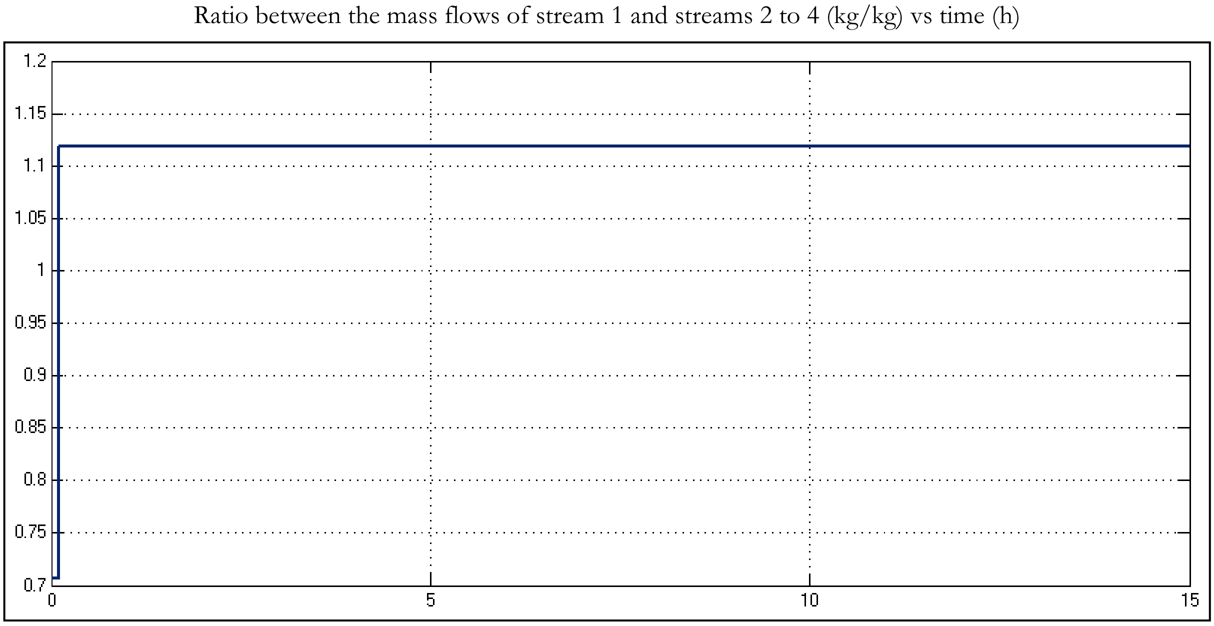
Ratio between the mass flows of stream 1 and streams 2 to 4 (kg/kg) vs time (h)

Figure 148: Plot of the ratio between the mass flow rates of stream 1 and streams 2 to 4, versus time (hours)

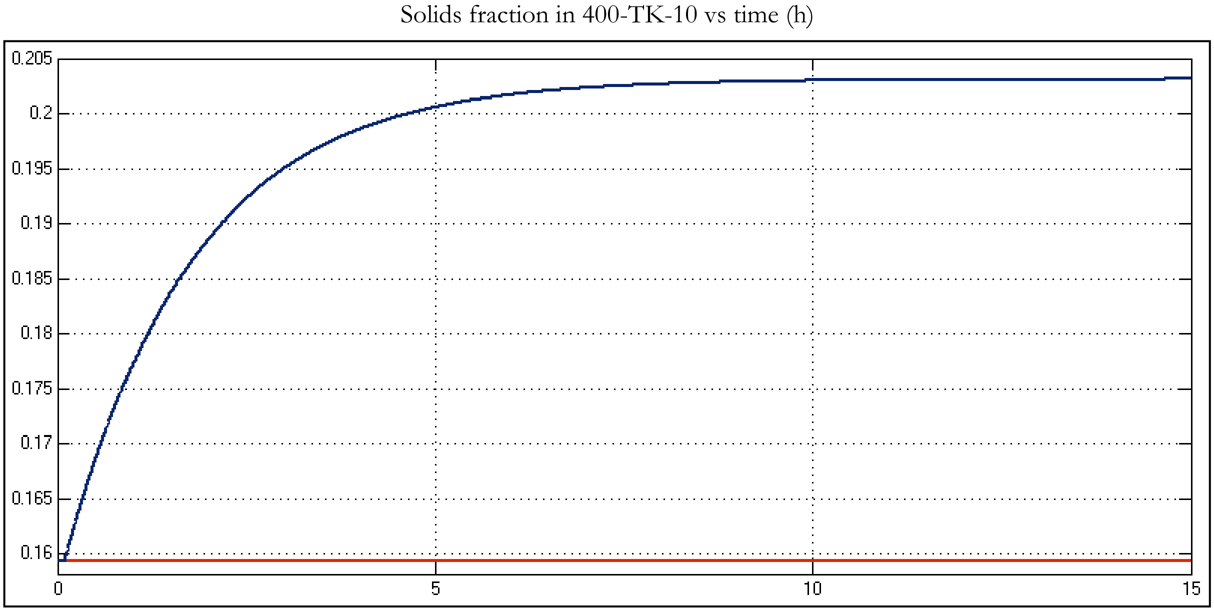
Solids fraction in 400-TK-10 vs time (h)

Figure 149: Plot of the solids fraction in 400-TK-10 (kg/kg) versus time (hours)

$\Delta Ratio_{\frac{m_1}{m_{2-4}}} = 1.1185 - 0.707 = 0.4115$

$\Delta Solids\ fraction = 0.2031 - 0.1593 = 0.0438$

$K_p = 0.1064$

$t_{63\%} = 1.704\ h$

$t_{28\%} = 0.5604\ h$

$\tau = 1.715$

$\theta = 0\ h$

$K_c K_p = 1.5$

$\frac{T_I}{t_{63\%}} = 0.24$

$\frac{T_d}{t_{63\%}} = 0$

$\boldsymbol{K_c = 14.1}$

$\boldsymbol{T_I = 0.409\ h}$

$\boldsymbol{T_d = 0\ h}$

$\boldsymbol{G_P = -0.1064/(1 + 1.715s)}$

For the development of an RGA the responses of 400-TK-10 and the acid concentration in this tank are noted.

400-TK-10 Response to Solids Fraction

No change is observed in the tank mass.

Response of Acid Concentration in 400-TK-10 to Solids Fraction

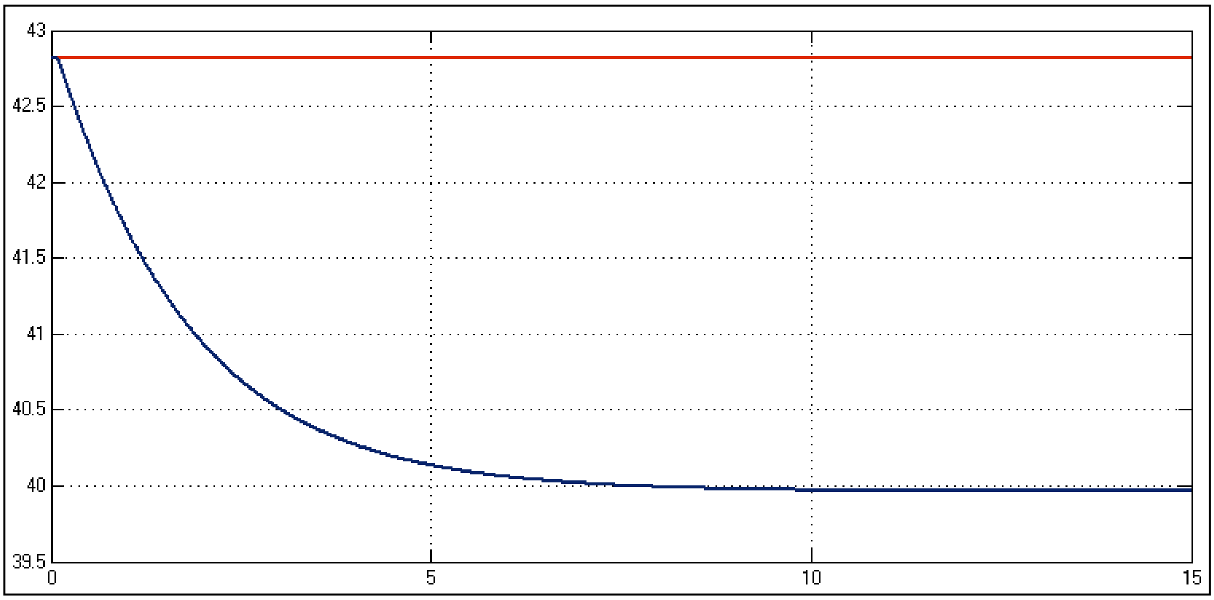

$\Delta Ratio_{\frac{m_1}{m_{2-4}}} = 1.1185 - 0.707 = 0.4115$

$\Delta Acid\ concentration = 39.963 - 42.813 = -2.85\ g/L$

$K_p = -6.926$

$t_{63\%} = 1.764\ h$

$t_{28\%} = 0.589\ h$

$\tau = 1.765$

$\theta = \sim 0\ h$

$\boldsymbol{G_P = -6.926/(1 + 1.763s)}$

G2.2 Acid Controller

The tuning for this part of the acid controller is done by manipulating the flow rates in such a way that the ratio between the mass flow rates of streams 3 and 2 changes with 55%. This is done under open-loop conditions.

Ratio between the mass flows of stream 3 and streams 2 (kg/kg) vs time (h)

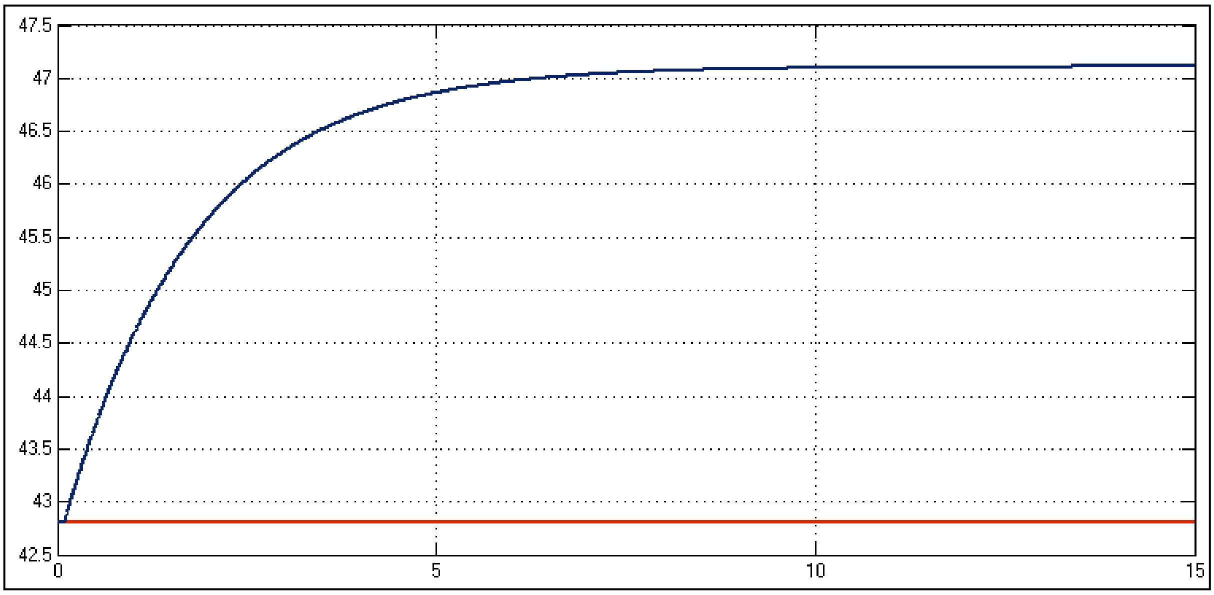

Figure 150: Plot of the ratio between the mass flow rates of streams 3 and 2, versus time (hours)

Acid concentration in 400-TK-10 (kg/l) vs time (h)

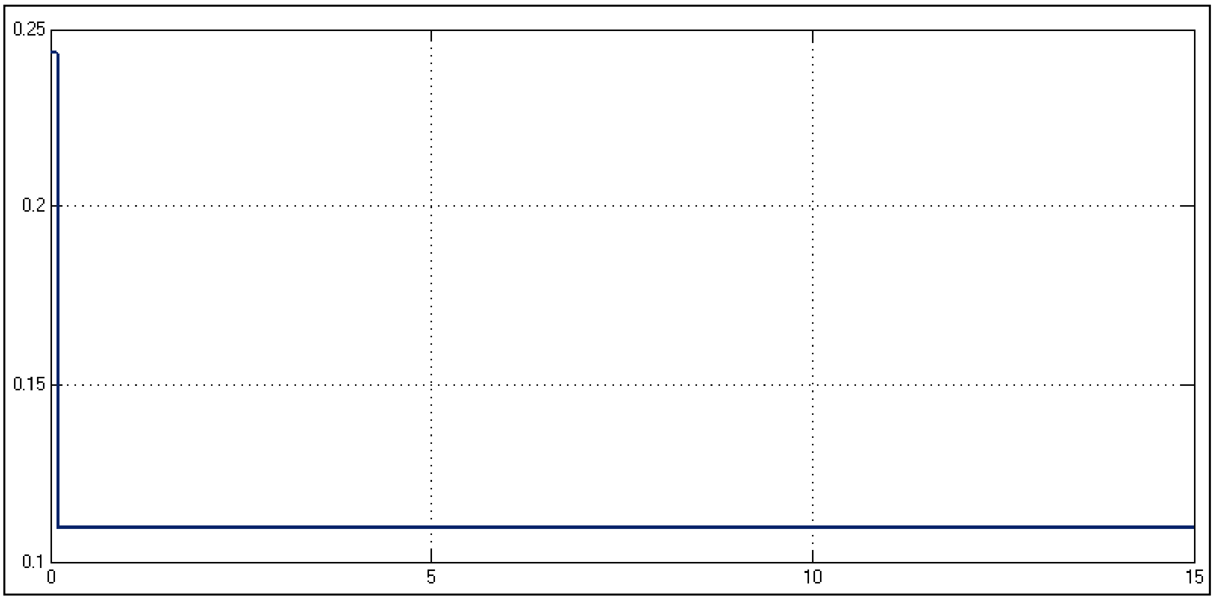

Figure 151: Plot of the acid concentration in 400-TK-10 (in kg/L) versus time (h)

$\Delta Ratio_{\frac{m_3}{m_2}} = 0.1095 - 0.2435 = -0.134$

$\Delta[Acid]_{400TK10} = 47.1106 - 42.8126 = 4.298\ g/L$

$K_p = -32.075\ g/L$

$t_{63\%} = 1.705\ h$

$t_{28\%} = 0.565\ h$

$\tau = 1.711\ h$

$\theta = 0\ h$

$K_c K_p = 1.5$

$\frac{T_I}{t_{63\%}} = 0.24$

$\frac{T_d}{t_{63\%}} = 0$

$\boldsymbol{K_c = -0.0468}$

$\boldsymbol{T_I = 0.409\ h}$

$\boldsymbol{T_d = 0\ h}$

$\boldsymbol{G_P = -32.075/(1 + 1.711s)}$

This change influences neither the solids fraction nor the mass in 400-TK-10.

For the tuning of this part of the acid controller, the flow rats of streams 4 and 2 are manipulated in such a manner that the ratio between them increase from 0 to approximately 0.0074.

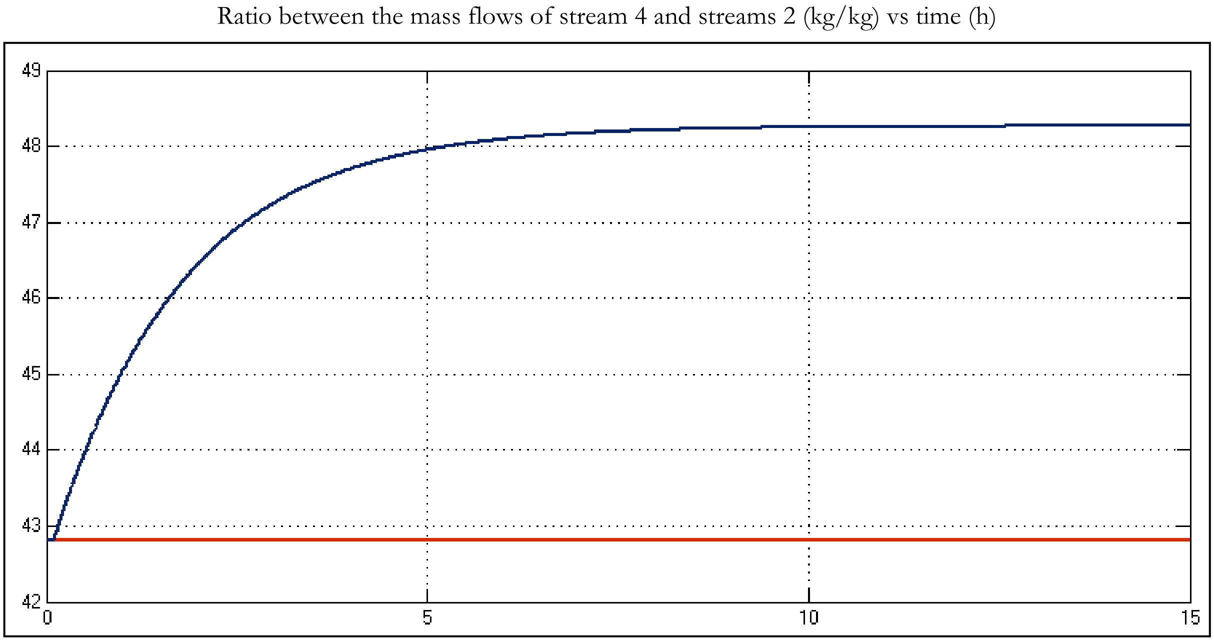

Figure 152: Plot of the ratio between the mass flows of streams 4 and 2, versus time (hours)

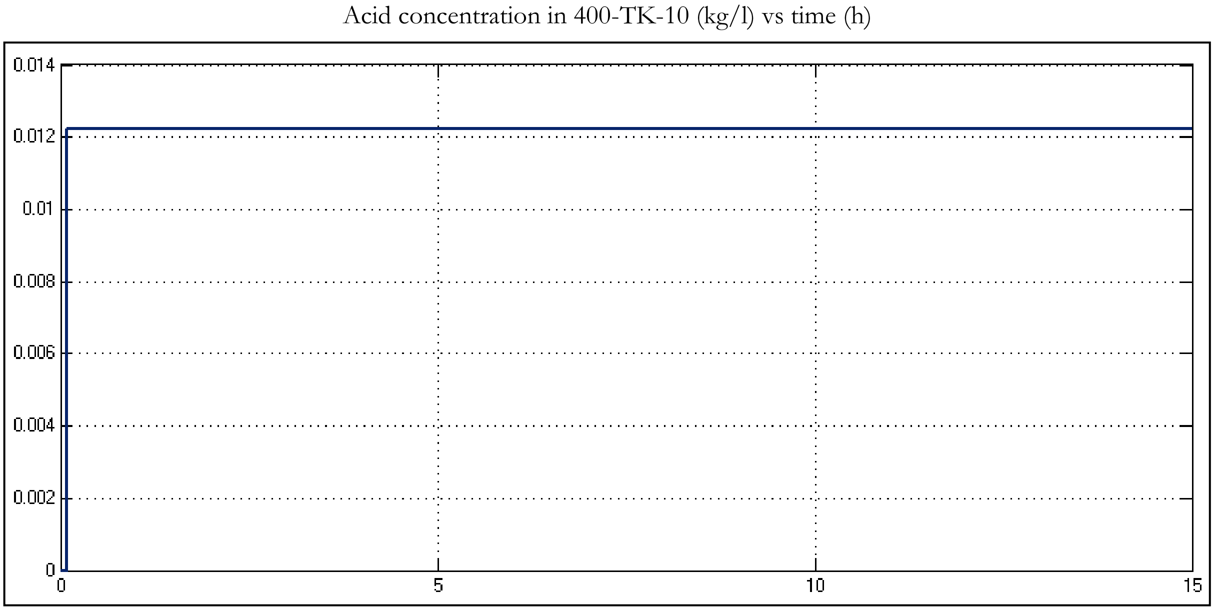

Figure 153: Plot of the acid concentration in 400-TK-10 (in kg/L) versus time (h)

$\Delta Ratio_{\frac{m_4}{m_2}} = 0.0122 - 0 = 0.0122\ kg/kg$

$\Delta[Acid] = 48.267 - 42.813 = 5.454\ g/L$

$K_p = 447.1\ g/L$

$t_{63\%} = 1.707\ h$

$t_{28\%} = 0.5637\ h$

$\tau = 1.715\ h$

$\theta = 0\ h$

$K_c K_p = 1.5$

$\frac{T_I}{t_{63\%}} = 0.24$

$\frac{T_d}{t_{63\%}} = 0$

$\boldsymbol{K_c = 0.0034}$

$\boldsymbol{T_I = 0.41\ h}$

$\boldsymbol{T_d = 0\ h}$

$\boldsymbol{G_P = -447.1/(1 + 1.715s)}$

G2.3 Fine-Tuning of Control on 400-TK-10

Acid Controller in 400-TK-10

In this test, the set point of the acid concentration in 400-TK-10 is multiplied by 1.1 at time step 0.1.

Set point and measured values for the acid concentration in 400-TK-10 (g/L) vs time (h)

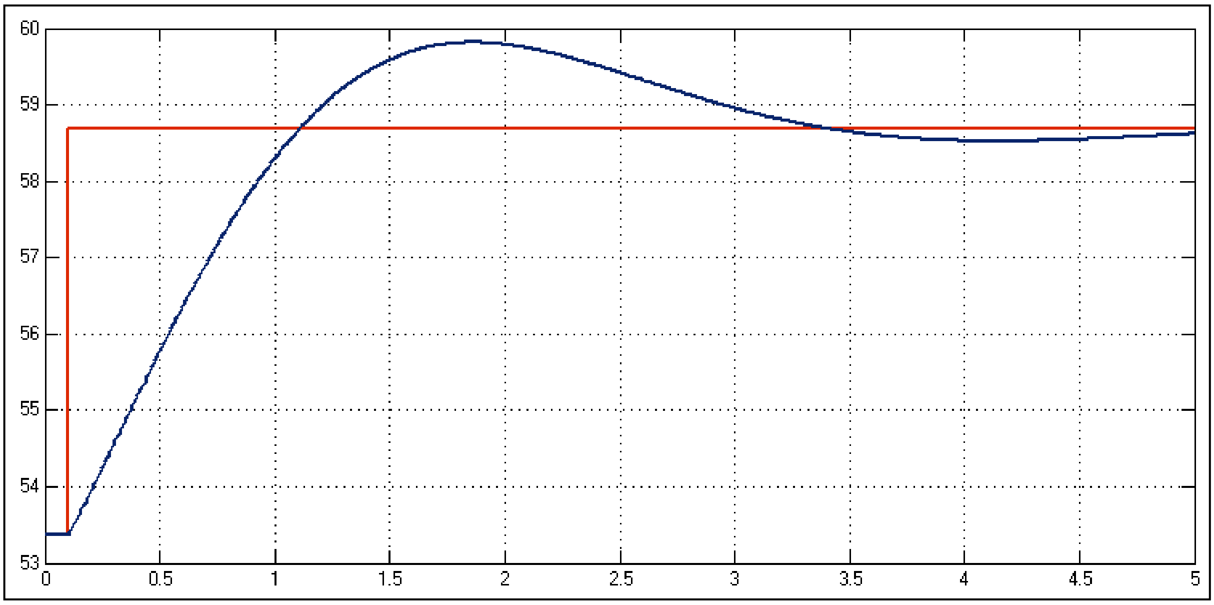

Figure 154: Plot of set point (red) and measurement (blue) of the acid concentration in 400-TK-10 vs time (in hours).

Ratio of the mass flow rates of streams 4 and 2 (kg/kg) vs time (h)

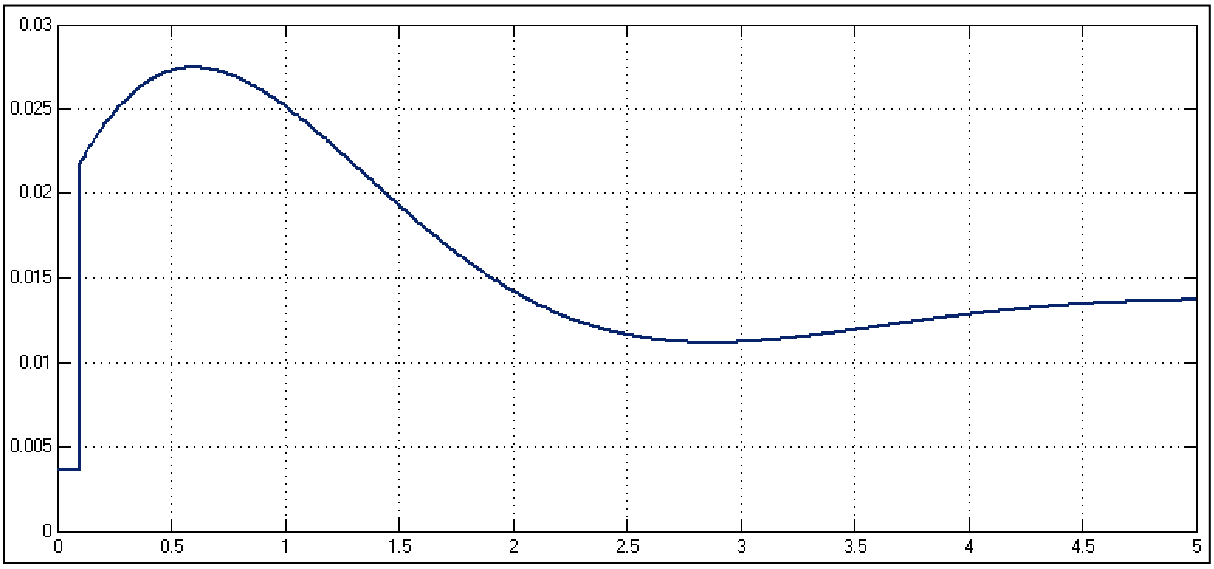

Figure 155: Plot of ratio between the mass flow rates of streams 4 and 2 vs time (in hours), with the ratio between flow rates 3 and 2 at zero.

It can be seen that the CV is slow in approaching the new SP, and the integral function is also very prominent. The controller gain is multiplied by a factor of 55 and the integral time is multiplied by 1.1, after which the test is repeated.

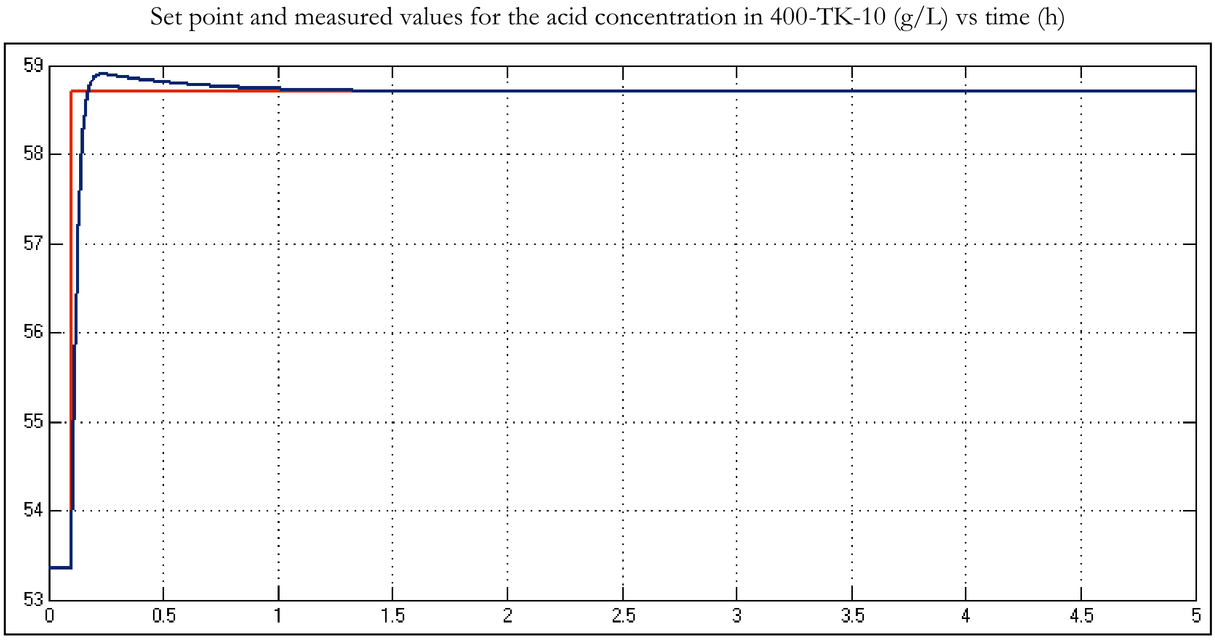

Figure 156: Plot of set point (red) and measurement (blue) of the acid concentration in 400-TK-10 vs time (in hours)

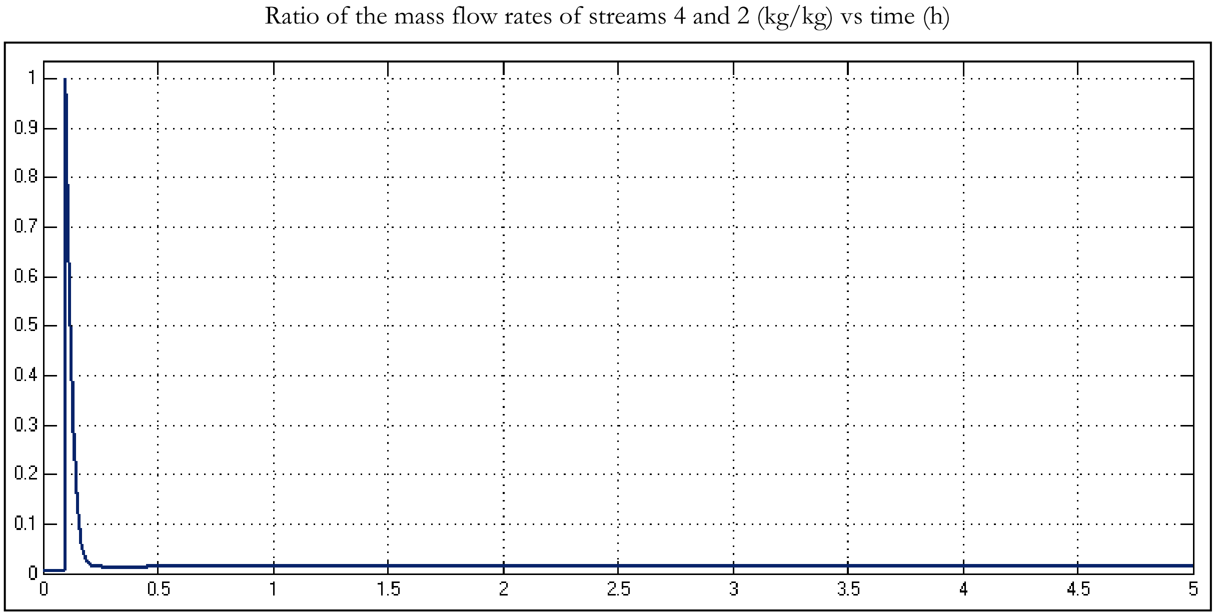

Figure 157: Plot of ratio between the mass flow rates of streams 4 and 2 vs time (in hours)

Even though the MV can be seen to respond aggressively, it should be noted that it is a ratio between two streams, and that it is permissible to vary in this manner. The CV behaviour is also much improved, with the new SP crossed after approximately 5 minutes.

Solids Fraction Controller

In this test, the set point of the solids fraction in 400-TK-10 is multiplied by 1.1 at time step 0.1.

Set point and measured values for the solids fraction in 400-TK-10 vs time (h)

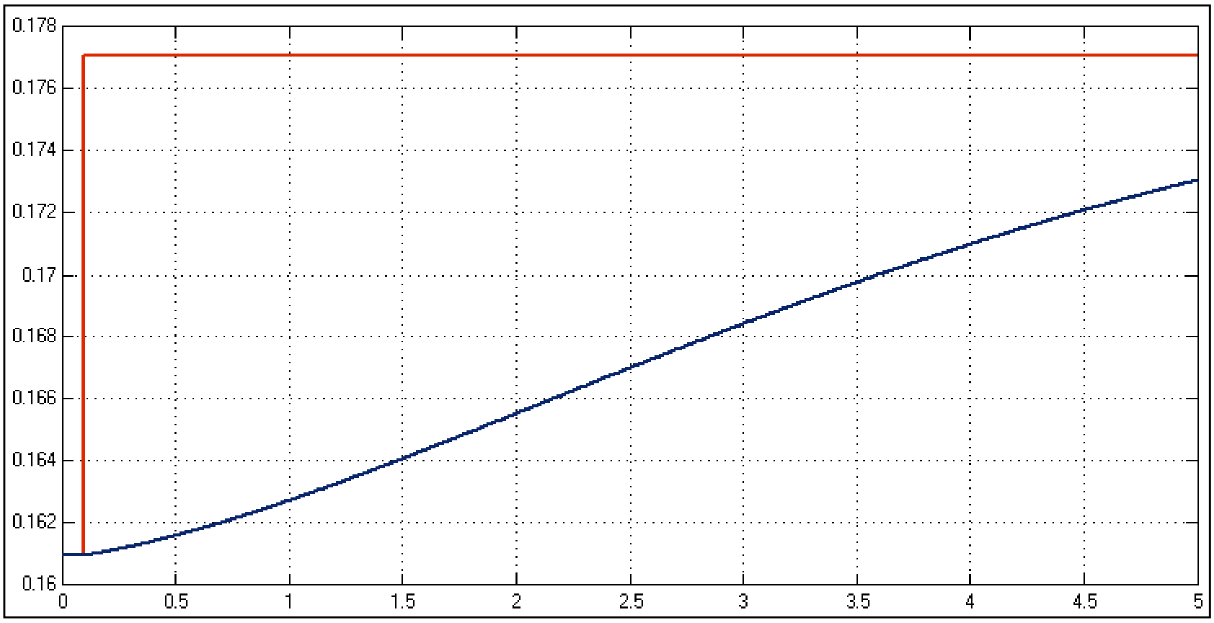

Figure 158: Plot of set point (red) and measurement (blue) of the solids fraction in 400-TK-10 vs time (in hours)

Ratio of the mass flow rates of stream 1 and the sum of streams 2 to 4 (kg/kg) vs time (h)

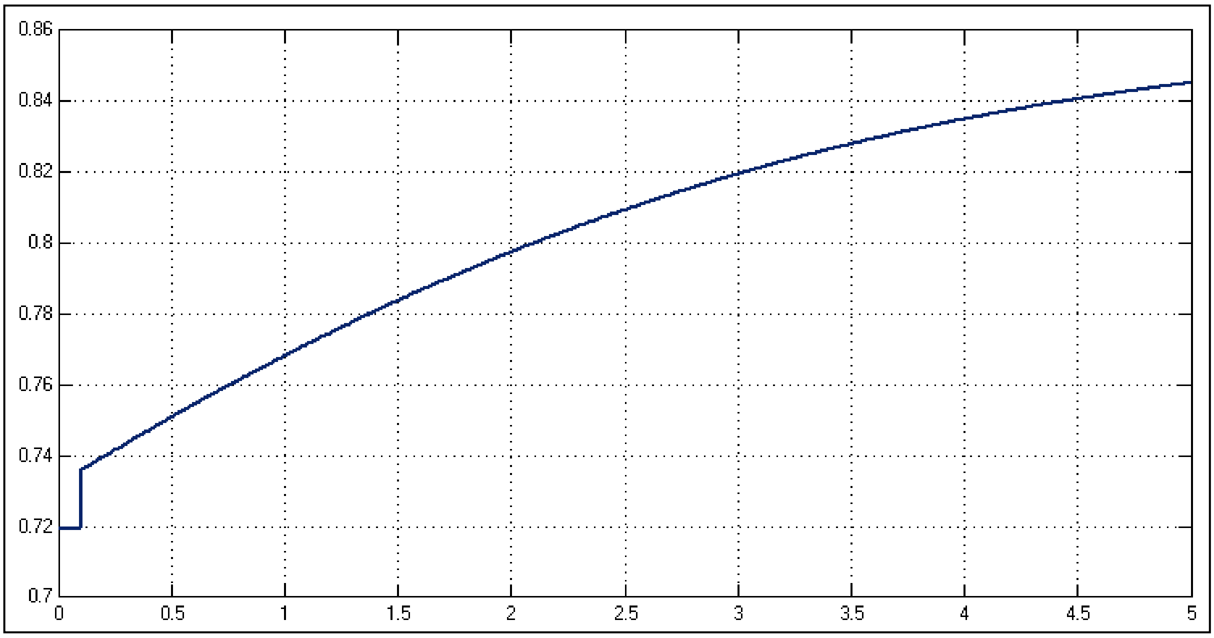

Figure 159: Plot of ratio between the mass flow rates of stream 1 and the sum of streams 2 to 4, vs time (in hours)

As with the fine-tuning of the acid controller, it can be seen that the control of the solids fraction is not aggressive enough. The controller gain of the acid controller is multiplied by a value of 1300, and the test is repeated.

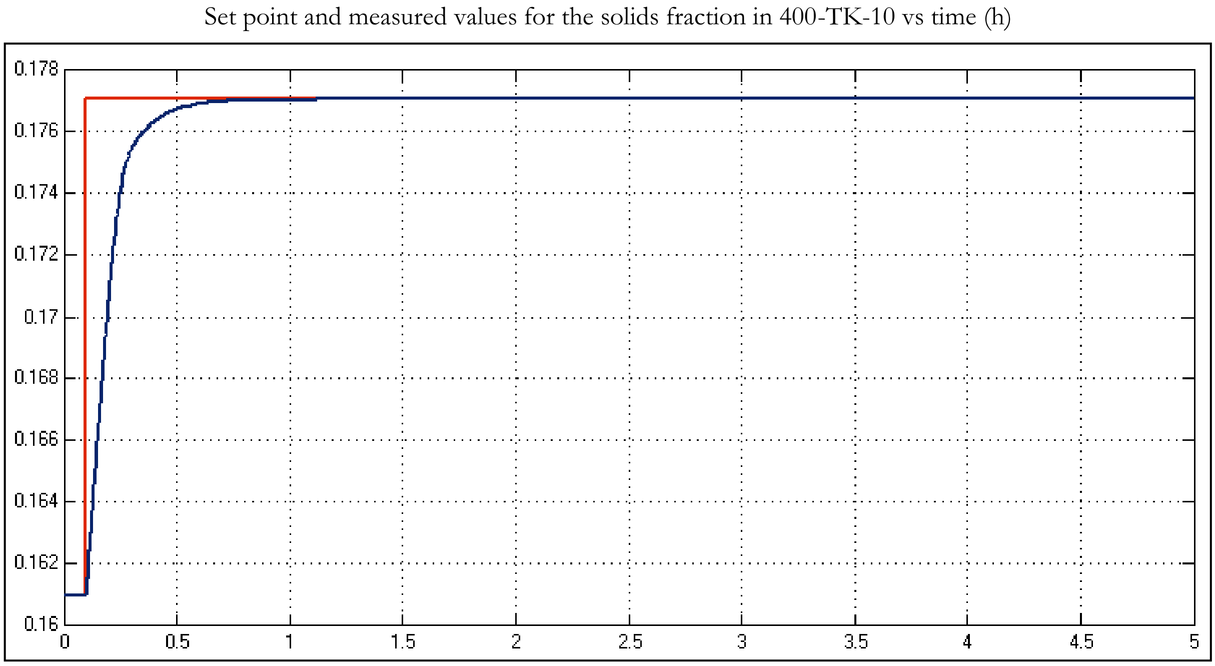

Figure 160: Plot of set point (red) and measurement (blue) of the solids fraction in 400-TK-10 vs time (in hours)

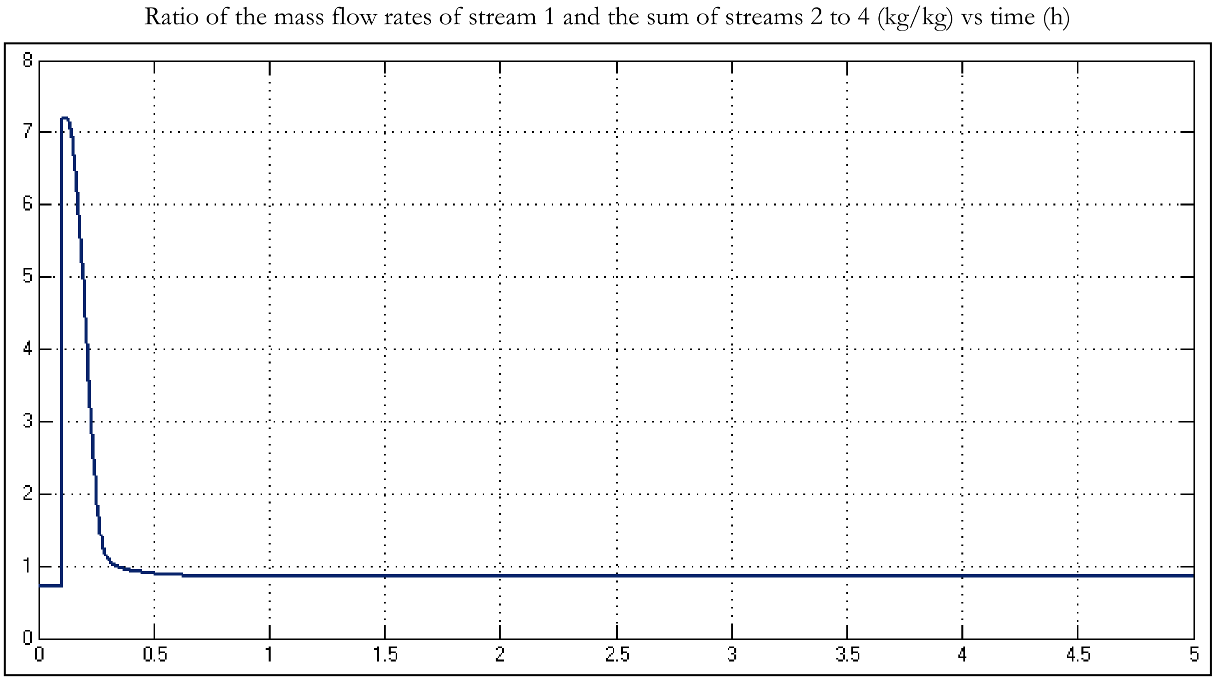

Figure 161: Plot of ratio between the mass flow rates of stream 1 and the sum of streams 2 to 4, vs time (in hours)

This control is satisfactory. Although the acid concentration requires 2 hours to reach its new set point, set point changes will not be this large – as will be made clear when cascade control is employed.

G2.4 Outside Solids Controller

For the tuning of the solids controller in 400-TK-20 its SP is multiplied by 1.1 at 0.1 hours.

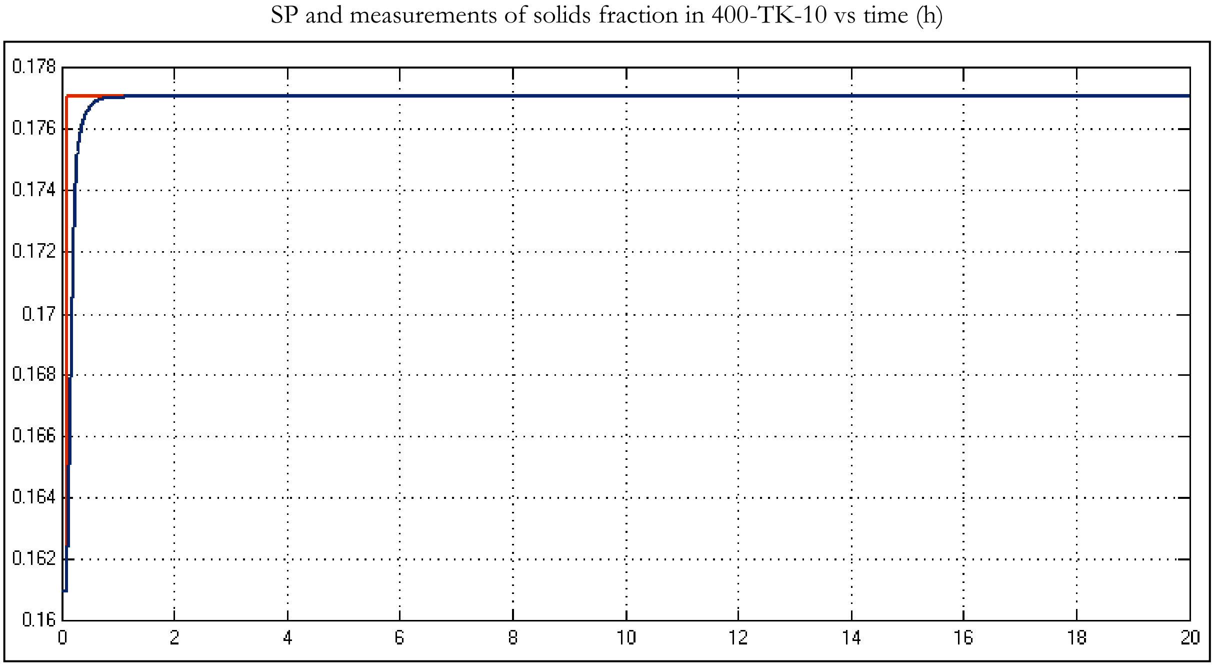

Figure 162: Plot of the set point (red) and measurement (blue) values of the solids fraction in 400-TK-10 vs time (in hours). This is the MV of the primary controller and CV of the secondary controller.

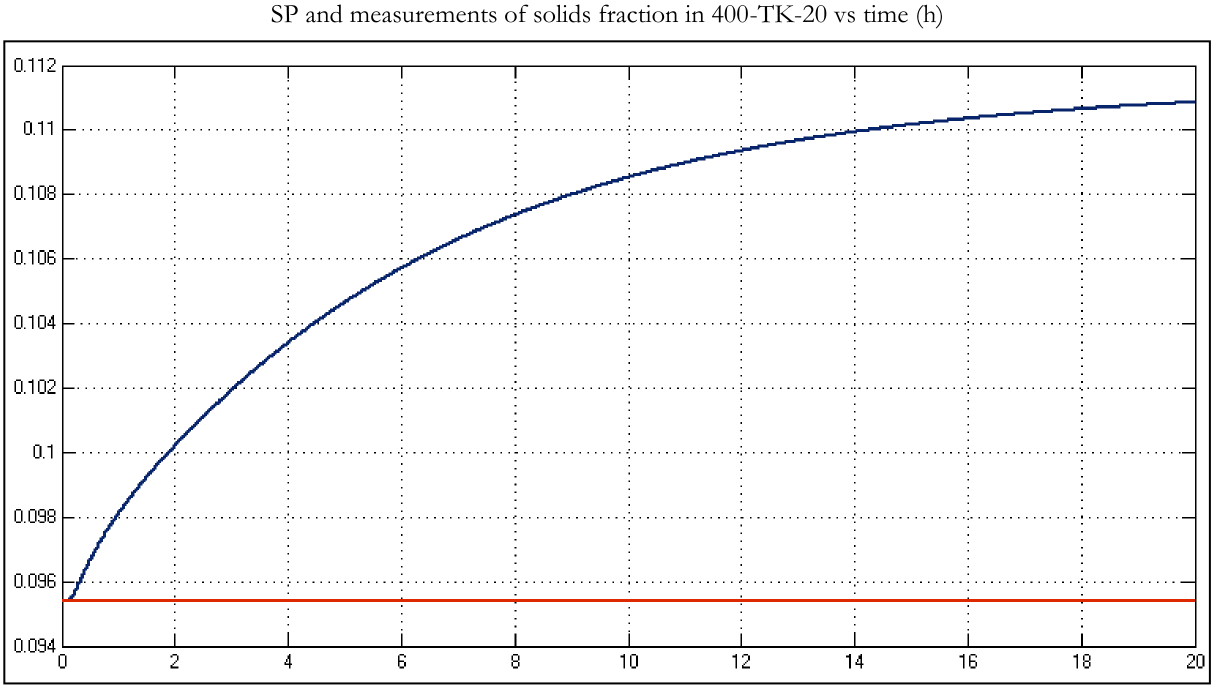

Figure 163: Plot of the set point (red) and measurement (blue) values of the solids fraction in 400-TK-20 vs time (in hours). This is the CV of the primary controller.

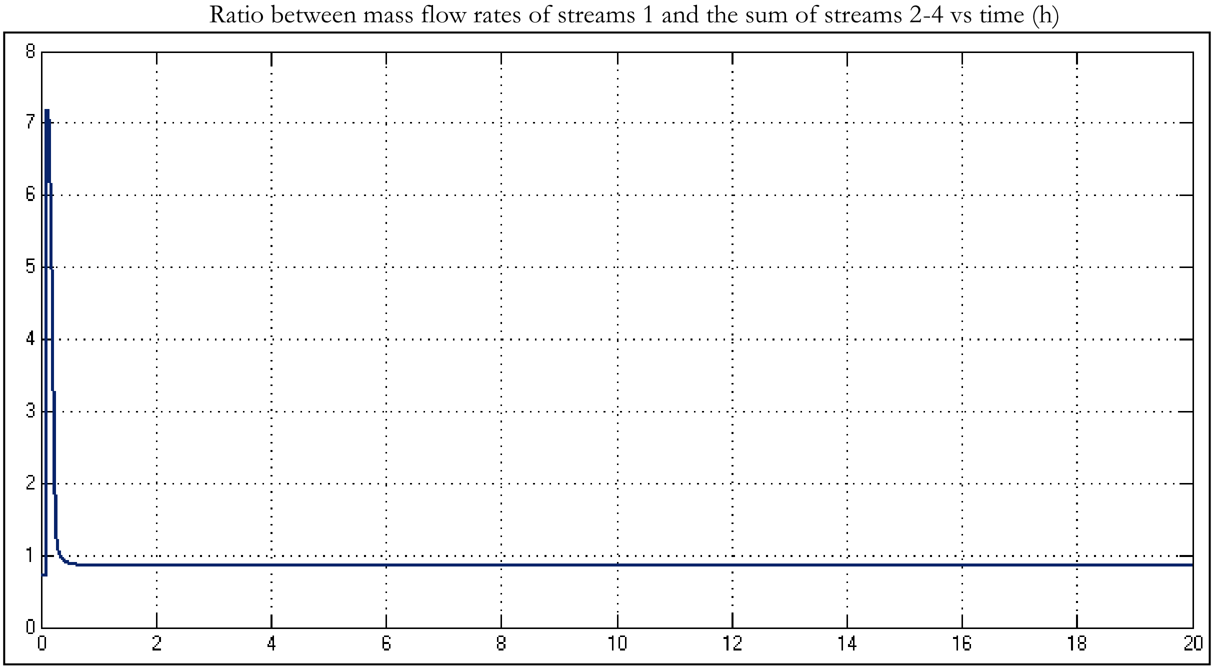

Figure 164: Plot of the ratio between the mass flow rates of streams 1 and the sum of streams 2-4 versus time (in hours). This is the MV of the secondary controller.

$\Delta Solidsfraction_{400TK10} = 0.1771 - 0.161 = 0.0161$

$\Delta Solidsfraction_{400TK20} = 0.1109 - 0.0954 = 0.0155$

$K_p = 0.963$

$t_{63\%} = 5.41\ h$

$t_{28\%} = 1.666\ h$

$\tau = 5.616\ h$

$\theta = 0\ h$

$K_c K_p = 1.5$

$\frac{T_I}{t_{63\%}} = 0.24$

$\frac{T_d}{t_{63\%}} = 0$

$\boldsymbol{K_c = 1.558}$

$\boldsymbol{T_I = 1.298\ h}$

$\boldsymbol{T_d = 0\ h}$

G2.5 Outside Acid Controller

For the tuning of this controller the SP of the acid concentration in 400-TK-20 is multiplied by 1.1 at time step 0.1.

SP and measurements of acid concentration in 400-TK-10 vs time (h)

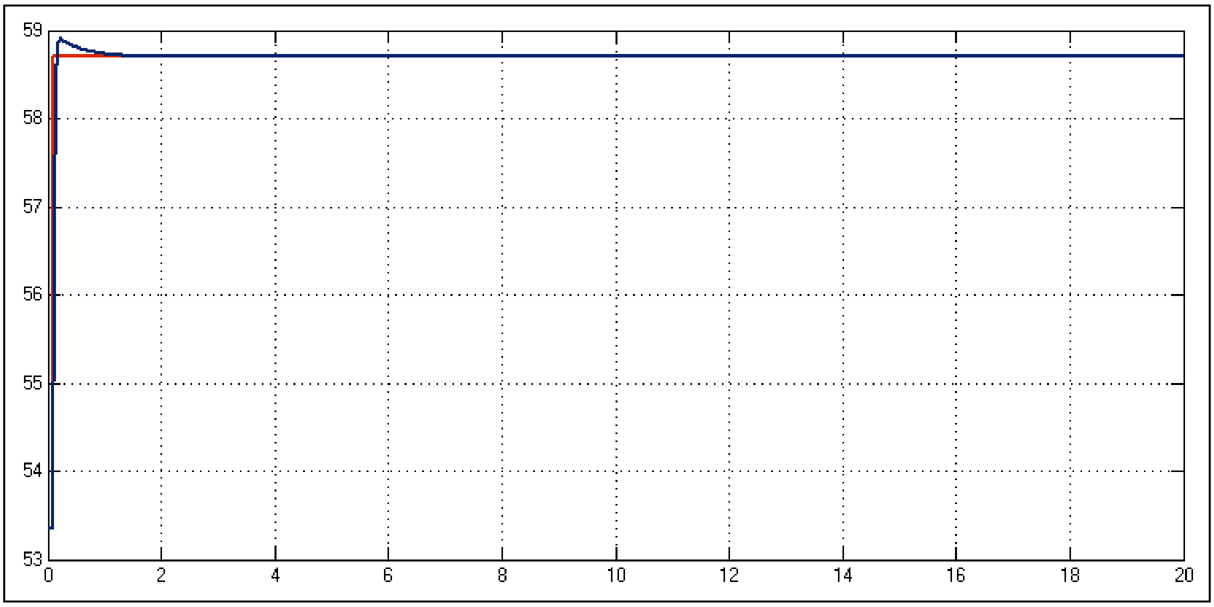

Figure 165: Plot of the set point (red) and measurement (blue) values of the acid concentration in 400-TK-10 vs time (in hours). This is the MV of the primary controller and CV of the secondary controller.

SP and measurements of acid concentration in 400-TK-20 vs time (h)

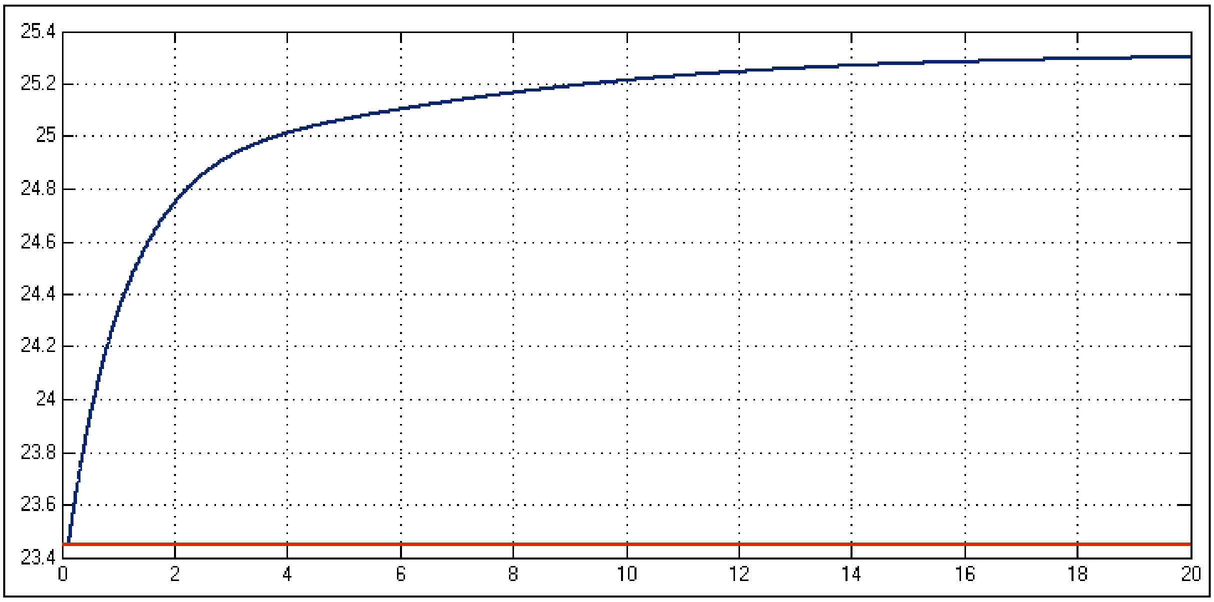

Figure 166: Plot of the set point (red) and measurement (blue) values of the acid concentration in 400-TK-20 vs time (in hours). This is the CV of the primary controller.

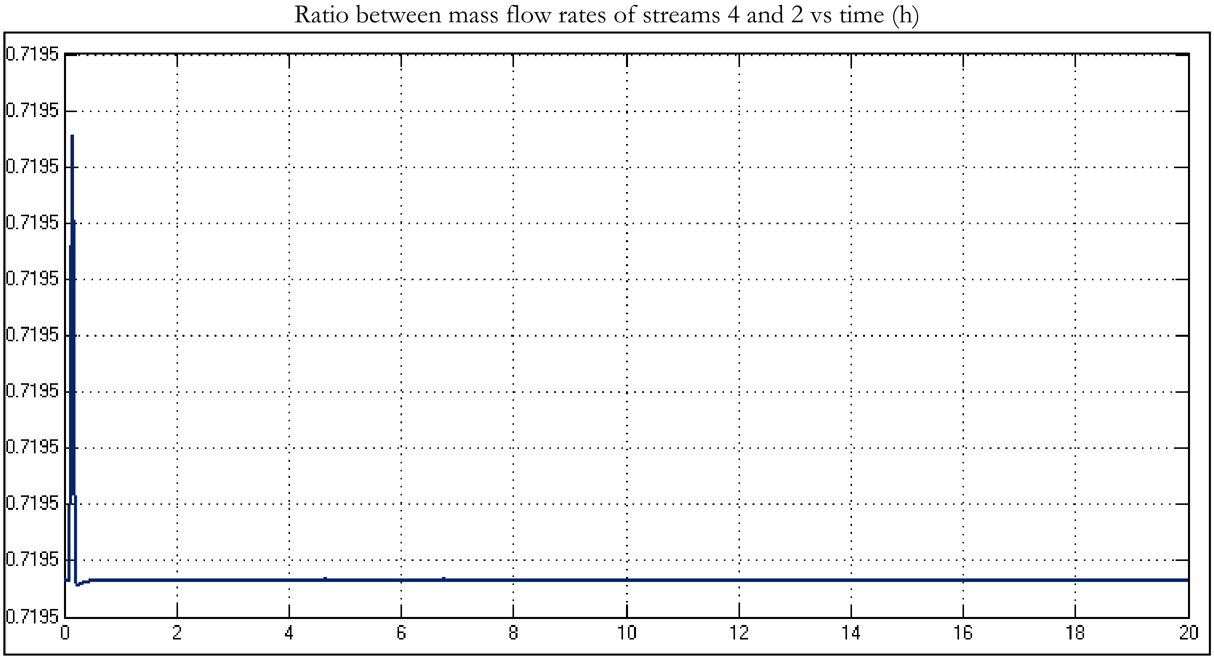

Figure 167: Plot of the ratio between the mass flow rates of streams 4 and 2 versus time (in hours). This is an MV of the secondary controller.

$\Delta[Acid]_{400TK10} = 58.6945 - 53.3586 = 5.3359\ g/L$

$\Delta[Acid]_{400TK20} = 25.2948 - 23.4454 = 1.8494\ g/L$

$K_p = 0.3466$

$t_{63\%} = 1.4607\ h$

$t_{28\%} = 0.4309\ h$

$\tau = 1.5447\ h$

$\theta = 0\ h$

$K_c K_p = 1.5$

$\frac{T_I}{t_{63\%}} = 0.24$

$\frac{T_d}{t_{63\%}} = 0$

$\boldsymbol{K_c = 4.328}$

$\boldsymbol{T_I = 0.351\ h}$

$\boldsymbol{T_d = 0\ h}$

G2.6 Fine-Tuning of Compositional Control on 400-TK-20

The fine-tuning of the compositional control is done by multiplying the SP of the acid concentration in 400-TK-20 by 1.1 at 0.1 hours. Note that the same is not done for the solids controller, since it is not ideal that the set point of solids should change.

Acid concentration in 400-TK-20 (g/L) vs time (h)

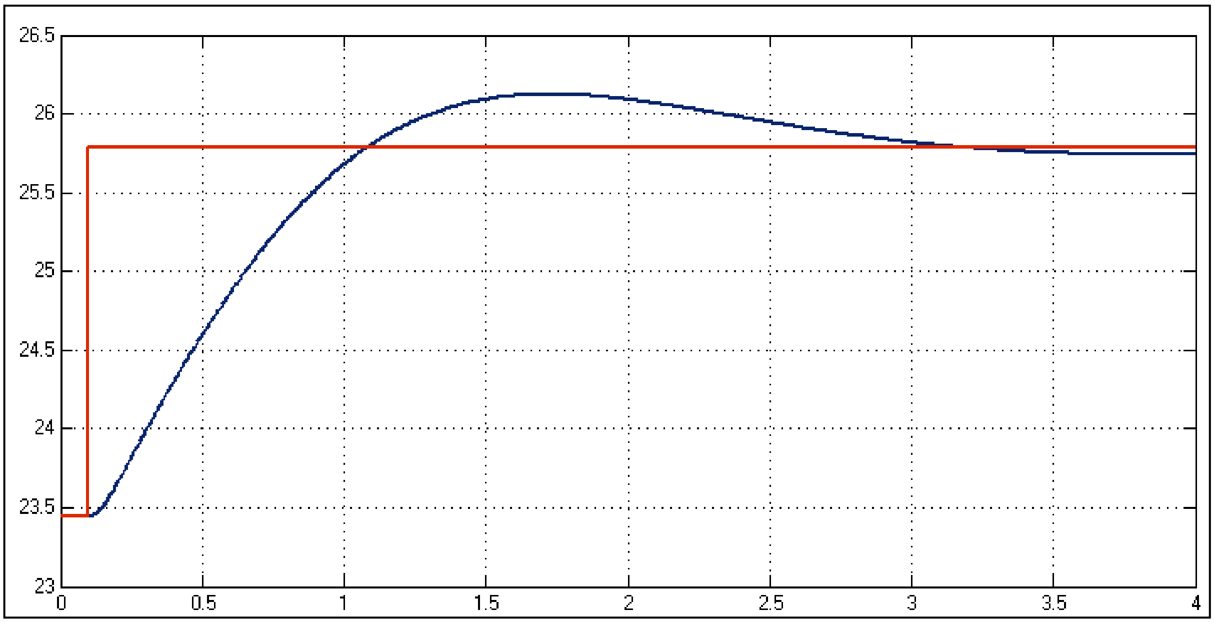

Figure 168: Plot of set point (red) and measured (blue) values for the acid concentration of 400-TK-20 (g/L) versus time (in hours).

Acid concentration in 400-TK-10 (g/L) vs time (h)

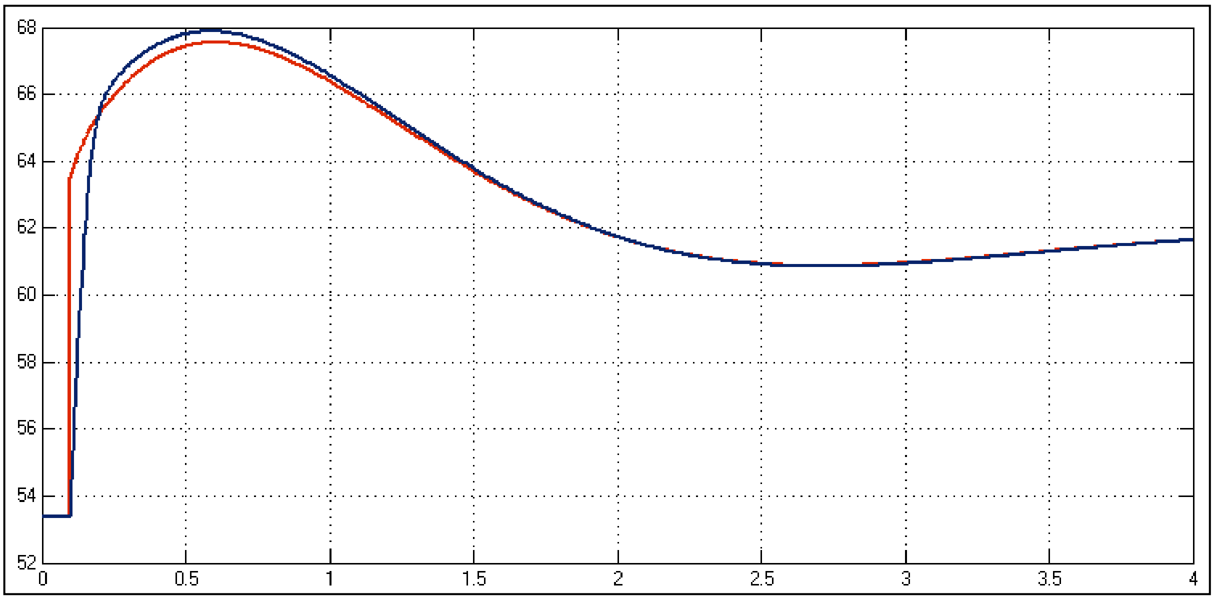

Figure 169: Plot of set point (red) and measured (blue) values for the acid concentration of 400-TK-20 (g/L) versus time (in hours).

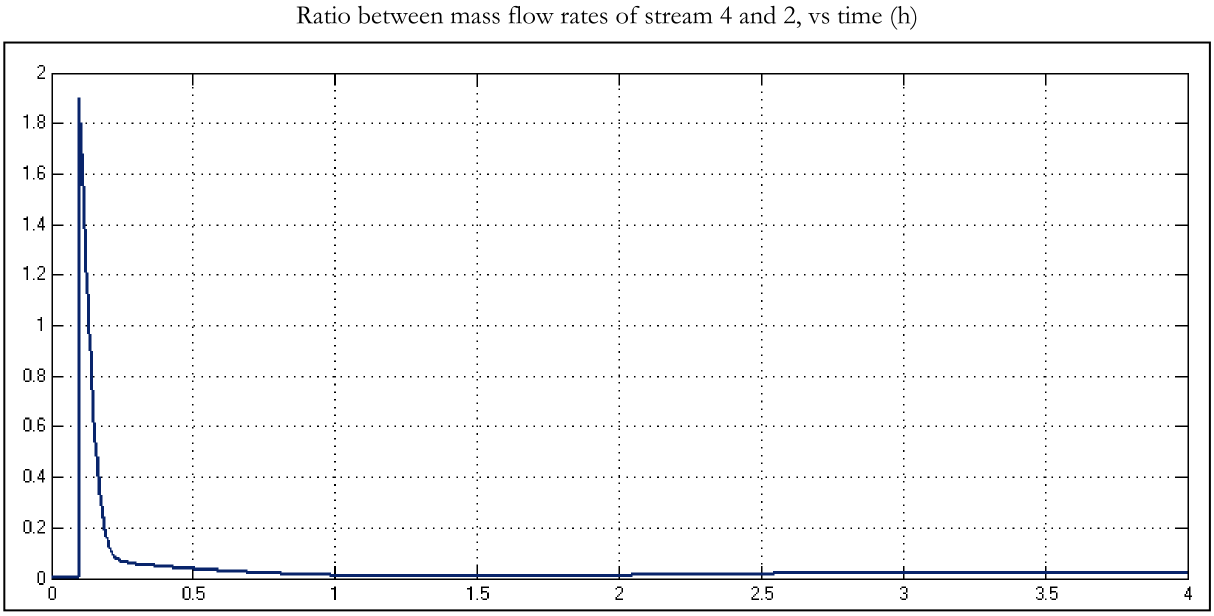

Figure 170: Plot of the ratio between the mass flow rates of streams 4 and 2 (kg/kg) versus time (in hours).

From this plot it can be seen that the acid concentration in 400-TK-20 takes approximately an hour to cross the new set point for the first time. This indicates that the controller is not aggressive enough. Note that the secondary acid controller tracks its set point fairly well, showing a delay initially. Before changing the tuning parameters, the solids fraction results are also viewed:

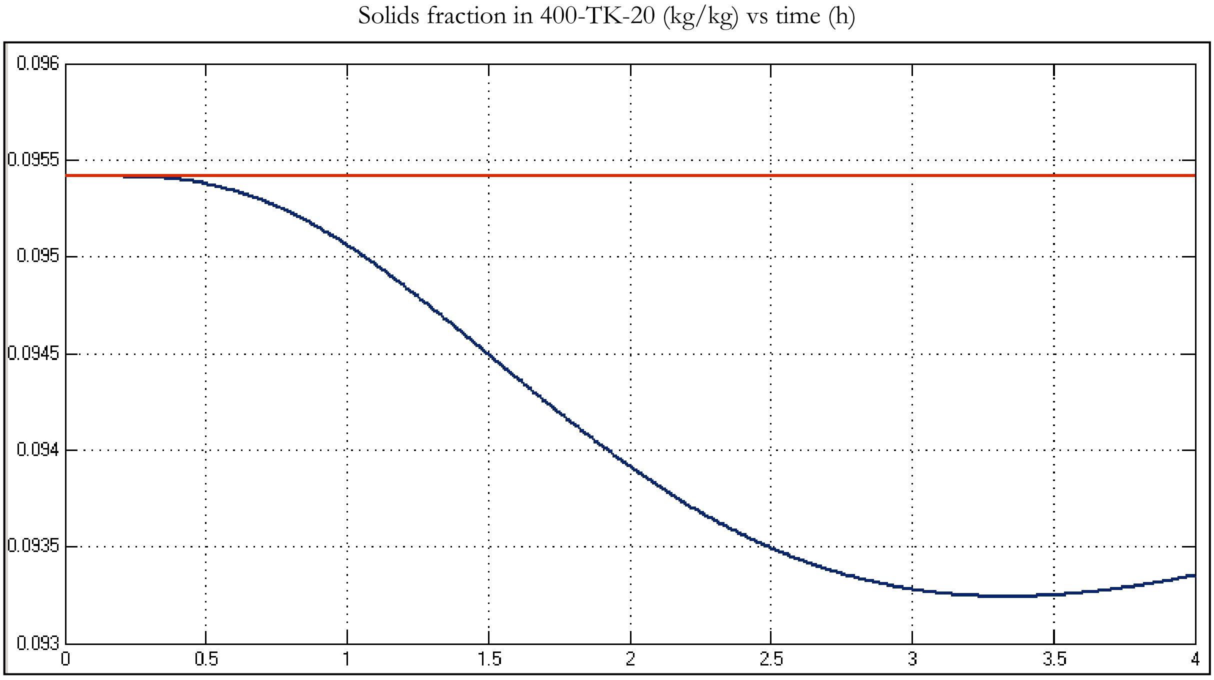

Figure 171: Plot of set point (red) and measured (blue) values for the solids fraction in 400-TK-20 (kg/kg) versus time (in hours).

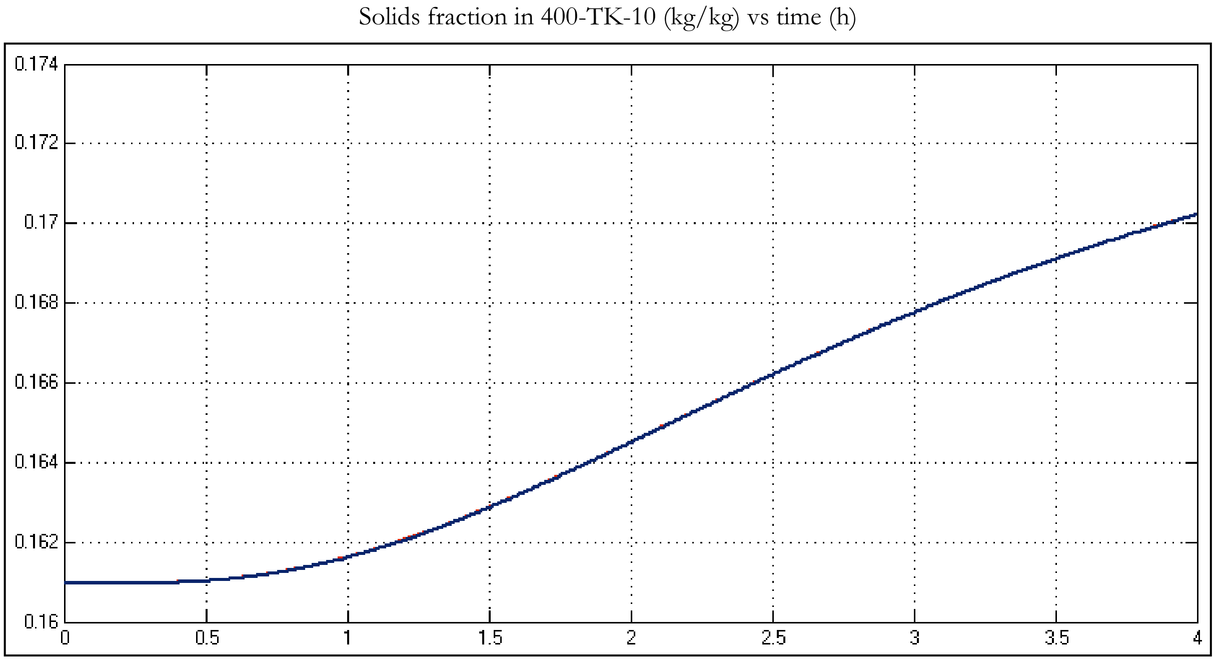

Figure 172: Plot of set point (red) and measured (blue) values for the solids fraction in 400-TK-10 (kg/kg) versus time (in hours).

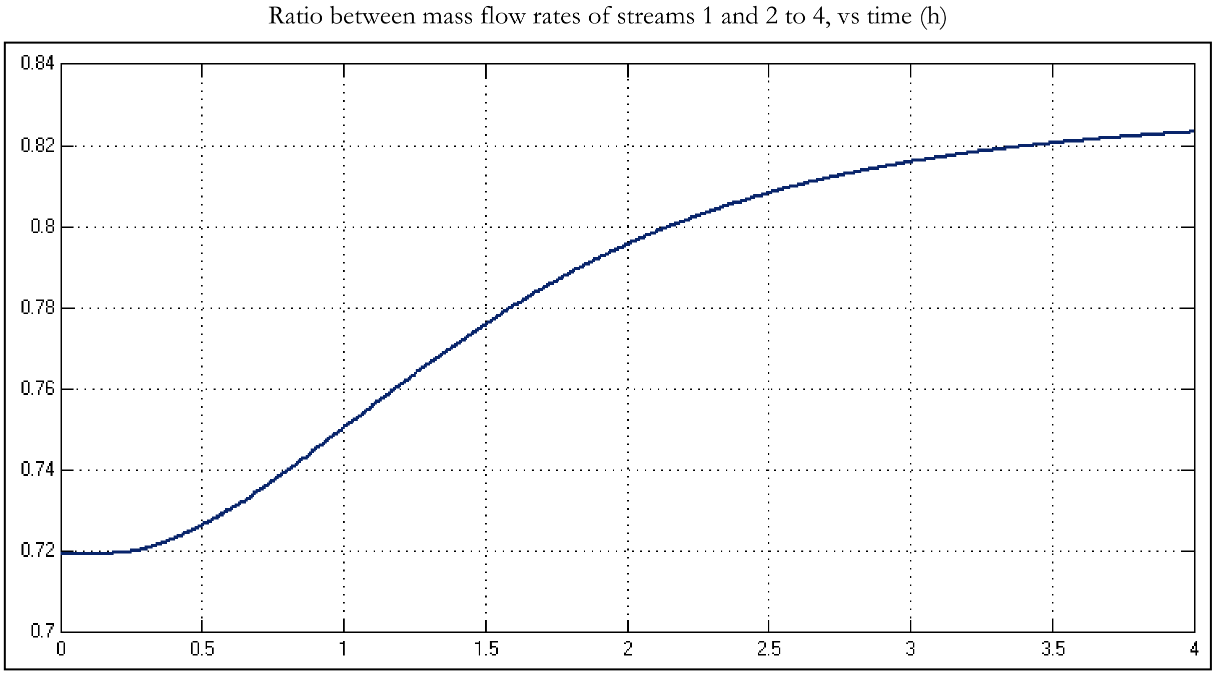

Figure 173: Plot of the ratio between the mass flow rates of streams 1 and 2 to 4 (kg/kg) versus time (in hours).

These plots demonstrate that the secondary controller works very well, tracking its set point value closely. The solids fraction in 400-TK-20 does, however, drift from its set point, but not more than 2.2%, which is acceptable.

The controller gain of the acid controller is multiplied by a factor of 2.8, while the integral time is multiplied by 1.5. The acid controller is not changed. This test is repeated.

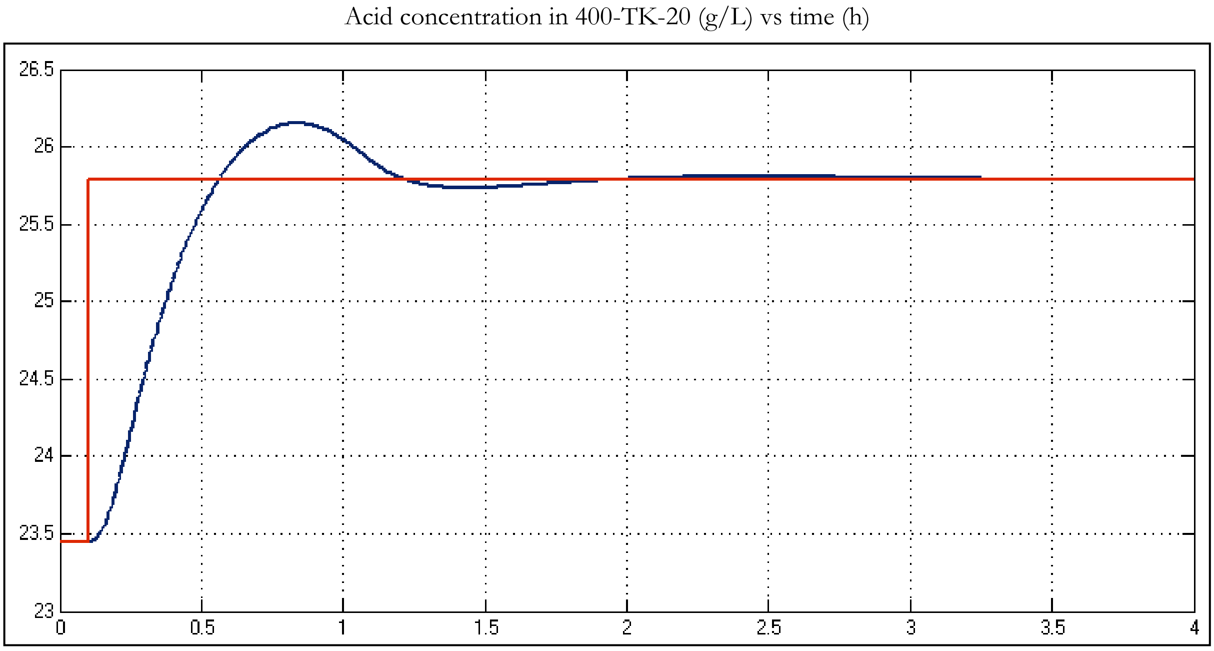

Figure 174: Plot of set point (red) and measured (blue) values for the acid concentration of 400-TK-20 (g/L) versus time (in hours).

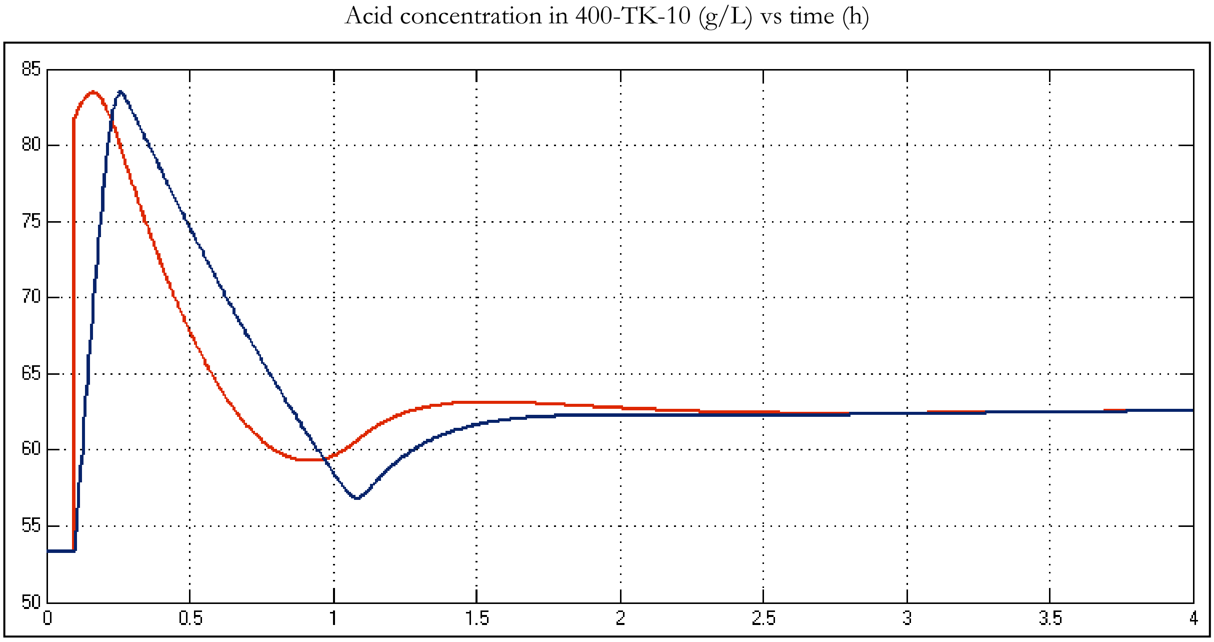

Figure 175: Plot of set point (red) and measured (blue) values for the acid concentration of 400-TK-20 (g/L) versus time (in hours).

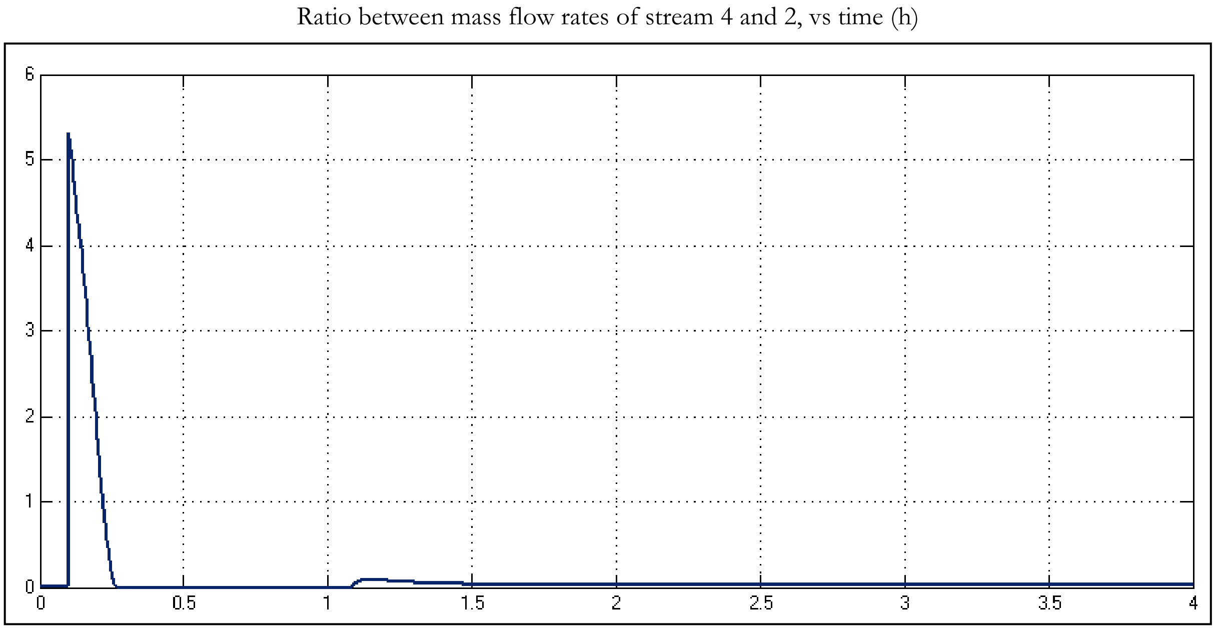

Figure 176: Plot of the ratio between the mass flow rates of streams 4 and 2 (kg/kg) versus time (in hours).

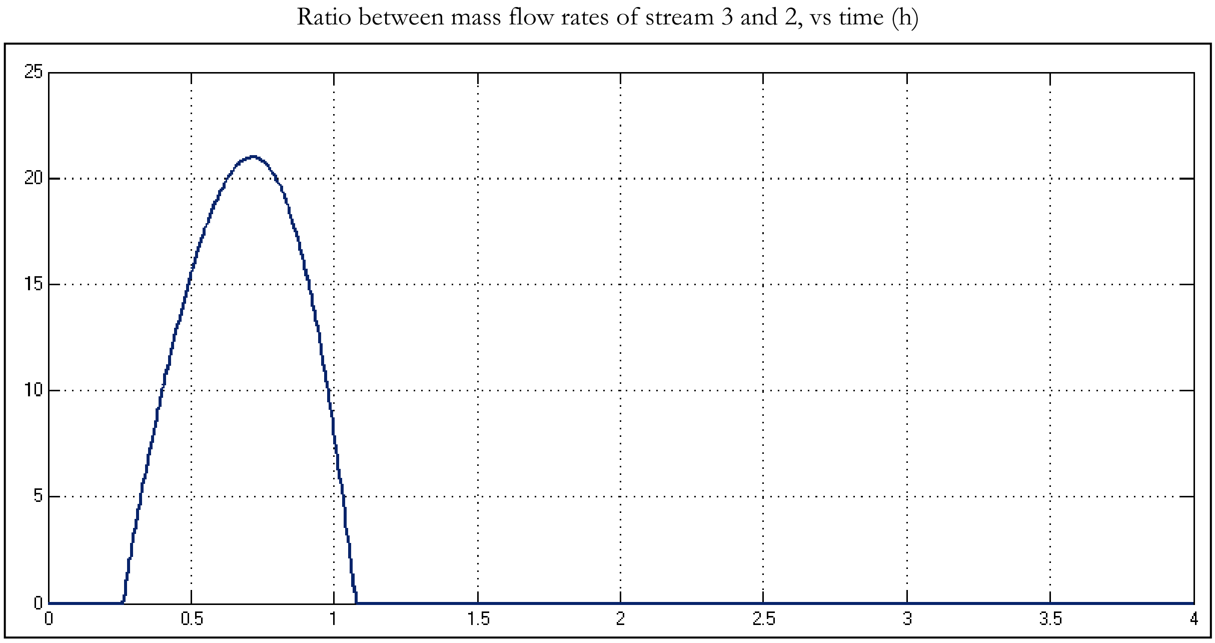

Figure 177: Plot of the ratio between the mass flow rates of streams 3 and 2 (kg/kg) versus time (in hours).

From the above results it can be seen that the changes made greatly improves the performance of the acid controller. It can be seen that there is an overshoot in the CV, which is 17% of the SP change. It can also be seen that the MV response is limited. Note that the limitation on the MV means that an increase in the controller gain would not lead to improved performance.

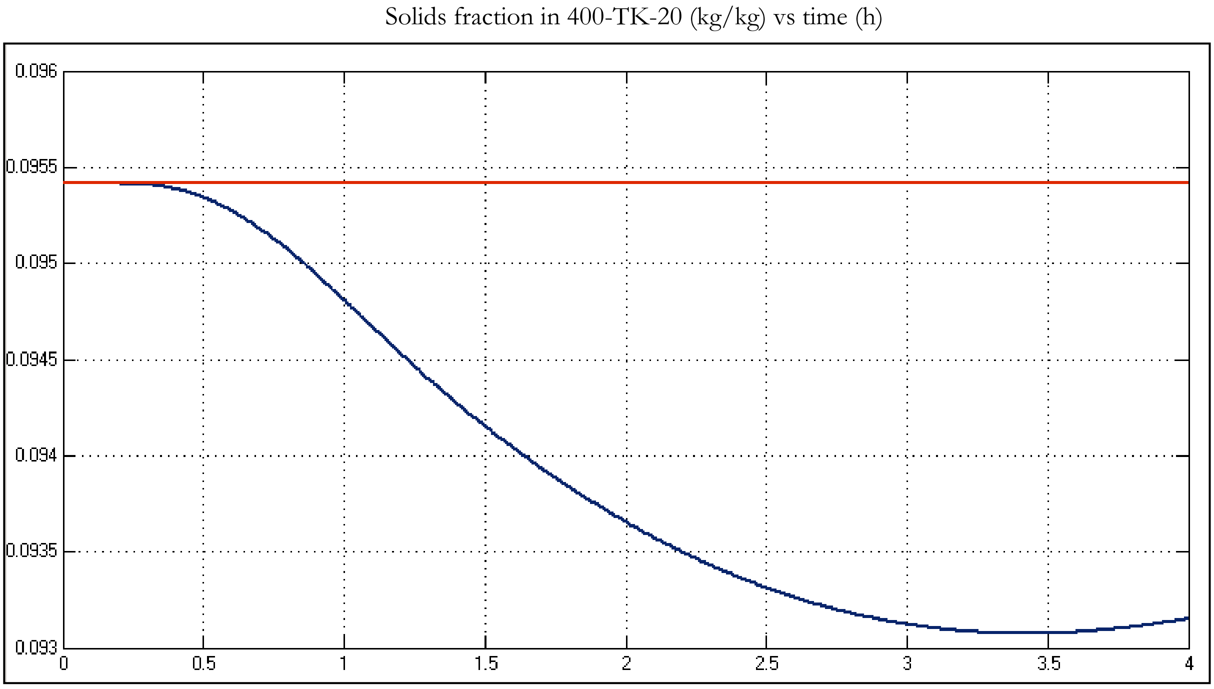

Figure 178: Plot of set point (red) and measured (blue) values for the solids fraction in 400-TK-20 (kg/kg) versus time (in hours).

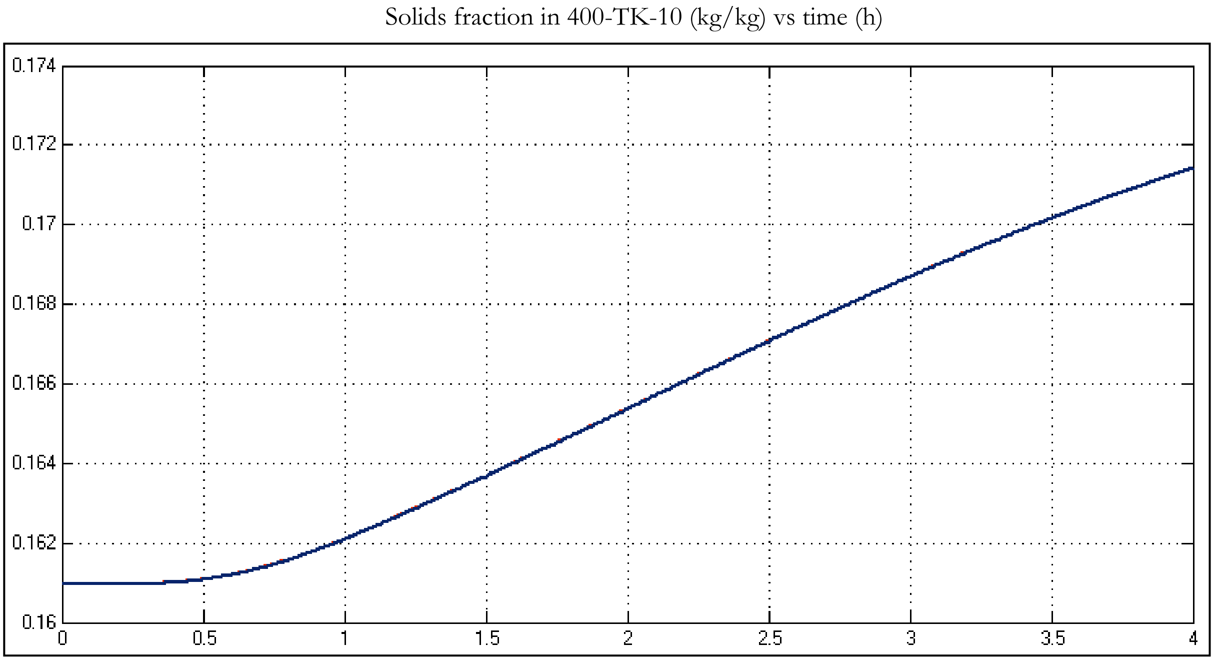

Figure 179: Plot of set point (red) and measured (blue) values for the solids fraction in 400-TK-10 (kg/kg) versus time (in hours).

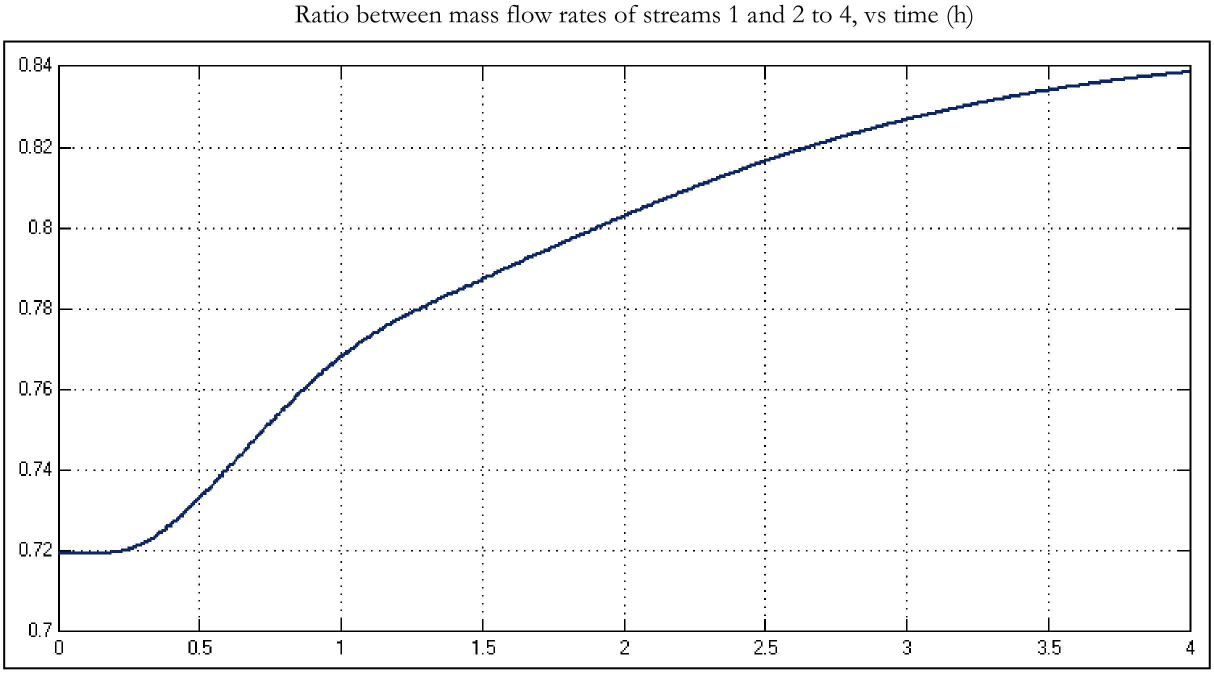

Figure 180: Plot of the ratio between the mass flow rates of streams 1 and 2 to 4 (kg/kg) versus time (in hours).

It can be seen that the solids control response is similar to how it was before the change in the acid controller tuning parameters.

The tuning of the compositional control is therefore deemed satisfactory for its purpose.

APPENDIX H

COMPOSITIONAL CONTROL EVALUATION FOR CHAPTER 5

H1 PLOTS FOR COMPOSITIONAL REGULATORY CONTROL EVALUATION – DISTURBANCE REJECTION

The purpose of the following plots is to supplement the evaluation discussion of section 5.7.2.

H1.1 Evaluation of Base Case – Disturbance Rejection

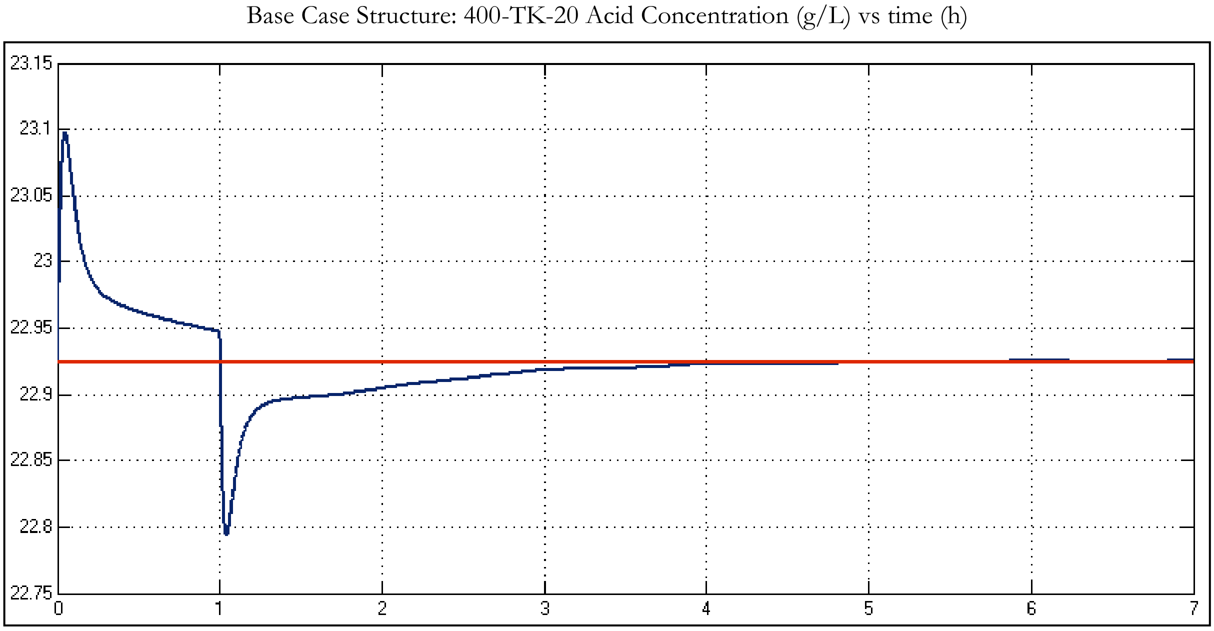

Figure 181: Plot of the set point (red) and measured (blue) base case acid concentration values for 400-TK-20 (g/L), versus time (hours). IAE = 0.0042, Maximum deviation = 0.56%. No steady-state offset.

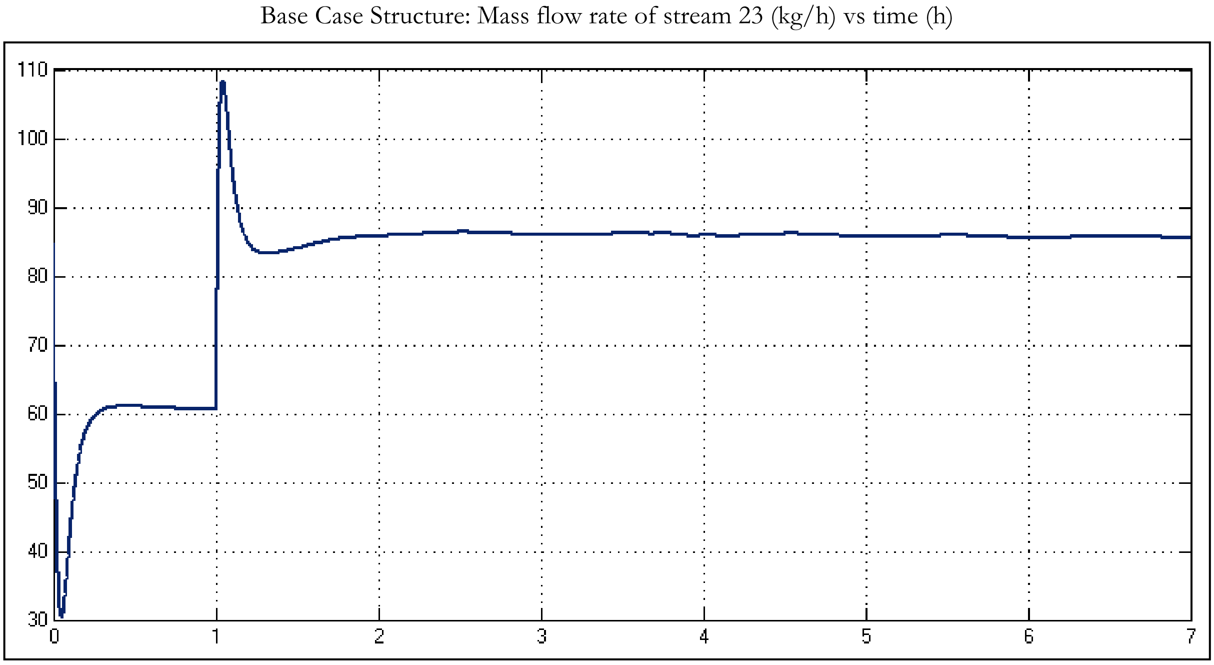

Figure 182: Plot of the mass flow rate of stream 23 (kg/h) versus time (in hours).

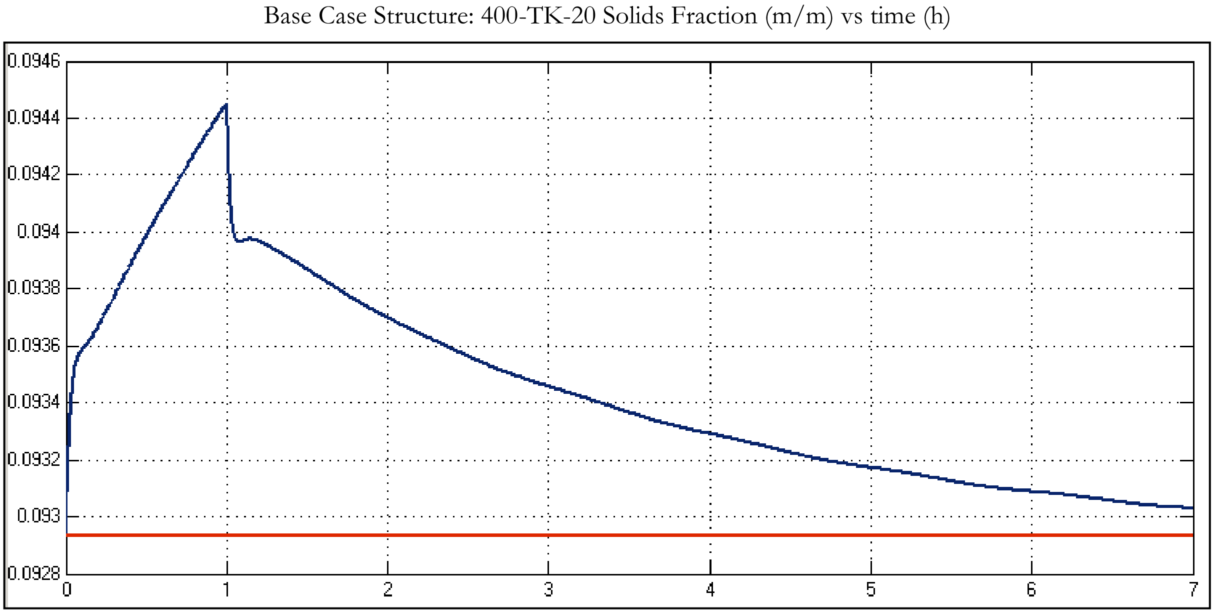

Figure 183: Plot of the set point (red) and measured (blue) base case solids fraction values for 400-TK-20, versus time (hours). IAE = 0.038, Maximum deviation = 1.64%.

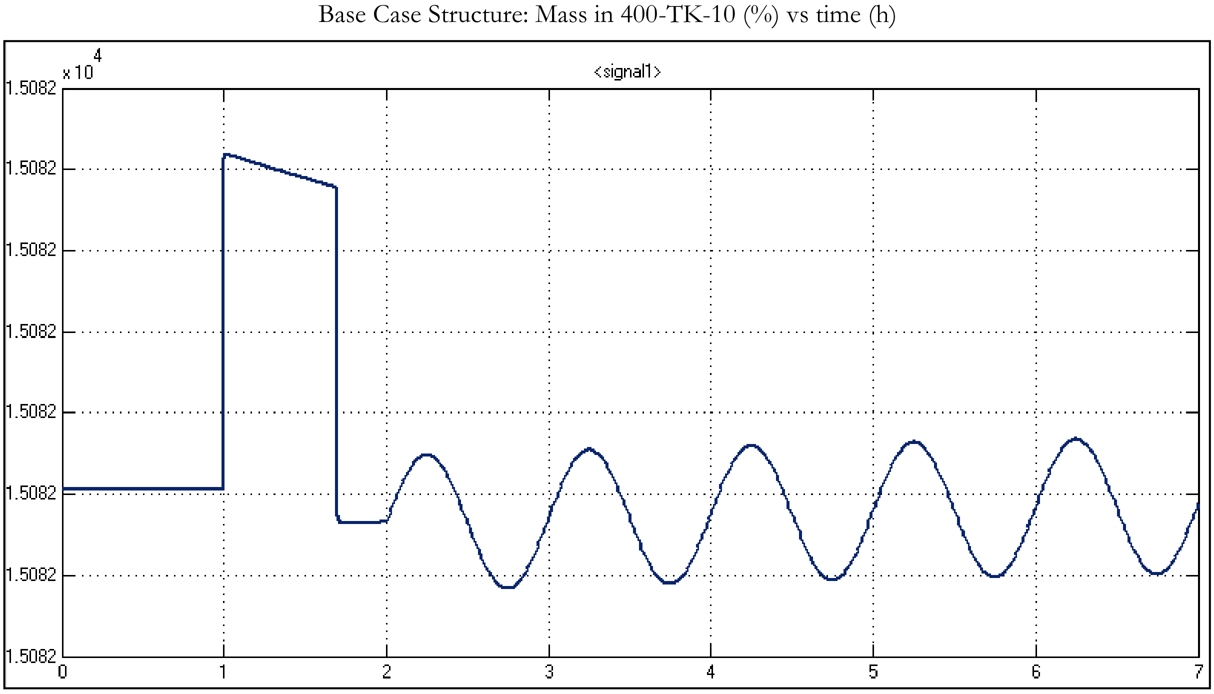

Figure 184: Plot of the mass of 400-TK-10 versus time (hours). IAE = 6.762e-6, Maximum deviation = 0.0005%.

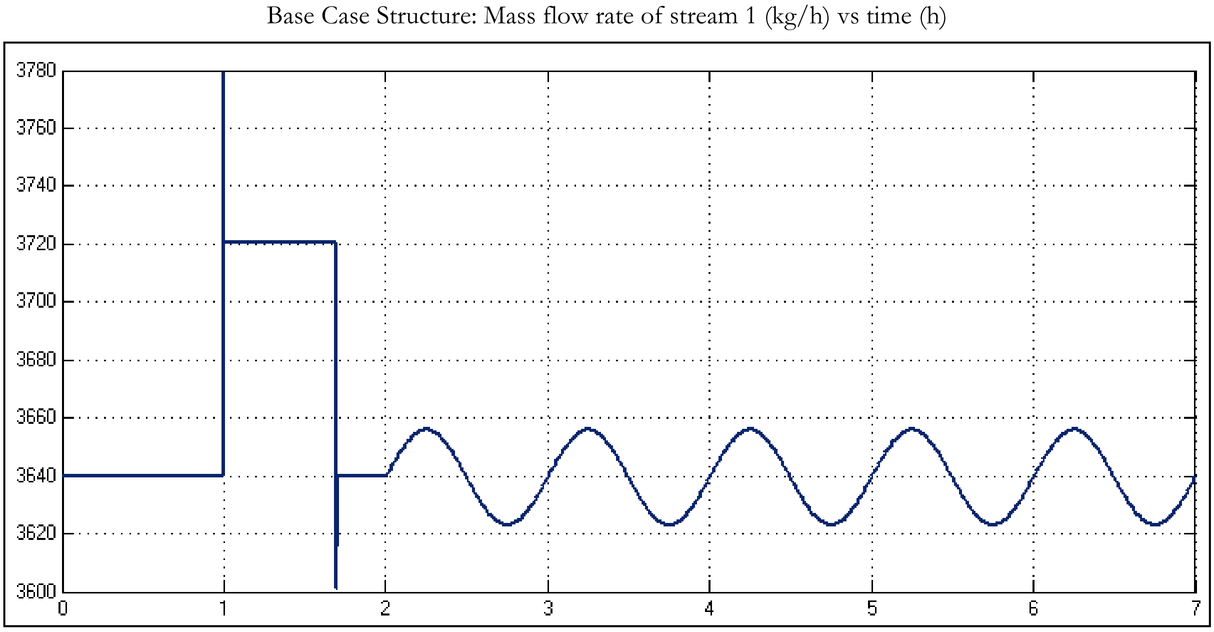

Figure 185: Plot of the flow rate of stream 1 (kg/h) versus time (in hours).

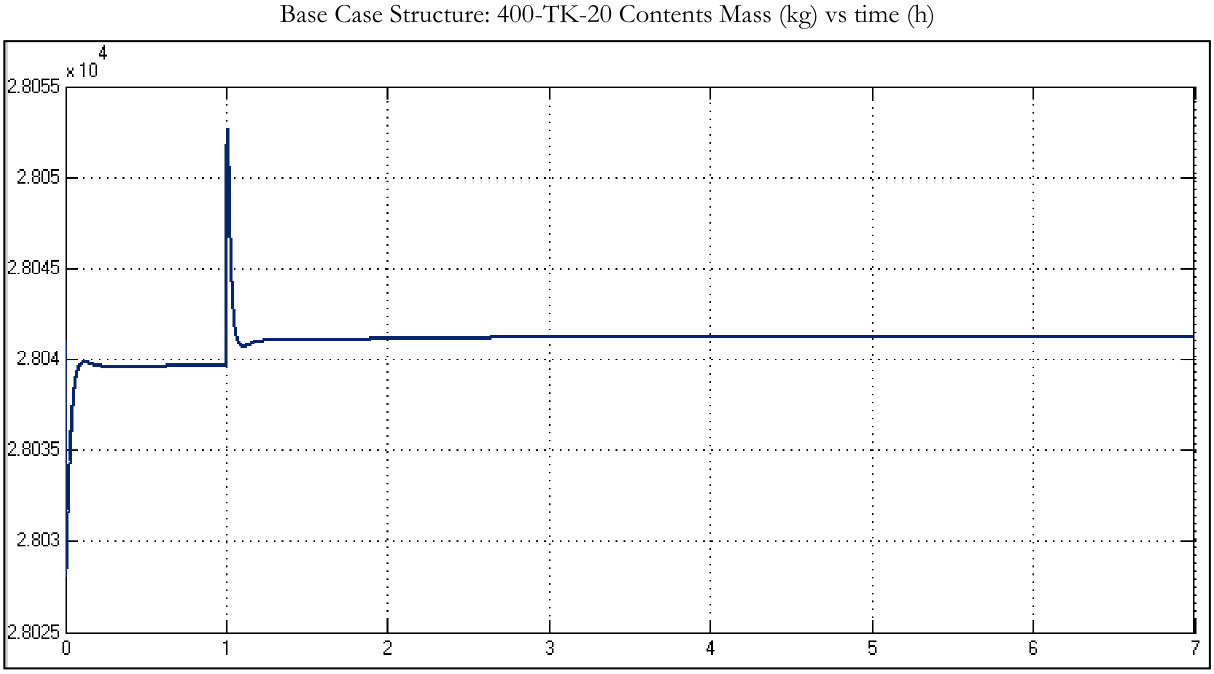

Figure 186: Plot of the base case model's mass of the contents of 400-TK-20 (kg), versus time (hours). IAE = 7.487e-5, Maximum deviation = 0.0053%.

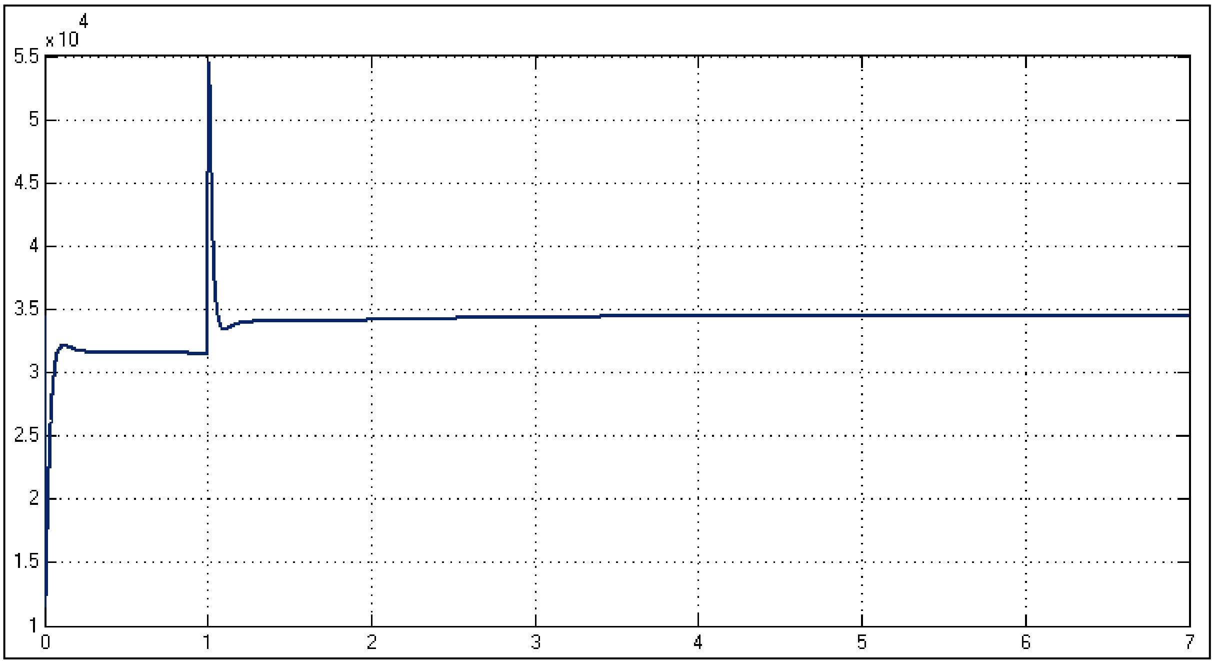
Base Case Structure: Mass flow rate of stream 7 (kg/h) vs time (h)

Figure 187: Plot of the flow rate of stream 1 (kg/h) versus time (in hours).

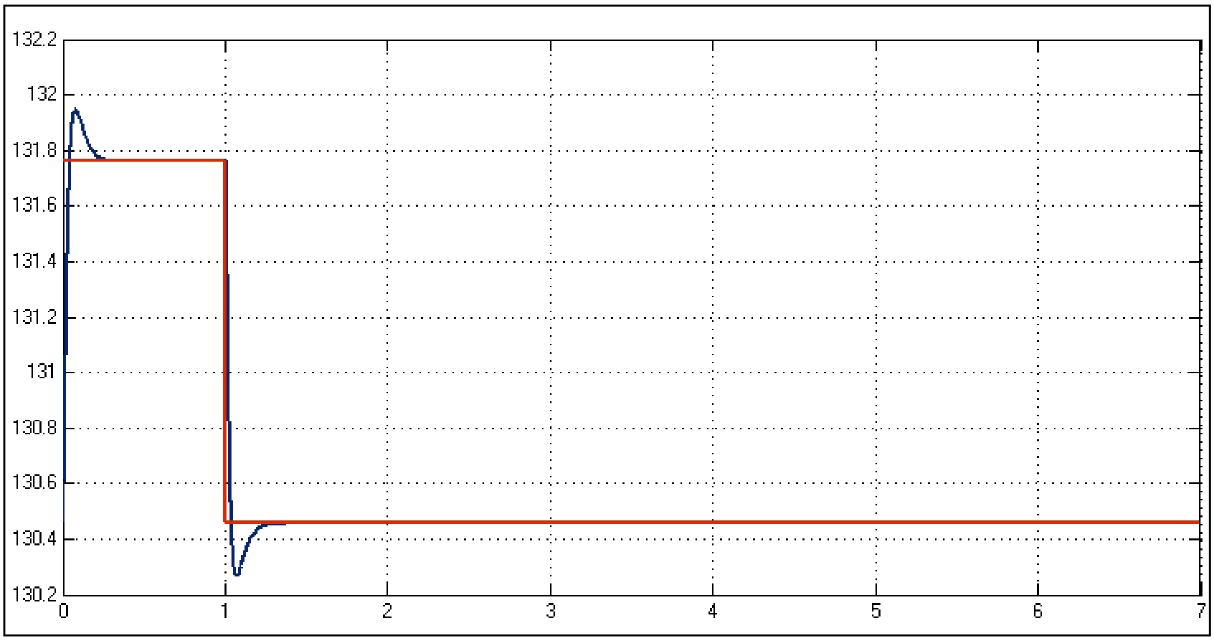
Base Case Structure: Temperature of Compartment 1 (°C) vs time (h)

Figure 188: Plot of the developed model's temperature of compartment 1 (°C) versus time (hours). IAE = 0.0023, Maximum deviation = 1%. No steady-state offset.

Base Case Structure: Flash recycle rate (kg/h) vs time (h)

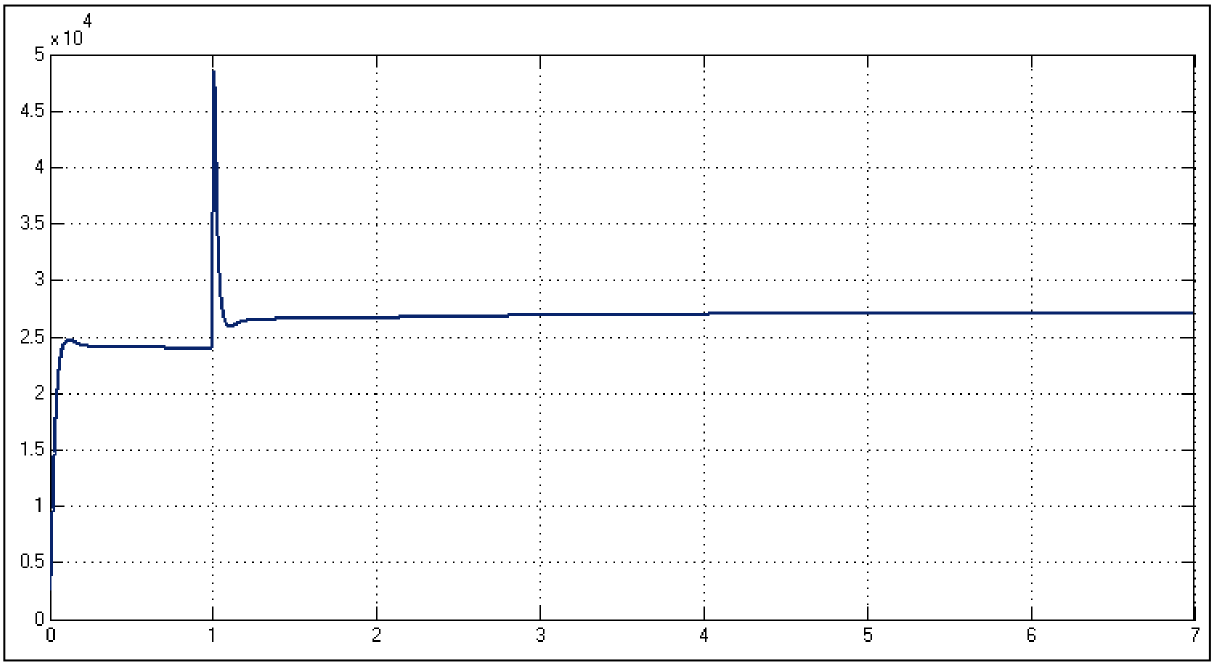

Figure 189: Plot of the flow rate of stream 9 (kg/h) versus time (in hours).

Base Case Structure: % Copper Dissolution in 2nd Stage Leach vs time (h)

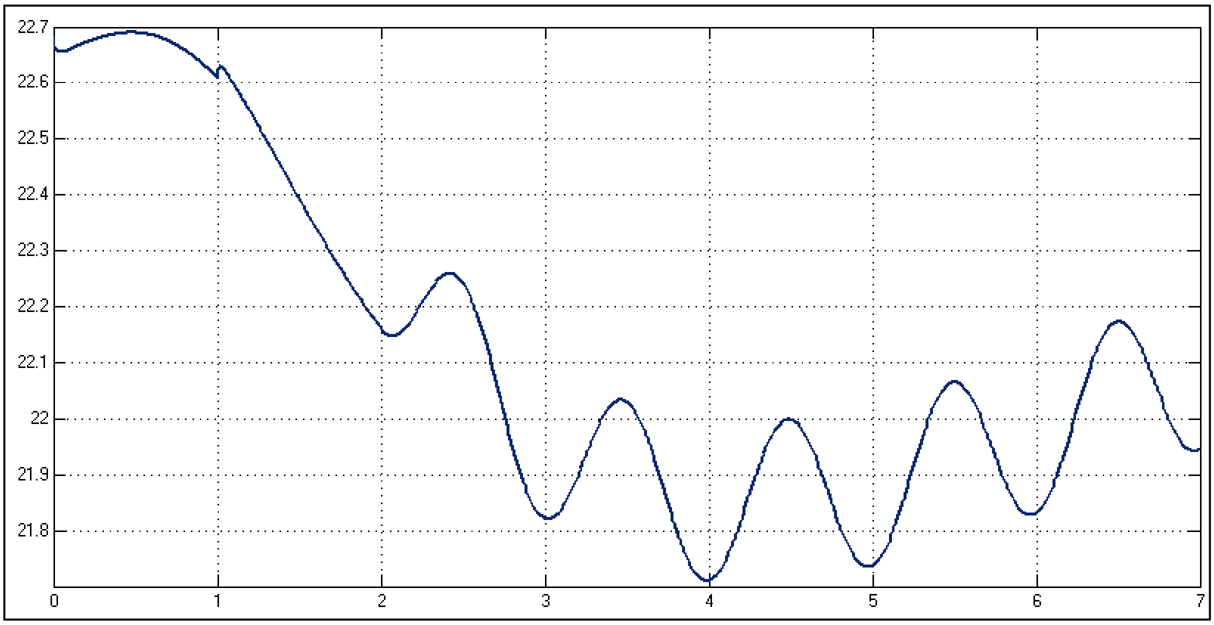

Figure 190: Plot of the percentage of the solid copper leached in the second stage leach in the base case model versus time (hours). Maximum deviation =4.3%

H1.2 Evaluation Cascade Compositional Control – Disturbance Rejection

Developed Structure: 400-TK-20 Acid Concentration (g/L) vs time (h)

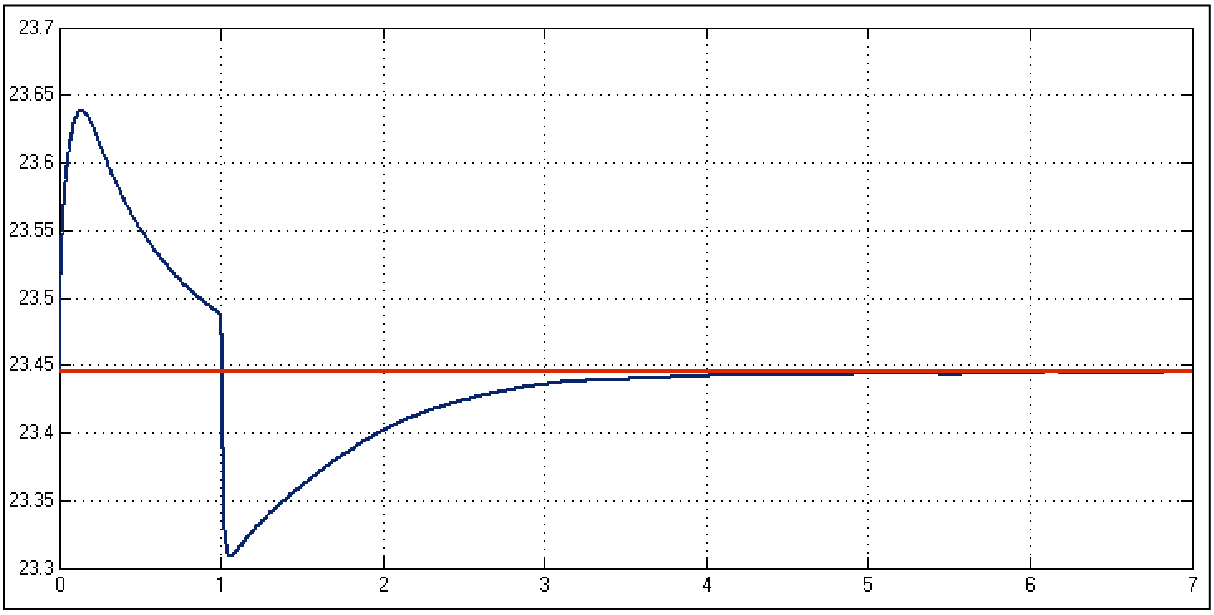

Figure 191: Plot of the set point (red) and measured (blue) developed model's acid concentration values for 400-TK-20 (g/L), versus time (hours). IAE = 0.0094, Maximum deviation = 0.80%. No steady-state offset.

Developed Structure: 400-TK-10 Acid Concentration (g/L) vs time (h)

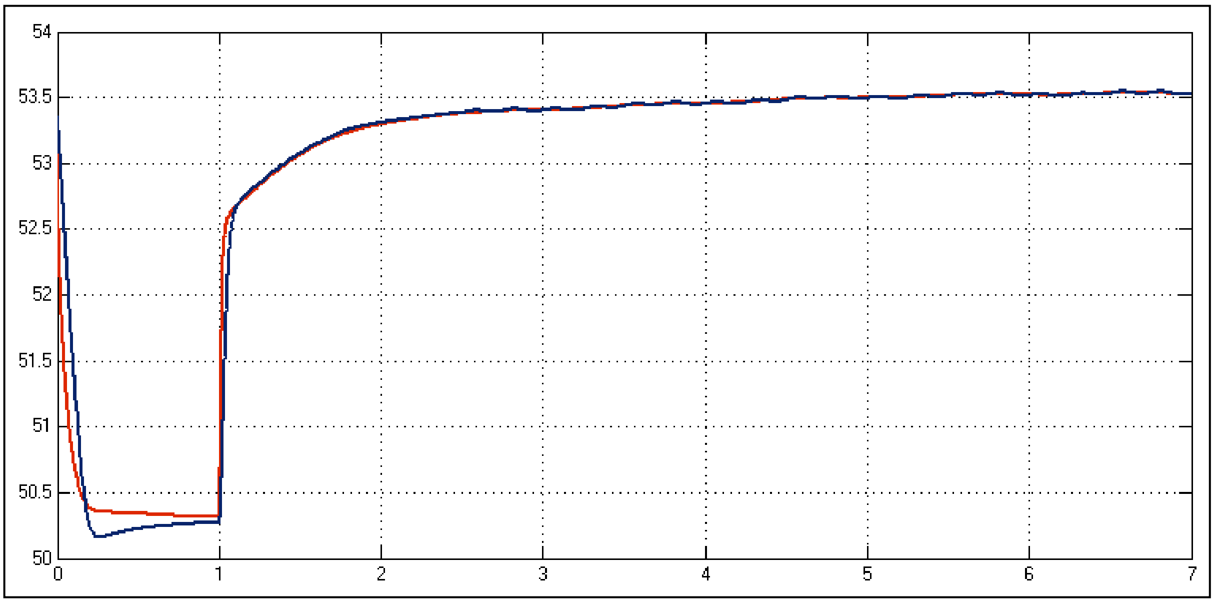

Figure 192: Plot of the set point (red) and measured (blue) developed model's acid concentration values for 400-TK-10 (g/L), versus time (hours).

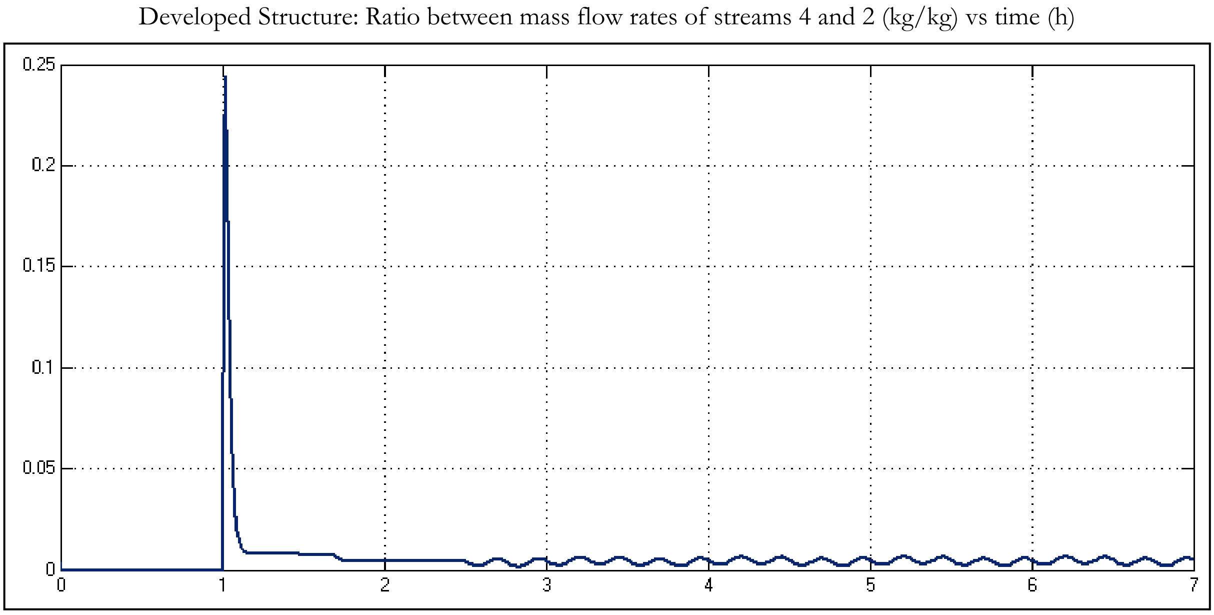

Figure 193: Plot of the ratio between the mass flow rates of streams 4 and 2 versus time (in hours).

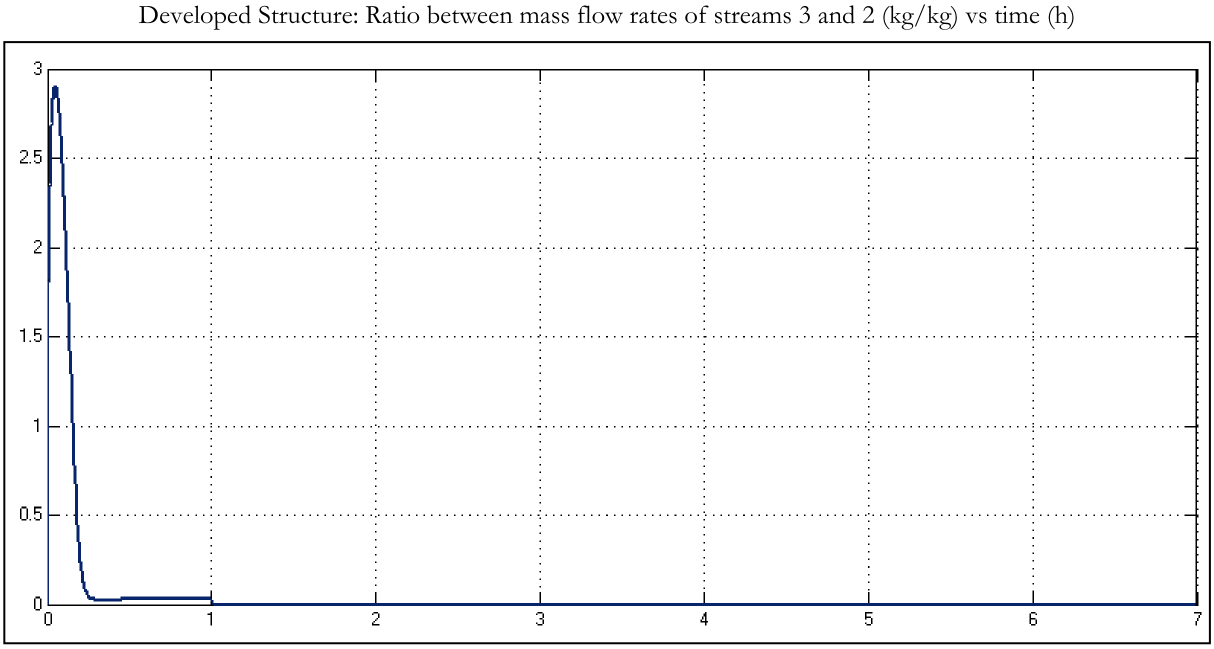

Figure 194: Plot of the ratio between the mass flow rates of streams 3 and 2 versus time (in hours)

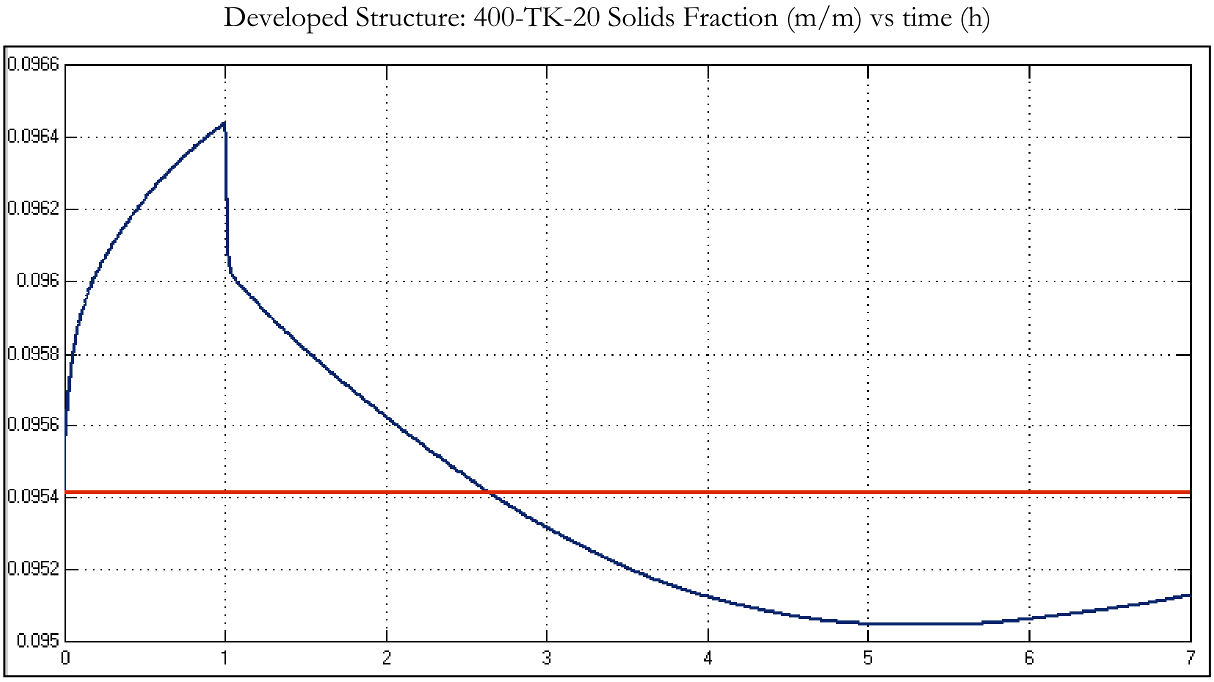

Figure 195: Plot of the set point (red) and measured (blue) developed model's solids fraction values for 400-TK-20, versus time (hours). IAE = 0.0225, Maximum deviation = 1.08%.

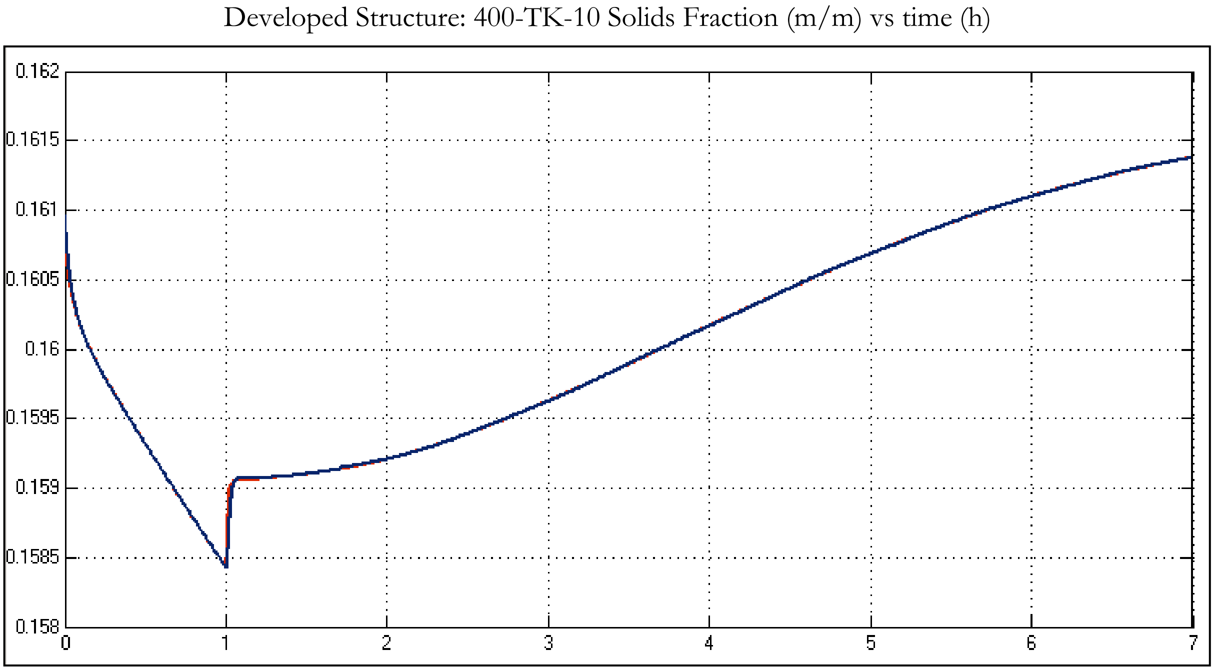

Figure 196: Plot of the set point (red) and measured (blue) developed model's solids fraction values for 400-TK-10, versus time (hours).

Developed Structure: Ratio between mass flow rates of streams 1 and 2 to 4 (kg/kg) vs time (h)

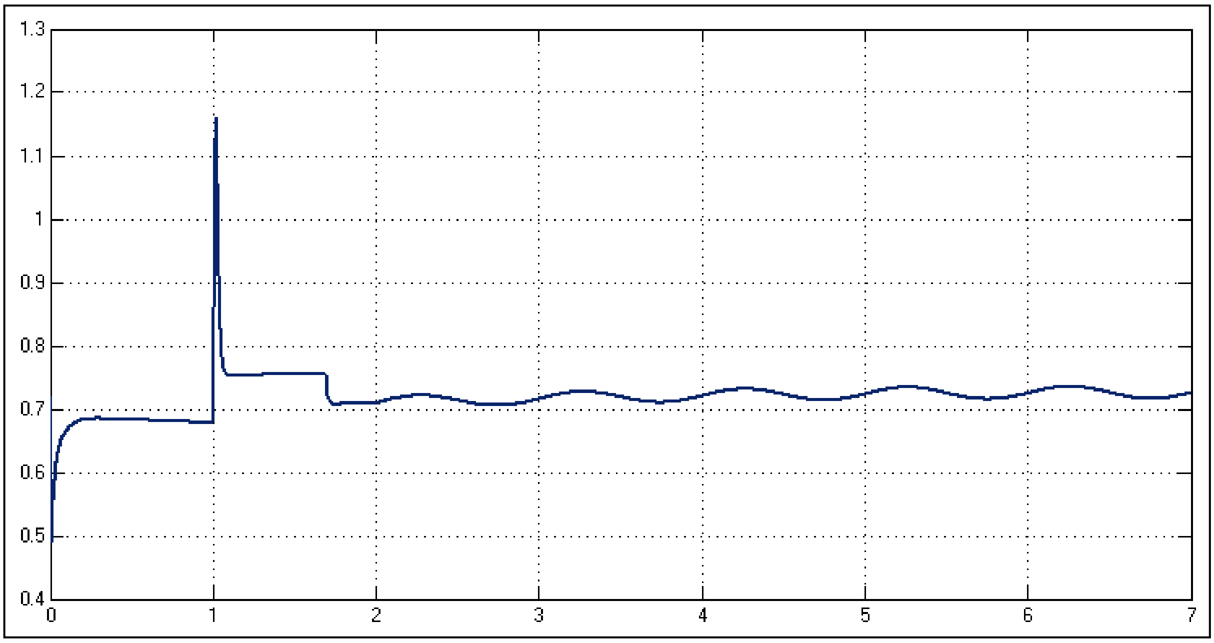

Figure 197: Plot of the ratio between the mass flow rates of streams 1 and 2 to 4 versus time (in hours).

Developed Control: Mass in 400-TK-10 (%) vs time (h)

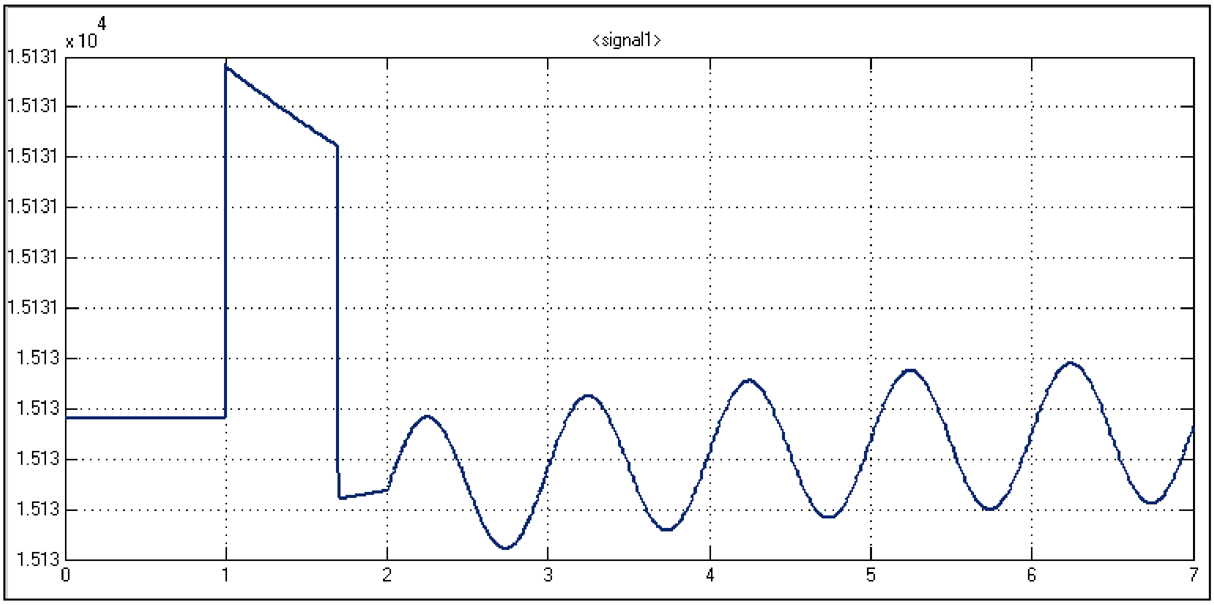

Figure 198: Plot of the mass of 400-TK-10 versus time (hours). IAE = 2.918e-6, Maximum deviation = 0.0002%.

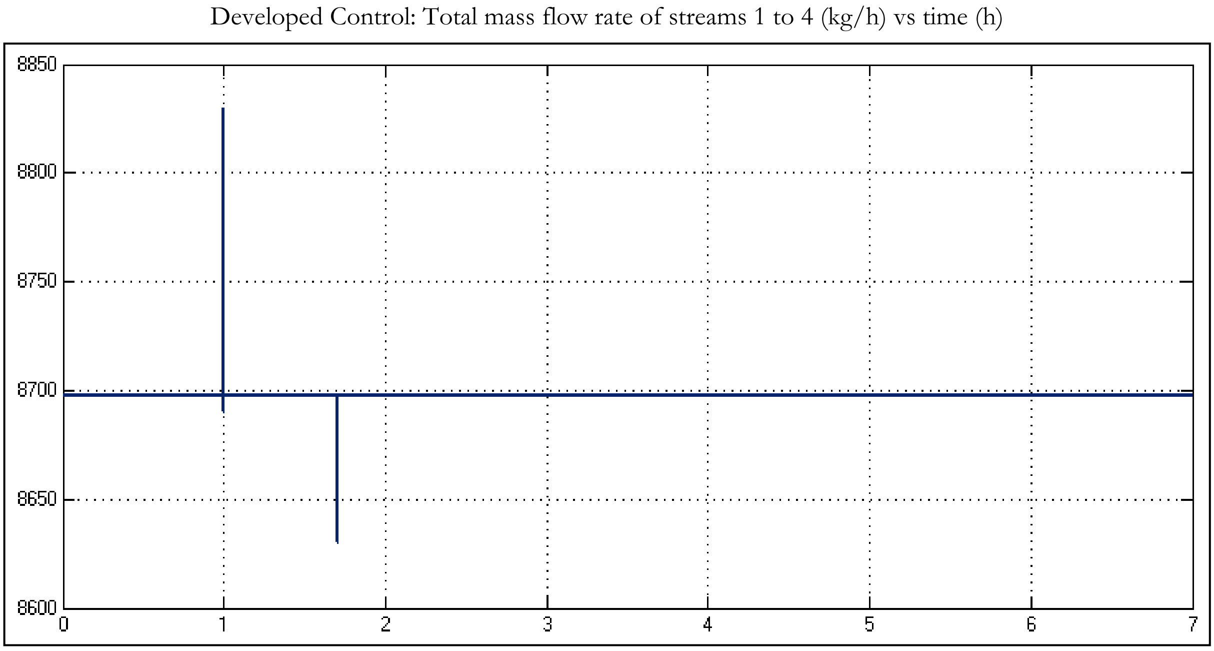

Figure 199: Plot of the sum of the mass flow rates of streams 1 to 4 (kg/h) versus time (in hours).

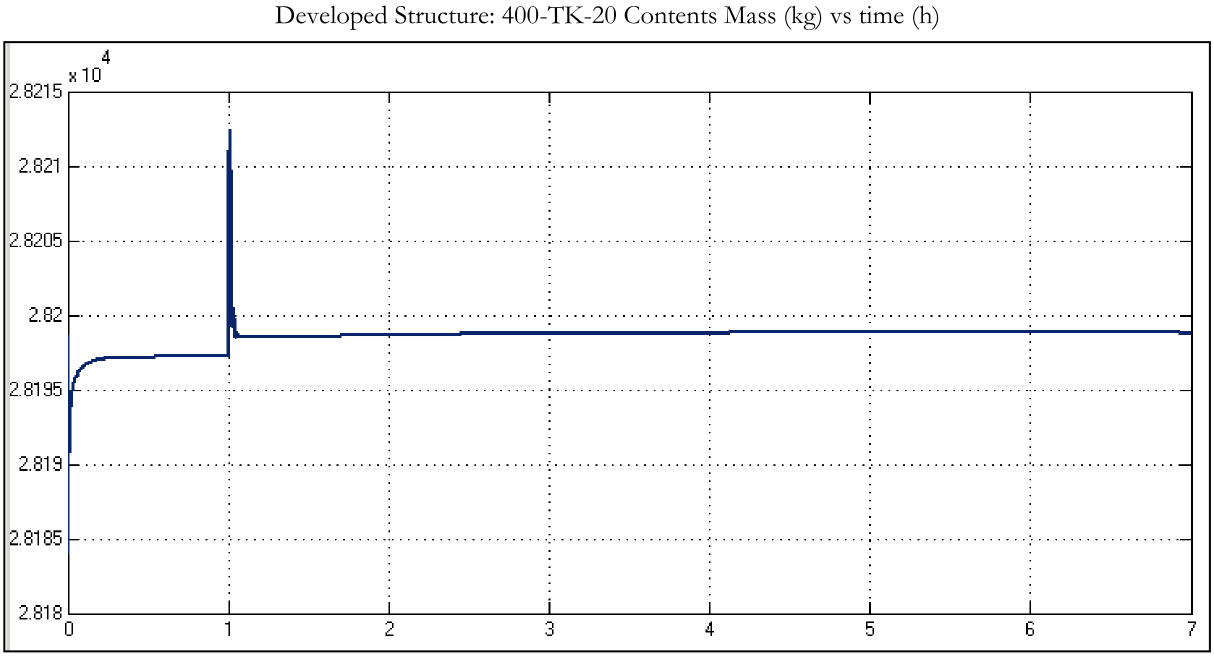

Figure 200: Plot of the developed model's mass of the contents of 400-TK-20 (kg), versus time (hours). IAE = 7.65e-5, Maximum deviation = 0.0023%

Developed Structure: Mass flow rate of stream 7 (kg/h) vs time (h)

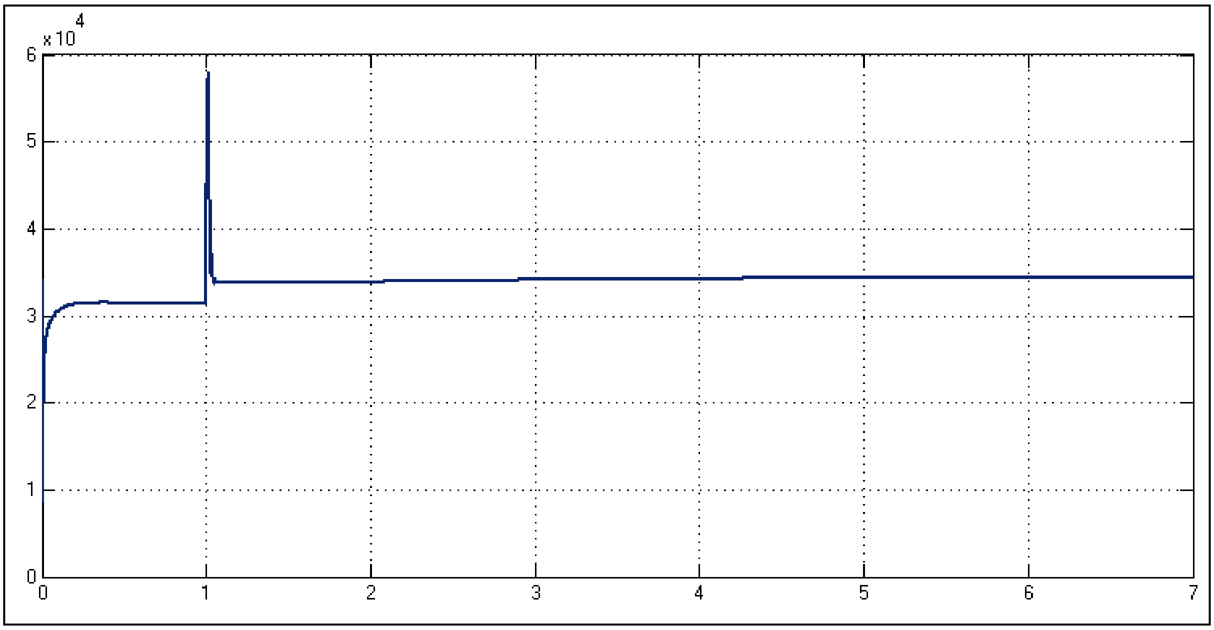

Figure 201: Plot of the mass flow rate of stream 7 (kg/h) versus time (in hours).

Developed Structure: Temperature of Compartment 1 (°C) vs time (h)

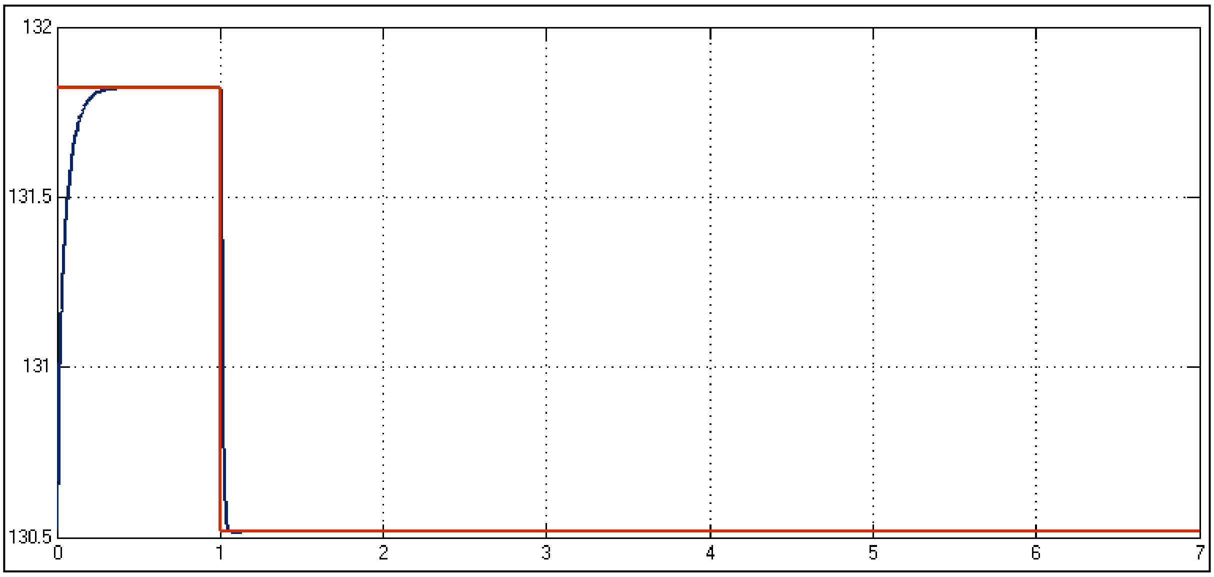

Figure 202: Plot of the developed model's temperature of compartment 1 (°C) versus time (hours). IAE = 0.0022, Maximum deviation = 1%. No steady-state offset.

Developed Structure: Mass flow rate of stream 9 (kg/h) vs time (h)

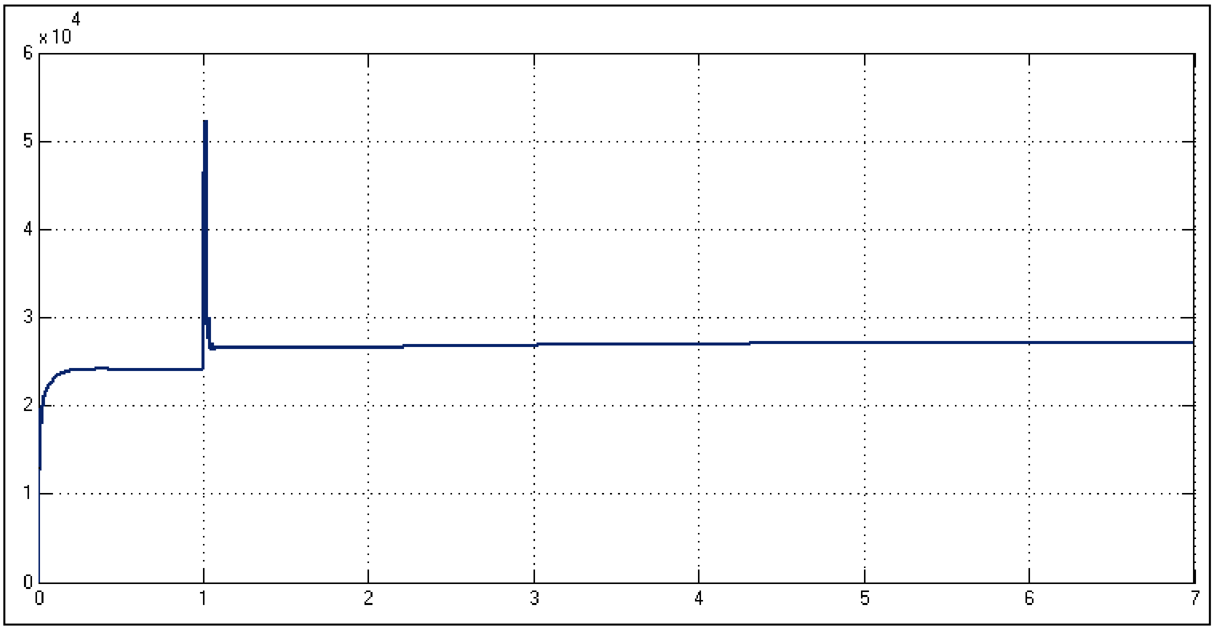

Figure 203: Plot of the mass flow rate of stream 9 (kg/h) versus time (in hours).

Developed Structure: % Copper Dissolution in 2nd Stage Leach vs time (h)

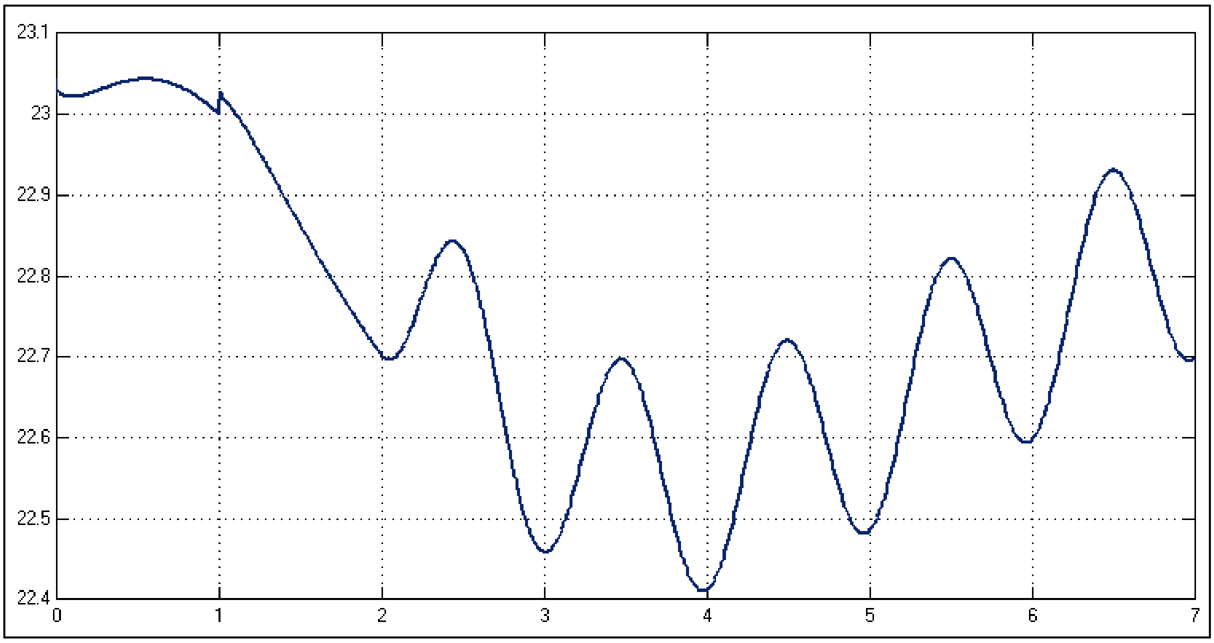

Figure 204: Plot of the percentage of the solid copper leached in the second stage leach in the newly developed model versus time (hours). Maximum deviation =2.75%

H2 PLOTS FOR COMPOSITIONAL REGULATORY CONTROL EVALUATION – ACID SET POINT TRACKING

The purpose of the following plots is to supplement the evaluation discussion of section 5.7.

H2.1 Evaluation of Base Case – Acid Set Point Tracking

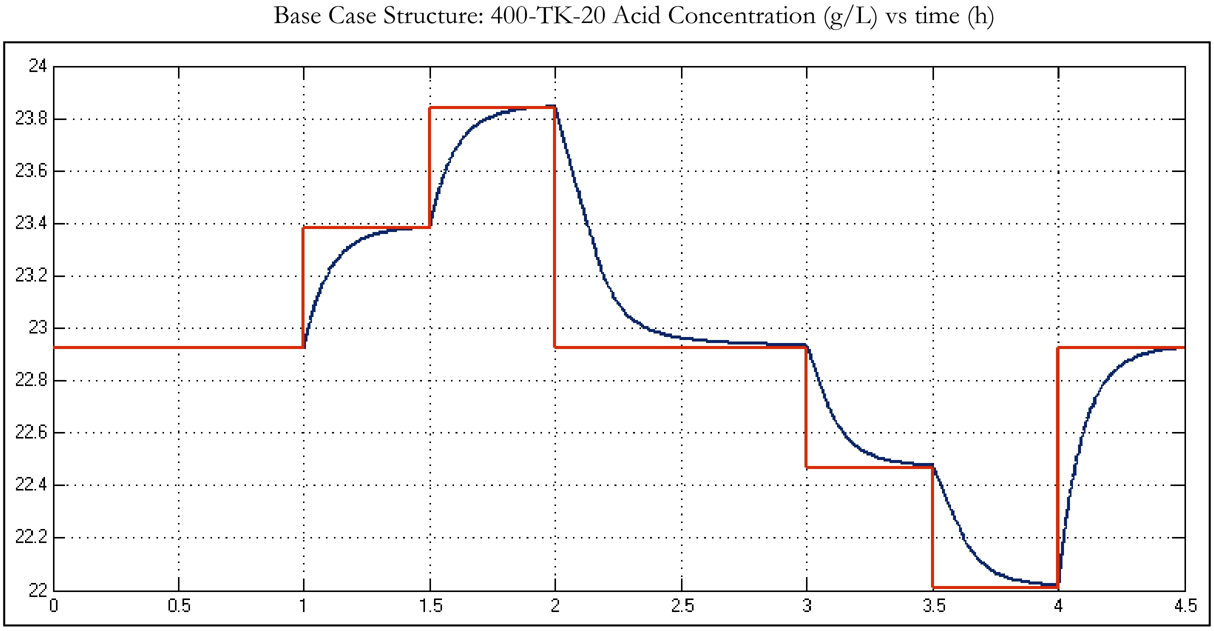

Figure 205: Plot of the set point (red) and measured (blue) base case acid concentration values for 400-TK-20 (g/L), versus time (hours). IAE = 0.0284, Maximum deviation= 4.01%.

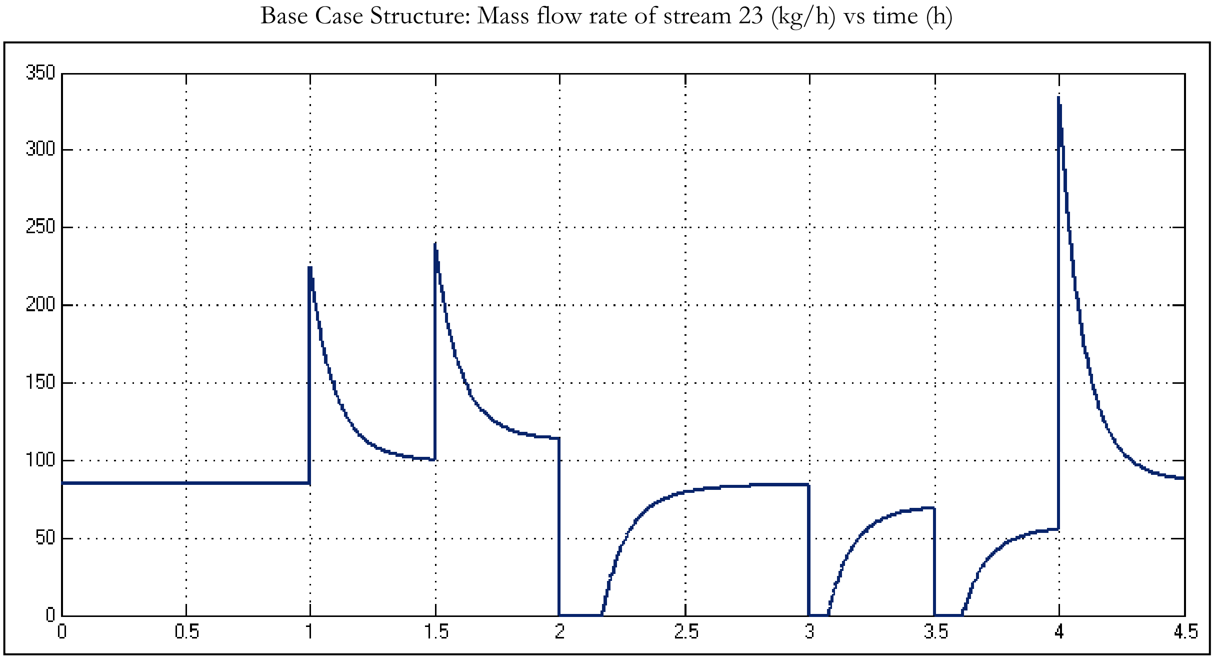

Figure 206: Plot of the mass flow rate of stream 23 (kg/h) versus time (in hours).

Base Case Structure: 400-TK-20 Solids Fraction (m/m) vs time (h)

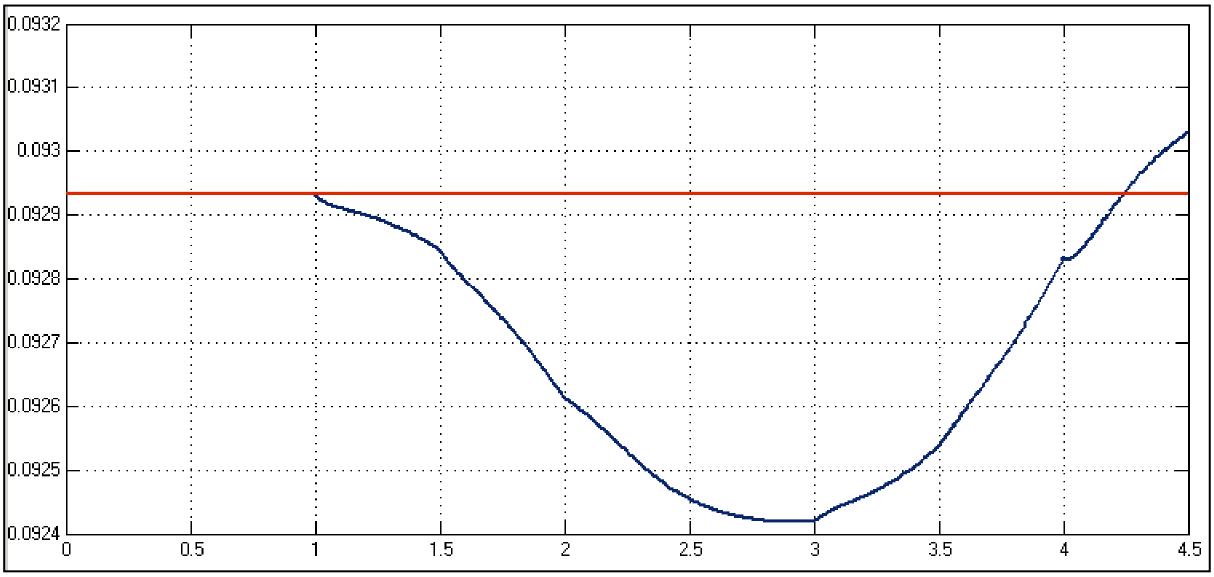

Figure 207: Plot of the set point (red) and measured (blue) base case solids fraction values for 400-TK-20, versus time (hours). IAE = 0.0103, Maximum deviation = 0.55%.

The mass in 400-TK-10 shows no noticeable change.

Base Case Structure: 400-TK-20 Contents Mass (kg) vs time (h)

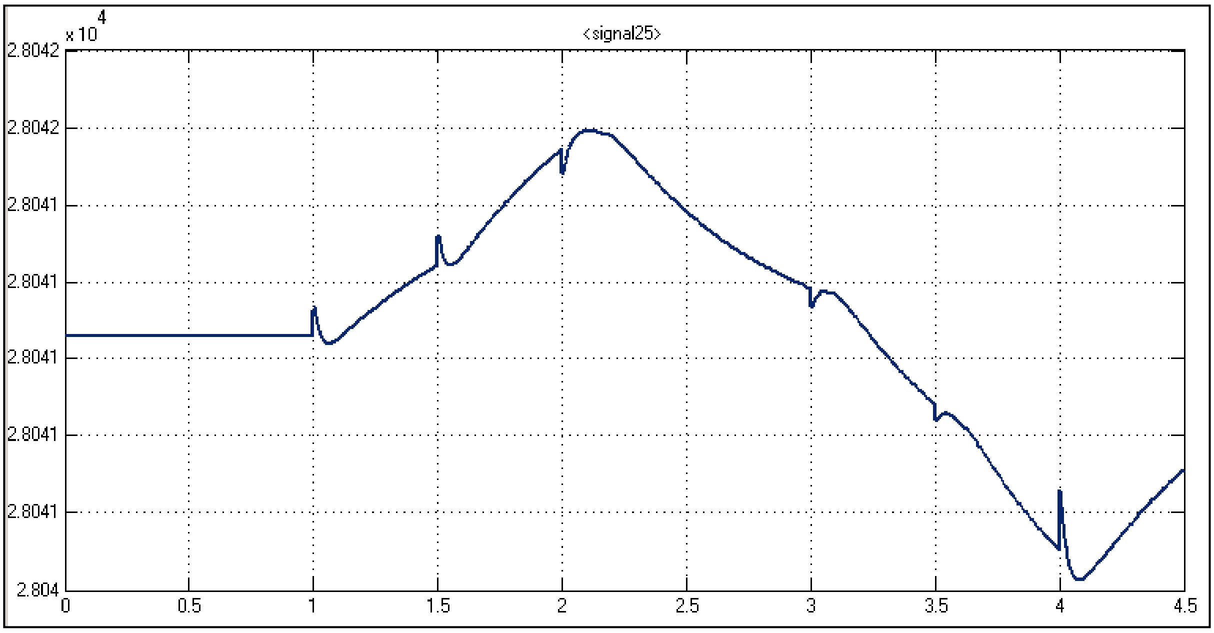

Figure 208: Plot of the base case model's mass of the contents of 400-TK-20 (kg), versus time (hours). IAE = 3.54e-5, Maximum deviation = 0.0022%.

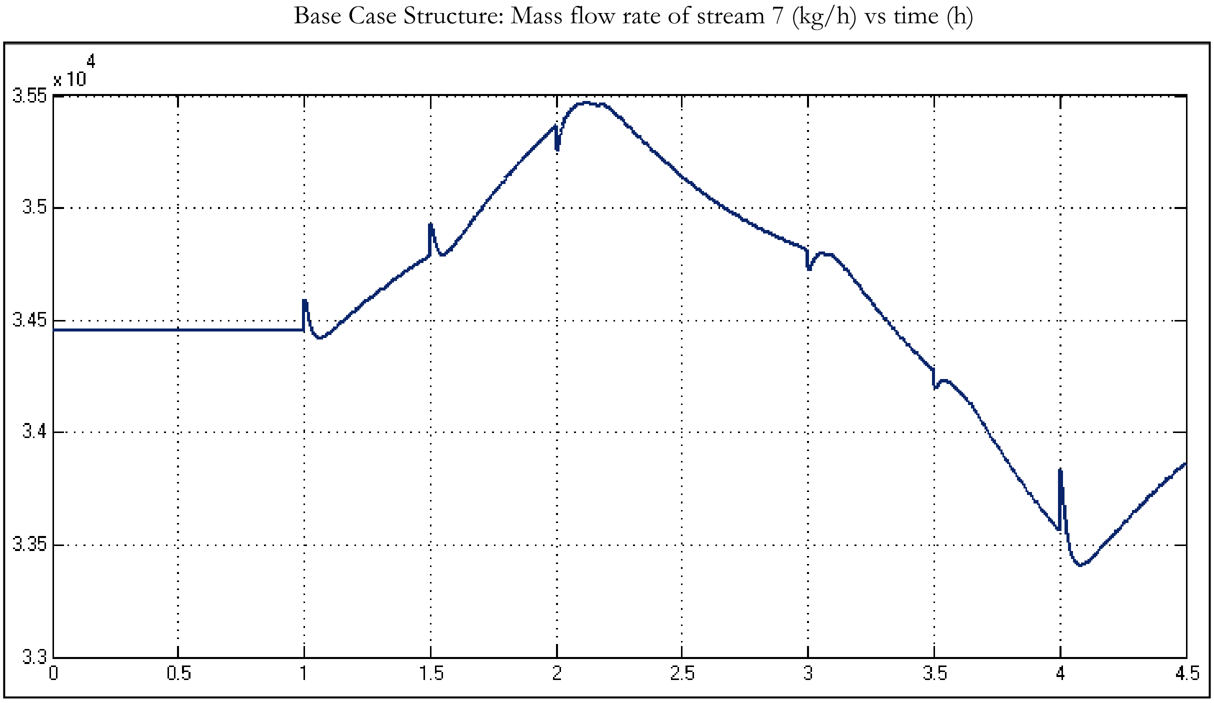

Figure 209: Plot of the flow rate of stream 1 (kg/h) versus time (in hours).

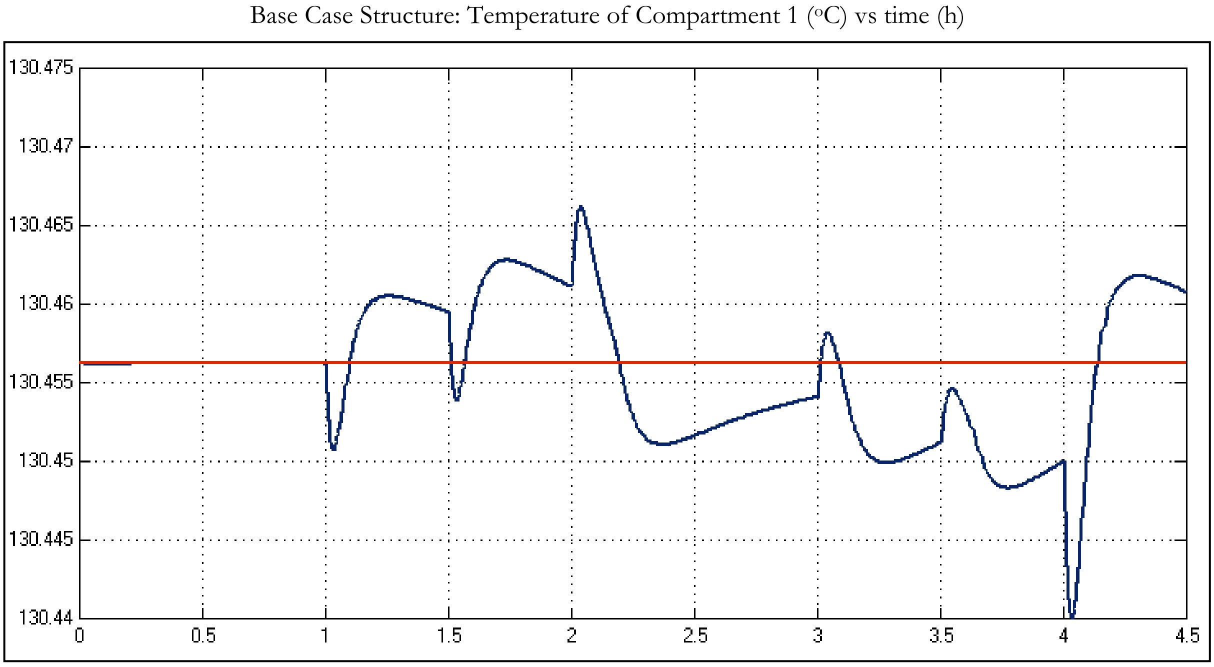

Figure 210: Plot of the set point (red) and measured (blue) values for the temperature of compartment 1 (°C) versus time (in hours). IAE = 1.171e-4, Maximum deviation= 0.006%.

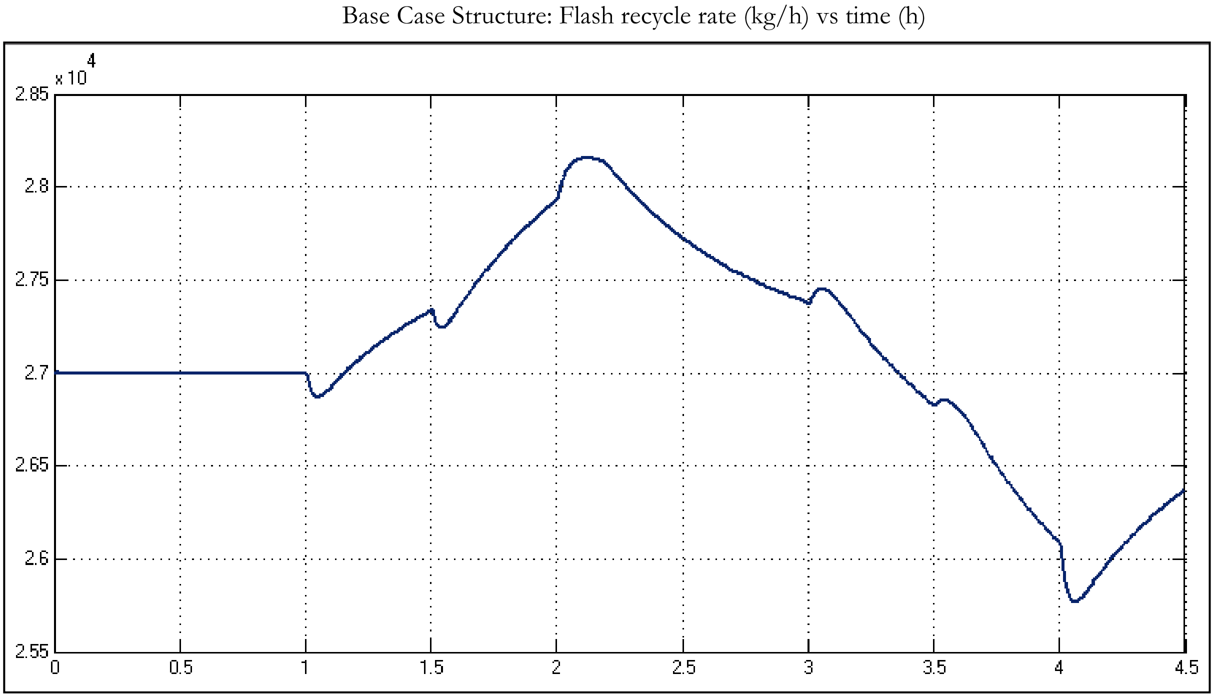

Figure 211: Plot of the flow rate of stream 9 (kg/h) versus time (in hours).

H2.2 Evaluation of Cascade Compositional Control – Acid Set Point Tracking

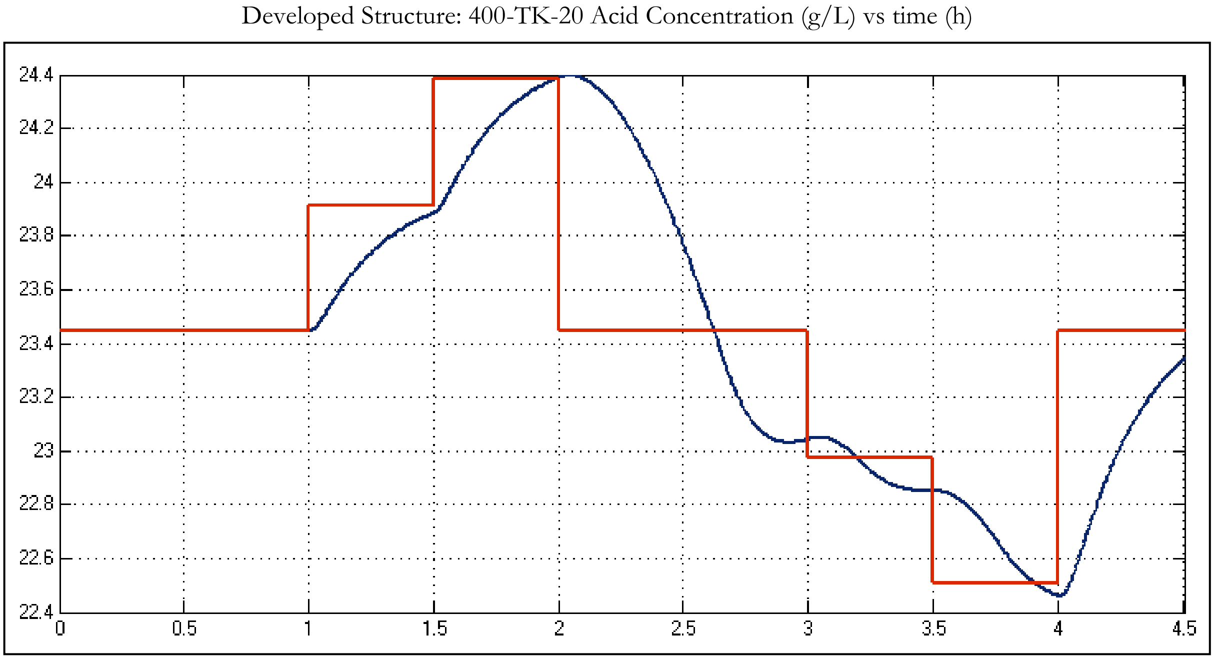

Figure 212: Plot of the set point (red) and measured (blue) developed model's acid concentration values for 400-TK-20 (g/L), versus time (hours). IAE = 0.0513, Maximum deviation = 4.2%.

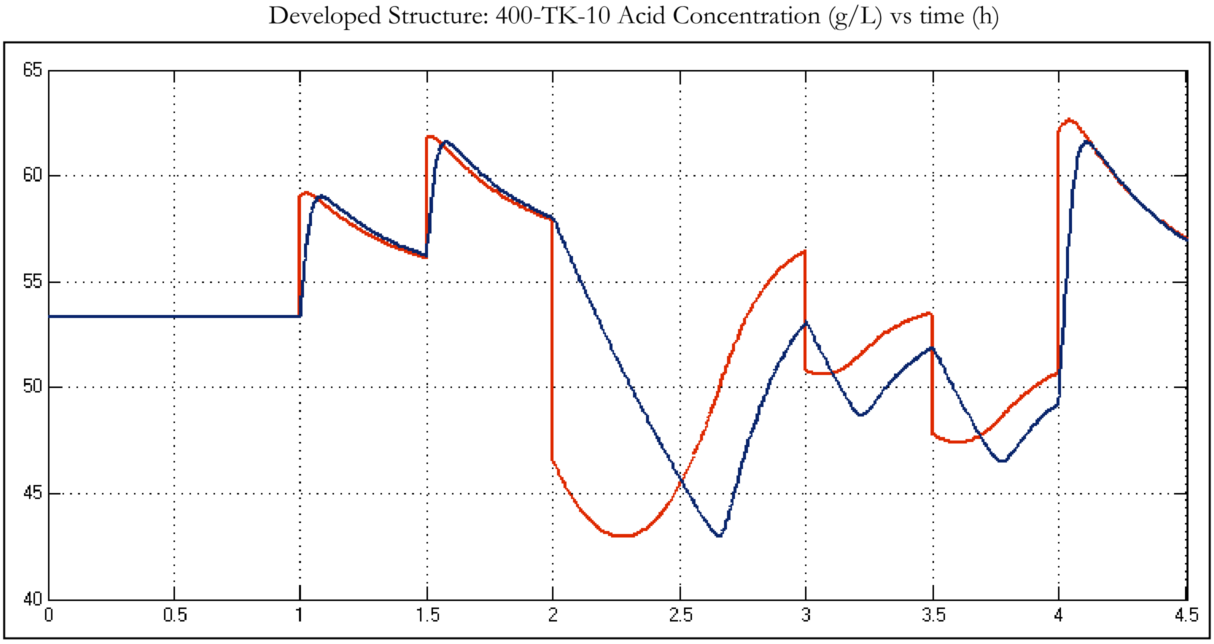

Figure 213: Plot of the set point (red) and measured (blue) developed model's acid concentration values for 400-TK-20 (g/L), versus time (hours).

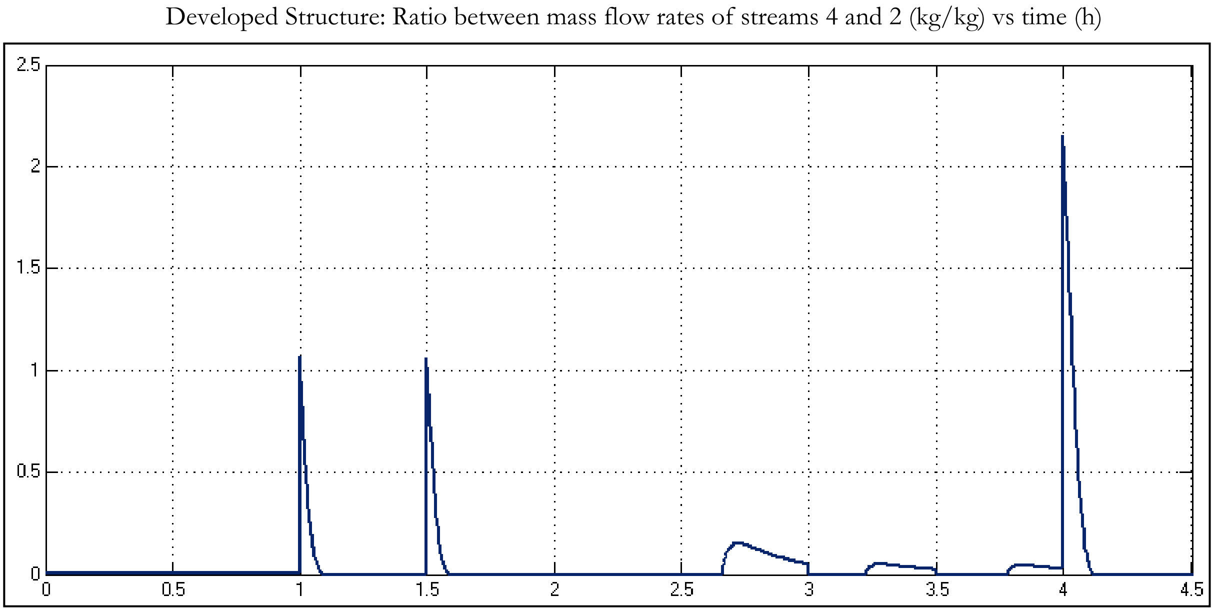

Figure 214: Plot of the ratio between the mass flow rates of streams 4 and 2 versus time (in hours).

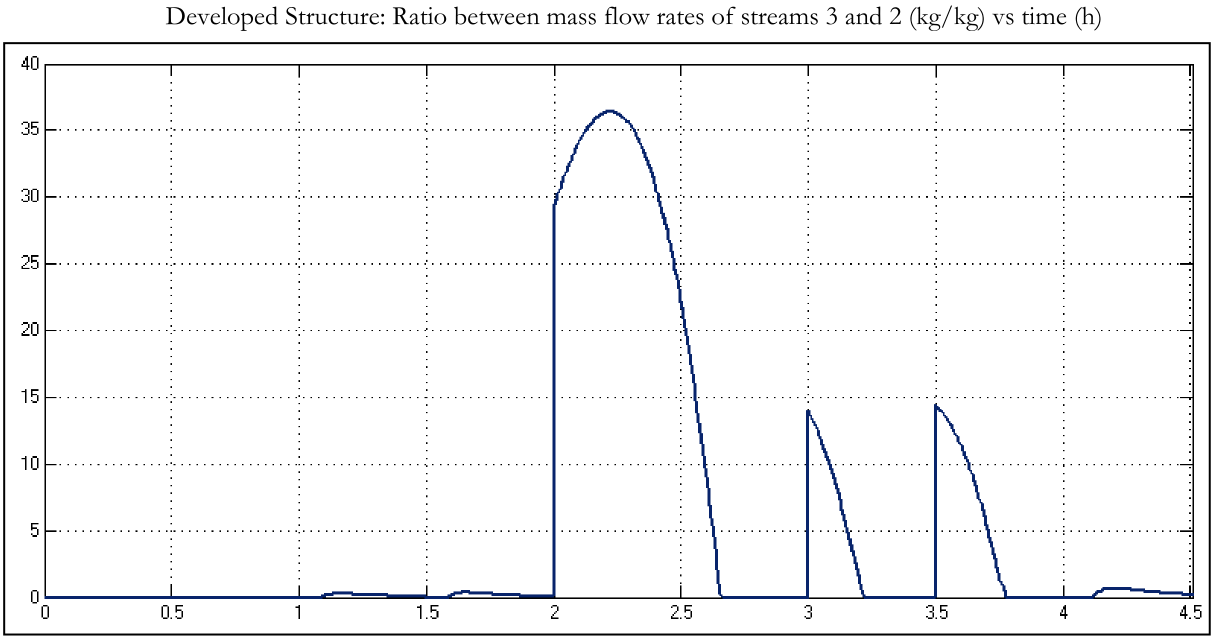

Figure 215: Plot of the ratio between the mass flow rates of streams 3 and 2 versus time (in hours).

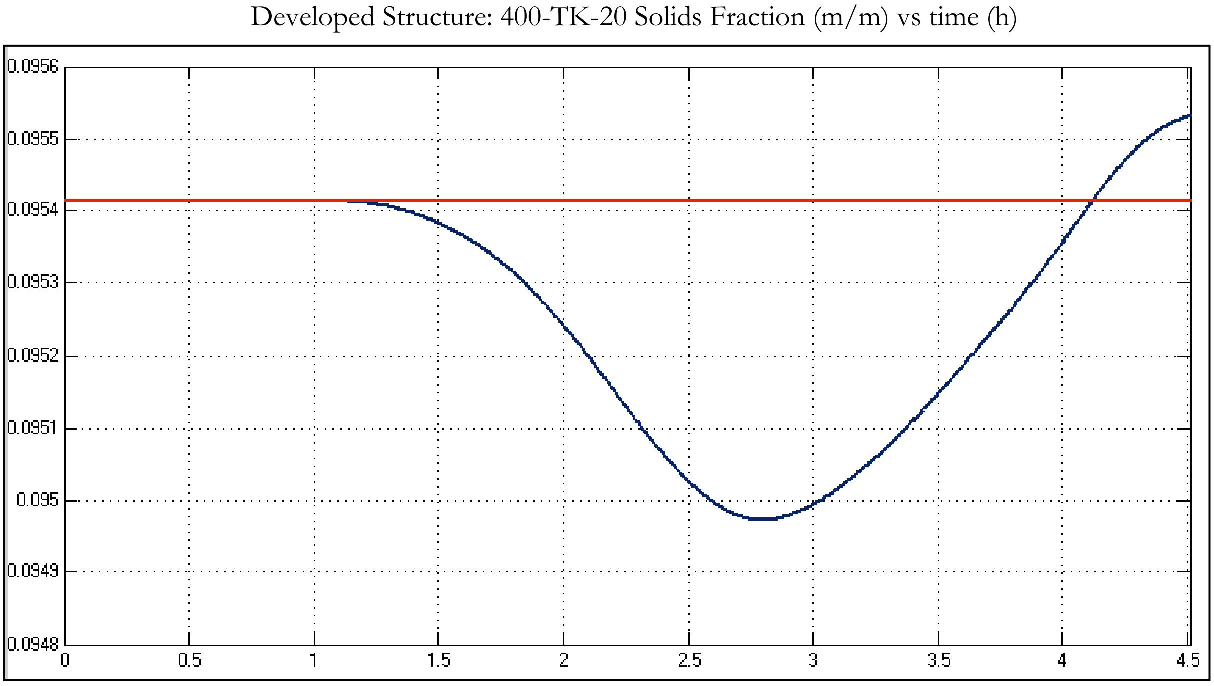

Figure 216: Plot of the set point (red) and measured (blue) developed model's solids fraction values for 400-TK-20, versus time (hours). IAE = 0.007, Maximum deviation = 0.46%.

The mass in 400-TK-10 shows no noticeable change.

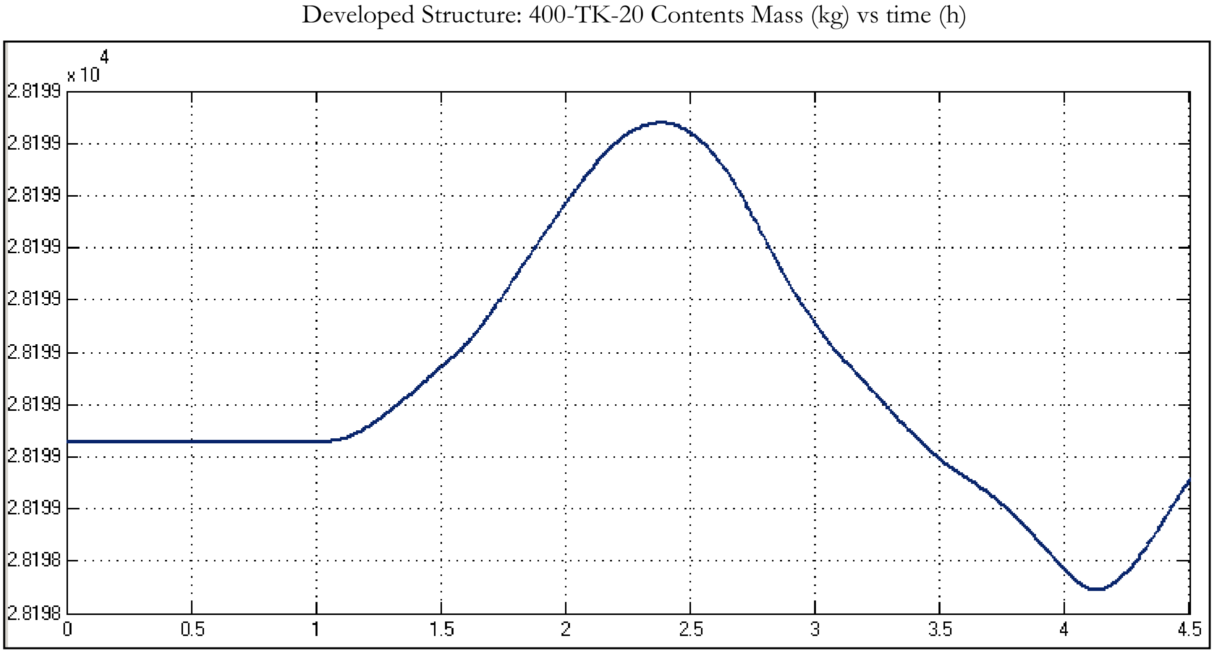

Figure 217: Plot of the developed model's mass of the contents of 400-TK-20 (kg), versus time (hours). IAE = 3.13e-5, Maximum deviation = 0.0022%.

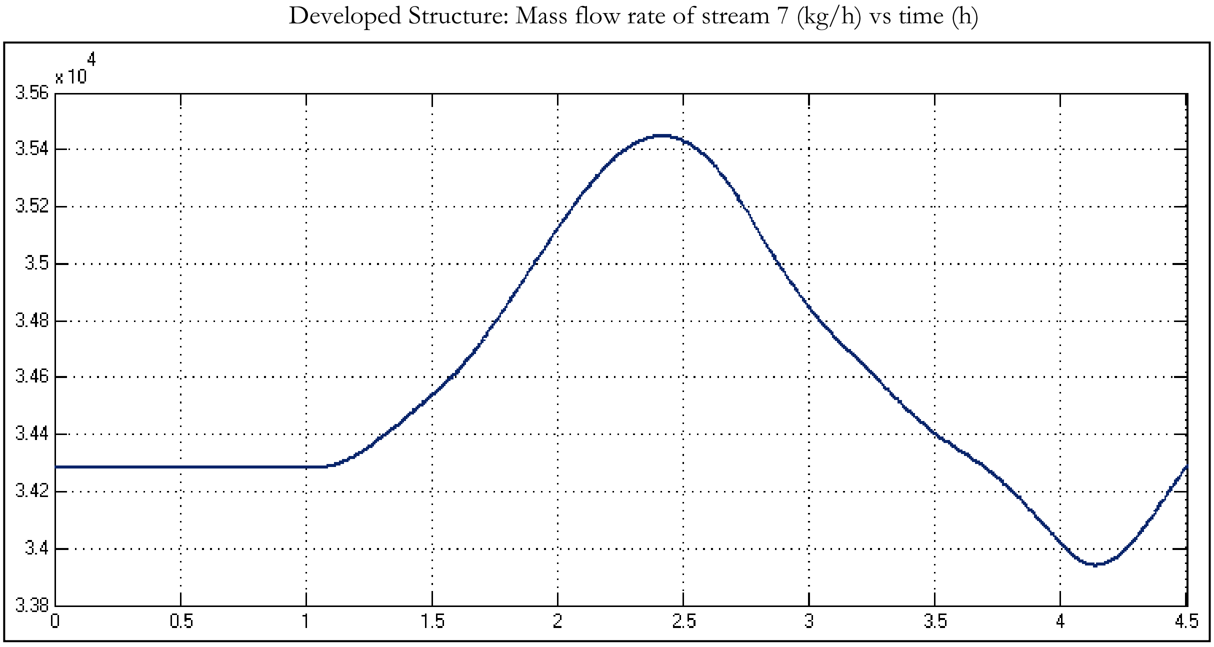

Figure 218: Plot of the mass flow rate of stream 7 (kg/h) versus time (in hours).

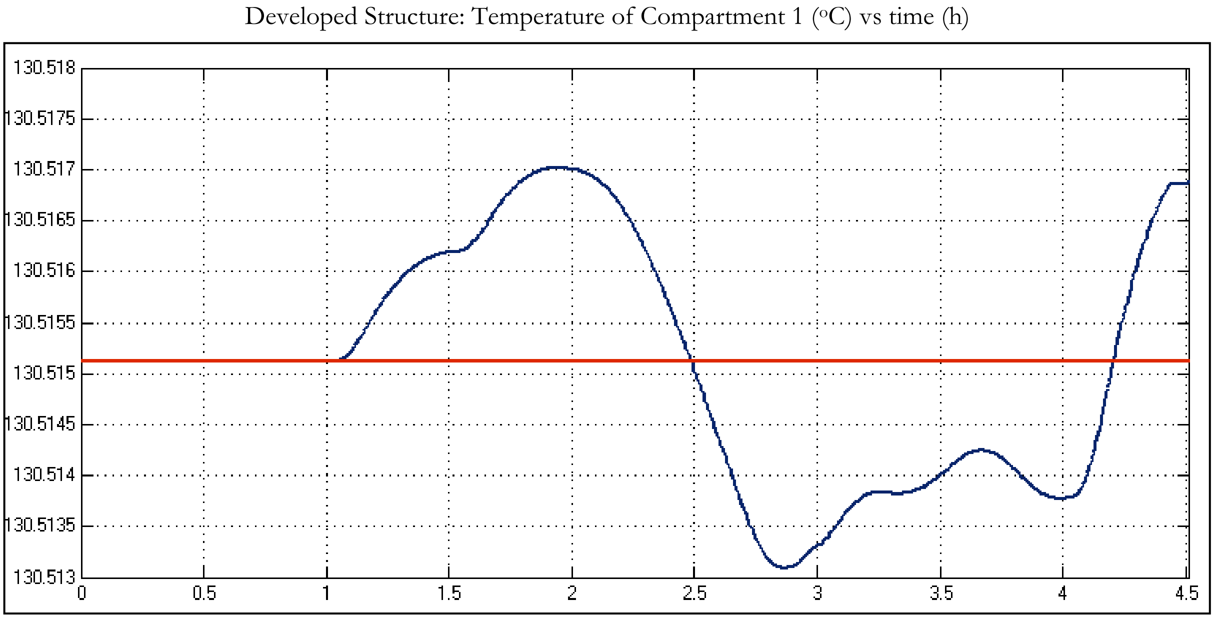

Figure 219: Plot of the set point (red) and measured (blue) values for the temperature of compartment 1 (^oC) versus time (in hours). IAE = 3.096e-5, Maximum deviation= 0.001%.

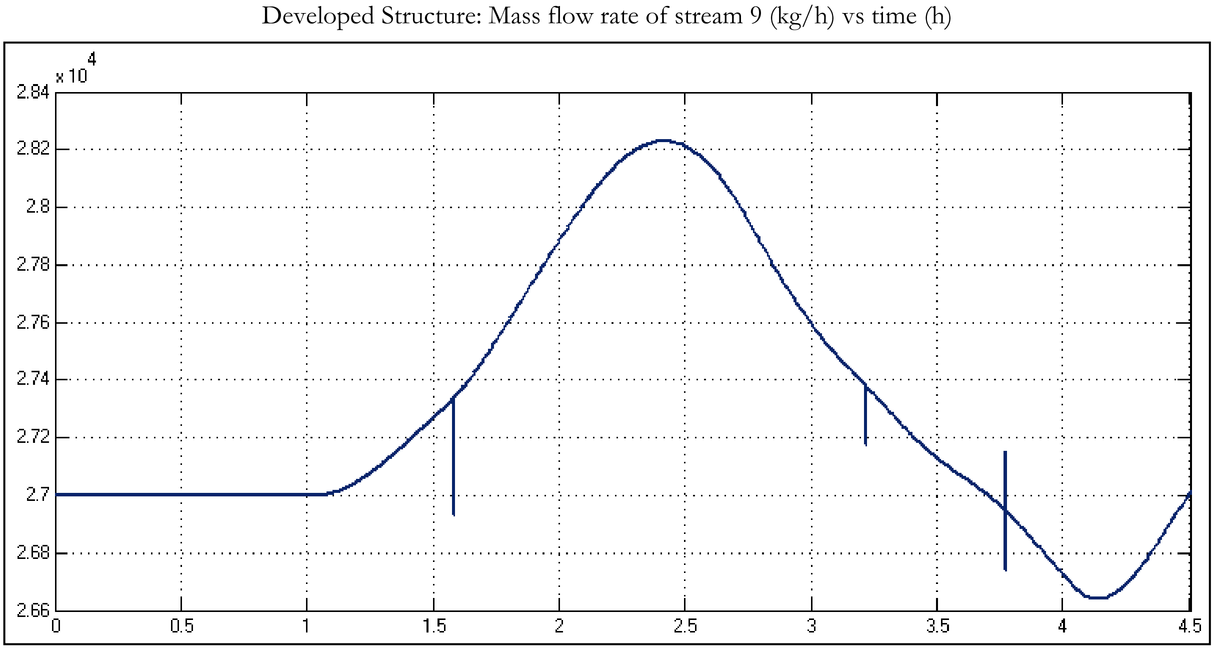

Figure 220: Plot of the mass flow rate of stream 9 (kg/h) versus time (in hours).

APPENDIX I

SIMULINK MODELS FOR CHAPTERS 4 & 5 ON DISK